



mobile communications series

Antti V. Räsänen  
Arto Lehto

# radio engineering

for Wireless  
Communication  
and Sensor  
Applications



**Radio Engineering for Wireless  
Communication and Sensor  
Applications**

For a listing of recent titles in the *Artech House Mobile Communications Series*,  
turn to the back of this book.

# **Radio Engineering for Wireless Communication and Sensor Applications**

Antti V. Räsänen  
Arto Lehto



Artech House  
Boston • London  
[www.artechhouse.com](http://www.artechhouse.com)

**Library of Congress Cataloging-in-Publication Data**

Räisänen, Antti V.

Radio engineering for wireless communication and sensor applications /  
Antti V. Räisänen, Arto Lehto.

p. cm. — (Artech House mobile communications series)

Includes bibliographical references and index.

ISBN 1-58053-542-9 (alk. paper)

1. Radio circuits. 2. Wireless communication systems—Equipment and supplies.  
3. Detectors. I. Lehto, Arto. II. Title. II. Series.

TK6560.R35 2003

621.384—dc21

2003048098

**British Library Cataloguing in Publication Data**

Räisänen, Antti V.

Radio engineering for wireless communication and sensor applications. — (Artech  
House mobile communications series)

1. Radio 2. Wireless communication systems

I. Title II. Lehto, Arto

621.3'84

ISBN 1-58053-542-9

**Cover design by Igor Valdman**

© 2003 ARTECH HOUSE, INC.

685 Canton Street

Norwood, MA 02062

All rights reserved. Printed and bound in the United States of America. No part of this book may be reproduced or utilized in any form or by any means, electronic or mechanical, including photocopying, recording, or by any information storage and retrieval system, without permission in writing from the publisher.

All terms mentioned in this book that are known to be trademarks or service marks have been appropriately capitalized. Artech House cannot attest to the accuracy of this information. Use of a term in this book should not be regarded as affecting the validity of any trademark or service mark.

International Standard Book Number: 1-58053-542-9

Library of Congress Catalog Card Number: 2003048098

10 9 8 7 6 5 4 3 2 1

*To our respective spouses, Hannele and Pirjo*



# Contents

	<b>Preface</b>	<b><i>xv</i></b>
	<b>Acknowledgments</b>	<b><i>xvii</i></b>
<b>1</b>	<b>Introduction to Radio Waves and Radio Engineering</b>	<b>1</b>
1.1	Radio Waves as a Part of the Electromagnetic Spectrum	1
1.2	What Is Radio Engineering?	4
1.3	Allocation of Radio Frequencies	4
1.4	History of Radio Engineering from Maxwell to the Present	6
	References	9
<b>2</b>	<b>Fundamentals of Electromagnetic Fields</b>	<b>11</b>
2.1	Maxwell's Equations	11
2.1.1	Maxwell's Equations in Case of Harmonic Time Dependence	14
2.1.2	Interpretations of Maxwell's Equations	15



2.2	Fields in Media	17
2.3	Boundary Conditions	20
2.4	Helmholtz Equation and Its Plane Wave Solution	22
2.5	Polarization of a Plane Wave	26
2.6	Reflection and Transmission at a Dielectric Interface	28
2.7	Energy and Power	31
	References	33
<b>3</b>	<b>Transmission Lines and Waveguides</b>	<b>35</b>
3.1	Basic Equations for Transmission Lines and Waveguides	38
3.2	Transverse Electromagnetic Wave Modes	40
3.3	Transverse Electric and Transverse Magnetic Wave Modes	42
3.4	Rectangular Waveguide	44
3.4.1	TE Wave Modes in Rectangular Waveguide	44
3.4.2	TM Wave Modes in Rectangular Waveguide	50
3.5	Circular Waveguide	52
3.6	Optical Fiber	56
3.7	Coaxial Line	58
3.8	Microstrip Line	61
3.9	Wave and Signal Velocities	65
3.10	Transmission Line Model	66
	References	68

---

<b>4</b>	<b>Impedance Matching</b>	<b>69</b>
4.1	Reflection from a Mismatched Load	69
4.2	Smith Chart	74
4.3	Matching Methods	78
4.3.1	Matching with Lumped Reactive Elements	79
4.3.2	Matching with Tuning Stubs (with Short Sections of Line)	86
4.3.3	Quarter-Wave Transformer	89
4.3.4	Resistive Matching	94
	References	95
<b>5</b>	<b>Microwave Circuit Theory</b>	<b>97</b>
5.1	Impedance and Admittance Matrices	97
5.2	Scattering Matrices	101
5.3	Signal Flow Graph, Transfer Function, and Gain	104
5.3.1	Mason's Rule	109
5.3.2	Gain of a Two-Port	111
	References	113
<b>6</b>	<b>Passive Transmission Line and Waveguide Devices</b>	<b>115</b>
6.1	Power Dividers and Directional Couplers	116
6.1.1	Power Dividers	117
6.1.2	Coupling and Directivity of a Directional Coupler	119
6.1.3	Scattering Matrix of a Directional Coupler	120
6.1.4	Waveguide Directional Couplers	122
6.1.5	Microstrip Directional Couplers	124
6.2	Ferrite Devices	128
6.2.1	Properties of Ferrite Materials	128

6.2.2	Faraday Rotation	131
6.2.3	Isolators	133
6.2.4	Circulators	134
6.3	Other Passive Components and Devices	134
6.3.1	Terminations	135
6.3.2	Attenuators	136
6.3.3	Phase Shifters	138
6.3.4	Connectors and Adapters	138
	References	139
<b>7</b>	<b>Resonators and Filters</b>	<b>141</b>
7.1	Resonators	141
7.1.1	Resonance Phenomenon	142
7.1.2	Quality Factor	142
7.1.3	Coupled Resonator	144
7.1.4	Transmission Line Section as a Resonator	147
7.1.5	Cavity Resonators	149
7.1.6	Dielectric Resonators	153
7.2	Filters	154
7.2.1	Insertion Loss Method	155
7.2.2	Design of Microwave Filters	161
7.2.3	Practical Microwave Filters	166
	References	169
<b>8</b>	<b>Circuits Based on Semiconductor Devices</b>	<b>171</b>
8.1	From Electron Tubes to Semiconductor Devices	171
8.2	Important Semiconductor Devices	172
8.2.1	Diodes	172
8.2.2	Transistors	177
8.3	Oscillators	180

---

8.4	Amplifiers	184
8.4.1	Design of Small-Signal and Low-Noise Amplifiers	184
8.4.2	Effect of Nonlinearities and Design of Power Amplifiers	191
8.4.3	Reflection Amplifiers	192
8.5	Frequency Converters (Mixers) and Frequency Multipliers	193
8.5.1	Mixers	194
8.5.2	Frequency Multipliers	197
8.6	Detectors	198
8.7	Monolithic Microwave Circuits	201
	References	202
<b>9</b>	<b>Antennas</b>	<b>205</b>
9.1	Fundamental Concepts of Antennas	205
9.2	Calculation of Radiation from Antennas	212
9.3	Radiating Current Element	214
9.4	Dipole and Monopole Antennas	217
9.5	Other Wire Antennas	222
9.6	Radiation from Apertures	225
9.7	Horn Antennas	232
9.8	Reflector Antennas	234
9.9	Other Antennas	236
9.10	Antenna Arrays	239
9.11	Matching of Antennas	242
9.12	Link Between Two Antennas	242
	References	245

<b>10</b>	<b><u>Propagation of Radio Waves</u></b>	<b>247</b>
10.1	Environment and Propagation Mechanisms	247
10.2	Tropospheric Attenuation	249
10.3	Bending (Refraction) of Radio Waves in Troposphere	252
10.4	LOS Path	255
10.5	Reflection from Ground	257
10.6	Multipath Propagation in Cellular Mobile Radio Systems	260
10.7	Propagation Aided by Scattering: Scatter Link	263
10.8	Propagation via Ionosphere	265
10.9	Propagation as a Ground (Surface) Wave	267
	References	270
<b>11</b>	<b><u>Radio System</u></b>	<b>271</b>
11.1	Transmitters and Receivers	271
11.2	Noise	275
11.2.1	Receiver Noise	275
11.2.2	Antenna Noise Temperature	284
11.3	Modulation and Demodulation of Signals	287
11.3.1	Analog Modulation	288
11.3.2	Digital Modulation	297
11.4	Radio Link Budget	304
	References	306

---

<b>12</b>	<b>Applications</b>	<b>307</b>
12.1	Broadcasting	307
12.1.1	Broadcasting in Finland	308
12.1.2	Broadcasting Satellites	310
12.2	Radio Link Systems	312
12.2.1	Terrestrial Radio Links	312
12.2.2	Satellite Radio Links	314
12.3	Wireless Local Area Networks	314
12.4	Mobile Communication	317
12.5	Radionavigation	320
12.5.1	Hyperbolic Radionavigation Systems	320
12.5.2	Satellite Navigation Systems	323
12.5.3	Navigation Systems in Aviation	326
12.6	Radar	328
12.6.1	Pulse Radar	328
12.6.2	Doppler Radar	332
12.6.3	Frequency-Modulated Radar	334
12.6.4	Surveillance and Tracking Radars	335
12.7	Remote Sensing	336
12.7.1	Radiometry	337
12.7.2	Total Power Radiometer and Dicke Radiometer	340
12.7.3	Remote-Sensing Radar	343
12.8	Radio Astronomy	345
12.8.1	Radio Telescopes and Receivers	346
12.8.2	Antenna Temperature of Radio Sources	349
12.8.3	Radio Sources in the Sky	350

12.9	Sensors for Industrial Applications	353
12.9.1	Transmission Sensors	354
12.9.2	Resonators	354
12.9.3	Reflection Sensors	355
12.9.4	Radar Sensors	355
12.9.5	Radiometer Sensors	356
12.9.6	Imaging Sensors	356
12.10	Power Applications	356
12.11	Medical Applications	357
12.11.1	Thermography	358
12.11.2	Diathermy	359
12.11.3	Hyperthermia	359
12.12	Electronic Warfare	359
12.12.1	ES	360
12.12.2	EA	360
12.12.3	EP	361
	References	361
<b>13</b>	<b>Biological Effects and Safety Standards</b>	<b>363</b>
	References	366
	<b>Appendix A: Vector Operations</b>	<b>367</b>
	<b>Appendix B: Physical Constants and Material Parameters</b>	<b>371</b>
	<b>List of Acronyms</b>	<b>373</b>
	<b>About the Authors</b>	<b>379</b>
	<b>Index</b>	<b>381</b>

# Preface

The word *radio* means techniques that are used in transmitting and receiving information or power in the atmosphere or free space, or in transmission lines utilizing electromagnetic waves—so-called radio waves—but also the equipment needed therein.

This book provides the reader with the basics in radio engineering, the techniques needed to generate, control, detect, and use radio waves. The text approaches the relevant problems both from the electromagnetic theory based on Maxwell's equations and from the circuit theory based on Kirchoff and Ohm's laws. Brief introductions to the electromagnetic theory as well as to the circuit theory are provided. Besides passive transmission lines and components, active RF circuits are also addressed. The treatment of the fundamentals of antennas and radio wave propagation in this book leads the reader to radio systems with noise and modulation considerations. Finally, a broad range of applications are described in addition to various wireless communication applications: radionavigation, radar, radiometry, remote sensing, radio astronomy, RF sensors, power and medical applications, and electronic warfare. The book ends with a short review of biological effects and safety standards. While numerous books specializing in various topics of radio engineering are available, this book gives a well-balanced, general overview of the whole topic. To the authors' knowledge, there are no similar books available.

This book got its origin from course lectures on the same topic at the Helsinki University of Technology. When we found that the Finnish text of our book (which was first published in 1992) written for our students



became very popular in the well-known Finnish wireless industry, we decided to write a similar book in English in order to provide an overview of this important technology to engineers, managers, sales representatives, and administrators globally.

In order to take full advantage from the contents of this book, one needs a solid background in physics and mathematics. The text can be used also without this background to obtain a general understanding of radio engineering, especially in Chapters 1, 12, and 13, and partly in Chapters 9, 10, and 11.

# Acknowledgments

We authors would like to thank our many colleagues and students, former and current, at the Helsinki University of Technology for their encouragement and many useful comments. We especially want to mention the help of Professors Sergei Tretyakov, Pertti Vainikainen, and Pekka Eskelinen. We would also like to express our appreciation of the professional drawings made by Harri Frestadius.

Dr. Räsänen is grateful to the Observatoire de Paris (LERMA) and Université de Paris 6, and especially to Professor Pierre Encrenaz for providing excellent conditions and good atmosphere for this writing task during his sabbatical leave.

Finally, we would like to thank our family members for their very important emotional support during the writing of this book.



# 1

## Introduction to Radio Waves and Radio Engineering

Electromagnetic waves propagate in a vacuum with the speed of light,  $c = 299,792,458$  m/s or about  $3 \times 10^8$  m/s. The electric and magnetic fields of a plane wave oscillate in phase and are perpendicular to each other and to the direction of propagation. The frequency of oscillation is  $f$ , and the wavelength is  $\lambda = c/f$ . Electromagnetic waves also may be considered to behave like particles of zero rest mass. The radiation consists of quanta, photons that have an energy of  $W = hf$  where  $h = 6.6256 \times 10^{-34}$  Js is Planck's constant.

There are many sources of electromagnetic radiation. Accelerating charges produce electromagnetic radiation, as when charges decelerating in an electric field produce bremsstrahlung and charges orbiting in a magnetic field produce synchrotron radiation. The random thermal motion of charged particles in matter produces thermal radiation. Atoms and molecules emit spectral line radiation as their energy level changes. The radiation generated by oscillators and emitted by antennas is based on high-frequency alternating currents.

### 1.1 Radio Waves as a Part of the Electromagnetic Spectrum

Electromagnetic waves cover a wide range of frequencies or wavelengths, as shown in Figure 1.1. The classification is based mainly on the sources of

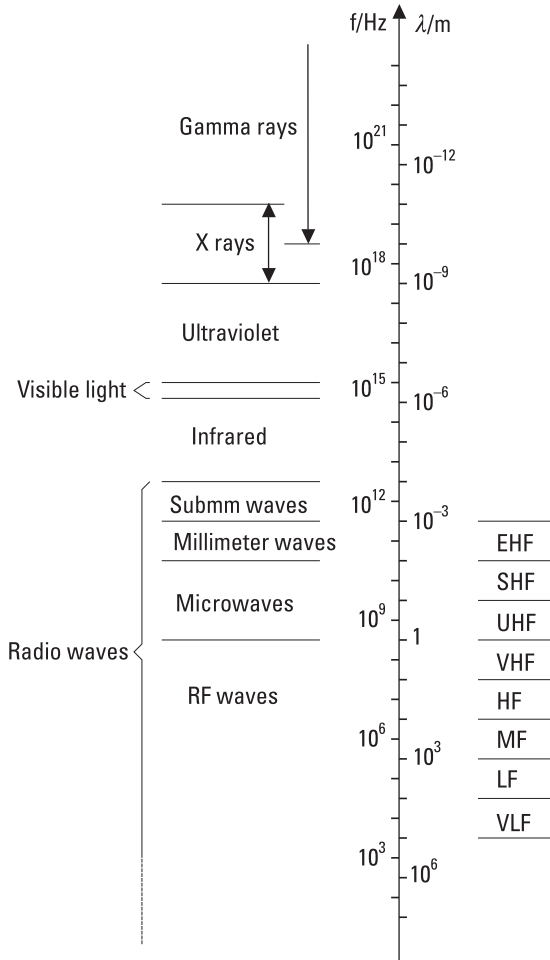


**Figure 1.1** Electromagnetic spectrum.

radiation. Boundaries of the ranges are not sharp, since different sources may produce waves in overlapping ranges of frequencies. The wavelengths of radio waves range from thousands of kilometers down to 0.1 mm. The frequency range is from a few hertz up to 3 THz. The waves having shorter wavelengths or higher frequencies than radio waves are classified as infrared, visible light, ultraviolet, x-rays, and gamma rays. Infrared waves are produced by molecules and hot bodies, light and ultraviolet waves by atoms and molecules, and x-rays by the inner electrons in atoms. Commercial x-ray tubes emit bremsstrahlung. Gamma rays originate in the nuclei of atoms and overlap the upper part of the x-ray spectrum.

The spectrum of radio waves is divided into ranges having a width of one decade, as indicated in Table 1.1 and Figure 1.1. Waves below 300 MHz are often called *radio frequency* (RF) waves. *Ultrahigh frequency* (UHF) and *superhigh frequency* (SHF) waves (300 MHz to 30 GHz) are called microwaves. Often the boundary between RF waves and microwaves is set to 1 GHz. The microwave range is further subdivided into bands according to waveguide bands, as shown in Table 1.2. *Extremely high frequency* (EHF) range is called the millimeter-wave range and the frequency range from 300 GHz to 3,000 GHz the submillimeter-wave range.

The interaction of electromagnetic waves with matter depends on the energy of photons. In general, shorter waves corresponding to energetic photons interact more strongly than longer waves. The photons of radio waves have low energies; for example, at 1,000 GHz the energy is only  $4 \times 10^{-3}$  eV ( $1 \text{ eV} = 1.6 \times 10^{-19} \text{ W}\cdot\text{s} = 1.6 \times 10^{-19} \text{ J}$ ). The energy needed to ionize molecules in biological tissue is at least 12 eV. Thus, ultraviolet

**Table 1.1**  
Ranges of Radio Waves

Name of Frequency Range and Abbreviation	Frequencies
Very low frequency (VLF)	3–30 kHz
Low frequency (LF)	30–300 kHz
Medium frequency (MF)	300–3,000 kHz
High frequency (HF)	3–30 MHz
Very high frequency (VHF)	30–300 MHz
Ultrahigh frequency (UHF)	300–3,000 MHz
Superhigh frequency (SHF)	3–30 GHz
Extremely high frequency (EHF)	30–300 GHz

**Table 1.2**  
Frequency Bands of Microwaves

Band	Frequencies
L	1–2 GHz
S	2–4 GHz
C	4–8 GHz
X	8–12 GHz
Ku	12–18 GHz
K	18–26 GHz
Ka	26–40 GHz

and radiation having even shorter wavelengths can ionize and dissociate molecules of biological tissues. Radio waves can only heat these materials. For example, water molecules are polar, and an electric field turns them back and forth, thus warming the food in a microwave oven.

Human beings gather a lot of information through electromagnetic waves. The retina of our eyes is sensitive to visible light, that is, wavelengths from 380 nm to 780 nm. The human skin can sense infrared or thermal radiation. Other parts of the spectrum cannot be sensed directly; they require their own specialized techniques to make the information carried by electromagnetic waves detectable. This book deals with the basic physics of radio waves and the techniques, which are needed to generate, transmit, and detect radio waves.

## 1.2 What Is Radio Engineering?

Radio engineering covers activities that use the possibilities offered by radio waves to serve the various goals of people. Some of these useful activities are:

- Broadcasting;
- Fixed communication (e.g., fixed radio links);
- Mobile communication;
- Radionavigation;
- Radiolocation (e.g., many radar applications);
- Amateur radio;
- Radio astronomy.

Radio engineering also covers the techniques needed to produce, process, investigate, measure, and use radio waves that make these services possible.

Electrical circuits and devices, in which the finite propagation speed of electric fields has to be taken into account or whose dimensions are of the same order as a wavelength, often are considered to belong to the field of radio engineering.

## 1.3 Allocation of Radio Frequencies

Radio waves have many applications and many users. However, the radio-frequency spectrum is a limited natural resource. Harmful interference

between users would take place if everybody sent signals at will. Therefore, the use of radio frequencies for different applications has been coordinated internationally.

The *International Telecommunication Union* (ITU) was reorganized in 1993. The *ITU Radiocommunication Sector* (ITU-R) comprises the former *Comité Consultatif International des Radiocommunications* (CCIR) and *International Frequency Registration Board* (IFRB), and is responsible for all of the ITU's work in the field of radiocommunication. The mission of ITU-R is to ensure rational, equitable, efficient, and economical use of the radio-frequency spectrum by all radiocommunication services, and to carry out studies and adopt recommendations on radiocommunication matters. Technical matters are drafted in ITU-R study groups and confirmed in *World Radiocommunication Conferences* (WRCs) every second or third year. The use of the radio-frequency spectrum is regulated in the *Radio Regulations* [1], which are updated according to the decisions made by WRCs.

In most applications, the use of radio frequencies cannot cause interference worldwide. For example, microwaves cannot propagate far beyond the horizon. For the allocation of frequencies, the world has been divided into three regions, as shown in Figure 1.2. For example, Region 1 includes Europe, Russia, Africa, the Middle East, and parts of Asia.

The radio-frequency spectrum is allocated for about 40 radio services in the *Radio Regulations*. Table 1.3 is an extract of the table of frequency allocation [1] and shows the use of frequency band 10 to 10.7 GHz for

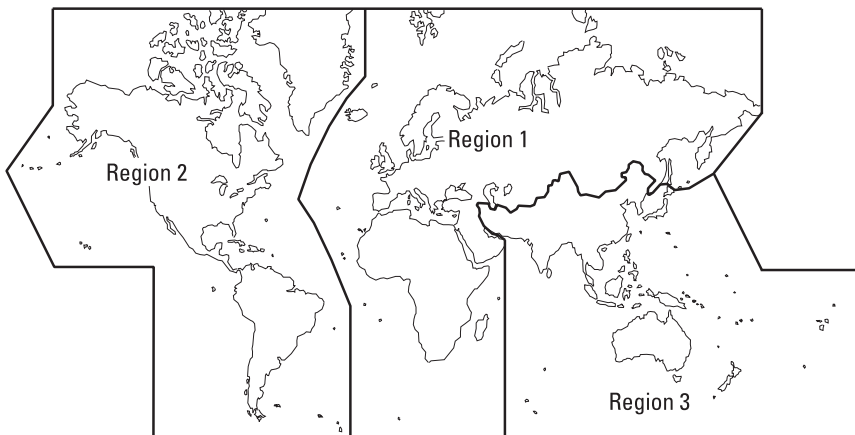


**Figure 1.2** Division of world in three regions for frequency allocation. (After: [1].)



**Table 1.3**  
Frequency Allocation for the Frequency Band 10–10.7 GHz

10–10.45 GHz	Fixed (Region 1 and 3) Mobile (Region 1 and 3) Radiolocation (Amateur)
10.45–10.5 GHz	Radiolocation (Amateur, amateur satellite)
10.5–10.55 GHz	Fixed Mobile Radiolocation (Region 2 and 3; secondary in Region 1)
10.55–10.6 GHz	Fixed Mobile, except aeronautical mobile (Radiolocation)
10.6–10.68 GHz	Earth exploration satellite, passive Fixed Mobile, except aeronautical mobile Radio astronomy Space research, passive (Radiolocation)
10.68–10.7 GHz	Earth exploration satellite, passive Radio astronomy Space research, passive

Source: [1].

primary and secondary services (regional limitations and secondary services are shown in parentheses).

In addition to the frequency allocation, all radio and other electrical equipment must comply with the *electromagnetic compatibility* (EMC) requirements and standards to assure interference-free operation [2]. Standards set limits to the emission of equipment and give requirements for their immunity against interference.

## 1.4 History of Radio Engineering from Maxwell to the Present

The Scottish physicist and mathematician James Clerk Maxwell (1831–1879) predicted the existence of electromagnetic waves. He combined Gauss' law for electric and magnetic fields, Ampère's law for magnetic fields, and the Faraday-Henry law of electromagnetic induction, and added displacement

current to Ampère's law. He formulated a set of equations, which he published in 1864. These equations showed the interrelation of electric and magnetic fields. Maxwell proposed that visible light is formed of electromagnetic vibrations and that electromagnetic waves of other wavelengths propagating with the speed of light were possible.

The German physicist Heinrich Hertz (1857–1894) was the first to prove experimentally the existence of radio waves, thus verifying Maxwell's equations [3]. In 1888, he released the results of his first experiments. The transmitter was an end-loaded dipole antenna with a spark gap. A current oscillating back and forth was produced as the charged antenna was discharged across the spark gap. The receiver consisted of a loop antenna and a spark gap. With this apparatus operating at about 50 MHz, Hertz was able to show that there are radio waves. Later he showed the reflection, diffraction, and polarization of radio waves, and he measured the wavelength from an interference pattern of radio waves.

The first person to use radio waves for communication was the Italian inventor Guglielmo Marconi (1874–1937). He made experiments in 1895 and submitted his patent application "Improvements in transmitting electrical impulses and signals and in apparatus therefor" in England in 1896. In 1901, Marconi, using his wireless telegraph, succeeded in sending the letter S in Morse code from Poldhu in Cornwall across the Atlantic to St. Johns in Newfoundland. Because the distance was over 3,000 km, this experiment demonstrated that radio waves could be sent beyond the horizon, contrary to the common belief of that time. The Russian physicist Alexander Popov (1859–1906) made experiments nearly simultaneously with Marconi. He demonstrated his apparatus in 1896 to a scientific audience in St. Petersburg.

Hertz used a spark gap between antenna terminals as a receiver. In 1891, the French physicist Edouard Branly (1846–1940) published a better detector, a coherer. It was based on the properties of small metal particles between two electrodes in an evacuated glass tube. Both Marconi and Popov used coherers in their early experiments. The invention of vacuum tubes was a great step forward toward better transmitters and receivers. In 1904, the British physicist John Ambrose Fleming (1849–1945) invented the rectifying vacuum tube, the diode. In 1906 the American inventor Lee De Forest (1873–1961) added a third electrode, called a grid, and thereby invented the triode. The grid controlled the current and made amplification possible. The efficiency of the electron tubes was greatly improved by using concentric cylinders as electrodes. One of the first inventors was the Finnish engineer Eric Tigerstedt (1886–1925), who filed his patent application for such a triode in 1914.

De Forest and the American engineer and inventor Edwin Armstrong (1890–1954) independently discovered regenerative feedback in 1912. This phenomenon was used to produce a continuous carrier wave, which could be modulated by a voice signal. Armstrong invented also the superheterodyne receiver. These techniques made broadcasting possible. AM stations began broadcasting in 1919 and 1920. Regular TV transmissions started in Germany in 1935. Armstrong's third great broadcasting invention was FM radio, but FM broadcasting was accepted not until after World War II.

Communication was not the only application of radio waves. Karl Jansky (1905–1950), while studying radio noise at Bell Labs in 1932, detected a steady hiss from our own galaxy, the Milky Way. This was the beginning of radio astronomy. The invention of microwave tubes, of klystron in 1939, and of magnetron in 1940 was essential for the development of microwave radar during World War II. The principle of radar had been introduced much earlier by the German engineer Christian Hülsmeyer (1881–1957), who made experiments in 1903. Due to the lack of financing, the idea was abandoned until 1922, when Marconi proposed using radar for detecting ships in fog.

The Radiation Laboratory, which was established at the Massachusetts Institute of Technology during World War II, had a great impact on the development of radio engineering. Many leading American physicists were gathered there to develop radar, radionavigation, microwave components, microwave theory, electronics, and education in the field, and gave written 27 books on the research conducted there.

The rectifying properties of semiconductors were noted in the late nineteenth century. However, the development of semiconductor devices was slow because vacuum tubes could do all the necessary operations, such as amplification and detection. A serious study of semiconductors began in the 1940s. The high-frequency capabilities of the point-contact semiconductor diode had already been observed. The invention of the transistor by Bardeen, Brattain, and Shockley started a new era in electronics. Their point-contact transistor worked for the first time in 1947. The principle of the bipolar junction transistor was proposed the next year.

The subsequent development of semiconductor devices is a prerequisite for the radio engineering of today. The continuous development of components and integrated circuits has made it possible to pack more complex functions to an ever-smaller space, which in turn has made possible many modern systems, such as mobile communication, satellite communication, and satellite navigation systems.

## References

- [1] *Radio Regulations*, Vol. I, Geneva, Switzerland: International Telecommunication Union, 2001.
- [2] Paul, C. R., *Introduction to Electromagnetic Compatibility*, New York: John Wiley & Sons, 1992.
- [3] Levy, R., (ed.), “Special Issue Commemorating the Centennial of Heinrich Hertz,” *IEEE Trans. on Microwave Theory and Techniques*, Vol. 36, No. 5, 1988, pp. 801–858.



# 2

## Fundamentals of Electromagnetic Fields

In this chapter, we outline the fundamentals of electromagnetic theory that we will need in the analysis of waveguides, antennas, and other devices. Here we use the following electric and magnetic quantities:

- E**, electric field strength [V/m];
- D**, electric flux density [ $C/m^2 = As/m^2$ ];
- H**, magnetic field strength [A/m];
- B**, magnetic flux density [ $Wb/m^2 = Vs/m^2$ ];
- J**, electric current density [ $A/m^2$ ];
- J<sub>s</sub>**, electric surface current density [A/m];
- ρ**, electric charge density [ $C/m^3 = As/m^3$ ].

### 2.1 Maxwell's Equations

Maxwell's equations relate the fields (**E** and **H**) and their sources (**ρ** and **J**) to each other. The electric field strength **E** and the magnetic flux density **B** may be considered the basic quantities, because they allow calculation of a force **F**, applied to a charge, *q*, moving at a velocity, **v**, in an electromagnetic field; this is obtained using Lorentz's force law:

$$\mathbf{F} = q(\mathbf{E} + \mathbf{v} \times \mathbf{B}) \quad (2.1)$$

The electric flux density  $\mathbf{D}$  and the magnetic field strength  $\mathbf{H}$  take into account the presence of materials. The electric and magnetic properties of media bind the field strengths and flux densities; the constitutive relations are

$$\mathbf{D} = \epsilon \mathbf{E} \quad (2.2)$$

$$\mathbf{B} = \mu \mathbf{H} \quad (2.3)$$

where  $\epsilon$  is the permittivity [ $\text{F/m} = \text{As/Vm}$ ] and  $\mu$  is the permeability [ $\text{H/m} = \text{Vs/Am}$ ] of the medium.

Maxwell's equations in differential form are

$$\text{I} \quad \nabla \cdot \mathbf{D} = \rho \quad \text{Gauss' law} \quad (2.4)$$

$$\text{II} \quad \nabla \cdot \mathbf{B} = 0 \quad (2.5)$$

$$\text{III} \quad \nabla \times \mathbf{E} = -\frac{\partial \mathbf{B}}{\partial t} \quad \text{Faraday's law} \quad (2.6)$$

$$\text{IV} \quad \nabla \times \mathbf{H} = \mathbf{J} + \frac{\partial \mathbf{D}}{\partial t} \quad \text{Ampère's law and Maxwell's addition} \quad (2.7)$$

As also mentioned in the above equations, a lot of the knowledge of electromagnetic theory was already developed before Maxwell by Gauss, Faraday, Ampère, and others. Maxwell's contribution was to put the existing knowledge together and to add the hypothetical displacement current, which then led to Hertz and Marconi's discoveries and to modern radio engineering.

How did Maxwell discover the displacement current? We may speculate and simplify this process of invention as follows (see [1], Chapter 18): Maxwell studied the known laws and expressed them as differential equations for each vector component, because the nabla notation (curl and divergence of a vector quantity) was not yet known. Nevertheless, we use the nabla notation here. He found that while Gauss' and Faraday's laws are true in general, there is a problem in Ampère's law:

$$\nabla \times \mathbf{H} = \mathbf{J} \quad (2.8)$$

If one takes the divergence of this equation, the left-hand side is zero, because the divergence of a curl is always zero. However, if the divergence of  $\mathbf{J}$  is zero, then the total flux of current through any closed surface is zero. Maxwell

correctly understood the law of charge conservation: The flux of current through a closed surface must be equal to the change of charge inside the surface (in the volume), that is,

$$\nabla \cdot \mathbf{J} = -\frac{\partial \rho}{\partial t} \quad (2.9)$$

In order to avoid the controversy, Maxwell added the displacement current term,  $\partial \mathbf{D} / \partial t$ , to the right-hand side of Ampère's law in a general case and got

$$\nabla \times \mathbf{H} = \mathbf{J} + \frac{\partial \mathbf{D}}{\partial t} \quad (2.10)$$

With this addition the principle of charge conservation holds, because by using Gauss' law we obtain

$$\nabla \cdot \nabla \times \mathbf{H} = \nabla \cdot \mathbf{J} + \frac{\partial}{\partial t} \nabla \cdot \mathbf{D} = \nabla \cdot \mathbf{J} + \frac{\partial \rho}{\partial t} = 0$$

The differential equations, (2.4) through (2.7), describe the fields locally or at a given point. In other words, they allow us to obtain the change of field versus space or time. Maxwell's equations in integral form describe how the field integrals over a closed surface  $S$  ( $\oint_S$ ) or along a closed loop  $\Gamma$  ( $\oint_\Gamma$ ) depend on the sources and changes of the fields versus time. Maxwell's equations in integral form are:

$$\text{I} \quad \oint_S \mathbf{D} \cdot d\mathbf{S} = \int_V \rho dV \quad (2.11)$$

$$\text{II} \quad \oint_S \mathbf{B} \cdot d\mathbf{S} = 0 \quad (2.12)$$

$$\text{III} \quad \oint_\Gamma \mathbf{E} \cdot d\mathbf{l} = -\frac{\partial}{\partial t} \int_S \mathbf{B} \cdot d\mathbf{S} \quad (2.13)$$

$$\text{IV} \quad \oint_\Gamma \mathbf{H} \cdot d\mathbf{l} = \int_S \left( \mathbf{J} + \frac{\partial \mathbf{D}}{\partial t} \right) \cdot d\mathbf{S} \quad (2.14)$$



where  $d\mathbf{S}$  is an element vector perpendicular to surface  $S$  having a magnitude equal to the surface element area,  $d\mathbf{l}$  is a length element parallel to the loop, and  $dV$  is a volume element. The volume,  $V$ , is enclosed by the closed surface  $S$ . Equations (2.11) and (2.12) are obtained by applying Gauss' theorem, according to which for any vector quantity  $\mathbf{A}$  it holds

$$\oint_S \mathbf{A} \cdot d\mathbf{S} = \int_V \nabla \cdot \mathbf{A} dV \quad (2.15)$$

and (2.13) and (2.14) are obtained by applying Stokes' theorem

$$\oint_{\Gamma} \mathbf{A} \cdot d\mathbf{l} = \int_S (\nabla \times \mathbf{A}) \cdot d\mathbf{S} \quad (2.16)$$

Maxwell's equations would be symmetric in relation to electric and magnetic quantities if magnetic charge density  $\rho_M$  [ $\text{Wb}/\text{m}^3 = \text{Vs}/\text{m}^3$ ] and magnetic current density  $\mathbf{M}$  [ $\text{V}/\text{m}^2$ ] were also introduced into them. However, there is no experimental evidence of their existence.

### 2.1.1 Maxwell's Equations in Case of Harmonic Time Dependence

Time harmonic fields, that is, fields having a sinusoidal time dependence at angular frequency of  $\omega = 2\pi f$ , may be presented as

$$\mathbf{A}(x, y, z, t) = \text{Re}[\mathbf{A}(x, y, z)e^{j\omega t}] \quad (2.17)$$

At a given point  $(x, y, z)$ , the field may be thought to be a vector rotating on the complex plane and having a constant amplitude, the real part of which is the field value at a given instant. Most phenomena in radio engineering are time harmonic or can be thought to be superpositions of several time harmonics. Therefore, in this book we will confine ourselves to the time harmonic cases. Assuming the  $e^{j\omega t}$  time dependence, the time derivatives can be replaced by multiplications by  $j\omega$ . For such sinusoidal fields and sources, Maxwell's equations in differential form are

$$\text{I} \quad \nabla \cdot \mathbf{D} = \rho \quad (2.18)$$

$$\text{II} \quad \nabla \cdot \mathbf{B} = 0 \quad (2.19)$$

$$\text{III} \quad \nabla \times \mathbf{E} = -j\omega\mathbf{B} = -j\omega\mu\mathbf{H} \quad (2.20)$$

$$\text{IV} \quad \nabla \times \mathbf{H} = \mathbf{J} + j\omega\mathbf{D} = (\sigma + j\omega\epsilon)\mathbf{E} \quad (2.21)$$

and in integral form

$$\text{I} \quad \oint_S \mathbf{D} \cdot d\mathbf{S} = \int_V \rho dV \quad (2.22)$$

$$\text{II} \quad \oint_S \mathbf{B} \cdot d\mathbf{S} = 0 \quad (2.23)$$

$$\text{III} \quad \oint_{\Gamma} \mathbf{E} \cdot d\mathbf{l} = -j\omega \int_S \mathbf{B} \cdot d\mathbf{S} = -j\omega\mu \int_S \mathbf{H} \cdot d\mathbf{S} \quad (2.24)$$

$$\text{IV} \quad \oint_{\Gamma} \mathbf{H} \cdot d\mathbf{l} = \int_S (\mathbf{J} + j\omega\mathbf{D}) \cdot d\mathbf{S} = (\sigma + j\omega\epsilon) \int_S \mathbf{E} \cdot d\mathbf{S} \quad (2.25)$$

In (2.21) and (2.25) we have taken into account that

$$\mathbf{J} = \sigma\mathbf{E} \quad (2.26)$$

where  $\sigma$  is the conductivity [ $\text{S/m} = \text{A/Vm}$ ] of the medium.

## 2.1.2 Interpretations of Maxwell's Equations

Maxwell's equations may be presented in words as follows:

- I The electric flux (surface integral of the electric flux) through a closed surface is equal to the total charge within the volume confined by the surface.
- II The magnetic flux (surface integral of the magnetic flux) through any closed surface is zero.
- III The line integral of the electric field along a closed contour is equal to the negative time derivative of the magnetic flux through the closed contour.
- IV The line integral of the magnetic field along a closed contour is equal to the sum of the total current through the closed contour and the time derivative of the electric flux.

Figure 2.1 illustrates Maxwell's equations in integral form. These qualitative interpretations are as follows:

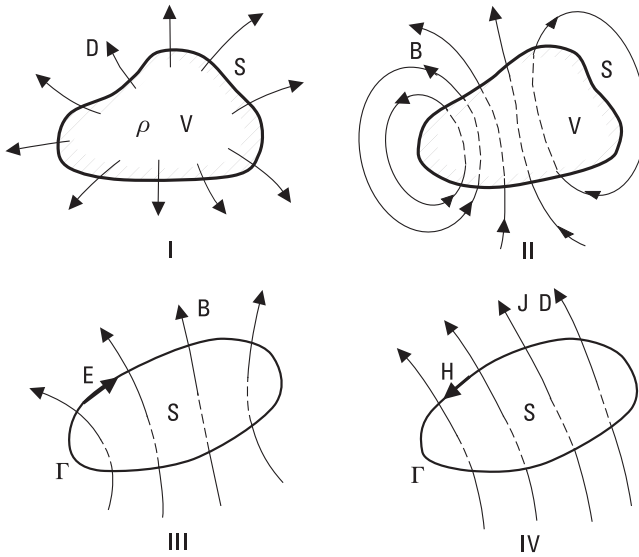


**Figure 2.1** Maxwell's equations (in integral form).

- I The distribution of the electric charge determines the electric field.
- II The magnetic flux lines are closed; in other words, there are no magnetic charges.
- III A changing magnetic flux creates an electric field.
- IV Both a moving charge (current) and a changing electric flux create a magnetic field.

The creation of an electromagnetic field is easy to understand qualitatively with the aid of Maxwell's equations. Let us consider a current loop with a changing current. The changing current creates a changing magnetic field (IV); the changing magnetic field creates a changing electric field (III); the changing electric field creates a changing magnetic field (IV); and so on. Figure 2.2 illustrates the creation of a propagating wave.

Maxwell's equations form the basis of radio engineering and, in fact, of the whole of electrical engineering. These equations cannot be derived from other laws; they are based on empirical research. Their validity comes from their capability to predict the electromagnetic phenomena correctly. Many books deal with fundamentals of the electromagnetic fields, such as those listed in [1–8].

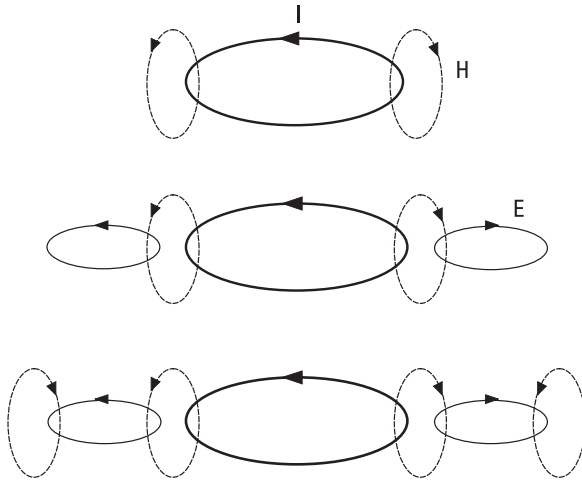


**Figure 2.2** Electromagnetic wave produced by a current loop.

## 2.2 Fields in Media

In the above equations, the permittivity  $\epsilon$  and permeability  $\mu$  represent the properties of the medium. A medium is homogeneous if its properties are constant, independent of location. An isotropic medium has the same properties in all directions. The properties of a linear medium are independent on field strength.

In a vacuum,  $\epsilon = \epsilon_0 \approx 8.8542 \times 10^{-12}$  F/m and  $\mu = \mu_0 = 4\pi \times 10^{-7}$  H/m. In other homogeneous media,  $\epsilon = \epsilon_r \epsilon_0$  and  $\mu = \mu_r \mu_0$ , where the dielectric constant  $\epsilon_r$ , that is, the relative permittivity, and the relative permeability,  $\mu_r$ , depend on the structure of the material. For air we can take  $\epsilon_r = \mu_r = 1$  for most applications. In general, in a lossy medium,  $\epsilon_r$  or  $\mu_r$  are complex, and in an anisotropic medium  $\epsilon_r$  or  $\mu_r$  are tensors.

Let us consider a dielectric that has no freely moving charges. The electric field, however, causes polarization of the material, that is, the electric dipole moments tend to align along the field. The field induces a dipole moment into the atoms by disturbing the movement of electrons. The so-called polar molecules, such as the water molecule, have a stationary dipole moment, because the charge is distributed unevenly in the molecule.

Electric polarization may be illustrated with a plate capacitor, the plates of which have an area of  $A$  and charges of  $+Q$  and  $-Q$ . If the fringing field lines are negligible, the electric flux density is  $D = Q/A$ . If there is vacuum (or air) between the plates, the electric field strength is  $E_0 = D/\epsilon_0$ ; see

Figure 2.3(a). When a dielectric material is introduced between the plates, the dipole moments align along the field lines; see Figure 2.3(b). The flux density does not change if  $Q$  does not change, because the charge density in the dielectric is zero. However, the field strength decreases, because the field caused by the dipole moments cancels part of the original field. Therefore, the electric flux density may be written as

$$\mathbf{D} = \epsilon_0 \mathbf{E} + \mathbf{P}_e \tag{2.27}$$

where  $\mathbf{P}_e$  is a dipole moment per unit volume due to polarization. If a constant voltage is applied between the plates, the electric field strength stays constant, and the electric flux density and the charge of the plates increase when dielectric material is introduced between the plates. In a linear medium, the electric polarization depends linearly on the field strength

$$\mathbf{P}_e = \epsilon_0 \chi_e \mathbf{E} \tag{2.28}$$

where  $\chi_e$  is the electric susceptibility, which may be complex. Now

$$\mathbf{D} = \epsilon_0 (1 + \chi_e) \mathbf{E} = \epsilon \mathbf{E} \tag{2.29}$$

where

$$\epsilon = \epsilon_0 (1 + \chi_e) = \epsilon_0 \epsilon_r = \epsilon_0 (\epsilon'_r - j\epsilon''_r) \tag{2.30}$$

is the complex permittivity. The imaginary part is due to loss in the medium; damping of the vibrating dipole moments causes heat, because the polar molecules cannot follow the changing electric flux due to friction.

The loss in a medium may also be due to conductivity of the material. In this case there are free charges in the material that are moved by the

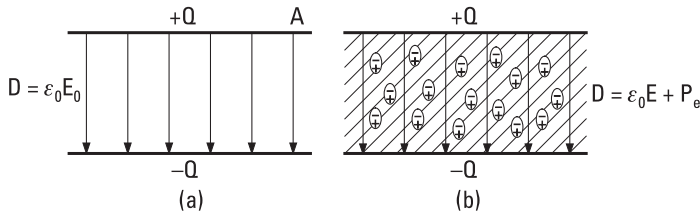


**Figure 2.3** Plate capacitor, which has as its insulator (a) vacuum, and (b) dielectric material that has electric dipole moments.

electric field. When the conduction current density  $\mathbf{J} = \sigma\mathbf{E}$  is introduced in Maxwell's IV equation, one obtains

$$\nabla \times \mathbf{H} = [\sigma + j\omega\epsilon_0(\epsilon'_r - j\epsilon''_r)]\mathbf{E} = j\omega\epsilon_0\left(\epsilon'_r - j\epsilon''_r - j\frac{\sigma}{\omega\epsilon_0}\right)\mathbf{E} \tag{2.31}$$

which shows that damping due to polarization and damping due to conduction are indistinguishable without a measurement at several frequencies. Often  $\sigma/(\omega\epsilon_0)$  is included in  $\epsilon''_r$ . Loss of a medium is often characterized by the loss tangent

$$\tan \delta = \frac{\epsilon''_r + \sigma/(\omega\epsilon_0)}{\epsilon'_r} \tag{2.32}$$

which allows us to write (2.31) in form

$$\nabla \times \mathbf{H} = j\omega\epsilon_0\epsilon'_r(1 - j \tan \delta)\mathbf{E} \tag{2.33}$$

In case of magnetic materials, the situation is analogous: The magnetic field aligns magnetic dipole moments, that is, polarizes the material magnetically. The permeability can be divided into a real part  $\mu'_r$  and an imaginary part  $\mu''_r$ ; the latter causes magnetic loss.

The same medium may be considered as a dielectric at a very high frequency but a conductor at a low frequency. One may argue that a material is a dielectric if  $\sigma/(\omega\epsilon'_r\epsilon_0) < 1/100$  and a conductor if  $\sigma/(\omega\epsilon'_r\epsilon_0) > 100$ . Table 2.1 shows conductivity, the real part of the dielectric constant, and the frequency at which the conduction current is equal to the displacement current for some media common in nature.

**Table 2.1**  
Conductivity, Real Part of Dielectric Constant, and Frequency  $f_T$  at Which the Conduction Current Is Equal to the Displacement Current of Some Materials

Material	$\sigma$ [S/m]	$\epsilon'_r$	$f_T$ [MHz]
Sea water	5	70	1300
Fresh water	$3 \times 10^{-3}$	80	0.7
Moist soil	$10^{-2}$	30	6
Dry soil	$10^{-4}$	3	0.6
Ice	$10^{-5} \dots 10^{-4}$	3	0.06–0.6

### 2.3 Boundary Conditions

In electronics and radio engineering we often have electromagnetic problems where the properties of the medium change abruptly. We have to know the behavior of fields at such interfaces, that is, we have to know the boundary conditions. They can be deduced from Maxwell's equations in integral form.

Let us consider a general interface between the two media presented in Figure 2.4. Medium 1 is characterized by  $\epsilon_1$  and  $\mu_1$ , and medium 2 by  $\epsilon_2$  and  $\mu_2$ . In the following, fields normal to the surface (of the interface) are denoted with subscript  $n$  and fields tangential to the surface with subscript  $t$ .

Let us consider a closed contour with dimensions  $\Delta l$  and  $h$  as shown in Figure 2.4. If  $h$  approaches 0, we obtain from Maxwell's III equation, (2.24):

$$\oint_{\Gamma} \mathbf{E} \cdot d\mathbf{l} = E_{1t} \Delta l - E_{2t} \Delta l = -j\omega \int_S \mathbf{B} \cdot d\mathbf{S}$$

which approaches zero because as the area  $\Delta h$  vanishes, the magnetic flux through the contour must also vanish. Therefore  $E_{1t} = E_{2t}$ , or

$$\mathbf{n} \times (\mathbf{E}_1 - \mathbf{E}_2) = 0 \tag{2.34}$$

Next we utilize Maxwell's IV equation, (2.25)

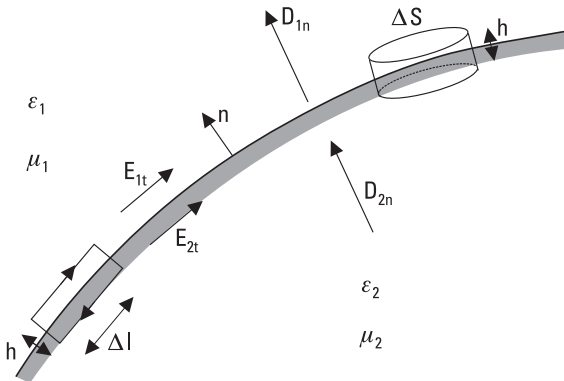


**Figure 2.4** Boundary between two media.

$$\oint_{\Gamma} \mathbf{H} \cdot d\mathbf{l} = H_{1t}\Delta l - H_{2t}\Delta l = \int_S (\mathbf{J} + j\omega\mathbf{D}) \cdot d\mathbf{S}$$

which approaches a value of  $J_s\Delta l$  as  $h$  approaches zero, because when the area  $\Delta l h$  vanishes the electric flux through the contour must vanish, but a current remains due to the surface current density  $J_s$  at the interface. Now we obtain

$$\mathbf{n} \times (\mathbf{H}_1 - \mathbf{H}_2) = \mathbf{J}_s \quad (2.35)$$

Next we consider a “pillbox,” a cylinder also shown in Figure 2.4. Its dimensions are height  $h$  and end surface area  $\Delta S$ . Utilizing Maxwell’s I equation, (2.22), in the case where  $h$  approaches 0, we obtain

$$\oint_S \mathbf{D} \cdot d\mathbf{S} = D_{2n}\Delta S - D_{1n}\Delta S = \int_V \rho dV = \rho_s\Delta S$$

where  $\rho_s$  is the surface charge density at the interface. Now we obtain the following boundary condition:

$$\mathbf{n} \cdot (\mathbf{D}_1 - \mathbf{D}_2) = \mathbf{n} \cdot (\epsilon_1\mathbf{E}_1 - \epsilon_2\mathbf{E}_2) = \rho_s \quad (2.36)$$

Similarly we can derive the following result for the magnetic flux density  $\mathbf{B}$  (Maxwell’s II equation):

$$\mathbf{n} \cdot (\mathbf{B}_1 - \mathbf{B}_2) = \mathbf{n} \cdot (\mu_1\mathbf{H}_1 - \mu_2\mathbf{H}_2) = 0 \quad (2.37)$$

In case of an interface between two media, we obtain the following boundary conditions:

$$\mathbf{n} \times (\mathbf{E}_1 - \mathbf{E}_2) = 0 \quad (2.38)$$

$$\mathbf{n} \times (\mathbf{H}_1 - \mathbf{H}_2) = 0 \quad (2.39)$$

$$\mathbf{n} \cdot (\mathbf{D}_1 - \mathbf{D}_2) = 0 \quad (2.40)$$

$$\mathbf{n} \cdot (\mathbf{B}_1 - \mathbf{B}_2) = 0 \quad (2.41)$$

These equations state that the tangential components of  $\mathbf{E}$  and  $\mathbf{H}$  as well as the normal components of  $\mathbf{D}$  and  $\mathbf{B}$  are equal on both sides of the interface, that is, they are continuous across the interface.



In radio engineering we often consider a case where we have an interface with a good conductor. Fields penetrate only a short distance into a good conductor such as metal and not at all into a perfect conductor ( $\sigma = \infty$ ). We often approximate a good conductor with a perfect conductor, which is lossless. The boundary conditions at the interface of a dielectric and a perfect conductor are:

$$\mathbf{n} \times \mathbf{E} = 0 \quad (2.42)$$

$$\mathbf{n} \times \mathbf{H} = \mathbf{J}_s \quad (2.43)$$

$$\mathbf{n} \cdot \mathbf{D} = \rho_s \quad (2.44)$$

$$\mathbf{n} \cdot \mathbf{B} = 0 \quad (2.45)$$

Such a boundary is also called an *electric wall*. Dual to the electric wall is the *magnetic wall*, where the tangential component of  $\mathbf{H}$  vanishes.

## 2.4 Helmholtz Equation and Its Plane Wave Solution

In a source-free ( $\rho = 0$ ,  $\mathbf{J} = 0$ ), linear, and isotropic medium, Maxwell's equations are simplified into the following forms:

$$\nabla \cdot \mathbf{E} = 0 \quad (2.46)$$

$$\nabla \cdot \mathbf{H} = 0 \quad (2.47)$$

$$\nabla \times \mathbf{E} = -j\omega\mu\mathbf{H} \quad (2.48)$$

$$\nabla \times \mathbf{H} = j\omega\epsilon\mathbf{E} \quad (2.49)$$

When the  $\nabla \times$  operator is applied on both sides of (2.48), we obtain in a homogeneous medium

$$\nabla \times \nabla \times \mathbf{E} = -j\omega\mu\nabla \times \mathbf{H} \quad (2.50)$$

which leads, after utilizing vector identity

$$\nabla \times \nabla \times \mathbf{A} = \nabla(\nabla \cdot \mathbf{A}) - \nabla^2\mathbf{A} \quad (2.51)$$

and (2.46), to

$$\nabla^2\mathbf{E} = -\omega^2\mu\epsilon\mathbf{E} = -k^2\mathbf{E} \quad (2.52)$$

This equation is called the Helmholtz equation, which is a special case of the wave equation

$$\nabla^2 \mathbf{E} - \mu\epsilon \frac{\partial^2 \mathbf{E}}{\partial t^2} = 0 \quad (2.53)$$

The constant  $k = \omega\sqrt{\mu\epsilon}$  is called the wave number [1/m].

Let us first consider propagation of a wave in a lossless medium, where  $\epsilon_r$  and  $\mu_r$  are real. Then  $k$  is also real. Let us assume that the electric field has only the  $x$  component, that the field is uniform in the  $x$  and  $y$  directions, and that the wave propagates in the  $z$  direction. The Helmholtz equation reduces to

$$\frac{\partial^2 E_x}{\partial z^2} + k^2 E_x = 0 \quad (2.54)$$

The solution of this equation is

$$E_x(z) = E^+ e^{-jkz} + E^- e^{jkz} \quad (2.55)$$

where  $E^+$  and  $E^-$  are arbitrary amplitudes of waves propagating into the  $+z$  and  $-z$  directions, respectively. The exact values of  $E^+$  and  $E^-$  are determined by the sources and the boundary conditions. In the time domain, (2.55) can be rewritten as

$$E_x(z, t) = E^+ \cos(\omega t - kz) + E^- \cos(\omega t + kz) \quad (2.56)$$

where  $E^+$  and  $E^-$  are now real constants.

The magnetic field of a plane wave can be solved from (2.49). The result is

$$H_y = \frac{1}{\eta} (E^+ e^{-jkz} - E^- e^{jkz}) \quad (2.57)$$

that is, the magnetic field has a component that is perpendicular to the electric field and to the direction of propagation. The ratio of the electric and magnetic fields is called the wave impedance, and it is  $\eta = \sqrt{\mu/\epsilon}$ . In vacuum  $\eta_0 = \sqrt{\mu_0/\epsilon_0} \approx 120\pi\Omega \approx 377\Omega$ . Figure 2.5 illustrates a plane

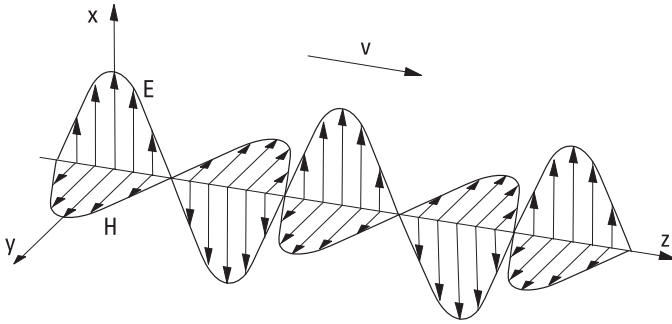


**Figure 2.5** Plane wave propagating into the +z direction.

wave propagating into the +z direction. The fields of a plane wave repeat themselves periodically in the z direction; the wavelength is

$$\lambda = \frac{2\pi}{k} = \frac{2\pi}{\omega\sqrt{\mu\epsilon}} = \frac{1}{f\sqrt{\mu\epsilon}} \quad (2.58)$$

The propagation velocity of the wave is

$$v = f\lambda = \frac{1}{\sqrt{\mu\epsilon}} \quad (2.59)$$

In a vacuum, the propagation velocity is the speed of light:

$$v = c = \frac{1}{\sqrt{\mu_0\epsilon_0}} \approx 2.998 \times 10^8 \text{ m/s} \quad (2.60)$$

In a lossy medium having conductivity  $\sigma$ , Maxwell's III and IV equations (the curl equations) are

$$\nabla \times \mathbf{E} = -j\omega\mu\mathbf{H} \quad (2.61)$$

$$\nabla \times \mathbf{H} = \sigma\mathbf{E} + j\omega\epsilon\mathbf{E} \quad (2.62)$$

Now the Helmholtz equation gets the following form:

$$\nabla^2\mathbf{E} + \omega^2\mu\epsilon\left(1 - j\frac{\sigma}{\omega\epsilon}\right)\mathbf{E} = 0 \quad (2.63)$$

Compared to (2.52), here  $jk$  is replaced by a complex propagation constant,

$$\gamma = \alpha + j\beta = j\omega\sqrt{\mu\epsilon}\sqrt{1 - j\frac{\sigma}{\omega\epsilon}} \quad (2.64)$$

where  $\alpha$  is the attenuation constant and  $\beta$  is the phase constant. In the case of a plane wave propagating into the  $z$  direction, we have

$$\frac{\partial^2 E_x}{\partial z^2} - \gamma^2 E_x = 0 \quad (2.65)$$

leading to

$$E_x(z) = E^+ e^{-\gamma z} + E^- e^{\gamma z} \quad (2.66)$$

In the time domain

$$E_x(z, t) = E^+ e^{-\alpha z} \cos(\omega t - \beta z) + E^- e^{\alpha z} \cos(\omega t + \beta z) \quad (2.67)$$

In the case of a good conductor, that is, when  $\sigma \gg \omega\epsilon$ , we obtain the propagation constant as

$$\gamma = \alpha + j\beta \approx j\omega\sqrt{\mu\epsilon}\sqrt{\frac{\sigma}{j\omega\epsilon}} = (1 + j)\sqrt{\frac{\omega\mu\sigma}{2}} \quad (2.68)$$

When a plane wave meets a surface of a lossy medium in the perpendicular direction and penetrates into it, its field is damped into  $1/e$  part over a distance called the skin depth:

$$\delta_s = \frac{1}{\alpha} = \sqrt{\frac{2}{\omega\mu\sigma}} \quad (2.69)$$

### Example 2.1

Find the attenuation of a  $4 \mu\text{m}$ -thick copper layer at 10 GHz.

### Solution

At a frequency of 10 GHz the skin depth in pure copper ( $\sigma = 5.8 \times 10^7$  S/m,  $\mu = \mu_0$ ) is only  $6.6 \times 10^{-7}$  m. Therefore, at this frequency a uniform

electromagnetic shield made of pure copper of thickness of  $4 \mu\text{m}$  ( $= 6$  skin depths) provides an attenuation of about  $-20 \log(1/e)^6 \approx 6 \times 8.68 \text{ dB} \approx 50 \text{ dB}$ .

In a general case, each field component can be solved from the general Helmholtz equation:

$$\frac{\partial^2 E_i}{\partial x^2} + \frac{\partial^2 E_i}{\partial y^2} + \frac{\partial^2 E_i}{\partial z^2} - \gamma^2 E_i = 0, \quad i = x, y, z \quad (2.70)$$

The solution is found by using the separation of variables. By assuming that  $E_i = f(x)g(y)h(z)$ ,

$$\frac{f''}{f} + \frac{g''}{g} + \frac{h''}{h} - \gamma^2 = 0 \quad (2.71)$$

where the double prime denotes the second derivative. The first three terms of this equation are each a function of one independent variable. As the sum of these terms is constant ( $\gamma^2$ ), each term must also be constant. Therefore, (2.71) can be divided into three independent equations of form  $f''/f - \gamma_x^2 = 0$ , which have solutions as shown previously.

## 2.5 Polarization of a Plane Wave

Electromagnetic fields are vector quantities, which have a direction in space. The polarization of a plane wave refers to this orientation of the electric field vector, which may be a fixed orientation (a linear polarization) or may change with time (a circular or elliptical polarization).

The electric field of a plane wave can be presented as a sum of two orthogonal components

$$\mathbf{E} = (E_1 \mathbf{u}_x + E_2 \mathbf{u}_y) e^{-jkz} \quad (2.72)$$

where  $\mathbf{u}_x$  and  $\mathbf{u}_y$  are the unit vectors in the  $x$  and  $y$  direction, respectively. In a general case this represents an elliptically polarized wave. The polarization ellipse shown in Figure 2.6(a) is characterized by the axial ratio  $E_{max}/E_{min}$ , tilt angle  $\tau$ , and direction of rotation. The direction of rotation, as seen in

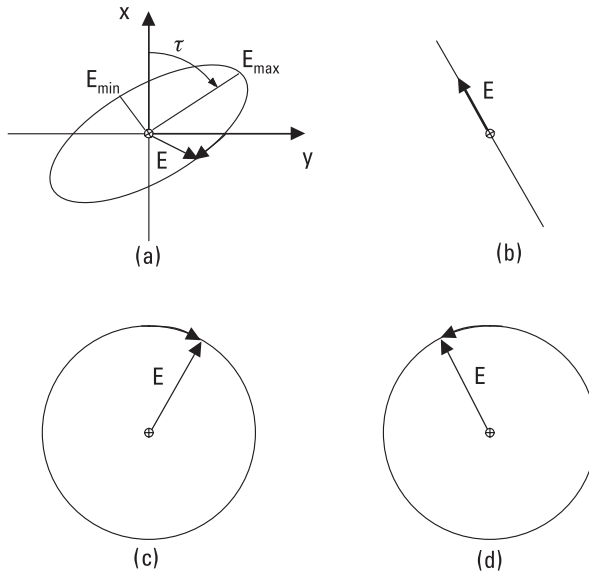


**Figure 2.6** Polarization of a plane wave: (a) elliptic; (b) linear; (c) clockwise circular; and (d) counterclockwise circular.

the direction of propagation and observed in a plane perpendicular to the direction of propagation, is either clockwise (right-handed) or counterclockwise (left-handed).

Special cases of an elliptical polarization are the linear polarization, Figure 2.6(b), and circular polarization, Figure 2.6(c, d). If  $E_1 \neq 0$  and  $E_2 = 0$ , we have a wave polarized linearly in the  $x$  direction. If both  $E_1$  and  $E_2$  are nonzero but real and the components are in the same phase, we have a linearly polarized wave, the polarization direction of which is in angle

$$\tau = \arctan(E_2/E_1) \quad (2.73)$$

In the case of circular polarization, the components have equal amplitudes and a  $90^\circ$  phase difference, that is,  $E_1 = \pm jE_2 = E_0$  ( $E_0$  real), and the electric field is

$$\mathbf{E} = E_0(\mathbf{u}_x - j\mathbf{u}_y)e^{-jkz} \quad (2.74)$$

or

$$\mathbf{E} = E_0(\mathbf{u}_x + j\mathbf{u}_y)e^{-jkz} \quad (2.75)$$

The former represents a clockwise, circularly polarized wave, and the latter a counterclockwise, circularly polarized wave. In the time domain the circularly polarized wave can be presented as (clockwise)

$$\mathbf{E}(z, t) = E_0[\mathbf{u}_x \cos(\omega t - kz) + \mathbf{u}_y \cos(\omega t - kz - \pi/2)] \quad (2.76)$$

and (counterclockwise)

$$\mathbf{E}(z, t) = E_0[\mathbf{u}_x \cos(\omega t - kz) - \mathbf{u}_y \cos(\omega t - kz - \pi/2)] \quad (2.77)$$

At  $z = 0$ , (2.76) and (2.77) are reduced to

$$\mathbf{E}(t) = E_0[\mathbf{u}_x \cos \omega t \pm \mathbf{u}_y \cos(\omega t - \pi/2)] \quad (2.78)$$

### 2.6 Reflection and Transmission at a Dielectric Interface

Let us consider a plane wave that is incident at a planar interface of two lossless media, as illustrated in Figure 2.7. The wave comes from medium 1, which is characterized by  $\epsilon_1$  and  $\mu_1$ , to medium 2 with  $\epsilon_2$  and  $\mu_2$ . The planar interface is at  $z = 0$ . The angle of incidence is  $\theta_1$  and the propagation vector  $\mathbf{k}_1$  is in the  $xz$ -plane. Part  $E_1'$  from the incident field is reflected at an angle  $\theta_1'$  and part  $E_2$  is transmitted through the interface and leaves at an angle of  $\theta_2$ .

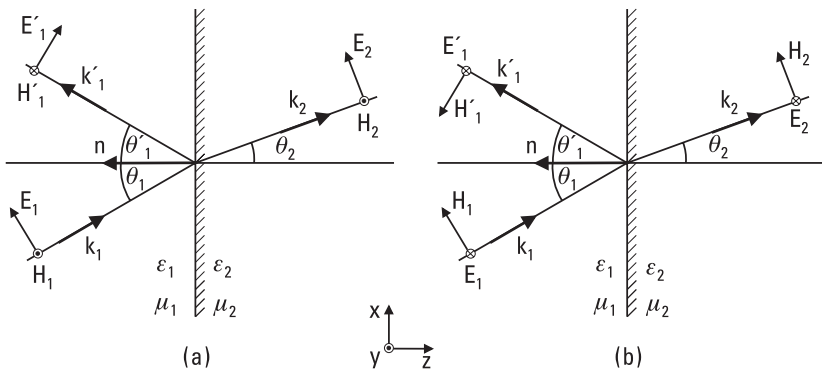


**Figure 2.7** Reflection and transmission of a plane wave in case of an oblique incidence at an interface of two lossless media: (a) parallel polarization, and (b) perpendicular polarization.

According to the boundary conditions, the tangential components of the electric and magnetic field are equal on both sides of the interface in each point of plane  $z = 0$ . This is possible only if the phase of the incident, reflected, and transmitted waves change equally in the  $x$  direction, in other words, the phase velocities in the  $x$  direction are the same, or

$$\frac{v_1}{\sin \theta_1} = \frac{v_1}{\sin \theta_1'} = \frac{v_2}{\sin \theta_2} \quad (2.79)$$

where  $v_1$  and  $v_2$  ( $v_i = \omega/k_i$ ) are the wave velocities in medium 1 and 2, respectively. From (2.79) it follows

$$\theta_1' = \theta_1 \quad (2.80)$$

which means the angle of incidence and angle of reflection are equal, and the angle of propagation of the transmitted wave is obtained from

$$\frac{\sin \theta_2}{\sin \theta_1} = \sqrt{\frac{\mu_1 \epsilon_1}{\mu_2 \epsilon_2}} \quad (2.81)$$

Let us assume in the following that  $\mu_1 = \mu_2 = \mu_0$ , which is valid in most cases of interest in practice. Then (2.81), which is called Snell's law, can be rewritten as

$$\frac{\sin \theta_2}{\sin \theta_1} = \sqrt{\frac{\epsilon_1}{\epsilon_2}} = \sqrt{\frac{\epsilon_{r1}}{\epsilon_{r2}}} = \frac{n_1}{n_2} \quad (2.82)$$

where  $n_1 = \sqrt{\epsilon_{r1}}$  and  $n_2 = \sqrt{\epsilon_{r2}}$  are the refraction indices of the materials.

The reflection and transmission coefficients depend on the polarization of the incident wave. Important special cases are the so-called parallel and perpendicular polarizations; see Figure 2.7. The parallel polarization means that the electric field vector is in the same plane with  $\mathbf{k}_1$  and the normal  $\mathbf{n}$  of the plane, that is, the field vector is in the  $xz$ -plane. The perpendicular polarization means that the electric field vector is perpendicular to the plane described previously, that is, it is parallel to the  $y$ -axis. The polarization of an arbitrary incident plane wave can be thought to be a superposition of the parallel and perpendicular polarizations.

In the case of the parallel polarization, the condition of continuity of the tangential electric field is



$$E_1 \cos \theta_1 + E_1' \cos \theta_1' = E_2 \cos \theta_2 \quad (2.83)$$

which leads, with the aid of (2.80) and (2.82), to

$$(E_1 + E_1') \cos \theta_1 = E_2 \sqrt{1 - \frac{\epsilon_1}{\epsilon_2} \sin^2 \theta_1} \quad (2.84)$$

The magnetic field has only a component in the  $y$  direction. The continuity of the tangential magnetic field leads to

$$(E_1 - E_1')\sqrt{\epsilon_1} = E_2\sqrt{\epsilon_2} \quad (2.85)$$

From (2.84) and (2.85) we can solve for the parallel polarization the reflection and transmission coefficients,  $\rho_{\parallel}$  and  $\tau_{\parallel}$ , respectively:

$$\rho_{\parallel} = \frac{E_1'}{E_1} = \frac{\sqrt{\frac{\epsilon_2}{\epsilon_1} - \sin^2 \theta_1} - \frac{\epsilon_2}{\epsilon_1} \cos \theta_1}{\sqrt{\frac{\epsilon_2}{\epsilon_1} - \sin^2 \theta_1} + \frac{\epsilon_2}{\epsilon_1} \cos \theta_1} \quad (2.86)$$

$$\tau_{\parallel} = \frac{E_2}{E_1} = \frac{2\sqrt{\frac{\epsilon_2}{\epsilon_1}} \cos \theta_1}{\sqrt{\frac{\epsilon_2}{\epsilon_1} - \sin^2 \theta_1} + \frac{\epsilon_2}{\epsilon_1} \cos \theta_1} \quad (2.87)$$

When the angle of incidence is  $90^\circ$ , that is, when the incident wave approaches perpendicularly to the surface, it holds for  $\rho$  and  $\tau$  that

$$1 + \rho = \tau \quad (2.88)$$

In case of the perpendicular polarization, the boundary conditions lead to

$$E_1 + E_1' = E_2 \quad (2.89)$$

$$(E_1 - E_1')\sqrt{\epsilon_1} \cos \theta_1 = E_2\sqrt{\epsilon_2} \cos \theta_2 \quad (2.90)$$

from which we can solve for the perpendicular polarization

$$\rho_{\perp} = \frac{\cos \theta_1 - \sqrt{\frac{\epsilon_2}{\epsilon_1} - \sin^2 \theta_1}}{\sqrt{\frac{\epsilon_2}{\epsilon_1} - \sin^2 \theta_1} + \cos \theta_1} \quad (2.91)$$

$$\tau_{\perp} = \frac{2 \cos \theta_1}{\sqrt{\frac{\epsilon_2}{\epsilon_1} - \sin^2 \theta_1} + \cos \theta_1} \quad (2.92)$$

Figure 2.8 shows the behavior of the reflection coefficient as a function of the angle of incidence for both polarizations, when  $n_1 < n_2$ , that is,  $\epsilon_1 < \epsilon_2$ . In case of the parallel polarization, the reflection coefficient is equal to zero at Brewster's angle

$$\theta_B = \arcsin \sqrt{\frac{\epsilon_2}{\epsilon_2 + \epsilon_1}} \quad (2.93)$$

If  $\epsilon_1 > \epsilon_2$ , a total reflection occurs at angles of incidence

$$\theta_1 \geq \arcsin \sqrt{\frac{\epsilon_2}{\epsilon_1}} \quad (2.94)$$

## 2.7 Energy and Power

Let us consider the principle of energy conservation in volume  $V$ , which is enclosed by a surface  $S$ . The medium filling the volume  $V$  is characterized

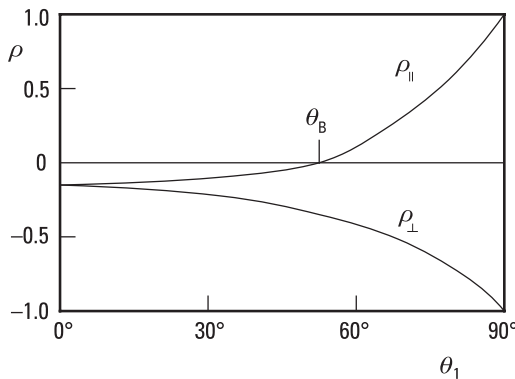


**Figure 2.8** The reflection coefficient for the parallel ( $\rho_{\parallel}$ ) and perpendicular ( $\rho_{\perp}$ ) polarization as a function of the angle of incidence  $\theta_1$ , when  $\epsilon_1 < \epsilon_2$ .

by  $\epsilon_r$ ,  $\mu_r$ , and  $\sigma$ . Let us assume that in the volume  $V$  there are the electromagnetic sources  $\mathbf{J}$  and  $\mathbf{M}$  ( $\mathbf{M}$  is the magnetic current density; see Section 2.1), which cause fields  $\mathbf{E}$  and  $\mathbf{H}$ . The complex power that these sources produce is

$$P_s = -\frac{1}{2} \int_V (\mathbf{E} \cdot \mathbf{J}^* + \mathbf{H}^* \cdot \mathbf{M}) dV \quad (2.95)$$

In a sinusoidal steady-state case, the time-averaged stored electric energy in the volume  $V$  is

$$W_e = \frac{\epsilon_0}{4} \int_V \epsilon_r' \mathbf{E} \cdot \mathbf{E}^* dV = \frac{\epsilon_0}{4} \int_V \epsilon_r' |\mathbf{E}|^2 dV \quad (2.96)$$

Accordingly, the time-averaged stored magnetic energy in the volume  $V$  is

$$W_m = \frac{\mu_0}{4} \int_V \mu_r' \mathbf{H} \cdot \mathbf{H}^* dV = \frac{\mu_0}{4} \int_V \mu_r' |\mathbf{H}|^2 dV \quad (2.97)$$

Using Poynting's vector we can calculate the power flow out of the closed surface  $S$

$$P_o = \frac{1}{2} \operatorname{Re} \oint_S \mathbf{E} \times \mathbf{H}^* \cdot d\mathbf{S} \quad (2.98)$$

Power dissipated in the volume  $V$  due to conduction, dielectric, and magnetic losses is

$$P_l = \frac{1}{2} \int_V \sigma |\mathbf{E}|^2 dV + \frac{\omega}{2} \int_V (\epsilon_0 \epsilon_r'' |\mathbf{E}|^2 + \mu_0 \mu_r'' |\mathbf{H}|^2) dV \quad (2.99)$$

According to the energy conservation principle, the power delivered by the sources in the volume  $V$  is equal to the sum of the power transmitted through the surface  $S$  and power dissipated in the volume, plus  $2\omega$  times the net reactive energy stored in the volume. This principle is called Poynting's theorem, which can be written as

$$P_s = P_o + P_l + 2j\omega(W_m - W_e) \quad (2.100)$$

Equation (2.100) combines the powers and energies presented in (2.95)–(2.99).

## References

- [1] Feynman, R. P., R. B. Leighton, and M. Sands, *The Feynman Lectures on Physics, Vol. II*, Reading, MA: Addison-Wesley, 1964.
- [2] Collin, R. E., *Foundations for Microwave Engineering*, 2nd ed., New York: IEEE Press, 2001.
- [3] Gardiol, F. E., *Introduction to Microwaves*, Dedham, MA: Artech House, 1984.
- [4] Kong, J. A., *Electromagnetic Wave Theory*, New York: John Wiley & Sons, 1986.
- [5] Kraus, J., and D. Fleisch, *Electromagnetics with Applications*, 5th ed., Boston, MA: McGraw-Hill, 1998.
- [6] Pozar, D. M., *Microwave Engineering*, 2nd ed., New York: John Wiley & Sons, 1998.
- [7] Ramo, S., J. Whinnery, and T. van Duzer, *Fields and Waves in Communication Electronics*, New York: John Wiley & Sons, 1965.
- [8] Van Bladel, J., *Electromagnetic Fields*, Washington, D.C.: Hemisphere Publishing, 1985.



# 3

## Transmission Lines and Waveguides

Transmission lines and waveguides carry signals and power between different devices and within them. We can form many kinds of components, such as directional couplers and filters, by connecting sections of transmission lines or waveguides (see Chapters 6 and 7). Usually, lines consisting of two or more conductors are called transmission lines, and lines or wave-guiding structures having a single metal tube or no conductors at all are called waveguides. However, the use of these terms is not always consistent, and often in analysis a transmission line model is used for a waveguide (see Section 3.10).

Several types of transmission lines and waveguides have been developed for various applications. They are characterized by their attenuation, bandwidth, dispersion, purity of wave mode, power-handling capability, physical size, and applicability for integration. Dispersion means the frequency dependence of wave propagation.

Figure 3.1 shows some types of transmission lines and waveguides, which are briefly described later. The electrical properties of the lines in Figure 3.1(a–d, f) are explained more detailed later in this chapter; see also [1–6]. A comparison of the lines in Figure 3.1(a, d, f) is given in Table 3.1.

A rectangular metal waveguide is a hollow metal pipe having a rectangular cross section. It has low losses and a high power-handling capability. Due to its closed structure, the fields are well isolated from the outside world. A large physical size and difficulty in integrating its components within the waveguide are the main disadvantages. The usable bandwidth for

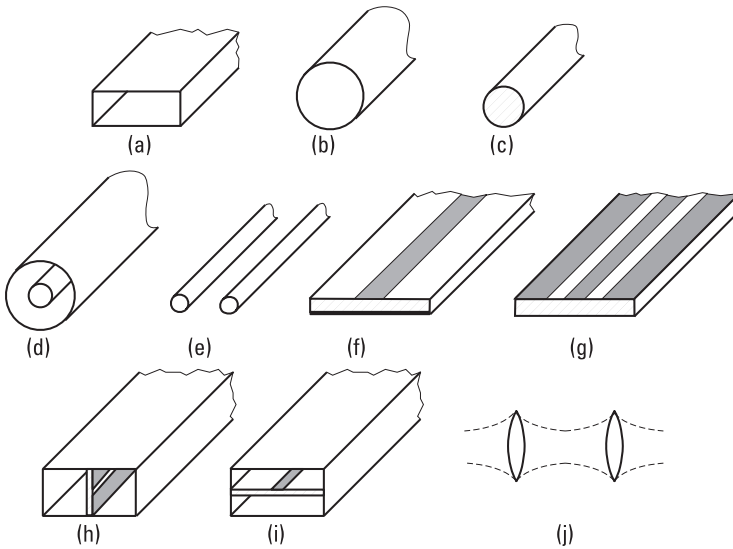


**Figure 3.1** Transmission lines and waveguides: (a) rectangular metal waveguide; (b) circular metal waveguide; (c) circular dielectric waveguide; (d) coaxial line; (e) parallel-wire line; (f) microstrip line; (g) coplanar waveguide; (h) fin line; (i) suspended stripline; and (j) quasioptical waveguide.

**Table 3.1**  
Comparison of Some Common Lines

Characteristic	Rectangular Waveguide	Coaxial Line	Microstrip Line
Mode	TE <sub>10</sub>	TEM	Quasi-TEM
Bandwidth	Medium	Broad	Broad
Dispersion	Medium	None	Low
Losses	Low	Medium	High
Power capability	High	Medium	Low
Size	Large	Medium	Small
Ease of fabrication	Medium	Medium	Easy
Integration	Difficult	Difficult	Easy

the pure fundamental mode TE<sub>10</sub> is less than 1 octave. Rectangular metal waveguides are used for various applications from below 1 GHz up to 1,000 GHz and even higher frequencies.

The properties of a circular metal waveguide are generally the same as those of the rectangular metal waveguide. However, the usable bandwidth for single-mode operation is even narrower, only about 25%. In an oversized circular metal waveguide, a very low-loss  $TE_{01}$  mode can propagate if the excitation of other modes can be prevented. (Later in this book we use the terms “rectangular waveguide” and “circular waveguide” omitting the word “metal,” as is often the practice in the literature.)

A circular dielectric waveguide is made of a dielectric low-loss material. Bends and other discontinuities in the line radiate easily. For example, an optical fiber is a dielectric waveguide.

A coaxial line consists of an outer and an inner conductor with circular cross sections. The space between the conductors is filled with a low-loss insulating material, such as air or Teflon. The coaxial line has a broad, single-mode bandwidth from 0 Hz to an upper limit, which depends on the dimensions of the conductors and may be as high as 60 GHz.

A parallel-wire line consists of two parallel conductors. It cannot be used at higher frequencies than in the VHF range because it has a high radiation loss at higher frequencies.

A microstrip line is made on an insulating substrate. The metal layer on the opposite side of the strip operates as a ground plane. The advantages of the microstrip line are a broad bandwidth, small size, and a good applicability for integration and mass production. The disadvantages are fairly high losses, radiation due to the open structure, and low power capability. Microstrip lines are used up to 100 GHz and even higher frequencies.

A coplanar waveguide has ground-plane conductors on both sides of a metal strip. All conductors are on the same side of the substrate. Both series and parallel components can easily be integrated with this line. Coplanar waveguides are used, for example, in monolithic integrated circuits operating at millimeter wavelengths.

A fin line is composed of a substrate in the E-plane of a rectangular (metal) waveguide. The field concentrates in a slot on the metallization of the substrate. The fin line has a low radiation loss, and components can be integrated quite easily with this line. Fin lines are used up to 200 GHz.

A suspended stripline has a substrate in the H-plane of a rectangular waveguide. There is a metal strip on the substrate.

A quasioptical waveguide is made of focusing lenses or mirrors, which maintain the energy in a beam in free space. Quasioptical waveguides are used from about 100 GHz up to infrared waves. Other lines become lossy and difficult to fabricate at such high frequencies.



### 3.1 Basic Equations for Transmission Lines and Waveguides

The Helmholtz equation (2.52) is valid in the sourceless medium of a transmission line or a waveguide. Let us assume that a wave is propagating in a uniform line along the  $z$  direction. Now, the Helmholtz equation is separable so that a solution having a form of  $f(z)g(x, y)$  can be found. The  $z$ -dependence of the field has a form of  $e^{-\gamma z}$ . Thus, the electric field may be written as

$$\mathbf{E} = \mathbf{E}(x, y, z) = \mathbf{g}(x, y) e^{-\gamma z} \quad (3.1)$$

where  $\mathbf{g}(x, y)$  is the field distribution in the transverse plane. By setting this to the Helmholtz equation, we get

$$\nabla^2 \mathbf{E} = \nabla_{xy}^2 \mathbf{E} + \frac{\partial^2 \mathbf{E}}{\partial z^2} = \nabla_{xy}^2 \mathbf{E} + \gamma^2 \mathbf{E} = -\omega^2 \mu \epsilon \mathbf{E} \quad (3.2)$$

where  $\nabla_{xy}^2$  includes the partial derivatives of  $\nabla^2$  with respect to  $x$  and  $y$ . Because similar equations can be derived for the magnetic field, the partial differential equations applicable for all uniform lines are

$$\nabla_{xy}^2 \mathbf{E} = -(\gamma^2 + \omega^2 \mu \epsilon) \mathbf{E} \quad (3.3)$$

$$\nabla_{xy}^2 \mathbf{H} = -(\gamma^2 + \omega^2 \mu \epsilon) \mathbf{H} \quad (3.4)$$

At first, the longitudinal or  $z$ -component of the electric or magnetic field is solved using the boundary conditions set by the structure of the line. When  $E_z$  or  $H_z$  is known, the  $x$ - and  $y$ -components of the fields may be solved from Maxwell's III and IV equations. Equation  $\nabla \times \mathbf{E} = -j\omega\mu\mathbf{H}$  may be divided into three parts:

$$\begin{aligned} \partial E_z / \partial y + \gamma E_y &= -j\omega\mu H_x \\ -\gamma E_x - \partial E_z / \partial x &= -j\omega\mu H_y \\ \partial E_y / \partial x - \partial E_x / \partial y &= -j\omega\mu H_z \end{aligned}$$

Correspondingly,  $\nabla \times \mathbf{H} = j\omega\epsilon\mathbf{E}$  is divided into three parts:

$$\begin{aligned}\partial H_z / \partial y + \gamma H_y &= j\omega\epsilon E_x \\ -\gamma H_x - \partial H_z / \partial x &= j\omega\epsilon E_y \\ \partial H_y / \partial x - \partial H_x / \partial y &= j\omega\epsilon E_z\end{aligned}$$

From these, the transverse components  $E_x$ ,  $E_y$ ,  $H_x$ , and  $H_y$  are solved as functions of the longitudinal components  $E_z$  and  $H_z$ :

$$E_x = \frac{-1}{\gamma^2 + \omega^2 \mu \epsilon} \left( \gamma \frac{\partial E_z}{\partial x} + j\omega\mu \frac{\partial H_z}{\partial y} \right) \quad (3.5)$$

$$E_y = \frac{1}{\gamma^2 + \omega^2 \mu \epsilon} \left( -\gamma \frac{\partial E_z}{\partial y} + j\omega\mu \frac{\partial H_z}{\partial x} \right) \quad (3.6)$$

$$H_x = \frac{1}{\gamma^2 + \omega^2 \mu \epsilon} \left( j\omega\epsilon \frac{\partial E_z}{\partial y} - \gamma \frac{\partial H_z}{\partial x} \right) \quad (3.7)$$

$$H_y = \frac{-1}{\gamma^2 + \omega^2 \mu \epsilon} \left( j\omega\epsilon \frac{\partial E_z}{\partial x} + \gamma \frac{\partial H_z}{\partial y} \right) \quad (3.8)$$

In a cylindrical coordinate system, the solution of the Helmholtz equation has the form of  $f(z)g(r, \phi)$ . As above, the transverse  $r$ - and  $\phi$ -components are calculated from the longitudinal components:

$$E_r = \frac{-1}{\gamma^2 + \omega^2 \mu \epsilon} \left( \gamma \frac{\partial E_z}{\partial r} + \frac{j\omega\mu}{r} \frac{\partial H_z}{\partial \phi} \right) \quad (3.9)$$

$$E_\phi = \frac{1}{\gamma^2 + \omega^2 \mu \epsilon} \left( -\frac{\gamma}{r} \frac{\partial E_z}{\partial \phi} + j\omega\mu \frac{\partial H_z}{\partial r} \right) \quad (3.10)$$

$$H_r = \frac{1}{\gamma^2 + \omega^2 \mu \epsilon} \left( \frac{j\omega\epsilon}{r} \frac{\partial E_z}{\partial \phi} - \gamma \frac{\partial H_z}{\partial r} \right) \quad (3.11)$$

$$H_\phi = \frac{-1}{\gamma^2 + \omega^2 \mu \epsilon} \left( j\omega\epsilon \frac{\partial E_z}{\partial r} + \frac{\gamma}{r} \frac{\partial H_z}{\partial \phi} \right) \quad (3.12)$$

In a given waveguide at a given frequency, several field configurations may satisfy Maxwell's equations. These field configurations are called wave

modes. Every mode has its own propagation characteristics: velocity, attenuation, and cutoff frequency. Because different modes propagate at different velocities, signals may be distorted due to the multimode propagation. Using the waveguide at low enough frequencies, so that only one mode—the dominant or fundamental mode—can propagate along the waveguide, prevents this multimode distortion.

### 3.2 Transverse Electromagnetic Wave Modes

In lossless and, with a good approximation, in low-loss two-conductor transmission lines, as in coaxial lines, fields can propagate as *transverse electromagnetic* (TEM) waves. TEM waves have no longitudinal field components. TEM waves may propagate at all frequencies, so the TEM mode has no cutoff frequency.

When  $E_z = 0$  and  $H_z = 0$ , it follows from (3.5) through (3.8) that the  $x$ - and  $y$ -components of the fields are also zero, unless

$$\gamma^2 + \omega^2 \mu \epsilon = 0 \quad (3.13)$$

Therefore, the propagation constant of a TEM wave is

$$\gamma = \pm j\omega \sqrt{\mu \epsilon} = \pm j \frac{2\pi}{\lambda} = \pm j\beta \quad (3.14)$$

The velocity  $v_p$  is independent of frequency, assuming that the material parameters  $\epsilon$  and  $\mu$  are independent of frequency:

$$v_p = \frac{\omega}{\beta} = \frac{1}{\sqrt{\mu \epsilon}} \quad (3.15)$$

Thus, there is no dispersion, and the TEM wave in a transmission line propagates at the same velocity as a wave in free space having the same  $\epsilon$  and  $\mu$  as the insulator of the transmission line. The wave equations for a TEM wave are

$$\nabla_{xy}^2 \mathbf{E} = 0 \quad (3.16)$$

$$\nabla_{xy}^2 \mathbf{H} = 0 \quad (3.17)$$

The fields of a wave propagating along the  $z$  direction satisfy the equation

$$\frac{E_x}{H_y} = -\frac{E_y}{H_x} = \eta \quad (3.18)$$

where  $\eta = \sqrt{\mu/\epsilon}$  is the wave impedance.

Laplace's equations, (3.16) and (3.17), are valid also for static fields. In electrostatics, the electric field may be presented as the gradient of the scalar transverse potential:

$$\mathbf{E}(x, y) = -\nabla_{xy}\Phi(x, y) \quad (3.19)$$

Because  $\nabla \times \nabla f = 0$ , the transverse curl of the electric field must vanish in order for (3.19) to be valid. Here this is the case, because

$$\nabla_{xy} \times \mathbf{E} = -j\omega\mu H_z \mathbf{u}_z = 0 \quad (3.20)$$

where  $\mathbf{u}_z$  is a unit vector pointing in the direction of the positive  $z$ -axis. Gauss' law in a sourceless space states that  $\nabla \cdot \mathbf{D} = \epsilon \nabla_{xy} \cdot \mathbf{E} = 0$ . From this and (3.19) it follows that  $\Phi(x, y)$  is also a solution of Laplace's equation, or

$$\nabla_{xy}^2 \Phi(x, y) = 0 \quad (3.21)$$

The voltage of a two-conductor line is

$$V_{12} = \int_1^2 \mathbf{E} \cdot d\mathbf{l} = \Phi_1 - \Phi_2 \quad (3.22)$$

where  $\Phi_1$  and  $\Phi_2$  are the potentials of the conductors. From Ampère's law, the current of the line is

$$I = \oint_{\Gamma} \mathbf{H} \cdot d\mathbf{l} \quad (3.23)$$

where  $\Gamma$  is a closed line surrounding the conductor.

### 3.3 Transverse Electric and Transverse Magnetic Wave Modes

A wave mode may have also longitudinal field components in addition to the transverse components. *Transverse electric* (TE) modes have  $E_z = 0$  but a nonzero longitudinal magnetic field  $H_z$ . *Transverse magnetic* (TM) modes have  $H_z = 0$  and a nonzero  $E_z$ .

From (3.4) it follows for a TE mode

$$\nabla_{xy}^2 H_z = -(\gamma^2 + \omega^2 \mu \epsilon) H_z = -k_c^2 H_z \quad (3.24)$$

Correspondingly, for a TM mode

$$\nabla_{xy}^2 E_z = -(\gamma^2 + \omega^2 \mu \epsilon) E_z = -k_c^2 E_z \quad (3.25)$$

The coefficient  $k_c$  is solved from (3.24) or (3.25) using the boundary conditions set by the waveguide. For a given waveguide, an infinite number of  $k_c$  values can usually be found. Each  $k_c$  corresponds to a propagating wave mode. We can prove that in the case of a waveguide such as a rectangular or circular waveguide, in which a conductor surrounds an insulator,  $k_c$  is always a positive real number.

The propagation constant is

$$\gamma = \sqrt{k_c^2 - \omega^2 \mu \epsilon} \quad (3.26)$$

If the insulating material is lossless,  $\omega^2 \mu \epsilon$  is real. The frequency at which  $\omega^2 \mu \epsilon = k_c^2$  is called the cutoff frequency:

$$f_c = \frac{k_c}{2\pi\sqrt{\mu\epsilon}} \quad (3.27)$$

The corresponding cutoff wavelength is

$$\lambda_c = \frac{2\pi}{k_c} \quad (3.28)$$

At frequencies below the cutoff frequency,  $f < f_c$ , no wave can propagate. The field attenuates rapidly and has an attenuation constant

$$\gamma = \alpha = \frac{2\pi}{\lambda_c} \sqrt{1 - \left(\frac{f}{f_c}\right)^2} \quad (3.29)$$

At frequencies much below the cutoff frequency,  $f \ll f_c$ , the attenuation constant is  $\alpha = 2\pi/\lambda_c$  or  $2\pi$  nepers (54.6 dB) per cutoff wavelength. Figure 3.2 shows the attenuation at frequencies below the cutoff frequency.

At frequencies higher than the cutoff frequency,  $f > f_c$ , waves can propagate and the propagation constant  $\gamma$  is complex. In a lossless line,  $\gamma$  is imaginary:

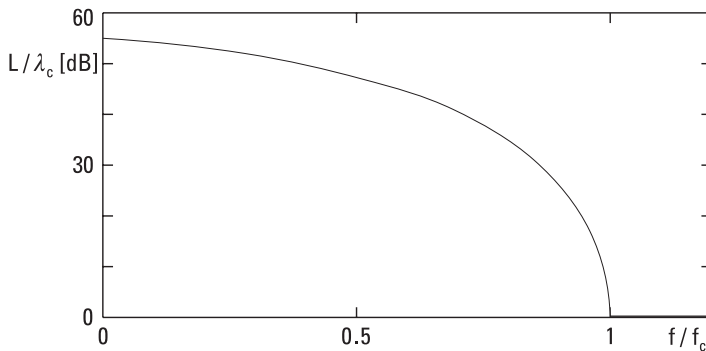
$$\gamma = j\beta_g = j \frac{2\pi}{\lambda} \sqrt{1 - \left(\frac{f_c}{f}\right)^2} \quad (3.30)$$

where  $\lambda$  is the wavelength in free space composed of the same material as the insulator of the line. The wavelength in the line is

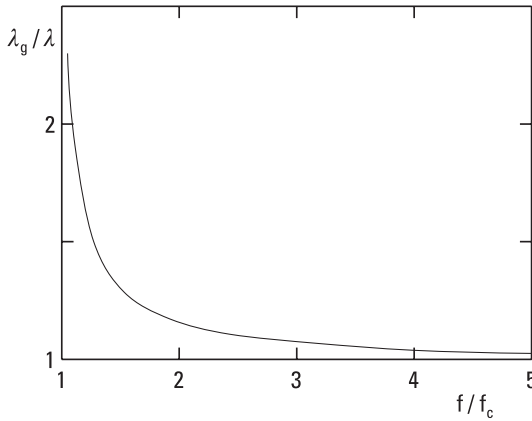
$$\lambda_g = \frac{2\pi}{\beta_g} = \frac{\lambda}{\sqrt{1 - (f_c/f)^2}} \quad (3.31)$$

Figure 3.3 shows how the wavelength  $\lambda_g$  depends on frequency. The phase velocity (see Section 3.9) is

$$v_p = \frac{v}{\sqrt{1 - (f_c/f)^2}} \quad (3.32)$$



**Figure 3.2** Attenuation of TE and TM waves below the cutoff frequency in a lossless waveguide.



**Figure 3.3** Wavelength of TE and TM waves above the cutoff frequency.

which is larger than the speed  $v$  of a plane wave in the same material as the insulator of the line. The propagation velocity of energy or the group velocity

$$v_g = v\sqrt{1 - (f_c/f)^2} \quad (3.33)$$

is smaller than the speed of the plane wave in this material. Thus, the propagation velocity of TE and TM waves depends on frequency, and waveguides carrying these modes are dispersive.

## 3.4 Rectangular Waveguide

Both TE and TM wave modes may propagate in the rectangular waveguide shown in Figure 3.4. The longitudinal electric field of a TE mode is zero,  $E_z = 0$ , while for a TM mode the longitudinal magnetic field is zero,  $H_z = 0$ .

### 3.4.1 TE Wave Modes in Rectangular Waveguide

Let us assume that the solution of the longitudinal magnetic field has a form of

$$H_z(x, y) = A \cos(k_1 x) \cos(k_2 y) \quad (3.34)$$

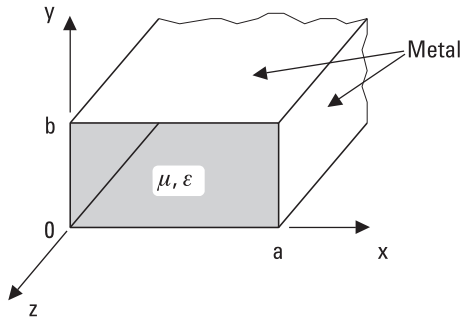


**Figure 3.4** Rectangular waveguide.

where  $A$  is an arbitrary amplitude constant. By introducing the field of (3.34) to the equation of the TE wave mode, (3.24), we note that the differential equation is fulfilled if

$$k_1^2 + k_2^2 = \gamma^2 + \omega^2 \mu \epsilon = k_c^2 \quad (3.35)$$

The transverse field components can be solved from (3.5) through (3.8):

$$E_x = j \frac{\omega \mu k_2}{k_c^2} A \cos(k_1 x) \sin(k_2 y) \quad (3.36)$$

$$E_y = -j \frac{\omega \mu k_1}{k_c^2} A \sin(k_1 x) \cos(k_2 y) \quad (3.37)$$

$$H_x = -\frac{E_y}{Z_{TE}} \quad (3.38)$$

$$H_y = \frac{E_x}{Z_{TE}} \quad (3.39)$$

The wave impedance of the TE wave mode is

$$Z_{TE} = \frac{\eta}{\sqrt{1 - (f_c/lf)^2}} \quad (3.40)$$



From the boundary conditions for the fields in a metal waveguide it follows that the transverse magnetic field cannot have a normal component at the boundary, that is,  $\mathbf{n} \cdot \mathbf{H} = 0$ . It follows from (3.7) and (3.8) that  $\partial H_z / \partial x = 0$ , when  $x = 0$  or  $a$ , and  $\partial H_z / \partial y = 0$ , when  $y = 0$  or  $b$ .

Also, the tangential component of the electric field must vanish at the boundary or  $\mathbf{n} \times \mathbf{E} = 0$ :  $E_x(x, 0) = 0$ ,  $E_x(x, b) = 0$ ,  $E_y(0, y) = 0$ ,  $E_y(a, y) = 0$ .

It results from these boundary conditions that  $k_1 a = n\pi$  and  $k_2 b = m\pi$ , where  $n = 0, 1, 2, \dots$  and  $m = 0, 1, 2, \dots$ , and therefore,

$$k_c^2 = \left(\frac{n\pi}{a}\right)^2 + \left(\frac{m\pi}{b}\right)^2 \quad (3.41)$$

The cutoff wavelength and cutoff frequency are:

$$\lambda_{cnm} = \frac{2\pi}{k_c} = \frac{2}{\sqrt{(n/a)^2 + (m/b)^2}} \quad (3.42)$$

$$f_{cnm} = \frac{1}{2\sqrt{\mu\epsilon}} \sqrt{\left(\frac{n}{a}\right)^2 + \left(\frac{m}{b}\right)^2} \quad (3.43)$$

The subscripts  $n$  and  $m$  refer to the number of field maxima in the  $x$  and  $y$  directions, respectively.

In most applications, we use the fundamental mode  $TE_{10}$  having the lowest cutoff frequency:

$$f_{cTE10} = \frac{1}{2a\sqrt{\mu\epsilon}} \quad (3.44)$$

In the case of an air-filled waveguide, we obtain  $f_{cTE10} = c/(2a)$ . The cutoff wavelength is  $\lambda_c = 2a$ . If the waveguide width  $a$  is twice the height  $b$ ,  $a = 2b$ , the  $TE_{20}$  and  $TE_{01}$  wave modes have a cutoff frequency of  $2f_{cTE10}$ .

The fields of the  $TE_{10}$  wave mode are solved from the Helmholtz equation and boundary conditions as follows:

$$E_x = 0 \quad (3.45)$$

$$E_y = E_0 \sin \frac{\pi x}{a} \quad (3.46)$$

$$H_z = j \frac{E_0}{\eta} \frac{\lambda}{2a} \cos \frac{\pi x}{a} \quad (3.47)$$

$$H_x = -\frac{E_0}{\eta} \sqrt{1 - \left(\frac{\lambda}{2a}\right)^2} \sin \frac{\pi x}{a} \quad (3.48)$$

$$H_y = 0 \quad (3.49)$$

$E_0$  is the maximum value of the electric field, which has only a  $y$ -component. All field components depend on time and the  $z$ -coordinate as  $\exp(j\omega t - \gamma z)$ . Figure 3.5 illustrates the fields and the surface currents of the  $TE_{10}$  wave mode.

The wave impedance of the  $TE_{10}$  mode is

$$Z_{TE10} = \left| \frac{E_y}{H_x} \right| = \frac{\eta}{\sqrt{1 - [\lambda/(2a)]^2}} \quad (3.50)$$

For example, at a frequency of  $1.5f_c$ , the wave impedance of an air-filled waveguide is  $506\Omega$ . The wave impedance depends on frequency and is characteristic for each wave mode.

The characteristic impedance  $Z_0$  of a transmission line is the ratio of voltage and current in an infinitely long line or in a line terminated with a

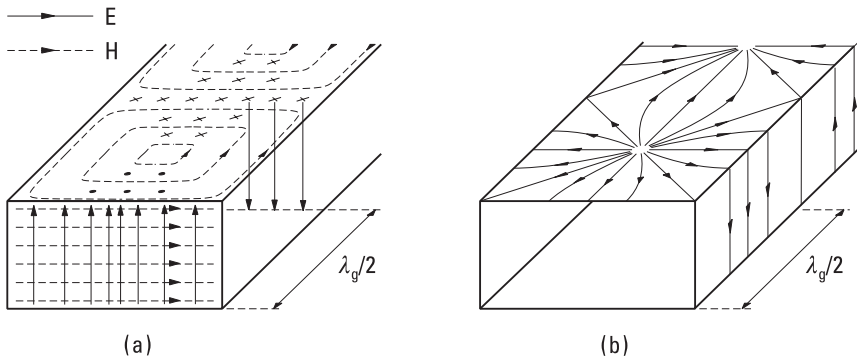


**Figure 3.5** (a) Fields and (b) surface currents of the  $TE_{10}$  wave mode in a rectangular waveguide at a given instant of time.

matched load having a wave propagating only in one direction. However, we cannot uniquely define the voltage and current of a waveguide as we can do for a two-conductor transmission line. Therefore, we may have many definitions for the characteristic impedance of a waveguide using any two of the following three quantities: power, voltage, current. The characteristic impedance can be calculated from the power propagating in the waveguide,  $P_p$  given in (3.53), and the voltage  $U$ , which is obtained by integrating the electric field in the middle of the waveguide from the upper wall to the lower wall, as

$$Z_{0TE10} = \frac{U^2}{P_p} = \frac{(E_0 b)^2/2}{P_p} = \frac{2b}{a} Z_{TE10} \quad (3.51)$$

Note that the characteristic impedance of the  $TE_{10}$  wave mode depends on the height  $b$ , whereas the wave impedance of (3.50) does not. The characteristic impedance in (3.51) has been found to be the best definition in practice when problems concerning impedance matching to various loads are being solved.

The power propagating in a waveguide is obtained by integrating Poynting's vector over the area of the cross section  $S$ :

$$P_p = \frac{1}{2} \operatorname{Re} \int_S \mathbf{E} \times \mathbf{H}^* \cdot d\mathbf{S} \quad (3.52)$$

The power propagating at the  $TE_{10}$  wave mode is

$$P_p = \frac{1}{2} \operatorname{Re} \int_S E_y H_x^* dS = \frac{E_0^2}{Z_{TE10}} \frac{ab}{4} \quad (3.53)$$

The finite conductivity of the metal,  $\sigma_m$ , causes loss in the walls of the waveguide. Also, the insulating material may have dielectric loss due to  $\epsilon_r''$  and conduction loss due to  $\sigma_d$ . The attenuation constant can be given as

$$\alpha = \frac{P_l}{2P_p} \quad (3.54)$$

where  $P_l$  is the power loss per unit length.

The power loss of conductors is calculated from the surface current density  $\mathbf{J}_s = \mathbf{n} \times \mathbf{H}$  ( $\mathbf{n}$  is a unit vector perpendicular to the surface) by integrating  $|\mathbf{J}_s|^2 R_s / 2$  over the surface of the conductor. Although in the preceding analysis the fields of the waveguide are derived assuming the conductors to be ideal, this method is accurate enough if the losses are low. The surface resistance of a conductor is  $R_s = \sqrt{\omega \mu_0 / (2\sigma_m)}$ . The attenuation constant of conductor loss for the  $TE_{10}$  wave mode is obtained as

$$\alpha_{cTE_{10}} = \frac{R_s}{\eta \sqrt{1 - [\lambda / (2a)]^2}} \left( \frac{1}{b} + \frac{\lambda^2}{2a^3} \right) \quad (3.55)$$

Close to the cutoff frequency, the attenuation is high, approaching infinite. If the dielectric material filling the waveguide has loss, the attenuation constant of dielectric loss is for all wave modes

$$\alpha_d = \frac{\pi}{\lambda} \frac{\tan \delta}{\sqrt{1 - (f_c / f)^2}} \quad (3.56)$$

The total attenuation constant is  $\alpha = \alpha_c + \alpha_d$ .

The recommended frequency range for waveguides operating at the  $TE_{10}$  wave mode is about from 1.2 to 1.9 times the cutoff frequency  $f_{cTE_{10}}$ . The increase of attenuation sets the lower limit, whereas the excitation of higher-order modes sets the higher limit. Hence, we need a large number of waveguides to cover the whole microwave and millimeter-wave range. Standard waveguides that cover the 10 GHz to 100 GHz range are listed in Table 3.2. In most cases  $a = 2b$ . Figure 3.6 shows the theoretical attenuation of some standard waveguides made of copper. In practice, the attenuation is higher due to the surface roughness.

### Example 3.1

Find the maximum power that can be fed to a WR-90 waveguide at 10 GHz. The maximum electric field that air can withstand without breakdown—the dielectric strength of air—is about 3 kV/mm.

### Solution

The dimensions of the waveguide are  $a = 22.86$  mm and  $b = 10.16$  mm. From (3.50), the wave impedance of the  $TE_{10}$  wave mode at 10 GHz ( $\lambda = 30$  mm) is  $Z_{TE_{10}} = 500\Omega$ . By setting  $E_0 = 3$  kV/mm into (3.53), we find the maximum power to be 1.05 MW. Because the attenuation is about

**Table 3.2**  
Standard Waveguides

Abbreviation	$a$ [mm]	$b$ [mm]	$f_c$ [GHz]	Range [GHz]
WR-90	22.86	10.16	6.56	8.2–12.4
WR-75	19.05	9.53	7.87	10–15
WR-62	15.80	7.90	9.49	12.4–18
WR-51	12.95	6.48	11.6	15–22
WR-42	10.67	4.32	14.1	18–26.5
WR-34	8.64	4.32	17.4	22–33
WR-28	7.11	3.56	21.1	26.5–40
WR-22	5.69	2.84	26.3	33–50
WR-19	4.78	2.39	31.4	40–60
WR-15	3.76	1.88	39.9	50–75
WR-12	3.10	1.55	48.4	60–90
WR-10	2.54	1.27	59.0	75–110
WR-8	2.03	1.02	73.8	90–140

0.1 dB/cm, the power absorbed into the walls of the waveguide is about 240 W/cm at the maximum power. If the load reflects some of the power, the maximum field strength is due to the standing wave higher than in the matched case. Then, the maximum power is lower than that calculated above.

### 3.4.2 TM Wave Modes in Rectangular Waveguide

TM wave modes have no longitudinal magnetic field component,  $H_z = 0$ . The solution of the longitudinal electric field has a form of

$$E_z = B \sin(k_1 x) \sin(k_2 y) \quad (3.57)$$

The other field components are

$$H_x = j \frac{\omega \epsilon k_2}{k_c^2} B \sin(k_1 x) \cos(k_2 y) \quad (3.58)$$

$$H_y = -j \frac{\omega \epsilon k_1}{k_c^2} B \cos(k_1 x) \sin(k_2 y) \quad (3.59)$$

$$E_x = Z_{TM} H_y \quad (3.60)$$

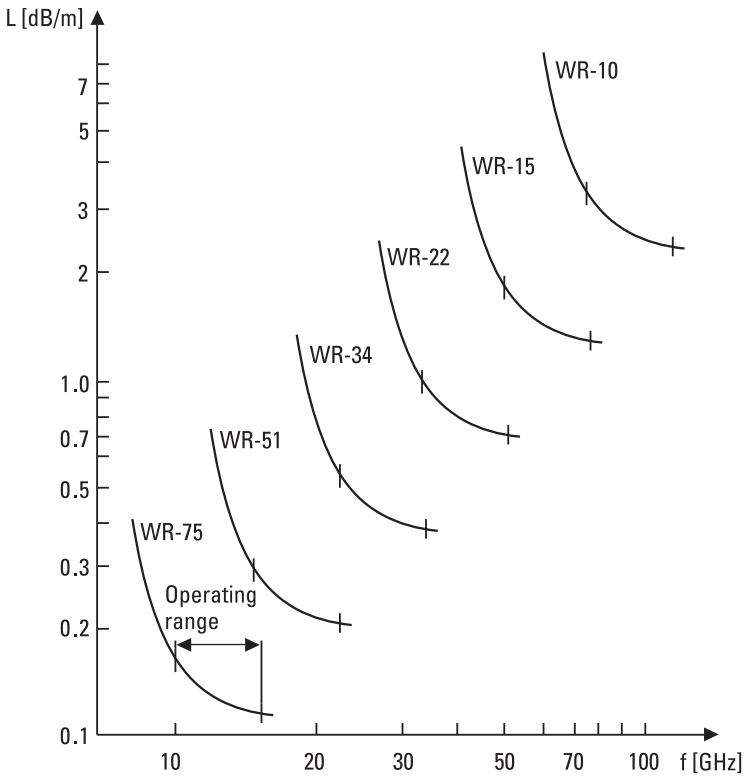


**Figure 3.6** Attenuation of standard waveguides.

$$E_y = -Z_{TM} H_x \quad (3.61)$$

The wave impedance of TM modes is

$$Z_{TM} = \eta \sqrt{1 - (f_c/f)^2} \quad (3.62)$$

From boundary conditions it follows that the equations for the cutoff wavelength and cutoff frequency are the same as those for the TE wave modes. Now, both indices  $n$  and  $m$  have to be nonzero. The TM wave mode having the lowest cutoff frequency is  $TM_{11}$ . Although  $TM_{11}$  and  $TE_{11}$  wave modes have equal cutoff frequencies, their field distributions are different. Figure 3.7 shows transverse field distributions of some TE and TM wave modes.

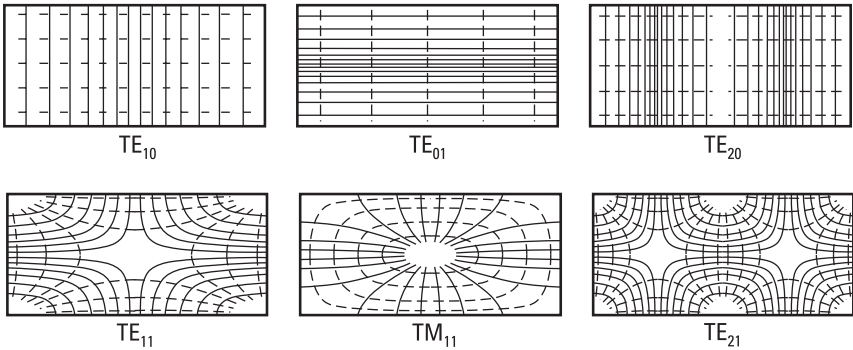


**Figure 3.7** Transverse field distributions of some TE and TM wave modes of a rectangular waveguide. Solid lines represent electric field lines, dashed lines magnetic field lines.

### 3.5 Circular Waveguide

The analysis of a circular waveguide shown in Figure 3.8 is best carried out using the cylindrical coordinate system. The principle of analysis is similar to that of the rectangular waveguide.

The solutions of the longitudinal magnetic fields of the TE wave modes are

$$H_z = AJ_n(k_c r) \cos(n\phi) \tag{3.63}$$

where  $J_n$  is the Bessel function of the order  $n$ . From the boundary condition  $H_r(r = a) = 0$ , it follows that  $\partial H_r / \partial r(r = a) = 0$ , and further that  $J'_n(k_c a) = 0$ , in which the apostrophe stands for derivative. From this we get

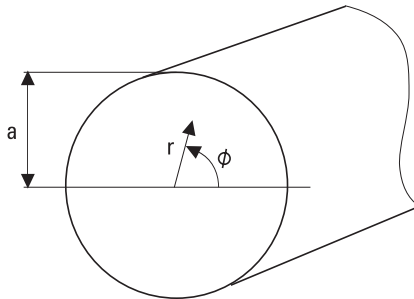


**Figure 3.8** Circular waveguide.

$$k_{cnm} = \frac{p'_{nm}}{a} \quad (3.64)$$

where  $p'_{nm}$  is the  $m$ th zero of  $J'_n$ . The corresponding cutoff wavelength is

$$\lambda_{cTEnm} = \frac{2\pi a}{p'_{nm}} \quad (3.65)$$

The solutions of the longitudinal electric fields of the TM wave modes are

$$E_z = BJ_n(k_c r) \cos(n\phi) \quad (3.66)$$

From the boundary condition  $E_z(r = a) = 0$  it follows that  $J_n(k_c a) = 0$ , or

$$k_{cnm} = \frac{p_{nm}}{a} \quad (3.67)$$

where  $p_{nm}$  is the  $m$ th zero of  $J_n$ . The cutoff wavelength is

$$\lambda_{cTMnm} = \frac{2\pi a}{p_{nm}} \quad (3.68)$$

The subscript  $n$  denotes the number of periods in the field distribution along the  $\phi$  angle. The subscript  $m$  gives the number of axial field minima in the radial direction. Figure 3.9 shows the transverse field distributions of some wave modes. Table 3.3 gives the cutoff wavelengths of the wave modes having the lowest cutoff frequencies.

The relative bandwidth of the circular waveguide operating at the fundamental mode  $TE_{11}$  is smaller than that of the rectangular waveguide operating at the  $TE_{10}$  mode, as shown in Figure 3.10. Therefore, many standard waveguide sizes are needed to cover a broad frequency range.

The conductor losses of the circular waveguide are calculated from the surface currents and surface resistance the same way as in the case of the rectangular waveguide. A special feature of the  $TE_{01}$  wave mode is that its attenuation decreases monotonously as the frequency increases. The attenuation constant of the  $TE_{01}$  wave mode is



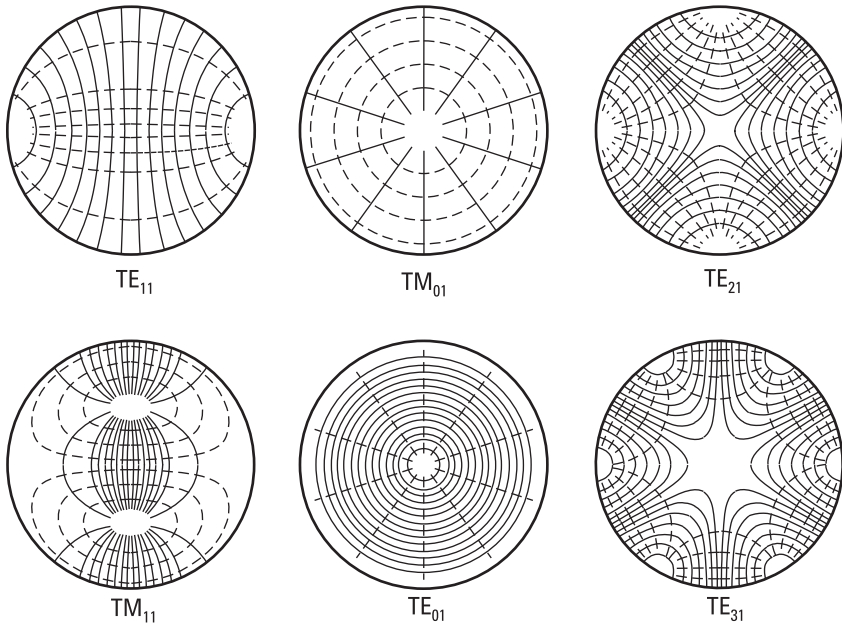


**Figure 3.9** Transverse field distributions of some TE and TM wave modes in a circular waveguide. Solid lines represent electric field lines, dashed lines magnetic field lines.

**Table 3.3**

Cutoff Wavelengths of Wave Modes in a Circular Waveguide with Radius  $a$

Wave Mode	$p_{nm}$ or $p'_{nm}$	$\lambda_c$
TE <sub>11</sub>	$p'_{11} = 1.841$	$3.41a$
TM <sub>01</sub>	$p_{01} = 2.405$	$2.61a$
TE <sub>21</sub>	$p'_{21} = 3.054$	$2.06a$
TE <sub>01</sub>	$p'_{01} = 3.832$	$1.64a$
TM <sub>11</sub>	$p_{11} = 3.832$	$1.64a$

$$\alpha_{cTE01} = \frac{R_s}{a\eta} \frac{(f_c/f)^2}{\sqrt{1 - (f_c/f)^2}} \quad (3.69)$$

The attenuation of the TE<sub>01</sub> wave mode is very low if the operating frequency is much higher than the cutoff frequency  $f_c$ . However, many other modes

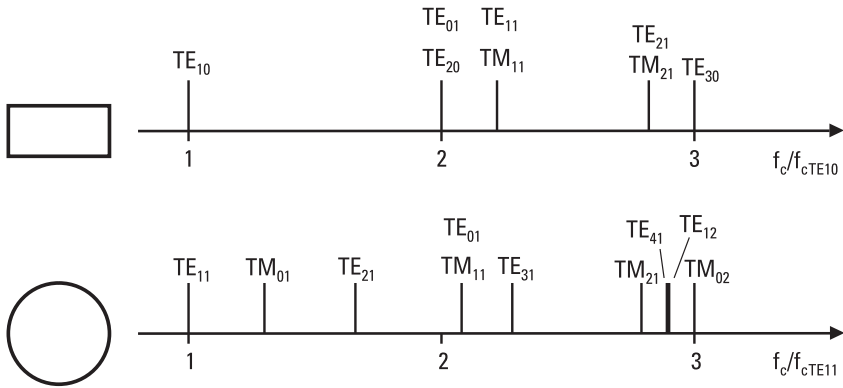


**Figure 3.10** Cutoff frequencies of the lowest wave modes of rectangular and circular waveguides.

can propagate in such an oversized waveguide. A low attenuation is achieved only if the excitation of unwanted modes is prevented.

### Example 3.2

Calculate the conductor losses at 60 GHz for the  $TE_{01}$  wave mode in a circular waveguide made of copper. The radius of the waveguide is (a) 3.5 mm, and (b) 20 mm.

### Solution

The surface resistance is

$$\begin{aligned}
 R_s &= \sqrt{\pi f \mu_0 / \sigma} \\
 &= \sqrt{\pi \times 60 \times 10^9 \times 4\pi \times 10^{-7} / 58 \times 10^6} \text{ } \Omega/\text{m} \\
 &= 0.064 \text{ } \Omega/\text{m}.
 \end{aligned}$$

The cutoff frequency of the  $TE_{01}$  wave mode is  $f_c = c/\lambda_c = c/(1.64a)$ . (a) When  $a = 3.5$  mm,  $f_c = 52.3$  GHz. From (3.69) we solve the attenuation constant  $\alpha_{cTE01} = 0.0753$  1/m. The attenuation of a waveguide having a length  $l$  is in decibels  $20 \log e^{\alpha l}$ , from which we obtain an attenuation of 0.65 dB/m. (b) When  $a = 20$  mm,  $f_c = 9.15$  GHz and  $\alpha_{cTE01} = 1.14 \times 10^{-3}$  1/m. The attenuation is now only 0.010 dB/m or 1.0 dB/100m.

### 3.6 Optical Fiber

TE and TM wave modes may propagate, not only in hollow metal waveguides, but also in dielectric waveguides. An optical fiber is actually a dielectric waveguide with a circular cross section, in which total internal reflection confines light in the fiber. Optical fibers are used in many kinds of communication networks, usually at wavelengths of 0.8 to 1.6  $\mu\text{m}$  at infrared. The optical carrier is modulated with data rates up to several gigabits per second.

Optical fibers are made of quartz, glass, or plastic. An optical fiber consists of a core and a cladding. The index of refraction  $n = \sqrt{\epsilon_r}$  of the core is larger than that of the cladding. The refractive index of the cladding is adjusted to a proper value by doping quartz with metal oxides as  $\text{TiO}_2$ ,  $\text{Al}_2\text{O}_3$ ,  $\text{GeO}_2$ , or  $\text{P}_2\text{O}_3$ . Optical fibers can be divided into three types, as shown in Figure 3.11:

1. Single-mode fiber: core radius 1–16  $\mu\text{m}$ , cladding radius 50–100  $\mu\text{m}$ .
2. Multimode fiber with a step in the index of refraction: core radius 25–60  $\mu\text{m}$ , cladding radius 50–150  $\mu\text{m}$ .
3. Multimode fiber with a continuous change in the index of refraction: core radius 10–35  $\mu\text{m}$ , cladding radius 50–80  $\mu\text{m}$ .

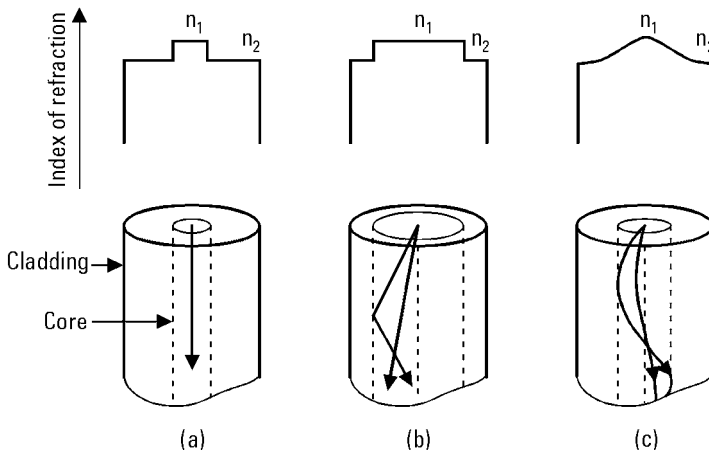


**Figure 3.11** Structures of optical fibers: (a) a single-mode fiber; (b) a multimode fiber with a step in the refractive index; (c) a multimode fiber with a continuous change in the refractive index.

An optical cable is usually made of several optical fibers. Steel wires and textile fibers as nylon give strength to the cable and support the fibers. Copper wires carry current for the repeater amplifiers if needed.

The solutions of the longitudinal field components in the core are

$$E_z = AJ_n(kr) \cos(n\phi) \quad (3.70)$$

$$H_z = BJ_n(kr) \sin(n\phi) \quad (3.71)$$

The solutions in the cladding are

$$E_z = CH_n(\chi r) \cos(n\phi) \quad (3.72)$$

$$H_z = DH_n(\chi r) \sin(n\phi) \quad (3.73)$$

In these equations,  $J_n(kr)$  is the Bessel function of the first kind of order  $n$ ;  $H_n(\chi r)$  is the Hankel function of the first kind of order  $n$ ;  $k$  is the transverse propagation constant in the core; and  $\chi$  is the transverse propagation constant in the cladding. Other field components are solved from these longitudinal fields, as in the case of metal waveguides, except now the boundary conditions are different, that is, the tangential components of  $E$  and  $H$  are continuous at the boundary of two dielectric materials.

From the expressions of longitudinal fields we can see that only cylindrically symmetric ( $n = 0$ ) wave modes are either TE or TM wave modes. Other wave modes are hybrid modes, denoted as EH or HE wave modes, for which both electric and magnetic fields have nonzero longitudinal components.

In a multimode fiber the number of propagating wave modes may be very large. The number of modes is approximately [7]

$$N = \frac{16}{\lambda_0^2} (n_1^2 - n_2^2) a^2 \quad (3.74)$$

where  $\lambda_0$  is the wavelength in free vacuum,  $n_1$  and  $n_2$  are the refractive indices of core and cladding, respectively, and  $a$  is the radius of the core.

### Example 3.3

Find the number of wave modes at a wavelength of  $1.55 \mu\text{m}$  in a quartz fiber having a core radius of  $40 \mu\text{m}$ . The refractive index of the cladding is 1% lower than that of the core.

**Solution**

The dielectric constant of quartz is  $\epsilon_r = 3.8$ . Hence  $n_1 = \sqrt{3.8} = 1.95$  and  $n_2 = 0.99 \times 1.95 = 1.93$ . From (3.74) we obtain the number of wave modes,  $N = 800$ .

The loss mechanisms of an optical fiber are:

- Dielectric absorption loss;
- Scattering loss due to the imperfections of the fiber;
- Radiation loss due to the bending of the fiber.

Properties making the optical fiber an excellent transmission medium for many applications are

- Small size and weight;
- Low attenuation—only 0.2 dB/km at 1.55  $\mu\text{m}$ —allowing cables hundreds of kilometers long without any repeater amplifiers;
- Immunity to interference and difficulty of interception;
- Reliability;
- Broad bandwidth;
- Low price compared to copper cable.

### 3.7 Coaxial Line

A coaxial line consists of two concentric conductors with circular cross sections and insulating material between them, as shown in Figure 3.12.

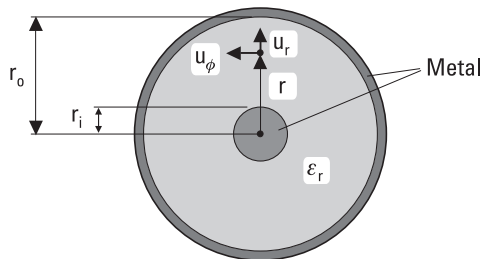


**Figure 3.12** Cross section of a coaxial line.

The inner radius of the outer conductor is  $r_o$  and the radius of the inner conductor is  $r_i$ ; the relative permittivity of the insulator is  $\epsilon_r$ . The fields are confined to the space between the conductors.

The fields of the TEM wave mode of the coaxial line can be derived from Laplace's equation (3.21) using the scalar potential  $\Phi(r, \phi)$ . In the cylindrical coordinate system, Laplace's equation is written as

$$\frac{1}{r} \frac{\partial}{\partial r} \left( r \frac{\partial \Phi(r, \phi)}{\partial r} \right) + \frac{1}{r^2} \frac{\partial^2 \Phi(r, \phi)}{\partial \phi^2} = 0 \quad (3.75)$$

Applying the boundary conditions  $\Phi(r_o, \phi) = 0$  and  $\Phi(r_i, \phi) = V$ , the potential is solved to be

$$\Phi(r, \phi) = V \frac{\ln(r_o/r)}{\ln(r_o/r_i)} \quad (3.76)$$

The electric field is the negative gradient of the potential:

$$\mathbf{E}(r, \phi) = -\nabla \Phi(r, \phi) = \mathbf{u}_r \frac{V}{\ln(r_o/r_i)} \frac{1}{r} \quad (3.77)$$

where  $\mathbf{u}_r$  is the unit vector in the radial direction. This is also the electric field of a cylindrical capacitor. The magnetic field of the coaxial line is

$$\mathbf{H}(r, \phi) = \frac{1}{\eta} \mathbf{u}_z \times \mathbf{E}(r, \phi) = \mathbf{u}_\phi \frac{V}{\eta r \ln(r_o/r_i)} = \mathbf{u}_\phi \frac{I}{2\pi r} \quad (3.78)$$

where  $\eta = \sqrt{\mu/\epsilon}$  is the wave impedance,  $I$  is the current in the inner conductor, and  $\mathbf{u}_\phi$  is the unit vector perpendicular to the radial direction. A current  $I$  flows also in the outer conductor but to the opposite direction.

The characteristic impedance of the coaxial line is

$$Z_0 = \frac{V}{I} = \frac{\eta}{2\pi} \ln(r_o/r_i) \quad (3.79)$$

The 50- $\Omega$  characteristic impedance has become a standard value. Most measurement instruments and thus also most devices have 50- $\Omega$  input and output connectors.

The attenuation constant due to conductor loss is

$$\alpha_c = \frac{R_s}{4\pi Z_0} \left( \frac{1}{r_o} + \frac{1}{r_i} \right) \quad (3.80)$$

For an air-filled coaxial line with a given outer conductor dimension, the minimum of the attenuation constant is obtained when the characteristic impedance is  $Z_0 = 77\Omega$ . The attenuation constant due to dielectric loss is

$$\alpha_d = \frac{\pi}{\lambda} \tan \delta \quad (3.81)$$

Also TE and TM wave modes may propagate in a coaxial line, if the operating frequency is larger than the cutoff frequency of these wave modes. To avoid losses and unanticipated phenomena due to these modes, the operating frequency should be chosen to be low enough. An approximate rule is that the circumference corresponding to the average radius should be smaller than the operating wavelength:

$$\lambda > \pi(r_o + r_i) \quad (3.82)$$

Consequently, the coaxial lines used at high frequencies should be thin enough to make sure that only the TEM wave mode may propagate.

#### Example 3.4

Show that the attenuation constant of an air-filled coaxial line having a fixed diameter is at minimum when the characteristic impedance is  $Z_0 = 77\Omega$ .

#### Solution

According to (3.79) and (3.80) the attenuation constant is proportional to the quantity

$$\frac{1}{r_o} \left( 1 + \frac{r_o}{r_i} \right) \frac{1}{\ln(r_o/r_i)}$$

Now  $r_o$  is constant. Let us denote  $r_o/r_i = x$  and derivate with respect of  $x$ :

$$D \left[ \frac{1}{r_o} \frac{1+x}{\ln x} \right] = \frac{1}{r_o} \frac{\ln x - (1+x)(1/x)}{\ln^2 x}$$

By setting this derivative equal to zero, we obtain

$$\ln x = \frac{1}{x} + 1$$

The solution of this equation is  $x = r_o/r_i = 3.591$ . By substituting this in (3.79), we obtain  $Z_0 = 76.7\Omega$ .

### 3.8 Microstrip Line

A microstrip line consists of a metal strip on one side and a ground plane on the other side of a substrate, as shown in Figure 3.13. The substrate is made of a low-loss dielectric material such as polytetrafluoroethylene (Teflon), aluminum oxide (alumina), or quartz.

A pure TEM wave mode can propagate in a microstrip line only if all fields are in the same medium. Then the solution for the field can be derived from Laplace's equation. In a case where the nonstatic fields are in two different media, the field has also longitudinal components. At low frequencies, or more precisely when  $\lambda \gg h$ , the fields are nearly the same as those in a static case, and we call them quasi-TEM. However, the analytical solution

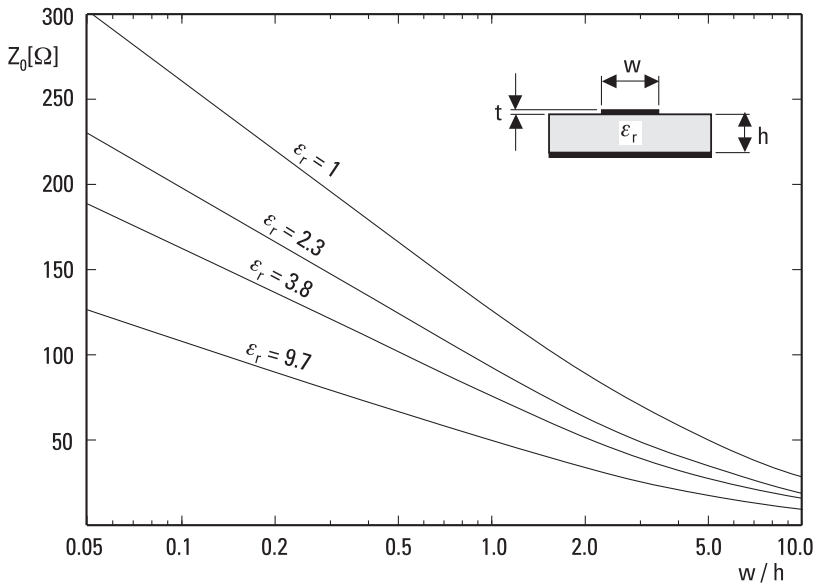


**Figure 3.13** The cross section of a microstrip line and the characteristic impedance  $Z_0$  as a function of the ratio of strip width to substrate height  $w/h$  for different substrate materials.



of the quasi-TEM wave mode is complicated and therefore a practical design of microstrip lines is based on graphs or approximate equations.

The phase constant of a quasi-TEM wave can be expressed as

$$\beta = \frac{2\pi}{\lambda} = \omega\sqrt{\mu\epsilon_0\epsilon_{\text{reff}}} \quad (3.83)$$

where  $\epsilon_{\text{reff}}$  is the effective relative permittivity. This is obtained by measuring or calculating the capacitance of the line per unit length  $C_{\text{eff}}$  and the capacitance of an air-filled but otherwise similar line per unit length  $C_0$ :

$$\epsilon_{\text{reff}} = \frac{C_{\text{eff}}}{C_0} \quad (3.84)$$

The designer often knows the required characteristic impedance  $Z_0$  and the required length of the line in wavelengths  $l/\lambda$ . Then the width of the strip  $w$  and the physical length  $l$  have to be determined.  $Z_0$  and  $\epsilon_{\text{reff}}$  depend mainly on the width of the strip  $w$  and on the height  $h$  and the relative permittivity  $\epsilon_r$  of the substrate. The velocity of the wave and the wavelength depend on  $\epsilon_{\text{reff}}$ , as given by (3.83). Sometimes the problem is inverse: The characteristic impedance has to be calculated from the dimensions and permittivity. Approximate design of a microstrip line can be carried out by using Figure 3.13 or the following equations [8]. These equations are valid when  $0.05 \leq w/h \leq 20$  and  $\epsilon_r \leq 16$ .

When  $w/h \leq 1$ , the effective relative permittivity and characteristic impedance are

$$\epsilon_{\text{reff}} \approx \frac{\epsilon_r + 1}{2} + \frac{\epsilon_r - 1}{2} \left[ \frac{1}{\sqrt{1 + 12h/w}} + 0.04 \left( 1 - \frac{w}{h} \right)^2 \right] \quad (3.85)$$

$$Z_0 \approx \frac{60}{\sqrt{\epsilon_{\text{reff}}}} \ln \left( \frac{8h}{w} + \frac{w}{4h} \right) \Omega \quad (3.86)$$

When  $w/h \geq 1$ ,

$$\epsilon_{\text{reff}} \approx \frac{\epsilon_r + 1}{2} + \frac{\epsilon_r - 1}{2} \frac{1}{\sqrt{1 + 12h/w}} \quad (3.87)$$

$$Z_0 \approx \frac{377}{\sqrt{\epsilon_{\text{reff}}} [w/h + 1.393 + 0.667 \ln(w/h + 1.444)]} \Omega \quad (3.88)$$

The width of the strip corresponding to a known  $Z_0$  is obtained for  $w/h \leq 2$  from

$$\frac{w}{h} \approx \frac{8e^A}{e^{2A} - 2} \quad (3.89)$$

where

$$A = \frac{Z_0}{60\Omega} \sqrt{\frac{\epsilon_r + 1}{2}} + \frac{\epsilon_r - 1}{\epsilon_r + 1} \left( 0.23 + \frac{0.11}{\epsilon_r} \right) \quad (3.90)$$

When  $w/h \geq 2$ ,

$$\frac{w}{h} \approx \frac{2}{\pi} \left\{ B - 1 - \ln(2B - 1) + \frac{\epsilon_r - 1}{2\epsilon_r} \left[ \ln(B - 1) + 0.39 - \frac{0.61}{\epsilon_r} \right] \right\} \quad (3.91)$$

where

$$B = \frac{377\pi\Omega}{2Z_0\sqrt{\epsilon_r}} \quad (3.92)$$

In the preceding equations, it has been assumed that the thickness  $t$  of the strip is very small. In practice, the capacitance of the line per unit length will be slightly larger due to the finite thickness  $t$  compared to the case  $t = 0$ . This will lower the characteristic impedance. Due to the extra capacitance, the width of the strip seems to increase by

$$\Delta w_e = \frac{t}{\pi} (1 + \ln D) \quad (3.93)$$

where  $D = 2h/t$ , when  $w/h \geq 1/(2\pi)$ , and  $D = 4\pi w/t$ , when  $w/h \leq 1/(2\pi)$ . Equation (3.93) is valid for  $t < h$  and  $t < w/2$ . Equations (3.86), (3.88), (3.89), and (3.91) can be used for a strip having a finite thickness by replacing  $w$  by  $w_e = w + \Delta w_e$ .

The sources of losses in a microstrip line are:

- Conductor loss in the strip and ground plane;
- Dielectric and conduction losses in the substrate;
- Radiation loss;
- Surface wave loss.

Assuming a constant current distribution over the strip width, the attenuation constant due to metal loss is

$$\alpha_c = \frac{R_s}{Z_0 w} \quad (3.94)$$

The accuracy of this equation is best for a wide strip. In practice, the value of the surface resistance  $R_s$  is larger than the theoretical one. For example, the surface roughness of the substrate increases  $R_s$ . The thickness of the conductors should be at least four times the skin depth  $\delta_s = \sqrt{2/(\omega\mu\sigma_m)}$ . A metallization thinner than twice the skin depth would yield excessive attenuation.

Dielectric loss is usually much lower than conductor loss. The attenuation constant due to dielectric loss is

$$\alpha_d = \pi \frac{\epsilon_r (\epsilon_{\text{reff}} - 1)}{\sqrt{\epsilon_{\text{reff}}} (\epsilon_r - 1)} \frac{\tan \delta}{\lambda_0} \quad (3.95)$$

where  $\lambda_0$  is the wavelength in free vacuum.

Discontinuities of the microstrip line produce radiation to free space. For a given line, radiation loss increases rapidly as the frequency increases. To avoid leakage and interference, microstrip circuits are usually shielded within a metal case. In microstrip antennas, leaking radiation is harnessed into use.

Surface waves are waves that are trapped by total reflection within the substrate. They may produce unwanted radiation from the edges of the substrate and spurious coupling between circuit elements.

### Example 3.5

Find the width of the strip for a 50- $\Omega$  microstrip line. The substrate has a thickness of  $h = 0.254$  mm and a relative permittivity of  $\epsilon_r = 9.7$ . The

thickness of the strip is  $t = 5 \mu\text{m}$ . Find the wavelength in the line at a frequency of 10 GHz.

### Solution

From Figure 3.13 we see that  $w/h$  is about 1. Equation (3.90) gives  $A = 2.124$ . From (3.89) we solve  $w/h = 0.985$  or  $w = 0.250 \text{ mm}$ . To account for the effect of the strip thickness, we calculate  $D = 2h/t = 101.6$  and solve from (3.93) to get  $\Delta w_e = 0.009 \text{ mm}$ . Therefore, the strip width should be  $0.250 \text{ mm} - 0.009 \text{ mm} = 0.241 \text{ mm}$ . A  $5 \mu\text{m}$  thick and  $0.241 \text{ mm}$  wide strip corresponds to a  $0.250 \text{ mm}$  wide strip with  $t = 0$ . From (3.85) we obtain  $\epsilon_{\text{reff}} = 6.548$ . The wavelength at  $f = 10 \text{ GHz}$  is  $\lambda = c/(f\sqrt{\epsilon_{\text{reff}}}) = 11.72 \text{ mm}$ . (In practice, microstrip lines are dispersive and  $\epsilon_{\text{reff}}$  increases as the frequency increases. Therefore,  $\lambda$  is slightly shorter.)

## 3.9 Wave and Signal Velocities

In a vacuum, radio waves propagate at the speed of light,  $c = 299,792,458 \text{ m/s}$ . In a medium with parameters  $\epsilon_r$  and  $\mu_r$  the velocity of propagation is

$$v = \frac{1}{\sqrt{\mu\epsilon}} = \frac{1}{\sqrt{\mu_r\epsilon_r}} c \quad (3.96)$$

The phase velocity

$$v_p = \frac{\omega}{\beta} \quad (3.97)$$

is that velocity with which the constant-phase points of a wave propagate. In case of a plane wave or a TEM wave propagating in a transmission line, the phase velocity is equal to the velocity of propagation in free space filled with the same medium,  $v_p = v$ . Generally, the phase velocity of a wave propagating in a waveguide may be smaller or larger than  $v$ .

If the phase velocity and attenuation of a propagating wave do not depend on frequency, the waveform of a broadband signal does not distort as it propagates. However, if the phase velocity is frequency-dependent, the waveform will distort. This phenomenon is called dispersion (see Section 3.3).

The group velocity,  $v_g$ , is that velocity with which the energy of a narrow-band signal (or signal experiencing no significant dispersion) propa-

gates. The group velocity of a plane wave or a TEM wave is equal to the velocity of propagation in free space filled with the same medium. For other wave modes, the group velocity is smaller than  $v$ . The group velocity can never exceed the speed of light. The group velocity is given by [2, 5]

$$v_g = \left( \frac{d\beta}{d\omega} \right)^{-1} \tag{3.98}$$

### 3.10 Transmission Line Model

A transmission line exhibits properties of capacitance, inductance, resistance, and conductance: The electric field between the conductors contains electric energy in the same way as a capacitor; the magnetic field produced by the currents contains magnetic energy as an inductor; the conductors have losses as a resistor; the leakage currents in the insulator produce losses as a resistor or a conductor. These properties cannot be separated because they are distributed along the line. Figure 3.14 shows the transmission line model, a short section of a transmission line with a length  $\Delta z$  having a series inductance  $L$ , a parallel capacitance  $C$ , a series resistance  $R$ , and a parallel conductance  $G$ , all being values per unit length.

In the transmission line model, voltages and currents are used instead of electric and magnetic fields to represent the propagating wave. This model best suits transmission lines carrying TEM wave modes. However, the transmission line model may also be applied for other transmission lines and waveguides by defining the voltage and current properly and by restricting the analysis for such a narrow band that dispersion may be neglected.

The voltage and current on a transmission line depend on the position and time,  $V(z, t)$  and  $I(z, t)$ . We can derive for voltage and current the so-called telegrapher equations:

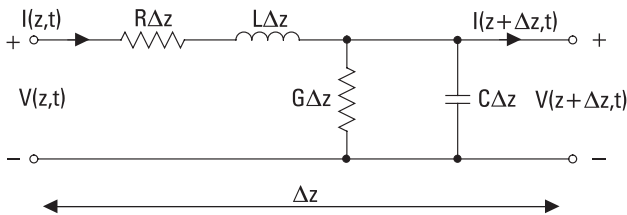


**Figure 3.14** Transmission line model.

$$\frac{\partial^2 V(z, t)}{\partial z^2} = LC \frac{\partial^2 V(z, t)}{\partial t^2} + (RC + LG) \frac{\partial V(z, t)}{\partial t} + RGV(z, t) \quad (3.99)$$

$$\frac{\partial^2 I(z, t)}{\partial z^2} = LC \frac{\partial^2 I(z, t)}{\partial t^2} + (RC + LG) \frac{\partial I(z, t)}{\partial t} + RGI(z, t) \quad (3.100)$$

The voltage and current of a sinusoidal signal are

$$V(z, t) = V(z) e^{j\omega t} \quad (3.101)$$

$$I(z, t) = I(z) e^{j\omega t} \quad (3.102)$$

For sinusoidal signals, the telegrapher equations simplify to

$$\frac{d^2 V(z)}{dz^2} - \gamma^2 V(z) = 0 \quad (3.103)$$

$$\frac{d^2 I(z)}{dz^2} - \gamma^2 I(z) = 0 \quad (3.104)$$

where

$$\gamma = \sqrt{(R + j\omega L)(G + j\omega C)} = \alpha + j\beta \quad (3.105)$$

The solutions of the telegrapher equations are of the form

$$V(z) = V^+ e^{-\gamma z} + V^- e^{+\gamma z} \quad (3.106)$$

$$I(z) = \frac{V^+}{Z_0} e^{-\gamma z} - \frac{V^-}{Z_0} e^{+\gamma z} = I^+ e^{-\gamma z} - I^- e^{+\gamma z} \quad (3.107)$$

where

$$Z_0 = \sqrt{\frac{R + j\omega L}{G + j\omega C}} \quad (3.108)$$

is the complex characteristic impedance of the transmission line. In (3.106) and (3.107)  $V^+$  and  $I^+$  are the complex amplitudes for a wave propagating into the positive  $z$  direction and  $V^-$  and  $I^-$  are those for a wave propagating into the negative  $z$  direction.

## References

- [1] Chatterjee, R., *Elements of Microwave Engineering*, Chichester, England: Ellis Horwood, 1986.
- [2] Collin, R. E., *Foundations for Microwave Engineering*, 2nd ed., New York: IEEE Press, 2001.
- [3] Collin, R. E., *Field Theory of Guided Waves*, New York: IEEE Press, 1991.
- [4] Gardiol, F. E., *Introduction to Microwaves*, Dedham, MA: Artech House, 1984.
- [5] Pozar, D. M., *Microwave Engineering*, 2nd ed., New York: John Wiley & Sons, 1998.
- [6] Ramo, S., J. Whinnery, and T. van Duzer, *Fields and Waves in Communication Electronics*, New York: John Wiley & Sons, 1965.
- [7] Liao, S. Y., *Microwave Circuit Analysis and Amplifier Design*, Englewood Cliffs, NJ: Prentice Hall, 1987.
- [8] Bahl, I. J., and D. K. Trivedi, "A Designer's Guide to Microstrip Line," *Microwaves*, May 1977, pp. 174–182.

# 4

## Impedance Matching

In Chapter 3 we considered homogeneous transmission lines and waveguides in which a wave propagates only in the  $z$  direction. In a homogeneous line the characteristic impedance is independent of  $z$ , and accordingly the ratio of the electric and magnetic field as well as the ratio of the voltage and current (in a TEM line) is constant.

If there is a discontinuity in the line disturbing the fields, the impedance changes and a reflection occurs. The discontinuity may be a change in the line dimensions or a terminating load, the impedance of which is different from that of the line. This mismatch of impedances may cause serious problems. Elimination of the reflection—that is, matching the load to the line—is a frequent and important task in radio engineering.

In this chapter we first consider the fundamental concepts needed in impedance matching: the reflection coefficient, input impedance, standing wave, and the Smith chart. Then we consider different methods of impedance matching, such as matching with lumped elements, with tuning stubs, with quarter-wave transformers, and with a resistive circuit.

### 4.1 Reflection from a Mismatched Load

In the following analysis we will use the transmission line model and use voltages and currents. In principle we could, of course, use electric and magnetic fields, but the advantage of using voltages and currents is that the characteristic impedance of a line is always (by definition) the ratio of the



voltage and current, but not always directly the ratio of the electric and magnetic field [see (3.51)]. In impedance matching it is the characteristic impedance of the line that matters, not the wave impedance.

Let us consider a situation shown in Figure 4.1 in which the line is terminated at  $z = 0$  with a load. The characteristic impedance of the line is  $Z_0$  and the impedance of the load is  $Z_L$ . Let us assume that there is a voltage wave propagating toward the load,  $V^+e^{-\gamma z}$ , and the corresponding current wave is  $I^+e^{-\gamma z}$  ( $Z_0 = V^+/I^+$ ). Then at the input of the load, normally one part of the propagating wave power is reflected while the other part is absorbed to the load. The reflected voltage wave is  $V^-e^{+\gamma z}$ , and the corresponding reflected current wave is  $I^-e^{+\gamma z}$  ( $Z_0 = V^-/I^-$ ).  $V^+$ ,  $I^+$ ,  $V^-$ , and  $I^-$  are complex amplitudes. At  $z = 0$  the voltages of the line and those of the load must be equal, and the same applies of course to the currents:

$$V^+ + V^- = V_L \tag{4.1}$$

$$I^+ - I^- = I_L \tag{4.2}$$

Note that the directions of positive  $I^+$  and  $I^-$  are defined to be opposites. As  $Z_L = V_L/I_L$ , we can present (4.2) as

$$\frac{V^+}{Z_0} - \frac{V^-}{Z_0} = \frac{V_L}{Z_L} \tag{4.3}$$

The voltage reflection coefficient of the load is defined as

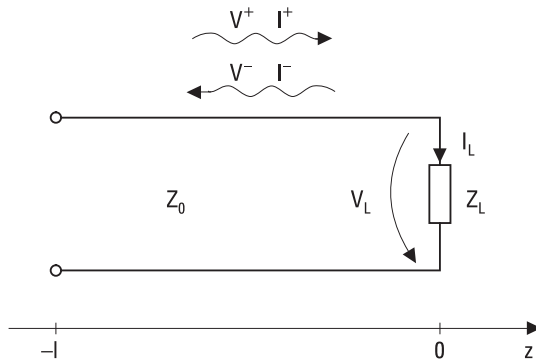


**Figure 4.1** A line terminated with a load.

$$\rho_L = \frac{V^-}{V^+} \quad (4.4)$$

If we eliminate  $V^-$  from (4.1) and (4.3), and then solve for  $\rho_L$ , we obtain

$$\rho_L = \frac{Z_L - Z_0}{Z_L + Z_0} = \frac{z_L - 1}{z_L + 1} \quad (4.5)$$

where  $z_L = Z_L/Z_0$  is the normalized load impedance (do not confuse the normalized impedances with the  $z$  coordinate). The voltage transmission coefficient is

$$\tau_L = \frac{V_L}{V^+} = 1 + \rho_L = \frac{2Z_L}{Z_L + Z_0} \quad (4.6)$$

If the load impedance and the characteristic impedance of the line are equal, there will be no reflected wave but all power will be absorbed into the load. In such a case the load is matched to the line.

If the load is mismatched or  $Z_L \neq Z_0$ , there will be a wave propagating in both directions, that is, the voltage and current as a function of  $z$  are

$$V(z) = V^+ e^{-\gamma z} + V^- e^{+\gamma z} \quad (4.7)$$

$$I(z) = I^+ e^{-\gamma z} - I^- e^{+\gamma z} = \frac{V^+}{Z_0} e^{-\gamma z} - \frac{V^-}{Z_0} e^{+\gamma z} \quad (4.8)$$

Let us assume that the length of the line is  $l$ . In the following we consider the load impedance seen through this line. At  $z = -l$  the voltage reflection coefficient is

$$\rho(-l) = \frac{V^- e^{-\gamma l}}{V^+ e^{+\gamma l}} = \rho_L e^{-2\gamma l} \quad (4.9)$$

Now the input impedance at  $z = -l$  is

$$Z(-l) = \frac{V(-l)}{I(-l)} = Z_0 \frac{V^+ e^{+\gamma l} + V^- e^{-\gamma l}}{V^+ e^{+\gamma l} - V^- e^{-\gamma l}} = Z_0 \frac{1 + \rho_L e^{-2\gamma l}}{1 - \rho_L e^{-2\gamma l}} = Z_0 \frac{1 + \rho(-l)}{1 - \rho(-l)} \quad (4.10)$$

When substituting (4.5) into (4.10) and taking into account that  $e^x = \sinh x + \cosh x$ , we obtain

$$Z(-l) = Z_0 \frac{Z_L + Z_0 \tanh \gamma l}{Z_0 + Z_L \tanh \gamma l} \tag{4.11}$$

In practice we use low-loss lines, which means that the attenuation (or damping) constant is small, often negligible, and then we can assume that  $\gamma = j\beta$ . In such a case the input impedance is

$$Z(-l) = Z_0 \frac{Z_L + jZ_0 \tan \beta l}{Z_0 + jZ_L \tan \beta l} \tag{4.12}$$

In a lossless case the line voltage as a function of  $z$  is

$$V(z) = V^+ e^{-j\beta z} (1 + \rho_L e^{2j\beta z}) \tag{4.13}$$

The voltage (or the field strength) repeats itself periodically at every half-wavelength, so there is a standing wave in the line, as shown in Figure 4.2. At the maximum, the voltages of the forward and reflected waves are in the same phase, and therefore the total amplitude is  $V_{max} = |V^+| + |V^-|$ . At the minimum, the voltages are in an opposite phase, and therefore the total amplitude  $V_{min}$  is the difference  $|V^+| - |V^-|$ . On the other hand, the current has a minimum where the voltage has a maximum, and vice versa. The voltage standing wave ratio is defined as

$$VSWR = \frac{V_{max}}{V_{min}} = \frac{|V^+| + |V^-|}{|V^+| - |V^-|} = \frac{1 + |\rho_L|}{1 - |\rho_L|} \tag{4.14}$$

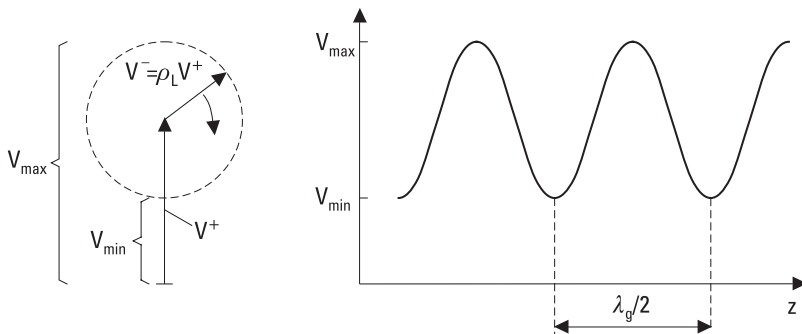


**Figure 4.2** Standing wave pattern (rhs) and its phasor presentation (lhs).

$VSWR$  is equal to 1 when the load is matched, and  $1 < VSWR \leq \infty$  when the load is mismatched. The input impedance of the line is  $Z_0 \times VSWR$  at the maximum and  $Z_0/VSWR$  at the minimum, that is, it is real in both cases.

There are many problems caused by the load mismatch:

- Part of the power is not absorbed by the load. Power is proportional to the square of the voltage (or field strength); therefore the power reflection coefficient is  $|\rho_L|^2$ . If the forward propagating power is  $P$ , then the reflected power is  $|\rho_L|^2 \times P$  and the power absorbed by the load is  $(1 - |\rho_L|^2) \times P$ . The power loss due to reflection or the reflection loss  $L_{refl}$  is (in decibels)

$$L_{refl} = 10 \log \frac{1}{1 - |\rho_L|^2} \quad (4.15)$$

The return loss  $L_{retn}$  describes how much smaller the reflected power is compared to the incident power  $P$ , and is defined (in decibels) as

$$L_{retn} = 10 \log \frac{1}{|\rho_L|^2} \quad (4.16)$$

- Due to reflection, the field strength may be doubled at the standing wave maximum, and therefore danger of electrical breakdown increases in high-power applications such as radar.
- The standing wave increases the conductor loss in the line. The loss is proportional to the square of the current. At the current maximum the loss increase is higher than the decrease at the current minimum compared to a matched case.
- A mismatch at the input of a sensitive receiver deteriorates the signal-to-noise ratio of the receiver.
- If the line is long, the input impedance fluctuates rapidly versus frequency. This is a disadvantage for active devices such as amplifiers because their performance depends on the feeding impedance. For example, the gain of an amplifier may change greatly if its input load impedance (feed impedance) changes.
- In digital radio systems the reflected pulses may cause symbol errors.

- In an antenna array a mismatched element causes deterioration of the overall antenna performance due to phase and amplitude errors.

A standing wave in a line can be measured and displayed using a slotted line, which is usually made of a rectangular metal waveguide or a coaxial line. In the case of a rectangular waveguide, there is a narrow slot in the middle of the wide wall, as shown in Figure 4.3; this slot does not disturb the fields of the waveguide because the surface currents of the  $TE_{10}$  mode do not cross the centerline of the wide wall. In the slot there is a movable probe, into which a voltage proportional to the electric field is induced. This voltage is then measured with a square-law diode detector and displayed with a proper device. By moving the probe, the maximum and minimum are found and their ratio gives the  $VSWR$ . The impedance at the standing wave minimum is  $Z_0/VSWR$ . Then the impedance at any position  $z$  can be calculated using (4.12). In practice, nowadays the impedance is measured using a network analyzer. For more information concerning measurement techniques, see [1].

## 4.2 Smith Chart

The Smith chart is a useful tool for displaying impedances measured versus frequency or for solving a matching problem in a circuit design. The Smith chart clearly shows the connection between the reflection coefficient and

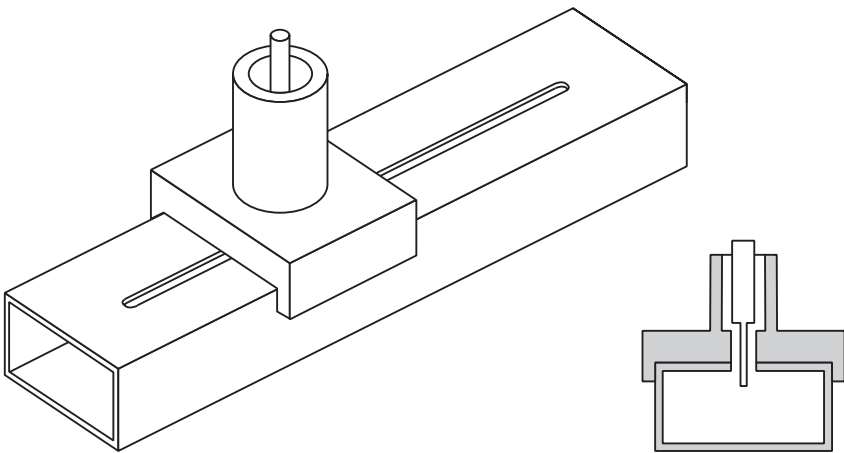


**Figure 4.3** A slotted line made of a rectangular waveguide.

impedance, and also displays readily how the input impedance changes when moving along the line.

If the load is passive, the absolute value of the voltage reflection coefficient is never more than 1. Then any complex reflection coefficient of a passive load can be presented in the polar form within a unity circle. All possible normalized impedances of passive loads can be presented within this unity circle. This is the great idea of the Smith chart, presented by P. Smith in 1939 [2].

The normalized input impedance at  $z = -l$  can be presented as

$$z(-l) = \frac{Z(-l)}{Z_0} = r + jx \quad (4.17)$$

The corresponding voltage reflection coefficient is

$$\rho(-l) = \rho_L e^{-2j\beta l} = u + jv \quad (4.18)$$

According to (4.10) we have

$$z(-l) = \frac{1 + \rho_L e^{-2j\beta l}}{1 - \rho_L e^{-2j\beta l}} \quad (4.19)$$

and after substituting (4.17) and (4.18) into this we obtain

$$r + jx = \frac{1 + (u + jv)}{1 - (u + jv)} \quad (4.20)$$

We can form the two following equations by separating (4.20) into real and imaginary parts:

$$r = \frac{1 - (u^2 + v^2)}{(1 - u)^2 + v^2} \quad (4.21)$$

$$x = \frac{2v}{(1 - u)^2 + v^2} \quad (4.22)$$

These can be solved for two equations of circles as

$$\left(u - \frac{r}{1+r}\right)^2 + v^2 = \frac{1}{(1+r)^2} \tag{4.23}$$

$$(u-1)^2 + \left(v - \frac{1}{x}\right)^2 = \frac{1}{x^2} \tag{4.24}$$

Graphically presented, these equations form the Smith chart shown in Figure 4.4.

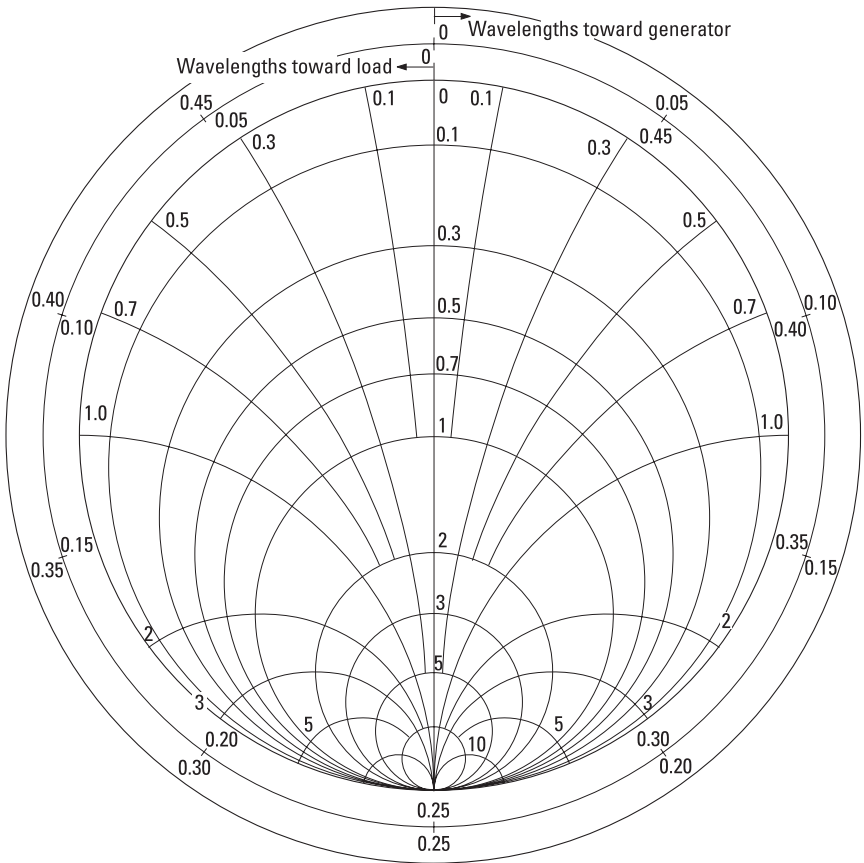
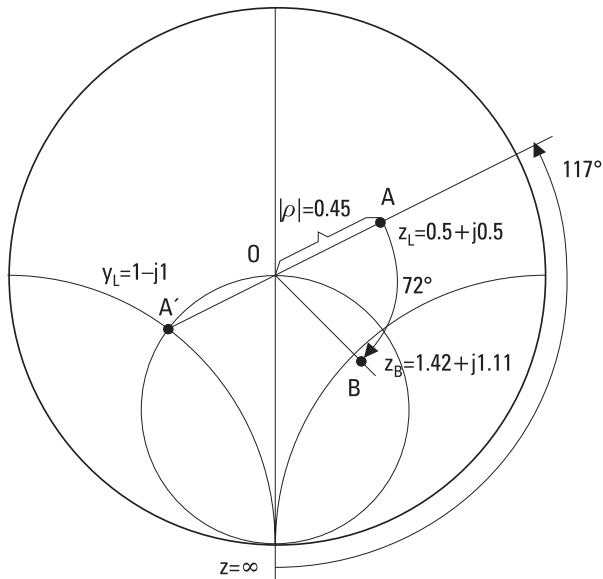


Figure 4.4 Smith chart.

At the center of the Smith chart the normalized impedance is  $z = 1$ ; that is, the load is matched to the line ( $\rho = 0$ ). At the top of the Smith chart there is a point representing a short circuit,  $z = 0$  or  $\rho = -1$ , and at the bottom there is a point representing an open circuit,  $z = \infty$  or  $\rho = 1$ . Points elsewhere on the unity circle perimeter represent pure imaginary impedances ( $|\rho| = 1$ ). All pure real impedances are on the vertical diameter, and from that to the left there are the capacitive impedances and to the right the inductive impedances.

Figure 4.5 shows how an impedance is related to the corresponding voltage reflection coefficient. Point A represents a normalized load impedance,  $z_L = 0.5 + j0.5$ . The magnitude of the reflection coefficient is the distance of point A from the center of the chart, point O, or  $|\rho| = 0.45$  (remember that the radius of the chart is 1). The phase of the reflection coefficient is the angle between the directions from point O to the point  $z = \infty$  and to point A measured counterclockwise, in this case  $\angle \rho = 117^\circ$ .

When moving along a lossless line, the absolute value of the reflection coefficient is constant and the phase changes  $360^\circ$  per one half-wavelength. Therefore the impedance locus following this move is along a circle, the



**Figure 4.5** Using the Smith chart: The relation between an impedance and the corresponding voltage reflection coefficient, movement along a lossless transmission line ( $A \rightarrow B$ ), and the relation between an impedance (point A) and the corresponding admittance (point A').



radius of which is equal to the absolute value of the load reflection coefficient. If the movement is toward the load, the direction on the Smith chart is counterclockwise. If the movement is away from the load, that is, toward the generator, the direction is clockwise. The impedance of the load,  $z_L = 0.5 + j0.5$ , seen through a line of  $0.1\lambda_g$  long, is obtained by moving from point A clockwise  $360^\circ/5 = 72^\circ$  to point B, where the impedance is  $z_B = 1.42 + j1.11$ .

One of the great features of the Smith chart is that the admittance  $y_L$  corresponding to the impedance  $z_L$  is obtained as the mirror image  $A'$  of point A. When  $z_L = 0.5 + j0.5$ , we can read from the Smith chart that  $y_L = 1.0 - j1.0$ . This can be easily checked using the definition of admittance

$$y^{(-l)} = \frac{1}{z^{(-l)}} = \frac{Z_0}{Z_{in}^{(-l)}} = g + jb \tag{4.25}$$

### 4.3 Matching Methods

The purpose of matching is to eliminate the wave reflected from a load. From the matching point of view, a load may be not only a circuit or device into which the power is absorbed from the line, but also a generator feeding the line. This is why we have to consider cautiously the directions “toward generator—clockwise” and “toward load—counterclockwise” on the Smith chart. In most cases we measure the reflection coefficient of the “load” first. In the measurement we use an auxiliary generator, and accordingly we can always use the direction “clockwise—toward generator” when designing a matching circuit. Figure 4.6 illustrates this in the case of an amplifier with both an input and output matching circuit in order to maximize gain. When designing the input matching circuit, we measure first the transistor reflection coefficient,  $\rho_{in}$ , from the input side, but when designing the output matching circuit we measure the reflection coefficient,  $\rho_{out}$ , from the output side.

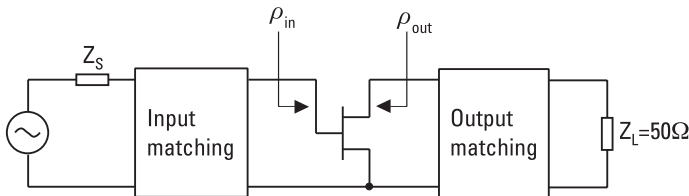


**Figure 4.6** A transistor amplifier with both input and output matching, illustrating the direction of measurement of the reflection coefficients.

Note that impedance tuners are needed in place of matching circuits to optimize the transistor performance before and during measurement. In the case of a bilateral transistor,  $\rho_{in}$  depends on the output load impedance and  $\rho_{out}$  depends on the input load impedance. Therefore, some iteration is needed to find the reflection coefficients providing the maximum gain. After these measurements, in both cases, we use the Smith chart in a clockwise manner when designing the matching circuits.

Usually the load is matched to the line with a matching circuit in front of the load. The matching circuit contains reactive elements such as inductors (coils), capacitors, transformers, tuning stubs, or special elements such as a tuning screw or an iris in a metal waveguide. The reactive elements represent discontinuities that cause reflections, which cancel the reflection from the load, so that ideally all power is absorbed into the load although there are multiple reflections between the load and the matching circuit (see Section 4.3.3). In case of a quarter-wave transformer these discontinuities are the abrupt changes in the characteristic impedance of the line. In some cases the load is matched resistively, but then the reflected wave is absorbed into the matching circuit and therefore lost.

Furthermore, in some cases the load impedance can be tuned actively. For example, the impedance of a diode detector depends on the diode bias current. By introducing a proper bias current, the matching of the detector can be optimized.

In Section 4.3 we assume that the load impedance will be matched to the real impedance of the line feeding the load. Generally, matching is realized between circuits having complex impedances—for example, between a source with an output impedance  $Z_S$  and a load with an input impedance  $Z_{in}$ . Then conjugate matching

$$Z_{in} = Z_S^* \quad (4.26)$$

results in maximum power transfer to the load for a fixed source impedance. In fact, in the following we realize the same because the matching circuit transforms the real line impedance to the complex conjugate of the load impedance.

### 4.3.1 Matching with Lumped Reactive Elements

In the megahertz range, a coil may perform as an ideal inductance and a capacitor as an ideal capacitance. In the microwave region, coils and capacitors may still be useful elements for realizing reactive matching circuits, but care

must be taken with the size of these elements. The size of the lumped element must be much smaller than a wavelength. In hybrid integrated circuits, chip capacitors or interdigital gap capacitors and wire coils are successfully used at least to several gigahertz, and in monolithic integrated circuits *metal-insulator-metal* (MIM) capacitors as well as loop and spiral inductors are used successfully at millimeter wavelengths. However, parasitic elements of such capacitors and inductors must also be taken into account in the circuit design, meaning that a careful modeling of these elements is necessary. Figure 4.7 illustrates some lumped elements used in integrated circuits.

Matching with a lumped reactive element is realized by placing a single element at a proper distance from the load in series or in parallel as shown in Figure 4.8. It is possible to move from any load impedance  $z_L$  toward the generator such a distance  $l_1 < \lambda_g/2$ , so that the load is seen as an impedance  $1 + jx_0$ . If we add at this point a series reactance of  $-x_0$ , the

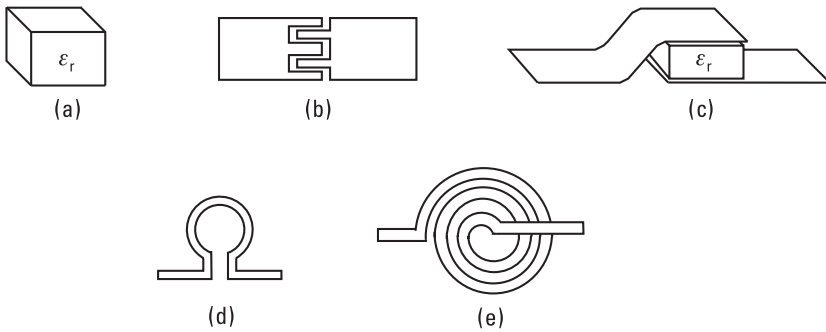


**Figure 4.7** Reactive lumped elements for integrated circuits: (a) chip capacitor; (b) interdigital gap capacitor; (c) metal-insulator-metal capacitor; (d) loop inductor; and (e) spiral inductor (with an airbridge).

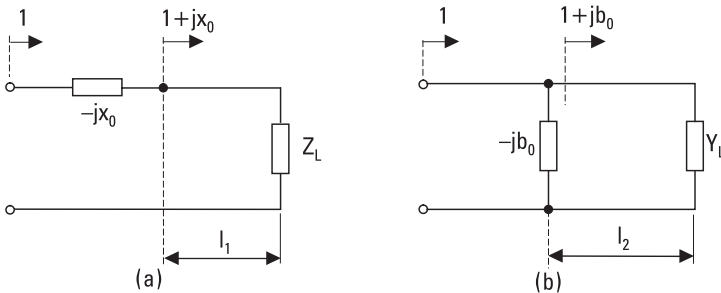


**Figure 4.8** Matching with a single reactive element placed at a proper distance from the load: (a) with a series element; and (b) with a shunt element.

input impedance is  $1 + jx_0 - jx_0 = 1$ , and the load is matched to the line; see Figure 4.8(a). On the other hand, from any load admittance it is possible to move toward the generator a distance  $l_2 < \lambda_g/2$ , so that the load admittance is seen as  $1 + jb_0$ . By adding in this point a shunt susceptance  $-b_0$ , we get a match, as in Figure 4.8(b).

#### Example 4.1

Match a load impedance of  $Z_L = R_L + jX_L = (150 + j100)\Omega$  to  $Z_0 = 50\Omega$  at 100 MHz according to Figure 4.8.

#### Solution

Let us first place the normalized load impedance  $z_L = Z_L/Z_0 = 3 + j2$  on the Smith chart in Figure 4.9; we are at point A. If we then move along a circle (radius OA) clockwise on the Smith chart (corresponding to moving along a lossless 50- $\Omega$  line away from the load), we first come to the unity circle after  $0.096\lambda_g$  at point B, where the impedance is  $1 - j1.62$ . By adding a series inductance with a normalized reactance of  $x = +1.62$  ( $L = xZ_0/\omega = 128$  nH) in this point, we match the load. Another possibility is to move further away (a distance of  $0.206\lambda_g$  from load) to point B', which is on the mirror image circle of circle  $r = 1$ . The corresponding admittance at point C' is  $1 + j1.62$ . By adding a shunt inductance with susceptance of  $b = -1.62$  ( $L = -Z_0/(\omega b) = 49$  nH) at this point we also match the load. A further possibility is to move to point B'' (distance from load  $0.346\lambda_g$ ) and add a shunt capacitance with susceptance of  $b = +1.62$  ( $C = b/(\omega Z_0)$ )

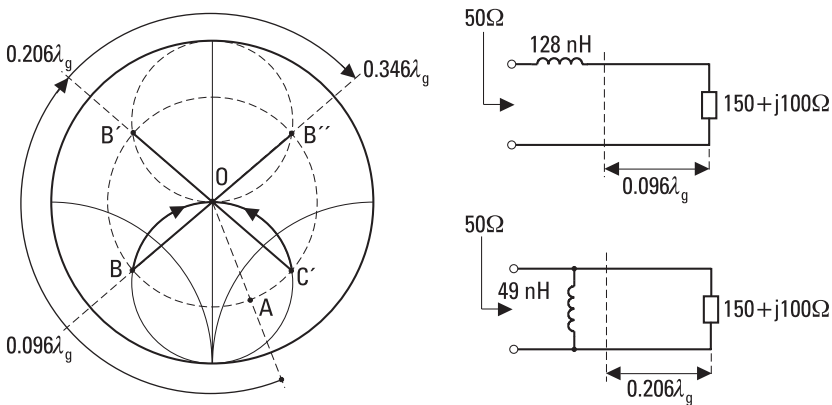


**Figure 4.9** Matching the load impedance of  $Z_L = R_L + jX_L = (150 + j100)\Omega$  to  $Z_0 = 50\Omega$  using a single lumped reactive element.

= 52 pF). However, the widest matching bandwidth is obtained when the reactive (susceptive) element is placed as close to the load as possible.

Another possibility in realizing a reactive match is to use an  $LC$  (or  $LL$  or  $CC$ ) circuit in front of the load, as shown in Figure 4.10. The series or shunt element next to the load now replaces the line section needed above, and the matching circuit is more compact.

If  $z_L = r_L + jx_L$  is inside the  $1 + jx$  circle, there are two distinct possibilities to match the load with two reactive elements: first either a capacitor or an inductor in parallel to the load and then in series an inductor or a capacitor, respectively, toward the line. If  $z_L = r_L + jx_L$  is inside the mirror image circle of the  $1 + jx$  circle, there are again two distinct possibilities: first either an inductor or a capacitor in series with the load and then a

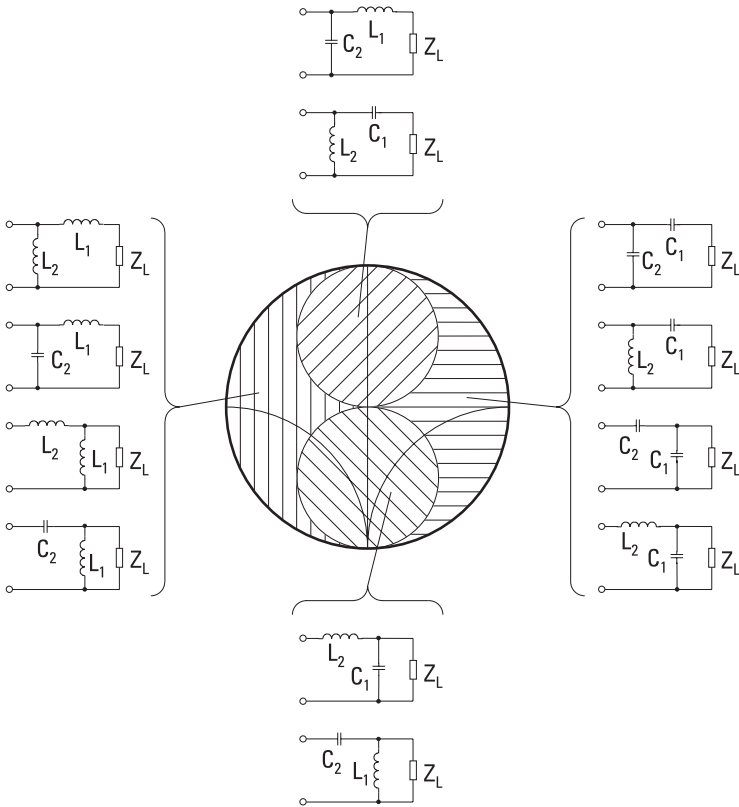


**Figure 4.10** Matching with two reactive elements: Depending on the value of the load impedance  $z_L = r_L + jx_L$ , the Smith chart is divided into four regions, each of which leads to different possibilities in matching with two reactive elements.

shunting capacitor or inductor, respectively, toward the line. If the load impedance is outside of both of the regions, in the vertically or horizontally shaded area of the Smith chart in Figure 4.10, there are more matching possibilities. If the load impedance  $z_L = r_L + jx_L$  is in the vertically shaded area, that is, if  $z_L$  is capacitive, there are four distinct possibilities to construct the matching circuit with two reactive elements, but we must start with an inductor next to the load. This inductor may be either in series or in parallel; the other component (respectively in parallel or in series) may be an inductor or a capacitor. Similarly, when  $z_L$  is in the horizontally shaded region—when the load impedance is inductive—there are again four different possibilities, but now we must start with a capacitor next to the load. Again, this capacitor may be either in series or in parallel; the other component (respectively in parallel or in series) may be an inductor or a capacitor. Let us study these in more detail through some examples, which also serve the reader for getting more confidence in using the Smith chart.

**Example 4.2**

Match a load impedance of  $Z_L = R_L + jX_L = (20 - j30)\Omega$  to  $Z_0 = 50\Omega$  at 100 MHz starting with a series inductor next to the load.

**Solution**

Let us first mark the normalized impedance  $z_L = Z_L/Z_0 = 0.4 - j0.6$  on the Smith chart as shown in Figure 4.11; we are at point A. If we add at this point a series reactance of  $x = 1.09$ , we get to the mirror image circle of the circle  $r = 1$  to point B, where the impedance is  $0.4 + j0.49$ . The

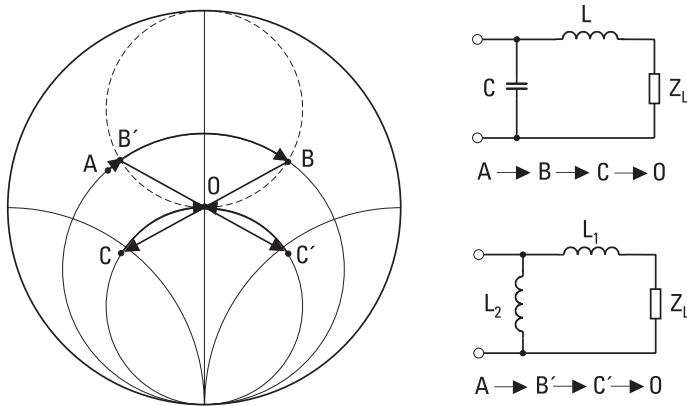


**Figure 4.11** Matching of a load  $Z_L = R_L + jX_L = (20 - j30)\Omega$  to  $Z_0 = 50\Omega$  using lumped reactive elements.

corresponding admittance is  $1.0 - j1.22$  (point C), so that by adding a parallel susceptance of  $b = 1.22$ , we match the load. The inductance corresponding to the normalized series reactance  $x$  is  $L = xZ_0/\omega$ , and the capacitance corresponding to the normalized parallel susceptance is  $C = b/(\omega Z_0)$ . The component values at 100 MHz are  $L = 87$  nH and  $C = 39$  pF. Another possibility is first to add a small series reactance of  $x = 0.11$  to get to point B' where the impedance is  $0.4 - j0.49$ . Then the corresponding admittance is  $1.0 + j1.22$  (point C'). After adding a parallel susceptance of  $b = -1.22$ , we also have obtained a match. Now both of the reactive components are inductances; the series component is  $L_1 = Z_0x/\omega = 8.8$  nH and the parallel component is  $L_2 = -Z_0/(b\omega) = 65$  nH. (Note: This load impedance can also be matched starting with a shunt inductance next to the load; in order to realize this, start from the load admittance.)

**Example 4.3**

Match a load impedance of  $Z_L = R_L + jX_L = (150 + j100)\Omega$  to  $Z_0 = 50\Omega$  at 100 MHz with two reactive elements.

**Solution**

Let us first mark the normalized impedance  $z_L = Z_L/Z_0 = 3 + j2$  on the Smith chart as shown in Figure 4.12; we are at point A. We first transform to the corresponding admittance,  $y_L = 0.23 - j0.15$ . From there we move along circle  $g = 0.23$  to the mirror image circle of  $g = 1$  either to point B' or point B''. Moving to B' corresponds to adding a shunt susceptance of  $b = -0.26$  (i.e.,  $L_1 = -Z_0/(b\omega) = 306$  nH), and moving to B'' corresponds

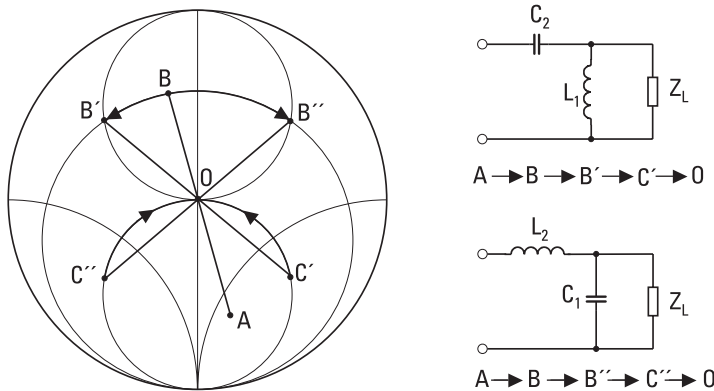


**Figure 4.12** Matching of a load  $Z_L = R_L + jX_L = (150 + j100)\Omega$  to  $Z_0 = 50\Omega$  using lumped reactive elements.

to adding a shunt susceptance of  $b = 0.56$  (i.e.,  $C_1 = b/(\omega Z_0) = 18$  pF). Then we transform back to the impedance and get to either point  $C'$  or  $C''$ , respectively. In order to get to the center of the Smith chart, we now have to add a series component. In the case of point  $C'$  we add a series capacitor with a reactance of  $x = -1.8$  ( $C_2 = -1/(Z_0 x \omega) = 18$  pF), and in the case of point  $C''$  we add a series inductor with a reactance of  $1.8$  ( $L_2 = x Z_0 / \omega = 143$  nH).

#### Example 4.4

Match a load impedance of  $Z_L = R_L + jX_L = (15 - j15)\Omega$  to  $Z_0 = 50\Omega$  at 100 MHz with two lumped reactive elements.

#### Solution

Let us first mark the normalized impedance  $z_L = Z_L/Z_0 = 0.3 - j0.3$  on the Smith chart as shown in Figure 4.13; we are at point A. If we now add a series reactance of  $x = 0.758$ , we move along the circle  $r = 0.3$  and get to the mirror image circle of the circle  $r = 1$  to point B, where the impedance is  $0.3 + j0.458$ . The corresponding admittance is  $1.0 - j1.528$  (point C), so that by adding a parallel susceptance of  $b = 1.528$  we match the load. The inductance corresponding to the normalized series reactance  $x$  is  $L_1 = x Z_0 / \omega = 60$  nH, and the capacitance corresponding to the normalized parallel susceptance is  $C_1 = b/(\omega Z_0) = 49$  pF at 100 MHz. Another possibility is to add first a series reactance of  $x = -0.158$  to get to point  $B'$  where the impedance is  $0.3 - j0.458$ . Then the corresponding admittance

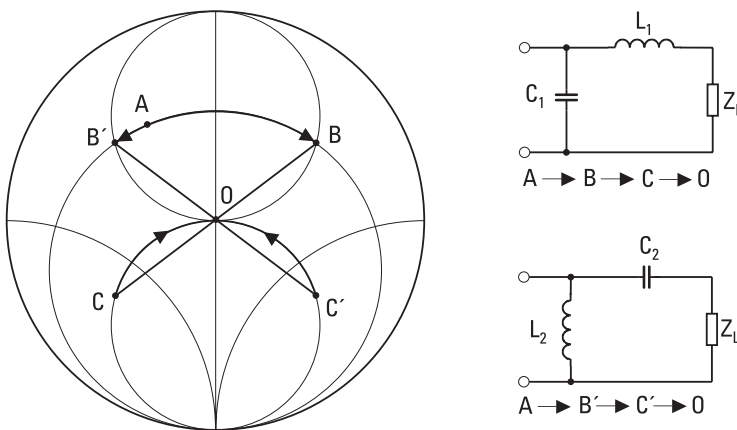


**Figure 4.13** Matching of a load  $Z_L = R_L + jX_L = (15 - j15)\Omega$  to  $Z_0 = 50\Omega$  using lumped reactive elements.



is  $1.0 + j1.528$  (point  $C'$ ). After adding a parallel susceptance of  $-1.528$ , we have obtained a match. Now the component values are for the series capacitance  $C_2 = -1/(Z_0x\omega) = 201$  pF and for the parallel inductance  $L_2 = -Z_0/(b\omega) = 52$  nH.

### 4.3.2 Matching with Tuning Stubs (with Short Sections of Line)

In the microwave region, the inductors and capacitors do not represent ideal inductances and capacitances but often behave as resonant circuits. At such high frequencies the desired reactance may often be more easily realizable by using a tuning stub, which is a short section of a line terminated with either a short circuit or an open circuit. As we can easily calculate using (4.12), a short-circuited tuning stub is inductive when its length is from 0 to  $\lambda_g/4$  and capacitive when its length is from  $\lambda_g/4$  to  $\lambda_g/2$ . An open-circuited tuning stub is capacitive when its length is from 0 to  $\lambda_g/4$  and inductive when its length is from  $\lambda_g/4$  to  $\lambda_g/2$ . Depending on the line type used, there may be only one choice: In a metal waveguide only a short-circuited stub is possible because an open end acts as an antenna. On the other hand, in microstrip circuits a short circuit is difficult to realize and therefore open-circuited stubs are used.

Matching with one tuning stub is realized according to Figure 4.8. In theory, we can use either a series stub or a parallel stub. In practice the choice is more limited. For example, in a microstrip circuit only a parallel stub is possible.

If the characteristic impedance of the tuning stub is the same as that of the line to which the load is to be matched, the length of a short-circuited stub is obtained from the following [see also (4.12)]

$$j \tan \beta l = -jx_0 = \frac{1}{-jb_0} \quad (4.27)$$

Accordingly, the length of an open-circuited stub is obtained from

$$\frac{1}{j \tan \beta l} = -jx_0 = \frac{1}{-jb_0} \quad (4.28)$$

The characteristic impedance of the stub may also differ from that of the line; then the proper length is calculated using (4.12). Since the impedance

of a stub is periodic with a period of  $\lambda_g/2$ , the stub length can also be  $l + n\lambda_g/2$ , but a short stub is preferred because it provides a wider matching bandwidth.

#### Example 4.5

Match the normalized admittance of  $y_L = 0.3 + j0.3$  to a  $50\text{-}\Omega$  line using a short-circuited tuning stub.

#### Solution

Figures 4.14 and 4.15 show how this problem is solved on the Smith chart. First we place the normalized admittance on the Smith chart, point A. Then we move along a circle (along a  $50\text{-}\Omega$  line) a distance of  $0.123\lambda_g$  and come to the unity circle  $g = 1$  to point B, where the admittance is  $1 + j1.4$ . If we now add at this point a parallel susceptance of  $-1.4$ , we obtain a match. Another possibility is to move along the  $50\text{-}\Omega$  line to point B', where the admittance is  $1 - j1.4$ , and add at this point a parallel susceptance of  $+j1.4$  in order to get a match. The required length of the parallel stub is either obtained from (4.27) or by using the Smith chart. Figure 4.15 shows how the length of a short-circuited stub with a normalized admittance of  $-j1.4$  is obtained. We start from  $y = \infty$  and move along the outer circle of the

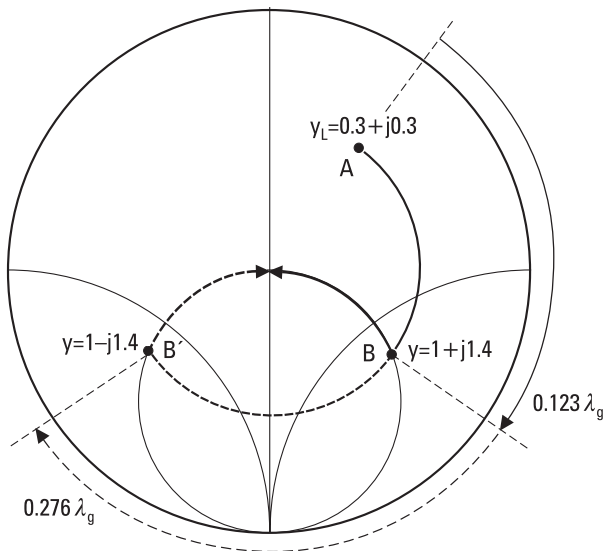


**Figure 4.14** Matching of a load with a shunt susceptance according to Figure 4.8(b) presented on the Smith chart.

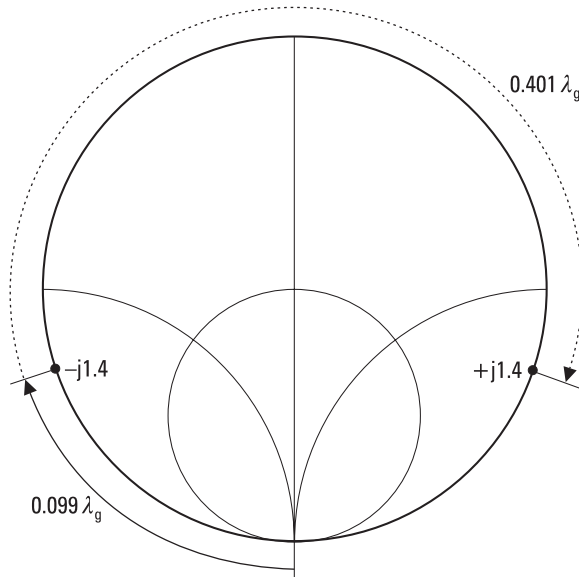


**Figure 4.15** Using the Smith chart to obtain the lengths of short-circuited tuning stubs corresponding to normalized admittances of  $-j1.4$  and  $+j1.4$ .

Smith chart to the point where the normalized admittance is  $-j1.4$ : The length  $l = 0.099\lambda_g$  can be read from the Smith chart. Accordingly, the admittance  $+j1.4$  can be realized with a short-circuited stub of length  $l = 0.401\lambda_g$ , as also shown in Figure 4.15. The obtained matching circuits are presented in Figure 4.16.

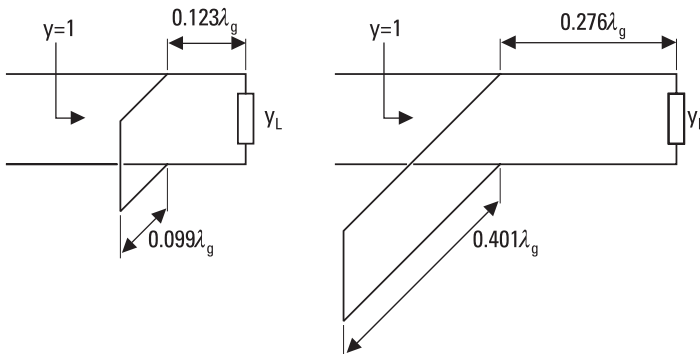


**Figure 4.16** Tuning-stub matching of a load with a normalized admittance of  $y_L = 0.3 + j0.3$ .

The above matching with a single tuning stub is simple but requires placing the stub in a new position when the frequency is changed, even if the stub length is adjustable. The tuning stubs can be placed in a fixed position when two or three stubs are used [3]. The remaining task is to find correct lengths of the stubs. Two tuning stubs allow matching of almost all possible load impedances. In practice, a limiting factor is the attenuation in the line; it limits the range of the obtainable stub susceptances. A wide matching bandwidth also requires that the distance between the stubs be close to either 0 or  $\lambda_g/2$ . In practice the tuning stubs are placed at a distance of  $\lambda_g/8$  or  $3\lambda_g/8$  from each other. For measurement setups, tuners are available with three adjustable stubs. Such a tuner can match any load impedance to the line.

### 4.3.3 Quarter-Wave Transformer

Let us consider the situation presented in Figure 4.17. A real load impedance  $R_L$  must be matched into a line with a characteristic impedance of  $Z_0$ . Matching is realized by using a line section of length  $\lambda_g/4$  and characteristic impedance  $Z_t$ . Because  $\tan(\beta\lambda_g/4) = \infty$ , we obtain from (4.12) that the impedance loading the original line is

$$R'_L = \frac{Z_t^2}{R_L} \tag{4.29}$$

If we choose  $Z_t = \sqrt{Z_0 R_L}$ , the load is matched to the line. The quarter-wavelength-long line section acts as a transformer, with a number-of-turns ratio equal to  $\sqrt{Z_0/R_L}$ . If the load impedance is not real, we use a line section with a proper length and characteristic impedance between the load and the transformer so that the load impedance seen through this section is real.

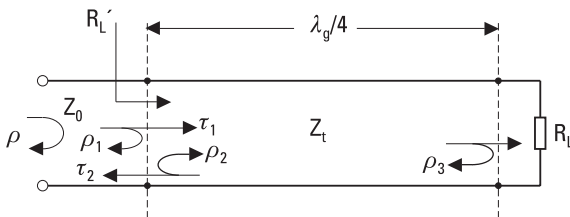


Figure 4.17 Quarter-wave transformer.

**Example 4.6**

Match a load impedance of  $Z_L = (20 + j40)\Omega$  to a line with  $Z_0 = 50\Omega$  using a quarter-wave transformer.

**Solution**

Figure 4.18 shows, on the Smith chart, how the problem is solved. First we need to make the load impedance real: We place a line section having a characteristic impedance of  $Z_0$  between the load and the transformer. The load impedance normalized to  $Z_0$  is  $z_L = 0.4 + j0.8$ . We need a line section of  $0.135\lambda_g$  to make the load impedance real. When we move from  $z_L = 0.4 + j0.8$  toward the generator a distance of  $0.135\lambda_g$ , we come to a real impedance (normalized) of  $r = 4.27$ , that is,  $R = rZ_0 = 214\Omega$ . According to (4.29) the required transformer impedance is  $\sqrt{Z_0 R} = \sqrt{r}Z_0 = 103\Omega$ . Then we normalize the impedance  $R$  to  $Z_t$  and obtain  $R/Z_t = \sqrt{r}$ . We move on the Smith chart to  $\sqrt{r} = 2.07$ , and then move a distance of  $\lambda_g/4$  toward the generator and get impedance  $1/\sqrt{r}$ . When we normalize this back to  $Z_0$ , we get an impedance of  $Z_t/(\sqrt{r}Z_0) = 1$ ; in other words, the load is matched.

Let us now consider what actually happens in the quarter-wave transformer of Figure 4.17 to the wave approaching the load. The wave is reflected

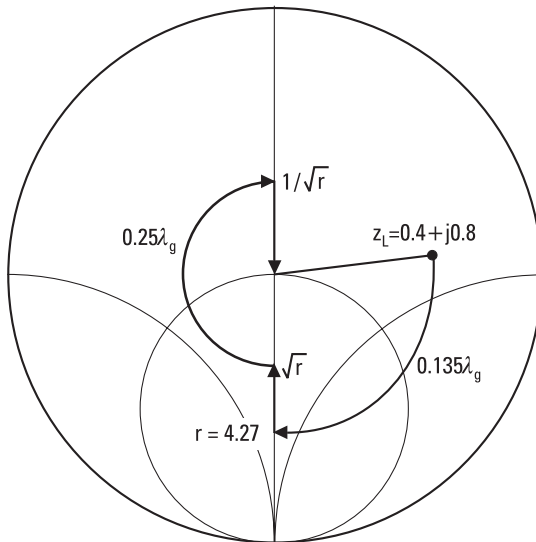


**Figure 4.18** Matching of a load  $Z_L = (20 + j40)\Omega$  to a  $50\text{-}\Omega$  line using a quarter-wave transformer, presented on the Smith chart.

and transmitted multiple times at the two boundaries, as shown in Figure 4.19. Let us first define the reflection and transmission coefficients as follows:

- $\rho$  = total reflection coefficient of the incident wave on the  $\lambda/4$  transformer
- $\rho_1$  = reflection coefficient of a wave incident on a load  $Z_t$  from a  $Z_0$  line
- $\rho_2$  = reflection coefficient of a wave incident on a load  $Z_0$  from a  $Z_t$  line
- $\rho_3$  = reflection coefficient of a wave incident on a load  $R_L$  from a  $Z_t$  line
- $\tau_1$  = transmission coefficient of a wave from a  $Z_0$  line into a  $Z_t$  line
- $\tau_2$  = transmission coefficient of a wave from a  $Z_t$  line into a  $Z_0$  line.

According to (4.5) and (4.6), these coefficients can be expressed as

$$\begin{aligned} \rho_1 &= (Z_t - Z_0)/(Z_t + Z_0) \\ \rho_2 &= (Z_0 - Z_t)/(Z_0 + Z_t) = -\rho_1 \\ \rho_3 &= (R_L - Z_t)/(R_L + Z_t) \\ \tau_1 &= 2Z_t/(Z_t + Z_0) \\ \tau_2 &= 2Z_0/(Z_t + Z_0) \end{aligned}$$

The total reflection coefficient is obtained as an infinite series of individual reflections and, taking into account that there is a phase shift of  $e^{-2j\theta}$  for each round-trip in the transformer, can be expressed as

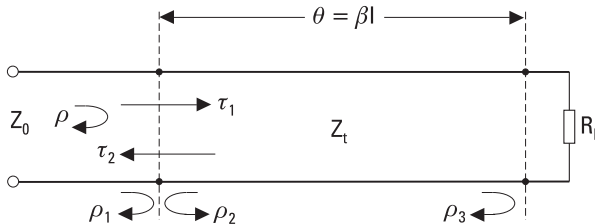


**Figure 4.19** Multiple-reflection analysis of the  $\lambda/4$  transformer.

$$\begin{aligned}
 \rho &= \rho_1 + \tau_1 \tau_2 \rho_3 e^{-2j\theta} + \tau_1 \tau_2 \rho_2 \rho_3^2 e^{-4j\theta} + \tau_1 \tau_2 \rho_2^2 \rho_3^3 e^{-6j\theta} + \dots \\
 &= \rho_1 + \tau_1 \tau_2 \rho_3 e^{-2j\theta} \sum_{n=0}^{\infty} (\rho_2 \rho_3 e^{-2j\theta})^n \\
 &= \rho_1 + \frac{\tau_1 \tau_2 \rho_3 e^{-2j\theta}}{1 - \rho_2 \rho_3 e^{-2j\theta}} \tag{4.30}
 \end{aligned}$$

The last result is obtained using the sum rule of an infinite geometric series, since  $|\rho_2| < 1$  and  $|\rho_3| < 1$ . If we furthermore take into account that  $\rho_2 = -\rho_1$ , and  $\tau_1 = 1 + \rho_1$  and  $\tau_2 = 1 - \rho_1$ , we get

$$\rho = \frac{\rho_1 + \rho_3 e^{-2j\theta}}{1 + \rho_1 \rho_3 e^{-2j\theta}} \tag{4.31}$$

From this we see, because the transformer characteristic impedance is  $Z_t = \sqrt{Z_0 R_L}$  and therefore  $\rho_1 = \rho_3$ , and at the center frequency  $e^{-2j\theta} = -1$ , that the total reflected wave fully disappears at the center frequency. If the discontinuities between the impedances  $Z_0$  and  $Z_t$  as well as between  $Z_t$  and  $R_L$  are small, then  $|\rho_1 \rho_3| \ll 1$ , and we can approximate  $\rho \approx \rho_1 + \rho_3 e^{-2j\theta}$ .

The problem with the quarter-wave transformer is its narrow matching bandwidth. The transformer offers a match only at the frequency where the transformer length is exactly  $\lambda_g/4$  (or  $\lambda_g/4 + n\lambda_g/2$ ). The bandwidth, over which the reflection coefficient is small, is narrow. Sometimes this is sufficient, but in many applications we need a wider bandwidth.

A wider bandwidth can be obtained by using several consecutive transformer sections, the characteristic impedances of which change with small steps between  $R_L$  and  $Z_0$ . Depending on how the impedance steps are chosen, different frequency responses of the reflection coefficient are obtained. A binomial transformer provides a maximally flat response. A Chebyshev transformer provides a frequency response where the reflection coefficient fluctuates between certain limits over the matching bandwidth. Figure 4.20 shows the frequency response of a single  $\lambda/4$  transformer, a two-section binomial transformer, and a three-section Chebyshev transformer. The design procedures of the binomial and Chebyshev transformers can be found in many books [3, 4].

Often a  $\lambda/4$  transformer is used to match two lines with different characteristic impedances. Figure 4.21(a) shows how a low- and high-imped-

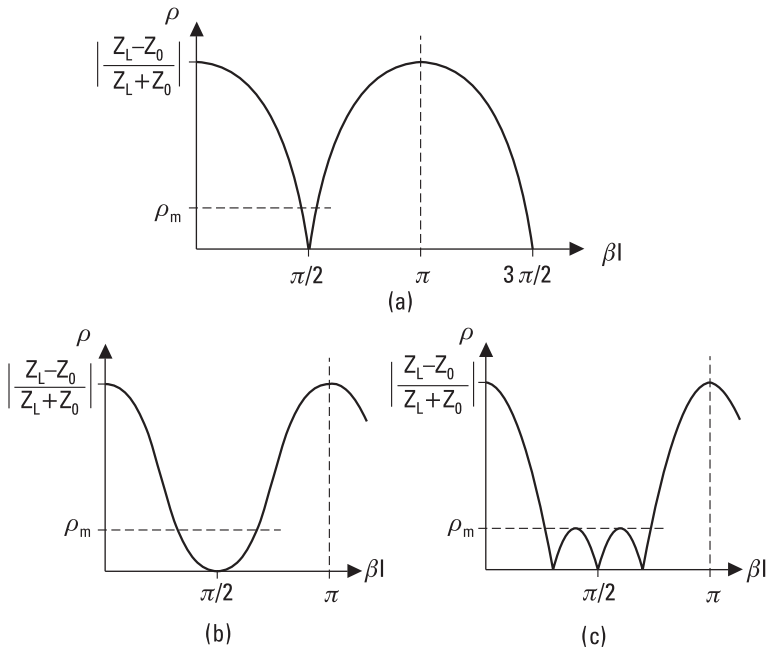


**Figure 4.20** Reflection coefficient of matching transformers as a function of the transformer section electrical length  $\beta l = 2\pi/\lambda_g$ : (a) a single  $\lambda/4$  transformer; (b) a two-section binomial transformer; and (c) a three-section Chebyshev transformer.

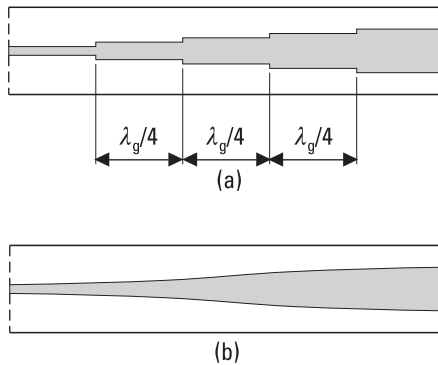


**Figure 4.21** Matching of a low- and high-impedance coaxial line using (a) a multisection  $\lambda/4$  transformer and (b) a tapered section.



ance coaxial line are matched to each other using a three-section  $\lambda/4$  transformer. Different impedances are realized by changing the inner conductor diameter. Abrupt changes in line dimensions cause not only reflections but also reactive fields and reactive energy storages. In an equivalent circuit these can be modeled using shunt susceptances. In an accurate analysis and design these reactive components must be taken into account.

Instead of using a multisection transformer, we can use a tapered section at least  $\lambda_g/2$  long, as shown in Figure 4.21(b). The tapering may be linear or follow other mathematical functions leading to different frequency responses.

### 4.3.4 Resistive Matching

Matching of a load can be improved simply by introducing an attenuator in front of the load, as shown in Figure 4.22. This may be a useful solution, for example, in a measurement application when a wide measurement bandwidth is required but the power loss is not a problem.

Let us assume that the load reflection coefficient is  $\rho_L$  and the insertion loss of an attenuator matched to the line is  $L$  [see (5.32)]. If the incident power to the attenuator is  $P$ , power after the attenuator is  $P/L$ . From this power, a part  $(1 - |\rho_L|^2) \times P/L$  is absorbed to the load and a part  $|\rho_L|^2 \times P/L$  is reflected. The reflected power is further attenuated in the attenuator to a value of  $|\rho_L|^2 \times P/L^2$ . When compared to a situation without an attenuator, the power reflection coefficient decreases from a value of  $|\rho_L|^2$  to a value of  $|\rho_L|^2/L^2$ . The drawback of this method is that the power absorbed to the load is at maximum  $P/L$ . The attenuator is realized in integrated circuits using resistors shown in Figure 4.23. Two applications of resistive matching are illustrated in Figure 4.24.

A better solution than the attenuator is an isolator (see Section 6.2.3) placed in front of the load. An ideal isolator is lossless in the forward direction but absorbs the backward reflected wave fully. The reflected power is also lost in this case but more power is available to the load, although in practice

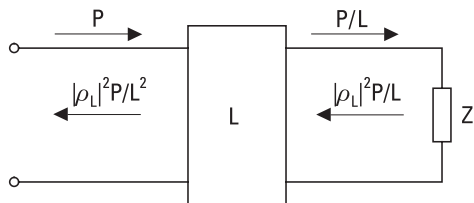


**Figure 4.22** Resistive matching with an attenuator.

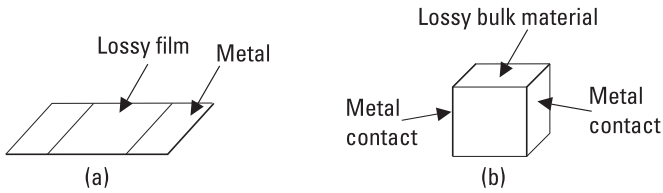


**Figure 4.23** Resistive lumped elements for integrated circuits: (a) planar resistor; and (b) chip resistor.

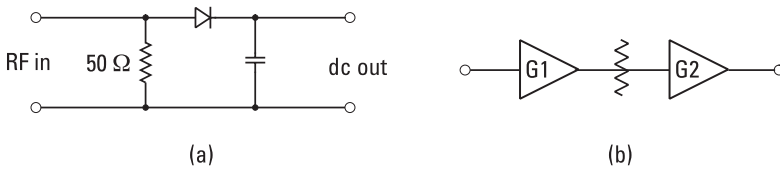


**Figure 4.24** Applications of resistive matching: (a) a diode detector; and (b) an amplifier chain.

an isolator also has some attenuation in the forward direction. Furthermore, it does not fully block the backward reflected wave and its ports are not fully matched to the line.

## References

- [1] Bryant, G. H., *Principles of Microwave Measurements*, London, England: Peter Peregrinus, 1988.
- [2] Smith, P. H., “Transmission Line Calculator,” *Electronics*, Vol. 12, No. 1, 1939, pp. 29–31.
- [3] Collin, R. E., *Foundations for Microwave Engineering*, 2nd ed., New York: IEEE Press, 2001.
- [4] Matthaei, G. L., L. Young, and E. M. T. Jones, *Microwave Filters, Impedance-Matching Networks, and Coupling Structures*, Dedham, MA: Artech House, 1980.



# 5

## Microwave Circuit Theory

Microwave circuits are composed of many parts and blocks, such as transmission lines, filters, and amplifiers. It was shown in Chapter 3 how the field distributions within the waveguides could be solved using Maxwell's equations and boundary conditions. In principle, whole circuits could be analyzed this way. However, this is very cumbersome, and often the knowledge of the field distributions is of no use.

Usually one wants to know how the wave is transmitted through the circuit or reflected from it. Therefore, the circuit can be considered to be a "black box" that has one or more ports. It is sufficient to know the transfer functions between the ports; it is not necessary to know what happens inside the circuit. Thus, the operation of the circuit can be described with only a few parameters. The transfer function of a system comprising of cascaded circuits can be obtained using these parameters. In the circuit theory,  $Z$ - and  $Y$ -parameters are commonly used. However, the scattering or  $S$ -parameters are best suited for describing the operation of a microwave circuit.

### 5.1 Impedance and Admittance Matrices

The voltages and currents of a low-frequency circuit can be defined uniquely. In case of a high-frequency circuit this is not necessarily true. Voltages and currents can be defined uniquely only for a transmission line that carries a pure TEM mode. For example, the voltage and current of a rectangular

waveguide can be defined in several ways. In such a line, the electric and magnetic fields and the power propagating in the waveguide are more fundamental quantities than the voltage and current. However, it would be useful if the operation of a high-frequency circuit could be described in terms of voltages, currents, and impedances because then the methods of the circuit theory could be used.

Figure 5.1 shows a circuit having  $n$  ports. There is a short homogeneous transmission line at each port. The reference plane (within this line) of each port has to be defined clearly because the parameters of the circuit depend on the positions of the reference planes. Let us assume that only the fundamental TEM mode is propagating into and out of the ports. The discontinuities of the circuit generate higher-order TE and TM modes, which usually are not able to propagate. The reference planes have to be far enough from these discontinuities so that the fields of the nonpropagating modes are well attenuated. For each port  $i$ , an entering voltage wave  $V_i^+$  and current wave  $I_i^+$  as well as a leaving voltage wave  $V_i^-$  and current wave  $I_i^-$  can be defined.

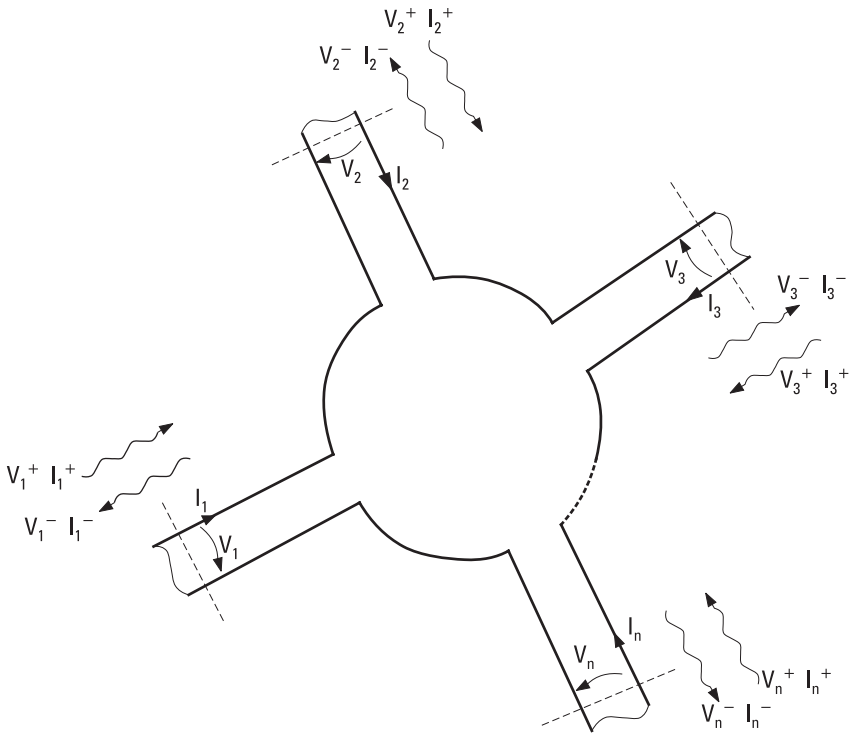


**Figure 5.1** Circuit having  $n$  ports.

$V_i^+$ ,  $I_i^+$ ,  $V_i^-$ , and  $I_i^-$  are the complex amplitudes of these sinusoidal waves. These equivalent voltage and current waves are defined so that (1) the voltage and current are proportional to the transverse electric and magnetic fields of the wave, respectively, (2) the product of the voltage and current gives the power of the entering or leaving wave, and (3) the ratio of the voltage and current is the characteristic impedance of the port.

The total voltage and the total current at port  $i$  are:

$$V_i = V_i^+ + V_i^- \quad (5.1)$$

$$I_i = I_i^+ - I_i^- \quad (5.2)$$

For a linear circuit, the voltage at port  $i$  is a linear function of the currents at all ports:

$$V_i = Z_{i1}I_1 + Z_{i2}I_2 + \dots + Z_{in}I_n \quad (5.3)$$

The whole circuit can be described with the impedance matrix  $[Z]$  as

$$\begin{bmatrix} V_1 \\ V_2 \\ \vdots \\ V_n \end{bmatrix} = \begin{bmatrix} Z_{11} & Z_{12} & \dots & Z_{1n} \\ Z_{21} & Z_{22} & \dots & Z_{2n} \\ \vdots & \vdots & \vdots & \vdots \\ Z_{n1} & Z_{n2} & \dots & Z_{nn} \end{bmatrix} \begin{bmatrix} I_1 \\ I_2 \\ \vdots \\ I_n \end{bmatrix} \quad (5.4)$$

Correspondingly, currents are obtained from voltages using the admittance matrix  $[Y]$ :

$$\begin{bmatrix} I_1 \\ I_2 \\ \vdots \\ I_n \end{bmatrix} = \begin{bmatrix} Y_{11} & Y_{12} & \dots & Y_{1n} \\ Y_{21} & Y_{22} & \dots & Y_{2n} \\ \vdots & \vdots & \vdots & \vdots \\ Y_{n1} & Y_{n2} & \dots & Y_{nn} \end{bmatrix} \begin{bmatrix} V_1 \\ V_2 \\ \vdots \\ V_n \end{bmatrix} \quad (5.5)$$

The impedance matrix [1] is an inverse matrix [2] of the admittance matrix,  $[Z] = [Y]^{-1}$ . The elements of the matrices,  $Z_{ij}$  and  $Y_{ij}$ , are called  $Z$ - and  $Y$ -parameters. For a reciprocal circuit, the matrices are symmetric:  $Z_{ij} = Z_{ji}$  and  $Y_{ij} = Y_{ji}$ .

A two-port is the most common of the  $n$ -port circuits. Many different equivalent circuits can be used to realize the equations of a two-port [3, 4].

Figure 5.2 shows an equivalent circuit for a reciprocal two-port. The three  $Z$ -parameters for this T-circuit,  $Z_{11}$ ,  $Z_{22}$ , and  $Z_{12}$ , are calculated or measured. If the load impedance  $Z_L = -V_2/I_2$  is connected at port 2, the input impedance measured at port 1 is

$$Z_{1in} = Z_{11} - \frac{Z_{12}^2}{Z_{22} + Z_L} \tag{5.6}$$

By measuring the input impedances corresponding to three different load impedances, a set of three equations is obtained. The  $Z$ -parameters may then be solved from these equations.

The properties of a circuit composed of two-ports connected in series can be calculated from the transmission matrices  $[T]$  of the two-ports. A transmission matrix is called also a chain or  $ABCD$  matrix. A transmission matrix ties the input and output quantities as

$$\begin{bmatrix} V_1 \\ I_1 \end{bmatrix} = \begin{bmatrix} A & B \\ C & D \end{bmatrix} \begin{bmatrix} V_2 \\ I_2 \end{bmatrix} = [T] \begin{bmatrix} V_2 \\ I_2 \end{bmatrix} \tag{5.7}$$

The transmission matrix of a two-port can be calculated from its  $Z$ -parameters:

$$[T] = \begin{bmatrix} Z_{11}/Z_{21} & Z_{11}Z_{22}/Z_{21} - Z_{12} \\ 1/Z_{21} & Z_{22}/Z_{21} \end{bmatrix} \tag{5.8}$$

It should be noted that the positive output current  $I_2$  is now defined to flow out of the two-port so that  $I_2$  will be the input current to the following two-port. The transmission matrix of a circuit consisting of several two-ports in a series is obtained by multiplying the transmission matrices of the two-ports in the same order.

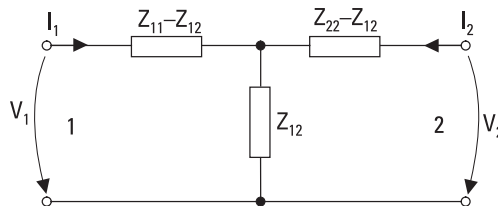


**Figure 5.2** Equivalent T-circuit for a two-port.

Generally, the measurement of  $Z$ - and  $Y$ -parameters is difficult at microwave frequencies because the measurement of the total voltages and currents at the ports is difficult, and in the case of waveguides carrying TE or TM modes it is impossible. Furthermore, in the case of some active circuits, the load impedances needed in the measurement may cause instability in the circuit.

## 5.2 Scattering Matrices

The scattering or  $S$ -parameters [1, 5, 6] are defined using the voltage waves entering the ports,  $V_i^+$ , and leaving the ports,  $V_i^-$ . If the circuit in Figure 5.1 is linear and all its ports have the same characteristic impedance of  $Z_0$ , the voltage wave leaving port  $i$  may be written as

$$V_i^- = S_{i1} V_1^+ + S_{i2} V_2^+ + \dots + S_{in} V_n^+ \quad (5.9)$$

The whole circuit is described by the scattering matrix  $[S]$  as

$$\begin{bmatrix} V_1^- \\ V_2^- \\ \vdots \\ V_n^- \end{bmatrix} = \begin{bmatrix} S_{11} & S_{12} & \dots & S_{1n} \\ S_{21} & S_{22} & \dots & S_{2n} \\ \vdots & \vdots & \vdots & \vdots \\ S_{n1} & S_{n2} & \dots & S_{nn} \end{bmatrix} \begin{bmatrix} V_1^+ \\ V_2^+ \\ \vdots \\ V_n^+ \end{bmatrix} \quad (5.10)$$

or  $[V^-] = [S][V^+]$ . The power flowing into port  $i$  is  $|V_i^+|^2/(2Z_0)$ , and the power flowing out of port  $i$  is  $|V_i^-|^2/(2Z_0)$ .

Usually, all the ports of a microwave circuit have similar connectors, such as 50- $\Omega$  coaxial connectors or waveguide flanges, and the characteristic impedances of the ports have the same value. However, in a general case, the characteristic impedances  $Z_{0i}$  may have different values. For example, the ports of a coaxial-to-waveguide adapter have different characteristic impedances. Then, the voltage waves should be normalized as

$$a_i = \frac{V_i^+}{\sqrt{Z_{0i}}} \quad (5.11)$$

$$b_i = \frac{V_i^-}{\sqrt{Z_{0i}}} \quad (5.12)$$



The total voltage and current are expressed using the normalized voltage waves as

$$V_i = V_i^+ + V_i^- = \sqrt{Z_{0i}}(a_i + b_i) \quad (5.13)$$

$$I_i = \frac{1}{Z_{0i}}(V_i^+ - V_i^-) = \frac{1}{\sqrt{Z_{0i}}}(a_i - b_i) \quad (5.14)$$

The power flowing into port  $i$  is  $|a_i|^2/2$ , and the power flowing out of port  $i$  is  $|b_i|^2/2$ . The scattering matrix presentation using normalized waves is now

$$\begin{bmatrix} b_1 \\ b_2 \\ \vdots \\ b_n \end{bmatrix} = \begin{bmatrix} S_{11} & S_{12} & \dots & S_{1n} \\ S_{21} & S_{22} & \dots & S_{2n} \\ \vdots & \vdots & \vdots & \vdots \\ S_{n1} & S_{n2} & \dots & S_{nn} \end{bmatrix} \begin{bmatrix} a_1 \\ a_2 \\ \vdots \\ a_n \end{bmatrix} \quad (5.15)$$

or  $[b] = [S][a]$ .

If all the ports are terminated with matched loads, the reflection coefficient for port  $i$  is  $\rho_i = S_{ii} = b_i/a_i$ , and the transducer power gain from port  $j$  to port  $i$  is  $G_{ij} = |S_{ij}|^2 = |b_i/a_j|^2$ .

The scattering matrix of a reciprocal circuit is symmetrical:  $S_{ij} = S_{ji}$ . In other words, the transposed matrix is the same as the matrix itself:  $[S]^T = [S]$ . A reciprocal circuit operates the same way, regardless of the direction of the power flow. Most passive circuits are reciprocal; circuits that include ferrite components are the exceptions.

If the circuit has no loss, the sum of the powers flowing into the ports equals the sum of the powers flowing out of the ports:

$$\sum_{i=1}^n |a_i|^2 = \sum_{i=1}^n |b_i|^2 = \sum_{i=1}^n \left| \sum_{j=1}^n S_{ij} a_j \right|^2 \quad (5.16)$$

If all the voltage waves  $a_i$  are chosen to be zero, except  $a_k$ , then

$$\sum_{i=1}^n |S_{ik}|^2 = \sum_{i=1}^n S_{ik} S_{ik}^* = 1 \quad (5.17)$$

Thus, for any column of the scattering matrix of a lossless circuit, the sum of the squares of the scattering parameters is 1. The same applies for all

rows. If the voltage waves  $a_k$  and  $a_l$  are chosen to be nonzero and other waves entering the circuit are zero, it can be proven that

$$\sum_{i=1}^n S_{ik} S_{il}^* = 0 \tag{5.18}$$

For any two columns, the scattering parameters of a lossless circuit fulfill this equation. A similar equation applies for any two rows. The scattering matrix of a lossless circuit is unitary; that is, the transposed scattering matrix is equal to the inverse of the complex conjugate of the scattering matrix.

Scattering matrices of some simple circuits:

- *A lossless transmission line having a length of  $l$  and a characteristic impedance of  $Z_0$ , as shown in Figure 5.3.  $Z_0$  is also the characteristic impedance of both ports. When one of the ports is terminated with a matched load, the reflection coefficient of the other port is zero. Thus,  $S_{11} = S_{22} = 0$ . If the voltage wave entering port 1 is  $a_1 = 1$ , the voltage wave leaving port 2 is  $b_2 = e^{-j\beta l}$ , and  $S_{21} = b_2/a_1 = e^{-j\beta l}$ . Due to the symmetry,  $S_{12} = S_{21}$ .*
- *A joint of two transmission lines, as shown in Figure 5.4. The characteristic impedances of the transmission lines and ports are  $Z_{01}$  and  $Z_{02}$ . The reference planes of the ports are located at a distance of*

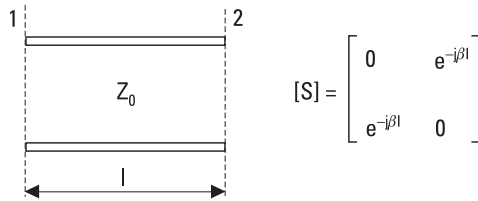


**Figure 5.3** Section of a lossless transmission line and its scattering matrix.

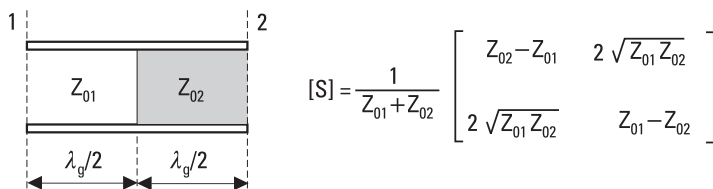


**Figure 5.4** Joint of two transmission lines and its scattering matrix.

$n\lambda_g/2$  from the junction. If  $a_1 = 1$  and  $a_2 = 0$ , then  $b_1 = \rho = (Z_{02} - Z_{01})/(Z_{01} + Z_{02}) = S_{11}$ . The voltage transmission coefficient is  $\tau = 1 + \rho$ . The normalized voltage wave  $b_2$  is obtained from  $\tau$  by using (5.11) and (5.12):  $b_2 = (1 + \rho)\sqrt{Z_{01}/Z_{02}} = 2\sqrt{Z_{01}Z_{02}}/(Z_{01} + Z_{02}) = S_{21}$ . Correspondingly, if  $a_1 = 0$  and  $a_2 = 1$ ,  $S_{22} = \rho$  and  $b_1 = (1 - \rho)\sqrt{Z_{02}/Z_{01}} = 2\sqrt{Z_{01}Z_{02}}/(Z_{01} + Z_{02}) = S_{12}$ , which may also be recognized directly due to the reciprocity.

- *A load having an impedance of  $Z_L$  is a one-port circuit.* Its scattering matrix has only one scattering parameter:  $S_{11} = \rho_L = (Z_L - Z_0)/(Z_L + Z_0)$ , the voltage reflection coefficient of the load terminating a transmission line.

The measurement of scattering parameters is much easier than the measurement of the  $Z$ - or  $Y$ -parameters. For example,  $S_{11}$  is obtained by measuring the voltage reflection coefficient  $\rho_1 = b_1/a_1$  at port 1, as all the other ports are terminated with their characteristic impedance  $Z_{0i}$  and therefore  $a_2 \dots a_n = 0$ . It is also an advantage that changing the position of a reference plane only changes the phases of the scattering parameters. For example, if the reference plane of port 1 of a two-port is moved outward an electrical distance of  $\beta l = \theta$ ,  $S_{11}$  changes to  $e^{-2j\theta}S_{11}$ ,  $S_{12}$  to  $e^{-j\theta}S_{12}$ , and  $S_{21}$  to  $e^{-j\theta}S_{21}$ , while  $S_{22}$  remains unchanged.

The transmission matrix  $[T]$  relates the input waves to output waves. Thus, in the case of a two-port we have

$$\begin{bmatrix} b_2 \\ a_2 \end{bmatrix} = \begin{bmatrix} T_{11} & T_{12} \\ T_{21} & T_{22} \end{bmatrix} \begin{bmatrix} a_1 \\ b_1 \end{bmatrix} \quad (5.19)$$

The transmission matrix is calculated from the scattering parameters as

$$[T] = \begin{bmatrix} S_{21} - S_{11}S_{22}/S_{12} & S_{22}/S_{12} \\ -S_{11}/S_{12} & 1/S_{12} \end{bmatrix} \quad (5.20)$$

The transmission matrix of a circuit consisting of blocks connected in series is obtained by multiplying the transmission matrices of the blocks.

### 5.3 Signal Flow Graph, Transfer Function, and Gain

A signal flow graph [7–9] is a graphical representation of the scattering matrix. It illustrates the equations governing the operation of a circuit. The

equations for such transfer functions as gain and reflection coefficient can be derived with the aid of signal flow graphs. Even the analysis of a circuit, which has more than one internal reflection leading to an infinite number of reflected waves, may be kept clear using a signal flow graph.

In a flow graph, there are two nodal points for each port. The values of the voltage waves,  $a_i$  and  $b_i$ , are assigned to these nodes. The nodes are connected with branches whose gains correspond to the scattering parameters. Signal may flow between two nodes along a branch only to that direction given by the arrow, that is, from node  $a$  to node  $b$ . Figure 5.5 shows the signal flow graphs for a two-port and three-port.

A given transfer function can be solved from a signal flow graph by using the simplification rules explained here and shown in Figure 5.6 [7]:

- Two branches in a series, Figure 5.6(a), with no other branches connected to the common node, can be replaced with one branch whose gain is the product of the gains of the two branches:

$$V_3 = S_{32} V_2 = S_{32} S_{21} V_1 \tag{5.21}$$

The normalized voltage waves  $a_i$  and  $b_i$  are denoted here with  $V_i$ .

- Two branches in parallel, Figure 5.6(b), can be replaced with a single branch whose gain is the sum of the gains of the two branches:

$$V_2 = S_a V_1 + S_b V_1 = (S_a + S_b) V_1 \tag{5.22}$$

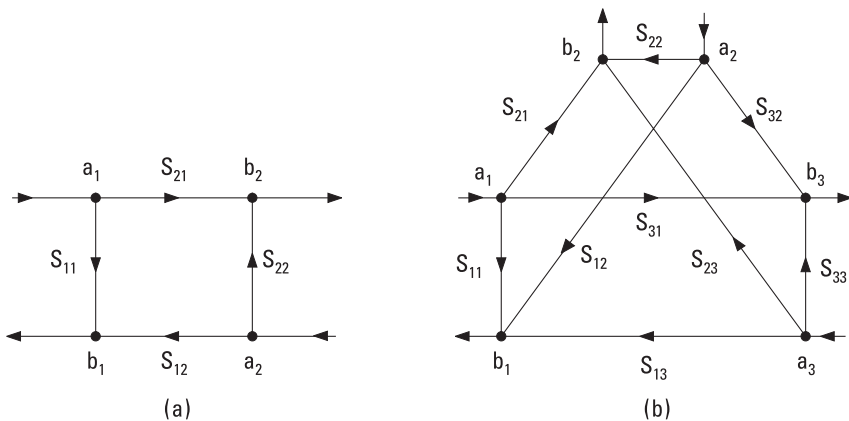
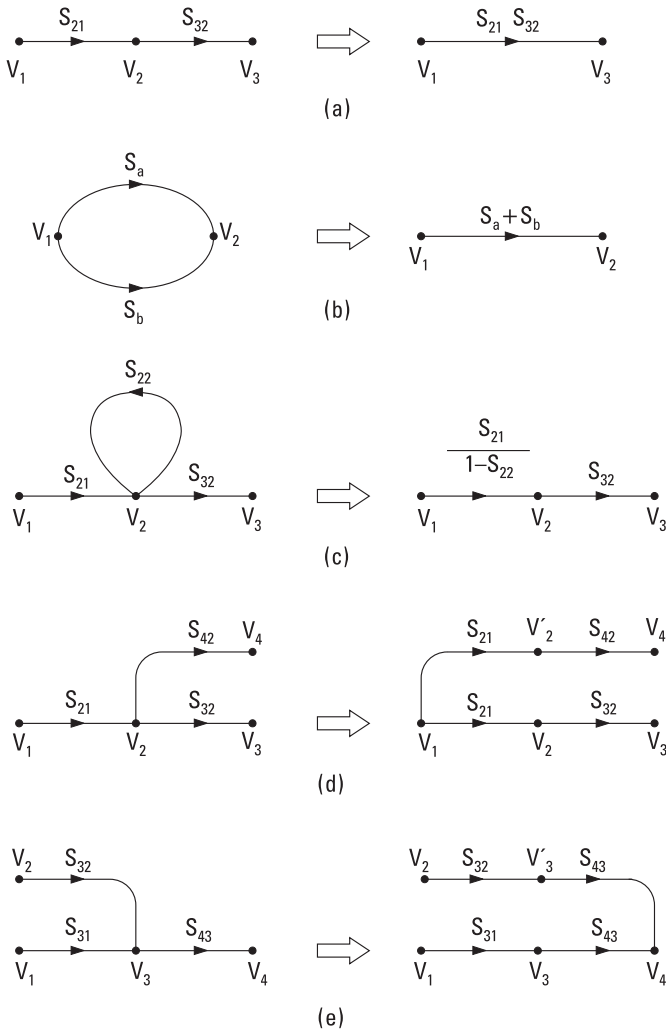


Figure 5.5 Signal flow graph for (a) a two-port and (b) a three-port.



**Figure 5.6** Simplification of flow graphs: (a) branches in series; (b) branches in parallel; (c) self-loop; (d) duplication of node with duplication of feeding branch; and (e) duplication of node with duplication of leaving branch.

- A self-loop connected to a node can be eliminated, if the gain of the branch(es) feeding the node is divided by 1 minus the gain of the loop, because from  $V_2 = S_{21} V_1 + S_{22} V_2$  it follows

$$V_2 = \frac{S_{21}}{1 - S_{22}} V_1 \tag{5.23}$$

- A node can be duplicated by duplicating the branch(es) feeding the node, Figure 5.6(d), or by duplicating the branch leaving the node, Figure 5.6(e).

The following examples illustrate how flow graphs can be simplified and transfer functions solved.

**Example 5.1**

Derive the input reflection coefficient  $\rho_{in}$  for a two-port when the output port (port 2) is terminated with a load impedance  $Z_L$ . The characteristic impedance of both ports is  $Z_0$ .

**Solution**

The voltage reflection coefficient for the load is  $\rho_L = (Z_L - Z_0)/(Z_L + Z_0)$ . This is also the gain of the branch connected to the output port in the flow graph of Figure 5.7(a). The node  $a_2$  is then duplicated by duplicating the branch  $\rho_L$  [Figure 5.7(b)]. The gain of the self-loop is  $S_{22}\rho_L$  according to the rule of branches in series. Then the self-loop is eliminated [Figure 5.7(c)].

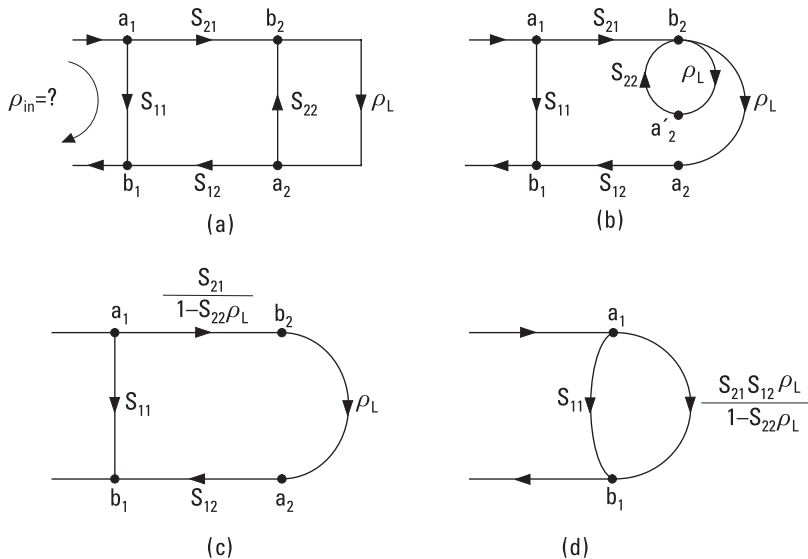


**Figure 5.7** Solving the input reflection coefficient for a two-port using a flow graph and its simplification rules: (a) a flow-graph presentation of a terminated two-port; (b) duplication of a node; (c) elimination of a self-loop; and (d) combination of branches in a series.

The rule of branches in series is used again [Figure 5.7(d)]. The input reflection coefficient is obtained by applying the rule of branches in parallel:

$$\rho_{in} = S_{11} + \frac{S_{21} S_{12} \rho_L}{1 - S_{22} \rho_L} \tag{5.24}$$

**Example 5.2**

A lossless transmission line is connected between a generator and load. The length of the line is  $l = n\lambda_g$  ( $n$  is integer) and its characteristic impedance is  $Z_0$ , Figure 5.8(a). The load impedance is  $Z_L$ . The output impedance of the generator is  $Z_S$ . What is the load voltage  $V_L$ , if the generator voltage is  $V_S$ ?

**Solution**

It is not necessary to normalize the voltages because both ports of the line (two-port) have the same characteristic impedance. The branches representing  $S_{11}$  and  $S_{22}$  are not drawn in Figure 5.8(b) because their gain is zero. Now  $S_{21} = S_{12} = e^{-j\beta l} = 1$ . The node having a voltage of  $V_S/2$  represents the generator because this voltage corresponds to available power of  $V_S^2/(8Z_S)$  of the generator. The voltage transmission coefficient from the generator to the line is  $1 - \rho_S$ . A branch having a gain of  $1 + \rho_L$  is added for the calculation of the load voltage  $V_L$ . By duplicating the node  $V_2^-$ , using the rule of branches in series, and eliminating the self-loop, the flow graph of Figure 5.8(c) is obtained. From this we get

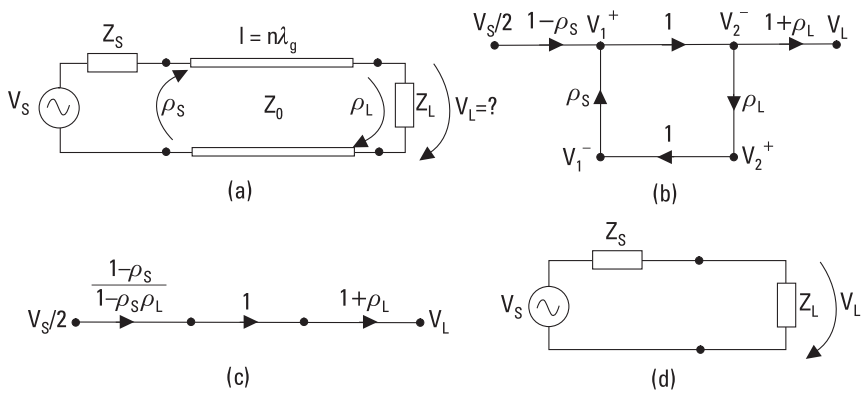


**Figure 5.8** Solving the load voltage using flow graphs: (a) a terminated  $n\lambda_g$  transmission line fed from a generator; (b) its flow-graph presentation; (c) elimination of a self-loop; and (d) an equivalent circuit of the flow graph presented in (c), equivalent to the circuit in (a).

$$V_L = \frac{(1 - \rho_S)(1 + \rho_L)}{1 - \rho_S \rho_L} \times \frac{V_S}{2}$$

Because the reflection coefficients are  $\rho_S = (Z_S - Z_0)/(Z_S + Z_0)$  and  $\rho_L = (Z_L - Z_0)/(Z_L + Z_0)$ , the load voltage is  $V_L = Z_L V_S / (Z_S + Z_L)$ , which may be seen also from Figure 5.8(d) by using voltage division.

### 5.3.1 Mason's Rule

Instead of the flow graph simplification, transfer functions can also be found by using Mason's rule [10]. According to Mason's rule, the ratio of a dependent variable (voltage of a node) to an independent variable produced by a source (voltage of the feed node) is

$$T = \frac{P_1 \left[ 1 - \sum L(1)^1 + \sum L(2)^1 - \dots \right] + P_2 \left[ 1 - \sum L(1)^2 + \sum L(2)^2 - \dots \right] + P_3 [1 - \dots]}{1 - \sum L(1) + \sum L(2) - \sum L(3) + \dots} \quad (5.25)$$

where

$P_1, P_2, \dots$  are the gains of the forward paths between the input and output nodes;

$\sum L(1), \sum L(2), \dots$  are the sums of the loop gains of the first order, second order, and so on;

$\sum L(1)^1, \sum L(2)^1, \dots$  are the sums of the loop gains of the first order, second order, and so on, for such loops, which do not touch path 1;

$\sum L(1)^2, \sum L(2)^2, \dots$  are the sums of the loop gains of the first order, second order, and so on, for such loops, which do not touch path 2.

A path is a continuous succession of branches having arrows pointing to the same direction. It is either a forward path connecting the input node to the output node, or a loop, which originates and terminates on the same node. A path passes each node in the loop only once. The path gain is the product of all the gains in the path. The loop gain is the product of the gains in the loop. The loop gain of the first order means the gain of an individual loop; the loop gain of the second order means the product of the



gains of two nontouching loops, and so on. Nontouching loops are separate loops that do not touch each other at any node.

**Example 5.3**

A generator and a load are connected to a two-port, as in Figure 5.9. Find the transducer power gain, that is, the ratio of the power coupled to the load,  $P_L$ , to the available power of the generator,  $P_{S,a}$ . The characteristic impedance is  $Z_0$ .

**Solution**

In the flow graph,  $a_S$  and  $a_L$  are normalized voltages corresponding to the available power of the generator and the power coupled to the load, respectively. There is only one path from the input node  $a_S$  to the output node  $a_L$ . Its gain is

$$P_1 = (1 - \rho_S) \sqrt{Z_S/Z_0} S_{21} (1 + \rho_L) \sqrt{Z_0/Z_L}$$

There are three loops, and the sum of their gains is

$$\sum L(1) = S_{11} \rho_S + S_{22} \rho_L + S_{21} \rho_L S_{12} \rho_S$$

The loops  $S_{11} \rho_S$  and  $S_{22} \rho_L$  are nontouching; thus,

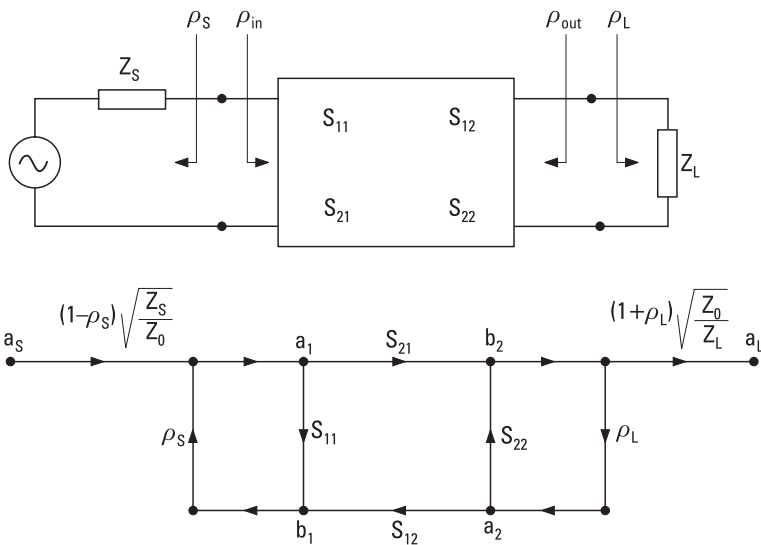


**Figure 5.9** Two-port connected between a generator and a load.

$$\sum L(2) = S_{11}\rho_S S_{22}\rho_L$$

All loops touch path  $P_1$  and therefore

$$\sum L(1)^1 = \sum L(2)^1 = \dots = 0$$

Using (5.25), the voltage of the output node is

$$a_L = \frac{(1 - \rho_S)S_{21}(1 + \rho_L)\sqrt{Z_S/Z_L}}{1 - S_{11}\rho_S - S_{22}\rho_L - S_{21}\rho_L S_{12}\rho_S + S_{11}\rho_S S_{22}\rho_L} \times a_S$$

### 5.3.2 Gain of a Two-Port

The final expression of the above solution gives us a good basis to present different definitions of the gain of a two-port. The *transducer power gain* ( $G_t$ ) can be presented in several ways:

$$\begin{aligned} G_t &= \frac{P_L}{P_{S,a}} = \frac{|a_L|^2}{|a_S|^2} = \frac{|S_{21}|^2(1 - |\rho_S|^2)(1 - |\rho_L|^2)}{|(1 - S_{11}\rho_S)(1 - S_{22}\rho_L) - S_{12}S_{21}\rho_S\rho_L|^2} \\ &= \frac{|S_{21}|^2(1 - |\rho_S|^2)(1 - |\rho_L|^2)}{|1 - \rho_S\rho_{in}|^2|1 - S_{22}\rho_L|^2} \\ &= \frac{|S_{21}|^2(1 - |\rho_S|^2)(1 - |\rho_L|^2)}{|1 - S_{11}\rho_S|^2|1 - \rho_{out}\rho_L|^2} \end{aligned} \quad (5.26)$$

where  $\rho_{out}$  is the reflection coefficient of the output port 2.

The *power gain* ( $G_p$ ) of a two-port is defined as the ratio of the power coupled to the load,  $P_L$ , to the power coupled to the two-port,  $P_{in}$ . Using the flow graph we obtain

$$G_p = \frac{P_L}{P_{in}} = \frac{|a_L|^2}{|a_1|^2(1 - |\rho_{in}|^2)} = \frac{|S_{21}|^2(1 - |\rho_L|^2)}{|1 - S_{22}\rho_L|^2(1 - |\rho_{in}|^2)} \quad (5.27)$$

The *available power gain* ( $G_a$ ) is defined as the ratio of the available output power of the two-port,  $P_{out,a}$ , to the available power of the generator,  $P_{S,a}$ :

$$G_a = \frac{P_{out,a}}{P_{S,a}} = \frac{P_L(\rho_L = \rho_{out}^*)}{P_{S,a}} = \frac{|S_{21}|^2(1 - |\rho_S|^2)}{|1 - S_{11}\rho_S|^2(1 - |\rho_{out}|^2)} \quad (5.28)$$

The *maximum available power gain* ( $G_{a,max}$ ) is the available power gain in that case when the input port is conjugate-matched to the generator:

$$G_{a,max} = \frac{P_L(\rho_L = \rho_{out}^*)}{P_{in}(\rho_S = \rho_{in}^*)} \quad (5.29)$$

How  $G_{a,max}$  can be expressed using the scattering parameters of a two-port is presented in Chapter 8, (8.28). In a unilateral case ( $S_{12} = 0$ ), the maximum available power gain is

$$G_{a,max} = \frac{|S_{21}|^2}{(1 - |S_{11}|^2)(1 - |S_{22}|^2)} \quad (5.30)$$

The *insertion gain* ( $G_i$ ) is the ratio of the power coupled to the load from the two-port,  $P_L$ , to the power coupled to the load directly from the generator,  $P_d$  (no two-port between):

$$G_i = \frac{P_L}{P_d} = \frac{|S_{21}|^2|1 - \rho_S\rho_L|^2}{|1 - \rho_S\rho_{in}|^2|1 - S_{22}\rho_L|^2} \quad (5.31)$$

If both the generator and load are matched to the characteristic impedance  $Z_0$ ,  $\rho_S = \rho_L = 0$  and  $G_i = |S_{12}|^2$ . The inverse of  $G_i$  is called the insertion loss:

$$L_i = \frac{1}{G_i} = \frac{P_d}{P_L} \quad (5.32)$$

The insertion gain and insertion loss are parameters, which can be measured directly. Other gains of a two-port may be calculated from measured scattering parameters and impedances  $Z_S$  and  $Z_L$ .

## References

- [1] Kuh, E. S., and R. A. Rohrer, *Theory of Linear Active Networks*, San Francisco, CA: Holden-Day, 1967.
- [2] Lay, D. C., *Linear Algebra and Its Applications*, 3rd ed., Reading, MA: Addison Wesley, 2002.
- [3] Collin, R. E., *Foundations for Microwave Engineering*, 2nd ed., New York: IEEE Press, 2001.
- [4] Ramo, S., J. Whinnery, and T. van Duzer, *Fields and Waves in Communication Electronics*, New York: John Wiley & Sons, 1965.
- [5] Belevitch, V., "Transmission Losses in  $2n$ -Terminal Networks," *Journal of Applied Physics*, Vol. 19, No. 7, 1948, pp. 636–638.
- [6] Montgomery, C. G., R. H. Dicke, and E. M. Purcell, *Principles of Microwave Circuits*, Radiation Laboratory Series, New York: McGraw-Hill, 1948.
- [7] Kuhn, N., "Simplified Signal Flow Graph Analysis," *Microwave Journal*, November 1963, pp. 59–66.
- [8] Bryant, G. H., *Principles of Microwave Measurements*, London, England: Peter Peregrinus, 1988.
- [9] Nyfors, E., and P. Vainikainen, *Industrial Microwave Sensors*, Norwood, MA: Artech House, 1989.
- [10] Mason, S. J., "Feedback Theory: Further Properties of Signal Flow Graphs," *IRE Proc.*, Vol. 44, July 1956, pp. 920–926.



# 6

## Passive Transmission Line and Waveguide Devices

Transmitters and receivers are composed of many kinds of passive and active devices. Some important passive devices based on sections of transmission lines or waveguides are covered in this chapter. Frequency-selective passive devices, resonators and filters, are the topic of Chapter 7. Standardized symbols for various passive devices are shown in Figure 6.1. Most passive devices are reciprocal; only isolators and circulators, which are based on ferrites, are nonreciprocal.

Components or devices used in radio equipment at various frequency ranges can be divided into three groups, according to their size in wavelengths:

1. Lumped components, such as capacitors and coils, are usable up to UHF and even higher frequencies. Their size is small compared to a wavelength. As the frequency increases, lumped elements become lossy and their parasitic reactances and radiation loss increase. For example, a capacitor may become a resonant circuit as a result of the parasitic inductances of the connecting wires.
2. Distributed components are made of sections of transmission lines or waveguides. Their size is comparable to a wavelength, and the phase differences between the parts of a component are significant. Distributed components are used at microwave and millimeter-wave ranges. However, waveguide components eventually become lossy and difficult to fabricate as the frequency increases.

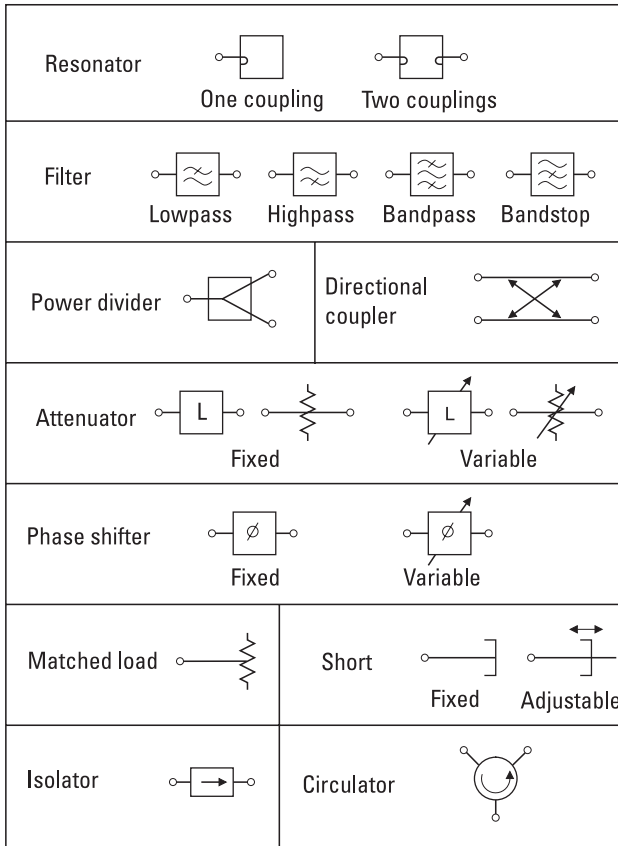


Figure 6.1 Standardized symbols for passive devices.

- Quasioptical components handle waves propagating in a beam in free space. The dimensions of quasioptical components are larger than a wavelength. They are used in millimeter-wave and submillimeter-wave systems.

### 6.1 Power Dividers and Directional Couplers

Power dividers and directional couplers are components that split the input signal into two or more output ports. They may also be used as power combiners. Power dividers usually are three-port devices. Directional couplers have four ports and can separate waves propagating into opposite directions on the line. Directional couplers are used in impedance measurement and

for taking a sample of a signal. Hybrids are 3-dB directional couplers with either a  $90^\circ$  or  $180^\circ$  phase difference between their output signals. Hybrids are needed in many mixers, modulators, and demodulators.

### 6.1.1 Power Dividers

The T-junctions shown in Figure 6.2 are simple power dividers. However, all the ports of a lossless three-port circuit cannot be matched. We can prove this by considering the properties of the scattering matrices. A passive, reciprocal, and matched three-port would have a scattering matrix, as

$$[S] = \begin{bmatrix} 0 & S_{12} & S_{13} \\ S_{12} & 0 & S_{23} \\ S_{13} & S_{23} & 0 \end{bmatrix} \quad (6.1)$$

As we stated in Chapter 5, the scattering matrix of a lossless circuit is unitary, from which it follows that

$$|S_{12}|^2 + |S_{13}|^2 = 1 \quad (6.2)$$

$$|S_{12}|^2 + |S_{23}|^2 = 1 \quad (6.3)$$

$$|S_{13}|^2 + |S_{23}|^2 = 1 \quad (6.4)$$

$$S_{13}^* S_{23} = 0 \quad (6.5)$$

$$S_{23}^* S_{12} = 0 \quad (6.6)$$

$$S_{12}^* S_{13} = 0 \quad (6.7)$$

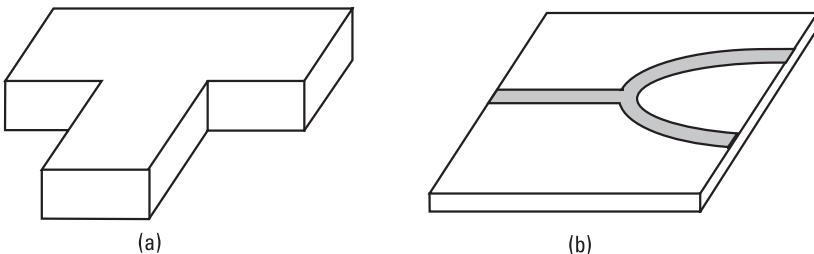


**Figure 6.2** T-junctions: (a) a waveguide junction; (b) a microstrip line junction.



According to (6.5) through (6.7) at least two of the parameters  $S_{12}$ ,  $S_{13}$ , and  $S_{23}$  are zero. However, this is in contradiction with at least one of (6.2) through (6.4). Thus, such a circuit cannot exist.

Let us consider the matching problem of a lossless T-junction with an equivalent circuit shown in Figure 6.3(a). The parallel susceptance  $B$  represents the reactive fields produced by the discontinuity of the junction. The characteristic impedances of the ports are  $Z_1$ ,  $Z_2$ , and  $Z_3$ . Let us assume that  $B = 0$ . We then choose  $Z_2 = Z_3 = 2Z_1$  and assume that the ports are terminated with load impedances equal to their characteristic impedances. Now port 1 is matched: The input impedance is  $Z_1$  and the power fed to port 1 is split evenly to the loads of ports 2 and 3. However, ports 2 and 3 are not matched because their input impedance is  $2Z_1/3$  ( $Z_1$  and  $2Z_1$  in parallel) instead of  $2Z_1$ .

All ports of a three-port divider can be matched by using resistive elements. Figure 6.3(b) shows a matched power divider containing lumped resistors. One half of the power coupled to the input port is absorbed in these resistors.

The isolation of the output ports of these power dividers is poor since a part of the power reflected from a mismatched output load is coupled to the other output port. The Wilkinson power divider shown in Figure 6.4 avoids this disadvantage. All the ports are matched to a characteristic impedance  $Z_0$  if the quarter-wave-long sections have a characteristic impedance of  $\sqrt{2}Z_0$ , and the output ports 2 and 3 are connected with a lumped resistor having a resistance  $2Z_0$ . This circuit is also lossless if the ports are terminated with a matched load, that is, with an impedance of  $Z_0$ .

For all the power dividers discussed so far, the ratio of output powers equals 1. However, this ratio can be chosen freely by modifying the parameters of the circuits.

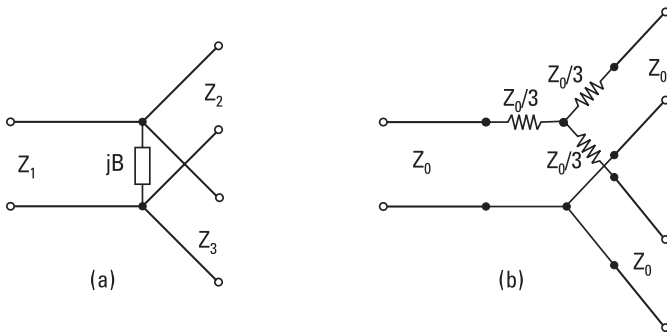


**Figure 6.3** Equivalent circuits of power dividers: (a) lossless T-junction and (b) resistive power divider.

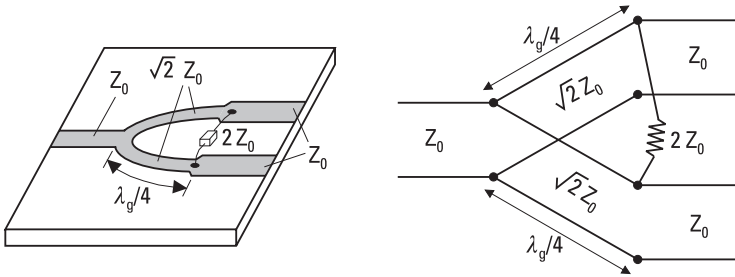


Figure 6.4 Wilkinson power divider.

### 6.1.2 Coupling and Directivity of a Directional Coupler

Let us consider the directional coupler shown in Figure 6.5 and assume that it is ideal. If a wave is fed from a signal source into port 1, it will couple to ports 2 and 4 but not at all to port 3. Similarly, if port 2 is the input port, ports 1 and 3 are output ports and port 4 is an isolated port. An ideal directional coupler is also lossless, and all of its ports can be matched. If all the ports are terminated with a matched load, the input reflection coefficients are zero. In practice, these properties can be achieved only approximately.

Let us assume that the power coupled into the input port 1 is  $P_1$  and the powers coupled from ports 2, 3, and 4 to the matched terminations are  $P_2$ ,  $P_3$ , and  $P_4$ , respectively. The coupling  $C$  and directivity  $D$  in decibels are defined as

$$C = 10 \log \frac{P_1}{P_4} \tag{6.8}$$

$$D = 10 \log \frac{P_4}{P_3} \tag{6.9}$$

Usually, most of the input power couples to the termination of the main line at port 2. The coupling describes the power coupled from the main line to the side line and is designed to a value that depends on the

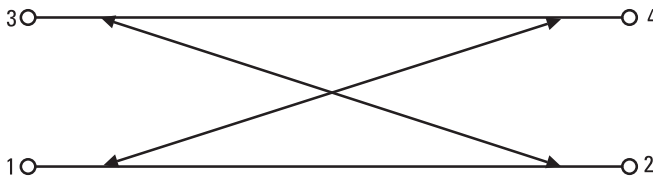


Figure 6.5 Directional coupler.

application, typically 3 dB to 30 dB. The directivity describes the leakage to the isolated port and should be as large as possible; a good directivity may be 30 dB to 40 dB. The isolation between the input port and the isolated port is  $C + D$  in decibels.

A directional coupler with a good directivity can discriminate between the waves propagating in opposite directions on a line. However, mismatches of the output loads may worsen the effective directivity. Let us consider the situation illustrated in Figure 6.6. A signal source is connected at port 1, an unknown load with a reflection coefficient of  $\rho_L$  is connected at port 2, and matched power meters are connected to ports 3 and 4. In an ideal case the power meter readings are

$$P_3 = |\rho_L|^2 \left( 1 - \frac{1}{10^{C/10}} \right) \frac{1}{10^{C/10}} P_1 \text{ and } P_4 = \frac{1}{10^{C/10}} P_1$$

from which the magnitude of the reflection coefficient can be solved. If the directional coupler has a finite directivity, and the signal source and power meters are mismatched, several waves will disturb the measurement and cause errors. An accurate analysis is complicated since there will be multiple reflections between the mismatches. The analysis may be carried out using a flow graph. Approximate error limits may be calculated by taking only the first reflections into account. When summing up the waves propagated to the power meters via different paths, both the amplitudes and phases of the waves must be taken into consideration. Summing up the powers of individual waves is not correct.

### 6.1.3 Scattering Matrix of a Directional Coupler

Let us next derive the scattering matrix of an ideal directional coupler. Because ports 1 and 3 as well ports 2 and 4 are isolated from each other,

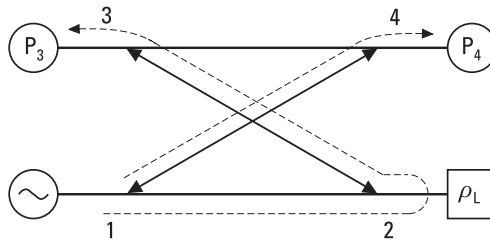


**Figure 6.6** Measuring the magnitude of the reflection coefficient with a directional coupler.

$S_{13} = S_{24} = 0$ . Let us assume that ports 1 and 2 are matched, or  $S_{11} = S_{22} = 0$ . Due to the reciprocity  $S_{ij} = S_{ji}$ . Thus, the scattering matrix is

$$[S] = \begin{bmatrix} 0 & S_{12} & 0 & S_{14} \\ S_{12} & 0 & S_{23} & 0 \\ 0 & S_{23} & S_{33} & S_{34} \\ S_{14} & 0 & S_{34} & S_{44} \end{bmatrix} \quad (6.10)$$

The scattering matrix of a lossless circuit is unitary. From rows 1 and 4 we get  $S_{14}S_{44}^* = 0$  and from rows 2 and 3  $S_{23}S_{33}^* = 0$ . Because  $S_{14}$  and  $S_{23}$  are nonzero, parameters  $S_{33}$  and  $S_{44}$  must be zero, and ports 3 and 4 must be matched. From rows 1 and 3 and from rows 2 and 4 we get the following equations, respectively,

$$S_{12}S_{23}^* + S_{14}S_{34}^* = 0 \quad (6.11)$$

$$S_{12}S_{14}^* + S_{23}S_{34}^* = 0 \quad (6.12)$$

Because, for example  $|S_{12}S_{23}^*| = |S_{12}||S_{23}|$ , (6.11) and (6.12) can be written as

$$|S_{12}||S_{23}| = |S_{14}||S_{34}| \quad (6.13)$$

$$|S_{12}||S_{14}| = |S_{23}||S_{34}| \quad (6.14)$$

By dividing the left side and right side of (6.13) with the corresponding sides of (6.14), we get  $|S_{23}|/|S_{14}| = |S_{14}|/|S_{23}|$ , which means that  $|S_{14}| = |S_{23}|$ . Hence the coupling between ports 1 and 4 is equal to that between ports 2 and 3. Now, from (6.13) it follows that  $|S_{12}| = |S_{34}|$ .

The reference planes of ports 1 and 3 can be chosen so that  $S_{12}$  and  $S_{34}$  are real and positive numbers equal to  $\alpha$ , and the reference plane of port 4 so that  $S_{14}$  is an imaginary number  $j\beta$  ( $\beta$  is real and positive). From (6.11) it follows that also  $S_{23} = j\beta$ . Due to the conservation of energy  $|S_{12}|^2 + |S_{14}|^2 = 1$  or  $\alpha^2 + \beta^2 = 1$ . Thus, the scattering matrix of an ideal directional coupler can be written as

$$[S] = \begin{bmatrix} 0 & \alpha & 0 & j\beta \\ \alpha & 0 & j\beta & 0 \\ 0 & j\beta & 0 & \alpha \\ j\beta & 0 & \alpha & 0 \end{bmatrix} \quad (6.15)$$

The coupling  $C$  (as a power ratio, not in decibels) is  $1/|S_{14}|^2 = 1/\beta^2$ , or  $\beta = \sqrt{1/C}$ , and from this it follows that  $\alpha = \sqrt{1 - 1/C}$ .

The special cases of a directional coupler having a 3-dB coupling are called hybrids. The hybrid couplers can be classified into two categories, depending on whether the phase difference of the output waves is  $90^\circ$  or  $180^\circ$ . The scattering matrix of a  $90^\circ$  hybrid is

$$[S] = \frac{1}{\sqrt{2}} \begin{bmatrix} 0 & 1 & 0 & j \\ 1 & 0 & j & 0 \\ 0 & j & 0 & 1 \\ j & 0 & 1 & 0 \end{bmatrix} \quad (6.16)$$

The scattering matrix of a  $180^\circ$  hybrid is

$$[S] = \frac{1}{\sqrt{2}} \begin{bmatrix} 0 & 1 & 0 & 1 \\ 1 & 0 & -1 & 0 \\ 0 & -1 & 0 & 1 \\ 1 & 0 & 1 & 0 \end{bmatrix} \quad (6.17)$$

Ports 1 and 4 of a  $180^\circ$  hybrid are called the  $\Sigma$  ports, whereas ports 2 and 3 are called the  $\Delta$  ports. When a wave enters a  $\Sigma$  port, the output waves have equal powers and are in the same phase. If a  $\Delta$  port is the input port, the output waves are in an opposite phase.

### 6.1.4 Waveguide Directional Couplers

We may make a directional coupler by placing side by side two rectangular metal waveguides having coupling holes in the common wall [1]. Figure 6.7 shows a simple directional coupler having two holes  $d = \lambda_g/4$  apart in the broad wall of the waveguides. Let us assume that the coupling factor of a single hole is  $B_f$  in the forward direction and  $B_b$  in the backward direction.

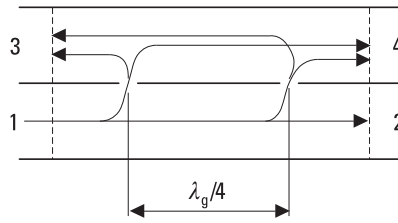


**Figure 6.7** Two-hole waveguide directional coupler.

For example, if a wave is applied to port 1 and its field is equal to 1 in the lower waveguide at a hole, in the upper waveguide the fields of the waves propagating toward ports 3 and 4 are  $B_b$  and  $B_f$ , respectively. If the coupling factors are small, the fields in the lower waveguide at both holes have nearly equal amplitudes. The two paths from port 1 to port 4 have equal lengths, and the fields strengthen each other at port 4. If the coupling holes are identical, the coupling is in decibels

$$C = -20 \log(2|B_f|) \quad (6.18)$$

On the other hand, the paths from port 1 to port 3 have a difference of  $\lambda_g/2$  in their lengths. The waves coupled through the holes to port 3 have opposite phases and cancel each other. Hence the directivity  $D$  is infinite.

The separation of the holes in the directional coupler of Figure 6.7 is  $\lambda_g/4$  only at a single frequency. As the frequency deviates from this frequency, the directivity decreases. The frequency response of the directivity is

$$D = 20 \log \frac{2|B_f|}{|B_b| |1 + e^{-j2\beta d}|} = 20 \log \frac{|B_f|}{|B_b|} + 20 \log \frac{1}{|\cos \beta d|} \quad (6.19)$$

The directivity can be interpreted as the sum of the directivity of a single hole and the directivity of the array of holes. A good directivity over a broad band can be achieved by using several coupling holes separated by  $\lambda_g/4$  at the center frequency. As before, the coupling and directivity of a multihole coupler can be calculated by summing the fields at ports 3 and 4. By choosing the sizes of the holes properly, different frequency responses, such as the Butterworth or Chebyshev response, can be realized for the directivity [2].

The waveguide junction shown in Figure 6.8 is called the magic T-junction. It operates as a  $180^\circ$  hybrid. A wave applied to port 1 ( $\Sigma$ ) is

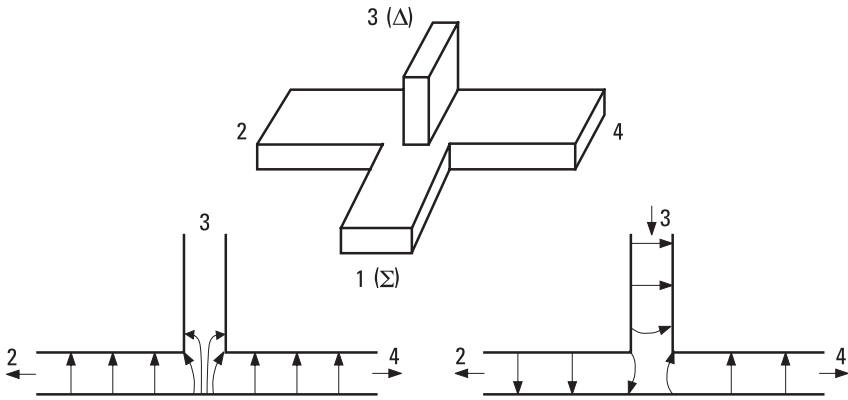


**Figure 6.8** Magic T-junction and its field patterns.

divided into ports 2 and 4 equally and in the same phase, due to symmetry. The electric field distribution has an even symmetry with respect to the middle line of port 3, whereas the field of the  $TE_{10}$  mode has an odd symmetry. Therefore, a wave cannot couple from port 1 to port 3. Also, a wave applied to port 3 ( $\Delta$ ) is divided into ports 2 and 4 with equal amplitude, but now the output waves have an opposite phase.

### 6.1.5 Microstrip Directional Couplers

Let us consider two parallel microstrip lines that are placed so close to each other that the fields of the lines couple to each other. Then a wave propagating in one line can excite a wave in the other line. The fields of a coupled line can be presented as a superposition of an even mode and an odd mode, shown in Figure 6.9. In case of the even mode the currents of the lines are equal and in the same direction; in case of the odd mode they are equal but in the opposite directions. A coupled line may be represented with an even-mode characteristic impedance  $Z_{0e}$  and an odd-mode characteristic impedance  $Z_{0o}$ , which are characteristic impedances of one of the strip

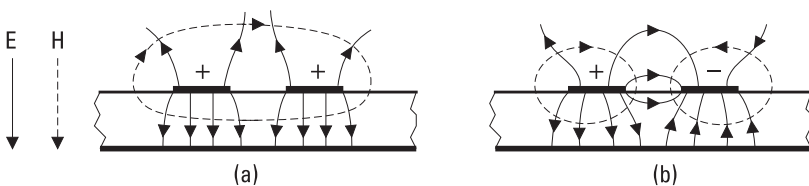


**Figure 6.9** Fields of (a) the even mode and (b) the odd mode in a coupled microstrip line.

conductors relative to the ground when the coupled line is operated in the even mode or odd mode, respectively. The graph in Figure 6.10 gives these impedances when the relative permittivity of the substrate is 10.

The microstrip lines shown in Figure 6.11(a) are coupled over a length of  $l$ . Let us assume that a signal source is at port 1 and other ports are terminated with loads having an impedance of  $Z_0$ . It can be proven that all the ports are matched if

$$Z_0 = \sqrt{Z_{0e} Z_{0o}} \tag{6.20}$$

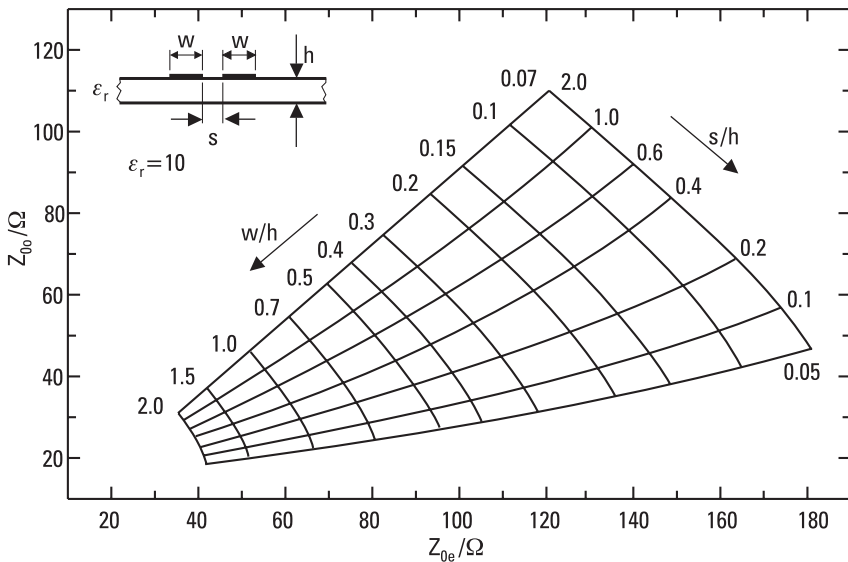


**Figure 6.10** Even-mode and odd-mode characteristic impedances of coupled microstrip lines;  $\epsilon_r = 10$ .

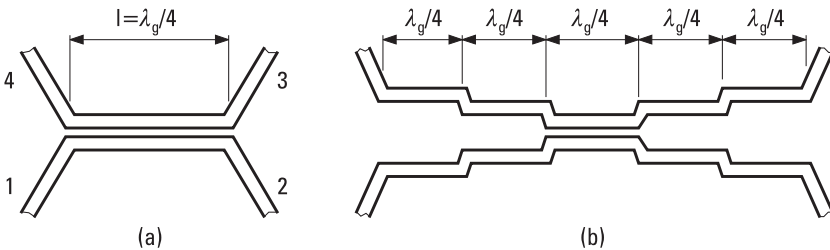


**Figure 6.11** Directional couplers based on coupled microstrip lines: (a) single-element coupler; and (b) multielement coupler.



When  $l = \lambda_g/4$  the coupling to port 4 reaches its maximum value and no signal is coupled to port 3. Thus, this device operates as a directional coupler. (Note that the coupled port is on the same end as the input port, unlike in Figures 6.6 and 6.7.) The characteristic impedances of the coupled line depend on  $Z_0$  and on the voltage coupling coefficient  $K = |V_4/V_1|$  as

$$Z_{0e} = Z_0 \sqrt{\frac{1 + K}{1 - K}} \tag{6.21}$$

$$Z_{0o} = Z_0 \sqrt{\frac{1 - K}{1 + K}} \tag{6.22}$$

Equations (6.20) through (6.22) are valid if the even-mode and odd-mode waves propagate at the same speed. In a coupled microstrip line, this is not exactly true, and the directivity is worse than in an ideal case. The structure of Figure 6.11(a) is best suited for realizing a weak coupling (large  $C$ ). The lines would be impractically close to each other to achieve a strong coupling. The single-element coupler has a bandwidth that may be too narrow for some applications. A broadband directional coupler is obtained by connecting quarter-wave sections with appropriate couplings, as in Figure 6.11(b).

The directional coupler shown in Figure 6.12 is called the Lange coupler and is suitable for realizing strong couplings as 3 dB to 6 dB. It is made of several coupled lines bonded together with thin wires.

The ring coupler illustrated in Figure 6.13(a) is a 180° hybrid. Its scattering matrix is obtained by multiplying the matrix of (6.17) by  $-j$ , if

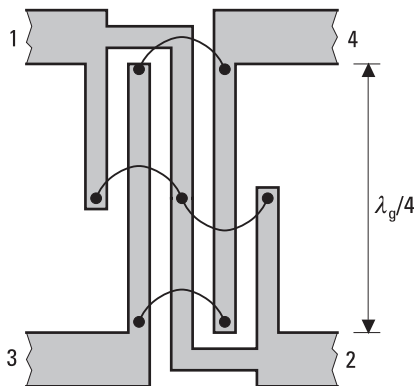


**Figure 6.12** Lange coupler.

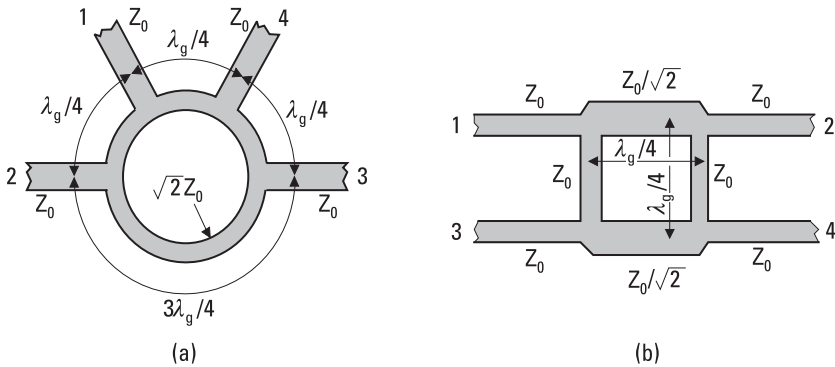


**Figure 6.13** Hybrids: (a) ring hybrid; and (b) branch-line hybrid.

the reference planes are at the T-junctions. The characteristic impedances of the ports are  $Z_0$  and that of the  $3\lambda_g/2$ -long ring is  $\sqrt{2}Z_0$ . A wave applied to port 1 ( $\Sigma$ ) does not couple to port 3 because the two paths have a difference in length of  $\lambda_g - \lambda_g/2 = \lambda_g/2$ , but it couples to ports 2 and 4 in the same phase. A wave applied to port 2 ( $\Delta$ ) couples to ports 1 and 3 in an opposite phase.

The branch-line coupler shown in Figure 6.13(b) is a  $90^\circ$  hybrid. The  $\lambda_g/4$ -long branches have characteristic impedances of  $Z_0$  and  $Z_0/\sqrt{2}$ . For example, a wave applied to port 1 couples to ports 2 and 4 with a phase difference of  $90^\circ$ , and port 3 is isolated from port 1. Both ring and branch-line couplers can be modified so that the ratio of output powers differs from 1.

### Example 6.1

Design a  $50\text{-}\Omega$  microstrip directional coupler operating at 1 GHz with a coupling of  $C = 15$  dB. The properties of the substrate are:  $\epsilon_r = 10$ ,  $h = 0.254$  mm,  $t = 5$   $\mu\text{m}$ . Use the structure presented in Figure 6.11(a).

### Solution

The voltage-coupling coefficient corresponding to a 15-dB coupling is  $K = \sqrt{1/10^{1.5}} = 0.1778$ . From (6.12) and (6.13) we get  $Z_{0e} = 59.8\Omega$  and  $Z_{0o} = 41.8\Omega$ . We use the graph of Figure 6.10 for  $\epsilon_r = 10$ , and read  $w/h = 0.9$  and  $s/h = 0.9$ . Thus, both the width of strips forming the coupled line and their separation is 0.23 mm. According to (3.85), the effective relative permittivity is  $\epsilon_{\text{reff}} = 6.69$ . The length of the coupled line section is  $\lambda/4 = c/(4f\sqrt{\epsilon_{\text{reff}}}) = 29.0$  mm. The strip width of  $50\text{-}\Omega$  lines is 0.234 mm.

## 6.2 Ferrite Devices

Ferrites are ceramic materials that possess a high resistivity and that behave nonreciprocally when embedded in a magnetic field. Ferrite devices such as isolators, circulators, attenuators, phase shifters, modulators, and switches are based on these properties [3].

### 6.2.1 Properties of Ferrite Materials

Ferrites are oxides of ferromagnetic materials, such as iron, to which another oxide has been added as an impurity. According to their molecular structure, ferrites are divided into garnets ( $3M_2O_3 \cdot 5Fe_2O_3$ ), spinels ( $MO \cdot Fe_2O_3$ ), and hexaferrites. In garnets  $M$  is a lanthanid like yttrium, gadolinium, or samarium. In spinels  $M$  is mangan, manganese, iron, zinc, nickel, or cadmium. The impurities increase the resistivity of the ferrite to as much as  $10^{14}$  times higher than the resistivity of metals. Typically, the relative permittivity  $\epsilon_r$  is 10 to 20, whereas the relative permeability  $\mu_r$  may be up to VHF band 1,000 or even more.

In ferromagnetic materials, strong interactions between atomic magnetic moments force them to line up parallel to each other. Ferromagnetic materials are able to retain magnetization when the magnetizing field is removed.

Atoms behave as magnetic dipoles because of the spin of their electrons. The orbital movement of the electrons about the nucleus also causes a small magnetic moment, but its effect is less important for the magnetic properties of materials. We can imagine that an electron is rotating about its axis producing a magnetic dipole moment

$$|\mathbf{m}| = \frac{eh}{4\pi m_e} = 9.27 \times 10^{-24} \text{ Am}^2 \quad (6.23)$$

where  $e$  is the magnitude of the electron charge,  $h$  is Planck's constant, and  $m_e$  is the mass of an electron. The spin angular momentum of an electron is

$$|\mathbf{P}| = \frac{h}{4\pi} \quad (6.24)$$

The vectors  $\mathbf{m}$  and  $\mathbf{P}$  point to opposite directions. The ratio of their magnitudes, the gyromagnetic ratio, is

$$\gamma = \left| \frac{m}{P} \right| = \frac{e}{m_e} = 17.6 \text{ MHz/gauss} \quad (6.25)$$

A static magnetic field having a flux density  $\mathbf{B}_0 = B_0 \mathbf{u}_z$  exerts on an electron a torque of ( $\mathbf{m} = -\gamma \mathbf{P}$ ):

$$\mathbf{T} = \mathbf{m} \times \mathbf{B}_0 = -\gamma \mathbf{P} \times \mathbf{B}_0 \quad (6.26)$$

Because of this torque, the electrons and their magnetic dipoles precess as gyroscopes. The angle of precession,  $\phi$ , is shown in Figure 6.14. The rate of change of the angular momentum equals the torque, or  $d\mathbf{P}/dt = \mathbf{T}$ . Thus the equation of motion for a magnetic dipole is

$$\frac{d\mathbf{m}}{dt} = -\gamma \mathbf{m} \times \mathbf{B}_0 \quad (6.27)$$

From this we can solve the angular frequency of precession (called the Larmor frequency):

$$\omega_0 = \gamma B_0 \quad (6.28)$$

Let us assume that both a static magnetic field with a flux density of  $B_0$  and a field of a high-frequency wave propagating into the  $z$  direction interact with an electron. The wave is circularly polarized in the  $xy$ -plane

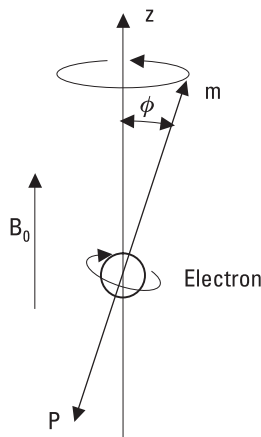


**Figure 6.14** An electron precessing in magnetic field.

and has a flux density of  $B_1$  ( $\ll B_0$ ). For a left-handed wave,  $\mathbf{B}_1 = \mathbf{B}_1^- = B_1(\mathbf{u}_x + j\mathbf{u}_y)$ . Now the total magnetic field is tilted by an angle of  $\theta = \arctan(B_1/B_0)$  with respect to the  $z$ -axis and precesses with the angular frequency of the wave,  $\omega$ . The torque due to the field produces precession of electrons in the counterclockwise direction in synchronism with the propagating wave, and therefore  $\phi < \theta$ . From the equation of motion we solve the component of the magnetic dipole moment  $m^-$  that rotates in synchronism with the left-handed circularly polarized wave

$$m^- = \frac{\gamma m_0 B_1}{\omega_0 + \omega} \quad (6.29)$$

where  $m_0 = m \cos \phi$ . Correspondingly, for a right-handed wave  $\mathbf{B}_1 = \mathbf{B}_1^+ = B_1(\mathbf{u}_x - j\mathbf{u}_y)$ , both fields produce precession in the clockwise direction, and therefore  $\phi > \theta$ , and

$$m^+ = \frac{\gamma m_0 B_1}{\omega_0 - \omega} \quad (6.30)$$

In ferromagnetic materials, the magnetic dipole moments are aligned parallel in regions called magnetic domains, even when no external field is present. When an external field is applied, the domains tend to orient parallel to the field. The magnetization of the material, or the magnetic dipole moment per unit volume, is  $\mathbf{M} = N\mathbf{m}$ , where  $N$  is the effective number of electrons per unit volume. When the external field increases, nearly all magnetic moments are aligned parallel to the field and a saturation magnetization  $\mathbf{M}_S$  is finally reached. Then the whole ferrite body behaves like a large magnetic dipole. The magnetic flux density in a saturated ferrite is

$$\mathbf{B} = \mu_0(\mathbf{H}_0 + \mathbf{M}_S) \quad (6.31)$$

As for a single electron, an equation of motion can be derived for magnetization. Equations analogous to (6.29) and (6.30) are obtained for circularly polarized waves by replacing  $m_0$  with  $Nm_0$ . From these it follows that the effective permeabilities for right-handed and left-handed circularly polarized waves are

$$\mu^+ = \mu_0 \mu_r^+ = \mu_0 \left( 1 + \frac{\gamma \mu_0 M_S}{\omega_0 - \omega} \right) \quad (6.32)$$

$$\mu^- = \mu_0 \mu_r^- = \mu_0 \left( 1 + \frac{\gamma \mu_0 M_S}{\omega_0 + \omega} \right) \quad (6.33)$$

when  $B_1 \ll B_0$  (small-signal conditions) and  $M = M_S$ . The matrix presentation is

$$\begin{bmatrix} B^+ \\ B^- \\ B_z \end{bmatrix} = \mu_0 \begin{bmatrix} \mu_r^+ & 0 & 0 \\ 0 & \mu_r^- & 0 \\ 0 & 0 & 1 \end{bmatrix} \begin{bmatrix} H^+ \\ H^- \\ H_z \end{bmatrix} \quad (6.34)$$

Thus the phase constant of a right-handed wave,  $\beta^+ = \omega \sqrt{\epsilon \mu^+}$ , and that of a left-handed wave,  $\beta^- = \omega \sqrt{\epsilon \mu^-}$ , are different.

## 6.2.2 Faraday Rotation

Let us consider a situation in which a plane wave propagates in ferrite in the  $z$  direction. A uniform, static magnetic field pointing to the  $z$  direction is applied over the ferrite. The wave is linearly polarized and the electric field is directed along the  $x$ -axis at  $z = 0$ . A linearly polarized wave can be divided into two orthogonal circularly polarized waves, as

$$\mathbf{E} = \mathbf{u}_x E_0 = (\mathbf{u}_x + j\mathbf{u}_y) \frac{E_0}{2} + (\mathbf{u}_x - j\mathbf{u}_y) \frac{E_0}{2} \quad (6.35)$$

The phase constants of these two components are  $\beta^-$  and  $\beta^+$ . At  $z = l$  the electric field is

$$\mathbf{E} = (\mathbf{u}_x + j\mathbf{u}_y) \frac{E_0}{2} e^{-j\beta^- l} + (\mathbf{u}_x - j\mathbf{u}_y) \frac{E_0}{2} e^{-j\beta^+ l} \quad (6.36)$$

This can be written as

$$\mathbf{E} = E_0 e^{-j(\beta^- + \beta^+)l/2} \{ \mathbf{u}_x \cos [(\beta^+ - \beta^-)l/2] - \mathbf{u}_y \sin [(\beta^+ - \beta^-)l/2] \} \quad (6.37)$$

The phase shift of the resultant wave is  $(\beta^- + \beta^+)l/2$  and the tilt angle with respect to the  $x$ -axis is

$$\theta = \arctan(E_y/E_x) = -(\beta^+ - \beta^-) \frac{l}{2} \quad (6.38)$$

Hence the tilt angle of the polarization vector changes as the wave propagates in a ferrite. This phenomenon is called the Faraday rotation. A typical change is  $100^\circ$  per centimeter at 10 GHz.

If the direction of propagation is reversed, the tilt angle rotates in the same direction with respect to the coordinate system. Therefore, as the wave propagates back from  $z = l$  to  $z = 0$ , the tilt angle does not return back from  $\theta$  to  $0^\circ$  but its value becomes  $2\theta$ . Consequently, the Faraday rotation is a nonreciprocal phenomenon.

Figure 6.15 shows how the phase and attenuation constants typically behave in a ferrite. When  $\omega_0 > \omega$ ,  $\beta^+ > \beta^-$ , and when  $\omega_0 < \omega$ ,  $\beta^+ < \beta^-$ . Thus, the direction of the Faraday rotation depends on whether the signal frequency is smaller or larger than the resonance frequency. Close to the resonance, the attenuation constant  $\alpha^+$  is large. Well below the resonance frequency, the attenuation constant is small, but then the difference between  $\beta^+$  and  $\beta^-$  is small and the tilt angle rotates slowly.

### Example 6.2

A linearly polarized wave at a frequency of  $f = 3$  GHz propagates in a ferrite into the direction of a static magnetic field with a flux density  $B_0 = 0.14$  Wb/m<sup>2</sup>. The ferrite has a saturation magnetization of  $\mu_0 M_S = 0.2$  Wb/m<sup>2</sup> and a relative permittivity of  $\epsilon_r = 10$ . Find the length of such a ferrite body that rotates the tilt angle by  $90^\circ$  as a wave passes through it.

### Solution

Using (6.25) and (6.28) we find the resonance frequency  $\omega_0 = \gamma B_0 = 24.64 \times 10^9$  1/s. Note that 1 Wb/m<sup>2</sup> = 1 T =  $10^4$  gauss. The angular frequency

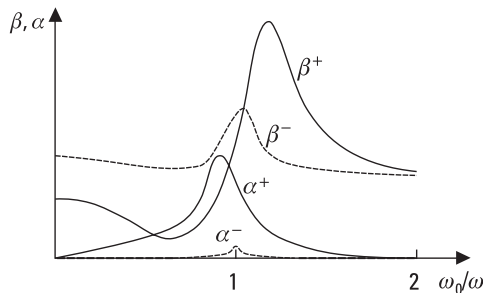


**Figure 6.15** Phase and attenuation constants for propagation in ferrite.

of the wave is  $\omega = 2\pi f = 18.85 \times 10^9$  1/s. From (6.32) and (6.33) we get the effective permeabilities for right-handed and left-handed circularly polarized waves as  $\mu^+ = 7.08\mu_0$  and  $\mu^- = 1.81\mu_0$ , respectively. Correspondingly, the phase constants are  $\beta^+ = \sqrt{\epsilon_r \mu_r^+} \omega/c = 8.41 \omega/c$  and  $\beta^- = \sqrt{\epsilon_r \mu_r^-} \omega/c = 4.25 \omega/c$ . Because  $\beta^+ > \beta^-$ , the angle  $\theta$  is negative and the tilt angle rotates counterclockwise as the wave propagates. By setting  $\theta = -\pi/2$  in (6.38) we solve  $l = \pi(\beta^+ - \beta^-) = 12$  mm. Also, lengths producing a rotation of  $\theta = -\pi/2 - n\pi$  ( $n$  is a positive integer) give a tilt angle of  $-90^\circ$  for the output wave. If the wave would propagate to the direction opposite to the field, the tilt angle would rotate clockwise, as seen to the direction of propagation, but in the same direction with respect to the coordinate system as before.

### 6.2.3 Isolators

An ideal isolator passes signals in the forward direction without loss but totally absorbs signals propagating in the reverse direction. In practice, the insertion loss may be below 0.5 dB in the forward direction and more than 20 dB in the reverse direction for a good isolator. Isolators are used for matching and for stabilizing oscillators against frequency changes due to varying load impedance.

The operation of an isolator may be based on a ferromagnetic resonance, on shifting of field pattern, or on the Faraday rotation. Figure 6.16 shows a waveguide isolator. There is a ferrite rod in a circular waveguide in a static magnetic field. Because of the Faraday rotation, the polarization of a wave propagating in the forward direction turns  $45^\circ$  clockwise in the ferrite. This wave does not attenuate significantly in the resistive cards at the input and output, because the electric field is now perpendicular to both cards. The polarization of a reverse wave turns  $45^\circ$  counterclockwise, as seen, to the

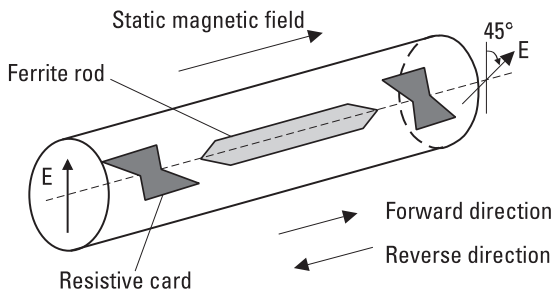


**Figure 6.16** Waveguide isolator based on the Faraday rotation.



direction of propagation. The electric field is now parallel to the resistive card at the output (output for reverse direction) and the wave is absorbed.

### 6.2.4 Circulators

An ideal circulator is an  $n$ -port device, which passes a signal applied in port 1 to port 2, a signal applied in port 2 to port 3, and finally a signal applied in port  $n$  to port 1. Usually, a circulator has three ports.

A three-port circulator can be used as an isolator by terminating one of the ports with a matched load. Circulators are used to separate the input and output ports of such devices that are based on reflection (e.g., reflection amplifier). Circulators are also used in radars to couple the transmitted power to the antenna and the echo signals from the antenna to the receiver.

A circulator may be based on the Faraday rotation or on a direction-dependent phase shift. The Y-junction circulator is the most common type. A cylindrical ferrite is placed in the middle of a symmetric junction, as shown in Figure 6.17. A static magnetic field is along the axis of the cylinder. The operation of this circulator may be explained by two degenerate resonance modes whose resonance frequencies differ due to the magnetic field [4, 5]. The operation range is between these two resonance frequencies.

## 6.3 Other Passive Components and Devices

In addition to the reciprocal power dividers and directional couplers and nonreciprocal ferrite devices, many other passive devices and components

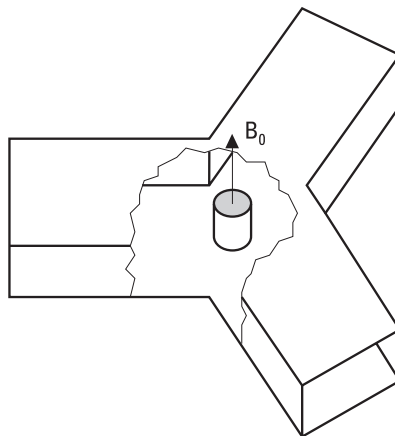


**Figure 6.17** Y-junction circulator.

are needed in radio engineering. Terminations, attenuators, phase shifters, connectors, and adapters are briefly discussed here.

### 6.3.1 Terminations

Terminations are single-port components that are used for terminating transmission lines, waveguides, and ports of different devices. Matched loads (in an ideal case  $\rho = 0$ ), shorts or short circuits ( $\rho = -1$ ), and open ends or open circuits ( $\rho = +1$ ) are terminations that are commonly used in measurements and in the calibration of measurement equipment.

A matched load absorbs all the power that is incident on it. Therefore, the impedance of a matched load equals the characteristic impedance of the line it terminates. A matched load can be realized by inserting a wedge, card, or pyramid made of lossy material in the waveguide, as shown in Figure 6.18(a). The length of the load should be at least one wavelength. A matched load is often adjustable; that is, the position of the absorber can be adjusted. Then, in measurements requiring a good accuracy, we may eliminate the effect of reflection from a nonideal matched load by performing the measurements with several positions of the load. A good matched load may have a *VSWR* less than 1.01. In a microstrip line, a matched load can be realized by terminating the line with a thin-film resistor followed by a shorting pin, as illustrated in Figure 6.18(b).

An ideal short circuit reflects the incident power totally. As a matched load, a short also may be fixed or adjustable. With an adjustable short we can realize a desired reactance: The impedance in a lossless line at a distance of  $l$  from the short is

$$Z = jZ_0 \tan \beta l \quad (6.39)$$

A metal block tightly fit in a coaxial line or waveguide serves as a simple short. However, in such a short the contact between the line and metal block is erratic if the short is moved. Figure 6.19 shows a structure

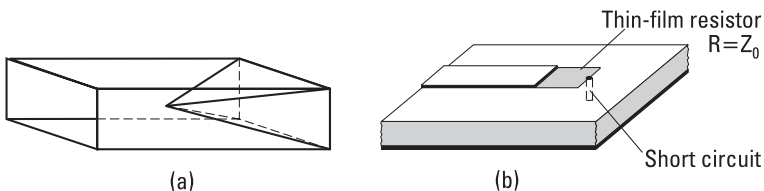


**Figure 6.18** Matched loads: (a) in waveguide; and (b) in microstrip line.

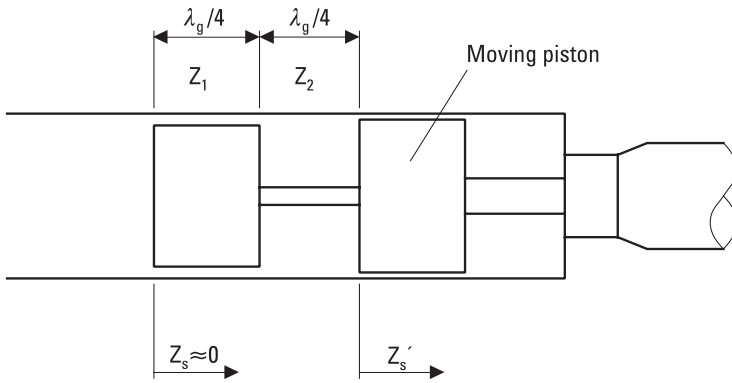


**Figure 6.19** Adjustable short.

that is better suited for an adjustable short. It is made of high- and low-impedance quarter-wave sections that operate as impedance inverters. If the characteristic impedances of the low-impedance and high-impedance sections are  $Z_1$  and  $Z_2$ , respectively, the input impedance is

$$Z_s = \left(\frac{Z_1}{Z_2}\right)^2 Z_s' \tag{6.40}$$

where  $Z_s'$  is the impedance indicated in Figure 6.19. Thus  $Z_s$  is much lower than  $Z_s'$ , which already has a low value. The disadvantage of this short is its narrow bandwidth, about 10%; the length of the sections is a quarter wavelength only at a single frequency.

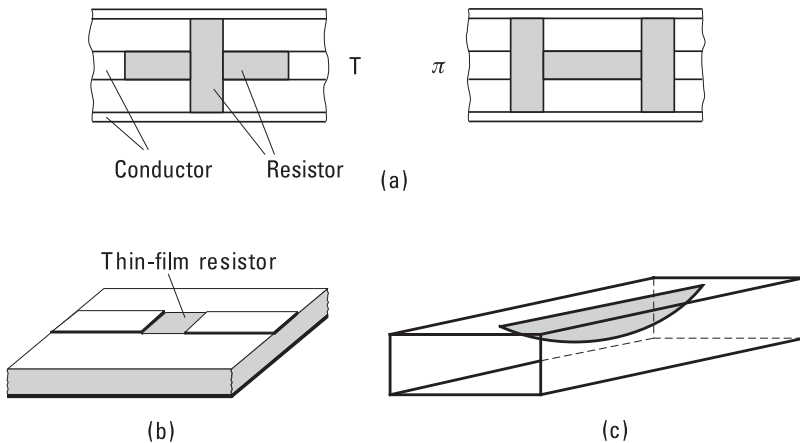
Often an open-ended line does not correspond well to an ideal open circuit. The fringing fields of an open end of a coaxial line may be modeled as a small capacitor or as an extension of the line. An open-ended waveguide radiates effectively and operates as an antenna; thus, it does not resemble an open circuit at all. An open-ended microstrip line is quite a good open circuit; it only needs to be slightly shortened to compensate for the length extension due to a fringing field.

### 6.3.2 Attenuators

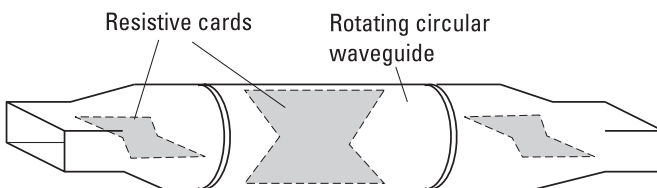
An ideal attenuator passes a given part of the incident power, absorbs the rest, and has matched ports. Lowering a power level, improving impedance matching, and measuring power ratios are applications of attenuators. The value of attenuation may be fixed or adjustable.

Figure 6.20(a) shows two fixed coaxial attenuators made of series-connected and parallel-connected resistors in a T and  $\pi$  configuration. In a microstrip circuit, T and  $\pi$  attenuators can be realized with the same principle using thin-film resistors. Figure 6.20(b) shows a simple microstrip line attenuator. The waveguide attenuator shown in Figure 6.20(c) has a resistive card in the middle of the broad wall along the direction of the  $E$  field. The card is tapered to ensure good matching.

Figure 6.21 shows a continuously adjustable waveguide attenuator. It has a rotating, circular waveguide section between a rectangular input and output waveguide. All three sections contain thin resistive cards. The input signal passes the first card with a negligible attenuation because the electric field of the  $TE_{10}$  wave mode is perpendicular to the card. Then the wave enters through a transition to the circular waveguide. The attenuation is adjusted by rotating the circular waveguide section and the resistive card within it. The field of the  $TE_{11}$  wave mode can be divided into two compo-



**Figure 6.20** Fixed attenuators: (a) coaxial attenuators, T- and  $\pi$ -type; (b) microstrip attenuator; and (c) waveguide attenuator.



**Figure 6.21** Adjustable waveguide attenuator.

nents, one perpendicular to the card and the other parallel to it. The latter component is absorbed by the card; the former component enters the output waveguide in which again its component parallel to the resistive card is absorbed. We can show that the attenuation in decibels is [1]

$$L = -40 \log (\sin \theta) \text{ dB} \quad (6.41)$$

where  $\theta$  is the angle between the electric field at the input and the plane of the resistive card in the circular section.

### 6.3.3 Phase Shifters

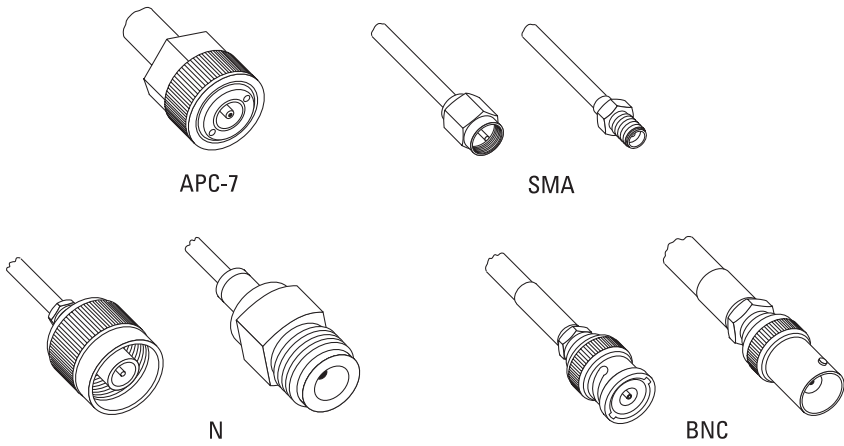
An ideal phase shifter is lossless and matched; it only shifts the phase of the output wave, or in other words, changes the phase difference between the output and input waves. Phase shifters are needed, for example, in phased antenna arrays.

An adjustable waveguide phase shifter can be realized by replacing the resistive card of the attenuator in Figure 6.20(c) with a dielectric card whose depth in the waveguide is adjustable. A structure resembling the attenuator in Figure 6.21 also operates as a phase shifter when the resistive cards are replaced with dielectric cards having proper lengths [1]. Electrically controlled phase shifters are much faster than mechanical phase shifters. They are often based on semiconductor devices such as *p-i-n* diodes or *field effect transistors* (FETs).

### 6.3.4 Connectors and Adapters

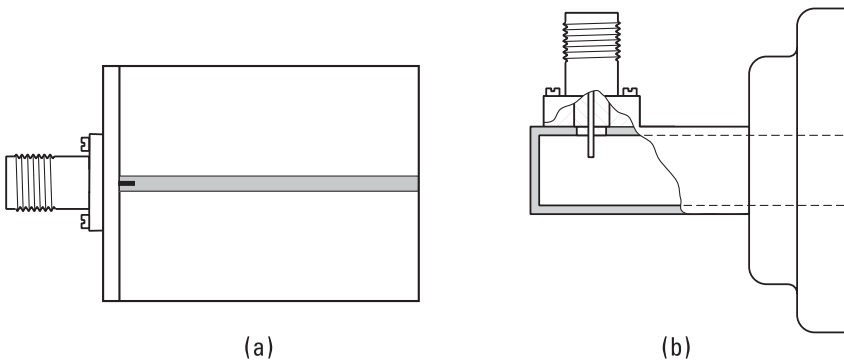
Connectors are needed to join different lines, devices, and circuit blocks together. An ideal connector is matched and lossless. Practical connectors cause small discontinuities. Therefore, unnecessary use of connectors should be avoided. The quality of connectors gets more and more important as the frequency gets higher.

Figure 6.22 shows some common coaxial connectors used at RF and microwave frequencies. An APC-7 connector is a precision connector that is used in measurements requiring good accuracy and repeatability. It is a sexless connector whose inner diameter of its outer conductor is 7 mm. SMA and N connectors are good enough for most cases. These connectors can be either male or female type. BNC connectors work best at frequencies below 1 GHz; at higher frequencies they may radiate. Waveguide components have flanges at their ports. Alignment pins on the flanges ensure accurate connection.



**Figure 6.22** Some common coaxial connectors.

Adapters are needed to connect components having connectors of different types or of the same sex. Figure 6.23(a) shows a transition from a coaxial line to a microstrip line. Coaxial and waveguide components can be connected using the adapter illustrated in Figure 6.23(b).



**Figure 6.23** (a) Coaxial-to-microstrip transition; and (b) waveguide-to-coaxial adapter.

## References

- [1] Collin, R. E., *Foundations for Microwave Engineering*, 2nd ed., New York: IEEE Press, 2001.
- [2] Pozar, D. M., *Microwave Engineering*, 2nd ed., New York: John Wiley & Sons, 1998.

- [3] Rodrigue, G. P., "A Generation of Microwave Ferrite Devices," *Proc. IEEE*, Vol. 76, No. 2, 1988, pp. 121–137.
- [4] Fay, C. E., and R. L. Comstock, "Operation of the Ferrite Junction Circulator," *IEEE Trans. on Microwave Theory and Techniques*, Vol. 13, No. 1, 1965, pp. 15–27.
- [5] Lahey, J., "Junction Circulator Design," *Microwave Journal*, Vol. 32, No. 11, 1989, pp. 26–45.

# 7

## Resonators and Filters

Transmission line and waveguide devices, discussed in Chapter 6, would ideally operate over a broad bandwidth. However, the useful bandwidth may be limited, for example, by the frequency dependence of the line sections that have proper electrical lengths only at the design frequency. Resonators and filters are intentionally frequency-selective devices.

### 7.1 Resonators

Resonators are used for stabilizing the frequency of oscillators, as building blocks of filters, as sensors in material measurements, and so on.

There are a large number of different resonator structures. Lumped components, coils and capacitors, are usable in realizing resonators at radio frequencies. Resonators based on the piezoelectric effect in a quartz crystal operate up to the VHF range. In micromechanical resonators made using *microelectromechanical systems* (MEMS) technology, electrical signals are coupled with the mechanical vibrations of a resonating beam [1]. Micromachined beam resonators may soon become usable at the UHF range. An open-circuited or short-circuited line, a closed metal cavity, a cylindrical pill made of a ceramic material, and a sphere made of ferrite (yttrium iron garnet, YIG) are examples of resonators operating at microwave frequencies. Open quasi-optical resonators become usable in the millimeter-wave range and at higher frequencies.



### 7.1.1 Resonance Phenomenon

A resonator is a structure having a natural frequency of oscillation. A circuit consisting of a coil and a capacitor, shown in Figure 7.1, forms a simple electromagnetic resonator. At first the switch is open and the capacitor is charged to a voltage  $V$ . The electric field of the capacitor contains an energy of  $W_e = CV^2/2$ , where  $C$  is the capacitance of the capacitor. After the switch is closed, a current starts to flow through the coil. When the capacitor has completely discharged, the current  $I$  is at maximum and the whole energy of the circuit is in the magnetic field of the coil. This energy is  $W_m = LI^2/2$ , where  $L$  is the inductance of the coil. Then the current will again charge the capacitor, but now the polarity of the voltage is reversed. At resonance, the average energy in the electric field  $CV^2/4$  is equal to the average energy in the magnetic field  $LI^2/4$ . The resonance frequency of the circuit is

$$f_r = \frac{1}{2\pi\sqrt{LC}} \quad (7.1)$$

If energy is applied to the circuit from an external source at the resonance frequency and in the correct phase, the energy contained in the circuit will increase. However, due to losses in the circuit, the energy does not increase indefinitely. The losses are modeled with a conductance  $G$  in a parallel resonant circuit and with a resistance  $R$  in a series resonant circuit, as shown in Figure 7.2. Also, resonators made of transmission lines and waveguides can be modeled with equivalent circuits containing lumped elements.

### 7.1.2 Quality Factor

The quality factor of a resonator is defined as

$$Q = \frac{\omega_r W}{P_l} \quad (7.2)$$

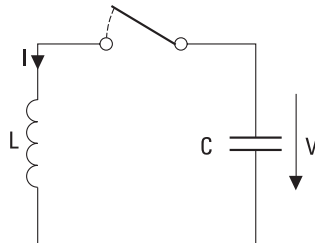


**Figure 7.1** Resonator composed of a coil and a capacitor.

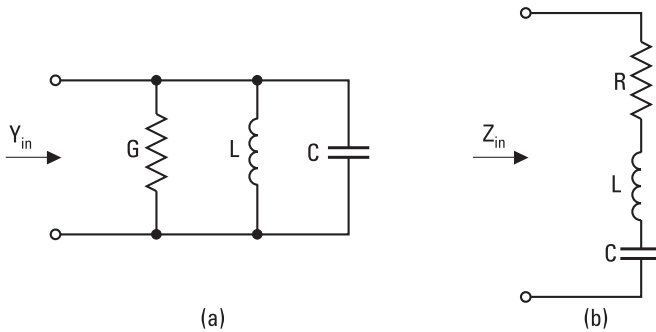


**Figure 7.2** (a) Parallel resonant circuit; and (b) series resonant circuit.

where  $\omega_r = 2\pi f_r$  is the angular resonance frequency,  $W$  is the energy stored in the resonator, and  $P_l$  is the power loss in the resonator.

When the energy source of the resonator is closed off, the stored energy decreases from its original value  $W_0$  exponentially as  $W(t) = W_0 e^{-j\delta t}$ . The damping factor  $\delta = \omega_r/(2Q)$  describes how fast the energy in the resonator decreases. Conversely, when the energy source is switched on, the energy increases from zero to its final value  $W_0$  as  $W(t) = W_0(1 - e^{-j\delta t})$ . The larger the quality factor, the longer the time required to charge or discharge the resonator.

Let us consider the parallel resonant circuit in Figure 7.2(a). The analysis of a series resonant circuit is a dual case: We replace  $G$  with  $R$ , interchange  $C$  and  $L$ , replace admittance quantities with impedance quantities, and replace current sources with voltage sources. Because the power loss of the parallel resonant circuit is  $P_l = GV^2/2$ , the quality factor is

$$Q = \frac{\omega_r W}{P_l} = \frac{\omega_r CV^2/2}{GV^2/2} = \frac{\omega_r C}{G} = \frac{1}{G\omega_r L} \quad (7.3)$$

The input admittance of the resonator is

$$Y_{in} = G + j\omega C + \frac{1}{j\omega L} \quad (7.4)$$

At the resonance frequency, the input admittance is real:  $Y_{in} = G$ . At frequencies close to the resonance, the input impedance is approximately

$$Y_{in} \approx G + j\Delta\omega 2C = G \left( 1 + j2Q \frac{\Delta\omega}{\omega_r} \right) = G + jB \quad (7.5)$$

where  $\Delta\omega = \omega - \omega_r$  ( $|\Delta\omega| \ll \omega_r$ ), Hence on the Smith chart the input impedance moves on a constant-conductance circle as the frequency changes. Close to the resonance frequency, the susceptance  $B$  is directly proportional to the frequency deviation  $\Delta f = \Delta\omega/(2\pi)$  from the resonance frequency  $f_r$ .

Let us assume that an ac current source is connected to the parallel resonant circuit above. At resonance  $B = 0$ , and current flows through the conductance  $G$ . The power loss in the resonator is now at its maximum. The more the frequency deviates from  $f_r$ , the larger the magnitude of the susceptance and the smaller the current through the conductance. As  $\Delta\omega = \pm\Delta\omega_{3dB} = \pm\omega_r/(2Q)$ , the real and imaginary parts of the input impedance are equal, the magnitude of the admittance is  $\sqrt{2}G$ , and the phase of the admittance is  $\pm\pi/4$ . Then the power loss in the resonator is half of that at the resonance frequency. Thus the quality factor may also be defined with the half-power frequencies illustrated in Figure 7.3 as

$$Q = \frac{\omega_r}{2\Delta\omega_{3dB}} = \frac{f_r}{2\Delta f_{3dB}} \tag{7.6}$$

In other words, the quality factor of a resonator is a measure of its selectivity. The higher the quality factor, the narrower the frequency response of a resonator.

### 7.1.3 Coupled Resonator

A resonator may have one, two, or more couplings to the external circuit. Figure 7.4 shows the normalized equivalent circuits of resonators having one

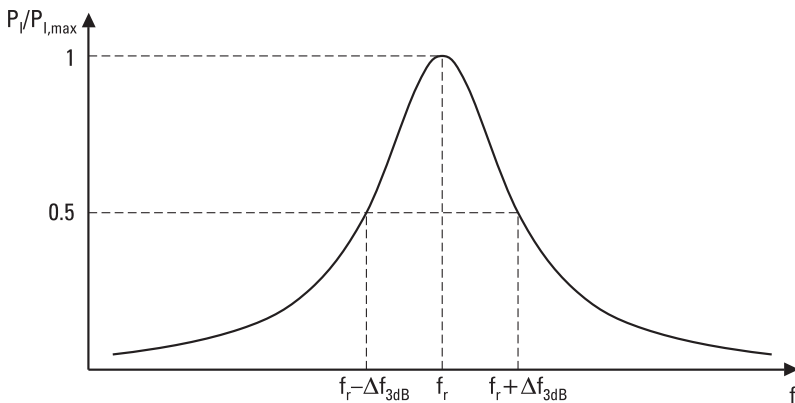


**Figure 7.3** Power absorbed in a resonator.

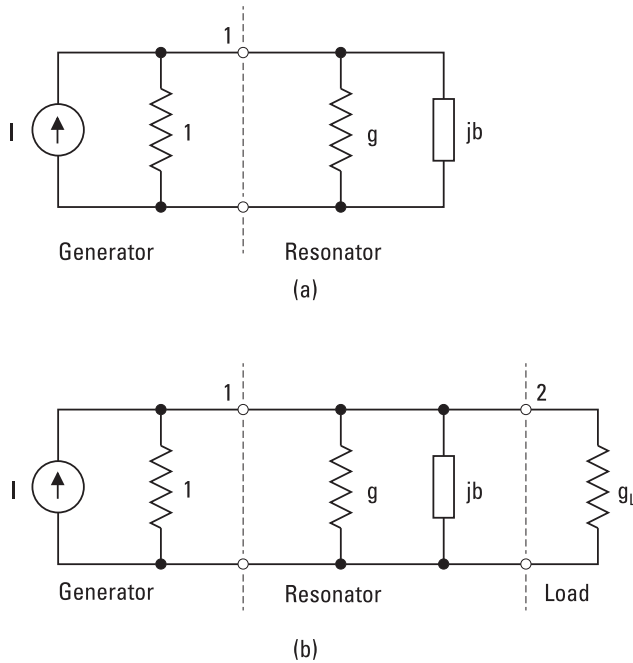


**Figure 7.4** Equivalent circuits of resonators: (a) one coupling; and (b) two couplings.

and two couplings. A generator (current source) having a normalized output admittance of 1 is connected to port 1. The load admittance at port 2 of the resonator having two couplings is  $g_L$ .

Let us consider at first the resonator with one coupling. The normalized input impedance is

$$y_{in} = g + jb \quad (7.7)$$

The total conductance of the circuit is  $1 + g$ , whereas that of the resonator alone is  $g$ . Therefore, the resonance curve such as that in Figure 7.3 has a peak that is broader by a factor of  $(1 + g)/g$  when the external coupling is taken into account.

The power loss in the circuit is divided into two parts, for each of which we can define a quality factor. The unloaded quality factor  $Q_0$  is related to the loss in the resonator. Absorption in the metal walls and in the dielectric medium and radiation into free space are the sources of this loss.  $Q_0$  can be obtained from those frequencies  $f_r \pm \Delta f_0$  at which  $g = b$ :

$$Q_0 = \frac{f_r}{2\Delta f_0} \quad (7.8)$$

The external quality factor  $Q_e$  is a measure of losses in the external circuit. From those frequencies  $f_r \pm \Delta f_e$  at which  $1 = b$ , we get

$$Q_e = \frac{f_r}{2\Delta f_e} \quad (7.9)$$

The loaded quality factor  $Q_L$  describes the losses of the whole circuit. From frequencies  $f_r \pm \Delta f_L$  at which  $1 + g = b$ , we get

$$Q_L = \frac{f_r}{2\Delta f_L} \quad (7.10)$$

Because the power loss is inversely proportional to the corresponding quality factor, we can combine different loss components as

$$\frac{1}{Q_L} = \frac{1}{Q_0} + \frac{1}{Q_e} \quad (7.11)$$

or in other words, the total loss equals the sum of the loss in the resonator and the loss in the external circuit.

Figure 7.5 illustrates how the quality factors can be obtained from the input admittance  $y_{in}(f)$  presented on the Smith chart. From the intersection points of  $y_{in}(f)$  with the lines  $b = g$ ,  $b = 1$ , and  $b = 1 + g$ , we get the frequency deviations  $\Delta f_0$ ,  $\Delta f_e$ , and  $\Delta f_L$ , from which we calculate  $Q_0$ ,  $Q_e$ , and  $Q_L$  using (7.8) through (7.10).

If  $Q_e > Q_0$  ( $1 < g$ ), the resonator loss at the resonance is larger than the loss in the external circuit; the resonator is undercoupled. For an overcoupled resonator,  $Q_e < Q_0$  ( $1 > g$ ), and the resonator loss at the resonance is smaller than the external loss. The coupling is called critical when  $Q_e = Q_0$ ; then the resonator is matched to the generator at resonance.

For a resonator having two couplings we can define two external quality factors:  $Q_{e1}$  for port 1 and  $Q_{e2}$  for port 2. The elements of the equivalent circuits can also be represented using the quality factors as  $g = Q_{e1}/Q_0$ ,  $g_L = Q_{e1}/Q_{e2}$ , and  $b = gQ_0 2\Delta f/f_r = Q_{e1} 2\Delta f/f_r$ . The transducer power loss of the resonator is

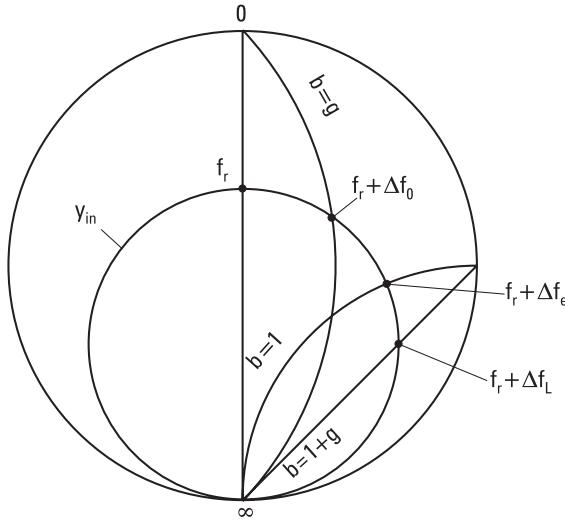


**Figure 7.5** Solving the quality factors of a resonator from the input admittance versus frequency on the Smith chart. Input admittance  $y_{in}$  of an overcoupled resonator is presented.

$$L = \frac{P_a}{P_L} = \frac{(1 + g + g_L)^2 + b^2}{4g_L} = \frac{Q_{e1}Q_{e2}}{4Q_L^2} \left[ 1 + Q_L^2 \left( \frac{2\Delta f}{f_r} \right)^2 \right] \quad (7.12)$$

where  $P_a = I^2/4$  is the available power from the current source and  $P_L$  is the power coupled to the load.

### 7.1.4 Transmission Line Section as a Resonator

Let us consider a section of a short-circuited transmission line with a length  $l$ , shown in Figure 7.6. Its series resistance, series inductance, and parallel capacitance per unit length are  $R'$ ,  $L'$ , and  $C'$ , respectively. For an air-filled line the parallel conductance may be neglected. The input impedance of the line is

$$Z_{in} = Z_0 \tanh(j\beta l + \alpha l) = Z_0 \frac{\tanh \alpha l + j \tan \beta l}{1 + j \tan \beta l \tanh \alpha l} \quad (7.13)$$

We assume that the total loss is small so that  $\tanh \alpha l \approx \alpha l$ . Close to the frequency  $f_r$ , at which  $l = \lambda_g/2$ ,  $\tan \beta l = \tan(\pi + \pi\Delta f/f_r) = \tan(\pi\Delta f/f_r) \approx \pi\Delta f/f_r$ . Now (7.13) simplifies to

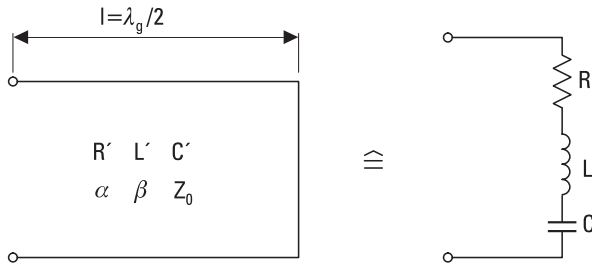


**Figure 7.6** Short-circuited  $\lambda_g/2$ -long transmission line and its equivalent circuit.

$$Z_{in} \approx Z_0(\alpha l + j\pi\Delta f/f_r) \tag{7.14}$$

The resistance is constant and the reactance is directly proportional to the frequency deviation; thus a short-circuited  $\lambda_g/2$ -long transmission line resembles a series resonant circuit. Because  $Z_0 = \sqrt{L'/C'}$ ,  $\alpha = (R'/2)\sqrt{C'/L'}$ , and  $\beta l = \omega_r l \sqrt{L'C'} = \pi$ , then

$$Z_{in} \approx R'l/2 + jL'l\Delta f \tag{7.15}$$

On the other hand, close to the resonance frequency, the input impedance of a series resonant circuit made of lumped elements is

$$Z_{in} \approx R + j2L\Delta f \tag{7.16}$$

By comparing (7.15) and (7.16), we see the relationship between the distributed quantities and the lumped elements of the equivalent circuit:  $R = R'l/2$ ,  $L = L'l/2$ , and  $C = 1/(\omega_r^2 L) = 1/(\omega_r^2 Z_0^2 C'l/2)$ .

The reactance of a short-circuited 50-Ω line and that of a corresponding LC series resonant circuit are compared in Figure 7.7. We see that close to the resonance frequency these two circuits have nearly similar properties. The quality factor of the transmission-line resonator is

$$Q = \frac{\omega_r L}{R} = \frac{\omega_r L'}{R'} = \frac{\beta}{2\alpha} \tag{7.17}$$

As before, we can show that an open-circuited  $\lambda_g/4$ -long line corresponds to a series resonant circuit, whereas a short-circuited  $\lambda_g/4$ -long line and an open-circuited  $\lambda_g/2$ -long line correspond to a parallel resonant circuit.

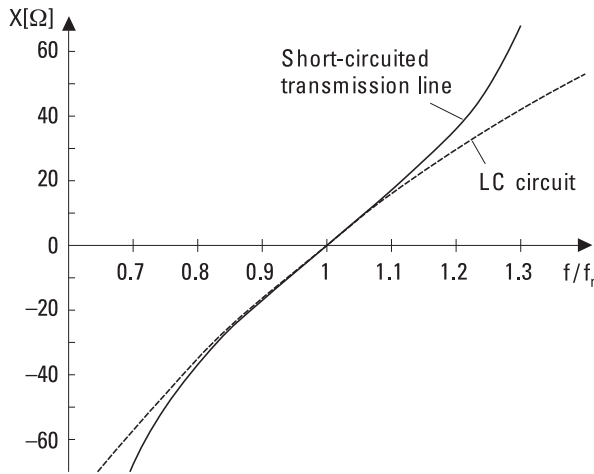


**Figure 7.7** The reactance  $X$  versus frequency for a short-circuited transmission line and an LC series resonant circuit. The length of the line is  $\lambda_g/2$  at  $f_r$ .

### 7.1.5 Cavity Resonators

Metal cavities can be used as resonators at microwave frequencies. A cavity resonator has a closed structure, except for the couplings to the external circuit, and thus has no radiative loss. The quality factor of a cavity resonator may be high—several thousands or even more.

Often a cavity resonator is made of a section of a waveguide or a coaxial line short-circuited at both ends. At resonance a standing wave is formed in the cavity as the wave bounces back and forth between the ends. Thus the length of the cavity is half of a wavelength or a multiple of that at the resonance frequency. A given cavity has an infinite number of resonance frequencies, unlike a resonator made of lumped elements.

Figure 7.8 shows three ways to couple a field into a cavity or from it: a loop, a probe, and a hole.

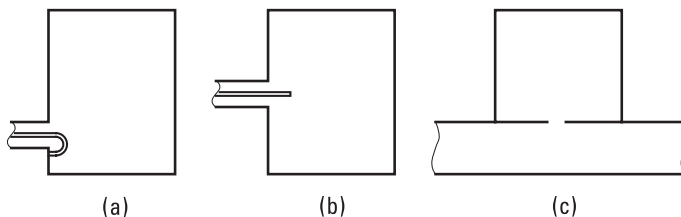


**Figure 7.8** Couplings to a cavity: (a) loop; (b) probe; and (c) hole.



the fields of the resonance mode have some common components with the fields of the coupling element. Therefore, a loop at the maximum of the magnetic field perpendicular to the field or a probe at the maximum of the electric field along the field works as a good coupling element. In order for the hole coupling to be successful, the fields of the waveguide and cavity should have some common components at the coupling hole. Different resonance modes that may be excited at a given frequency can often be discriminated by choosing the proper position for the coupling element. The coupling coefficient  $\beta_{ci} = Q_0/Q_{ei}$  at port  $i$  is used to describe the strength of the coupling.

Close to the resonance, a cavity resonator may be modeled with a parallel resonant or series resonant  $RLC$  circuit. A parallel resonant circuit may be transformed into a series resonant circuit and vice versa by changing the position of the reference plane at which the resonator input is assumed to be. Often it is more practical to treat a cavity resonator with its quality factors.

Let us consider the air-filled rectangular cavity shown in Figure 7.9 [2]. We can regard it as a section of a rectangular waveguide having short circuits at planes  $z = 0$  and  $z = d$ . The phase constant of the  $TE_{nm}$  and  $TM_{nm}$  wave modes is

$$\beta_{nm} = \sqrt{k_0^2 - \left(\frac{n\pi}{a}\right)^2 - \left(\frac{m\pi}{b}\right)^2} \tag{7.18}$$

where  $k_0 = \omega\sqrt{\mu_0\epsilon_0} = 2\pi/\lambda_0$ . Since at resonance the length of the cavity is  $l\lambda_g/2$  ( $l$  is integer),

$$\beta_{nm} = \frac{l\pi}{d} \tag{7.19}$$

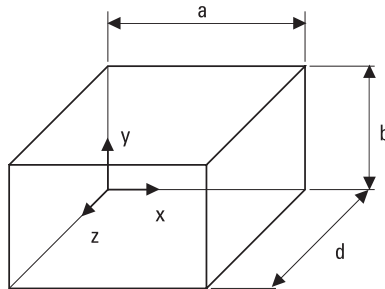


**Figure 7.9** Rectangular cavity resonator.

From (7.18) and (7.19) we solve

$$k_0 = k_{nml} = \sqrt{\left(\frac{n\pi}{a}\right)^2 + \left(\frac{m\pi}{b}\right)^2 + \left(\frac{l\pi}{d}\right)^2} \quad (7.20)$$

Resonance frequencies corresponding to these discrete values of  $k_{nml}$  are

$$f_{nml} = \frac{ck_{nml}}{2\pi} = \frac{c}{2} \sqrt{\left(\frac{n}{a}\right)^2 + \left(\frac{m}{b}\right)^2 + \left(\frac{l}{d}\right)^2} \quad (7.21)$$

This equation is valid for both the  $TE_{nm}$  and  $TM_{nm}$  wave modes. Resonance modes having the same resonance frequency but a different field distribution are called degenerate modes.

Let us study in more detail the resonance mode  $TE_{101}$ , that is, a resonance that is excited in a cavity that is half-wave long at the fundamental wave mode  $TE_{10}$ . This is the mode having the lowest resonance frequency if  $b < a < d$ . We find the field distribution by summing up waves propagating into the  $+z$  and  $-z$  directions:

$$E_y = (E^+ e^{-j\beta z} + E^- e^{j\beta z}) \sin \frac{\pi x}{a} \quad (7.22)$$

$$H_x = -\frac{1}{Z_{TE}} (E^+ e^{-j\beta z} - E^- e^{j\beta z}) \sin \frac{\pi x}{a} \quad (7.23)$$

$$H_z = \frac{j\lambda}{\eta 2a} (E^+ e^{-j\beta z} + E^- e^{j\beta z}) \cos \frac{\pi x}{a} \quad (7.24)$$

Because  $E_y = 0$  at  $z = 0$ ,  $E^- = -E^+$ .  $E_y$  must also be zero at  $z = d$ , which leads to  $\beta = \pi/d$ . By denoting  $E_0 = -2jE^+$ , we get

$$E_y = E_0 \sin \frac{\pi x}{a} \sin \frac{\pi z}{d} \quad (7.25)$$

$$H_x = -j \frac{E_0}{\eta} \frac{\lambda}{2d} \sin \frac{\pi x}{a} \cos \frac{\pi z}{d} \quad (7.26)$$

$$H_z = j \frac{E_0}{\eta} \frac{\lambda}{2a} \cos \frac{\pi x}{a} \sin \frac{\pi z}{d} \quad (7.27)$$

The energy stored is the maximum energy of the electric field because then the energy of the magnetic field is zero. This energy is

$$W = \frac{\epsilon_0}{2} \int_0^d \int_0^b \int_0^a |E_y|^2 dx dy dz = \frac{\epsilon_0 abd}{8} E_0^2 \quad (7.28)$$

The loss can be calculated if the surface current  $J_s$  and the surface resistance  $R_s$  are known on all walls of the cavity. The surface current, or current per unit width, is

$$\mathbf{J}_s = \mathbf{n} \times \mathbf{H} \quad (7.29)$$

where  $\mathbf{n}$  is a unit vector perpendicular to the surface. Equations (7.25) through (7.27) are valid in case of ideal, lossless conductors but they can be applied with good accuracy in case of low-loss conductors. The power loss is obtained by integrating over all the surfaces of the cavity:

$$P_l = \frac{R_s}{2} \int_S |J_s|^2 dS = \frac{R_s \lambda^2}{8\eta^2} E_0^2 \left[ \frac{ab}{d^2} + \frac{bd}{a^2} + \frac{1}{2} \left( \frac{a}{d} + \frac{d}{a} \right) \right] \quad (7.30)$$

By combining (7.28) and (7.30) we get the quality factor of TE<sub>101</sub> mode as

$$Q = \frac{\omega_r W}{P_l} = \frac{\pi \eta}{4R_s} \left[ \frac{2b(a^2 + d^2)^{3/2}}{ad(a^2 + d^2) + 2b(a^3 + d^3)} \right] \quad (7.31)$$

The quality factor of a cubical ( $a = b = d$ ) cavity is

$$Q = \frac{\sqrt{2}\pi}{6} \frac{\eta}{R_s} = 0.742 \frac{\eta}{R_s} \quad (7.32)$$

If the cavity is filled with a lossy dielectric having a permittivity of  $\epsilon = \epsilon' - j\epsilon''$ , the quality factor describing the dielectric loss is [3]

$$Q_d = \frac{\epsilon'}{\epsilon''} \quad (7.33)$$

This equation is valid for all resonance modes.

**Example 7.1**

A cubical cavity resonator made of copper has a side length of 20 mm. Find the resonance frequency of the fundamental mode and the quality factor.

**Solution**

The fundamental mode is  $TE_{101}$ . When  $a = b = d = 20$  mm,  $n = l = 1$ , and  $m = 0$ , we get, from (7.21), the resonance frequency as  $f_{101} = 10.6$  GHz. The conductivity of copper is  $\sigma = 5.8 \times 10^7$  S/m. At the resonance frequency the surface resistance is  $R_s = \sqrt{\omega\mu_0/(2\sigma)} = 0.027\Omega$ . From (7.31) or (7.32) we solve  $Q = 10,400$ . In practice  $Q$  is lower because  $R_s$  is higher due to surface roughness and because couplings have some loss.

In principle, the quality factor of other resonance modes may be calculated the same way as the quality factor of the  $TE_{101}$  mode. Note that the name of a resonance mode also depends on the choice of the coordinate system. For example, the  $TE_{101}$  mode is called the  $TM_{110}$  mode if the  $y$ -axis is chosen to be “the direction of propagation.” At a given frequency, the higher the order of the resonance mode, the larger the cavity needed. As the size of the cavity increases, the ratio of the volume to the surface area increases, leading to a higher quality factor. In the case of a large cavity, however, the resonance frequencies of different modes are close to each other, and it is difficult to excite only a particular mode.

A cylindrical cavity is a section of a circular waveguide. The lowest order resonance mode is  $TE_{111}$ . At this mode the height of the cylinder is  $\lambda_g/2$  at the fundamental mode  $TE_{11}$ . The resonance mode  $TE_{011}$  of a cylindrical cavity is exceptionally important. This mode has a high quality factor and no axial surface currents, which facilitates the realization of an adjustable cavity because the moving short does not need to make a good contact with the cylinder walls.

**7.1.6 Dielectric Resonators**

It is not possible to make high-quality resonators with microstrip techniques because microstrip lines are rather lossy and radiate easily. However, dielectric resonators [4] can easily be used in connection with microstrip circuits.

Dielectric resonators are usually small, cylindrical pills made of ceramic materials such as  $Ba_2Ti_9O_{20}$ ,  $BaTi_4O_9$ , or  $(Zr-Sn)TiO_4$ . Such materials have a good temperature stability, low loss, and high dielectric constant, typically  $\epsilon_r = 10$  to 100. Because of the large dielectric constant, the size of

a dielectric resonator is much smaller than the size of a cavity resonator operating at the same frequency. Electric and magnetic fields concentrate within the resonator, but part of the field is outside the cylinder and this part may be employed in coupling. The radiation loss is low and the quality factor is mainly determined by the loss in the dielectric material. The unloaded quality factor  $Q_0$  is typically 4,000 to 10,000 at 10 GHz. A given resonator can operate at several resonance modes, of which the  $TE_{01\delta}$  mode is the most used.

Dielectric resonators are used in filters and transistor oscillators at frequencies from 1 to 50 GHz. If the frequency of an oscillator is stabilized with a dielectric resonator, it is called a *dielectric resonator oscillator* (DRO). Figure 7.10 shows how a DRO is coupled to a microstrip line. The magnetic fields of the line and the resonator have common components. The resonator is simply placed on the substrate, and the strength of the coupling can be adjusted by changing the distance of the resonator from the strip. To reduce radiation loss, the structure is enclosed within a metal case.

## 7.2 Filters

A resonator with two couplings passes through signals having frequencies near the resonance frequency; in other words, it acts as a bandpass filter. A hollow metal waveguide acts as a highpass filter, because it has a cutoff frequency that depends on the dimensions.

In general a filter is a two-port, which prevents propagation of undesired signals while desired signals pass it. In an ideal case, there is no insertion loss in the passband, but the attenuation in the stopband is infinite. Depending on the appearance of these bands, the filter is said to be a bandpass, bandstop, lowpass, or highpass filter. An ideal filter has a linear phase response, which allows a signal containing several frequency components to pass through

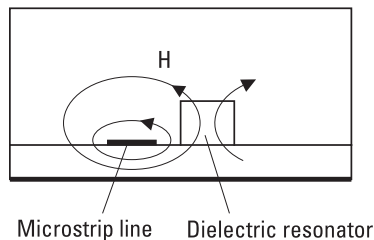


**Figure 7.10** Dielectric resonator coupled to a microstrip line.

without distortion. Filters are used also for multiplexing (combining signals at different frequencies) and demultiplexing (separating signals at different frequencies). Also, reactive impedance matching circuits, tuning circuits in oscillators and amplifiers, delay lines, and slow-wave structures act as filters.

In the design of filters, two basic methods are used: the image parameter method and insertion loss method [3, 5, 6]. In the image parameter method, simple filter sections are cascaded to provide the desired passband-stopband characteristics. However, the required frequency response for the whole frequency range cannot be exactly synthesized. An iterative design process is used to improve the frequency response. On the contrary, the insertion loss method allows the synthesis of an exact response. We study the insertion loss method in more detail in the following section.

A filter design using the insertion loss method gives as a result a circuit consisting of lumped elements. At microwave frequencies, distributed elements are used instead of lumped ones as already discussed in Chapter 4. To realize distributed elements corresponding to the desired lumped elements, we use transmission line sections and aid the design with Richards' transformation, the Kuroda identities, as well as the impedance and admittance inverters.

### 7.2.1 Insertion Loss Method

In the insertion loss method, the filter design and synthesis is started by choosing the desired frequency response. This is followed by calculation of the normalized (in terms of frequency and impedance) component values for a lowpass filter prototype. These normalized component values can also be obtained from tables presented in the literature [6]. Then the normalized filter is converted to the desired frequency band and impedance level.

The insertion loss of a filter containing only reactive elements is obtained from its reflection coefficient as

$$L = \frac{1}{1 - |\rho(\omega)|^2} \quad (7.34)$$

The power reflection coefficient  $|\rho(\omega)|^2$  of all realizable linear, passive circuits can be expressed as a polynomial of  $\omega^2$ , that is, it is an even function of  $\omega$ . It follows from this fact that the insertion loss of (7.34) can always be written as [3, 7]

$$L = 1 + \frac{P(\omega^2)}{Q^2(\omega)} \quad (7.35)$$

where  $P$  is a polynomial of  $\omega^2$  and  $Q$  is a polynomial of  $\omega$ .

The most frequently used filter responses are the maximally flat and Chebyshev responses. In the following we study these filter responses in more detail.

**Maximally Flat Response** The maximally flat response is also called the *binomial* or *Butterworth response*. It provides the flattest possible passband for a given order of the filter, that is, in practice for a given number of reactive elements. The insertion loss for the lowpass filter prototype is

$$L = 1 + k^2 \left( \frac{\omega}{\omega_c} \right)^{2N} \quad (7.36)$$

where  $N$  is the order of the filter and  $\omega_c$  is its cutoff (angular) frequency. Note that here  $Q^2(\omega) = 1$ . The passband is from 0 to  $\omega_c$ , and at  $\omega_c$  the insertion loss is  $L = 1 + k^2$ . Most often the band edge is chosen to be the 3-dB point, and then  $k = 1$ . At frequencies well above the cutoff frequency ( $\omega \gg \omega_c$ ) the insertion loss is  $L \approx k^2(\omega/\omega_c)^{2N}$  and, thus, it increases  $20N$  dB per decade.

**Chebyshev Response** The Chebyshev response is often also called the *equal-ripple response*. The insertion loss is

$$L = 1 + k^2 T_N^2 \left( \frac{\omega}{\omega_c} \right) \quad (7.37)$$

where  $T_N$  is the  $N$ th order Chebyshev polynomial, which can also be written as

$$T_N \left( \frac{\omega}{\omega_c} \right) = \cos \left[ N \arccos \left( \frac{\omega}{\omega_c} \right) \right] \quad (7.38)$$

when  $0 \leq \omega/\omega_c \leq 1$ , and

$$T_N \left( \frac{\omega}{\omega_c} \right) = \cosh \left[ N \operatorname{arcosh} \left( \frac{\omega}{\omega_c} \right) \right] \quad (7.39)$$

when  $\omega/\omega_c \geq 1$ . In the passband,  $L$  varies between values 1 and  $1 + k^2$ . At  $\omega = 0$  the insertion loss is  $L = 1$  if  $N$  is odd, and  $L = 1 + k^2$ , if  $N$  is even. When  $\omega \gg \omega_c$ ,  $L \approx k^2(2\omega/\omega_c)^{2N}/4$ , which is to say, the insertion loss increases  $20N$  dB per decade, as is also the case with a maximally flat response. The insertion loss is, however,  $2^{2N}/4$  times larger than that of a maximally flat response of the same order. In Figure 7.11 these responses are compared to each other.

Other important filter responses are the elliptic amplitude response and the linear phase response. The insertion loss of the maximally flat and Chebyshev responses increases monotonically in the stopband. In some applications a given minimum stopband insertion loss is adequate but a sharper cutoff response is desired. In such a case an elliptic filter is a good choice [8]. In some other applications (e.g., in multiplexers) a phase response as linear as possible is desired. Then a linear phase filter is the correct choice. However, a good phase response and a sharp cutoff response are incompatible requirements, so in designing a filter for a good phase response one must compromise with the amplitude response.

A normalized lowpass filter consists of shunt (parallel) capacitors and series inductors  $g_k$ . The generator source impedance is  $g_0 = 1\Omega$  or the source admittance is  $g_0 = 1S$ , depending on whether the filter prototype starts with a shunt capacitor or with a series inductor, respectively, and the cutoff

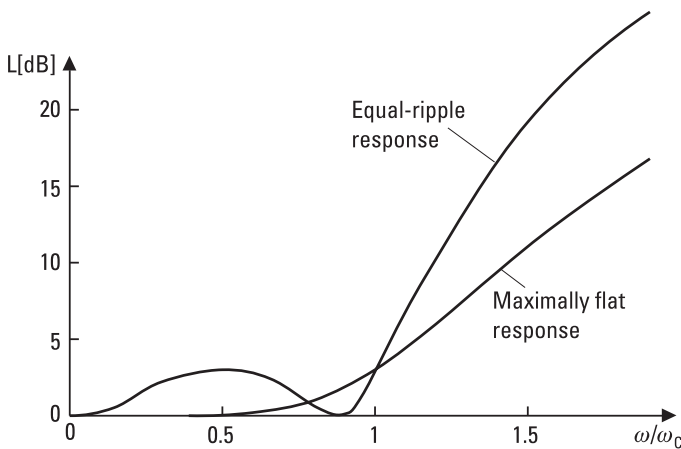


**Figure 7.11** Maximally flat and Chebyshev (equal-ripple) responses of a lowpass filter ( $N = 3$ ,  $k = 1$ ).



frequency is  $\omega_c = 1$ . The order  $N$  of the filter is the number of reactive elements in the filter. As already discussed, the first element may be a shunt element, as in Figure 7.12(a), or a series element, as in Figure 7.12(b). The response in both cases is the same. The element  $g_{N+1}$  is the load resistance if  $g_N$  is a shunt capacitor, and the load conductance if  $g_N$  is a series inductor.

With the equivalent circuits presented in Figure 7.12, it is possible to calculate the component values that provide a given response. For the maximally flat response the prototype component values are  $g_0 = 1$ ,  $g_{N+1} = 1$ , and

$$g_k = 2 \sin \left[ \frac{(2k - 1)\pi}{2N} \right] \tag{7.40}$$

where  $k = 1 \dots N$ . For the Chebyshev response, calculation of the component values is more difficult, so we omit it here. Tables 7.1 through 7.3 represent element values for maximally flat and Chebyshev (equal ripple) lowpass filter prototypes.

After the lowpass filter prototype design is completed, the circuit designed is converted to the correct frequency and correct impedance level.

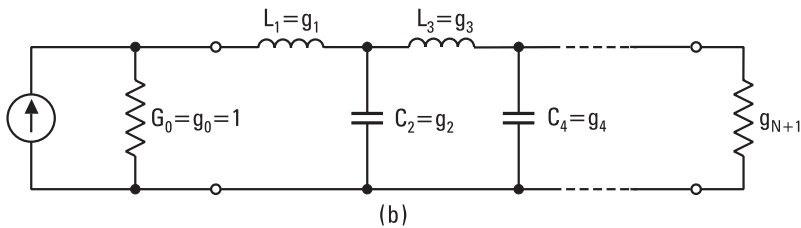
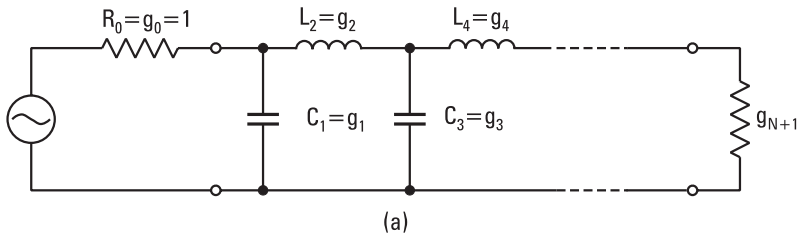


**Figure 7.12** Lowpass filter prototypes: beginning with (a) a parallel element, and (b) a series element.

**Table 7.1**  
Element Values for the Maximally Flat Lowpass Filter Prototype  
( $g_0 = 1, \omega_c = 1$ )

$N$	$g_1$	$g_2$	$g_3$	$g_4$	$g_5$	$g_6$	$g_7$
1	2.0000	1.0000					
2	1.4142	1.4142	1.0000				
3	1.0000	2.0000	1.0000	1.0000			
4	0.7654	1.8478	1.8478	0.7654	1.0000		
5	0.6180	1.6180	2.0000	1.6180	0.6168	1.0000	
6	0.5176	1.4142	1.9318	1.9318	1.4142	0.5176	1.0000

Source: [6].

**Table 7.2**  
Element Values for a Chebyshev Lowpass Filter Prototype  
( $g_0 = 1, \omega_c = 1, \text{ripple } 0.5 \text{ dB}$ )

$N$	$g_1$	$g_2$	$g_3$	$g_4$	$g_5$	$g_6$	$g_7$
1	0.6986	1.0000					
2	1.4029	0.7071	1.9841				
3	1.5963	1.0967	1.5963	1.0000			
4	1.6703	1.1926	2.3661	0.8419	1.9841		
5	1.7058	1.2296	2.5408	1.2296	1.7058	1.0000	
6	1.7254	1.2479	2.6064	1.3137	2.4758	0.8696	1.9841

Source: [6].

**Table 7.3**  
Element Values for a Chebyshev Lowpass Filter Prototype  
( $g_0 = 1, \omega_c = 1, \text{ripple } 3.0 \text{ dB}$ )

$N$	$g_1$	$g_2$	$g_3$	$g_4$	$g_5$	$g_6$	$g_7$
1	1.9953	1.0000					
2	3.1013	0.5339	5.8095				
3	3.3487	0.7117	3.3487	1.0000			
4	3.4389	0.7483	4.3471	0.5920	5.8095		
5	3.4817	0.7618	4.5381	0.7618	3.4817	1.0000	
6	3.5045	0.7685	4.6061	0.7929	4.4641	0.6033	5.8095

Source: [6].

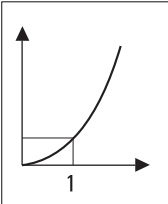
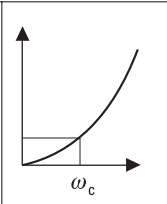
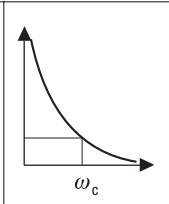
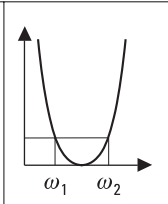
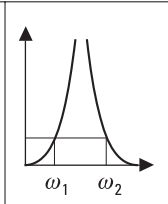
If the generator resistance is  $R_0$ , the scaled element values (symbols with prime) are

$$L'_k = R_0 L_k \tag{7.41}$$

$$C'_k = C_k / R_0 \tag{7.42}$$

$$R'_L = R_0 R_L \tag{7.43}$$

where  $L_k$ ,  $C_k$ , and  $R_L$  are the prototype values  $g_k$  and  $g_{N+1}$ . Figure 7.13 shows the scaling of the cutoff frequency from 1 to  $\omega_c$ , and the transformations to a highpass, bandpass, and bandstop filter. In a bandpass filter, an  $LC$  series circuit corresponds to a series inductor of the lowpass prototype, and an  $LC$  parallel circuit corresponds to a shunt capacitor of the lowpass prototype. On the other hand, in a bandstop filter, an  $LC$  parallel circuit corresponds to a series inductor, and an  $LC$  series circuit corresponds to a shunt capacitor of the lowpass prototype. In the equations for Figure 7.13,  $\omega_0 = \sqrt{\omega_1 \omega_2}$ ,  $\Delta = (\omega_2 - \omega_1) / \omega_0$ , and  $\omega_1$  and  $\omega_2$  are the limits of the filter frequency band.

				
$L_k$	$L'_k = \frac{L_k}{\omega_c}$	$C'_k = \frac{1}{\omega_c L_k}$	$L'_k = \frac{L_k}{\Delta \omega_0}$ $C'_k = \frac{\Delta}{\omega_0 L_k}$	$L'_k = \frac{\Delta L_k}{\omega_0}$ $C'_k = \frac{1}{\Delta \omega_0 L_k}$
$C_k$	$C'_k = \frac{C_k}{\omega_c}$	$L'_k = \frac{1}{\omega_c C_k}$	$C'_k = \frac{C_k}{\Delta \omega_0}$ $L'_k = \frac{\Delta}{\omega_0 C_k}$	$C'_k = \frac{\Delta C_k}{\omega_0}$ $L'_k = \frac{1}{\Delta \omega_0 C_k}$

**Figure 7.13** Frequency scaling and transformations of a lowpass filter prototype,  $\omega_0 = \sqrt{\omega_1 \omega_2}$ ,  $\Delta = (\omega_2 - \omega_1) / \omega_0$ .

The insertion-loss frequency response of a lowpass filter provides a frequency response of a highpass filter, when in (7.36) and (7.37)  $\omega/\omega_c$  is replaced with  $\omega_c/\omega$ . The frequency response of a bandpass filter is obtained by replacing  $\omega/\omega_c$  with the term  $(\omega/\omega_0 - \omega_0/\omega)/\Delta$ , and that of a bandstop filter by replacing  $\omega/\omega_c$  with the term  $\Delta/(\omega/\omega_0 - \omega_0/\omega)$ .

## 7.2.2 Design of Microwave Filters

At microwave frequencies we have two major problems in realizing the synthesized filters. First, good lumped elements do not exist; instead we must use distributed elements. The frequency behavior of the distributed elements is more complicated than that of the lumped ideal ones, which makes the filter synthesis difficult. However, design of a narrow-band filter is easy, because over a narrow bandwidth many distributed elements may be modeled by ideal inductors and capacitors. Second, the filter elements should be physically close to each other (in wavelength scale), which is often impossible in practice. Therefore, transmission line sections must be used to separate the filter elements.

Richards' transformation is used to transform the lumped elements into sections of transmission lines. Richards' transformation [9]

$$\Omega = \tan \beta l = \tan (\omega l / v_p) \quad (7.44)$$

maps the  $\omega$  plane to the  $\Omega$  plane. By replacing  $\omega$  with  $\Omega$ , we can write the reactance of an inductor and the susceptance of a capacitor, respectively, as

$$jX_L = j\Omega L = jL \tan \beta l \quad (7.45)$$

$$jB_C = j\Omega C = jC \tan \beta l \quad (7.46)$$

This means that an inductor can be replaced with a short-circuited stub having an electrical length of  $\beta l$  and a characteristic impedance of  $L$ . Accordingly, a capacitor can be replaced with an open-circuited stub having an electrical length of  $\beta l$  and a characteristic impedance of  $1/C$ . The cutoff frequency of the transformed filter is the same as that of the prototype ( $\omega_c = 1$ ), if  $\Omega = 1 = \tan \beta l$ , or  $l = \lambda_g/8$ . At frequencies where  $\omega$  differs a lot from  $\omega_c$ , the response of the transformed filter differs considerably from the response of the prototype. The response is periodic, repeating every  $4\omega_c$ .

With the aid of the Kuroda identities [5, 10, 11] we can separate the transmission line stubs physically from each other, transform the series stubs

into parallel stubs (or vice versa), and also transform characteristic impedances to a more easily realizable level. Figure 7.14 shows the four Kuroda identities, where an inductance represents a short-circuited stub, a capacitance represents an open-circuited stub, and a box represents a transmission line with a characteristic impedance marked in the box. All stubs are of the same length—for example,  $\lambda_g/8$  at the angular frequency of  $\omega_c$ —and  $n^2 = 1 + Z_2/Z_1$ .

**Example 7.2**

Design a lowpass microstrip filter with the following characteristics: cutoff frequency of 3 GHz, Chebyshev response with  $N = 3$ , ripple of 0.5 dB, and filter impedance of  $50\Omega$ .

**Solution**

The element values for the prototype filter are  $g_0 = G_0 = 1$ ,  $g_1 = L_1 = 1.5963$ ,  $g_2 = C_2 = 1.0967$ ,  $g_3 = L_3 = 1.5963$ , and  $g_4 = G_L = 1$ ; see Table 7.2 and Figure 7.15(a). Using Richards' transformation, we can transform the inductances into series stubs and the capacitance into a parallel stub, as shown in Figure 7.15(b). The length of all stubs is  $\lambda_g/8$  at 3 GHz. Because

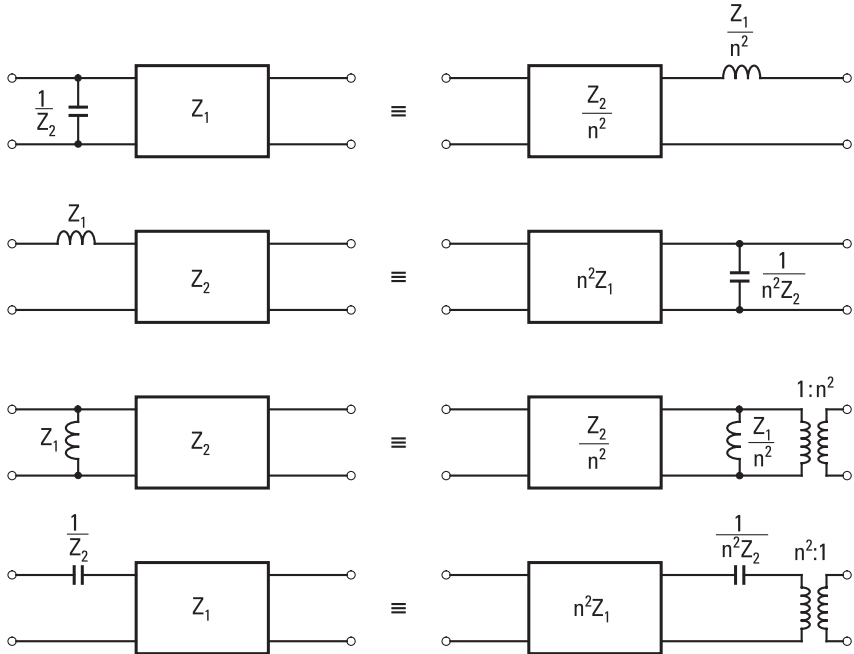


**Figure 7.14** The four Kuroda identities.

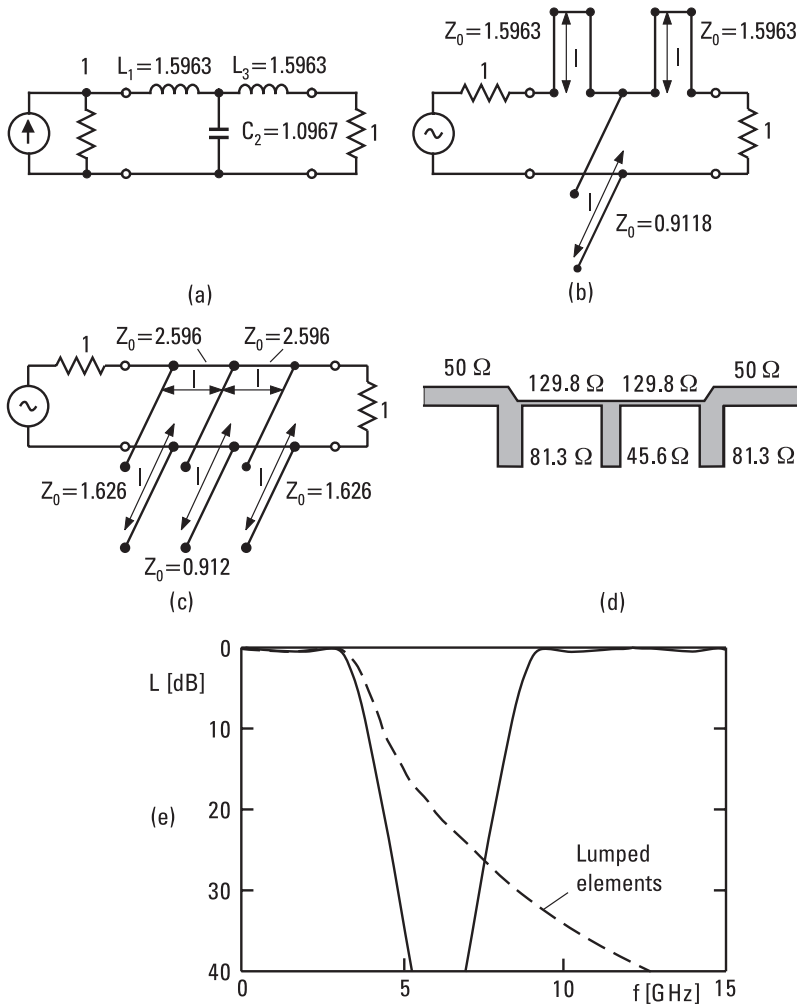


**Figure 7.15** Design of a lowpass filter: (a) a lowpass filter prototype; (b) lumped inductors and capacitors converted to transmission line stubs ( $l = \lambda_g/8$  at 3 GHz) using Richards' transformation; (c) series stubs transformed to parallel stubs using a Kuroda identity; (d) microstrip layout of the filter; and (e) calculated frequency response.

the series stubs cannot be realized with microstrip lines, we transform them into parallel stubs using a Kuroda identity. In order to be able to do that, we first add a transmission line section with a length of  $\lambda_g/8$  and a characteristic impedance of  $Z_0 = 1$  into both ends of the filter. These sections do not affect the filter response because the generator and load are matched to these

lines. The second Kuroda identity of Figure 7.14, with  $Z_1 = 1.5963$ ,  $Z_2 = 1$ ,  $n^2 = 1 + Z_2/Z_1 = 1.6264$ ,  $n^2 Z_1 = 2.596$ , and  $1/(n^2 Z_2) = 0.615$ , is then used for both ends of the filter. The result is shown in Figure 7.15(c). Finally, the impedances are scaled by multiplying by  $50\Omega$ , and the line lengths are calculated to be  $\lambda_g/8$  at 3 GHz. The stub characteristic impedances are  $50n^2 Z_2 = 81.3\Omega$ ,  $50/C_2 = 45.6\Omega$ , and  $81.3\Omega$ , and the transmission line sections between the stubs have a characteristic impedance of  $50n^2 Z_1 = 129.8\Omega$ . In order to find the exact line lengths and widths we should know the characteristics of the substrate and use (3.85) through (3.93). However, a schematic layout is presented in Figure 7.15(d), and its calculated frequency response is presented in Figure 7.15(e). When this response is compared with that of a filter made of lumped elements, we observe that in the passband the responses are nearly equal, but above the cutoff frequency the insertion loss of the microstrip filter increases more quickly and the response has another passband at 12 GHz.

As in the preceding example, in most filters we want to use only parallel (or series) elements. In the microwave region we often prefer parallel stubs. In addition to the Kuroda identities, this transformation can also be done using impedance or admittance inverters. The impedance inverters are also called the  $K$ -inverters and the admittance inverters the  $J$ -inverters. For example, an ideal quarter-wave transformer is both a  $K$ - and a  $J$ -inverter. It transforms a load impedance  $Z_L$  into an impedance  $Z_{in} = K^2/Z_L$  or a load admittance  $Y_L$  into an admittance  $Y_{in} = J^2/Y_L$ . Here  $K$  is the characteristic impedance and  $J$  the characteristic admittance of the transformer. A quarter-wave transformer, however, behaves approximately as an ideal inverter only over a narrow bandwidth, and therefore this method is suitable only for narrow-band filters. Figure 7.16 shows how a bandpass filter is transformed into a filter circuit consisting only of either series or parallel resonators. The characteristic impedance values of the impedance and admittance inverters are presented in Table 7.4.

$R_{aG}$ ,  $R_{aL}$ ,  $L_{ak}$ , and  $C_{ak}$  can be chosen freely, as long as the resonance frequency of the resonant circuits is the same as the filter center frequency or  $\omega_0 = 1/\sqrt{L_{ak}C_{ak}}$  and the impedance values of the inverters are calculated according to Table 7.4. We may also choose a value 1 for  $R_{aG}$  and  $R_{aL}$ , as well as for the inverters, and then calculate values for  $L_{ak}$  and  $C_{ak}$  starting from one end of the filter. The  $LC$  parallel or series resonant circuits can be realized, for example, with open- and short-circuited transmission line stubs with a length of  $\lambda_g/4$  or its multiple (see also Section 7.1.4). The characteristic impedance of a short-circuited stub with a length of  $\lambda_g/4$  must

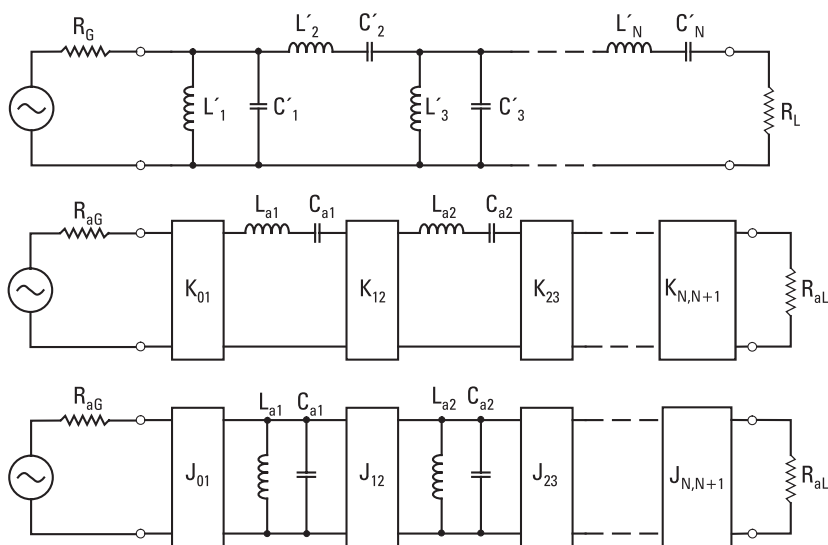


**Figure 7.16** A bandpass filter, and the same filter transformed using impedance and admittance inverters.

**Table 7.4**

Characteristics of the Impedance and Admittance Inverters ( $k = 1 \dots N - 1$ )

	$k/N$ odd	$k/N$ even
$K_{01}$	$(L'_1 R_{aG} / C_{a1} R_G)^{1/2}$	$(L'_1 R_{aG} / C_{a1} R_G)^{1/2}$
$K_{k,k+1}$	$(L_{ak} L_{ak+1} / C'_k L'_{k+1})^{1/2}$	$(L_{ak} L_{ak+1} / L'_k C'_{k+1})^{1/2}$
$K_{N,N+1}$	$(L_{aN} R_{aL} / C'_N R_L)^{1/2}$	$(L_{aN} R_{aL} R_L / L'_N)^{1/2}$
$J_{01}$	$(C_{a1} / C'_1 R_{aG} R_G)^{1/2}$	$(C_{a1} / C'_1 R_{aG} R_G)^{1/2}$
$J_{k,k+1}$	$(C_{ak} C_{ak+1} / C'_k L'_{k+1})^{1/2}$	$(C_{ak} C_{ak+1} / L'_k C'_{k+1})^{1/2}$
$J_{N,N+1}$	$(C_{aN} / C'_N R_{aL} R_L)^{1/2}$	$(C_{aN} R_L / L'_N R_{aL})^{1/2}$

be  $Z_0 = (\pi/4) \sqrt{L_{ak} / C_{ak}}$ , which may be difficult to realize because of its low value.

### Example 7.3

Design a bandpass filter with the following specifications: maximally flat response with  $N = 3$ , frequency range from 950 to 1,050 MHz, filter impedance of  $50\Omega$ .



**Solution**

Now  $f_1 = 950$  MHz,  $f_2 = 1,050$  MHz, and  $f_0 = 998.7$  MHz. From Table 7.1 we can read the element values for the lowpass filter prototype:  $g_0 = R_G = 1$ ,  $g_1 = C_1 = 1$ ,  $g_2 = L_2 = 2$ ,  $g_3 = C_3 = 1$ ,  $g_4 = R_L = 1$ . Let us transform the lowpass prototype into a bandpass filter using the equations presented in Figure 7.13:  $C_1' = C_1/\Delta\omega_0 = C_1/(\omega_2 - \omega_1) = 1.592 \times 10^{-9} = C_3'$ ,  $L_2' = L_2/(\omega_2 - \omega_1) = 3.183 \times 10^{-9}$ .  $L_1'$ ,  $C_2'$ , and  $L_3'$  are obtained from condition  $L_k' C_k' = 1/\omega_0^2$ .  $L_2'$  and  $C_2'$  form a series resonant circuit in series. Let us transform this into a shunt element using a  $J$ -inverter. We can choose  $R_{aG} = 1$  and  $J = 1$ . From Table 7.4 we obtain  $C_{a1} = C_1'$ ,  $C_{a2} = L_2'$ ,  $C_{a3} = C_3'$ , and  $R_{aL} = 1$ . The parallel resonant circuits can be realized with short-circuited stubs with a length of  $\lambda_g/4$ . From equation  $z_k = (\pi/4)\sqrt{L_{ak}/C_{ak}} = \pi/(4\omega_0 C_{ak})$  we obtain the normalized characteristic impedances of the lines:  $z_1 = z_3 = 0.079$  and  $z_2 = 0.039$ . The characteristic impedances of the short-circuited parallel stubs are  $Z_1 = Z_3 = 4.0\Omega$  and  $Z_2 = 2.0\Omega$ . Between these stubs there are inverters with a  $50\text{-}\Omega$  characteristic impedance and a  $\lambda_g/4$  length. The short-circuited stubs may also be  $3\lambda_g/4$  long and then the characteristic impedances are three times these values. However, they are still extremely hard to realize and the response differs even more from the response obtained with a filter formed with lumped elements.

**7.2.3 Practical Microwave Filters**

A large number of different possible structures can be used to realize a synthesized filter. In the following we briefly describe some commonly used filter structures. Other filters and their design rules are presented in the literature [6].

A simple lowpass filter can be realized by coupling short transmission line sections in series, with alternating low and high characteristic impedances. A short (electrical length  $\beta l < \pi/4$ ) line with a high characteristic impedance  $Z_0$  corresponds approximately to a series reactance of

$$X \approx Z_0 \beta l \quad (7.47)$$

Accordingly, a short line with a low characteristic impedance corresponds to a parallel susceptance of

$$B \approx \beta l / Z_0 \quad (7.48)$$

From the element values of the prototype filter we can calculate the required electrical lengths of the lines. The ratio of the high and low impedance should be as high as possible. The longer the line sections, the further from the ideal the response will be. Usually there are also passbands at higher frequencies. Figure 7.17 shows a microstrip layout of such a stepped-impedance filter with six line sections. One must also remember that an abrupt change in the microstrip line width causes a fringing capacitance, which must be taken into account in determining the lengths of the sections.

The bandpass and bandstop filters consist of series and parallel resonant circuits. In the microwave region the resonators can be realized in various ways, and then filters can be constructed from them in a number of ways. Figure 7.18(a) shows a bandpass filter consisting of open-circuited  $\lambda_g/2$  long microstrip lines that are side-coupled over a length of  $\lambda_g/4$  to each other [12]. This structure is suitable for filters with a passband width less than 20%. Figure 7.18(b) shows a microstrip bandpass filter consisting of end-coupled  $\lambda_g/2$  resonators. The small gap between the line ends corresponds to a series capacitance. This capacitance is necessarily rather small due to

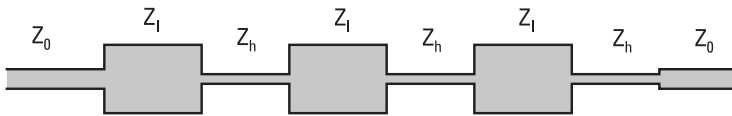


**Figure 7.17** Microstrip layout of a stepped-impedance lowpass filter.

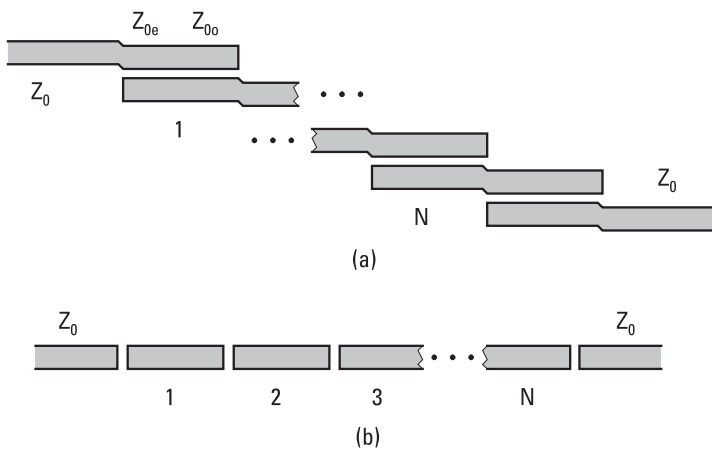


**Figure 7.18** Microstrip layouts of bandpass filters: (a) side-coupled line resonators; and (b) capacitive-gap coupled (end-coupled) line resonators.

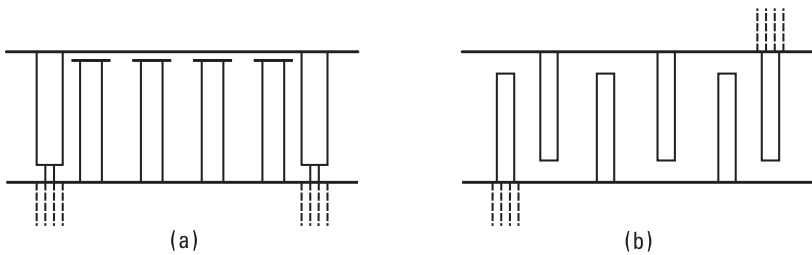
limitations in fabricating small gaps using microstrip techniques, and therefore the resulting bandwidth is rather small.

A comb-line filter consists of resonators with a length less than  $\lambda_g/4$ , which are grounded in one end and capacitively loaded in the other end. Figure 7.19(a) shows a comb-line filter consisting of rectangular or circular metal posts in a rectangular metal box. By adding a metal plate to the end of each capacitively loaded resonator, the end capacitance can be increased. A fine-tuning of the resonance frequency may be done with tuning screws.

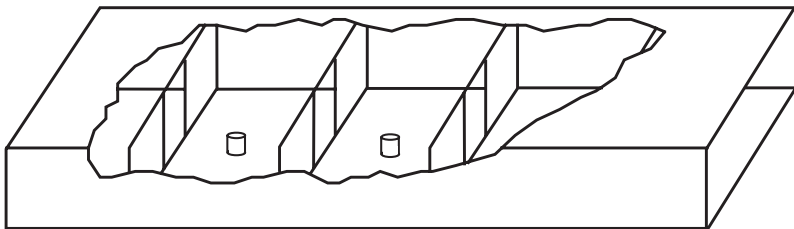
An interdigital filter also consists of  $\lambda_g/4$ -long resonators, which are grounded in one end and open in the other end, as shown in Figure 7.19(b). This structure is suitable for a broad bandpass filter. The comb-line and interdigital filters can also be manufactured using microstrip medium.

Figure 7.20 shows a bandpass filter made in a metal waveguide from iris-coupled resonators. The resonator cavities are  $\lambda_g/2$  long and separated by thin metal walls, each containing a rectangular or circular inductive iris. The resonance frequency of each individual resonator can be tuned with a tuning screw through the broad waveguide wall in the middle of the resonator.

A waveguide-cavity filter, a comb-line filter, or an interdigital filter can be made much smaller if the metal housing is filled with a ceramic of



**Figure 7.19** (a) Comb-line filter; and (b) interdigital filter.



**Figure 7.20** Bandpass filter made from waveguide cavities coupled through inductive irises.

high permittivity ( $\epsilon_r = 10$  to 100). Such a ceramic interdigital filter at 5 GHz with a 100 MHz passband may have dimensions of  $10 \times 4 \times 3 \text{ mm}^3$ , and its insertion loss is typically 1 dB. Ceramic filters are used also in mobile phones as duplex filters, with dimensions like  $10 \times 5 \times 2 \text{ mm}^3$ , but in this application such dimensions are considered large, and the tendency is to move to using *surface acoustic wave* (SAW) or *bulk acoustic wave* (BAW) filters [13, 14].

A SAW filter is based on an acoustic wave propagating on the surface of a piezoelectric medium. The SAW filters are bandpass filters of a small size. The electric signal is transformed into an acoustic wave with an interdigital transducer and vice versa, as shown in Figure 7.21. The SAW filters are usable to frequencies over 2 GHz. A 2-GHz SAW filter chip has an area of  $1 \times 1 \text{ mm}^2$ , but with the package it requires a somewhat larger area. Insertion loss is typically 2 dB to 3 dB. A BAW filter is even smaller and provides somewhat higher frequency selectivity because of higher  $Q$  compared to SAW.

Although the basic filter theory has been around for a long time, there are continuing advances in the synthesis methods. In particular, there are continuous technological advances in SAW and BAW filters, in MEMS tuning of micromechanical microwave filters, and in the more conventional filter structures where high-temperature superconductors are now successfully utilized.

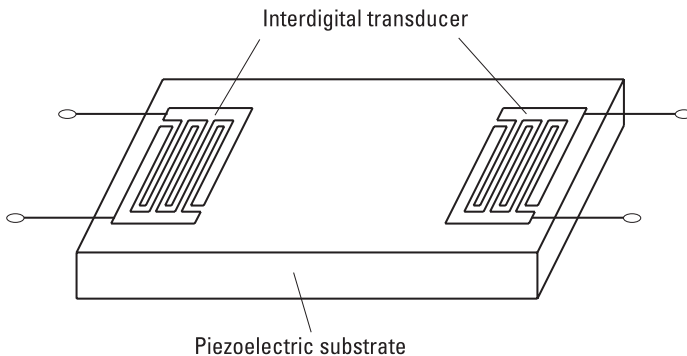


**Figure 7.21** SAW filter.

## References

- [1] Nguyen, C. T.-C., "Frequency-Selective MEMS for Miniaturized Low-Power Communication Devices," *IEEE Trans. Microwave Theory and Techniques*, Vol. 47, No. 8, 1999, pp. 1486–1503.

- [2] Ramo, S., J. Whinnery, and T. van Duzer, *Fields and Waves in Communication Electronics*, New York: John Wiley & Sons, 1965.
- [3] Collin, R. E., *Foundations for Microwave Engineering*, 2nd ed., New York: IEEE Press, 2001.
- [4] Kajfez, D., and P. Guillon, (eds.), *Dielectric Resonators*, Oxford, MS: Vector Fields, 1990.
- [5] Pozar, D. M., *Microwave Engineering*, 2nd ed., New York: John Wiley & Sons, 1998.
- [6] Matthaei, G. L., L. Young, and E. M. T. Jones, *Microwave Filters, Impedance-Matching Networks, and Coupling Structures*, Dedham, MA: Artech House, 1980.
- [7] Fano, R. M., and A. W. Lawson, "The Theory of Microwave Filters," G. L. Ragan, (ed.), *Microwave Transmission Circuits*, Radiation Laboratory Series, New York: McGraw-Hill, 1948.
- [8] Zverev, A. I., *Handbook of Filter Synthesis*, New York: John Wiley & Sons, 1967.
- [9] Richards, P. I., "Resistor-Transmission-Line Networks," *Proc. IRE*, Vol. 36, February 1948, pp. 217–220.
- [10] Ozaki, H., and J. Ishii, "Synthesis of a Class of Stripline Filters," *IRE Trans. on Circuit Theory*, Vol. CT-5, June 1958, pp. 104–109.
- [11] Matsumoto, A., *Microwave Filters and Circuits*, New York: Academic Press, 1970.
- [12] Cohn, S. B., "Parallel-Coupled Transmission-Line-Resonator Filter," *IRE Trans. on Microwave Theory and Techniques*, Vol. 6, April 1958, pp. 223–231.
- [13] Campbell, C. K., "Application of Surface Acoustic and Shallow Bulk Acoustic Wave Devices," *Proc. IEEE*, Vol. 77, No. 10, 1989, pp. 1453–1484.
- [14] Special Issue on Modeling, Optimization, and Design of Surface and Bulk Acoustic Wave Devices, *IEEE Trans. on Ultrasonics, Ferroelectrics, and Frequency Control*, Vol. 48, No. 5, 2001, pp. 1161–1479.

# 8

## Circuits Based on Semiconductor Devices

In Section 1.4 we discussed early development of the radio. At first both the transmitter and receiver were based on a spark gap. Then came a coherer as a detector, and an electron tube was invented in 1904. Nowadays semiconductor devices have replaced electron tubes in most applications.

### 8.1 From Electron Tubes to Semiconductor Devices

Electron tubes came into wide use in radio engineering in the 1910s. They were used as oscillators, modulators, amplifiers, mixers, and detectors. A suitable electron tube was developed for different applications: diode, triode, tetrode, pentode, hexode, heptode, and octode. The names of the different electron tubes are based on the number of electrodes: a diode has only a cathode and an anode; a triode has in addition one grid, which can be used to control the current from the anode to the cathode by a small applied voltage the same way as is done today in the field-effect transistor (see Section 8.2.2); a tetrode has two grids; and so on. Although the transistor was invented in 1948 and a semiconductor diode earlier, electron tubes are still in use. They are used as transmitter tubes in LF, MF, HF, and VHF radio broadcasting stations, and in some military electronics because of their high tolerance for strong electromagnetic pulses.

Currently, in most radio applications we use semiconductor devices for signal generation, amplification, detection, and so on. The advantages

of the semiconductor devices over the electron tubes are their small size, low weight, low supply voltage, and long lifetime.

Circuits based on semiconductor devices may be either active or passive. A circuit is said to be active if it generates RF power from dc power (oscillator) or it amplifies an RF signal (amplifier). In a broader sense, we can consider some other circuits as active: A mixer, frequency multiplier, detector, modulator, and demodulator are all active because they convert power from one frequency to another. However, not all circuits containing semiconductor devices, that is, diodes and transistors, are active. They are also used to realize switches, attenuators, phase shifters, and loads needed in impedance matching (e.g., active matching in MMICs). Figure 8.1 presents standardized drawing symbols of some circuits based on semiconductor components.

## 8.2 Important Semiconductor Devices

Semiconductor technology has advanced rapidly during the last decades. Several types of diodes and transistors are available for RF and microwave applications. The fastest transistors are usable at frequencies over 200 GHz and the fastest diodes at frequencies over 3 THz. The structures and operation principles of the most important diodes and transistors are treated in this section. A more detailed analysis of their physics can be found in the literature [1–3].

### 8.2.1 Diodes

The simplest semiconductor diode is the  $p$ - $n$  diode shown in Figure 8.2(a). It is based on the interface of  $p$ - and  $n$ -type semiconductors. The semiconductor is most often silicon (Si), germanium (Ge), or gallium arsenide (GaAs).

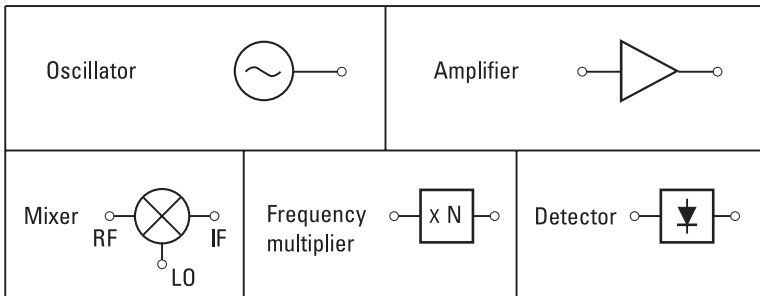


**Figure 8.1** Drawing symbols for circuits based on semiconductor devices.

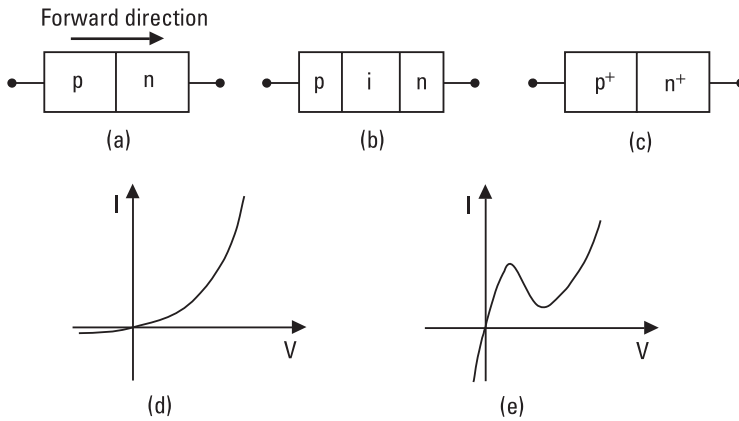


**Figure 8.2** (a)  $p$ - $n$  diode; (b)  $p$ - $i$ - $n$  diode; (c) tunnel diode; (d)  $I$ - $V$  characteristic of a  $p$ - $n$  diode; and (e)  $I$ - $V$  characteristic of a tunnel diode.

In a  $p$ - $n$  junction, current is carried by minority carriers, that is, by holes injected into the  $n$ -side and by electrons injected into the  $p$ -side. In the forward direction the current increases exponentially as the applied voltage increases as shown in Figure 8.2(d). In the reverse direction only a small saturation current flows. Because of the large diffusion capacitance due to the minority carriers, the use of the  $p$ - $n$  diode is limited to low frequencies, a few hundred MHz at maximum. The  $p$ - $n$  diode is used in rectifiers and detectors.

A reverse-biased  $p$ - $n$  diode is used as a varactor, that is, as a voltage-dependent capacitor. It is used as an electrically controlled tuning element, but also in modulators, switches, frequency multipliers, and parametric amplifiers.

When an intrinsic (undoped) semiconductor layer is added in between the  $p$ - and  $n$ -regions, a  $p$ - $i$ - $n$  diode, shown in Figure 8.2(b), is formed. The intrinsic semiconductor layer decreases considerably the junction capacitance, and therefore the  $p$ - $i$ - $n$  diode is well suited to many microwave circuits. It is used in rectifiers, modulators, attenuators, switches, phase shifters, and limiters.

A tunnel diode is a  $p$ - $n$  junction with both sides very heavily doped, as shown in Figure 8.2(c). The depletion region becomes very narrow and therefore allows a remarkable tunneling current at a low forward bias. Its  $I$ - $V$  curve has a negative differential resistance region, as shown in Figure 8.2(e). The tunnel diode is well suited to oscillators and detectors.

In a forward-biased  $p$ - $i$ - $n$  diode, carriers are accumulated in the  $i$ -region and therefore the diffusion capacitance is high. However, this accumulated



charge is suddenly released when the bias is reversed: A short reverse current pulse is generated. This extremely nonlinear behavior is utilized in the step-recovery diode, which is used in frequency multipliers and comb generators for producing frequencies of high harmonic number [4].

The most important diode suitable for microwave detectors, mixers, and frequency multipliers is the Schottky diode. It is an interface between an *n*-type semiconductor (Si or GaAs) and a metal (Au, Pt, or Ti). Minority carriers (holes) play a negligible role, and therefore a Schottky diode is very fast, that is, it can switch from a conducting state to a nonconducting state very quickly. GaAs-Schottky diodes are used up to 3 THz.

A Schottky diode can be contacted and packaged in many ways. In Figure 8.3(a) an unpackaged, whisker-contacted Schottky diode is shown. There are many small anodes on the surface of the GaAs chip; one of them is contacted to the embedding circuit with a sharp wire, a whisker. The planar Schottky diode shown in Figure 8.3(d) can be used as a flip-chip component on a microstrip circuit, it can be encapsulated as a beam-lead diode, or it can be integrated monolithically.

Figure 8.3(b) shows an equivalent circuit of a Schottky diode. It consists of a voltage-dependent junction resistance  $R_j$ , a voltage-dependent junction

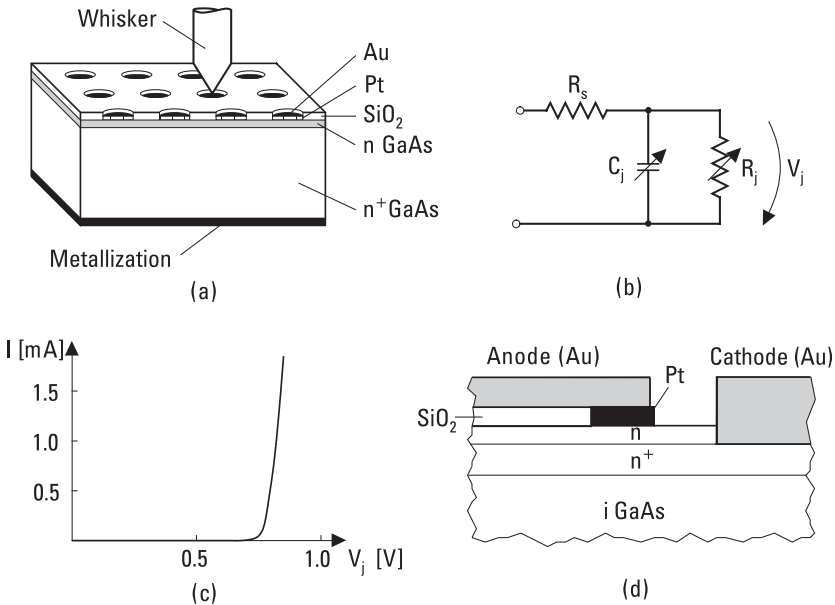


**Figure 8.3** Schottky diode: (a) GaAs diode chip; (b) equivalent circuit; (c) *I*–*V* characteristic; and (d) planar diode.

capacitance  $C_j$ , and a series resistance  $R_s$ . When the Schottky diode is connected to a circuit, it always has a series inductance as well and may have an extra fringing capacitance which both decrease its performance.

The  $I$ - $V$  characteristic shown in Figure 8.3(c) is exponential as

$$I(V_j) = I_s(e^{\alpha V_j} - 1) \quad (8.1)$$

$$\alpha = \frac{q}{\eta k T} = \frac{1}{V_0} \quad (8.2)$$

where  $I_s$  is the saturation current,  $q$  is the magnitude of the electron charge,  $\eta$  is the ideality factor,  $k$  is Boltzmann's constant, and  $T$  is the absolute temperature. The ideality factor of a good diode at room temperature is slightly above unity. The junction differential resistance is obtained from the  $I$ - $V$  characteristic as

$$R_j = \left( \frac{dI}{dV_j} \right)^{-1} = \frac{1}{\alpha(I + I_s)} \approx \frac{V_0}{I} \quad (8.3)$$

The junction capacitance is also voltage dependent and behaves as

$$C_j(V_j) = \frac{C_{j0}}{(1 - V_j/\phi_i)^\gamma} \quad (8.4)$$

where  $C_{j0}$  is the junction capacitance at zero voltage,  $\phi_i$  is the contact potential, and  $\gamma$  is a constant depending on the doping profile of the epitaxial layer. For a GaAs-Pt junction  $\phi_i$  is about 1 V. If the doping profile is abrupt, we have  $\gamma = 0.5$ .

When a Schottky diode is used as a detector or mixer, its figure of merit is the cutoff frequency:

$$f_c = \frac{1}{2\pi R_s C_j} \quad (8.5)$$

The series resistance  $R_s$  is mainly due to the low mobility of electrons in the undepleted epitaxial layer; it is also called the spreading resistance. At the cutoff frequency, one half of the voltage applied over the diode is over the series resistance. The cutoff frequency should be much higher than

the operating frequency ( $f_c \geq 10f$ ). A Schottky varactor has basically the same structure and equivalent circuit as the mixer diode; its behavior is based on the voltage-dependent capacitance, and it is used in frequency multipliers.

In oscillators a device with negative resistance is needed. Besides the tunnel diode, a Gunn diode and an *impact ionization avalanche transit time* (IMPATT) diode have a negative resistance region in their  $I$ - $V$  characteristics.

The Gunn diode, named for its inventor but also called a *transferred electron device* (TED), is not a rectifying diode but rather a piece of  $n$ -type bulk semiconductor. Its negative resistance is based on the properties of the energy band structure of the III-V semiconductors, such as GaAs or *indium phosphide* (InP). In these semiconductors, electrons with sufficiently high energy transfer from the main valley of the conduction band to a satellite valley, where their effective mass is higher and their mobility lower than in the main valley. Therefore, above a given electric field  $E = E_T$  the average drift velocity of electrons decreases while  $E$  increases; in other words, the differential resistance of the semiconductor is negative. Figure 8.4 illustrates the energy band structure and current density versus electric field in  $n$ -type GaAs.

Figure 8.5(a) presents different structures of the IMPATT diode. When a sufficiently high reverse voltage is applied over the diode, an avalanche breakdown (electron-hole pairs are rapidly and increasingly created) occurs in the  $p$ - $n$  interface, where the electric field is highest. For example, in a  $p^+n$ - $n^+$  structure the holes go directly to the  $p^+$ -region but the electrons drift through the  $n$ -region (so-called drift region) to the  $n^+$ -contact. When an alternating voltage is applied over the diode in addition to the dc bias, the phase of the generated electron pulse is  $90^\circ$  behind the voltage phase. With a proper thickness of the  $n$ -layer, an additional phase shift of  $90^\circ$  occurs, due to the drift time. Then the current and voltage of the diode are

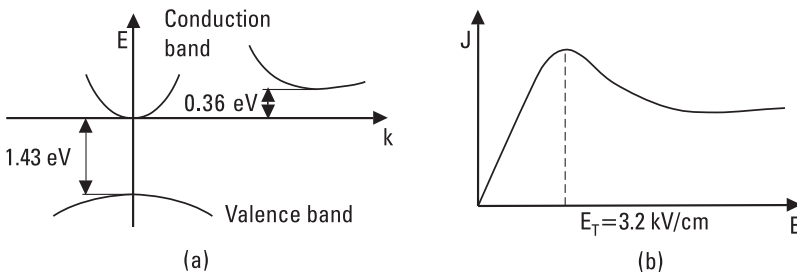


**Figure 8.4** (a) Energy band structure and (b) current density versus electric field in  $n$ -type GaAs.

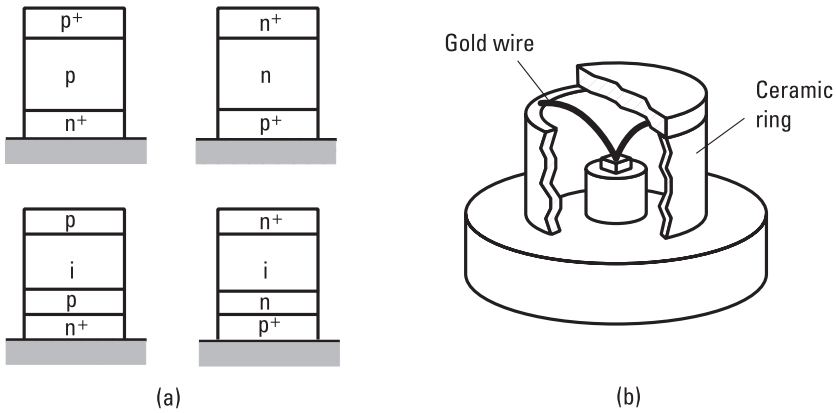


**Figure 8.5** IMPATT diode: (a) different structures; and (b) encapsulated diode.

in opposite phase, that is, its resistance is negative. An IMPATT diode must be encapsulated so that the heat generated in the diode is effectively transferred away.

## 8.2.2 Transistors

The most common transistor in RF applications up to a few gigahertz is the bipolar transistor. In a bipolar transistor both electrons and holes act as current carriers. A bipolar transistor is usually made of silicon. Figure 8.6 shows an *n-p-n* type bipolar transistor. Between the emitter (E) and collector (C) there is a thin base (B) layer. In RF applications the transistor is usually in common-emitter connection, that is, the emitter is grounded. Proper bias voltages are applied to the base-emitter and collector-base junctions; then a small change in the base current,  $\Delta I_B$ , causes a large change in the collector current,  $\Delta I_C$ . The small-signal gain is

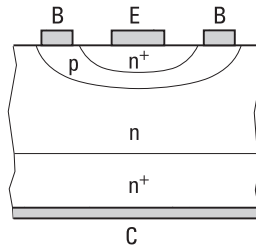


**Figure 8.6** Bipolar transistor.

$$\beta = \frac{\Delta I_C}{\Delta I_B} \tag{8.6}$$

Parasitic capacitances and resistances and the drift times of carriers limit the highest usable frequency of the bipolar transistor.

A *heterojunction bipolar transistor* (HBT) is a faster version of the bipolar transistor. Here *heterojunction* means an interface of two different semiconductors; for example, the emitter is of Si and the base of SiGe, or the emitter is of AlGaAs and the base of GaAs. Because of the heterojunction, the base can be doped very heavily, and therefore the base resistance is small and the transistor is operational at high frequencies.

*Metal-oxide-semiconductor field-effect transistors* (MOSFETs) and *metal-semiconductor field-effect transistors* (MESFETs) are field-effect transistors for RF and microwave applications. MOSFETs fabricated using *complementary metal-oxide-semiconductor* (CMOS) technology, commonly used for digital microcircuits, are applicable for analog RF circuits up to several gigahertz.

GaAs MESFETs are useful up to millimeter wavelengths. Figure 8.7 shows a cross section of a MESFET and its small-signal equivalent circuit. There is a thin *n*-type layer on an undoped substrate. This layer forms the transistor channel, where electrons act as carriers. On the surface of the channel layer there are two ohmic contacts, the source (S) and the drain (D), and between them a short gate (G) contact, which forms with the semiconductor a reverse-biased Schottky junction. As in the Schottky diode, there is a depletion layer in the channel under the gate; the width of the depletion layer depends on the gate voltage. Therefore, the gate voltage  $V_{GS}$  can be used to control the current between the source and drain,  $I_{DS}$ . The ratio of the changes in  $I_{DS}$  and  $V_{GS}$  with a constant  $V_{DS}$  is called the transconductance

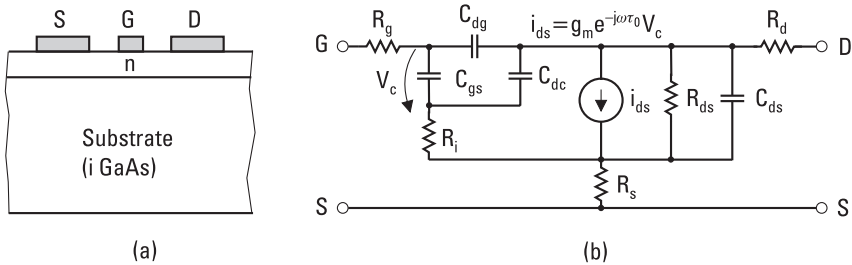


**Figure 8.7** Metal-semiconductor field-effect transistor (MESFET): (a) structure; (b) equivalent circuit.

$$g_m = \frac{\partial I_{DS}}{\partial V_{GS}} \quad (8.7)$$

The frequency at which the short-circuit current gain is 1, is approximately

$$f_T \approx \frac{g_m}{2\pi C_{gs}} \approx \frac{v_s}{2\pi L} \quad (8.8)$$

where  $C_{gs}$  is the capacitance between the gate and source,  $v_s$  is the saturation velocity of carriers, and  $L$  is the gate length. The maximum oscillation frequency, or frequency at which the power gain is unity, is

$$f_{max} \approx \frac{f_T}{2} \sqrt{\frac{R_{ds}}{R_g + R_i + R_s}} \quad (8.9)$$

The cutoff frequency can be made high if the gate is made short. Typically  $L$  is below  $1 \mu\text{m}$ .

A *high electron mobility transistor* (HEMT) or *heterojunction field-effect transistor* (HFET) is a MESFET based on a heterojunction. In the HEMT shown in Figure 8.8 an interface between  $n$ -type AlGaAs and undoped GaAs forms the heterojunction. At the interface, on the side of GaAs, a very thin potential well is formed, due to the mismatch of energy bands. The potential well is so thin that the electrons attracted by the lower potential form a two-dimensional electron gas in the well. Because the electrons drift in the undoped semiconductor, they are not experiencing collisions with impurity ions and therefore their mobility is higher than in a doped semiconductor. Thus, a HEMT is faster than a conventional MESFET. HEMTs made using InP technology are operational up to 200 GHz.

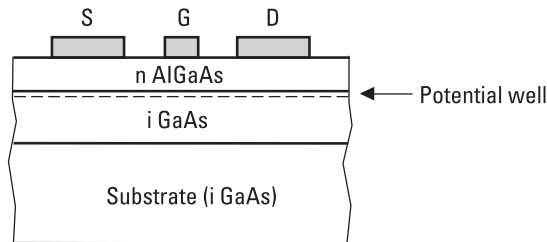


**Figure 8.8** Structure of the HEMT.

### 8.3 Oscillators

An oscillator is a circuit that transfers dc power to RF power [5–8]. The generated RF signal may be sinusoidal or distorted because of containing harmonic components. Important characteristics of an oscillator are its frequency and tuning range, output power, frequency stability, and spectral purity.

An oscillator may be modeled either as a feedback circuit providing a nonzero output voltage for zero-input voltage or as a one-port circuit having negative resistance. In this text we use the latter concept. An active element having a negative resistance may be a diode or a potentially unstable transistor (more about the stability of a transistor in Section 8.4). Figure 8.9 shows a simplified equivalent circuit of an oscillator: A passive load impedance  $Z_L$  is connected to the input impedance  $Z_{in}$  of an active component. The impedance of the active element depends on both current and frequency, that is,

$$Z_{in}(I, f) = R_{in}(I, f) + jX_{in}(I, f) \quad (8.10)$$

The load impedance depends on frequency:

$$Z_L(f) = R_L(f) + jX_L(f) \quad (8.11)$$

Before an oscillation starts, the circuit must be in an unstable state, that is,  $R_{in} + R_L < 0$ . Because  $R_L$  is always positive,  $R_{in}$  must be negative. Then any disturbance or noise may cause oscillation at some frequency  $f$ . When the current increases due to oscillation,  $R_{in}$  must change to less

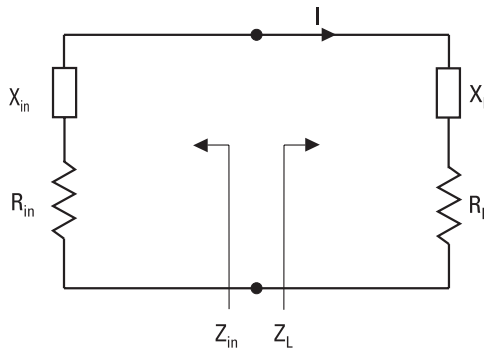


**Figure 8.9** A simplified equivalent circuit of an oscillator.

negative. A properly designed oscillator settles down in a stable operation. Then, according to Kirchoff's law  $(Z_{in} + Z_L)I = 0$ , or

$$R_{in}(I_0, f_0) + R_L(f_0) = 0 \quad (8.12)$$

$$X_{in}(I_0, f_0) + X_L(f_0) = 0 \quad (8.13)$$

The final, stable oscillation frequency  $f_0$  is usually different from the original frequency. In a stable condition, any disturbances of current or voltage are damped, and after a disturbance the oscillator rapidly returns into its stable state.

The load is a circuit with a high quality factor  $Q$ ; it is for example an  $LC$  circuit, quartz crystal, cavity, YIG, or dielectric resonator. Then  $X_L$  changes fast as a function of frequency, and the reactance equation, (8.13), determines the oscillation frequency. In practice,  $R_L$  is nearly independent of frequency. The higher the  $Q$ , the more stable the oscillation state. The oscillation may also be stabilized by using injection locking or phase locking. In the injection locking, a weak signal from an accurate frequency standard is fed into the oscillator. In the phase locking, the output frequency is compared to an accurate signal derived from a frequency standard (see Section 11.1). The frequency standard is usually a crystal-controlled oscillator, the frequency of which may be further stabilized by controlling the temperature of the quartz crystal.

Suitable diodes having a potential negative resistance for an oscillator are Gunn, IMPATT, and tunnel diodes. Only a proper bias voltage is needed to produce a negative resistance. A transistor oscillator may be based on a bipolar transistor in the common-emitter connection, or on an FET in the common-gate connection. Other configurations are also possible. A negative resistance is realized by connecting to the input port of the transistor a load, which makes the transistor unstable. Then the reflection coefficient seen toward the transistor in the output port is greater than unity; that is, the real part of the impedance is negative. The instability may be increased with feedback.

Bipolar transistors are used in oscillators up to about 20 GHz. HBT operates at higher frequencies, up to 50 GHz. These both have 10 dB to 15 dB lower phase noise, that is, a cleaner spectrum near the oscillation frequency, than an FET oscillator has. MESFET is suitable for oscillators up to 100 GHz and HEMT to 200 GHz. The Gunn oscillator operates in the fundamental mode to about 100 GHz, and in harmonic mode up to 200 GHz. IMPATT oscillators are used even at 300 GHz. The spectrum



of an IMPATT oscillator is rather noisy. The amplitude noise is especially strong; that is, the spectrum is noisy even far away from the oscillation frequency. Output powers available from semiconductor oscillators are presented in Figure 8.10. Tube oscillators provide much higher powers; for example, a klystron at 1 GHz or a gyrotron at 100 GHz may produce over 1 MW.

There are several alternative ways to tune the oscillation frequency. According to (8.13), the frequency  $f_0$  depends on the reactance of both the active element and the load. Therefore the frequency can be tuned either mechanically or electrically. The resonance frequency of a cavity is tuned by changing its length, for example, by moving a short circuit in the end of the cavity. A Gunn oscillator may be tuned mechanically over an octave, and an IMPATT oscillator over  $\pm 10\%$ . The resonance frequency of a dielectric resonator is tunable mechanically about  $\pm 2\%$  by changing the distance of a metal plate or a screw above the resonator pill. With bias tuning the Gunn oscillator frequency changes about  $\pm 1\%$ , and that of an IMPATT oscillator over  $\pm 5\%$ . As mentioned before, a varactor is a voltage-dependent capacitor. With a varactor in the embedding circuit, a transistor oscillator may be tuned electrically about an octave. The varactor tuning is also often

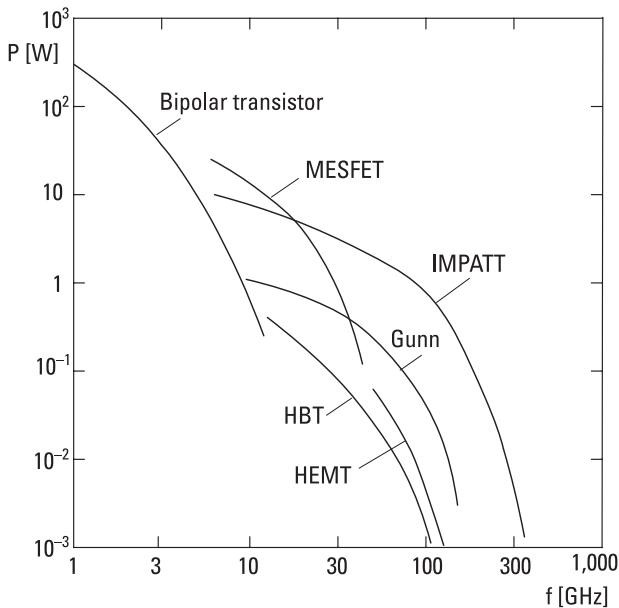


**Figure 8.10** Output powers available from semiconductor oscillators.

used in oscillators stabilized with a DRO, but then the tuning range is small. A varactor tuning (Schottky varactor) is used up to 50 GHz. Such a voltage-tuned oscillator is often called a *voltage-controlled oscillator* (VCO).

Figure 8.11 shows a 5.43-GHz transistor oscillator on a microstrip. A bipolar transistor is in the common-collector connection. The base impedance is made to be in an unstable region. The frequency is determined by a DRO and may be tuned electrically about  $\pm 1$  MHz by changing the dc bias of a varactor.

Signal generators, especially sweepers, often utilize transistor oscillators, the frequency of which is tuned using a *yttrium iron garnet* (YIG) resonator. The YIG material is ferrite. In a static magnetic field the YIG resonator has a resonance at microwave frequencies. The YIG resonators are spherical, having a diameter of 0.2 mm to 2 mm. The resonator is coupled to the embedding network with a current loop around the sphere, as shown in Figure 8.12. The unloaded  $Q$  is about 10,000. The resonance frequency depends linearly on the magnetic field strength, which in turn depends linearly on the dc current of the magnet coil. The frequency tuning range can be 2–3 octaves, making it very useful for sweep generators. The YIG resonators are used up to 50 GHz.

The electric frequency tuning of an oscillator is also utilized in phase locking, frequency modulation, and demodulation. *Frequency modulation* (FM) (see Section 11.3) may be realized by modulating the control voltage of a VCO. Demodulation of an FM signal can be made by phase locking the frequency of a VCO to the received signal. The VCO control voltage is then the demodulated FM signal.

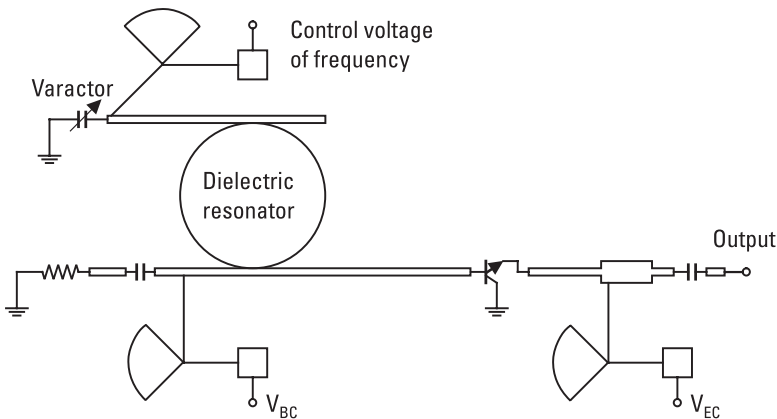


**Figure 8.11** Microstrip layout of a transistor oscillator stabilized with a dielectric resonator and voltage tuned with a varactor.

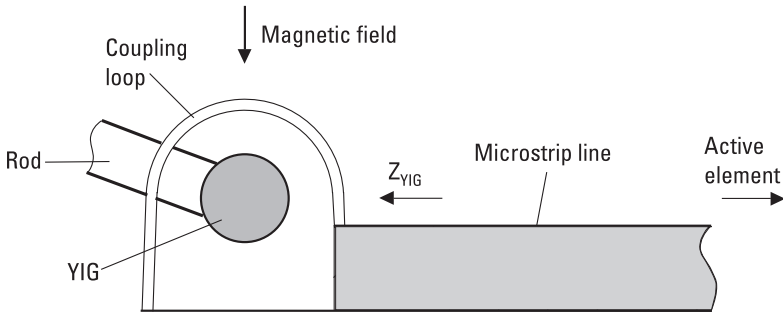


Figure 8.12 YIG resonator coupled to an oscillator circuit.

## 8.4 Amplifiers

Amplifiers based on semiconductor devices are of either transmission (transconductance) or reflection type. In transconductance type amplifiers, bipolar and field-effect transistors are used as active elements. Silicon bipolar transistors are applicable up to 10 GHz, HBTs to 50 GHz, GaAs-MESFETs to 100 GHz, and HEMTs to 200 GHz. Transistor amplifiers are used as *low-noise preamplifiers* (LNAs) in receivers, as *power amplifiers* (PAs) in transmitters, and as *intermediate frequency* (IF) amplifiers in both receivers and transmitters.

### 8.4.1 Design of Small-Signal and Low-Noise Amplifiers

In the following we study the design of a narrowband, small-signal amplifier (for more details, see [7–10]). The design of matching circuits may be based on the equivalent circuit of the transistor or its scattering parameters. We use the  $S$ -parameters as the starting point. Figure 8.13 presents a two-port

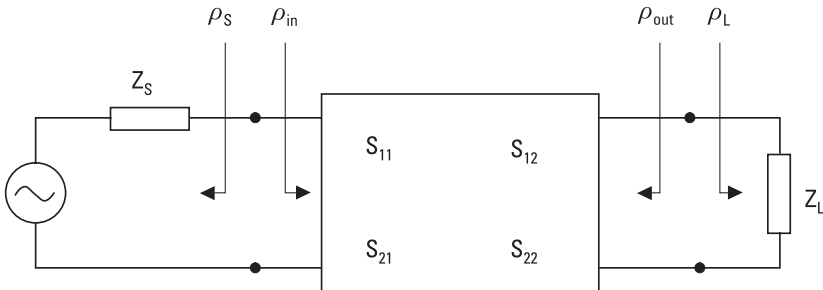


Figure 8.13 A two-port as an amplifier.

(a transistor), the  $S$ -parameters of which are determined in reference to the reference impedance  $Z_0$  (characteristic impedance of the transmission line). The small-signal  $S$ -parameters of a transistor depend on frequency and operating point, that is, on bias voltages and currents. The manufacturer usually reports typical values of the  $S$ -parameters (in reference to  $50\Omega$ ) versus frequency in a few operating points. The load impedance of the two-port is  $Z_L$ , and the impedance of the feeding generator is  $Z_S$ . The reflection coefficients of the terminations in the input and output are

$$\rho_S = \frac{Z_S - Z_0}{Z_S + Z_0} \quad (8.14)$$

$$\rho_L = \frac{Z_L - Z_0}{Z_L + Z_0} \quad (8.15)$$

The input reflection coefficient seen toward the two-port can be presented using the normalized voltage waves as

$$\rho_{in} = \frac{b_1}{a_1} \quad (8.16)$$

Accordingly, in the output we have

$$\rho_L = \frac{a_2}{b_2} \quad (8.17)$$

We can solve  $\rho_{in}$  using a signal flow graph, as we did in Section 5.3; see (5.24):

$$\rho_{in} = S_{11} + \frac{S_{21}S_{12}\rho_L}{1 - \rho_L S_{22}} = \frac{S_{11} - \rho_L \Delta}{1 - \rho_L S_{22}} \quad (8.18)$$

where

$$\Delta = S_{11}S_{22} - S_{12}S_{21} \quad (8.19)$$

The output reflection coefficient seen toward the two-port is

$$\rho_{out} = \frac{S_{22} - \rho_S \Delta}{1 - \rho_S S_{11}} \quad (8.20)$$

A transistor amplifier provides the maximum available power gain  $G_{a,max}$  when both ports are conjugately matched. This condition can be written as

$$\rho_{in} = \rho_S^* \text{ and } \rho_{out} = \rho_L^* \quad (8.21)$$

By substituting these into (8.18) and (8.20) we obtain generator and load reflection coefficients (in reference to  $50\Omega$ )  $\rho_{SM}$  and  $\rho_{LM}$ , respectively, that both the input and output are simultaneously matched:

$$\rho_{SM} = \frac{B_1 \mp \sqrt{B_1^2 - 4|C_1|^2}}{2C_1} \quad (8.22)$$

$$\rho_{LM} = \frac{B_2 \mp \sqrt{B_2^2 - 4|C_2|^2}}{2C_2} \quad (8.23)$$

where

$$B_1 = 1 + |S_{11}|^2 - |S_{22}|^2 - |\Delta|^2 \quad (8.24)$$

$$B_2 = 1 - |S_{11}|^2 + |S_{22}|^2 - |\Delta|^2 \quad (8.25)$$

$$C_1 = S_{11} - \Delta S_{22}^* \quad (8.26)$$

$$C_2 = S_{22} - \Delta S_{11}^* \quad (8.27)$$

If  $B_1 > 0$  and  $|B_1/2C_1| > 1$ , one must select the negative sign in front of the square root in (8.22) in order to have  $|\rho_{SM}| < 1$ , that is, to be able to realize the input matching circuit using passive elements. Accordingly, for the output, if  $B_2 > 0$  and  $|B_2/2C_2| > 1$ , one must select the negative sign in (8.23). For a unilateral transistor ( $S_{12} = 0$ ),  $\rho_{SM} = S_{11}^*$  and  $\rho_{LM} = S_{22}^*$ .

The maximum available power gain can be presented in the following form:

$$G_{a,max} = \frac{|S_{21}|}{|S_{12}|} (K - \sqrt{K^2 - 1}) \quad (8.28)$$

where

$$K = \frac{1 - |S_{11}|^2 - |S_{22}|^2 + |\Delta|^2}{2|S_{12}S_{21}|} \quad (8.29)$$

The use of (8.28) requires that  $K \geq 1$ ; otherwise  $G_{a,max}$  becomes complex.

Generally, the matching circuit provides the maximum available power gain only at the design frequency. When the frequency moves away from the design frequency, gain decreases rapidly. The bandwidth can be made wider if we are satisfied with a gain lower than  $G_{a,max}$ . In that case a small mismatch is purposely designed in both the input and output. Design is aided by using constant gain circles drawn on the Smith chart.

A transistor amplifier is not necessarily stable. Oscillation is possible if the real part of the input or output impedance is negative. This means that  $|\rho_{in}| > 1$  or  $|\rho_{out}| > 1$ . If  $|\rho_{in}| < 1$  and  $|\rho_{out}| < 1$  with all generator and load impedance values, the amplifier is unconditionally stable. In other cases the amplifier is potentially unstable. From conditions  $|\rho_{in}| = 1$  or  $|\rho_{out}| = 1$  we can calculate boundaries for the stable regions of input and output impedances. On the Smith chart these boundaries are circles, as shown in Figure 8.14. The output impedance stability circle is defined by the center point  $c_L$  and radius  $r_L$  as

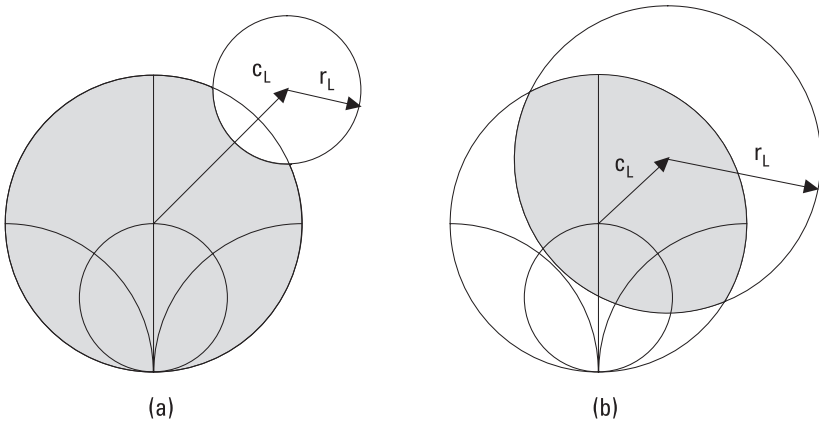


**Figure 8.14** Output stability circles on the Smith chart. Shaded areas are stable when  $|S_{11}| < 1$ . The center point of the Smith chart is (a) outside the stability circle, and (b) inside the circle.

$$c_L = \frac{(S_{22} - \Delta S_{11}^*)^*}{|S_{22}|^2 - |\Delta|^2} \quad (8.30)$$

$$r_L = \left| \frac{S_{12}S_{21}}{|S_{22}|^2 - |\Delta|^2} \right| \quad (8.31)$$

Either the inside or outside of the stability circle presents the stable region. If  $|S_{11}| < 1$ , the center point of the Smith chart is in the stable region. If, however,  $|S_{11}| > 1$ , the Smith chart center point is in the unstable region. The center point  $c_S$  and radius  $r_S$  of the input stability circle are obtained by replacing  $S_{22}$  with  $S_{11}$  and vice versa in (8.30) and (8.31). It can be proven that the necessary and sufficient conditions for the unconditional stability are  $K > 1$  and  $|\Delta| < 1$ . It may be worth checking that  $\rho_S$  and  $\rho_L$  are in the stable region not only at the operating frequency but also at other frequencies.

In addition to gain and stability, a third important characteristic of an LNA is its noise factor  $F$  (for more detail see Section 11.2). A transistor has four noise parameters: minimum noise factor  $F_{min}$ , magnitude and phase of optimum input reflection coefficient  $\rho_{opt}$  ( $F = F_{min}$ , when  $\rho_S = \rho_{opt}$ ), and equivalent noise resistance  $R_n$  [11]. The noise factor can be presented as a function of the generator admittance  $Y_S = 1/Z_S$  as

$$F = F_{min} + \frac{R_n}{G_S} |Y_S - Y_{opt}|^2 \quad (8.32)$$

where  $G_S$  is the real part of  $Y_S$  and  $Y_{opt}$  is the admittance corresponding to  $\rho_{opt}$ . The load impedance  $Z_L$  affects the gain but not the noise factor. In general, it is not possible to obtain the minimum noise factor and maximum gain simultaneously, but one must make a compromise. This can be helped by using constant noise circles calculated from (8.32) on the Smith chart, together with constant gain circles as shown Figure 8.15.

In addition to the design of matching circuits according to proper  $\rho_S$  and  $\rho_L$ , the completion of the design work requires also design of circuits for bias voltages. Figure 8.16 shows an example of a practical realization: a 22-GHz HEMT amplifier. The low-impedance microstrip line sections in the input and output provide  $\rho_S$  for the minimum noise factor and  $\rho_L$  for the conjugate match of output (in order to optimize gain). Bias voltages to the gate and drain are supplied through high-impedance lines. At a distance of  $\lambda/4$  from the feed point there is a radial stub short circuit in each of

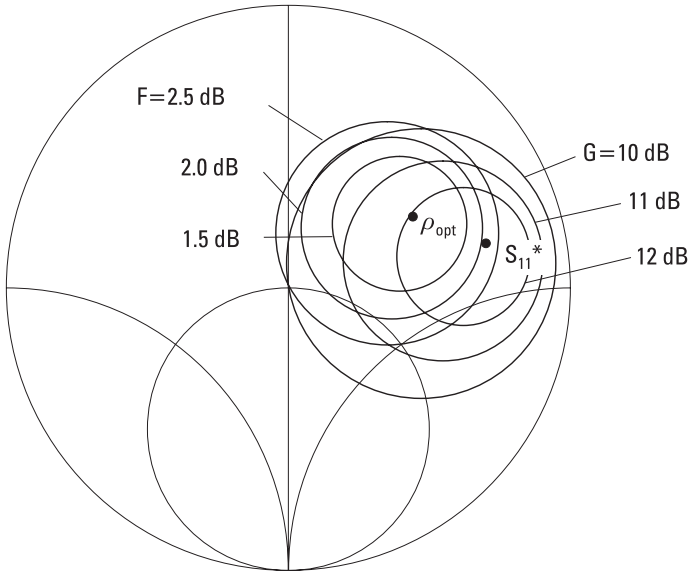


**Figure 8.15** Constant gain and noise circles of an amplifier on the Smith chart.  $F$  and  $G$  versus  $Z_S$  when the output is matched.

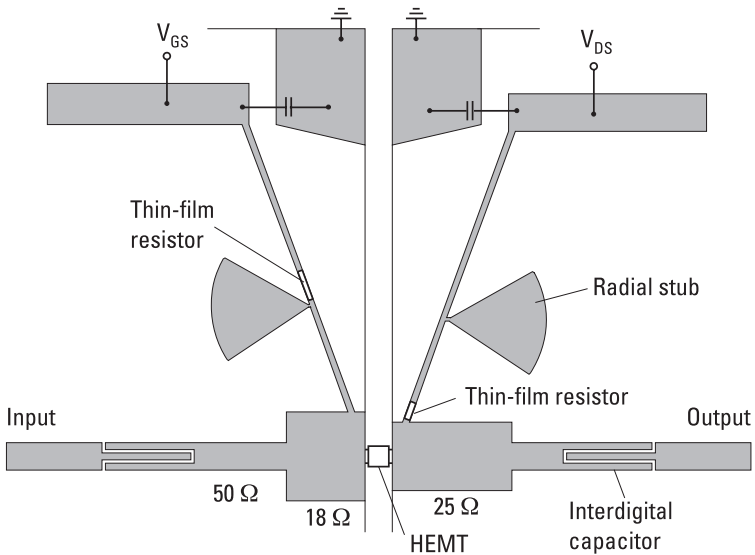


**Figure 8.16** A 22-GHz HEMT amplifier (a microstrip circuit).



these lines. These are needed in order to have the bias circuits seen as open circuits from the transistor. The function of the thin-film resistors is to prevent low-frequency oscillations. The interdigital capacitors in input and output prevent dc from flowing out, but are only negligible series reactances at RF.

**Example 8.1**

Design a transistor amplifier at 4 GHz for maximum available gain. The scattering parameters in the desired operation point  $V_{DS} = 3\text{ V}$  and  $I_{DS} = 10\text{ mA}$  are  $S_{11} = 0.70 \angle -115^\circ$ ,  $S_{21} = 2.50 \angle 70^\circ$ ,  $S_{12} = 0.04 \angle 55^\circ$ , and  $S_{22} = 0.65 \angle -40^\circ$ .

**Solution**

First we must check the stability of the transistor. From (8.19) we obtain  $\Delta = 0.544 \angle -150^\circ$ , and from (8.29)  $K = 1.917$ . Therefore, the transistor is unconditionally stable at 4 GHz. We do not need to calculate the stability circles; they are totally outside the Smith chart. Next we calculate the reflection coefficients, providing a conjugate match in the input and output. From (8.24) through (8.27) we calculate  $B_1 = 0.772$ ,  $B_2 = 0.637$ ,  $C_1 = 0.349 \angle -120^\circ$ , and  $C_2 = 0.273 \angle -47^\circ$ . From (8.22) and (8.23) we obtain reflection coefficients  $\rho_{SM} = 0.636 \angle 120^\circ$  and  $\rho_{LM} = 0.566 \angle 47^\circ$ . Equation (8.28) gives  $G_{a,max} = 17.6 = 12.5\text{ dB}$ . Because both ports are conjugate matched, it holds that  $G_{a,max} = G_t = G_p = G_a$ , which may be verified using (5.26) through (5.28). The matching circuits can be realized, for example, according to Figure 8.17 using open-circuited parallel stubs. All transmission

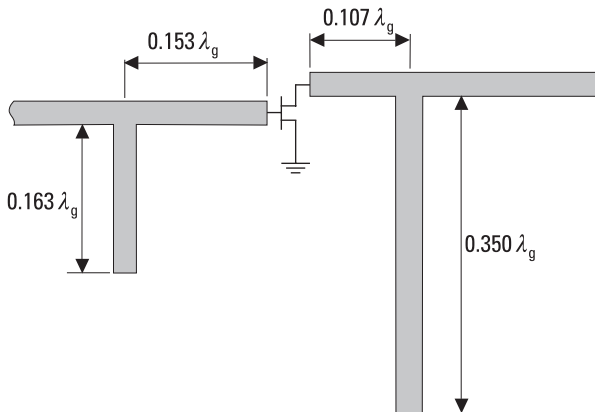


**Figure 8.17** Microstrip matching circuits for an FET amplifier.

lines are 50- $\Omega$  microstrip lines. In this realization we have not taken into account the fringing components of the microstrip T-junctions and open ends [12]. Another often used matching method in transistor amplifiers is an alternating high-low-impedance line. A manual design of amplifiers and other circuits becomes excessively laborious if all parasitic effects are taken into account and the circuit has to operate over a broad band. Then use of a *computer-aided design* (CAD) package significantly facilitates the design.

### 8.4.2 Effect of Nonlinearities and Design of Power Amplifiers

In the previous study we assumed that the transistor characteristics did not depend on the signal level, that is, the transistor operates in linear, small-signal conditions. However, as the input power level increases, the nonlinearities of the transistor cause gain compression and generation of spurious frequency components.

As the input power level increases, the gain of an amplifier is constant at small signal levels but finally starts to decrease. Often the bias voltages limit the maximum output voltage. This saturation or gain compression is characterized by the 1-dB compression point, which is the output power at which the gain has decreased by 1 dB from its small-signal value.

Because of the compression, the output waveform is distorted. This distortion produces harmonics  $nf$  of a single input signal at frequency  $f$  and intermodulation products  $mf_1 + nf_2$  ( $m, n = \pm 1, \pm 2, \dots$ ) of a two-tone input signal. The order of intermodulation products is defined to be  $|m| + |n|$ . Especially important are the third-order intermodulation products at frequencies  $2f_1 - f_2$  and  $2f_2 - f_1$  because they are close to frequencies  $f_1$  and  $f_2$ , if  $f_1 \approx f_2$ . At low input signal levels, the power of third-order intermodulation products increases by 3 dB as the power of input signals having equal magnitudes increases by 1 dB. If there were no compression, the output powers of the desired signals at  $f_1$  and  $f_2$  and the third-order products would be equal at an output power level called the third-order intercept point,  $IP_3$ .

The dynamic range of an amplifier is that operating power range over which the amplifier has desirable characteristics. Noise usually sets the lower limit of dynamic range. The upper limit of the linear dynamic range may be defined as the 1-dB compression point. The spurious-free dynamic range is limited by the power level, which produces unacceptable intermodulation products.

In the design of a power amplifier, the theory presented here for getting proper  $\rho_S$  and  $\rho_L$  is valid only if the scattering parameters are measured in

large-signal conditions, that is, at a power level corresponding to the real operation. A power amplifier is designed so that both input and output is conjugate matched, because this provides the maximum gain. Power amplifiers are divided into different classes. A class-A amplifier operates linearly. The bias voltages and signal amplitude are chosen so that output current flows during the full signal period, as shown in Figure 8.18. In a class-B amplifier the output current flows only during one-half of the period, and in a class-C amplifier less than one-half of the period. These amplifiers operate very nonlinearly but they transform dc power more effectively into RF power than a class-A amplifier. A good efficiency is obtained also with class-D, class-E, and class-F amplifiers in which the transistors operate as switches.

In comparing different power amplifiers, an often used figure-of-merit is the power-added efficiency

$$PAE = \frac{P_L - P_{in}}{P_{dc}} \quad (8.33)$$

where  $P_L$  is the RF power coupled to the load,  $P_{in}$  is the RF power coupled to the amplifier, and  $P_{dc}$  is the dc power absorbed by the amplifier. When a very high power level is needed, several amplifiers may be combined parallel using a power combiner (see Section 6.1).

### 8.4.3 Reflection Amplifiers

The reflection-type amplifier is based on the negative resistance of, for example, a Gunn or IMPATT diode. The power gain of a reflection-type amplifier is

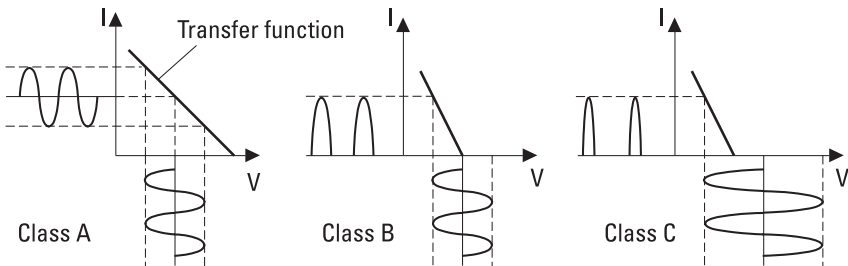


**Figure 8.18** Current waveforms in class-A, class-B, and class-C amplifiers.

$$G = |\rho|^2 = \left| \frac{Z_d - Z_0}{Z_d + Z_0} \right|^2 \quad (8.34)$$

where  $Z_0$  is the characteristic impedance of the transmission line and  $Z_d$  is the diode impedance. If for example  $Z_0 = 50\Omega$  and  $Z_d = -25\Omega$ , gain is  $G = (75/25)^2 = 9 = 9.5$  dB. The input and output signals can be separated by using a circulator according to Figure 8.19.

## 8.5 Frequency Converters (Mixers) and Frequency Multipliers

The output signal from a linear circuit has shape similar to that of the input signal; however, its amplitude may be higher (amplifier) or lower (attenuator). In a nonlinear circuit the signal is distorted, and the output signal (voltage  $V_o$ ) is a nonlinear function of the input signal (voltage  $V_i$ ) and can be presented as a power series

$$V_o = f(V_i) = AV_i + BV_i^2 + CV_i^3 + \dots \quad (8.35)$$

Figure 8.20 illustrates the difference between a linear and nonlinear transfer function. If, in the case of a nonlinear transfer function, the input signal is weak and causes only a small perturbation in the vicinity of the operating point, the circuit can be considered linear for the signal; that is,  $\delta V_o = A' \delta V_i$ , where  $A'$  is the slope of the curve  $f(V_i)$  in the operating

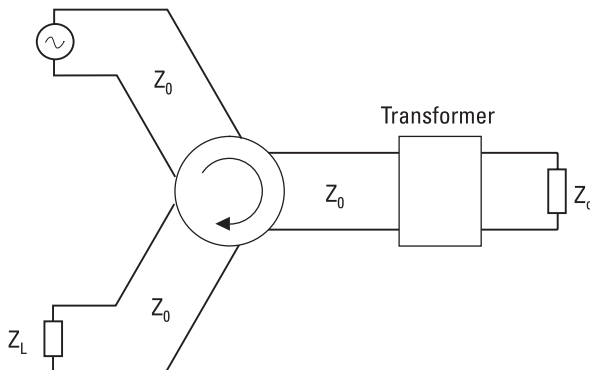


**Figure 8.19** A reflection-type amplifier.

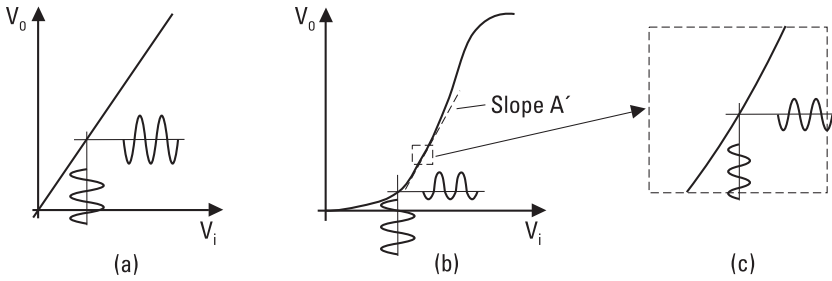


**Figure 8.20** Transfer function of (a) a linear and (b) a nonlinear circuit, and (c) a linear small-signal condition.

point. We call this situation the small-signal condition. In a large-signal condition, several terms of (8.35) must be taken into account.

Let us assume that  $V_i = V_1 \cos \omega_1 t + V_2 \cos \omega_2 t$ . Then the term  $AV_i$  contains signal components at frequencies  $f_1$  and  $f_2$ , term  $BV_i^2$  contains components at frequencies 0 (dc),  $2f_1$ ,  $2f_2$ , and  $f_1 \pm f_2$ , and term  $CV_i^3$  contains components at frequencies  $f_1$ ,  $f_2$ ,  $3f_1$ ,  $3f_2$ ,  $2f_1 \pm f_2$ , and  $2f_2 \pm f_1$  (a frequency may be also negative). We note that when a sinusoidal signal at frequency  $f_1$  is fed to a nonlinear circuit, the output contains harmonics at frequencies  $mf_1$ , and when two sinusoidal signals at frequencies  $f_1$  and  $f_2$  are fed to a nonlinear circuit, the output contains components at frequencies  $mf_1 + nf_2$  ( $m$  and  $n$  are integers). These nonlinear characteristics make possible the operation of a frequency converter, or a mixer and a frequency multiplier. Note that a mixer may also be based on a time-dependent linear circuit. In a circuit meant to be linear, such as a low-noise amplifier, the distortion due to nonlinearity produces unwanted frequency components.

### 8.5.1 Mixers

A mixer is a circuit that converts the frequency of a signal up or down so that the information contained in the signal is preserved. Upconverters are used in modulators and transmitters, downconverters in heterodyne receivers and demodulators. In Figure 8.21, a signal at frequency  $f_s$  and a local oscillator signal at  $f_{LO}$  are fed to a downconverter; then at the output we have a signal at a low intermediate frequency  $f_{IF} = |f_s - f_{LO}|$ . Processing of the signal at  $f_{IF}$  is much easier than that of the original signal at  $f_s$ . The conversion loss  $L_c$  is defined as

$$L_c = \frac{P_{s,av}}{P_{IF}} = \frac{\text{Available power at } f_s}{\text{Power coupled to load at } f_{IF}} \quad (8.36)$$

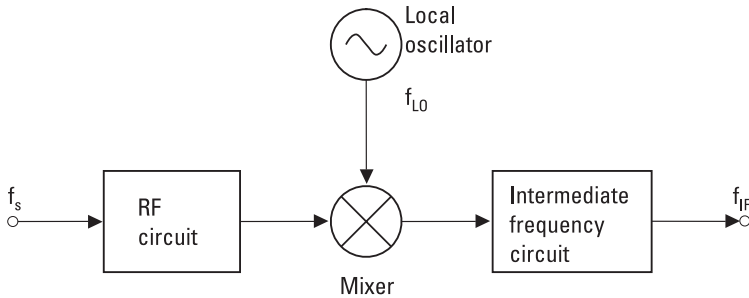


**Figure 8.21** Mixer as a downconverter.

As in case of an amplifier, a mixer is linear for a low-power signal ( $P_s < P_{LO}/100$ ) but at higher powers the output signal will be distorted. Thus we can define a 1-dB compression point and a third-order intercept point for a mixer, too.

The nonlinear element may be a diode or a transistor, most often a Schottky diode, bipolar transistor, or FET. Diode mixers are passive; transistor mixers may operate in an active mode and have some conversion gain. Transistor mixers suit well in integrated circuits. Operation of a diode mixer is based on the exponential  $I$ - $V$  characteristic, but frequency conversion takes place also in the nonlinear capacitance. In a bipolar transistor the emitter-base junction forms a diode. Therefore, in a common-emitter connection the collector current depends exponentially on the base voltage. In an FET the drain current  $I_{DS}$  is a nonlinear function of the gate voltage  $V_{GS}$ . Especially a *dual-gate FET* (DGFET) is well suited as a mixer, because the RF signal can be fed to one gate and the local oscillator signal to another gate.

In case of a diode mixer, frequency conversion can be analyzed as follows; for equations see [13, 14]. Using the embedding impedances loading the diode at frequencies  $mf_{LO}$  we calculate the waveforms of the conductance  $G_j(t) = 1/R_j(t)$  and capacitance  $C_j(t)$  caused by the local oscillator signal and a possible dc bias. The better the diode corresponds to an ideal switch operating at  $f_{LO}$ , the more effective frequency conversion is. The signal ( $f_s$ ) power is usually very small compared to the LO signal ( $f_{LO}$ ) power; then from the signal's point of view the mixer is a linear, time-dependent circuit.

The operation of a mixer depends on conditions not only at the signal and IF frequency, but also at the sidebands  $mf_{LO} \pm f_{IF}$  because power may convert from any sideband to another. Especially important is the image sideband  $f_i = 2f_{LO} - f_s$ . Frequencies  $mf_{LO} \pm nf_{IF}$  ( $n \geq 2$ ) are important only if the signal power level is of the same order as that of the LO. Using

the Fourier series of  $G_j(t)$  and  $C_j(t)$  we can then calculate a frequency conversion matrix. With this and the load impedances we obtain conversion efficiencies between any two sidebands. Figure 8.22 illustrates the conversion from a frequency  $f_s$  to different sidebands.

In designing a mixer, it is important to find the correct load impedances at different sidebands. The conversion loss is at minimum when there is a conjugate match between the nonlinear element and the embedding network at signal and intermediate frequencies, and the other sidebands are terminated with proper, purely reactive loads. The noise optimum requires slightly different conditions the same way as in case of an amplifier. In practice, mixer design today is carried out with a CAD package employing a harmonic balance [13, 14] simulator.

Depending on which sidebands are selected as the signal bands, we have different mixers. A *single-sideband* (SSB) mixer converts the signal only from one sideband, either from the upper sideband  $f_{LO} + f_{IF}$  or from the lower sideband  $f_{LO} - f_{IF}$ , to the intermediate frequency band. A *double-sideband* (DSB) mixer converts both sidebands to the IF band. Two DSB mixers can be combined to form an SSB mixer, which is then called an image-rejection mixer: The outputs of the individual mixers are combined in phase in case of the desired sideband while the outputs cancel each other in case of the image sideband. A harmonic mixer converts the sidebands of an LO harmonic  $mf_{LO} \pm f_{IF}$  ( $m \geq 2$ ) to the IF band.

There are a number of different mixer structures or architectures [14]. Figure 8.23 presents the principle of a single-ended, a balanced, and a double-balanced diode mixer, as well as of a double-balanced transistor mixer. For simplicity, the matching and bias circuits are omitted in Figure 8.23. At millimeter wavelengths the mixers are often single-ended waveguide mixers, where the signal and LO are fed to the diode along the same waveguide after combining them in a directional coupler. At RF and microwave frequencies most often balanced and double-balanced mixers are used, and signal and LO power are fed to the nonlinear elements using 3-dB hybrids (described

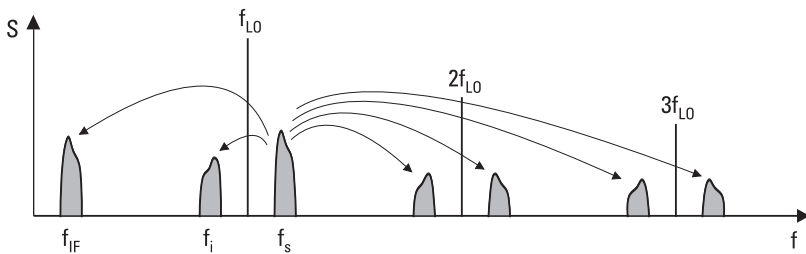


**Figure 8.22** Conversion of signal power to different sidebands in a mixer.

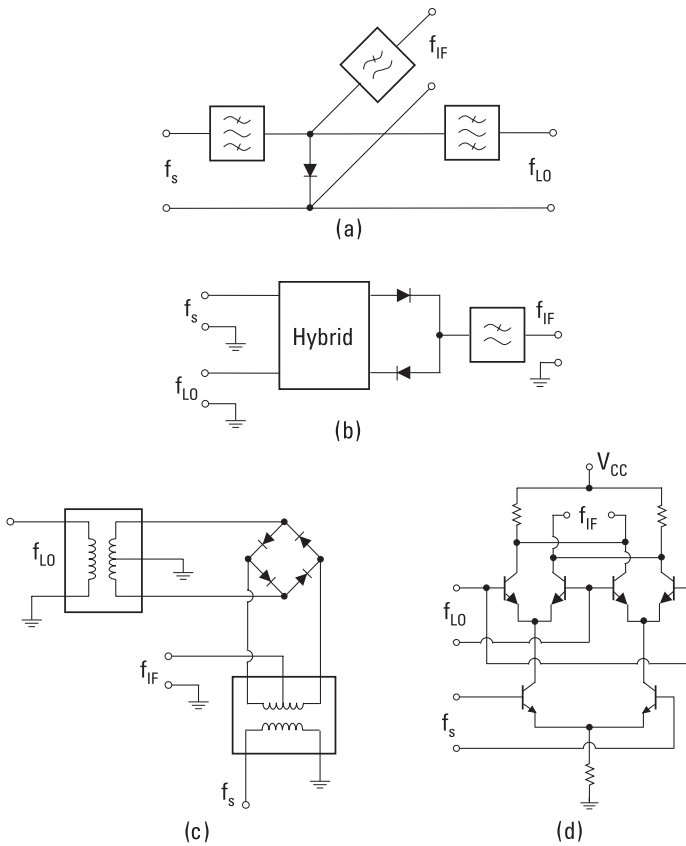


**Figure 8.23** Different mixer circuits: (a) single-ended mixer; (b) balanced mixer; (c) double-balanced mixer; and (d) Gilbert cell mixer.

in Section 6.1). At low radio frequencies tapped transformers are used. The balanced and double-balanced mixers have many advantages over the single-ended mixer: There is a good isolation between the signal and LO ports, the AM noise of the LO is rejected, certain spurious signals are rejected, and the compression and intercept points are higher. In a double-balanced mixer there is a good isolation also between the IF and other ports. A disadvantage of balanced and double-balanced mixers is their higher LO power requirement. The Gilbert cell mixer shown in Figure 8.23(d) is a double-balanced transistor mixer, which is widely used in integrated circuits.

## 8.5.2 Frequency Multipliers

In a frequency multiplier, harmonic signals at frequencies  $nf$  are generated, and using a filter one of them is selected as the output signal. This way we



can realize frequency doublers (x2), triplers (x3), quadruplers (x4), quintuplers (x5), and so on [15, 16]. A frequency multiplier helps in generating signals at high frequencies where it is otherwise difficult or impossible. Also a signal generated by a multiplier may have a more accurate frequency than a signal produced directly with an oscillator.

The nonlinear element may be either a diode (either resistive or capacitive diode, i.e., a varistor or a varactor, respectively) or a transistor. The multiplication efficiency  $\eta$  is defined as

$$\eta = \frac{\text{Power coupled to load at } nf}{\text{Available power from source at } f} \quad (8.37)$$

In order to optimize the frequency multiplication efficiency, the nonlinear element must be conjugate matched to the embedding network at the input and output frequencies and terminated with proper, pure reactive loads at other harmonic frequencies. Especially important are the proper reactive terminations at the idler frequencies (intermediate harmonics between the fundamental and output frequency) in higher-order multipliers. The efficiency  $\eta$  of a multiplier based on a nonlinear reactive element is at maximum unity at any multiplication factor  $n$ , if both the nonlinear element and the embedding network are lossless (Manley–Rowe equations; see [17]). In practice the efficiency decreases rapidly versus an increasing multiplication factor. A positive, monotonically voltage-dependent nonlinear resistance can produce a multiplication efficiency of  $1/n^2$  at maximum. The efficiency of a transistor multiplier may be greater than unity.

## 8.6 Detectors

Detecting a signal requires transforming it into a useful or observable form. In a diode detector an RF signal is transformed into a voltage proportional to the signal power. Operation of a detector is based on the nonlinearity of a diode, such as a Schottky or  $p$ - $n$  diode. When a sinusoidal voltage is applied over the diode, the current contains, besides a component at the signal frequency, harmonic components and a dc component that is proportional to the signal power. Diode detectors are used for power measurement, automatic level control, AM demodulation, and so on.

Let us consider a Schottky diode, where the series resistance  $R_s$  and the junction capacitance  $C_j$  are assumed negligible. When a bias voltage  $V_B$

and a small sinusoidal signal  $V_s \cos \omega t$  are applied over the junction resistance (see Figure 8.24), the diode current can be presented as a series:

$$I(V_B + V_s \cos \omega t) = I_B + \alpha^2(I_s + I_B) \frac{V_s^2}{4} + \alpha(I_s + I_B) V_s \cos \omega t \quad (8.38)$$

$$+ \alpha^2(I_s + I_B) \frac{V_s^2}{4} \cos 2\omega t + \dots$$

Further terms are negligible if  $\alpha V_s \ll 1$  [see  $\alpha$  in (8.2)] or at room temperature  $V_s \ll 25$  mV.  $I_B$  is the direct current caused by the bias voltage,  $I(V_B)$ . The second term is the dc component proportional to the signal power; that is, it is the useful component. According to (8.38), the junction can be considered as a voltage source with a voltage

$$V_o = \frac{\alpha V_s^2}{4} \quad (8.39)$$

and with an internal resistance  $R_j$ . The diode is said to follow the square law, because the useful signal is directly proportional to the RF power, that is, to the square of the signal voltage ( $V_o \propto V_s^2$ ). The voltage sensitivity is the ratio of the detector output voltage  $V_o$  and the applied signal power  $P_s$ , in an impedance-matched case, as in

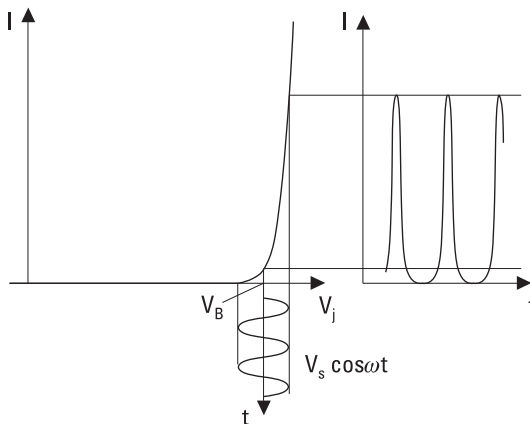


**Figure 8.24** Current in a diode with an exponential  $I$ - $V$  characteristic, when a dc bias and a sinusoidal signal are applied to the diode.

$$\beta_v = \frac{V_o}{P_s} = \frac{\alpha R_j}{2} \tag{8.40}$$

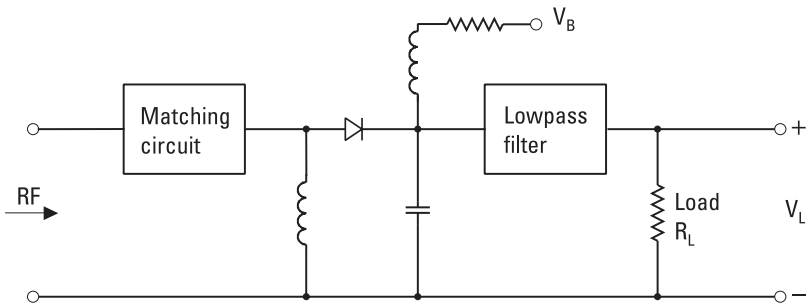
If the parasitic elements  $R_s$  and  $C_j$  of the diode as well as the load resistance  $R_L$  are taken into account, we get the following expression [18] for the voltage sensitivity

$$\beta_v = \frac{V_L}{P_s} = \frac{\alpha R_j}{2} \times \frac{R_L}{(1 + R_s/R_j)(1 + R_s/R_j + \omega^2 C_j^2 R_s R_j)(R_j + R_s + R_L)} \tag{8.41}$$

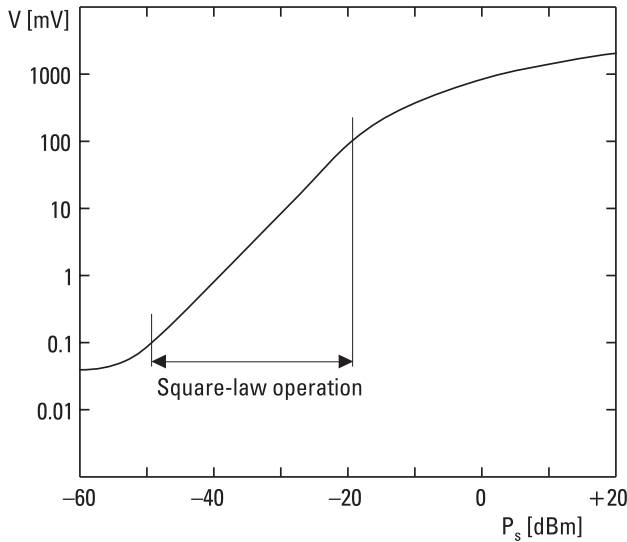
where  $V_L$  is the voltage over the load.  $R_s$  and  $C_j$  reduce the voltage sensitivity, which also decreases as the frequency or temperature are increased ( $\alpha$  is proportional to temperature).

Figure 8.25 shows how a diode detector is connected into a circuit. In order to get all signal power absorbed into the diode, it must be matched to the transmission line, usually to  $50\Omega$ . Without a bias voltage, the junction resistance  $R_j$  may be very high and difficult to match. Furthermore, (8.41) shows that in order to maximize the voltage sensitivity, it should be  $R_L \gg R_j$ . Therefore, such a diode needs a small bias current in order to provide a proper  $R_j$ . Matching the diode over a wide frequency band is difficult. However, in practice we want a flat frequency response and, therefore, we must satisfy on lower voltage sensitivity than that given by (8.41). A lowpass filter is used in the output to prevent the RF and harmonic components from coupling to the load. A coil and a capacitor are needed to guarantee that both dc and RF currents can flow through the diode.

Figure 8.26 shows a typical power response of a diode detector. When the power level increases to a level over  $-20$  dBm (dBm = decibels over



**Figure 8.25** Equivalent circuit of a diode detector.



**Figure 8.26** Response of a diode detector.

1 mW), the response no longer follows the square law. Finally, the output voltage will saturate. On the other hand, at very low power levels noise is the limiting factor.

## 8.7 Monolithic Microwave Circuits

Circuits consisting of microstrip lines, lumped passive elements (resistors, inductors, and capacitors), and semiconductor diodes and transistors may be integrated (connected without connectors) and be made very small. If components are soldered or bonded on a microstrip circuit, we call it a hybrid circuit. If a circuit is integrated directly on the surface of a semiconductor substrate, it is called a monolithic integrated circuit.

Up to about 2 GHz the monolithic circuits are made on Si; at higher frequencies the substrate is usually GaAs and these circuits are called *monolithic microwave integrated circuits* (MMICs). The advantages of the MMICs are their extremely small size, suitability to mass production, good repeatability, and high reliability. For example, a whole microwave amplifier can easily be fabricated on a GaAs chip with an area of  $1 \text{ mm}^2$  and a thickness of  $100 \mu\text{m}$ . Design and fabrication of a single MMIC becomes very expensive, but in mass production its price becomes reasonable. Microwave applications

gaining from mass production of integrated circuits include mobile phones, satellite TV receivers, GPS receivers, and WLAN terminals.

From diodes the Schottky diode and from transistors both MESFET and HEMT are easily suited to GaAs-MMICs. The transmission lines are either microstrip lines or coplanar waveguides. Resistors are either ion-implanted directly in GaAs or are thin metal films in the transmission lines. Inductors (coils) may be narrow microstrip lines in the form of a loop or a spiral; capacitors have either an interdigital or *metal-insulator-metal* (MIM) structure (see Figure 4.7). Grounding is realized by a metallized via in the substrate. Figure 8.27 presents a GaAs-MMIC with typical elements. Digital microwave circuits have been made using MMIC technology up to tens of gigahertz, analog circuits up to 200 GHz. Integrated optoelectronic circuits are made using similar technology. In designing MMICs, commercially available software packages are used for both electrical and layout design.

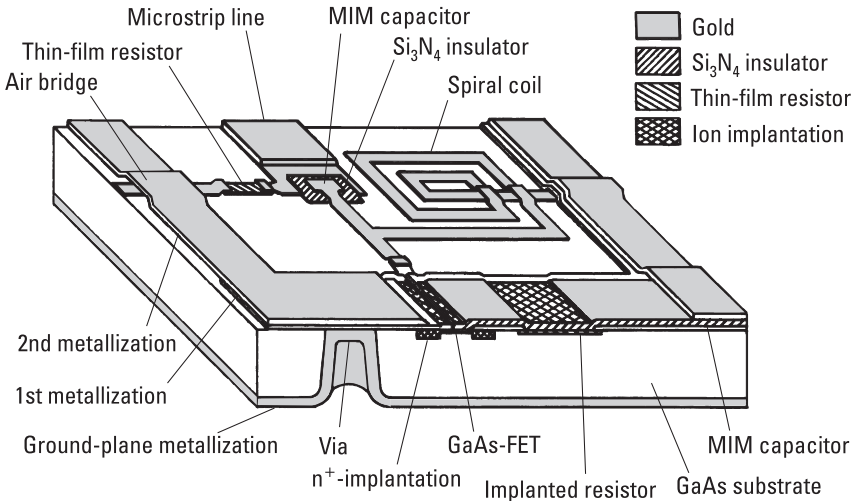


**Figure 8.27** Monolithic microwave integrated circuit on gallium arsenide (GaAs-MMIC).

## References

- [1] Sze, S. M., *Semiconductor Devices, Physics, and Technology*, New York: John Wiley & Sons, 1985.
- [2] Howes, M. J., and D. V. Morgan, *Gallium Arsenide Materials, Devices, and Circuits*, Chichester, England: John Wiley & Sons, 1986.

- [3] Yngvesson, S., *Microwave Semiconductor Devices*, Boston, MA: Kluwer Academic Publishers, 1991.
- [4] Zhang, J., and A. V. Räisänen, "Computer-Aided Design of Step Recovery Diode Frequency Multipliers," *IEEE Trans. on Microwave Theory and Techniques*, Vol. 44, No. 12, 1996, pp. 2612–2616.
- [5] Gentili, C., *Microwave Amplifiers and Oscillators*, New York: McGraw-Hill, 1987.
- [6] Rogers, R. G., *Low Phase Noise Microwave Oscillator Design*, Norwood, MA: Artech House, 1991.
- [7] Liao, S. Y., *Microwave Circuit Analysis and Amplifier Design*, Englewood Cliffs, NJ: Prentice Hall, 1987.
- [8] Abrie, P. L. D., *Design of RF and Microwave Amplifiers and Oscillators*, Norwood, MA: Artech House, 1999.
- [9] Ha, T., *Solid-State Microwave Amplifier Design*, New York: John Wiley & Sons, 1981.
- [10] Pozar, D. M., *Microwave Engineering*, 2nd ed., New York: John Wiley & Sons, 1998.
- [11] Lange, J., "Noise Characterization of Linear Two-Ports in Terms of Invariant Parameters," *IEEE J. of Solid-State Circuits*, Vol. 2, No. 2, 1967, pp. 37–40.
- [12] Hoffmann, R. K., *Handbook of Microwave Integrated Circuits*, Norwood, MA: Artech House, 1987.
- [13] Held, D. N., and A. R. Kerr, "Conversion Loss and Noise of Microwave and Millimeter-Wave Mixers: Part I—Theory," *IEEE Trans. on Microwave Theory and Techniques*, Vol. 26, No. 2, 1978, pp. 49–55.
- [14] Maas, S. A., *Microwave Mixers*, 2nd ed., Norwood, MA: Artech House, 1993.
- [15] Räisänen, A. V., "Frequency Multipliers for Millimeter and Submillimeter Wavelengths," *Proc. IEEE*, Vol. 80, No. 11, 1992, pp. 1842–1852.
- [16] Faber, M. T., J. Chramiec, and M. E. Adamski, *Microwave and Millimeter-Wave Diode Frequency Multipliers*, Norwood, MA: Artech House, 1995.
- [17] Collin, R. E., *Foundations for Microwave Engineering*, 2nd ed., New York: IEEE Press, 2001.
- [18] Bahl, I., and P. Bhartia, *Microwave Solid State Circuit Design*, New York: John Wiley & Sons, 1988.



# 9

## Antennas

Antennas transmit and receive radio waves. They operate as matching devices from a transmission line to the free space and vice versa. An ideal antenna radiates all the power incident from the transmission line feeding the antenna. It radiates to (or receives from) desired directions; in other words, an antenna has a certain radiation pattern.

Antennas are needed in nearly all applications of radio engineering. The congestion of the radio spectrum due to the increasing number of users and applications sets increasingly strict requirements for antennas. A large number of antenna structures have been developed for different frequencies and applications. Antennas can be categorized, for example, into current element antennas, traveling-wave antennas, aperture antennas, and antenna arrays.

In this chapter, the fundamental concepts of antennas, the calculation of radiation pattern and other antenna quantities, different types of antennas, and the link between two antennas are treated. Antennas are the subject of many books [1–8].

### 9.1 Fundamental Concepts of Antennas

Antennas are *reciprocal* devices. That means that the properties of an antenna are similar both in the transmitting mode and in the receiving mode. For example, if a transmitting antenna radiates to certain directions, it can also receive from those directions—the same radiation pattern applies for both



cases. The reciprocity does not apply if nonreciprocal components such as ferrite devices or amplifiers are integrated into the antenna. Also, a link between two antennas is reciprocal: The total loss is the same in both directions. However, magnetized plasma, such as in the ionosphere, between the antennas may cause Faraday rotation, making the link nonreciprocal.

The space surrounding an antenna can be divided into three regions according to the properties of the radiated field. Because the field changes smoothly, the boundaries between the regions are more or less arbitrary. The *reactive near-field region* is closest to the antenna. In this region, the reactive field component is larger than the radiating one. For a short current element, the reactive and radiating components are equal at a distance of  $\lambda/(2\pi)$  from the element. For other current distributions this distance is shorter. As the distance increases, the reactive field decreases as  $1/r^2$  or  $1/r^3$  and becomes negligible compared to the radiating field. In the *radiating near-field region* or *Fresnel region*, the shape of the normalized radiation pattern depends on the distance. As the distance of the observation point changes, the difference in distances to different parts of the antenna changes essentially compared to the wavelength. In the *far-field region* or *Fraunhofer region*, the normalized radiation pattern is practically independent of the distance and the field decreases as  $1/r$ . The boundary between the near-field and far-field regions is usually chosen to be at the distance of

$$r = \frac{2D^2}{\lambda} \quad (9.1)$$

where  $D$  is the largest dimension of the antenna perpendicular to the direction of observation. At the boundary, the edges of a planar antenna are  $\lambda/16$  farther away from the observation point P than the center of the antenna, as illustrated in Figure 9.1. This difference in distance corresponds to a phase

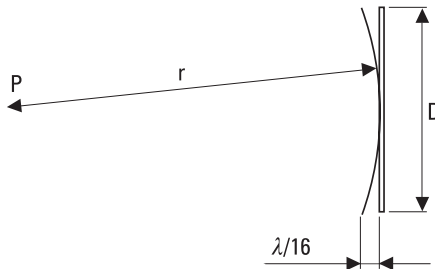


**Figure 9.1** At the boundary of near-field and far-field regions.

difference of  $22.5^\circ$ . Because antennas are usually operated at large distances, the far-field pattern is of interest. It should be noted that at lower frequencies in case of small antennas, the outer limit of the reactive near-field region,  $\lambda/(2\pi)$ , is larger than the distance obtained from (9.1).

The coordinate system used for antenna analysis or measurements should be defined clearly. In analysis, the complexity of equations depends on the system. Figure 9.2 shows the spherical coordinate system that is often used. The elevation angle  $\theta$  increases along a great circle from  $0^\circ$  to  $180^\circ$ . The azimuth angle  $\phi$  is obtained from the projection of the directional vector in the  $xy$ -plane, and it is between  $0^\circ$  and  $360^\circ$ .

An antenna can be described by several properties, which are related to the field radiated by the antenna, for example, directional pattern, gain, and polarization. Due to the reciprocity, these properties also describe the ability of the antenna to receive waves coming from different directions and having different polarizations. The importance of different radiation properties depends on the application. As a circuit element an antenna also has an impedance, efficiency, and bandwidth. Often mechanical properties such as the size, weight, and wind load are also very important.

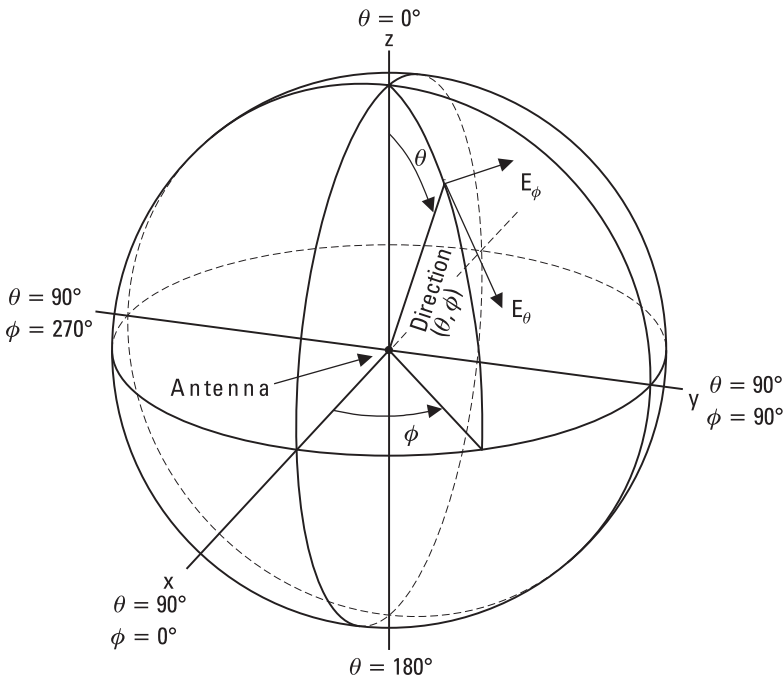


**Figure 9.2** Spherical coordinate system used for antenna analysis and measurements.

An isotropic antenna that radiates at an equal strength to all directions is a good reference antenna but is not realizable in practice. A real antenna has a certain *radiation pattern*, which describes the field distribution as the antenna radiates. Often the radiation pattern means the same as the *directional pattern*. The directional pattern describes the power density  $P(\theta, \phi)$  in watts per square meter or the electric field intensity  $E(\theta, \phi)$  in volts per meter as a function of direction. Usually, the directional pattern is normalized so that the maximum value of the power density or electric field is 1 (or 0 dB). The normalized field  $E_n(\theta, \phi)$  is equal to the square root of the normalized power density  $P_n(\theta, \phi)$ .

Often the antenna radiates mainly to one direction only. Then one main beam or the main lobe and possibly a number of lower maxima, sidelobes, can be distinguished, as in Figure 9.3(a). The directions of the lobes and nulls, the width of the main lobe, the levels of the sidelobes, and

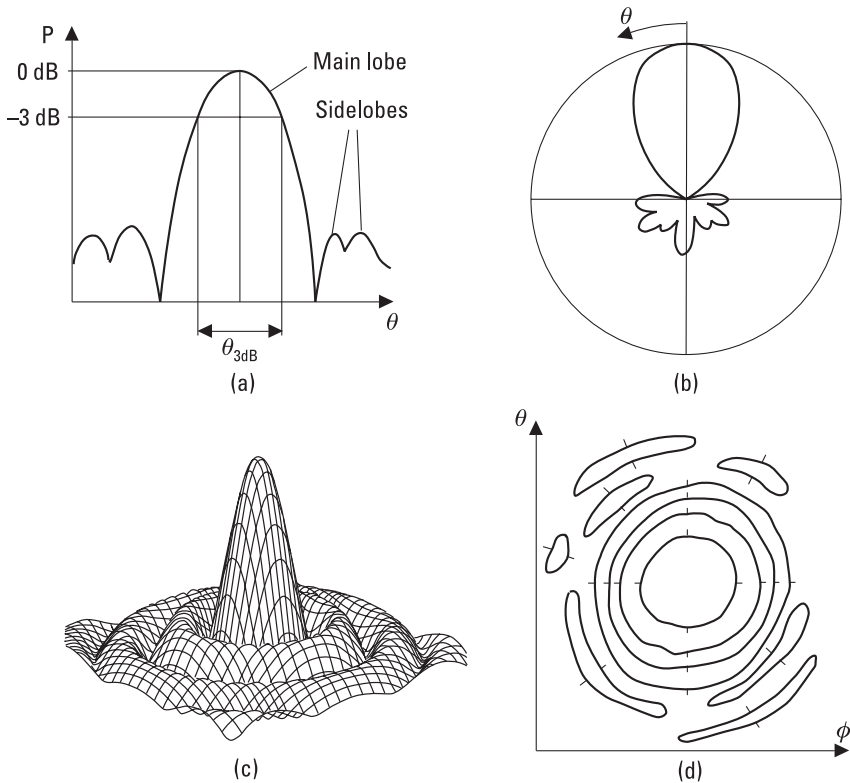


**Figure 9.3** Different representations of the directional pattern: (a) rectangular; (b) polar; (c) three-dimensional; and (d) constant-value contours.

the depths of nulls can be obtained from the directional pattern. The half-power beamwidth,  $\theta_{3\text{dB}}$  or  $\phi_{3\text{dB}}$ , is often used as the measure of the main lobe width.

Figure 9.3 shows different representations of directional patterns. The rectangular representation is suitable for directive antennas having a narrow main beam. The polar representation is natural for an antenna radiating over a wide range of angles. Both rectangular and polar plots are two-dimensional cuts of the three-dimensional pattern. The directional patterns are often  $\theta$ -cuts or  $\phi$ -cuts. For a  $\theta$ -cut, for example, the angle  $\theta$  is constant and the angle  $\phi$  is variable. The most important cuts are the cuts in the principal planes. The principal planes are orthogonal planes that intersect at the maximum of the main lobe, that is, at the boresight. For example, for a linearly polarized antenna, the principal planes are the  $E$ -plane and  $H$ -plane, which are the planes parallel to the electric field vector and magnetic field vector, respectively. The whole pattern can be represented as a three-dimensional or contour plot. The scale of different plots may be a linear power, a linear field, or a logarithmic (decibel) scale.

The number of different shapes of directional patterns is countless. A pencil beam antenna has a narrow and symmetrical main lobe. Such highly directional antennas are used, for example, in point-to-point radio links, satellite communication, and radio astronomy. The directional pattern of a terrestrial broadcasting antenna should be constant in the azimuth plane and shaped in the vertical plane to give a field strength that is constant over the service area. The directional pattern of an antenna in a satellite should follow the shape of the geographic service area.

The *directivity*  $D$  of an antenna is obtained by integrating the normalized power pattern  $P_n(\theta, \phi)$  over the whole solid angle  $4\pi$ :

$$D = \frac{4\pi}{\int\int_{4\pi} P_n(\theta, \phi) d\Omega} \quad (9.2)$$

where  $d\Omega$  is an element of the solid angle. Because  $P_n(\theta, \phi) = P(\theta, \phi)/P_{\text{max}}$ , the directivity is the maximum power density divided by the average power density.

### Example 9.1

The beam of an antenna is rotationally symmetric. Within the  $1^\circ$ -wide beam, the pattern level is  $P_n = 1$ , and outside the beam the pattern level is

$P_n = 0$ . (In practice, this kind of a beam is not realizable.) What is the directivity of this antenna?

**Solution**

Because the beamwidth is small, the section of the sphere corresponding to the beam can be approximated with a circular, planar surface. The beamwidth is  $1^\circ = \pi/180 = 0.01745$  radians. The solid angle of the beam is  $\Omega_A = \iint_{4\pi} P_n(\theta, \phi) d\Omega = \pi \times 0.01745^2/4 = 2.392 \times 10^{-4}$  steradians (square radians). The directivity is  $D = 4\pi/\Omega_A = 52,500$ , which in decibels is  $10 \log(52,500) = 47.2$  dB.

The *gain*  $G$  of an antenna is the ratio of the maximum radiation intensity produced by the antenna to the radiation intensity that would be obtained if the power accepted by the antenna were radiated equally in all directions. For an antenna having no loss, the gain is equal to the directivity. In practical antennas there are some conductor and dielectric losses. All the power coupled to the antenna is not radiated and the gain is smaller than the directivity:

$$G = \eta_r D \quad (9.3)$$

where  $\eta_r$  is the *radiation efficiency*. If the power coupled to the antenna is  $P$ , the power radiated is  $\eta_r P$ , and the power lost in the antenna is  $(1 - \eta_r)P$ . Losses due to impedance and polarization mismatches are not taken into account in the definition of gain. The directivity and gain can also be given as functions of direction:  $D(\theta, \phi) = P_n(\theta, \phi) \cdot D$ ,  $G(\theta, \phi) = P_n(\theta, \phi) \cdot G$ .

The *effective area*  $A_{ef}$  is a useful quantity for a receiving antenna. An ideal antenna with an area of  $A_{ef}$  receives from a plane wave, having a power density of  $S$ , the same power,  $A_{ef}S$ , as the real antenna. As shown in Section 9.6, the effective area is directly related to the gain as

$$A_{ef}(\theta, \phi) = \frac{\lambda^2}{4\pi} G(\theta, \phi) \quad (9.4)$$

Thus, the effective area of an isotropic antenna is  $\lambda^2/(4\pi)$ . For an antenna having a radiating aperture, the aperture efficiency is defined as

$$\eta_{ap} = \frac{A_{ef}}{A_{phys}} \quad (9.5)$$

where  $A_{phys}$  is the physical area of the aperture.

The *phase pattern*  $\psi(\theta, \phi)$  is the phase difference of the constant phase front radiated by the antenna and the spherical phase front of an ideal antenna. The position of the reference point where the spherical wave is assumed to emanate must be given. The *phase center* of an antenna is the reference point that minimizes the phase difference over the main beam. For example, the phase center of the feed antenna and the focal point of the reflector that is illuminated by the feed should coincide.

The *polarization* of an antenna describes how the orientation of the electric field radiated by the antenna behaves as a function of time. We can imagine that the tip of the electric field vector makes an ellipse during one cycle on a plane that is perpendicular to the direction of propagation (Figure 9.4). The polarization ellipse is defined by its axial ratio  $E_{max}/E_{min}$ , its tilt angle  $\tau$ , and its sense of rotation. The special cases of the elliptical polarization are the linear polarization and the circular polarization. The polarization of an antenna is also a function of angle  $(\theta, \phi)$ .

The field radiated by the antenna can be divided into two orthogonal components: the copolar and cross-polar field. Often the copolar component is used for the intended operation and the cross-polar component represents an unwanted radiation or an interference. Linear polarizations that are perpendicular to each other, as for example the vertical and horizontal polarizations, are orthogonal. The right-handed and left-handed circular polarization are orthogonal to each other as well.

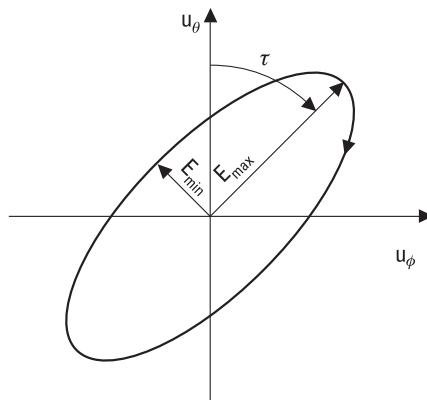


**Figure 9.4** Polarization ellipse.

Generally, the polarization of an incoming wave and the polarization of the antenna are different, which causes a polarization mismatch. If the polarizations are the same, there will be no mismatch and the polarization efficiency is  $\eta_p = 1$ . In the case of orthogonal polarizations, no energy couples to the antenna and  $\eta_p = 0$ . If the wave is circularly polarized and the antenna is linearly polarized, one-half of the power incident on the effective area couples to the antenna, that is,  $\eta_p = 1/2$ .

The quantities  $P_n(\theta, \phi)$ ,  $E_n(\theta, \phi)$ ,  $D(\theta, \phi)$ ,  $G(\theta, \phi)$ ,  $A_{ef}(\theta, \phi)$ , and  $\psi(\theta, \phi)$  can be given for both copolar and cross-polar fields. An ideal antenna has no cross polarization. The cross-polar field of a practical antenna depends on the angle  $(\theta, \phi)$  and is often at minimum in the direction of the main beam. An antenna should have a low level of cross-polarization, for example in such applications where two channels are transmitted at the same frequency using two orthogonal polarizations.

All the power couples from the transmission line to the antenna and vice versa, if the *impedance*  $Z$  of the antenna is equal to the characteristic impedance of the transmission line (note that the characteristic impedance of a transmission line is real). A part of the power reflects back from an impedance mismatch. The impedance  $Z = R + jX$  has a resistive part and a reactive part. The resistive part,  $R = R_r + R_l$ , is divided into the *radiation resistance*  $R_r$  and the loss resistance  $R_l$ . The power “absorbed” in the radiation resistance is radiated and the power absorbed in the loss resistance is transformed into heat in the antenna. The impedance of an antenna depends on its surroundings. The reflections coming from nearby objects, such as the head of a mobile phone user, alter the impedance. Due to the mutual couplings of elements in an antenna array, the impedance of an element embedded in the array differs from that of the element alone in free space.

The *bandwidth* of an antenna can be defined to be the frequency band in which the impedance match, gain, beamwidth, sidelobe level, cross-polarization level, or some other quantity is within the accepted limits.

The parameters of an antenna may also be adjustable. In case of an adaptive antenna, its impedance, radiation pattern, or some other characteristic can adapt according to the electromagnetic environment.

## 9.2 Calculation of Radiation from Antennas

The fields radiated by an antenna can be calculated using auxiliary quantities called the magnetic vector potential  $\mathbf{A}$  and the electric vector potential  $\mathbf{F}$ .

An antenna can be considered to be a sinusoidal current density distribution  $\mathbf{J}$  in a volume  $V$ . At a point of space, the magnetic vector potential is

$$\mathbf{A} = \frac{\mu}{4\pi} \int_V \frac{\mathbf{J} e^{-jkR}}{R} dV \quad (9.6)$$

where  $R$  is the distance from a volume element  $dV$  to the point of observation and  $k = 2\pi/\lambda$ . If the currents flow on a surface  $S$  and the surface current density is  $\mathbf{J}_s$ , (9.6) can be written as

$$\mathbf{A} = \frac{\mu}{4\pi} \int_S \frac{\mathbf{J}_s e^{-jkR}}{R} dS \quad (9.7)$$

The electric field  $\mathbf{E}$  and magnetic field  $\mathbf{H}$  are calculated as

$$\mathbf{E} = -\frac{j\omega}{k^2} \nabla \times \nabla \times \mathbf{A} = -\frac{j\omega}{k^2} \nabla(\nabla \cdot \mathbf{A}) - j\omega \mathbf{A} \quad (9.8)$$

$$\mathbf{H} = \frac{1}{\mu} \nabla \times \mathbf{A} \quad (9.9)$$

In principle, the radiated fields can be calculated for all antennas using these equations. They are well suited for wire antennas that have a known current distribution.

An aperture antenna, such as a horn antenna, has an aperture or a surface from which the radiation seems to emanate. It may be difficult to find out the current distribution. Then it may be easier to calculate the radiated fields from the aperture fields  $\mathbf{E}_a$  and  $\mathbf{H}_a$ . The aperture fields are replaced with surface currents that would produce the aperture fields. The magnetic field is replaced with a surface current having a density of

$$\mathbf{J}_s = \mathbf{n} \times \mathbf{H}_a \quad (9.10)$$

where  $\mathbf{n}$  is a unit vector normal to the surface of the aperture. The vector potential  $\mathbf{A}$  corresponding to  $\mathbf{J}_s$  is then calculated. The radiated field components are obtained from (9.8) and (9.9). The electric field of the aperture is replaced with a magnetic surface current having a density of



$$\mathbf{M}_s = -\mathbf{n} \times \mathbf{E}_a \quad (9.11)$$

The electric vector potential is defined as

$$\mathbf{F} = \frac{\epsilon}{4\pi} \int_S \frac{\mathbf{M}_s e^{-jkR}}{R} dS \quad (9.12)$$

The radiated field components corresponding to  $\mathbf{M}_s$  are

$$\mathbf{E} = -\frac{1}{\epsilon} \nabla \times \mathbf{F} \quad (9.13)$$

$$\mathbf{H} = -\frac{j\omega}{k^2} \nabla \times \nabla \times \mathbf{F} = -\frac{j\omega}{k^2} \nabla(\nabla \cdot \mathbf{F}) - j\omega \mathbf{F} \quad (9.14)$$

The total radiated field is obtained by summing up the field components due to  $\mathbf{J}_s$  and  $\mathbf{M}_s$ .

### 9.3 Radiating Current Element

Figure 9.5 shows a short current element at the origin. The element of a length  $dz$  along the  $z$ -axis carries an alternating sinusoidal current  $I_0$ , which is constant along the element. This kind of current element is also called

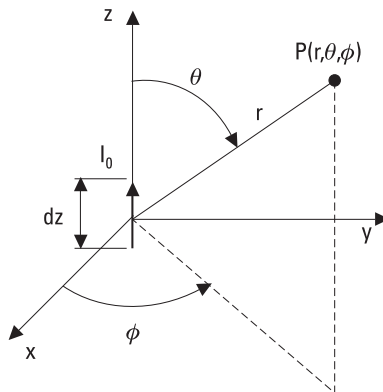


**Figure 9.5** Radiating current element.

the Hertz dipole. In his experiments, Heinrich Hertz used end-loaded dipoles. Because of the capacitive loadings, currents could flow even at the ends of the dipole making a nearly constant current distribution possible. As explained in Chapter 2, a fluctuating current produces electromagnetic waves: The current produces a changing magnetic field, the changing magnetic field produces a changing electric field, the changing electric field produces a changing magnetic field, and so on.

The volume integral of the current density is  $\int_V \mathbf{J} dV = I_0 dz \mathbf{u}_z$  in the case of a current element. Therefore, the vector potential at a point  $P(r, \theta, \phi)$  is

$$\mathbf{A} = \frac{\mu}{4\pi} \cdot \frac{I_0 dz e^{-jkr}}{r} \mathbf{u}_z = A_z \mathbf{u}_z \quad (9.15)$$

The components of the vector potential in the spherical coordinate system are  $A_r = A_z \cos \theta$ ,  $A_\theta = -A_z \sin \theta$ , and  $A_\phi = 0$ . Equations (9.8) and (9.9) give the components of the fields:

$$E_r = \frac{I_0 dz}{4\pi} e^{-jkr} \left( \frac{2\eta}{r^2} + \frac{2}{j\omega\epsilon r^3} \right) \cos \theta \quad (9.16)$$

$$E_\theta = \frac{I_0 dz}{4\pi} e^{-jkr} \left( \frac{j\omega\mu}{r} + \frac{\eta}{r^2} + \frac{1}{j\omega\epsilon r^3} \right) \sin \theta \quad (9.17)$$

$$H_\phi = \frac{I_0 dz}{4\pi} e^{-jkr} \left( \frac{jk}{r} + \frac{1}{r^2} \right) \sin \theta \quad (9.18)$$

$$E_\phi = H_r = H_\theta = 0 \quad (9.19)$$

where  $\eta$  is the wave impedance in free space.

Those components of the field having a  $1/r^2$  or  $1/r^3$  dependence dominate at small distances but become negligible at larger distances. Far away from the element, the fields are

$$E_\theta = \frac{j\omega\mu I_0 dz}{4\pi r} e^{-jkr} \sin \theta \quad (9.20)$$

$$H_\phi = \frac{E_\theta}{\eta} \quad (9.21)$$

Other components are negligible. The electric and magnetic fields are in phase and perpendicular to each other, just like in the case of a plane wave.

The power radiated by the current element is calculated by integrating the Poynting vector  $\mathbf{S} = (1/2) \text{Re}(\mathbf{E} \times \mathbf{H}^*)$  over a sphere surrounding the element. If the radius of the sphere,  $r$ , is much larger than  $dz$ ,  $\mathbf{S}$  is perpendicular to the surface of the sphere and the outflowing power per unit area is  $S = |\mathbf{S}| = (1/2)|E_\theta H_\phi|$ . The surface element for integration is selected as shown in Figure 9.6. The power radiated is

$$P = \int_0^\pi S 2\pi r^2 \sin \theta d\theta = 40\pi^2 I_0^2 \left(\frac{dz}{\lambda}\right)^2 \quad (9.22)$$

The radiation resistance of the current element is obtained by equating the radiated power with  $P = (1/2)R_r I_0^2$ :

$$R_r = 80\pi^2 \left(\frac{dz}{\lambda}\right)^2 \Omega \quad (9.23)$$

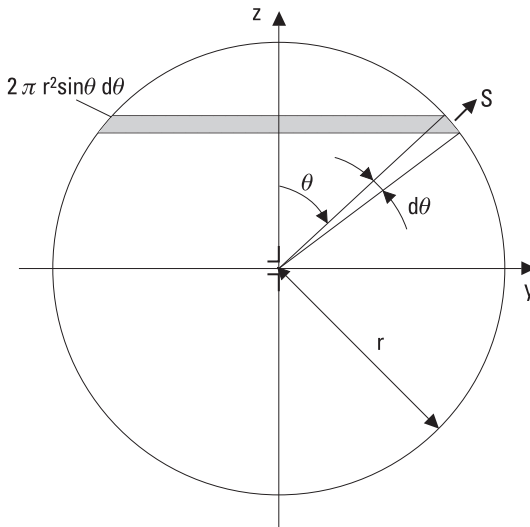


**Figure 9.6** Integration of power density over a sphere.

## 9.4 Dipole and Monopole Antennas

Wire antennas are popular at frequencies below 1 GHz. The dipole antenna is the most often used wire antenna. It is a straight wire, which is usually split in the middle so that it can be fed by a transmission line.

It can be thought that a dipole shown in Figure 9.7 consists of current elements in a line. The far field is calculated by summing the fields produced by the current elements, that is, by integrating (9.20):

$$E_{\theta} = \frac{j\omega\mu}{4\pi} \int_{-l/2}^{l/2} \frac{I(z)e^{-jkR(z)}}{R(z)} \sin \theta(z) dz \quad (9.24)$$

where  $l$  is the length of the dipole. It can be assumed that the current distribution  $I(z)$  is sinusoidal and at the ends of the wire the current is zero. This assumption applies well for a thin wire. The current distribution can be considered to be a standing wave pattern, which is produced as the current wave reflects from the end of the wire. The current distribution is

$$I(z) = \begin{cases} I_0 \sin [k(l/2 - z)], & \text{for } z > 0 \\ I_0 \sin [k(l/2 + z)], & \text{for } z < 0 \end{cases} \quad (9.25)$$

where  $I_0$  is the maximum current. Far away from the antenna at a point  $P(r, \theta, \phi)$  it applies  $\theta(z) \approx \theta$  and  $1/R(z) \approx 1/r$ , so these terms can be

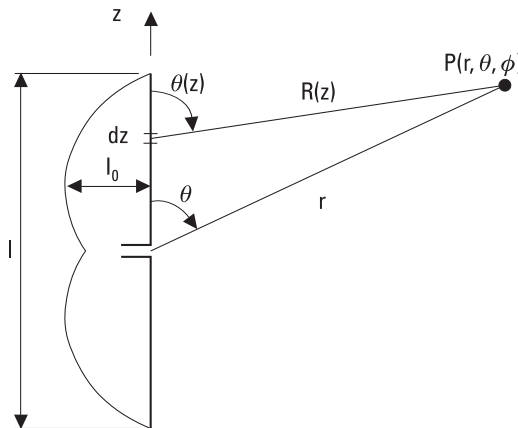


Figure 9.7 Dipole antenna.

assumed to be constant in (9.24). However, small changes in  $R(z)$  as a function of  $z$  have to be taken into account in the phase term  $e^{-jkR(z)}$ . The distance from  $P$  to the element is

$$R(z) = \sqrt{r^2 + z^2 - 2rz \cos \theta} \approx r - z \cos \theta \quad (9.26)$$

From (9.24), the field radiated by the dipole is

$$E_\theta = \frac{j\eta I_0}{2\pi r} e^{-jkr} \frac{\cos\left(\frac{1}{2}kl \cos \theta\right) - \cos\left(\frac{1}{2}kl\right)}{\sin \theta} \quad (9.27)$$

If the dipole is short compared to a wavelength, the current distribution is approximately triangular. Its radiation resistance is a quarter of that of the Hertz dipole having the same length:

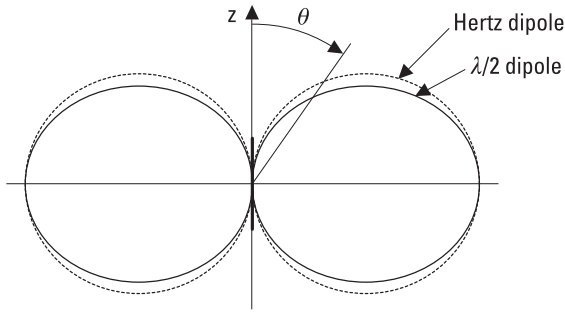
$$R_r \approx 20\pi^2 \left(\frac{l}{\lambda}\right)^2 \Omega \quad (9.28)$$

This is valid up to about a length of  $l = \lambda/4$ .

The half-wave dipole is the most important of dipole antennas. When  $l = \lambda/2$ , it follows from (9.27) that

$$E_\theta = \frac{j\eta I_0}{2\pi r} e^{-jkr} \frac{\cos\left(\frac{\pi}{2} \cos \theta\right)}{\sin \theta} \quad (9.29)$$

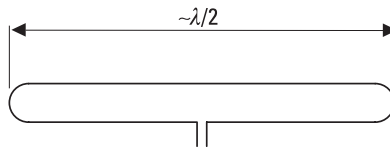
The maximum of the field is in the plane perpendicular to the wire and the nulls are along the direction of the wire. The half-power beamwidth is  $\theta_{3\text{dB}} = 78^\circ$ . The directivity is  $D = 1.64$  (2.15 dB), which is also the gain  $G$  for a lossless half-wave dipole. The directional patterns of the half-wave dipole and the Hertz dipole ( $\theta_{3\text{dB}} = 90^\circ$ ,  $D = 1.5$ ) are compared in Figure 9.8. The radiation resistance of the half-wave dipole is  $R_r = 73.1\Omega$  in a lossless case. The input impedance also includes some inductive reactance. The impedance could be made purely resistive by reducing the length of the wire by a few percent; this will reduce the radiation resistance too. In practice, the properties of the half-wave dipole also depend on the thickness of the wire.



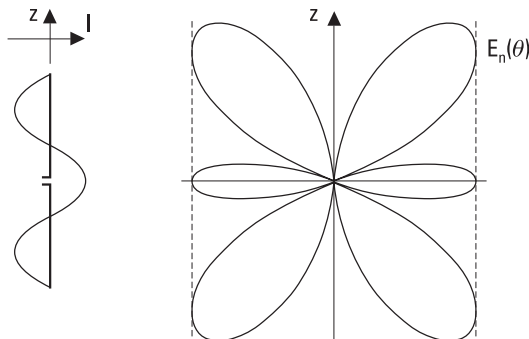
**Figure 9.8** Normalized directional patterns of the half-wave and Hertz dipole.

Figure 9.9 shows a folded dipole. Both of the half-wave-long wires have a similar current distribution. Therefore, the folded dipole produces a field twice of that of the half-wave dipole for a given feed current. Thus, the radiated power is four times that of the half-wave dipole and the radiation resistance is about  $300\Omega$ . A parallel-wire line having a characteristic impedance of  $300\Omega$  is suitable for feeding a folded dipole antenna.

If a dipole antenna has a length of a few half-wavelengths, its directional pattern has several lobes. Figure 9.10 shows the current distribution and directional pattern of a  $3\lambda/2$ -long dipole. As the length  $l$  further increases,



**Figure 9.9** Folded dipole antenna.



**Figure 9.10** A  $3\lambda/2$ -long dipole antenna: current distribution and directional pattern.

the number of lobes increases. The envelope of the lobes forms a cylinder around the  $z$ -axis. The feed point of a dipole antenna is usually in the middle but can be at some other point. The directional pattern and impedance depend on the position of the feed point.

**Example 9.2**

Let us consider two dipole antennas having lengths of  $0.1\lambda$  and  $0.5\lambda$ . Both have a feed current of 1A. What are the radiated powers?

**Solution**

From (9.28), the radiation resistance is  $R_r = 1.97\Omega$  as  $l = 0.1\lambda$ . The radiated power  $P = \frac{1}{2}R_r I^2 = 1.0\text{W}$ . For the half-wave dipole,  $R_r = 73.1\Omega$  and  $P = 36.5\text{W}$ . Thus, a short dipole is ineffective and its small resistance is difficult to match to a transmission line.

The monopole antenna is a straight wire above a ground plane as shown in Figure 9.11(a). In the analysis, the image principle can be applied. The conducting plane can be removed if an image of the current distribution is placed on the other side of the plane, as in Figure 9.11(b). This way the tangential electric field vanishes at the plane where the conducting plane was.

The monopole antenna and the dipole antenna formed according to the image principle have similar fields in the half-space above the ground plane. For a given feed current, the power radiated by the monopole is half of that of the corresponding dipole because the monopole produces no fields below the ground plane. Therefore, the radiation resistance of a quarter-wave monopole is  $36.5\Omega$ , which is half of that of a half-wave dipole. The gain of the monopole is twice of that of the dipole.

In practice, the ground plane of a monopole antenna is finite and has a finite conductivity. Therefore, the main lobe is tilted upward and there

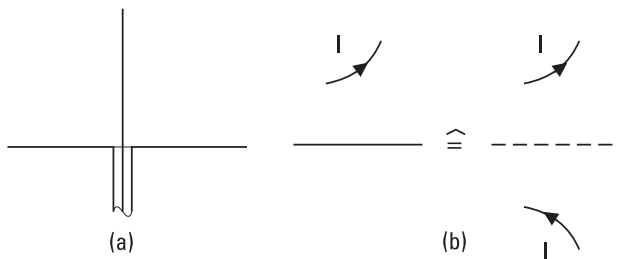


**Figure 9.11** (a) Monopole antenna; and (b) image principle.

may be a null along the direction of the surface. At low frequencies, a flat ground acts as a ground plane. The conductivity may be improved by introducing metal wires into the ground.

Monopole antennas operating at VLF and LF ranges are short compared to a wavelength and have a low radiation resistance. Their efficiency can be improved by adding a horizontal wire at the top, as shown in Figure 9.12. Due to the top loading, the current in the vertical part is increased. The fields produced by the vertical part and its image add constructively. However, the fields from the horizontal part and its image cancel each other, because their currents flow to opposite directions and their distance is small compared to a wavelength.

Dipole and monopole antennas are omnidirectional in the plane perpendicular to the wire and thus have a low directivity. Figure 9.13 shows a Yagi (or Yagi-Uda) antenna, which is an antenna commonly used for TV reception. It consists of an array of parallel dipoles, which together form a directional antenna. Only one element, the driven element, is fed from the transmission line. There is a reflector behind the driven element and directors in front of it. Currents are induced to these parasitic elements. The fields

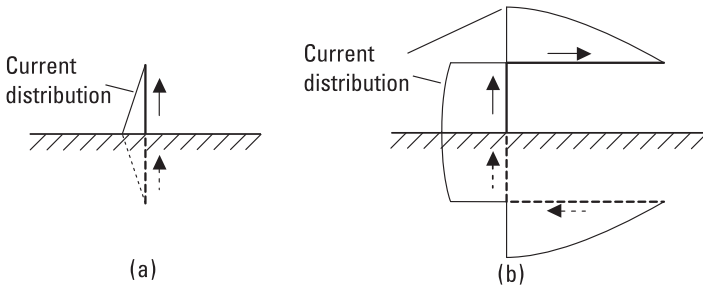


**Figure 9.12** (a) Short monopole antenna; and (b) top-loaded monopole antenna.

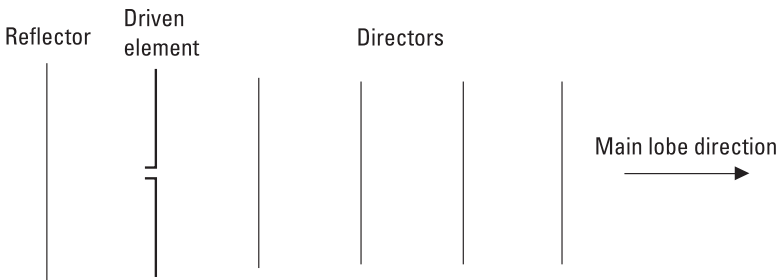


**Figure 9.13** Yagi antenna.



produced by the driven and parasitic elements add in phase in the forward direction and cancel in the reverse direction.

The driven element of a Yagi antenna is in a resonance, that is, the input impedance is resistive, when the length of the element is 0.45 to 0.48 wavelength. The driven element is often a folded dipole. The reflector is 0.15 to 0.30 wavelength behind the driven element and it is about 5% longer than the driven element. The directors are about 5% shorter than the driven element and their spacings are 0.15 to 0.30 wavelength. Often the directors have equal lengths and equal spacings, although the optimization of dimensions would give a slightly higher directivity. A larger number of director elements means a higher directivity. Usually there are three to twelve directors. The directivity of a seven-element Yagi is typically 12 dB. The narrow bandwidth is a drawback of the Yagi antenna. In a cold climate snow and ice covering the elements may easily spoil the directional pattern.

A log-periodic antenna is a broadband antenna whose properties repeat at frequencies having a constant ratio of  $\tau$ . The structure is periodic so that if all the dimensions are multiplied or divided by  $\tau$ , the original structure, excluding the outermost elements, is obtained. Figure 9.14 shows a log-periodic dipole antenna. The antenna is fed from the high-frequency end, and the feed line goes through all elements, so that the phase is reversed from an element to the next one. Only the element being in resonance radiates effectively. The element behind it acts as a reflector and the element in front of it acts as a director. Thus, the active part of the antenna depends on the frequency. The directivity is typically 8 dB.

## 9.5 Other Wire Antennas

A loop antenna is a circular or rectangular wire, which may consist of several turns. If the loop is small compared to a wavelength, the current is nearly

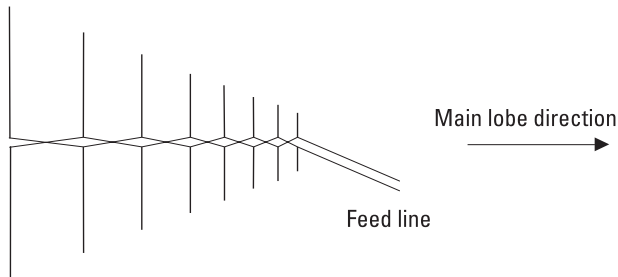


**Figure 9.14** Log-periodic dipole antenna.

constant along the loop. The maximum of the directional pattern is in the plane of the loop and the nulls are perpendicular to that plane as in Figure 9.15(a). The pattern is like the pattern of a small dipole having the electric and magnetic fields interchanged. Therefore, a small loop can be considered to be a magnetic dipole. The radiation resistance is

$$R_r = 320\pi^4 \left( \frac{NA}{\lambda^2} \right)^2 \Omega \quad (9.30)$$

where  $A$  is the area of the loop and  $N$  is the number of turns.

The current of a larger loop is not constant. Then the directional pattern differs from that of a small loop. If the length of the circumference is one wavelength, the maximum of the directional pattern is perpendicular to the plane of the loop and the null is in the plane of the loop. Figure 9.15(b) shows a quad antenna, which is made of such loops. Like the Yagi antenna, the quad antenna has a driven element, a reflector, and one or more directors. Quad antennas operating at different frequency ranges can be placed inside each other because the coupling of such loops is small.

A helix antenna, shown in Figure 9.16, is a helical wire having either the left-handed or right-handed sense. If the length of the circumference  $L$  is less than  $\lambda/2$ , the helix antenna radiates in the normal mode; that is, the maximum of the directional pattern is perpendicular to the axis of the helix. This kind of a helix antenna operates as a shortened monopole, except the field is elliptically polarized. If  $L$  is from  $0.75\lambda$  to  $1.25\lambda$ , the helix antenna operates in the axial mode; that is, the main beam is along the axis of the helix and the field is circularly polarized.

Long-wire and rhombic antennas are traveling-wave antennas, which are used at HF range. The current has constant amplitude but the phase changes linearly along the wire (in a dipole antenna, the amplitude of the current changes but the phase is constant).

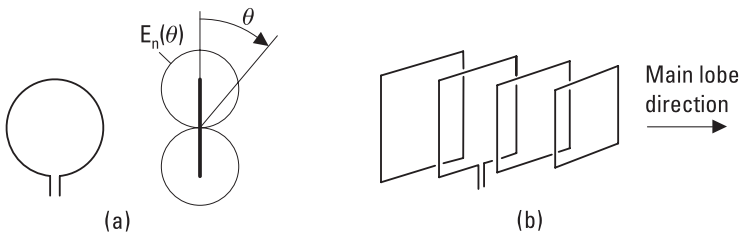


**Figure 9.15** (a) Small loop antenna and its directional pattern; and (b) quad antenna.

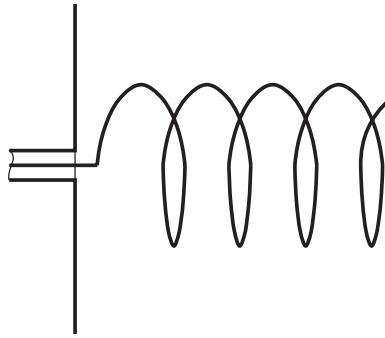


**Figure 9.16** Helix antenna fed from a coaxial cable through a conducting plane.

The long-wire antenna is usually a horizontal wire, which is terminated with a matched load, as shown in Figure 9.17. The conical directional pattern is

$$E_n(\alpha) = \frac{\sin \alpha}{1 - \cos \alpha} \sin [\pi L(1 - \cos \alpha)/\lambda] \tag{9.31}$$

where  $\alpha$  is the angle from the direction of the wire and  $L$  is the length of the wire. The longer the wire, the smaller the angle  $\alpha_m$  is between the directions of the main lobe and the wire. For an antenna having a length of several wavelengths, the main lobe direction is  $\alpha_m \approx \sqrt{\lambda/L}$ . A V-antenna is made of two long-wire antennas placed in an angle of  $2\alpha_m$  to each other. It has a better directional pattern than a single long-wire antenna because the main lobes of the two wires reinforce each other.

A rhombic antenna is made of four horizontal long-wire antennas (or two V-antennas), as shown in Figure 9.18. It is fed from a parallel-wire line and is terminated with a matched load. The fields produced by the long-

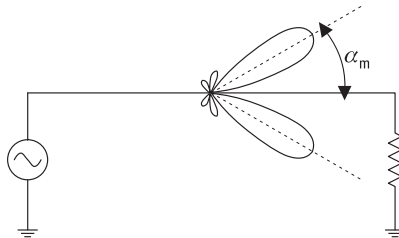


**Figure 9.17** Long-wire antenna.

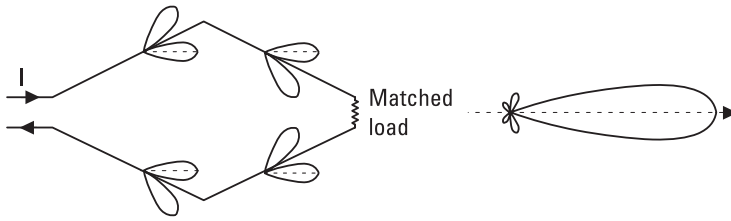


**Figure 9.18** Rhombic antenna and its directional pattern.

wire antennas are all in phase in the forward direction. In practice, the main lobe tilts slightly upward, due to the ground.

## 9.6 Radiation from Apertures

Figure 9.19 shows a surface element  $dS$  at the origin in the  $xy$ -plane. The electric field  $E_x$  and magnetic field  $H_y = E_x / \eta$  are constant over the element. These aperture fields can be replaced with surface currents  $\mathbf{M}_s = -E_x \mathbf{u}_y$  and  $\mathbf{J}_s = -E_x / \eta \mathbf{u}_x$ . The vector potentials at a point  $P(r, \theta, \phi)$  are

$$\mathbf{A} = -\frac{\mu E_x}{4\pi r \eta} e^{-jkr} dS \mathbf{u}_x \quad (9.32)$$

$$\mathbf{F} = -\frac{\epsilon E_x}{4\pi r} e^{-jkr} dS \mathbf{u}_y \quad (9.33)$$

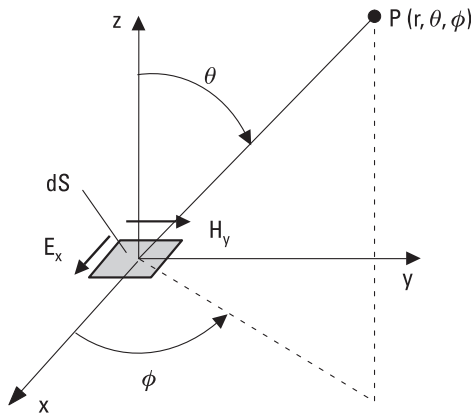


**Figure 9.19** Radiating surface element.

These vector potentials are then expressed in the spherical coordinate system. For example, the components of the magnetic vector potential are  $A_r = \sin \theta \cos \phi A_x$ ,  $A_\theta = \cos \theta \cos \phi A_x$ , and  $A_\phi = -\sin \phi A_x$ . As the curl of the vector potential is expressed in the spherical coordinate system, it can be noted, that far away from the element the radial component is negligible. Then the curl simplifies to

$$\nabla \times \mathbf{A} = -\frac{\partial A_\phi}{\partial r} \mathbf{u}_\theta + \frac{\partial A_\theta}{\partial r} \mathbf{u}_\phi \quad (9.34)$$

The  $\theta$  and  $\phi$ -components of the electric field are solved using (9.9) and (9.13):

$$E_\theta = \frac{jE_x}{2\lambda r} e^{-jkr} (1 + \cos \theta) \cos \phi dS \quad (9.35)$$

$$E_\phi = \frac{jE_x}{2\lambda r} e^{-jkr} (1 + \cos \theta) (-\sin \phi) dS \quad (9.36)$$

The power density produced by the surface element is

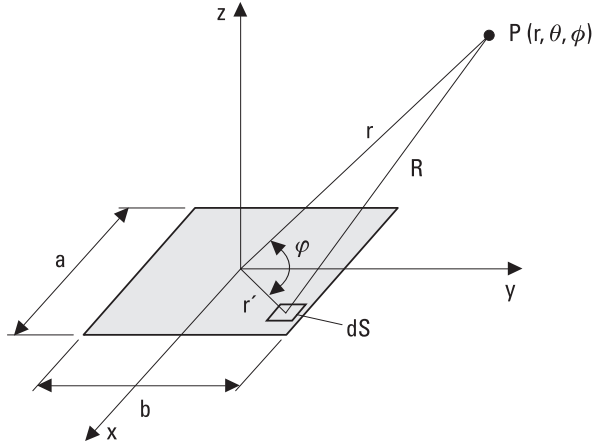
$$S = \frac{1}{2} \frac{|E_\theta|^2 + |E_\phi|^2}{\eta} = \frac{1}{2\eta} \left( \frac{E_x dS}{\lambda r} \right)^2 \cos^4(\theta/2) \quad (9.37)$$

Figure 9.20 shows a rectangular radiating aperture, which is in the  $xy$ -plane and whose center is at the origin. The width of the aperture is  $a$  in the  $x$ -direction and  $b$  in the  $y$ -direction. The electric field  $E_x$  has a constant amplitude and phase over the whole aperture. The magnetic field is  $H_y = E_x/\eta$ . Thus, the aperture is like a part of a plane wave.

Far away from the aperture the field is obtained by integrating the field of the surface element, (9.35) and (9.36), over the aperture. Because the aperture field is constant, the integration simplifies to an integration of the phase term  $e^{-jkR}$ , where the distance from the surface element to the point of observation P varies. Far from the aperture

$$R \approx r - r' \cos \varphi \quad (9.38)$$

where  $r'$  is the distance of the surface element from the origin and  $\varphi$  is the angle between the vectors  $\mathbf{r}$  and  $\mathbf{r}'$ . The variable term  $r' \cos \varphi$  can be written as



**Figure 9.20** Radiating aperture.

$$\begin{aligned}
 r' \cos \phi &= \mathbf{u}_r \cdot \mathbf{r}' \\
 &= (\mathbf{u}_x \sin \theta \cos \phi + \mathbf{u}_y \sin \theta \sin \phi + \mathbf{u}_z \cos \theta) \cdot (\mathbf{u}_x x' + \mathbf{u}_y y') \\
 &= x' \sin \theta \cos \phi + y' \sin \theta \sin \phi
 \end{aligned} \tag{9.39}$$

where  $x'$  and  $y'$  are the coordinates of the surface element. Integration gives the  $\theta$ -component of the electric field:

$$\begin{aligned}
 E_\theta &= \frac{jE_x}{2\lambda r} e^{-jkr} (1 + \cos \theta) \cos \phi \int_{-b/2}^{b/2} \int_{-a/2}^{a/2} e^{jk(x' \sin \theta \cos \phi + y' \sin \theta \sin \phi)} dx' dy' \\
 &= \frac{jabE_x}{2\lambda r} e^{-jkr} (1 + \cos \theta) \cos \phi \left[ \frac{\sin \left( \frac{1}{2} ka \sin \theta \cos \phi \right)}{\frac{1}{2} ka \sin \theta \cos \phi} \right] \\
 &\quad \cdot \left[ \frac{\sin \left( \frac{1}{2} kb \sin \theta \sin \phi \right)}{\frac{1}{2} kb \sin \theta \sin \phi} \right]
 \end{aligned} \tag{9.40}$$

Correspondingly, the  $\phi$ -component is

$$E_{\phi} = \frac{jabE_x}{2\lambda r} e^{-jkr} (1 + \cos \theta) (-\sin \phi) \left[ \frac{\sin \left( \frac{1}{2} ka \sin \theta \cos \phi \right)}{\frac{1}{2} ka \sin \theta \cos \phi} \right] \cdot \left[ \frac{\sin \left( \frac{1}{2} kb \sin \theta \sin \phi \right)}{\frac{1}{2} kb \sin \theta \sin \phi} \right] \quad (9.41)$$

In the  $E$ - or  $xz$ -plane ( $\phi = 0^\circ$ ), the electric field has only the  $E_{\theta}$ -component, and in the  $H$ - or  $yz$ -plane ( $\phi = 90^\circ$ ), only the  $E_{\phi}$ -component.

If the aperture is large ( $a$  and  $b \gg \lambda$ ), the field is significant at small  $\theta$  angles only. Then  $\cos \theta \approx 1$  and  $\sin \theta \approx \theta$ , and the normalized directional patterns in the  $E$ - and  $H$ -planes simplify to

$$E_n(\theta, \phi = 0^\circ) = \left| \frac{\sin \left( \frac{1}{2} ka\theta \right)}{\frac{1}{2} ka\theta} \right| \quad (9.42)$$

$$E_n(\theta, \phi = 90^\circ) = \left| \frac{\sin \left( \frac{1}{2} kb\theta \right)}{\frac{1}{2} kb\theta} \right| \quad (9.43)$$

Figure 9.21 shows the directional pattern in the  $E$ -plane. It can be solved from (9.42) that the first null in the  $E$ -plane is at an angle of

$$\theta_0 = \frac{\lambda}{a} \quad (9.44)$$

and the half-power beamwidth is

$$\theta_{3\text{dB}} \approx 0.89 \frac{\lambda}{a} \quad (9.45)$$

and the level of the first sidelobe is  $-13.3$  dB.

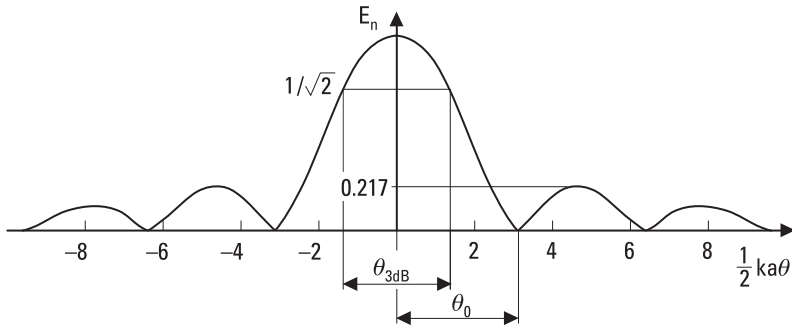


**Figure 9.21** Normalized directional pattern of a rectangular aperture.

The maximum power density produced by the rectangular aperture is

$$S_{max} = \frac{1}{2\eta} \left( \frac{E_x ab}{\lambda r} \right)^2 \quad (9.46)$$

Because  $\int_{-\infty}^{\infty} \sin^2 x/x^2 dx = \pi$ , the average power density produced by a large aperture is

$$S_{av} = \frac{1}{4\pi} \iint_{4\pi} S d\Omega \approx \frac{1}{4\pi} S_{max} \frac{2\pi}{ka} \frac{2\pi}{kb} \quad (9.47)$$

The ratio of these power densities, the directivity, is

$$D = \frac{S_{max}}{S_{av}} = \frac{4\pi}{\lambda^2} ab \quad (9.48)$$

Assuming a lossless aperture ( $D = G$ ) and comparing (9.48) to (9.4), we can see that the physical and effective areas are equal, that is,  $ab = A_{eff}$ .

The radiation pattern of an aperture antenna having an arbitrary shape, amplitude distribution, and phase distribution is calculated using the same principle as above: The fields produced by the surface elements are summed at the point of observation.

If a rectangular aperture has a field distribution of a form  $f(x)g(y)$ , the normalized patterns in the  $xz$ - and  $yz$ -planes are those of the line sources



(one-dimensional apertures) having aperture distributions of  $f(x)$  and  $g(y)$ , respectively. The normalized pattern is the product of the normalized patterns in the  $xz$ - and  $yz$ -planes.

Table 9.1 shows properties of line sources having different amplitude distributions. The constant amplitude distribution gives the narrowest beam but the highest level of sidelobes. If the amplitude of the field decreases toward the edge of the aperture, the beamwidth increases, the gain decreases, and the sidelobe level decreases.

Earlier it was assumed that the phase of the aperture was constant. In practice, a quadratic phase distribution is usual. Then constant phase fronts are nearly spherical in the aperture. Figure 9.22 shows directional patterns for line sources having a constant amplitude but quadratic phase distribution. As the parameter  $\Delta$  (phase difference between the center and edge in wavelengths) increases, gain decreases, sidelobes increase, and nulls get filled.

The properties of circular apertures are listed in Table 9.2 for different amplitude distributions (the phase is constant). If the aperture has a constant amplitude, the normalized directional pattern is

$$E_n(\theta) = 2 \left| \frac{J_1\left(\frac{1}{2} kD \sin \theta\right)}{\frac{1}{2} kD \sin \theta} \right| \tag{9.49}$$

where  $D$  is the diameter of the aperture and  $J_1$  is the Bessel function of the first kind of order one.

**Table 9.1**  
Properties of Line Sources

Amplitude Distribution in Aperture	Half-Power Beamwidth	Level of First Sidelobe	Position of First Null
Constant	$0.89\lambda/a$	-13.3 dB	$\lambda/a$
$\cos(\pi x/a)$	$1.19\lambda/a$	-23.1 dB	$1.5\lambda/a$
$\cos^2(\pi x/a)$	$1.44\lambda/a$	-31.5 dB	$2.0\lambda/a$
$1 - 0.5(2x/a)^2$	$0.97\lambda/a$	-17.1 dB	$1.14\lambda/a$
Taylor, $n = 3$ , edge -9 dB	$1.07\lambda/a$	-25.0 dB	—

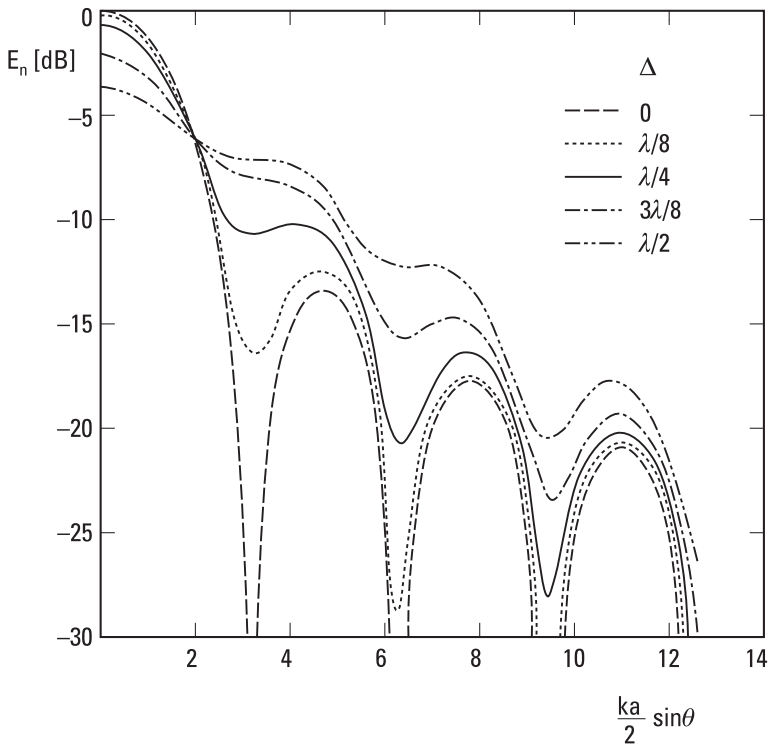


**Figure 9.22** Directional pattern of a line source having a constant amplitude and quadratic phase distribution;  $\Delta$  is the phase difference between the center and edge of the aperture in wavelengths.

**Table 9.2**  
Properties of Circular Apertures

Amplitude Distribution in Aperture	Half-Power Beamwidth	Level of First Sidelobe	Position of First Null
Constant	$1.02\lambda/D$	-17.6 dB	$1.22\lambda/D$
$1 - r^2$	$1.27\lambda/D$	-24.6 dB	$1.63\lambda/D$
$(1 - r^2)^2$	$1.47\lambda/D$	-30.6 dB	$2.03\lambda/D$
$0.5 + 0.5(1 - r^2)^2$	$1.16\lambda/D$	-26.5 dB	$1.51\lambda/D$
Taylor	$1.31\lambda/D$	-40.0 dB	—

### 9.7 Horn Antennas

An open waveguide end operates as a simple antenna. It has a broad, unsymmetrical beam and a rather large impedance mismatch. A much better antenna, a horn antenna, is obtained by widening the waveguide end, as shown in Figure 9.23.

*H*-plane, *E*-plane, and pyramidal horns are fed from a rectangular waveguide. An *H*-plane horn is widened along the broad side of the waveguide, an *E*-plane horn along the narrow side. A pyramidal horn is broadened in both directions. The distribution of the aperture field follows the field distribution of the fundamental waveguide mode, TE<sub>10</sub>. Because the amplitude in the *E*-plane is constant, the sidelobes are higher in this plane than in the *H*-plane, which has a cosine amplitude distribution tapering to zero at the edges. However, the phase in the aperture is not constant; rather it is quadratic. The *H*- and *E*-plane horns have cylindrical phase fronts, which seem to emanate from the apex. The apex is in the intersection of the slanting side planes. The phase difference between the center and edge of the aperture is in wavelengths

$$\Delta = (1 - \cos \theta_0) \frac{L}{\lambda} \tag{9.50}$$

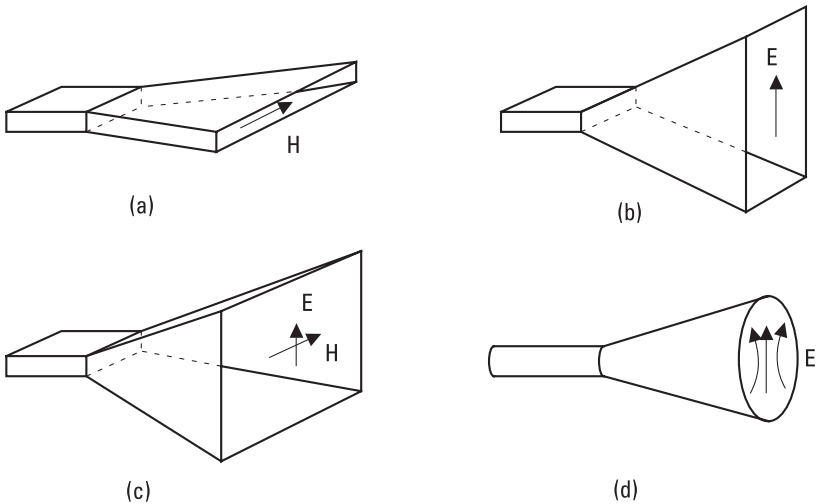


**Figure 9.23** Horn antennas: (a) *H*-plane horn; (b) *E*-plane horn; (c) pyramidal horn; and (d) conical horn.

where  $\theta_0$  is half of the opening angle and  $L$  is the distance from the apex to the aperture.

Figure 9.24 gives the directivities  $D_E$  and  $D_H$  for  $E$ - and  $H$ -plane horns. Because of the aperture phase error  $\Delta$ , it is impractical to make a horn, which has a very high directivity. For a fixed length  $L$ , the directivity increases as the aperture size increases until it collapses due to the phase error. The directivity of a pyramidal horn is obtained from the directivities of the corresponding  $E$ - and  $H$ -plane horns:

$$D \approx \frac{\pi D_E D_H \lambda^2}{32ab} \quad (9.51)$$

where  $a$  is the width and  $b$  is the height of the input waveguide. Usually, the losses of horn antennas are small, and the gain and directivity are approximately equal.

A conical horn like that shown in Figure 9.23(d) is obtained by widening a circular waveguide. Although the structure is symmetrical, the fields of the fundamental mode  $TE_{11}$  are not. Therefore, the  $E$ - and  $H$ -plane directional patterns are different.

Figure 9.25 shows horn antennas, which produce more symmetrical beams than pyramidal and conical horns. The rectangular waveguide feeding the diagonal horn, shown in Figure 9.25(a), transforms first to a circular waveguide and then to a square waveguide, which is at a  $45^\circ$  angle to the feeding waveguide. The field of the aperture is a combination of the fields of  $TE_{10}$  and  $TE_{01}$  modes. The beam of a diagonal horn is fairly symmetrical,

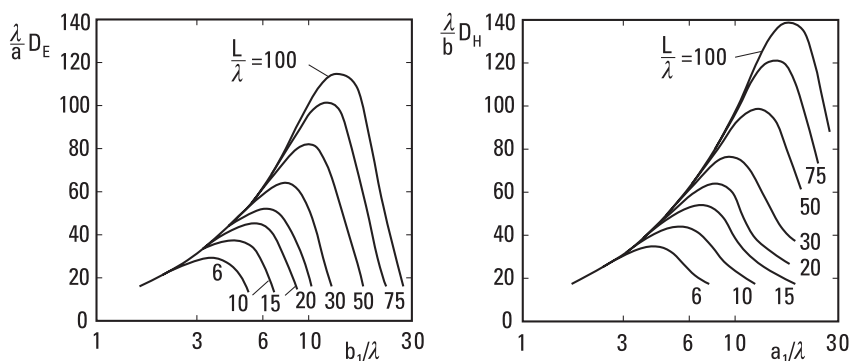


**Figure 9.24** Directivities of  $E$ -plane horns,  $D_E$ , and  $H$ -plane horns,  $D_H$ . Aperture size in  $E$ -plane =  $b_1$ , aperture size in  $H$ -plane =  $a_1$ .

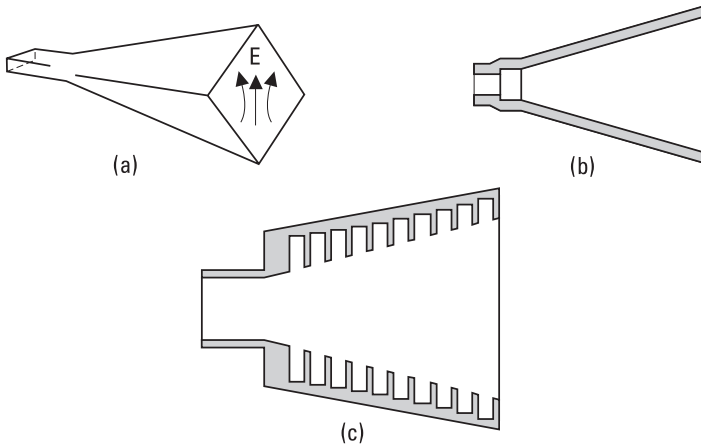


**Figure 9.25** (a) Diagonal horn; (b) Potter horn; and (c) corrugated horn.

but the level of cross polarization is high in the  $45^\circ$  and  $135^\circ$  planes between the  $E$ - and  $H$ -planes.

A Potter horn or a dual-mode horn, shown in Figure 9.25(b), is a conical horn, which has a step in the feeding circular waveguide. The fundamental mode  $TE_{11}$  and the  $TM_{11}$  mode excited at the step together produce an aperture field having parallel field lines, if the modes have proper amplitudes and a proper phase difference in the aperture. The Potter horn has a symmetrical pattern, low sidelobe level, and low cross-polarization level. However, it has a narrow bandwidth because the phasing of modes depends on the frequency.

A corrugated horn, shown in Figure 9.25(c), is a conical horn having a corrugated inner wall. The number of grooves should be at least two per wavelength. The depth of grooves is about  $\lambda/4$ . Near the throat the depth changes gradually to  $\lambda/2$  to ensure a good impedance match between the input waveguide and the flaring section. The mode propagating in the horn is  $HE_{11}$ , a hybrid of  $TE_{11}$  and  $TM_{11}$  modes. A corrugated horn has many good properties: a symmetrical pattern, low sidelobe level, low cross-polarization level, and broad operating bandwidth.

## 9.8 Reflector Antennas

Reflector antennas are used as high-gain, narrow-beam antennas in fixed radio links, satellite communication, radars, and radio astronomy.

A parabolic reflector antenna is the most common of reflector antennas. Figure 9.26(a) shows a parabolic antenna fed from the primary focus. The equation of the surface is

$$\rho = \frac{2F}{1 + \cos \theta} \quad (9.52)$$

where  $F$  is the focal length. The rays coming from the focal point are converted parallel by the reflector or vice versa. A more physical interpretation is that the fields radiated by the feed antenna induce surface currents, which in turn produce the aperture fields. The feed antenna is often a horn antenna. The phase center of the feed antenna should coincide with the focal point to obtain maximum gain.

The Cassegrainian antenna shown in Figure 9.26(b) is fed from the secondary focus behind the reflector. The subreflector is a hyperbolic reflector. This configuration has several advantages compared to the primary focused antenna: Transmitters and receivers can be placed behind the reflector; transmission lines between the feed and the radio equipment are short; positioning of the feed antenna is less critical; the phase and amplitude distribution of the aperture field can be adjusted with a shaped subreflector; and the feed pattern over the edge of the subreflector is directed toward a cold sky in satellite reception, which leads to a lower antenna noise temperature. A more complicated structure and often a larger blockage of the aperture are the disadvantages of the Cassegrainian antenna.

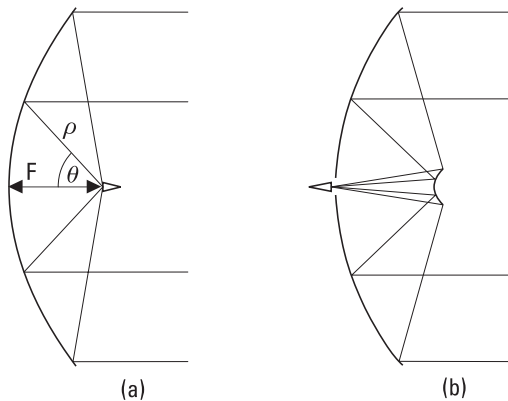


**Figure 9.26** Parabolic reflector antennas: (a) a primary focus fed antenna; and (b) a Cassegrainian antenna.

The theoretical directional patterns of circular apertures are only rough approximations of real patterns. Aperture field distribution depends on the radiation pattern of the feed antenna and on the ratio of the focal length and diameter of the reflector,  $F/D$ . A constant aperture field gives the highest gain but also the highest sidelobe level. A high edge illumination leads also to a high feed radiation over the edge of the reflector. Tapering the aperture illumination toward the edge leads to a lower aperture efficiency and gain but improves the pattern by lowering the sidelobes. Typically, the field at the edge is 10 dB to 12 dB lower than that at the center, and the aperture efficiency is about 0.6.

Many factors have an effect on the pattern of a reflector antenna: amplitude and phase pattern of the feed; positioning of the feed; aperture blockage due to the struts, feed, and subreflector; multiple reflections between the feed and reflector; and errors in the shape of the reflector and subreflector. Small random errors in the surface of the reflector reduce the gain and move energy from the main beam to the sidelobes. If the rms value of the surface errors is  $\epsilon$ , the aperture efficiency is

$$\eta_{ap} = \eta_0 \exp [-(4\pi\epsilon/\lambda)^2] \quad (9.53)$$

where  $\eta_0$  is the aperture efficiency for an ideal surface. The surface error  $\epsilon$  should not exceed  $\lambda/16$ .

The struts and the feed or the subreflector block a part of the aperture, which reduces  $\eta_{ap}$  and changes the level of sidelobes. They also scatter and diffract energy over a large solid angle. Also the edge of the reflector diffracts, which often produces a back lobe opposite to the main lobe.

The aperture blockage can be avoided by using offset geometry. Figure 9.27 shows offset-fed reflector antennas. The single-offset antenna has a simpler structure but the offset geometry inherently produces cross polarization. The dual-offset antenna has two distinct advantages compared to the single-offset antenna: The cross-polar field can be compensated and the aperture field distribution can be adjusted by shaping the reflectors. Dual-offset reflectors may have excellent sidelobe properties.

## 9.9 Other Antennas

In addition to the antennas discussed already, there are a large number of other antenna types. Some of them are briefly described here.

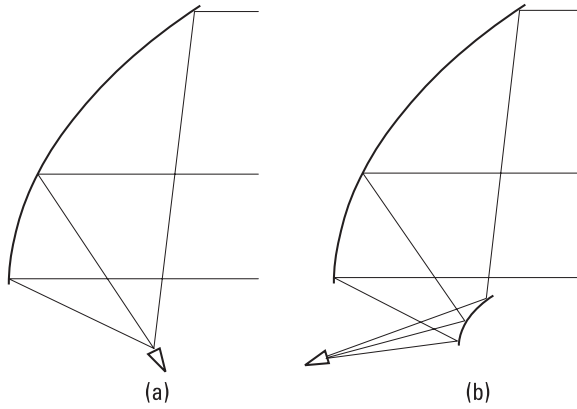


**Figure 9.27** Offset-fed reflector antennas: (a) single-offset; and (b) dual-offset.

Microstrip antennas are small, light, and suitable for integration and mass-production [6, 7]. Figure 9.28(a) shows the basic microstrip antenna: a rectangular, half-wave-long patch. It is made on a substrate having a ground plane on the other side. The patch is fed with a microstrip line from the edge and it radiates from both open-ended edges. The linearly polarized main beam is perpendicular to the surface. Because the antenna radiates effectively only at the resonance frequency, it has a narrow bandwidth. Fairly high loss is another disadvantage of microstrip antennas.

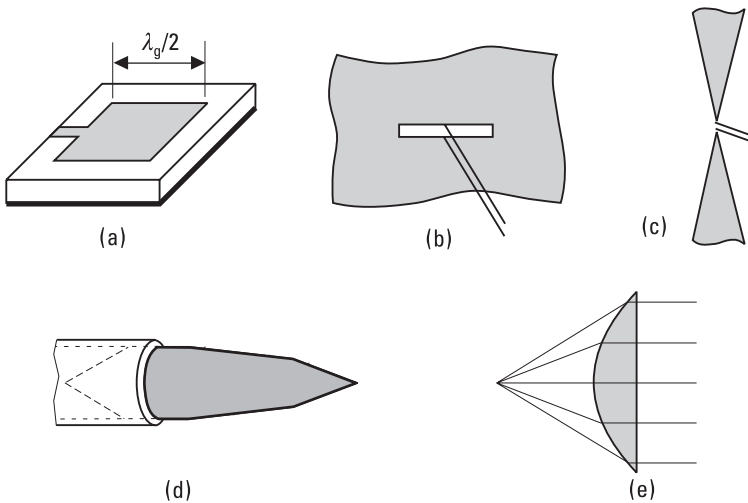


**Figure 9.28** (a) Microstrip antenna; (b) slot antenna; (c) bow-tie antenna; (d) dielectric rod antenna; and (e) lens antenna.



There are many variations on the basic microstrip antenna: different shapes of the patch, ways to feed the patch, and possibilities to combine elements to an array. A circularly polarized wave can be produced with a square patch, which is fed from the adjacent sides so that the phase difference of the feeds is  $90^\circ$ . A patch can also be fed with a coaxial cable through the substrate, in which case the input impedance depends on the position of the feed point. Feeding through a slot in the ground plane allows the radiating patches to be separated from the feed lines and other circuits. The directivity of a single element is low. A higher directivity is obtained by combining a large number of elements (see Section 9.10).

A slot antenna is a radiating slot in a metal plane, as shown in Figure 9.28(b). It is dual with a dipole antenna; that is, the radiation pattern is that of a dipole except that the electric and magnetic fields are interchanged. A slot antenna can be fed from a parallel-wire line, coaxial line, microstrip line, or waveguide. A waveguide having an array of slots is a common antenna. A slot in a waveguide wall radiates if it disturbs surface currents; a narrow slot, which is along the current flow, does not radiate.

The bow-tie antenna shown in Figure 9.28(c) is an example of a broadband antenna. The feed point is in the center of two planar conductors. The input impedance and directional pattern may be frequency-independent over a frequency range of one decade or more. In an ideal case, the bow-tie antenna has no dimensions, which can be expressed in wavelengths; the opening angle of the conductors is the only dimension. In practice, the structure of the feed point and the finite length of the conductors set limits for the frequency range. Often bow-tie antennas are placed on a dielectric substrate. Then the main lobe is on the dielectric side. Other frequency-independent shapes used in broadband antennas are spirals and cones.

Antennas made of dielectric materials have some mechanical and electrical advantages [8]. Figure 9.28(d) shows a dielectric rod antenna, which is placed at the open end of a circular waveguide. This kind of an antenna works well as a feed antenna.

Like a parabolic reflector, a lens antenna operates as a phase modifier, which changes a spherical phase front to a planar one. The paths of the rays from the focal point of the lens to a plane in front of the lens have equal electrical lengths. Lenses are usually made of low-loss dielectric materials. The phase velocity of the wave is  $c/\sqrt{\epsilon_r}$  in the dielectric material. Figure 9.28(e) shows a simple plano-convex lens. The reflections in the air-dielectric interfaces can be eliminated with quarter-wave matching layers. Lenses are often used to correct the phase error at the aperture of a horn antenna.

## 9.10 Antenna Arrays

An antenna array is an entity consisting of two or more element antennas. Antenna arrays may have many good properties, which cannot be achieved with a single element, such as high gain, narrow beam, shaped beam, scanning beam, or adaptive beam.

Figure 9.29 shows an array that consists of two elements having a separation of  $d$ . Let us assume that the far-field patterns of the antennas are  $E_1(\phi)$  and  $E_2(\phi)$  and that the phase difference of the feed currents is  $\delta$  (in this case the lengths of the feed lines are different). The total field produced by the array is

$$E(\phi) = E_1(\phi)e^{-j(kd \cos \phi + \delta)} + E_2(\phi) \quad (9.54)$$

The path length difference of  $d \cos \phi$  in free space produces the phase difference of  $kd \cos \phi$ . The fields of the elements are in the same phase in directions  $\phi_{max}$  that meet the condition of

$$kd \cos \phi_{max} + \delta = n2\pi \quad (9.55)$$

where  $n$  is an integer. The fields have opposite phases in directions  $\phi_{min}$  which meet the condition of

$$kd \cos \phi_{min} + \delta = n2\pi + \pi \quad (9.56)$$

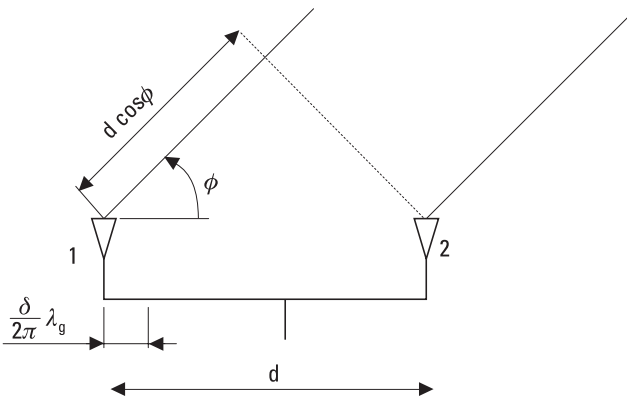


**Figure 9.29** An array of two elements.

If the elements of Figure 9.29 are similar,  $E_1(\phi) = E_2(\phi)$ , and they are fed in phase,  $\delta = 0$ , (9.54) can be written as

$$E(\phi) = E_1(\phi)(1 + e^{-jkd \cos \phi}) \tag{9.57}$$

The array pattern is the product of the element pattern and the array factor. If the element pattern maximum and the array factor maximum coincide in the same direction, the maximum field is twice that produced by a single element,  $E = 2E_1(\phi_{max})$ . However, even if the power density is now four times that produced by a single element, the gain of the array is only twice the gain of an element. The power density produced by an element would be doubled if all the input power of the array were fed to that element alone. The normalized pattern may look like that shown in Figure 9.30. The envelope follows the element pattern, and at minima the fields of the elements cancel each other out. As the separation  $d$  increases, the number of maxima and minima in the pattern increases.

Many kinds of directional patterns can be realized by changing the distance (or frequency) and phase difference of the elements. Figure 9.31 shows some patterns when the elements radiate isotropically in the  $\phi$ -plane (for example dipoles which are perpendicular to the  $\phi$ -plane).

Also, the pattern of an array consisting of more than two elements can be expressed as the product of the element pattern and the array factor. The array factor depends on the positions, amplitudes, and phases of the elements. The array may be linear, planar, or conformal (shaped according to the surface). The elements of a linear array are on a line. Figure 9.32 shows a

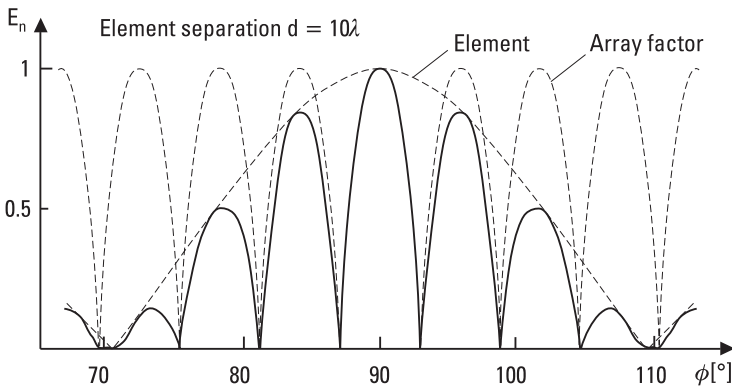


**Figure 9.30** Pattern of a two-element array (solid line) equals the element pattern multiplied by the array factor.

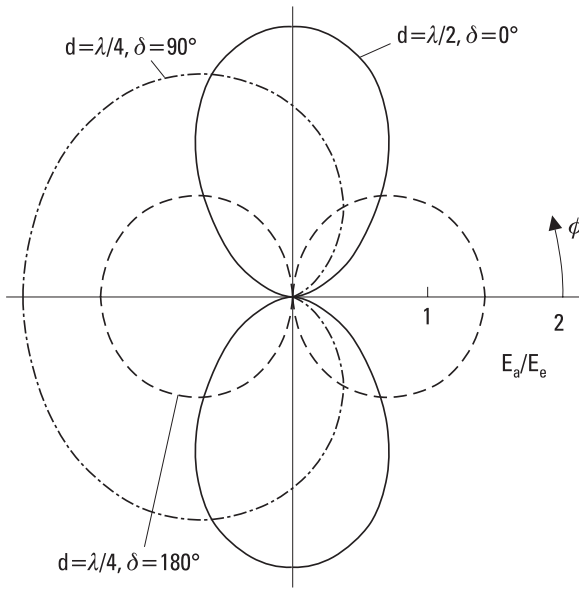


**Figure 9.31** Directional patterns of two-element arrays in polar form. The elements are isotropic in the  $\phi$ -plane.  $E_a/E_e$  = field of array divided by the field of the element.

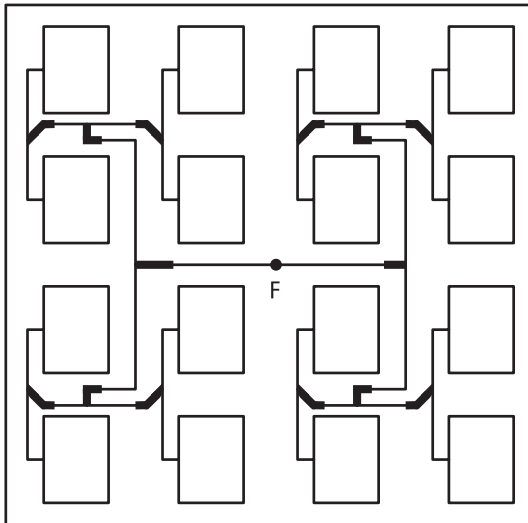


**Figure 9.32** Microstrip antenna array (F = feed point).

planar array, which consists of 16 microstrip antenna elements fed in phase and with equal amplitudes. This array is like the rectangular aperture antenna treated in Section 9.6. Many kinds of different patterns can be realized by choosing proper amplitudes and phases for the elements. Besides microstrip elements, an array may consist of many other types of elements such as dipoles, slots, or horns [9].

If there are electronically controlled phase shifters in the feed network of an array, the direction of the beam can be changed rapidly without rotating the antenna. This kind of electronic scanning is much faster than mechanical scanning. A phased array combined with digital signal processing may operate as an adaptive antenna. The pattern of an adaptive antenna changes according to the electromagnetic environment; for example, the beam of a base-station antenna may follow a moving user and a null may be formed in the direction of an interfering signal. An adaptive antenna may also partly correct the deterioration of its pattern, if one or more of its elements breaks down. Adaptive antennas are also called “smart” antennas.

## 9.11 Matching of Antennas

In principle, an antenna may be matched as any load impedance. However, some wire antennas, such as dipole and loop antennas, need a special attention if they are fed from an unsymmetrical line. For example, if a dipole antenna is connected directly to a coaxial line, currents will flow on the outer surface of the outer conductor. Then the outer conductor will radiate and the directional pattern will be distorted.

The radiation of the outer conductor can be prevented with a balun, a balanced-to-unbalanced transformer. The balun of Figure 9.33(a) has a short-circuited quarter-wave line outside the outer conductor. Thus, the impedance between A and B is large. Now, a symmetric load as a dipole antenna can be connected between A and C so that the outer conductor does not radiate. The balun of Figure 9.33(b) transforms the characteristic impedance of the coaxial line,  $Z_0$ , to an impedance of  $4Z_0$  between A and B. In the balun of Figure 9.33(c) the coaxial line changes gradually to a parallel-wire line.

## 9.12 Link Between Two Antennas

Let us assume that a signal is transmitted from one antenna to another. The antennas are in free space and their separation  $r$  is large compared to the

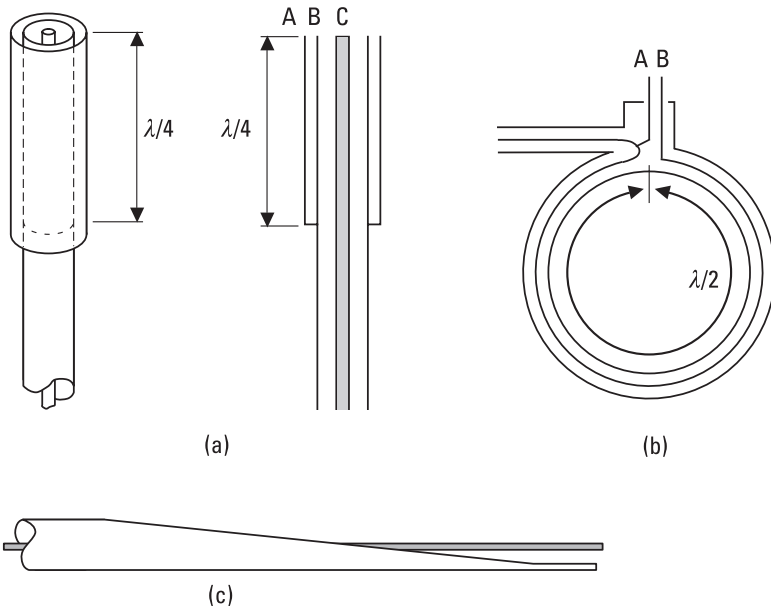


**Figure 9.33** Baluns: (a) a short-circuited sleeve of a length  $\lambda/4$  over a coaxial cable; (b) a loop of a length  $\lambda/2$  of a coaxial line; and (c) the outer conductor of a coaxial line changes gradually to a parallel-wire line.

distances obtained from (9.1). The main beams of the antennas are pointing toward each other and their polarizations are matched.

If the power accepted by the transmitting antenna,  $P_t$ , were transmitted isotropically, the power density at a distance of  $r$  would be

$$S_{isot} = \frac{P_t}{4\pi r^2} \quad (9.58)$$

The maximum power density produced by the transmitting antenna having a gain of  $G_t$  is

$$S = \frac{G_t P_t}{4\pi r^2} \quad (9.59)$$

The corresponding electric field amplitude produced by the antenna is

$$E = \sqrt{2\eta S} \quad (9.60)$$

The power available from the receiving antenna is its effective area  $A_r$ , times the power density of the incoming wave:

$$P_r = A_r S \quad (9.61)$$

Using (9.4) and (9.59), this can be written as the Friis free-space equation:

$$P_r = G_t G_r \left( \frac{\lambda}{4\pi r} \right)^2 P_t \quad (9.62)$$

where  $G_r$  is the gain of the receiving antenna.

In practice, many factors may reduce the power received, such as errors in the pointing of the antennas, polarization mismatch, loss due to the atmosphere, and fading due to multipath propagation. Losses due to impedance mismatches also have to be taken into account; generally, the power accepted by the transmitting antenna is smaller than the available power of the transmitter, and the power accepted by the receiver is smaller than the available power from the receiving antenna.

### Example 9.3

What is the loss  $P_t/P_r$  at 12 GHz from a geostationary satellite at a distance of 40,000 km? Both the transmitting and receiving antennas have a diameter of  $D = 1$  m and an aperture efficiency of  $\eta_{ap} = 0.6$ .

### Solution

The antennas have an effective area of  $A_{eff} = \eta_{ap} \pi D^2/4 = 0.47 \text{ m}^2$  and a gain of  $G = 4\pi A_{eff}/\lambda^2 = 9\,500$ . The loss  $P_t/P_r = (4\pi r/G\lambda)^2 = 4.5 \times 10^{12}$ , in decibels  $10 \log(4.5 \times 10^{12}) \text{ dB} = 126.5 \text{ dB}$ . Here, the attenuation of the atmosphere is not taken into account. During a clear weather, the atmospheric attenuation is about 0.3 dB at 12 GHz.

### Example 9.4

How accurately the receiving antenna of the preceding example has to be pointed to the satellite, if the allowed maximum pointing loss is 0.5 dB? The satellite transmits two orthogonal, linearly polarized signals. How accurately must the tilt angle of the linearly polarized receiving antenna be adjusted if (a) the maximum loss due to polarization mismatch is 0.5 dB, and if (b) the maximum power coupled between the orthogonal channels is  $-30 \text{ dB}$ ?

### Solution

The beamwidth of the receiving antenna is  $\theta_{3\text{dB}} \approx 1.2\lambda/D = 0.03 \text{ rad} = 1.7^\circ$ . The pattern level depends approximately quadratically on the angle near the main beam maximum. Thus, the maximum allowed pointing error is  $(0.5/3)^{1/2} \times 1.7^\circ/2 = 0.35^\circ$ . The antenna receives only the component of the incoming wave that has the same polarization as the antenna. (a) From  $20 \log(\cos \Delta\tau) = -0.5$  we solve that an error of  $\Delta\tau = 19.3^\circ$  in the tilt angle reduces the received power by 0.5 dB. (b) From  $20 \log(\sin \Delta\tau) = -30$  we solve that  $\Delta\tau = 1.8^\circ$  gives a cross-polar discrimination of 30 dB. Thus, to avoid interference between the orthogonal channels, the error in the tilt angle should not be too large.

## References

- [1] Kraus, J. D., and R. J. Marhefka, *Antennas for All Applications*, 3rd ed., New York: McGraw-Hill, 2002.
- [2] Lo, Y. T., and S. W. Lee, (eds.), *Antenna Handbook: Theory, Applications, and Design*, New York: Van Nostrand Reinhold, 1988.
- [3] Rudge, A. W., et al., (eds.), *The Handbook of Antenna Design, Vol. 1*, London, England: Peter Peregrinus, 1982.
- [4] Rudge, A. W., et al., (eds.), *The Handbook of Antenna Design, Vol. 2*, London, England: Peter Peregrinus, 1983.
- [5] Fujimoto, K., and J. R. James, (eds.), *Mobile Antenna Systems Handbook*, Norwood, MA: Artech House, 1994.
- [6] Garg, P., et al., *Microstrip Antenna Design Handbook*, Norwood, MA: Artech House, 2001.
- [7] Lee, K. F., and W. Chen, (eds.), *Advances in Microstrip and Printed Antennas*, New York: John Wiley & Sons, 1997.
- [8] Chatterjee, R., *Dielectric and Dielectric-Loaded Antennas*, New York: John Wiley & Sons, 1985.
- [9] Sehm, T., A. Lehto, and A. Räsänen, "A High-Gain 58-GHz Box-Horn Array Antenna with Suppressed Grating Lobes," *IEEE Trans. on Antennas and Propagation*, Vol. 47, No. 7, 1999, pp. 1125–1130.





# 10

## Propagation of Radio Waves

In the previous chapter we studied a radio link between two antennas. Equation (9.62) applies for the link between two antennas when the wave propagates unhindered and without atmospheric attenuation; only the decrease of power density as  $1/r^2$  is taken into account. In practice, many factors, such as troposphere, ionosphere, terrain, and buildings, affect propagation of the radio waves. From a system point of view, the concept of the radio propagation channel or just the radio channel covers the radio wave propagation phenomena between a transmitting and receiving antenna. This channel may be considered as a system element that transforms input signals into output signals. It is analogous to a time-variant linear filter.

### 10.1 Environment and Propagation Mechanisms

The troposphere is the lowest part of the atmosphere, where all weather phenomena occur. It extends on the poles to about 9 km and on the equator to about 17 km. The troposphere is inhomogeneous and constantly changing. Temperature, pressure, humidity, and precipitation affect the propagation of radio waves. In the troposphere the radio waves attenuate, scatter, refract, and reflect; the amplitude and phase of the received signal may fluctuate randomly due to multipath propagation; the polarization of the wave may change; noise originating from the atmosphere is added to the signal.

The ionosphere extends from about 60 km to 1,000 km. It contains plasma, which is gas ionized by the solar ultraviolet and particle radiation.

The free electrons of the ionosphere form a mirror, which reflects the radio waves at frequencies below about 10 MHz. The upper frequency limit of reflection depends on time of day and season, and on solar activity.

Also terrain and man-made objects diffract, scatter, and reflect radio waves. At low frequencies the attenuation of the ground waves (waves propagating close to the Earth's surface) depends on the electrical properties of the ground.

Radio waves can propagate from one point to another in many ways. The most important mechanisms of propagation used in radio systems are, in order of decreasing frequency, the following:

1. *Propagation along a line-of-sight (LOS) path.* This resembles the propagation in free space. Because of refraction, the radio horizon is farther away than the geometrical horizon. In UHF, SHF, and EHF bands most radio systems require an LOS path. From the millimeter-wave band to infrared, the radio link hops are short because of attenuation due to precipitation and gas molecules. In VHF and UHF bands multipath propagation is common: The LOS path may be complemented or interfered by diffraction and reflection from buildings and ground as well as by propagation through vegetation and building walls.
2. *Scattering from inhomogeneities of the atmosphere.* The applicable frequency range is from 300 MHz to 10 GHz.
3. *Propagation via the ionosphere.* A radio wave may reflect from the ionosphere at frequencies below 30 MHz. A wave may also reflect multiple times between the ionosphere and ground, and thus propagate round the globe.
4. *Ground-wave propagation.* The attenuation of the ground wave increases rapidly versus frequency; this phenomenon is important at frequencies below 10 MHz.

Figure 10.1 illustrates different propagation mechanisms. In a given radio link, the waves may propagate through several different mechanisms. In long hops, a ground wave is dominating up to 150 kHz, and the ionospheric wave in the frequency range of 1.5 MHz to 30 MHz, depending on the state of the ionosphere. At frequencies from 150 kHz to 1,500 kHz both mechanisms are equally important. As it does in VHF and UHF bands, the wave propagates through several paths, but now the reason is diffraction and reflection from buildings and ground. Due to the interference of waves

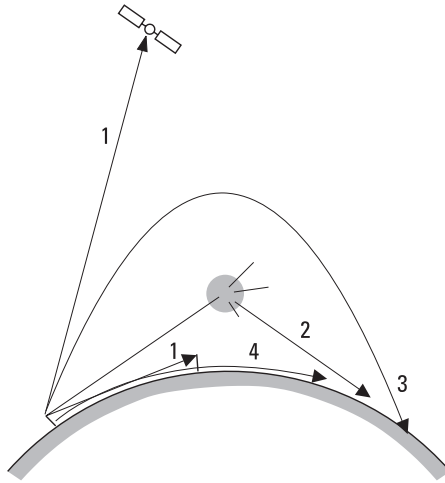


**Figure 10.1** Propagation mechanisms of radio waves (numbers refer to different mechanisms described in text).

propagating via different routes, the power level of the received signal may alternate considerably over time and location (fast fading).

Propagation beyond the radio horizon is also possible due to tropospheric reflections at frequencies from 30 MHz to 1,000 MHz, and due to ducting at frequencies above 1 GHz. These propagation mechanisms are, however, so unreliable, that one cannot build a continuous radio path based on them. On the contrary, they cause interference to other radio links in the same frequency band.

In general, the available power received cannot be accurately predicted. The signal power level may alternate several tens of decibels in a given radio path. In order to reach a high reliability in a radio system, one must know the statistical distribution of the link attenuation and design the antenna sizes and power of transmission accordingly.

## 10.2 Tropospheric Attenuation

At frequencies above a few gigahertz, the attenuation due to atmospheric absorption and scattering must be taken into account. This attenuation can be divided into two parts: attenuation due to clear air and attenuation due to precipitation (raindrops, hail, and snow flakes) and fog. Attenuation of the clear air is mainly due to resonance states of oxygen ( $O_2$ ) and water vapor ( $H_2O$ ) molecules. An energy quantum corresponding to the resonance

frequency may change the rotational energy state of a gas molecule. When the molecule absorbs an energy quantum, the molecule is excited to a higher energy state. When it returns back to equilibrium—that is, drops back to the ground state—it radiates the energy difference, but not necessarily at the same frequency because returning to equilibrium may happen in smaller energy steps. Under pressure the molecular emission lines have a wide spectrum. Therefore the energy quantum is lost from the propagating wave, and for the same reason the atmosphere is always noisy at all frequencies.

The lowest resonance frequencies of oxygen are 60 GHz and 119 GHz, and those of water vapor are 22, 183, and 325 GHz. The amount of oxygen is always nearly constant, but that of water vapor is highly variable versus time and location. The attenuation constant due to water vapor is directly proportional to the absolute amount of water vapor, which is a function of temperature and humidity. Figure 10.2 presents the clear air attenuation versus frequency. Between the resonance frequencies there are so-called spectral windows centered at frequencies 35, 95, 140, and 220 GHz. At resonance frequencies the attenuation may be tens of decibels per kilometer. These frequencies are, however, suitable for intersatellite links, for short terrestrial links, and for WLANs.

Figure 10.3 presents attenuation due to rain and fog. Attenuation of rain is mainly due to scattering: The electric field of the radio wave polarizes

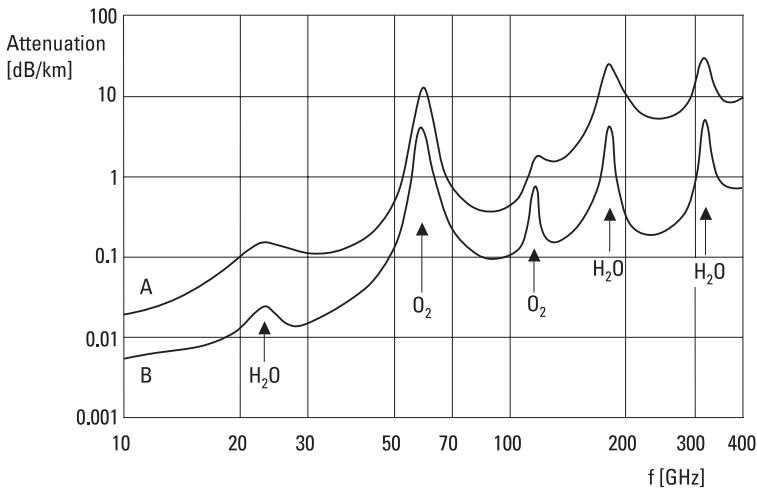


**Figure 10.2** Attenuation in clear atmosphere versus frequency. Curve A: at sea level ( $T = 20^{\circ}\text{C}$ , water vapor density  $7.5 \text{ g/m}^3$ ). Curve B: at altitude of 4 km ( $T = 0^{\circ}\text{C}$ , water vapor density  $1 \text{ g/m}^3$ ).

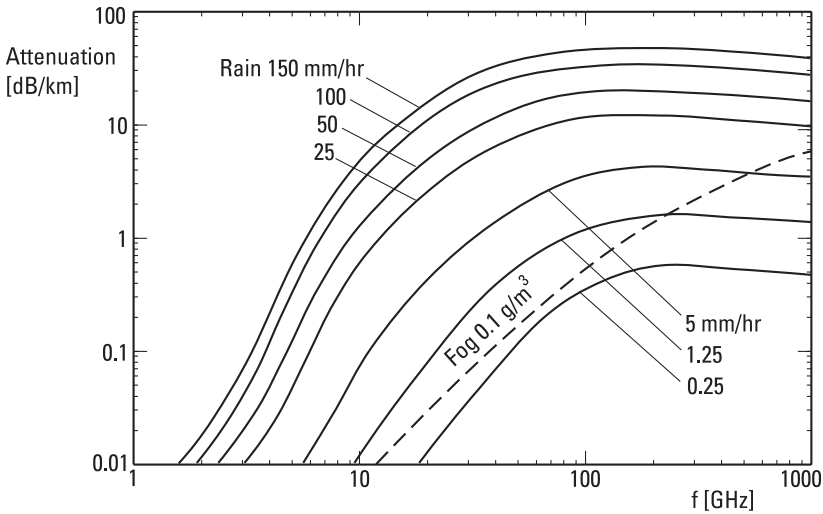


**Figure 10.3** Attenuation due to rain and fog.

the water molecules of the raindrop, and then the raindrop acts like a small electric dipole radiating over a large solid angle. A heavy rain makes long radio hops impossible at frequencies above 10 GHz. In a moderate rain (5 mm/hr) attenuation is 0.08 dB/km at 10 GHz and 3 dB/km at 100 GHz. In a pouring rain (150 mm/hr) these values are about tenfold, but on the other hand the time percentage of such strong rains is small. In a heavy rain the drops are large and their shape is ellipsoidal. Then a horizontally polarized wave attenuates more than a vertically polarized wave. This phenomenon, depending on the wind speed, also causes depolarization of the wave, if the electric field is not along either axis of the raindrop. Depolarization results in unwanted coupling between orthogonally polarized channels and an extra loss in reception because the receiving antenna can accept only that polarization for which it is designed. The attenuation constant due to fog and clouds is nearly directly proportional to the amount of water.

Both real and imaginary parts of the dielectric constant of ice are clearly smaller than those of water. Therefore, attenuation due to dry snow is low. Wet snow causes more attenuation, and its attenuation is directly proportional to the amount of water.

Turbulence in the troposphere may cause also scintillation, that is, random changes in amplitude and phase of the wave as it propagates via different routes due to turbulence (refractive index may vary strongly over short distances). Atmospheric propagation phenomena were the subject of

many studies at Helsinki University of Technology in the 1990s; some examples of the results are presented in [1–4].

### 10.3 Bending (Refraction) of Radio Waves in Troposphere

The refraction index  $n = \sqrt{\epsilon_r}$  of the troposphere fluctuates over time and location. In normal conditions the refraction index decreases monotonically versus altitude, because the air density decreases. Because a phenomenon of this kind is a weak function of altitude, it causes slow bending of the ray. Fast changes in the refraction index cause scattering and reflections. Turbulence, where temperature or humidity differs strongly from those of the surroundings, gives rise to scattering. Reflections are caused by horizontal boundaries in the atmosphere due to weather phenomena.

Because  $n$  is always close to unity, we often use the so-called refractivity  $N$ , which is the difference of the refraction index value from unity in parts per million:

$$N = (n - 1) \times 10^6 \quad (10.1)$$

The refractivity for air is obtained from equations

$$N = \frac{77.6}{T} \left( p + 4,810 \frac{e}{T} \right) \quad (10.2)$$

$$e = 6.11R \exp [19.7(T - 273)/T] \quad (10.3)$$

where  $T$  is the absolute temperature,  $p$  is the barometric pressure (unit mb = hPa),  $e$  is the partial pressure of water vapor (mb), and  $R$  is the relative humidity. The error of (10.2) is less than 0.5%, if  $f < 30$  GHz,  $p = 200$ – $1,100$  mb,  $T = 240$ – $310$ K, and  $e < 30$  mb. If there is no resonance frequency of oxygen or water vapor molecules in the vicinity, this equation is useful up to 1,000 GHz.

According to an ITU-R specification, the average refractivity of the atmosphere versus altitude follows equation

$$N(h) = N_A e^{-b_A h} \quad (10.4)$$

where  $N_A = 315$  and  $b_A = 0.136 \text{ km}^{-1}$ . These values are calculated using the standard-atmosphere model:  $p = 1,013$  mb, its change  $-12$  mb/100m

upward,  $T = 15^\circ\text{C}$ , its change  $-0.55^\circ\text{C}/100\text{m}$  upward,  $R = 60\%$ . A more accurate model may be obtained by using maps published by ITU-R.

Let us now consider a wave that propagates in the troposphere in a direction that makes an angle  $\phi$  with the horizontal plane, as shown in Figure 10.4. Because the refraction index changes with altitude, the angle  $\phi$  changes while the wave propagates. According to Snell's law,

$$n \cos \phi = \text{constant} \quad (10.5)$$

By derivating this equation with altitude  $h$ , we get

$$\frac{dn}{dh} \cos \phi - n \sin \phi \frac{d\phi}{dh} = 0 \quad (10.6)$$

Let us mark the traveled distance in propagation direction as  $s$ ; then we get

$$\frac{d\phi}{dh} = \frac{d\phi}{ds} \frac{ds}{dh} = \frac{d\phi}{ds} \frac{1}{\sin \phi} \quad (10.7)$$

We substitute this into (10.6), from which we solve

$$\frac{d\phi}{ds} = \frac{1}{n} \frac{dn}{dh} \cos \phi \approx \frac{dn}{dh} \quad (10.8)$$

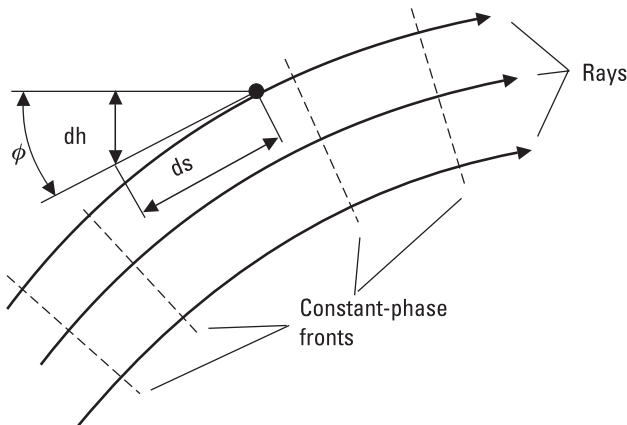


**Figure 10.4** Refraction (bending) of a wave in the troposphere.



as  $n \approx 1$ , and for terrestrial radio paths in general  $\phi \approx 0^\circ$ , that is,  $\cos \phi \approx 1$ . In an average atmosphere at sea level, the curvature ( $= -1/\text{bending radius}$ , i.e., the rate of change of direction with distance) of the ray is

$$\frac{d\phi}{ds} \approx \frac{dn}{dh} = -10^{-6} N_A b_A = -43 \times 10^{-6} \text{ km}^{-1} \quad (10.9)$$

that is, the ray bends downward.

Also the Earth's surface bends downward, and its curvature is  $-1/R$ , where the Earth's radius is  $R = 6,370 \text{ km}$ . Therefore the curvature of the ray in reference to the Earth's surface is

$$\frac{dn}{dh} + \frac{1}{R} = \frac{1}{KR} \quad (10.10)$$

When analyzing radio paths in the troposphere, we can imagine that the ray is straight, if we use an effective Earth radius  $KR$  (see Figure 10.5). In the average atmosphere  $KR = 8,760 \text{ km}$  or  $K = 1.375$ . Often we use a value of  $K = 4/3$ .

Temporarily the distribution of the refraction index versus altitude may differ considerably from that of the average atmosphere. If  $dn/dh = -157 \times 10^{-6} \text{ km}^{-1}$ , the ray bends as fast as the Earth's surface ( $K = \infty$ ). If  $dn/dh < -157 \times 10^{-6} \text{ km}^{-1}$ , the ray bends toward the Earth's surface ( $K < 0$ ). The wave may propagate long distances with successive reflections, as illustrated in Figure 10.6. Propagation with this mechanism is called ducting. Ducting may happen in the so-called inversion layer, where temperature increases rapidly as altitude increases. Such an inversion layer may range in height from a few meters to about 100m and may appear near the ground or at a high altitude.

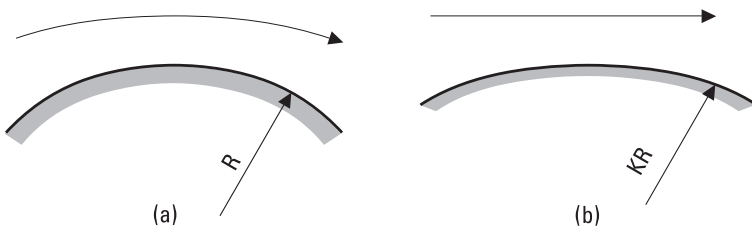


**Figure 10.5** Propagation in the troposphere: (a) refraction; (b) a model of straight propagation above the surface of an extended globe.

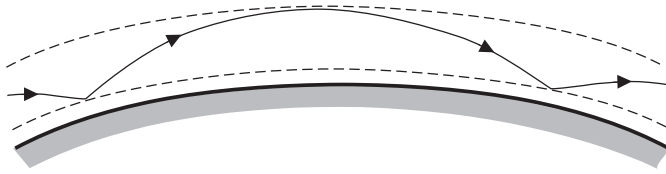


**Figure 10.6** Ducting of a radio wave.

## 10.4 LOS Path

In an LOS path the receiving antenna is above the radio horizon of the transmitting station. Links between two satellites and between an earth station and a satellite are LOS paths, and a path between two terrestrial stations may be such. In the two latter cases the tropospheric effects discussed previously must be taken into account.

According to the ray theory, it is enough that just a ray can propagate unhindered from the transmitting antenna to the receiving antenna. In reality a radio wave requires much more space in order to propagate without extra loss. The free space must be the size of the so-called first Fresnel ellipsoid, shown in Figure 10.7. It is characterized by

$$r_1 + r_2 - r_0 = \lambda/2 \quad (10.11)$$

where  $r_1$  and  $r_2$  are distances of a point on the ellipsoid from the transmitting and receiving points, and  $r_0$  is their direct distance. The radius of the first Fresnel ellipsoid is

$$h_F = \sqrt{\frac{\lambda r_1 r_2}{r_1 + r_2}} \quad (10.12)$$

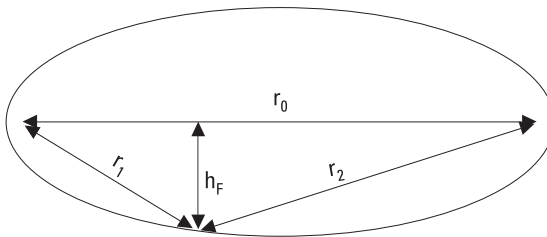


**Figure 10.7** The first Fresnel ellipsoid.

We observe that the radius of the ellipsoid in a given path is the smaller the higher the frequency; that is, the ray theory holds better at higher frequencies.

Figure 10.8 shows the extra attenuation due to a knife-edge obstacle in the first Fresnel ellipsoid. According to the ray theory, an obstacle hindering the ray causes an infinite attenuation, and an obstacle just below the ray does not have any effect on the attenuation. However, the result shown in Figure 10.8 is reality and is better explained by Huygens' principle: Every point of the wavefront above the obstacle is a source point of a new spherical wave. This explains diffraction (or bending) of the wave due to an obstacle. Diffraction also helps the wave to propagate behind the obstacle to a space, which is not seen from the original point of transmission. When the knife-edge obstacle is just on the LOS path ( $h = 0$ ), it causes an extra attenuation of 6 dB. When the obstacle reaches just to the lower boundary of the first Fresnel ellipsoid, the wave arriving at the receiving point may be even stronger than that in a fully obstacle-free case. If there is a hill in the propagation path that cannot be considered a knife-edge, extra attenuation is even higher than in case of a knife-edge obstacle.

When terrestrial radio-link hops are designed, bending of the Earth's surface as well as bending of the ray in the troposphere must be taken into

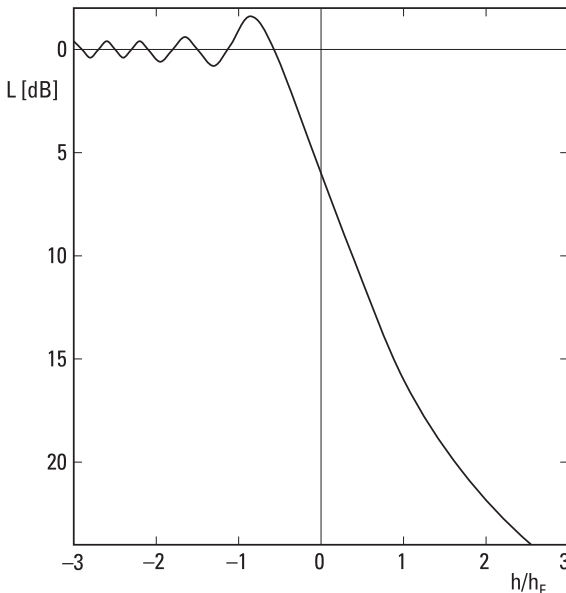


**Figure 10.8** Extra attenuation due to the knife-edge diffraction.

account. The radio horizon is at the distance of  $r_H$  if the transmitting antenna is at the height of

$$h_H = \frac{r_H^2}{2KR} \quad (10.13)$$

### Example 10.1

Consider a 50-km radio-link hop at 10 GHz, when the antenna heights are the same. What are the required antenna heights?

### Solution

Taking  $K = 4/3$  we get from (10.13) that the radio horizon of the antennas is in the middle point of the path between the antennas, when  $h_H = 36.8\text{m}$ . By introducing  $\lambda = 0.03\text{m}$  and  $r_1 = r_2 = 25\text{ km}$  into (10.12) we get the radius of the first Fresnel ellipsoid in the middle point as  $h_F = 19.4\text{m}$ . The antenna heights must be then at least  $h = h_H + h_F = 56.2\text{m}$ . In addition, if there are woods in the path, the height of the trees must be taken into account.

At low frequencies, fulfillment of the requirement of leaving the first Fresnel ellipsoid empty is difficult. Often we must compromise. For example, at 100 MHz in the 50-km hop of the example, the maximum radius of the first Fresnel ellipsoid is 194m.

A radio-link hop design is aided by using a profile diagram of the terrain, which takes into account the bending of the radio ray in standard conditions. In the diagram, the height scale is much larger than the horizontal scale, and the terrain along the hop is drawn so that perpendicular directions against the Earth's surface are parallel. The middle point of the hop is placed in the middle of the diagram. After drawing the terrain, the antenna heights are selected so that the first Fresnel ellipsoid is fully in free space, if possible. Figure 10.9 presents a profile diagram between Korppoo and Turku in the Finnish archipelago.

## 10.5 Reflection from Ground

In an LOS path, the receiving antenna often receives, besides a direct wave, waves that are reflected from the ground or from obstacles such as buildings. This is called multipath propagation.

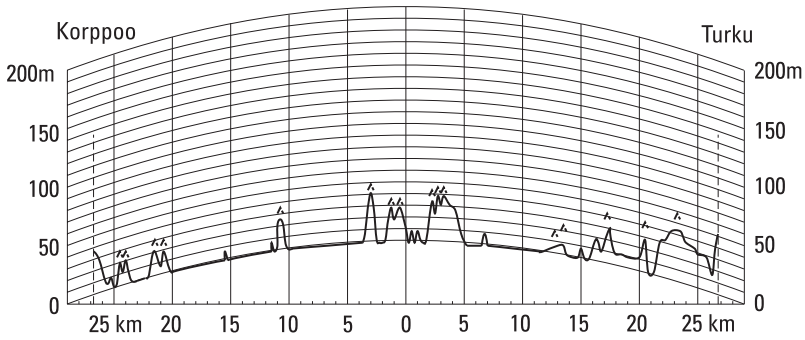


**Figure 10.9** Profile diagram for radio-link hop planning.

Let us consider a simple situation, where there is a flat, smooth ground surface between the transmitting and receiving antenna masts, which are located so that their distance is  $d$ , and the distance between the transmitting and receiving points is  $r_0$ , as presented in Figure 10.10. In practice this situation may be quite typical in VHF and UHF radio broadcasting, where an antenna mast with a height  $h_1$  is at the broadcasting station. Let us further assume that the transmitting antenna radiates isotropically. The electric field strength due to the direct wave at the distance  $r_0$  from the transmitter is  $E_0$ . Taking also the reflected wave into account, the total electric field strength at the receiving point is

$$E \approx E_0 \left[ 1 + \rho e^{-j\beta(r_1+r_2-r_0)} \right] \tag{10.14}$$

where  $\rho$  is the reflection coefficient of the ground surface, and we have assumed that  $r_1 + r_2 \approx r_0$ . The reflection coefficient depends on the electric

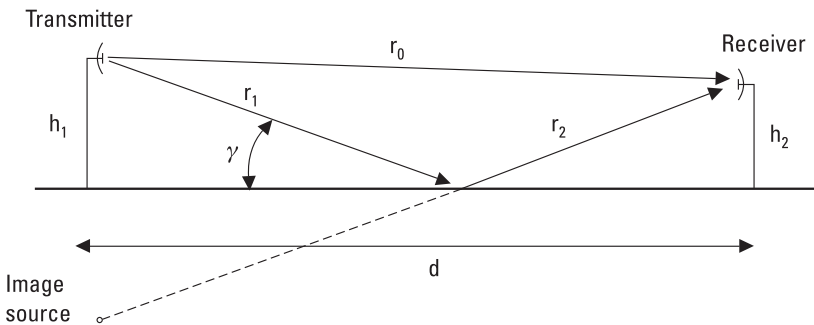


**Figure 10.10** A direct and reflected wave.

properties of the surface and on the polarization of the wave. At frequencies above 30 MHz the reflection coefficient can be assumed to be  $-1$  if the polarization is horizontal (or perpendicular) and the antenna heights are much less than the distance  $d$ ; that is, the grazing angle  $\gamma$  is small. For the vertical or parallel polarization the amplitude and phase angle of the reflection coefficient vary rapidly at small angles  $\gamma$  [5].

In the following we assume a horizontal polarization. In practice the antenna heights  $h_1$  and  $h_2$  are often small compared to the distance  $d$ , and therefore the angle  $\gamma$  is small and  $r_1 + r_2 - r_0 \approx 2h_1 h_2/d$ . Now the field strength is

$$E \approx E_0(1 - e^{-j\beta 2h_1 h_2/d}) \tag{10.15}$$

The actual radiation pattern corresponds to that of the array formed by the transmitting antenna and its mirror image. The electric field strength  $E$  varies as a function of distance between values 0 and  $2E_0$ , as shown in Figure 10.11(a). Note that  $E_0$  decreases as  $1/d$ . The nulls of the field strength (maxima for vertical polarization in case of an ideal conducting surface) are at heights  $h_2 \approx n\lambda d/(2h_1)$ , where  $n = 0, 1, 2, \dots$ , as shown in Figure 10.11(b). The receiving antenna height must be selected correctly. In order to reduce the effects of reflections, it is possible to use a transmitting antenna that has radiation nulls at directions of the reflection points. Also, a forest at the theoretical reflection points helps because it effectively eliminates reflections.

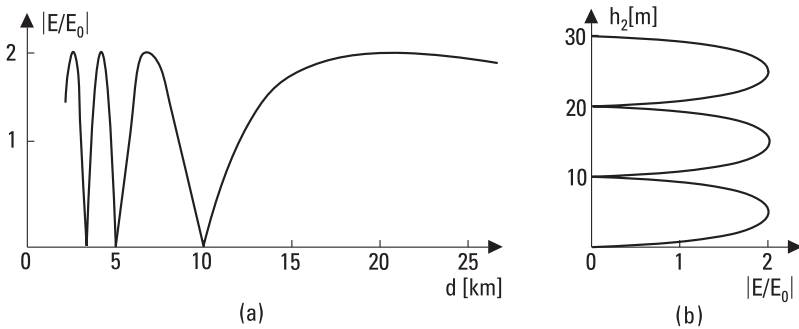


**Figure 10.11** Field strength (a) as a function of the distance  $d$  when the receiving antenna height is  $h_2 = 10\text{m}$  and (b) as a function of the receiving antenna height  $h_2$  when  $d = 10\text{ km}$ . The situation resembles Figure 10.10:  $\rho = -1$ ,  $f = 500\text{ MHz}$ ,  $h_1 = 300\text{m}$ .

**Example 10.2**

The transmitting antenna is located at a height of 300m. The frequency is 225 MHz, and the polarization is horizontal. What is the best height for a receiving antenna at a distance of 12 km, if the terrain between the antennas is a flat field?

**Solution**

Reflection from the surface causes a phase shift of  $180^\circ$ . Therefore the electric fields of the direct and reflected wave add up in phase when the path difference  $r_1 + r_2 - r_0 \approx 2h_1h_2/d$  is equal to  $\lambda/2$ . The optimum height of the receiving antenna mast is  $h_2 = \lambda d/(4h_1) = 13.3\text{m}$ . Other solutions are  $(2n + 1) \times 13.3\text{m}$ .

In the preceding discussion we have assumed that the wave propagates as a ray. However, as we discussed in Section 10.4, the ray requires the volume of the first Fresnel ellipsoid as free space. The surface area, where the reflection may happen, is therefore large. If the distance between the antennas is long, bending of the Earth's surface must also be taken into account in determining the location of reflection.

The surface may be considered smooth, if the rms value of the surface roughness,  $\Delta h$ , fulfils the following condition:

$$\Delta h < \frac{\lambda}{32 \sin \gamma} \quad (10.16)$$

If the surface is rough, a considerable part of power will scatter; that is, it will radiate into a large solid angle.

## 10.6 Multipath Propagation in Cellular Mobile Radio Systems

Figure 10.11 presents the field strength as a function of distance when a strong reflected wave interferes with an LOS wave. As the receiver moves away from the transmitter, the signal fades wherever the two waves are in opposite phase. In mobile radio systems, the situation is generally much more complex due to the multipath propagation [6, 7].

We can categorize fading phenomena in many ways. Prominent obstacles between the transmitter and receiver cause large-scale fading. Because

of this, the path loss increases rapidly over distance and is log-normally distributed about the mean value. Small-scale fading refers to signal amplitude and phase variations due to small changes (order of a wavelength) in position. Interference of several waves—multipath propagation—causes this type of fading. Because of the multipath propagation the signal spreads in time (dispersion) and the channel is time-variant due to the motion of the mobile unit. Both phenomena degrade the performance of the system. Depending on the effect of dispersion, we categorize fading either as frequency-selective or flat. If the radio channel is frequency-selective over the signal bandwidth, *intersymbol interference* (ISI) will degrade the performance. In the case of flat fading all signal components fade equally. According to the rapidity of changes in the time-variant channel, we categorize fading as fast or slow.

When there is a dominant LOS wave in a multipath environment, the amplitude of the signal envelope has a Rician probability distribution. If there is no LOS wave, as in Figure 10.12, the envelope has a Rayleigh probability distribution. There are reflected, diffracted, and scattered waves as well as waves propagating through vegetation and buildings. The Rayleigh distribution is obtained by summing up a large number of independent field components, and its probability distribution is

$$P(r) = \frac{r}{\sigma^2} \exp[-r^2/(2\sigma^2)] \quad (10.17)$$

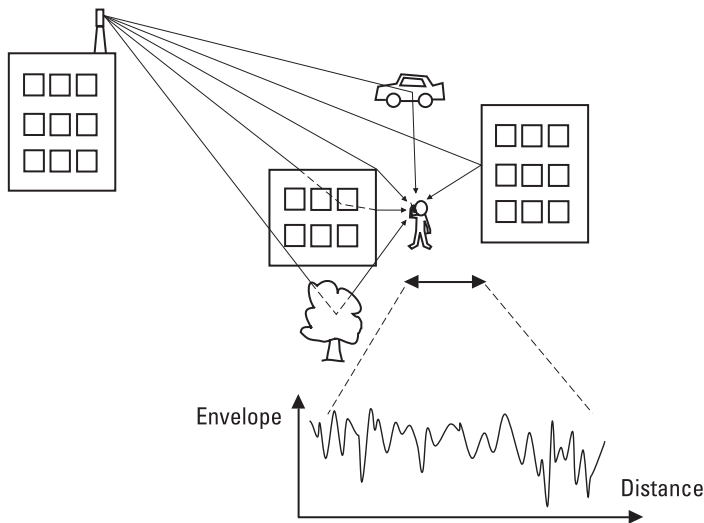


**Figure 10.12** Multipath propagation in an urban environment and the signal envelope in a fading radio channel.



where the envelope  $r(t)$  of the complex signal  $E(t)$  is given as  $r(t) = \sqrt{[\operatorname{Re} E(t)]^2 + [\operatorname{Im} E(t)]^2}$ , and  $\sigma^2$  is the mean power, and  $r^2(t)/2$  is the short-term signal power.

The effect of small-scale fading may be mitigated by using in receiving or transmitting multiple antennas, time redundancy, several polarizations, or several frequencies (space, time, polarization, and frequency diversity). The diversity increases the probability that at least one of the received signals will be strong enough to be detected. Spread spectrum or multicarrier systems can mitigate the small-scale fading due to their large bandwidth, that is, their frequency diversity. A rake receiver can mitigate it using time diversity by detecting replicas of the transmitted signal with different time delays [7]. A smart antenna system such as *multiple-in-multiple-out* (MIMO) can mitigate it through space and polarization diversity [8]. Moreover, a MIMO system can increase the spectral efficiency by utilizing different independently fading propagation paths as parallel data channels.

In rural areas the base station antennas are located in high antenna masts so that most of the path is in free space or along the treetops. The final meters or tens of meters of the path to the mobile terminal may cause a lot of attenuation; in a forest the average excess attenuation through vegetation at 2 GHz is about 0.4 dB/m; however, the attenuation of a tree with or without foliage is very different. In urban areas the base station antennas may be located at the roofs or walls of the buildings, while the mobile terminals move along the street canyons or are inside the buildings.

Both deterministic and stochastic propagation models are used in design, optimization, and performance evaluation of cellular mobile radio systems. Deterministic models are based on electromagnetic simulations (utilizing ray tracing together with geometrical optics and uniform theory of diffraction, finite difference time domain method, and so forth) making use of information of the specific physical environment or on measurements. Stochastic models describe the propagation phenomena on average; they are based on defining the fading distributions (log-normal, Rayleigh, Rician). The model parameters are based on measurements or on a deterministic model in a given type of environment [9, 10].

The deterministic propagation models can be divided into simplified semiempirical path loss models and computational site-specific models. An example of the empirical models is the Okumura-Hata model [11]. In the Okumura-Hata model the physical environment can be selected among a large city, a medium to small city, a suburban area, or a rural area, and the model takes into account the antenna heights and frequency. The Walfisch-

Bertoni model [12] allows slightly more detailed characterization of the environment; for example, the average building height and the width and orientation of the streets can be taken into account. It counts the propagation loss as a function of distance (free-space loss), multiscreen diffraction due to rows of houses, and finally the roof-to-street diffraction. Inside the buildings, site-specific computational models are often used, but simplified models such as the Motley-Keenan model [13], which calculates the path loss from the free-space path loss according to the distance added by attenuation of each wall along the path, are also in use.

## 10.7 Propagation Aided by Scattering: Scatter Link

Inhomogeneities of the atmosphere cause scattering. Scattering means that part of the coherent plane wave is transformed into incoherent form and will radiate into a large solid angle. Normally, scattering will weaken the radio link by attenuating the signal. However, the scattered field may also be useful: A scatter link takes advantage of scattering.

Let us first consider scattering by a single object or particle. The scattering cross section  $\sigma$  of an object to a given direction describes the effective area of the object when it is illuminated by a plane wave. The power intercepted by this area, when scattered equally in all directions, produces the same power density as the object. The scattering cross section also depends on the direction of the incident wave and its polarization. Figure 10.13 shows how the scattering cross section of a conducting (metal) sphere behaves as a function of frequency, when the direction of incidence and the direction of observation are the same. The scattering cross section of a small (in comparison to a wavelength), metallic sphere (or of an object of another shape) is proportional to  $f^4$  (Rayleigh scattering). The scattering cross section  $\sigma$  of a large (in comparison to a wavelength) sphere is equal to its geometric cross section  $\sigma_g$ . This is called the optical region. Between these regions there is a resonance region (Mie scattering). Because the relative permittivity  $\epsilon_r$  of water is large, the curve in Figure 10.13 also describes the scattering of a raindrop. The total scattering cross section  $\sigma_s$  multiplied by the power density of the incident wave gives the total power scattered by the object into the solid angle of  $4\pi$ . The total scattering cross section  $\sigma_s$  of a large object is  $2\sigma_g$ .

If the density of small scattering particles is  $\rho$  (particles per cubic meter), the scattering cross-section density is  $\sigma_d = \rho\sigma$ . In a symmetric radio path utilizing scattering as shown in Figure 10.14, the power received is

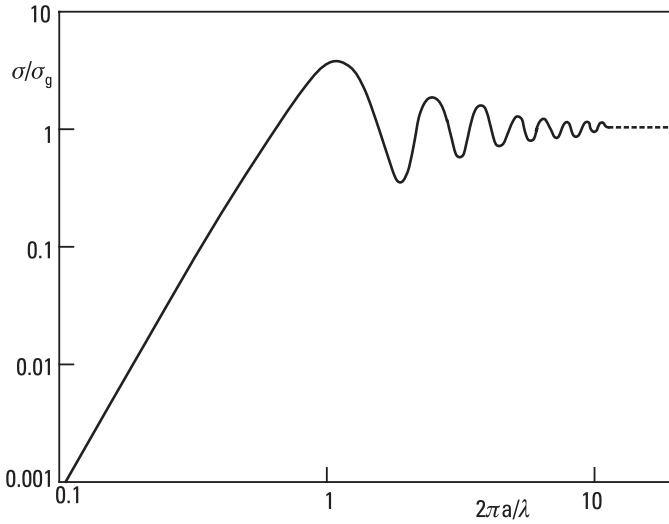


**Figure 10.13** Scattering cross section  $\sigma$  versus frequency of a conducting sphere with a radius  $a$ .

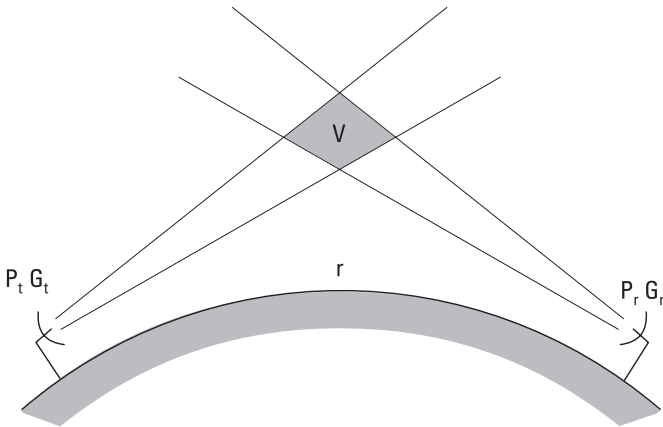


**Figure 10.14** A radio path utilizing tropospheric scattering: a scatter link.

$$P_t = G_t G_r \frac{\lambda^2}{4\pi^3 r^4} P_t \int_V \sigma_d dV \tag{10.18}$$

where  $V$  is the volume where scattering occurs.

In radio links, three kinds of scattering are utilized: tropospheric, ionospheric, and meteor scattering. The tropospheric scattering is due to turbulence in the troposphere and is the most widely utilized scattering mechanism in communication. This may provide a 500-km hop in the microwave region. The ionospheric scattering is caused by the cloudlike structures of the lowest layers of the ionosphere, and the meteor scattering is caused by the ionized trails of meteors. (The ionized trail is due to the high temperature produced by friction as the meteor enters the atmosphere at high velocity.) These scattering mechanisms may provide radio hops of 2,000 km at frequencies from 30 to 80 MHz. Furthermore, raindrops and snowflakes cause scattering, which may introduce interference between different radio links.

Fading or a random variation of the signal power level is typical for radio systems based on scattering. This phenomenon may be divided into a slow fading, which is due to large changes in the propagation conditions, and into a fast fading, which is due to multipath propagation. Fading can be partially compensated by a feedback, which is used to stabilize the signal power level, or by using diversity, as described in Section 10.6.

## 10.8 Propagation via Ionosphere

The highest layers of the Earth's atmosphere are called the ionosphere, because they contain plasma, which is ionized gas (free electrons and ions). The ionosphere extends from 60 to 1,000 km. Below 60 km the ionization is insignificant because the solar ionizing radiation is getting weaker due to absorption in the higher layers, and because recombination of plasma is fast due to high density of molecules. Above 1,000 km the density of molecules is too low for a significant phenomenon. It is possible to distinguish different layers in the ionosphere, as shown in Figure 10.15; they are called D, E, F<sub>1</sub>, and F<sub>2</sub> layers. The electron density and the height of these layers depend on the solar activity, on the time of day and season, and on the geographical location. During night the D layer nearly disappears, and the F<sub>1</sub> and F<sub>2</sub> layers merge together. The highest electron density is about  $10^{12}$  electrons/m<sup>3</sup>, and it can be found at daytime at the altitude of about 250 to 400 km in the F<sub>2</sub> layer.

Let us consider radio wave propagation in plasma. The electric field having a strength  $E$  affects (accelerates) a charge  $q$  by force  $qE$ . If there are  $N$  charges in a unit volume, the current density in case of a sinusoidal field is ( $F = ma = mdv/dt = mj\omega v$ )

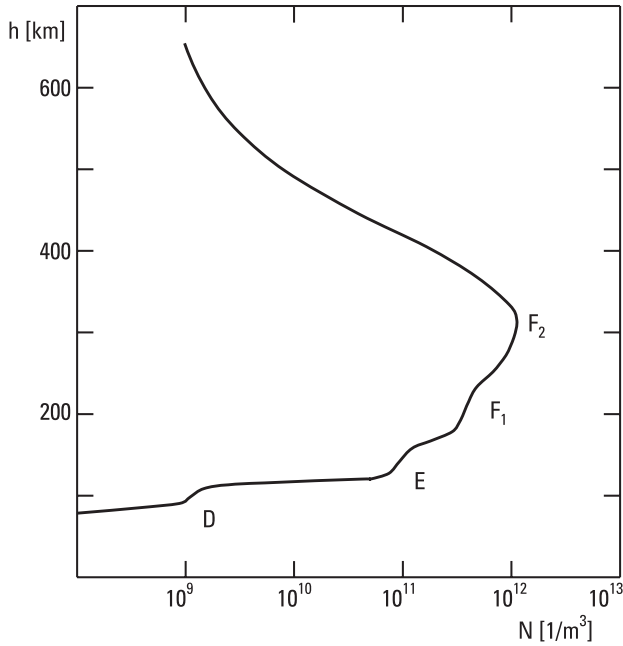


**Figure 10.15** Electron density in the ionosphere versus altitude.

$$\mathbf{J} = Nq\mathbf{v} = \frac{Nq^2\mathbf{E}}{j\omega m} \quad (10.19)$$

where  $\mathbf{v}$  is the velocity of the charge and  $m$  is its mass. Maxwell's IV equation, (2.21), can now be written as

$$\nabla \times \mathbf{H} = \mathbf{J} + j\omega\epsilon\mathbf{E} = j\omega\epsilon_0 \left( 1 - \frac{Nq^2}{\omega^2 m \epsilon_0} \right) \mathbf{E} \quad (10.20)$$

The charges cause a decrease of the permittivity of medium. Because the electron rest mass is only 1/1,836 of that of a hydrogen ion, the electrons determine the permittivity. The relative permittivity of plasma is

$$\epsilon_r = 1 - \frac{Ne^2}{\omega^2 m_e \epsilon_0} = 1 - \left( \frac{f_p}{f} \right)^2 \quad (10.21)$$

where  $e$  is the electron charge and  $m_e$  is the electron mass, and

$$f_p = \frac{1}{2\pi} \sqrt{\frac{Ne^2}{m_e \epsilon_0}} \quad (10.22)$$

is the plasma frequency. The plasma frequency in hertz is

$$f_p \approx 9\sqrt{N} \quad (10.23)$$

where  $N$  is the number of electrons in one cubic meter; that is, the plasma frequency is 9 MHz for an electron density of  $10^{12}/\text{m}^3$ .

This treatment does not take into account collisions of electrons with neutral molecules, which causes attenuation. Furthermore, the Earth's magnetic field affects the electron motion, which leads to a direction depending on  $\epsilon_r$ ; that is, plasma is an anisotropic and nonreciprocal medium and  $\epsilon_r$  is a tensor. The nonreciprocity causes Faraday rotation (see Section 6.2). The electric field of a linearly polarized wave may rotate, causing wrong polarization in reception. Therefore, in radio systems utilizing the ionosphere, a circular polarization is preferred.

A wave can propagate in plasma only if its frequency is higher than the plasma frequency. Otherwise  $\epsilon_r$  is negative and the wave will be totally reflected. At frequencies well above the plasma frequency,  $\epsilon_r \approx 1$ , and the effect of plasma on radio wave propagation is negligible. In practice, there is no need to take the ionosphere into account at VHF and higher frequencies.

A wave propagating vertically into the ionosphere will be reflected at altitude where  $\epsilon_r = 0$ , that is,  $f_p = f$ . If the wave approaches the ionosphere in an angle  $\phi_0$ , as shown in Figure 10.16, reflection takes place at a height where

$$f_p = f \cos \phi_0 \quad (10.24)$$

Via the ionosphere it is possible to obtain a radio hop to a distance of 4,000 km just with one reflection. Also, longer hops are possible if the wave reflects from the ground back to the ionosphere. In a given radio link the frequency must be higher than the *lowest usable frequency* (LUF) but lower than the *maximum usable frequency* (MUF). The LUF and MUF depend on the temporary characteristics of the ionosphere.

## 10.9 Propagation as a Ground (Surface) Wave

If the transmitting and receiving antennas are close (in comparison to a wavelength) to the ground, the wave propagates bound to the ground, as a

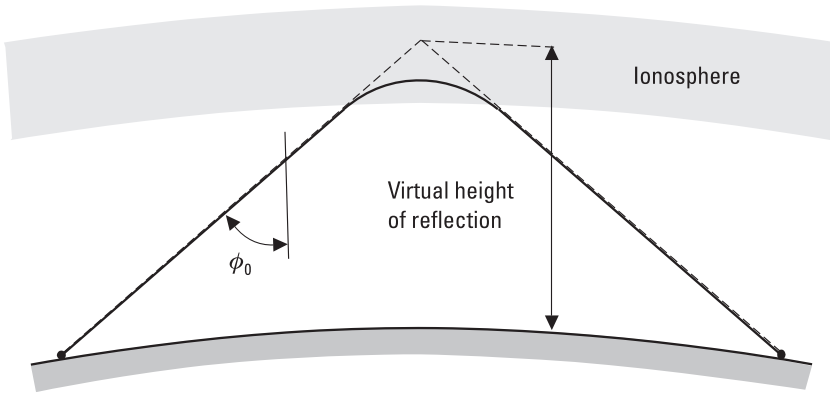


**Figure 10.16** Wave propagation via the ionosphere.

surface wave. The electric field strength of the wave decreases rapidly as the distance from the surface increases. At low frequencies the attenuation of such a ground wave is small, and the wave can propagate beyond the horizon thousands of kilometers, especially over seawater. However, the attenuation of a ground wave increases rapidly with frequency. Therefore this propagation mechanism is useful only below 10 MHz.

Attenuation of the wave depends on conductivity and permittivity of the surface (land, lake, or sea). Table 10.1 shows some typical characteristics at frequencies below 30 MHz. At microwave frequencies these characteristics change strongly as a function of frequency. ITU-R publishes field strength graphs for different surface types. Figure 10.17 presents the electric field strength versus distance when the wave propagates along the surface of a medium dry land and sea [14]. The transmitting antenna is a vertical monopole, and the power transmitted is 1 kW. The graphs show that at 10 kHz the electric field strength decreases as  $1/r$  (as in free space) up to a distance

**Table 10.1**  
Electrical Properties of Different Ground Surfaces ( $f < 30$  MHz)

	$\epsilon_r'$	$\sigma/\text{Sm}^{-1}$
Seawater	70	5
Fresh water	80	$3 \times 10^{-3}$
Wet land	30	$10^{-2}$
Dry land	3	$10^{-4}$
Ice on a lake	3	$10^{-5}-10^{-4}$

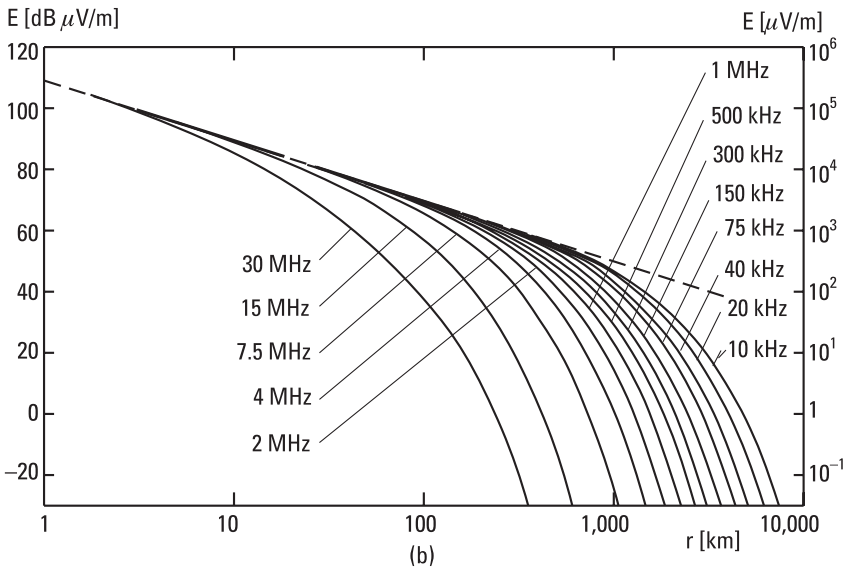
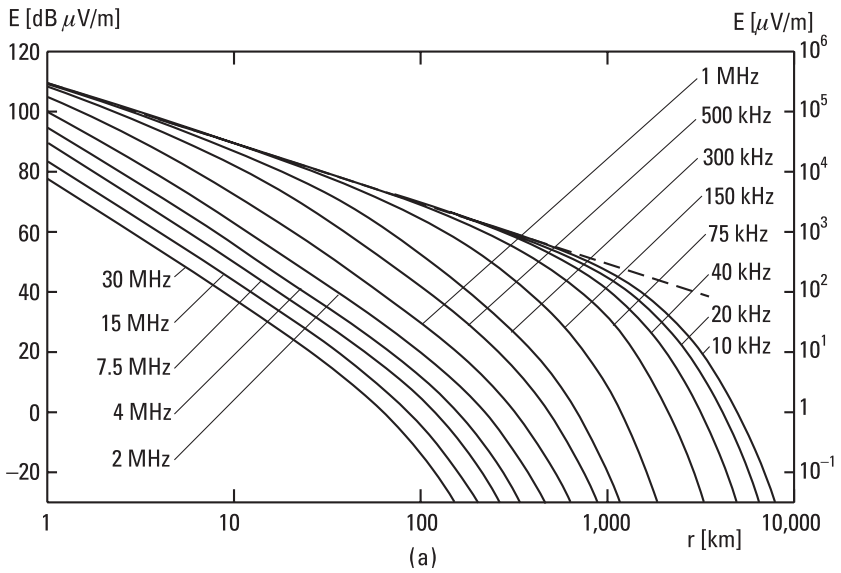


**Figure 10.17** Electric field strength of the ground wave when the transmitting antenna is a vertical monopole and the power transmitted is 1 kW: (a) over a medium dry land,  $\sigma = 10^{-3}$  S/m,  $\epsilon_r = 15$ ; (b) over sea water,  $\sigma = 5$  S/m,  $\epsilon_r = 70$ . (After: [14].)



of 1,000 km. At higher frequencies the attenuation is much higher. Over the sea the wave attenuates much slower than over medium dry land. In practice the electrical characteristics of the surface may vary a lot between the transmitting and receiving stations, and therefore a prediction of the power to be received is difficult.

## References

- [1] Salonen, E., et al., "Modeling and Calculation of Atmospheric Attenuation for Low-Fade-Margin Satellite Communications," *ESA Journal*, Vol. 16, 1992, pp. 299–317.
- [2] Zhang, W., S. I. Karhu, and E. T. Salonen, "Predictions of Radiowave Attenuations Due to a Melting Layer of Precipitation," *IEEE Trans. on Antennas and Propagation*, Vol. 42, No. 4, 1994, pp. 492–500.
- [3] Salonen, E. T., J. K. Tervonen, and W. J. Vogel, "Scintillation Effect on Total Fade Distributions for Earth-Satellite Links," *IEEE Trans. on Antennas and Propagation*, Vol. 44, No. 1, 1996, pp. 23–27.
- [4] van de Kamp, M. M. J. L., et al., "Frequency Dependence of Amplitude Scintillation," *IEEE Trans. on Antennas and Propagation*, Vol. 47, No. 1, 1999, pp. 77–85.
- [5] Skolnik, M. I., *Introduction to Radar Systems*, 2nd ed., New York: McGraw-Hill, 1981.
- [6] Rappaport, T. S., *Wireless Communications, Principles, and Practice*, Upper Saddle River, NJ: Prentice Hall, 1996.
- [7] Parsons, J. D., *The Mobile Radio Propagation Channel*, 2nd ed., Chichester, England: John Wiley & Sons, 2000.
- [8] Foschini, G. J., and M. J. Gans, "On Limits of Wireless Communications in a Fading Environment When Using Multiple Antennas," *Wireless Personal Communications*, Vol. 6, No. 3, 1998, pp. 311–335.
- [9] Bach Andersen, J., T. S. Rappaport, and S. Yoshida, "Propagation Measurements and Models for Wireless Communications Channels," *IEEE Communications Magazine*, Vol. 33, No. 1, 1995, pp. 42–49.
- [10] Bertoni, H. L., *Radio Propagation for Modern Wireless Systems*, Upper Saddle River, NJ: Prentice Hall, 2000.
- [11] Hata, M., "Empirical Formulae for Propagation Loss in Land Mobile Radio Services," *IEEE Trans. on Vehicular Technology*, Vol. VT-29, No. 3, 1980, pp. 317–325.
- [12] Walfisch, J., and H. L. Bertoni, "A Theoretical Model of UHF Propagation in Urban Environments," *IEEE Trans. on Antennas and Propagation*, Vol. 36, No. 12, 1988, pp. 1788–1796.
- [13] Keenan, J. M., and A. J. Motley, "Radio Coverage in Buildings," *British Telecom Technology Journal*, Vol. 8, No. 1, 1990, pp. 19–24.
- [14] International Telecommunication Union, "Ground-Wave Propagation Curves for Frequencies Between 10 kHz and 30 MHz," Recommendation ITU-R P.368-7.

# 11

## Radio System

Performance of a whole radio system, such as a cellular network, navigation system, or radar, depends on the characteristics of the transmitters, receivers, and antennas as well as of propagation of radio waves between the transmitting and receiving antennas. If the transmitted power and the gains and attenuations in different parts of the system are known, the received power can be calculated. However, in addition to the received power, there are other factors affecting the signal detection: modulation of the signal, frequency stability, interference from other radio systems, noise, dispersion due to the radio channel, and so on.

In this chapter we first briefly discuss transmitters and receivers. Then we study noise in more detail as it decreases the performance of any radio system. We also study different modulation techniques, that is, how information can be attached to the carrier. Finally we consider the link budget. In Chapter 12 some radio systems are studied in more detail.

### 11.1 Transmitters and Receivers

A radio transmitter must produce a signal that has enough power, has generally a very accurate frequency, and has a clean enough spectrum so that the transmitter does not disturb users of other radio systems. Information to be transmitted, the baseband signal, is attached to a sinusoidal carrier signal by modulating the carrier amplitude, frequency, or phase either analogically or digitally (see Section 11.3).

Low-power transmitters are usually based on a semiconductor device, a transistor or diode oscillator. When a transmitter power of hundreds of watts is needed, power is generated with electron tubes or so-called microwave tubes. Tetrodes are used from LF to VHF, and klystrons at UHF and SHF. In radar transmitters, a magnetron oscillator is the most common. In klystrons, magnetrons, and other microwave tubes, microwave oscillation is generated by an electron beam interacting with a resonance cavity or a slow-wave structure [1].

In order to have a sufficiently accurate and clean signal, the oscillator frequency must be stabilized and the signal must be bandpass filtered before transmitting. Oscillators may be stabilized using a resonator with a sufficiently high quality factor. Often the accurate frequency is based on a quartz crystal oscillator at a frequency of 1 to 40 MHz and with a frequency stability of  $10^{-9}$  to  $10^{-10}$  per day. The signal of the quartz oscillator is frequency multiplied to the transmission frequency and then amplified, or it is used to injection lock or phase lock another oscillator to the correct frequency.

Figure 11.1 presents a direct-conversion transmitter. A digital baseband signal modulates the carrier in an IQ-modulator (see Section 11.3.2). The modulated signal is then filtered and amplified. In a superheterodyne transmitter the signal is further upconverted to the final frequency. The carrier frequency is stabilized by phase locking [2]. A basic *phase-locked loop* (PLL) is a feedback system consisting of a VCO, a phase detector (for example, a double-balanced mixer), and a low-pass filter. In the loop of Figure 11.1 there is also in the feedback branch a digital circuit that divides the frequency of the VCO by  $N$ . The output of the divider is compared with the signal from the reference oscillator in the phase detector. A possible difference in frequency (in phase) is transformed into a voltage proportional to the phase difference, and after lowpass filtering this voltage is used to control the VCO frequency until the frequency difference is zero. The output frequency of the locked loop is  $Nf_{ref}$ . The loop also stabilizes within its bandwidth the random phase variations of the VCO and, thus, the reference oscillator determines the phase-noise characteristics.

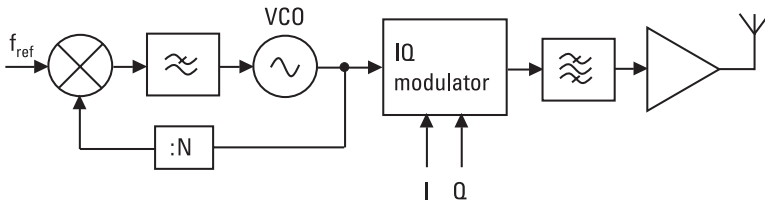


**Figure 11.1** Direct-conversion transmitter with a phase-locked oscillator.

If the system must operate at several nearby frequencies (channels), the transmitter and receiver signals are generated in a frequency synthesizer [3]. The synthesis may be based on a PLL, on a direct synthesis, or on a *direct digital synthesis* (DDS). If a programmable divider is employed in Figure 11.1, this PLL can produce several frequencies spaced by  $f_{ref}$ . Smaller frequency steps are obtained by combining several PLLs or by using a fractional- $N$  loop, where the division ratio is a fraction and is not limited to integer values. The direct synthesis uses mixers, frequency multipliers, dividers, filters, and switches to produce accurate frequencies. This method may not be practical if a large number of closely spaced frequencies are needed, because the synthesizer would become very complex. In the DDS a *digital-to-analog converter* (DAC) generates the waveform using a look-up table. Accurately modulated signals with very good frequency resolution may be produced using DDS, but the upper frequency is limited by the available DACs to a few hundred megahertz.

The receiver must be sensitive and selective. It must be able to detect even a weak signal among many other, possibly stronger signals. Therefore, a good receiver must have good filters, an accurate local oscillator frequency, and low-noise components. It should have also a large, spurious-free dynamic range.

Receivers are usually superheterodyne receivers (here “super” comes originally from “supersonic,” meaning that there is an intermediate frequency higher than the audio frequency, that is, the baseband signal frequency in a voice radio). Figure 11.2 presents such a receiver, where the signal from the antenna is first filtered and then amplified by an LNA by 10 to 20 dB. In front of a mixer an image-rejection filter blocks the image band. A frequency synthesizer generates an accurate *local oscillator* (LO) signal. The mixer downconverts the signal to an IF, where it is again filtered with a narrowband filter (e.g., a SAW filter) and amplified by an IF amplifier (e.g. by 70 to 100 dB) before demodulation. The demodulator recovers the original analog or digital baseband signal. If the signal power level may vary

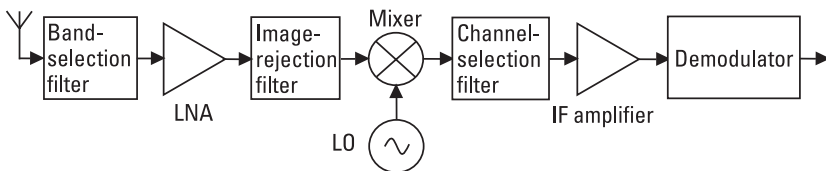


**Figure 11.2** Block diagram of a typical superheterodyne receiver used in radio communication.

significantly, the IF gain should be controllable with an *automatic gain control* (AGC) circuit in order to avoid saturation in the back end.

There are many other receiver architectures. Often in a superheterodyne receiver the signal is downconverted twice. In such a dual-conversion receiver the first IF is high and the second IF is low. This facilitates the realization of filters. Distribution of the gain to several frequencies also reduces the tendency of the receiver to oscillate.

Figure 11.3 shows a direct-conversion receiver, which is called also a homodyne or zero-IF receiver. The signal is now downconverted directly to the baseband. There is no IF stage and, thus, this structure is simpler and better suited for integration than the superheterodyne architecture. Lower power consumption and the possibility of making the channel filter at the baseband are other advantages. However, as the LO frequency equals the carrier frequency, leaking of the LO power may cause severe problems. In a dual-conversion receiver the channel selection can be realized with a synthesizer operating at the IF, but in a direct-conversion receiver the synthesizer must operate at the higher carrier frequency.

In a direct IF sampling receiver, which is also called a software radio, the whole band at the IF is sampled with an *analog-to-digital converter* (ADC). Channel filtering and demodulation is then realized with digital signal processing. This architecture is flexible and suited multimode operation, because the system standard may easily be changed. However, the ADC is now a critical component; it has to operate very linearly over a large dynamic range.

A transceiver is a combination of a transmitter and receiver sharing the same antenna. Now the isolation of the transmitter and receiver has to be very large, for example, 120 dB. If the transmitter and receiver operate

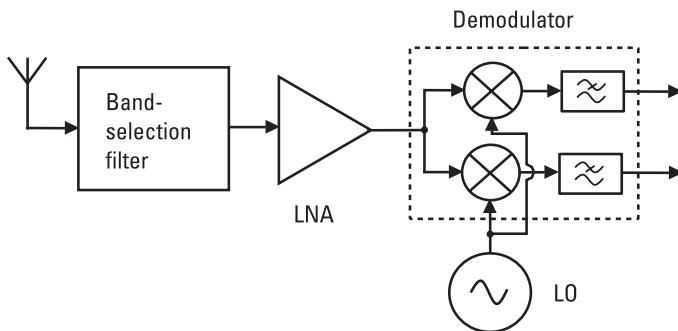


**Figure 11.3** Direct-conversion receiver.

at different frequencies, called *frequency division duplexing* (FDD), a duplexing filter separates them from each other. A duplexing filter consists of two bandpass filters. If the transmitter and receiver operate in different time slots, called *time division duplexing* (TDD), a switch can be used to isolate the receiver during transmission. The loss of a switch is usually less than the loss of a duplexing filter.

A high level of integration is essential in the mass production of low-cost transceivers and receivers. The ultimate goal is to integrate all the transceiver electronics on a single chip, because external components increase the cost. High-quality filters and resonators are often too difficult to integrate on a chip. The practical solution is to combine several chips made using different technologies with some external components. Low-cost silicon-based technologies such as bipolar, BiCMOS, and CMOS technology are used to produce chips up to about 3 GHz. When top performance is required or the frequency is higher, chips are made using GaAs and InP technologies.

## 11.2 Noise

Random fields and voltages, that is, noise, disturb all radio systems. The antenna receives noise from its surroundings, and all receiver components, which are either active or lossy, generate noise. We call the former the antenna noise and the latter the receiver noise; their sum is called the system noise. In a radio system (e.g., a communication link) the system noise power in the receiver bandwidth may be stronger than the signal to be received. The ratio of the signal power to the noise power at the receiver bandwidth, that is, the  $S/N$  often determines the quality of a radio link. However, noise signals may also be useful, as is the case in radiometry, for example, in remote sensing and radio astronomy (see Sections 12.7 and 12.8).

In system considerations, a radio channel, where white noise corrupting the signal is the only nonideality, is called the *additive white Gaussian noise* (AWGN) channel. In addition to noise, in practical radio channels there are other nonidealities. When the small-scale fading or Rayleigh fading in multipath propagation conditions is the limiting factor for the channel performance, we call it a Rayleigh fading channel.

### 11.2.1 Receiver Noise

In a receiver, many kinds of noise are generated, for example, thermal noise, shot noise,  $1/f$  noise, and quantum noise.

Thermal noise is generated by the thermal motion of charge carriers. The warmer the material is, the more electrons collide with the crystal lattice of the material. Each collision causes a change in the kinetic energy state of the electron, and the energy difference is radiated as an electromagnetic wave. Similarly, collisions are also the reason for resistivity of a material and, therefore, thermal noise is generated in all materials and circuits absorbing RF power. Thermal noise is directly proportional to the absolute temperature of the medium, but its power density is independent of frequency—it is so-called white noise.

Shot noise is often the most important noise mechanism in semiconductor devices and electron tubes. Shot noise is caused by the fact that charge is not a continuous quantity but always a multiple of an electron charge. For example, a current going through the Schottky interface is not continuous but is a sum of the current impulses of single electrons. The power density of shot noise is directly proportional to the current.

At low frequencies there is  $1/f$  noise (flicker noise) in all semiconductor devices. It is caused, for example, by the fluctuating amount of electrons in the conduction band. Its power density is inversely proportional to frequency.

Quantum noise is due to the quantized energy of the radio wave. It is important only in cases of submillimeter and shorter waves, because their energy quantum  $W = hf$  is large.

Noise properties of a device are described by the noise factor  $F$  or the equivalent noise temperature  $T_e$  [4]. The latter is also called the effective input noise temperature, the input noise temperature, or just the noise temperature. The noise factor of a linear two-port is defined [5] by

$$F = \frac{N_{out}}{G_a N_{in}} \quad (11.1)$$

where  $N_{in}$  is the available noise power in a bandwidth  $df$  from a matched resistive termination (here “matched” means that the termination is matched to the characteristic impedance of the line) at temperature  $T_0 = 290\text{K}$  connected to the input of the device, and  $N_{out}$  is the total noise power available at the output port in a bandwidth  $df$  when the input power is  $N_{in}$ .  $G_a$  is the available power gain of the two-port for incoherent signals from an input bandwidth of  $df$  to an output bandwidth of  $df$ . The noise factor indicates how many times larger the output noise power of the device is compared to that of a noiseless device, when both have in the input a matched resistive termination at the absolute reference temperature of  $T_0 = 290\text{K}$ .

The equivalent noise temperature is defined by means of the noise factor as follows:

$$T_e = (F - 1) T_0 \quad (11.2)$$

or

$$F = 1 + \frac{T_e}{T_0} \quad (11.3)$$

In other words, the equivalent noise temperature can be defined as the physical temperature, at which the matched resistive input termination of a noiseless device should be in order to have the same available noise power in the output as the noisy device itself produces into its output when its matched resistive input termination is at the absolute zero temperature.

A resistor  $R$  at temperature  $T$  generates noise, the rms voltage of which in a bandwidth of  $df$  is

$$v_n = \sqrt{\frac{4Rhfdf}{e^{hf/kT} - 1}} \approx \sqrt{4kTdfR} \quad (11.4)$$

where  $h = 6.626 \times 10^{-34}$  Js is Planck's constant and  $k = 1.381 \times 10^{-23}$  J/K is Boltzmann's constant. The approximation of (11.4) is valid when  $hf \ll kT$ . The available noise power from this resistor, that is, the noise power from this resistor to another resistor with the same resistance, is

$$P = \left( \frac{v_n}{2R} \right)^2 R = kTdf \quad (11.5)$$

This noise power  $P$  is equal to  $N_{in}$  in (11.1), and therefore the noise factor is

$$F = \frac{N_{out}}{kT_0 df G_a} \quad (11.6)$$

In (11.6)  $N_{out}$  is sometimes for practical reasons the power delivered (coupled) to the load; then, instead of the available power gain, one must use the transducer power gain  $G_t$  (see (5.26)). Because the available noise



power in the input is  $N_{in} = kT_0df$  and the ratio of the signal powers in output and in input is  $G_a = S_{out}/S_{in}$ , the noise factor can also be presented as a ratio of the signal-to-noise ratios ( $S/N$ ) in input and in output, as

$$F = \frac{(S/N)_{in}}{(S/N)_{out}} \tag{11.7}$$

Thus, the noise factor describes the degradation of the  $S/N$  in the device, when the matched input termination is at 290K. The noise figure is the noise factor in decibels, that is,

$$F \text{ (dB)} = 10 \log F \tag{11.8}$$

So far we have assumed that the noise properties of the device are constant over the bandwidth  $df$ . An average noise factor is

$$F = \frac{\int_0^\infty F(f) G_t(f) df}{\int_0^\infty G_t(f) df} \tag{11.9}$$

where  $F(f)$  is the noise factor at a point frequency.

An often-useful quantity in noise analysis is the noise bandwidth  $B_n$  of the device illustrated in Figure 11.4:

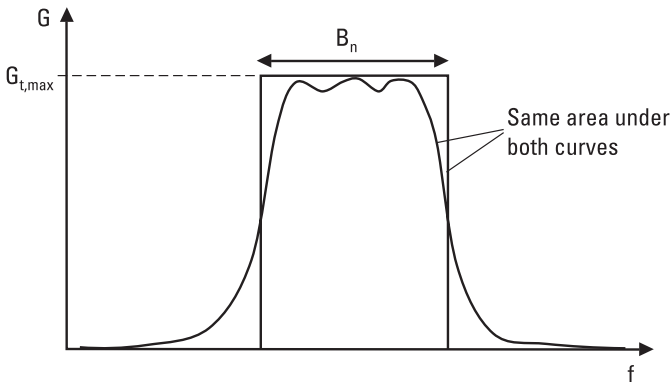


**Figure 11.4** Definition of the noise bandwidth  $B_n$ .

$$B_n = \frac{1}{G_{t,max}} \int_0^{\infty} G_t(f) df \quad (11.10)$$

where  $G_{t,max}$  is the maximum value of the transducer power gain. In respect to white noise in the input, the device behaves like a device that has a gain of  $G_{t,max}$  over the noise bandwidth  $B_n$  and a gain of zero at all frequencies outside this band.

Let us next consider the equivalent noise temperature of a resistive attenuator at a physical temperature  $T$ . If both the attenuator itself and its matched resistive input termination are at the same physical temperature, the attenuator absorbs and emits the same amount of energy. When we measure the noise power from this attenuator in a bandwidth of  $df$ , we get the following result (assuming  $hf \ll kT$ ) as in (11.5)

$$N_{out} = kdfT = N_{in}e^{-\tau} + N_{int} = kdfTe^{-\tau} + kdfT(1 - e^{-\tau}) \quad (11.11)$$

where  $\tau$  is the so-called optical depth, which describes the rate of absorption and emission in the attenuator. For a section of a transmission line with a length  $l$  and an attenuation constant  $\alpha$ , the optical depth is  $\tau = \alpha l$ , and therefore the attenuation of this attenuator is  $L = e^{\alpha l} = e^{\tau}$ . Now we know that the intrinsic noise power  $N_{int}$  is

$$N_{int} = kdfT(1 - e^{-\tau}) = kdfT\left(1 - \frac{1}{L}\right) \quad (11.12)$$

By the definition of the equivalent noise temperature, the input noise temperature  $T_L$  of a resistive attenuator at a physical temperature  $T$  is then

$$T_L = T(L - 1) \quad (11.13)$$

A receiver is, from the signal and noise point of view, all the way from the antenna terminals to the detector a chain of linear two-ports, as shown in Figure 11.5. The noise factor of such a chain is

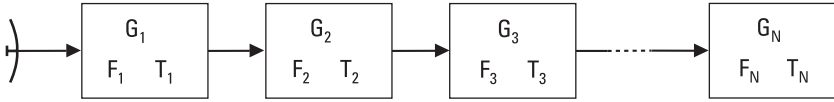


**Figure 11.5** Chain of two-ports in series.

$$\begin{aligned}
 F &= \frac{N_{out}}{kT_0 df G_1 G_2 \dots G_N} \\
 &= \frac{kdf[(T_0 + T_1)G_1 G_2 \dots G_N + T_2 G_2 \dots G_N + \dots + T_N G_N]}{kT_0 df G_1 G_2 \dots G_N} \\
 &= 1 + \frac{T_1}{T_0} + \frac{T_2}{T_0 G_1} + \frac{T_3}{T_0 G_1 G_2} + \dots + \frac{T_N}{T_0 G_1 G_2 \dots G_{N-1}} \\
 &= F_1 + \frac{F_2 - 1}{G_1} + \frac{F_3 - 1}{G_1 G_2} + \dots + \frac{F_N - 1}{G_1 G_2 \dots G_{N-1}} \quad (11.14)
 \end{aligned}$$

and its equivalent noise temperature is

$$T_e = T_1 + \frac{T_2}{G_1} + \frac{T_3}{G_1 G_2} + \dots + \frac{T_N}{G_1 G_2 \dots G_{N-1}} \quad (11.15)$$

In (11.14) and (11.15)  $F_i$ ,  $T_i$ , and  $G_i$  are the noise factor, noise temperature, and available gain of the  $i$ th two-port of the chain. Equations (11.14) and (11.15) are called the Friis noise equations. They are valid only if the two-ports are matched to each other.

According to (11.15), the first stage determines the noise temperature of a receiver, if  $G_1$  is high enough and  $T_2$  low enough. If possible, a good amplifier should be placed as the first stage of the receiver. In a comparison of different amplifiers, a quantity called the noise measure is used. The noise measure is

$$M = \frac{F - 1}{1 - 1/G_a} \quad (11.16)$$

which is the noise factor of an infinitely long chain of similar amplifiers minus one. When cascading two amplifiers, it is better to put as the first stage an amplifier, which has the lowest noise measure, and not necessarily the one, which has the lowest noise factor.

### Example 11.1

You have two low-noise amplifiers, LNA1 and LNA2, with characteristics  $T_1 = 100\text{K}$ ,  $G_1 = 13\text{ dB}$ , and  $T_2 = 90\text{K}$ ,  $G_2 = 7\text{ dB}$ , respectively. You want to use these LNAs together in a series connection in the input of a low-noise receiver. Which one should be placed as the first stage in order to obtain the best possible noise performance of the receiver?

### Solution

Let us first calculate the corresponding noise factors:  $F_1 = 1 + T_1/T_0 = 1 + 100/290 = 1.34$ , and  $F_2 = 1 + 90/290 = 1.31$ . Gains of the amplifiers in absolute values are  $G_1 = 20.0$  and  $G_2 = 5.0$ . Now we can calculate the noise measures:  $M_1 = (F_1 - 1)/(1 - 1/G_1) = 0.34/0.95 = 0.36$ , and  $M_2 = 0.31/0.8 = 0.39$ . Therefore, LNA1 should be placed as the first stage.

The noise factor and noise temperature of a mixer are quantities, which continuously cause confusion, especially in the case of millimeter-wave receivers, where a mixer is often the first stage [6]. The reason for the confusion is the presence of an image sideband in the mixer. The most frequent errors in the noise factor and noise temperature usage are made in the following areas:

- The SSB quantities of a DSB mixer (also called a *broadband mixer*) are confused with the respective quantities of an SSB mixer (also called a *narrowband* or *image-rejection mixer*);
- Depending on the situation, the noise generated in the image termination is to be included as a part of either the receiver noise or the source noise;
- Many old rules of thumb, valid for calculating SSB quantities from DSB quantities of a DSB mixer (or vice versa) in a special case, are unfortunately used also in other cases where they are not valid.

In a mixer, power is converted to the intermediate frequency not only from the signal sideband but also from other sidebands, especially from the image sideband. Let us consider a DSB mixer, which has conversion losses  $L_s$  and  $L_i$  from the signal and image sideband, respectively, to the intermediate frequency band, and the conversion loss values from other (harmonic) sidebands are infinitely large. The DSB noise temperature  $T_{M,DSB}$  of this mixer is, according to the definition of the equivalent noise temperature, the

temperature of a termination that is connected to the noiseless mixer at both the signal and image sidebands. However, the SSB noise temperature  $T_{M,SSB}$  is the temperature of a termination, according to the definition that is connected to the noiseless mixer only at the signal sideband, and at the image sideband there is a termination at the temperature of 0K. Then the DSB and SSB noise temperatures of the DSB mixer are related to each other as

$$T_{M,SSB} = T_{M,DSB} \left( 1 + \frac{L_s}{L_i} \right) \quad (11.17)$$

If the first stage of the receiver is a mixer, the receiver noise temperature is

$$T_R = T_M + L_c T_{IF} \quad (11.18)$$

where  $L_c$  is the conversion loss of the mixer,  $T_M$  is the mixer noise temperature, and  $T_{IF}$  is the noise temperature of the IF amplifier. The receiver SSB noise temperature is obtained with  $T_M = T_{M,SSB}$  and  $L_c = L_{M,SSB} = L_s$ , and the DSB noise temperature is obtained with  $T_M = T_{M,DSB}$  and  $L_c = L_{M,DSB} = L_s L_i / (L_s + L_i)$ . For diode mixers  $L_c$  is larger than unity and, therefore, the noise temperature of the IF amplifier plays a very important role in the receiver noise temperature.

It is worth emphasizing that if an image-rejection filter is placed in front of the DSB mixer, the mixer turns into an SSB mixer, and its conversion loss  $L_c$  is no more equal to the original  $L_s$ , neither is its noise temperature the one obtained from (11.17).

So far we have assumed that when we use a DSB mixer in an SSB mode, there is a termination at 0K at the image sideband. However, this is not the case in practice. For example, a radiometer observing the atmospheric molecular lines often utilizes a DSB mixer as its first stage, and although the useful signal now enters the receiver only at the signal sideband, the same atmospheric background noise enters the receiver at both sidebands, and the termination impedance at both sidebands is nearly the same, that is, the antenna radiation impedance. In this case we have to add a term  $(L_s/L_i) T_i$  into the receiver noise temperature of (11.18) in order to have a noise quantity, which really describes the receiver's ability to detect the useful signal at the signal sideband. Here  $T_i$  is the image sideband termination temperature, which is often nearly equal to the antenna noise temperature (see Section 11.2.2), that is,  $T_i \approx T_A$ .

Now we are ready to summarize the receiver noise temperatures and noise factors in the case of a DSB mixer used as the first stage [6]:

$$T_{R,DSB} = T_{M,DSB} + L_{M,DSB} T_{IF} \quad (11.19)$$

$$F_{R,DSB} = 1 + \frac{T_{R,DSB}}{T_0} \quad (11.20)$$

$$T_{R,SSB} = \left(1 + \frac{L_s}{L_i}\right) T_{R,DSB} + \frac{L_s}{L_i} T_i = \left(1 + \frac{L_s}{L_i}\right) T_{M,DSB} + \frac{L_s}{L_i} T_i + L_s T_{IF} \quad (11.21)$$

$$F_{R,SSB} = 1 + \frac{T_{R,SSB}}{T_0} = \left(1 + \frac{L_s}{L_i}\right) F_{R,DSB} + \frac{L_s}{L_i} \left(\frac{T_i}{T_0} - 1\right) \quad (11.22)$$

### Example 11.2

Calculate the receiver noise temperature and noise figure of a receiver consisting of an LNA, followed by an image-rejection mixer, and an IF amplifier. The characteristics of the components are  $T_{LNA} = 50\text{K}$  and  $G_{LNA} = 10\text{ dB}$ ,  $T_M = 500\text{K}$  and  $L_M = 6\text{ dB}$ ,  $T_{IF} = 200\text{K}$  and  $G_{IF} = 50\text{ dB}$ . How much worse is the receiver performance if at a room temperature of  $295\text{K}$  there is a cable with a loss of  $0.2\text{ dB}$  in front of the LNA?

### Solution

The component gains in absolute values are  $G_{LNA} = 10$ ,  $L_M = 4$ , and  $G_{IF} = 100,000$ , but the latter is not needed in this calculation.  $T_R = T_{LNA} + (1/G_{LNA}) T_M + (L_M/G_{LNA}) T_{IF} = 50\text{K} + (1/10)500\text{K} + (4/10)200\text{K} = (50 + 50 + 80)\text{K} = 180\text{K}$ .  $F_R\text{ (dB)} = 10 \log(1 + T_R/T_0) = 10 \log 1.62 = 2.1\text{ dB}$ . When the cable with loss of  $L = 0.2\text{ dB}$  (in absolute value  $L$  is  $1.05$ ) is added in front of this receiver, we get a new receiver noise temperature  $T_R' = (L - 1) T_{room} + L T_R = (1.05 - 1)295\text{K} + 1.05 \times 180 = 15\text{K} + 189\text{K} = 204\text{K}$ .

When the aim is to have a very low-noise receiver, the receiver front end is cooled down to, for example, a temperature of  $20\text{K}$ . The cooling reduces the noise temperature of an amplifier or a mixer but also the thermal noise from resistive loss in transmission lines and other components. Some

amplifier and mixer types are able to operate only at very low temperatures, for example, a maser and a *superconductor-insulator-superconductor* (SIS) quasi-particle mixer. Figure 11.6 presents noise temperatures of different microwave amplifiers and mixers.

### 11.2.2 Antenna Noise Temperature

Besides the useful signal, an antenna also receives noise power from its surroundings. The antenna noise temperature  $T_A$  is defined as the temperature of such a matched resistive termination, which provides the same noise power as the noise power available from the antenna terminals, which is equal to the noise power received by the antenna in case of a lossless antenna. In the following we assume a lossless antenna.

A so-called black surface does not reflect any radiation incident on it. At optical wavelengths such a surface is black in color. In a thermal equilib-

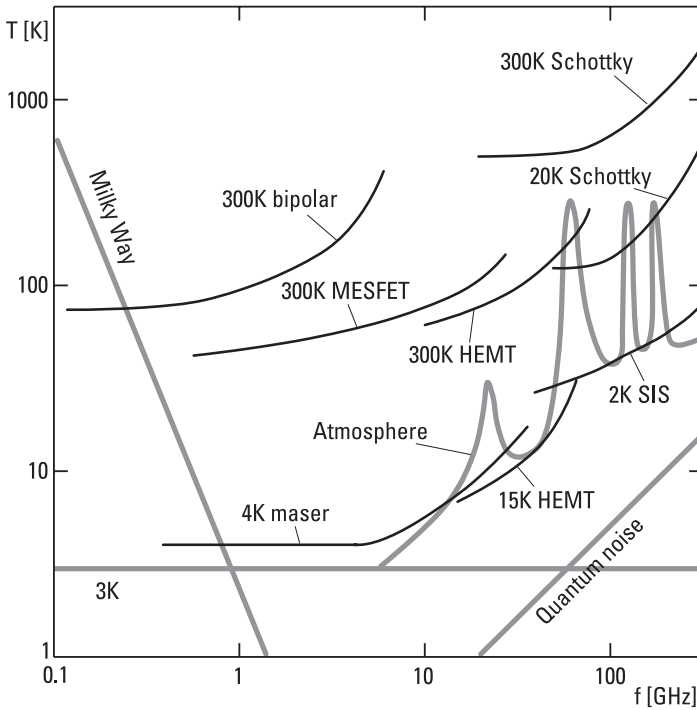


**Figure 11.6** Noise temperatures versus frequency of microwave amplifiers and mixers at different physical temperatures. Natural background noise values as a reference.

rium, the black surface must emit the same power as it absorbs. At temperature  $T$  its brightness, or the power radiated per square meter, hertz, and steradian, is [7]

$$B = \frac{2hf^3}{c^2} \frac{1}{e^{hf/kT} - 1} \quad (11.23)$$

At radio frequencies  $hf \ll kT$ , and therefore

$$B \approx \frac{2kT}{\lambda^2} \quad (11.24)$$

Let us consider a situation like that in Figure 11.7, where a black surface fully surrounds a lossless antenna. The noise power received by the antenna in a bandwidth of  $df$  is

$$P = \frac{1}{2} A_{ef} df \int \int_{4\pi} B(\theta, \phi) \frac{G(\theta, \phi)}{G_{max}} d\Omega \quad (11.25)$$

where  $A_{ef}$  is the effective aperture area of the antenna,  $G(\theta, \phi)$  is the antenna gain in a direction  $(\theta, \phi)$ , and  $G_{max}$  is the maximum antenna gain. The

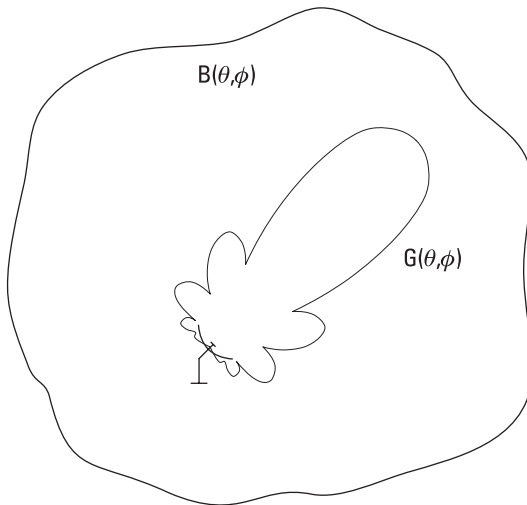


**Figure 11.7** A receiving antenna surrounded by a black surface.



factor of 1/2 is due to the fact that an antenna has a certain polarization but the polarization of noise is random. Therefore, one-half of the noise power is in a given polarization. By substituting (11.24) into (11.25) we get

$$P = \frac{1}{2} A_{ef} df \frac{2kT}{\lambda^2} \frac{4\pi}{G_{max}} = kT df \tag{11.26}$$

Thus,  $T_A = T$ , and the received noise power is independent of the antenna gain and is directly proportional to the temperature of the black surface and to the bandwidth. If the temperature of the black surface depends on the direction within the radiation pattern of the antenna, the received noise power is calculated by integrating from (11.25).

The antenna receives noise from everywhere, including from space and the atmosphere. For these it is possible to define an equivalent black surface temperature, which depends on frequency and direction, as shown in Figure 11.8.

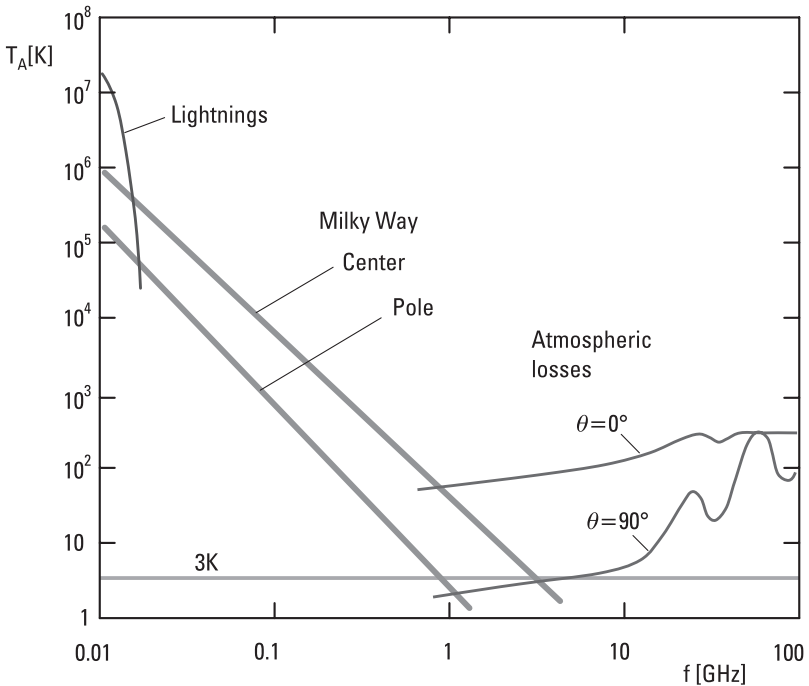


**Figure 11.8** Noise temperature of the sky.

At frequencies that do not penetrate the ionosphere, that is, in the HF band and at lower frequencies, noise from electric discharge in the atmosphere (lightning) is dominant. The amount depends on the season and day, location, and frequency.

Noise from space dominates at frequencies from 20 MHz to 1 GHz. The Milky Way produces RF noise, which is at its maximum in the plane of the Milky Way and decreases as the direction goes away from this plane. The Milky Way noise also decreases as frequency increases. At all frequencies there is a 3K cosmic background radiation, which has its origin in the Big Bang, that is, it is a remnant of the birth of the universe.

Thermal noise due to the atmospheric attenuation is the dominating noise source above 1 GHz. It depends on the atmospheric humidity and elevation angle. The atmosphere can be considered as an attenuator at a physical temperature of about 270K.

Noise due to human activity may be considerable, especially near densely populated areas. In the VHF band and at lower frequencies, noise from the spark plugs of cars and power lines may be stronger than that from nature.

### **11.3 Modulation and Demodulation of Signals**

Information to be transmitted in a radio system, such as voice or music, is first transformed to a low frequency, for example, an audio frequency, electric signal. This baseband signal cannot be directly transmitted through a radio channel, or at least that would be very inefficient. The signal is first fed into a modulator, which modulates some property (amplitude, frequency, phase) of a high-frequency carrier according to the baseband signal. The high-frequency signal obtained is then transmitted by a transmitting antenna. A receiving antenna receives the high-frequency signal and feeds it into a receiver. In the receiver the signal is often downconverted to an intermediate frequency and then demodulated, that is, the original baseband signal is detected; for example, in the case of voice radio, the original voice signal is recovered. In other words, with a modulator the information is attached into a carrier, and with a demodulator it is detached.

There are a number of different modulation schemes, which can be divided into analog and digital methods. Modulation is important not only in communication (radio broadcasting, radio links, mobile phone systems) but also in radar, radionavigation, and so on. Modulation is treated in many communication textbooks, for example, [8–10].

### 11.3.1 Analog Modulation

A sinusoidal waveform can be presented as

$$A(t) = A_0 \cos(\omega_0 t + \psi_0) = A_0 \cos(2\pi f_0 t + \psi_0) \quad (11.27)$$

Information can be attached into this carrier by modulating one of its basic properties according to the baseband signal. Modulation methods are:

1. *Amplitude modulation* (AM): Information is attached to the carrier amplitude.
2. *Frequency modulation* (FM): Information is attached to the carrier frequency.
3. *Phase modulation* (PM): Information is attached to the carrier phase.

AM is in principle the simplest method, but it has high requirements, especially for the linearity of the transmitter. It is used in radio broadcasting in the LF, MF, and HF bands, and in TV broadcasting. FM is used, for example, in FM radio.

#### 11.3.1.1 AM

Let us consider a signal that is amplitude modulated by a sinusoidal signal at frequency  $f_m$ :

$$A(t) = A_0 [1 + m \cos(2\pi f_m t)] \cos 2\pi f_0 t \quad (11.28)$$

Thus, the amplitude varies between values of  $A_0(1 - m)$  and  $A_0(1 + m)$ . Factor  $m$  is the modulation index or modulation depth. The signal envelope follows the modulating signal as shown in Figure 11.9(a), if  $m < 1$ . The carrier frequency should be much higher than the modulating frequency. Equation (11.28) can be presented as

$$A(t) = A_0 \left[ \cos \omega_0 t + \frac{m}{2} \cos(\omega_0 + \omega_m)t + \frac{m}{2} \cos(\omega_0 - \omega_m)t \right] \quad (11.29)$$

The graphical interpretation of this equation is presented in Figure 11.9(b). A constant voltage phasor  $A_0$  corresponds to the carrier frequency. Two voltage phasors with an amplitude of  $(m/2)A_0$  rotate in opposite

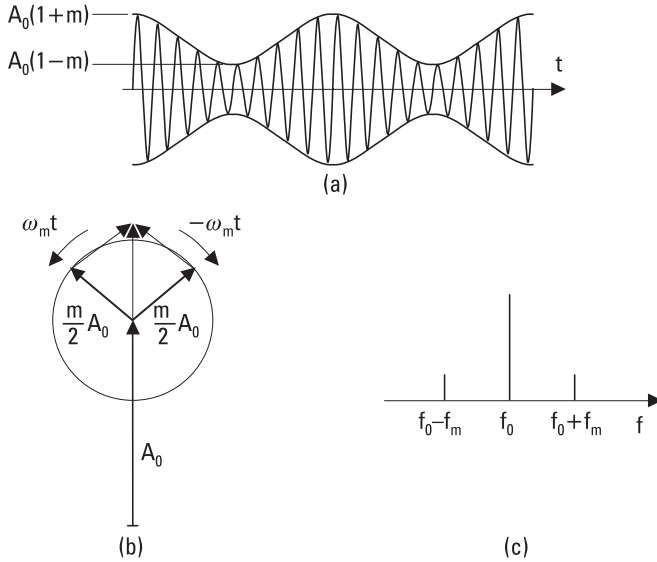


**Figure 11.9** Amplitude-modulated signal: (a) in time domain; (b) phasor presentation; and (c) frequency spectrum.

directions at an angular frequency of  $\omega_m$ . The resultant of these three voltage phasors gives the total voltage. The spectrum contains the components at frequencies  $f_0$ ,  $f_0 + f_m$ , and  $f_0 - f_m$ , as shown in Figure 11.9(c).

If the modulating baseband signal is more complicated, it can be considered as consisting of several sinusoidal components, which have a given amplitude and phase. The modulating signal has a given spectrum and each spectral component modulates the carrier independently.

Figure 11.10 presents the spectrum of an AM signal when the modulating signal is distributed over a given frequency range. The AM is using lavishly both the power and frequency spectrum, because also the carrier not containing information is transmitted and one sideband is only a mirror image of the other. Transmitter power can be saved using DSB modulation, in which the carrier is suppressed, that is, it is not transmitted. This modulation scheme is also called *double-sideband suppressed carrier* (DSBSC) modulation. The frequency spectrum is saved by removing the other sideband, which leads to SSB modulation.

If the modulating signal contains frequency components near the zero frequency, use of SSB modulation becomes complicated, because it is difficult to separate the sidebands. *Vestigial sideband* (VSB) modulation is a compromise between SSB and DSB modulations. In VSB, one sideband is trans-

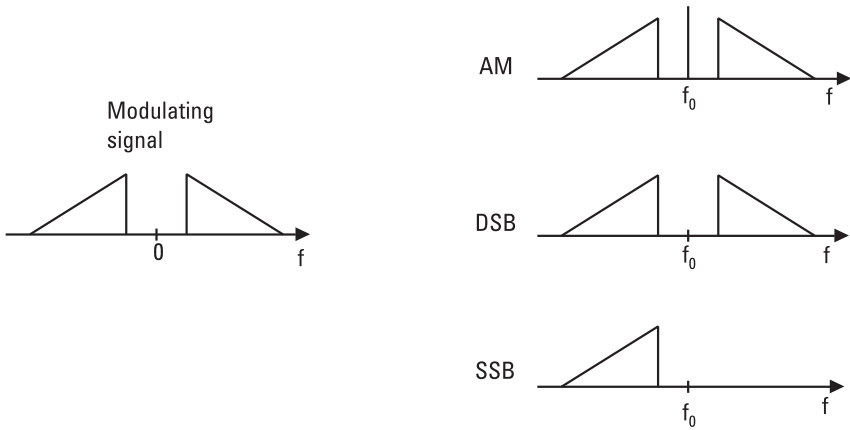


**Figure 11.10** Spectra of basic AM, DSB, and SSB modulation.

mitted nearly in full, but only a small part of the other sideband is transmitted, as illustrated in Figure 11.11. VSB can be realized more easily than SSB by filtering from DSB.

### 11.3.1.2 Amplitude Modulators and Demodulators

A mixer can be used as an amplitude modulator. The modulating waveform is fed into the IF port and the carrier into the LO port, and the modulated signal is obtained from the RF (signal) port, as in Figure 11.12. In a double-balanced mixer there is a good isolation between the LO and RF ports. In that case the carrier is suppressed, and a DSB signal is obtained. The SSB modulation can be realized using the circuit shown in Figure 11.13.



**Figure 11.11** VSB modulation.

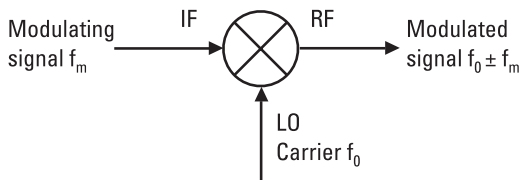


**Figure 11.12** A mixer as an amplitude modulator.

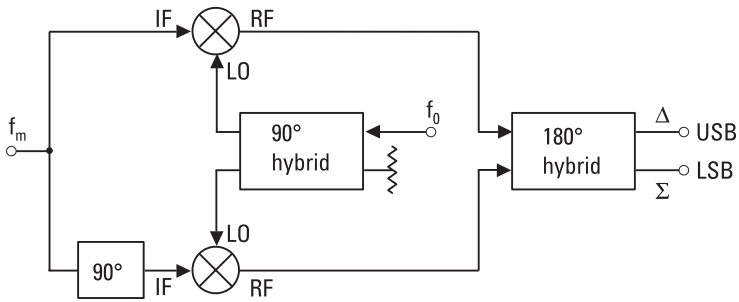


**Figure 11.13** An SSB modulator.

An AM signal can be demodulated by an envelope detector. The output of an envelope detector follows the envelope of the input signal, as shown in Figure 11.14. During one half forward cycle the capacitance  $C$  is charged rapidly to the peak voltage value of the signal. The time constant  $R_S C$  must be much shorter than the cycle length  $1/f_0$ . In the reverse direction the capacitor  $C$  discharges slowly, but it has to be able to follow the modulating signal. This leads to a condition  $1/f_0 \ll R_L C \ll 1/B$ , where  $B$  is the bandwidth of the modulating signal.

In order to demodulate a DSB signal, the carrier must be generated in the receiver. Both the frequency and phase must be correct. The DSB demodulator shown in Figure 11.15 is called the Costas loop, and it resembles the PLL. The input signal is mixed with orthogonal LO signals from a VCO. The difference signals selected by the lowpass filters are proportional to  $m(t) \cos \phi$  and  $m(t) \sin \phi$ , where  $\phi$  is the phase error of the LO. The third mixer produces a signal that adjusts the VCO phase and frequency until the output signal of the upper branch is at maximum and that of the lower branch vanishes. Also, demodulation of an SSB signal requires generation

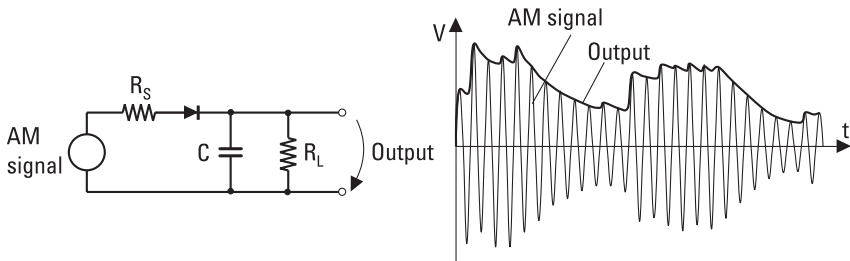


**Figure 11.14** An envelope detector as an amplitude demodulator.

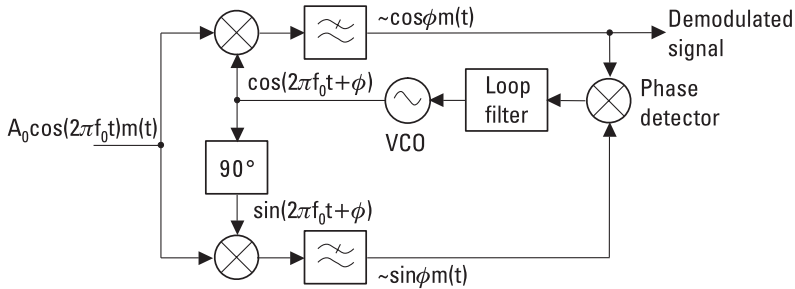


**Figure 11.15** A DSB demodulator.

of the carrier. In order to aid this process, a pilot carrier may be transmitted together with the sideband.

**11.3.1.3 Quadrature AM (QAM)**

QAM is a modulation method that combines two orthogonal DSB signals into the same band. In the transmitter shown in Figure 11.16(a), the phase difference between the two carriers is 90°. In the receiver there is also a 90° phase difference between the two LO signals, and the original baseband signals can be separated. QAM is used in TV broadcasting.

**11.3.1.4 FM**

The amplitude of a frequency-modulated signal is constant, and the instantaneous frequency varies according to the modulating signal. If the modulating signal is sinusoidal, the instantaneous frequency is

$$f(t) = \frac{1}{2\pi} \frac{d\phi(t)}{dt} = f_0 + \Delta f \cos(2\pi f_m t) \tag{11.30}$$

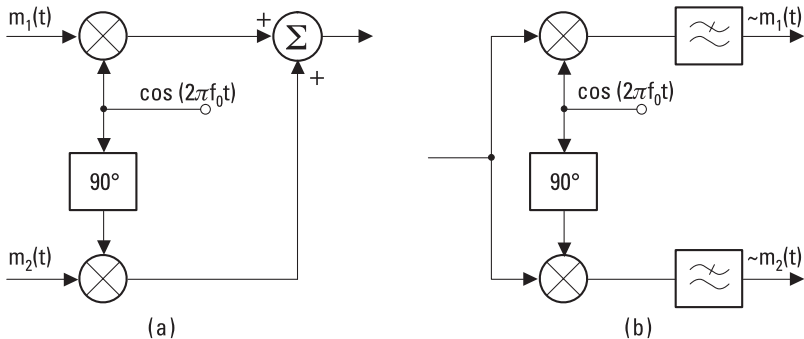


**Figure 11.16** QAM: (a) transmitter and (b) receiver.

where  $\Delta f$  is the maximum frequency deviation. The equation for an FM signal waveform is

$$A(t) = A_0 \cos \phi(t) = A_0 \cos \left[ 2\pi f_0 t + \frac{\Delta f}{f_m} \sin(2\pi f_m t) \right] \quad (11.31)$$

The spectrum of the FM signal contains, besides the carrier, an infinite number of sidebands with a separation of  $f_m$ . The required bandwidth is wider than that in AM, but tolerance to noise and interference is better. The amplitudes of the carrier and sidebands depend on the modulation index  $m = \Delta f/f_m$ . The amplitude  $A_{sp}$  of a sideband  $p$  relative to the amplitude  $A_0$  of an unmodulated carrier is obtained from

$$\frac{A_{sp}}{A_0 (m=0)} = J_p(\Delta f/f_m) \quad (11.32)$$

where  $J_p$  is the  $p$ th order Bessel function of the first kind. Figure 11.17 presents Bessel functions and Figure 11.18 shows an FM power spectrum when the modulation index is  $m = 5.52$ . In this case the normalized amplitude  $J_0$  of the carrier component is small.

If  $m$  is small—less than unity—there is in the spectrum only one important sideband on both sides of the carrier, and  $A_{s1}/A_0 \approx m/2$ . The

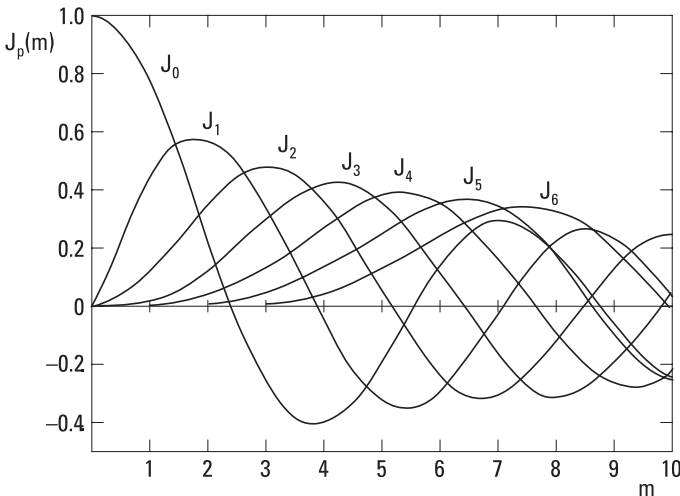


**Figure 11.17** Bessel functions (first kind).



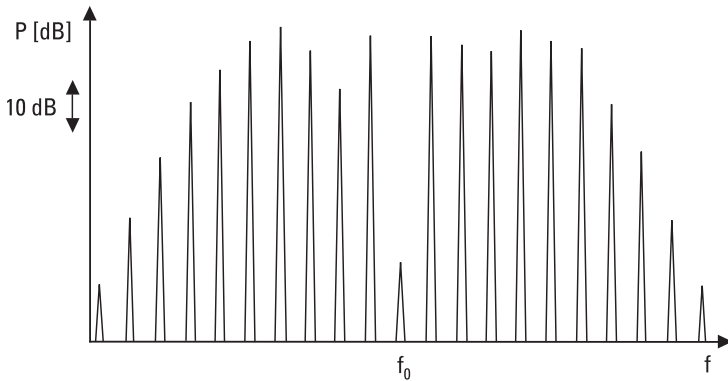


**Figure 11.18** Spectrum of a frequency-modulated signal when the modulation index is  $m = 5.52$ .

spectrum looks like the AM spectrum, but the phases of the sidebands are different.

In theory the FM signal requires an infinite bandwidth. If we allow a given maximum distortion, we can limit the bandwidth. According to Carson’s rule the required bandwidth is [10]

$$B \approx 2\Delta f + 2f_m = 2\Delta f(1 + 1/m) = 2f_m(1 + m) \quad (11.33)$$

### 11.3.1.5 Frequency Modulators and Demodulators

FM can be realized with a VCO. The output frequency of some oscillators can be controlled directly by changing the operation point of the nonlinear element. In other VCOs the frequency is controlled by voltage tuning the resonance frequency of the high-Q embedding circuit, which contains a voltage-dependent element such as a varactor.

Figure 11.19 shows a Hartley oscillator. The input network contains a varactor. The resonance frequency of the input resonator is

$$f = \frac{1}{2\pi\sqrt{(L_1 + L_2)C(t)}} \quad (11.34)$$

Let us assume that  $C$  changes sinusoidally an amount of  $\Delta C$  around  $C_0$  and that the ratio  $\Delta C/C_0$  is small. Then

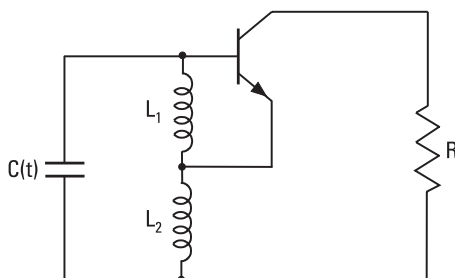


**Figure 11.19** A Hartley oscillator.

$$\begin{aligned}
 f &= \frac{1}{2\pi\sqrt{(L_1 + L_2)(C_0 + \Delta C \cos 2\pi f_m t)}} \\
 &= \frac{1}{2\pi\sqrt{(L_1 + L_2)C_0}} \frac{1}{\sqrt{1 + (\Delta C/C_0) \cos 2\pi f_m t}} \quad (11.35) \\
 &\approx f_0 \left( 1 - \frac{\Delta C}{2C_0} \cos 2\pi f_m t \right) \\
 &= f_0 + \Delta f \cos 2\pi f_m t
 \end{aligned}$$

which shows that we have a frequency modulator.

A frequency demodulator produces a voltage, the instantaneous value of which is proportional to the instantaneous frequency of the signal. Networks capable of doing so include, for example, a frequency discriminator, such as the one shown in Figure 11.20, and a PLL, shown in Figure 11.21. In the frequency discriminator there are two resonance circuits, each followed by an envelope detector. One resonance circuit is tuned to a frequency above the carrier frequency, the other one below. One detector produces a positive output voltage, the other one a negative output voltage. The sum of these voltages is linear in the vicinity of the carrier frequency, if the difference between the resonance frequencies has a proper value. Usually there is an amplitude limiter before the frequency discriminator to eliminate the effects of signal amplitude variations. In the PLL, the control voltage of the VCO contains the demodulated signal, if the frequency depends linearly on the control voltage.

### 11.3.1.6 PM

PM is closely linked to FM because frequency  $f(t)$  is obtained from the derivative of phase  $\phi(t) = \omega(t)t + \psi(t)$  and accordingly the phase is obtained as an integral of the frequency:

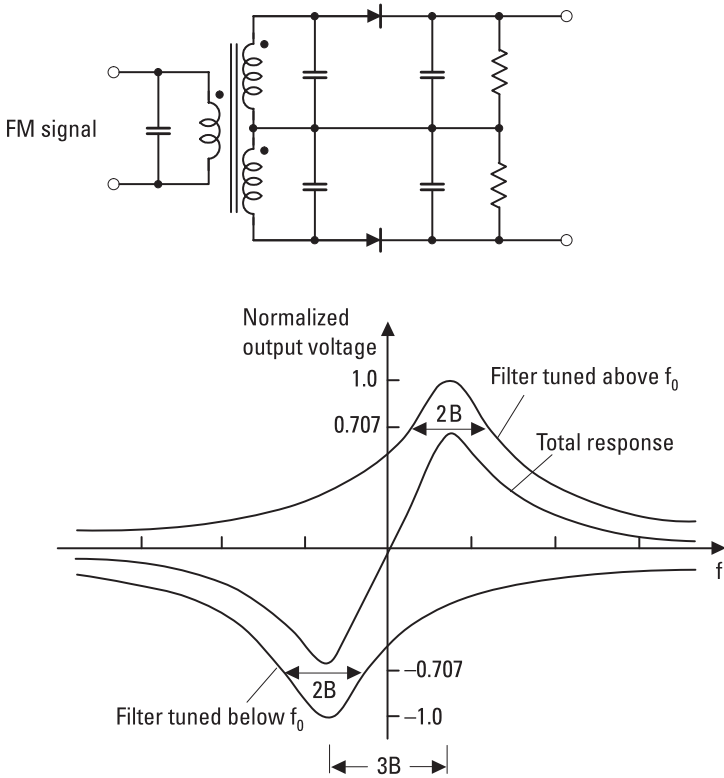


**Figure 11.20** FM demodulator based on a frequency discriminator and its normalized output voltage.

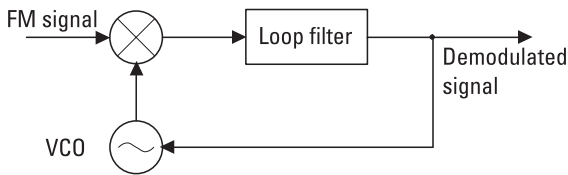


**Figure 11.21** A PLL as an FM demodulator.

$$f(t) = \frac{1}{2\pi} \frac{d\phi(t)}{dt} \tag{11.36}$$

$$\phi(t) = 2\pi \int_0^t f(t') dt' + \phi(0) \tag{11.37}$$

A PM signal can be presented as

$$\begin{aligned} A(t) &= A_0 \cos [2\pi f_0 t + \psi(t)] \\ &= A_0 [\cos (2\pi f_0 t) \cos \psi(t) - \sin (2\pi f_0 t) \sin \psi(t)] \end{aligned} \quad (11.38)$$

If  $\psi(t)$  is small,  $\cos \psi(t) \approx 1$  and  $\sin \psi(t) \approx \psi(t)$ , and (11.38) is simplified into form

$$A(t) \approx A_0 [\cos (2\pi f_0 t) - \sin (2\pi f_0 t) \psi(t)] \quad (11.39)$$

When the modulating signal is sinusoidal  $\psi(t) = 2\pi M \cos (2\pi f_m t)$ , we obtain

$$A(t) \approx A_0 \{ \cos (2\pi f_0 t) - \pi M \sin [2\pi (f_0 + f_m) t] - \pi M \sin [2\pi (f_0 - f_m) t] \} \quad (11.40)$$

Equation (11.40) shows that the spectrum of a PM signal contains frequencies  $f_0$ ,  $f_0 + f_m$ , and  $f_0 - f_m$ , as an AM signal does, but now the phases of these components are different. Figure 11.22 represents a phasor diagram of the PM signal.

### 11.3.2 Digital Modulation

An analog signal, such as a voice signal in the form of an audio-frequency electric signal, can be transformed into a digital form by sampling it frequently

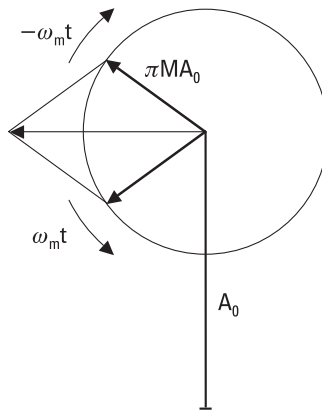


**Figure 11.22** Phasor presentation of a PM signal.

enough. A digital signal may be binary, that is, containing only symbols 0 and 1, or  $m$ -ary, containing  $m$  different levels or states. The digital modulation has many advantages over the analog modulation; the total use of spectrum is effective, immunity to interference is good, frequency reuse is effective, TDM is easily realized, and it allows the use of encryption for privacy.

The basic digital modulation methods are *amplitude-shift keying* (ASK), *frequency-shift keying* (FSK), and *phase-shift keying* (PSK). Figure 11.23 shows the waveforms of binary ASK, FSK, and PSK signals when a symbol chain 01101001 is transmitted. In ASK, the maximum amplitude corresponds to symbol 1 and a zero amplitude corresponds to symbol 0. In FSK, the symbols are presented by signals with frequencies  $f_1$  and  $f_2$ . In PSK, signals corresponding to symbols 1 and 0 have a phase difference of  $180^\circ$ . While analog FM and PM signals closely resemble each other, FSK and PSK signals are easily distinguishable.

In digital modulation, rapid waveform changes occur and thus the power spectrum of a digitally modulated signal is broad. Figure 11.24 shows the spectra of a binary baseband signal consisting of rectangular pulses and a PSK signal modulated with it. The envelopes of the spectra have the shape of a sinc function. The width between the first nulls of the PSK spectrum is twice the bit rate  $1/T_b$ , where  $T_b$  is the symbol period. In practice, the signal is filtered and the spectrum is narrower.

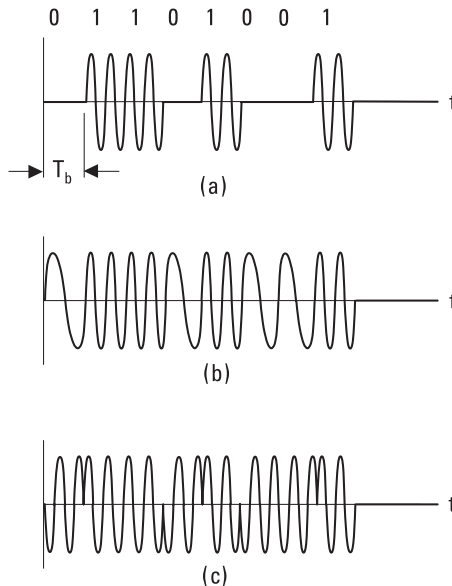


**Figure 11.23** Waveforms of digitally modulated signals: (a) ASK, (b) FSK, and (c) PSK.

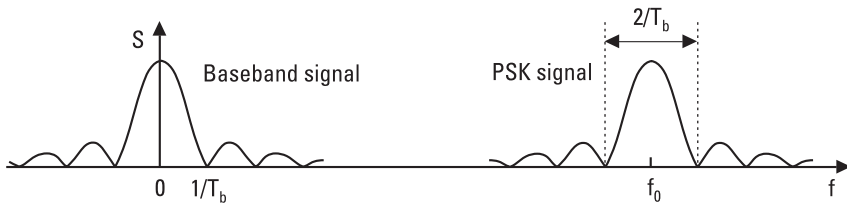


**Figure 11.24** Spectra of a digital baseband signal and a PSK signal modulated with it.

In a binary modulation each symbol contains one bit of information. In a modulation scheme having  $2^m$  different states each symbol contains  $m$  bits. Then it is possible to transmit more information in a given bandwidth or to use a narrower band to transmit a given signal having a given bit rate. A *four-state FSK* (4FSK), *four-state PSK* (4PSK or QPSK), and *eight-state PSK* (8PSK) are examples of modulation methods that save spectrum compared to the binary methods. In a digital QAM, both the amplitude and phase get several discrete values and the number of states may be 16, 64, or even higher. Therefore QAM is used in high-capacity links requiring effective use of the spectrum.

### 11.3.2.1 FSK

FSK can be realized by frequency modulating an oscillator or by switching between two oscillators operating at two different frequencies. The receiver may consist of two bandpass filters tuned for the frequencies  $f_1$  and  $f_2$ , and followed by envelope detectors. Decision between symbols 1 and 0 is made based on the output voltage of each detector. Such an FSK demodulator, presented in Figure 11.25, is said to be noncoherent.

A coherent demodulator, shown in Figure 11.26, provides a smaller *bit error rate (BER)*. In the receiver, the frequencies  $f_1$  and  $f_2$  are regenerated, and their phases are synchronized with the incoming signal. The output

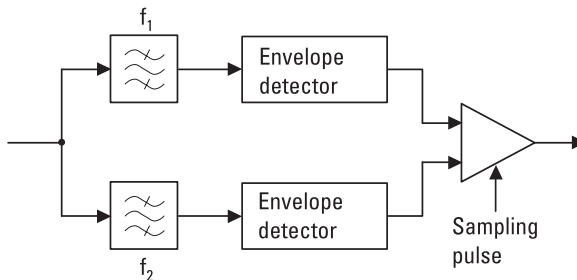


**Figure 11.25** A noncoherent FSK demodulator.

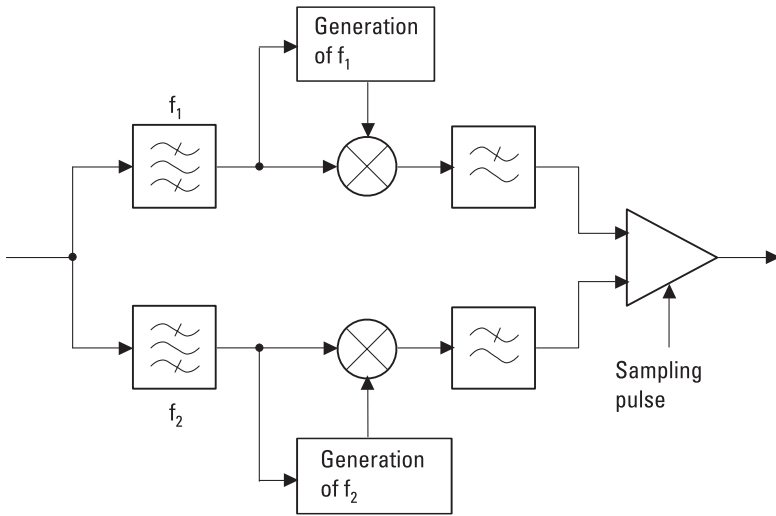


**Figure 11.26** A coherent FSK demodulator.

voltage of a phase detector (a double-balanced mixer) is proportional to the phase difference of these two signals. After filtering, the amplitudes are compared at the sampling time, and a decision is made between 1 and 0.

*Minimum-shift keying* (MSK) is a special case of FSK having the smallest separation of frequencies  $f_1$  and  $f_2$  so that the correlation between the symbols corresponding to 1 and 0 is zero. For MSK, the difference between  $f_1$  and  $f_2$  is half of the bit rate.

### 11.3.2.2 PSK

PSK can be realized by switching between two oscillators that have the same frequency but opposite phase, or with a double-balanced mixer, as shown in Figure 11.27(a). The double-balanced mixer acts as a polarity-reversing switch: When the sign of the voltage fed into the IF port changes, the phase of the carrier output from the RF port changes  $180^\circ$ . Demodulation takes

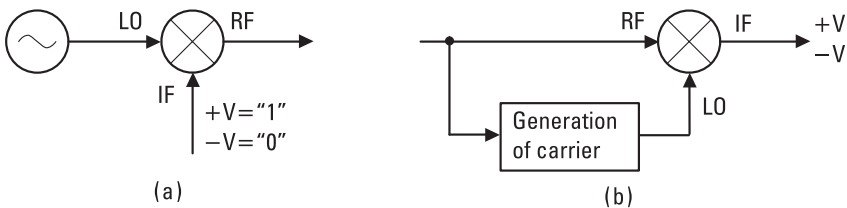


**Figure 11.27** PSK: (a) modulation and (b) demodulation with a double-balanced mixer.

place in a reversed order, as in Figure 11.27(b). The carrier is regenerated in the receiver and fed into the LO port. The double-balanced mixer acts as a phase detector, and therefore the voltage from the IF port is either positive ( $+V = "1"$ ) or negative ( $-V = "0"$ ).

It may be difficult to get a phase synchronism between the carrier and the local oscillator during a period of only a few symbols. This difficulty can be avoided, and it is not necessary to generate the carrier in the receiver, if the phase of successive symbols is compared. Figure 11.28 shows such a *differential PSK* (DPSK) demodulator, where the signal is compared in a phase detector with the signal delayed by one symbol period  $T_b$ .

In *quadrature phase-shift keying* (QPSK), the phase has four possible values, and each symbol corresponds to two bits: phase  $\pi/4$  corresponds to 10,  $3\pi/4$  corresponds to 00,  $5\pi/4$  corresponds to 01, and  $7\pi/4$  corresponds to 11. A QPSK signal can be generated using the circuitry shown in Figure 11.29(a). The first bit of the pair is fed to the mixer of the upper branch (I = in-phase), and the second bit of the pair to the mixer of the lower branch (Q = quadrature phase). In the demodulator, shown in Figure 11.29(b), the carrier is regenerated and the phase detectors provide output voltages proportional to the bits.

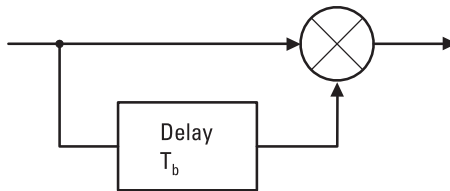


**Figure 11.28** A DPSK demodulator.

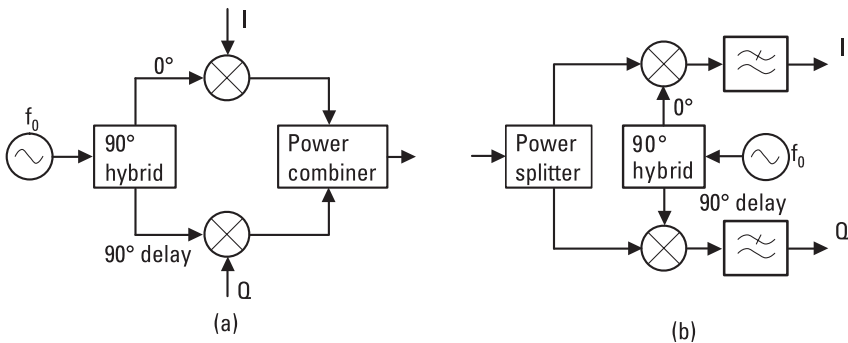


**Figure 11.29** QPSK: (a) modulation and (b) demodulation.



### 11.3.2.3 QAM

The circuits in Figure 11.29 are also called an IQ-modulator and an IQ-demodulator. They may be used to generate and detect digital QAM signals. For example, a 16QAM signal may be produced as a sum of a four-level I-signal and a four-level Q-signal. Figure 11.30 shows the constellation of the 16QAM signal on the IQ-diagram. Each point of the constellation presents one symbol now containing 4 bits. The distance of a point from the origin is proportional to the amplitude of the modulated carrier, and the angle between the positive I-axis and the direction of the point from the origin is analogous to the phase of the signal.

### 11.3.2.4 Comparison of Digital Modulation Methods

An ideal modulation method uses the radio spectrum efficiently, is robust against noise, interference, and fading, and can be realized with low-cost and power-efficient circuitry. However, these requirements are partly contradictory, and some tradeoffs have to be made to optimize the overall system performance.

Binary ASK, FSK, and PSK signals can be generated with simple circuits. Because ASK and FSK signals can be demodulated incoherently with an envelope detector, these receivers can also be made simple and inexpensive. Coherent detection of ASK and FSK requires more complex circuits but provides a lower *BER*. PSK has the lowest *BER* but requires generation of a synchronized carrier in the receiver.

Figure 11.31 shows how the bit error rate of a PSK system depends on the  $S/N$  in an ideal AWGN channel and in a Rayleigh channel. In the AWGN channel, white noise is the only nonideality. An  $S/N$  of only about 7 dB is needed to achieve a *BER* of  $10^{-3}$ . Coherent FSK needs 3 dB higher

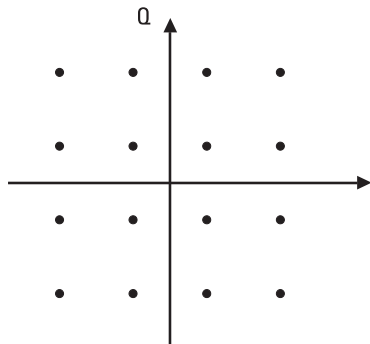


**Figure 11.30** Constellation of 16QAM.

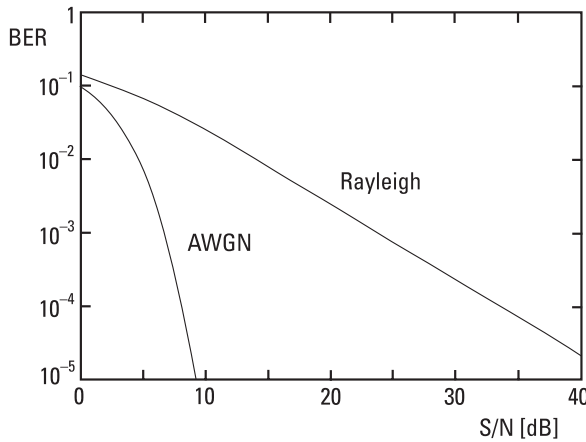


**Figure 11.31** The BER of PSK systems in AWGN and Rayleigh channels.

$S/N$  than PSK for a similar performance. In the AWGN channel  $BER$  decreases exponentially as  $S/N$  increases. In the Rayleigh fading channel a much higher average  $S/N$  is required for a given  $BER$ , because during deep fades the error rate is large. ASK has a very poor performance in the Rayleigh channel, because the threshold level between 0 and 1 depends on the signal level; FSK and PSK have no such problem.

The bandwidth efficiency describes how well a modulation method uses a limited bandwidth. The bandwidth efficiency of binary modulation methods is slightly less than 1 bit in 1 second per 1 hertz bandwidth. As noted before, increasing the number of modulation states lowers the symbol rate, making the spectrum narrower. Thus multistate methods have better bandwidth efficiencies than binary methods. However, for a given signal power the states become closer to each other, making the system more susceptible to noise and interference. Also, the equipment requirements of a multistate method are demanding. For example, an imbalance of the branches of an IQ-modulator and IQ-demodulator, and the phase noise of an oscillator may easily increase the  $BER$ .

In case of multistate QAM, the amplitude variations are large. Therefore transmitters and receivers have to operate linearly; otherwise, the signal will distort and the occupied bandwidth will grow. Modulation methods such as MSK, producing a constant-envelope waveform, allow the use of nonlinear power amplifiers in transmitters. As discussed in Section 8.4, nonlinear amplifiers are more efficient than linear amplifiers. Power efficiency is an important factor in battery-powered transmitters.

In mobile communication, connections have to operate reliably in spite of signal fading and Doppler shifts. Therefore, simple FSK and QPSK modulations or their variations are used in mobile systems. In fixed LOS radio links, good bandwidth efficiency is often required. Size and power consumption are not as critical as they are in mobile units. Multistate QAM can be used in LOS links, because in such links propagation problems are less severe than in mobile systems.

### 11.4 Radio Link Budget

A radio link between two stations consists of a transmitter, transmission path, and receiver, as presented in Figure 11.32. In a given link it is possible to transmit several channels, which are separated using *frequency division multiplexing* (FDM) or *time division multiplexing* (TDM). The received signal power is

$$P_r = G_t G_r \left( \frac{\lambda}{4\pi r} \right)^2 \frac{1}{L_p} P_t \tag{11.41}$$

where  $L_p$  is the loss of the transmission path in addition to the free space loss, which equals  $(4\pi r/\lambda)^2$ . Loss  $L_p$  contains, among other things, the tropospheric absorption and scattering loss as well as the effects of diffraction and multipath propagation. Thus, it is possible that  $L_p$  is less than unity.

The system noise temperature of a receiving system is

$$T_S = T_A + T_R \tag{11.42}$$

Then the equivalent noise power in the receiver input is

$$P_n = kT_S B_{RF} \tag{11.43}$$

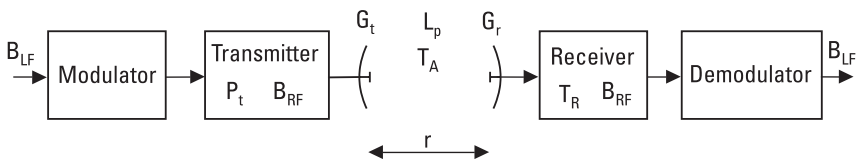


Figure 11.32 Radio link.

where  $B_{RF}$  is the noise bandwidth of the receiver (see Figure 11.4). The noise bandwidth is approximately equal to the bandwidth of the modulated RF signal, which, on the other hand, depends on the baseband signal and the modulation method used. For example, the bandwidth of an analog baseband signal required for voice is 3 kHz, and that for a TV picture is 5 MHz.

The  $S/N$  in the input of the receiver is

$$S/N = \frac{P_r}{P_n} = \frac{G_t P_t \lambda^2}{(4\pi r)^2 k B_{RF} L_p} \frac{G_r}{T_S} \quad (11.44)$$

The  $S/N$  required for a good transmission depends on the application. For example, a good analog TV picture requires  $S/N$  over 40 dB for the video signal. For FM radio,  $S/N$  over 10 dB is satisfactory. Often in the receiving end one can affect the ratio  $G_r/T_S$  by properly selecting the antenna and receiver. Equation (11.44) in various forms is often called the link-budget formula.

### Example 11.3

Let us consider a 12-GHz satellite TV link, where a geostationary satellite is broadcasting to Scandinavia. The distance between the transmitter and receiver is 40,000 km, and the satellite is seen at an elevation angle of about 20°. The transmitted power is 200W, and the transmitting satellite antenna is a 1.5-m paraboloid with an aperture efficiency of 0.6. The required availability of the system is 99.9%. What is the minimum ratio  $G_r/T_S$  and the maximum  $T_R$  that will result in a good TV reception?

### Solution

From long-term statistics it is known that the atmospheric attenuation on the radio path of such a geostationary satellite is during 99.9% of time less than or equal to 3 dB. In order to obtain the required video signal  $S/N$  of 40 dB, the received FM signal must have at least  $S/N = 14$  dB. By expressing the variables and constants of (11.44) in decibels, we get the link budget in decibels. Now the system properties can be calculated by adding and subtracting the decibel values. Properties of the system in decibels are given in Table 11.1. When the values from Table 11.1 are substituted into (11.44) and it is taken into account that  $k = -228.6 \text{ dBWK}^{-1} \text{ Hz}^{-1}$ , it is obtained that  $G_r/T_S = 2.4 \text{ dBK}^{-1}$ . If the receiving antenna is a paraboloidal reflector with a diameter of 0.4m and an aperture efficiency of 0.6, its gain is 31.8 dB. Then  $T_S$  may be at maximum 29.4 dBK or 870K. The antenna noise

**Table 11.1**  
Characteristics of a Satellite TV System

Quantity	Absolute Value	Decibel Value
$P_t$	= 200W	= 23 dBW
$G_t$	= 21,300	= 43.3 dB
$(4\pi r)^2$	= $(4\pi \times 40,000 \text{ km})^2$	= 174.0 dBm <sup>2</sup>
$L_p$	= 2	= 3.0 dB
$\lambda^2$	= $(0.025\text{m})^2$	= -32.0 dBm <sup>2</sup>
$B_{RF}$	= 27 MHz	= 74.3 dBHz
S/N	= 25	= 14 dB

temperature may be assumed to be at maximum 150K, and therefore the receiver noise temperature may be at maximum 720K. At the edges of the satellite antenna beam  $G_t$  is smaller than at the center of the beam, and therefore a larger receiving antenna or a more sensitive receiver is needed.

## References

- [1] Collin, R. E., *Foundations for Microwave Engineering*, 2nd ed., New York: IEEE Press, 2001.
- [2] Gardner, F. M., *Phaselock Techniques*, 2nd ed., New York: John Wiley & Sons, 1979.
- [3] Manassewitsch, V., *Frequency Synthesizers: Theory and Design*, 3rd ed., New York: John Wiley & Sons, 1987.
- [4] Mumford, W. W., and E. H. Scheibe, *Noise Performance Factors in Communication Systems*, Dedham, MA: Horizon House—Microwave, 1968.
- [5] "IRE Standards on Methods of Measuring Noise in Linear Twoports, 1959," *IRE Proc.*, Vol. 48, No. 1, 1960, pp. 61–68.
- [6] Räisänen, A. V., "Experimental Studies on Cooled Millimeter Wave Mixers," *Acta Polytechnica Scandinavica*, Electrical Engineering Series, No. 46, Helsinki, 1980.
- [7] Kraus, J. D., *Radio Astronomy*, 2nd ed., Powell, OH: Cygnus-Quasar Books, 1986.
- [8] Bhargava, V. K., et al., *Digital Communications by Satellite*, New York: John Wiley & Sons, 1981.
- [9] Carlson, A. B., *Communication Systems*, 3rd ed., New York: McGraw-Hill, 1986.
- [10] Haykin, S., *Communication Systems*, 4th ed., New York: John Wiley & Sons, 2001.

# 12

## Applications

Communication is the most important application of radio engineering. Radio communication includes broadcasting, terrestrial and satellite radio link systems, wireless local area networks, and mobile communication. Radio-navigation, sensor applications such as locating by radar, remote sensing, and radio astronomy are other important applications. Radio waves are used also in many kinds of other sensors as in industrial sensors, for heating, and in medical applications.

### 12.1 Broadcasting

Broadcasting means supplying the public with information and entertainment by means of radio and television. Transmitting stations may be either terrestrial or satellite borne. Frequency ranges that are reserved for broadcasting in Region 1 (see Figure 1.2) are listed in Table 12.1. Analog radio transmissions are amplitude modulated in the LF, MF, and HF ranges and frequency modulated in the VHF range. Analog television transmissions use a VSB modulation for picture signal and either an analog FM or a digital QPSK for voice signal. Up to the HF range, waves can propagate long distances, even around the globe, as surface waves or by reflecting from the ionosphere. At VHF and higher frequencies, a nearly free LOS path between the transmitter and receiver is needed.

Broadcasting is currently transitioning from analog transmissions to digitally modulated transmissions. Digital transmission techniques have

**Table 12.1**  
Frequency Ranges for Broadcasting in Region 1

Range	Frequencies	Application	Channel Spacing
LF	148.5–283.5 kHz	AM radio	9 kHz
MF	526.5–1,606.5 kHz	AM radio	9 kHz
HF	Several ranges	AM radio	
VHF I	47–68 MHz	Television	7 MHz
VHF II	87.5–108 MHz	FM radio	100 kHz
VHF III	174–230 MHz	Television	7 MHz
UHF IV	470–582 MHz	Television	8 MHz
UHF V	582–790 MHz	Television	8 MHz
SHF	11.7–12.5 GHz	Satellite TV	27 MHz

several advantages: The radio spectrum is used more effectively than in analog systems, the quality of the sound and picture is excellent even if the receiver is moving, and many kinds of services can be attached to the signal.

*Digital Audio Broadcasting* (DAB) is a European standard for digital radio transmissions. DAB uses a *coded orthogonal frequency division multiplex* (COFDM), in which information is coded effectively to reduce the number of errors. Bits are then distributed to several orthogonal carriers, which are modulated using a differential QPSK. A signal with 1,536 carriers has a bandwidth of about 1.5 MHz and can carry, for example, 6 stereo programs or 18 speech programs. *Digital Video Broadcasting* (DVB) is a standard for broadcasting digital TV. It is also based on COFDM. The maximum number of carriers is 6,817, and alternative modulation methods are QPSK, 16QAM, and 64QAM. Four or five TV programs fit to an 8 MHz wide channel. Because there are many carriers in COFDM, in each carrier the symbol rate is low and the symbol duration long. This makes COFDM insensitive to the adverse effects of multipath propagation and allows a use of single-frequency networks where all synchronized transmitters use the same frequency.

### 12.1.1 Broadcasting in Finland

In Finland, radio and television programs are delivered by the Finnish Broadcasting Company, *Yleisradio* (YLE) and some commercial companies. The network includes about 40 large transmission stations, 160 substations, and link stations. There are also two MF stations and one HF station. DAB test transmissions were started in 1994 and regular transmissions in the

VHF III range (174–240 MHz) began in 1998. Test transmissions of digital TV were started in 1998 and regular transmissions in the UHF range began in 2001.

The antenna masts for FM, DAB, and TV broadcasting are usually 100m to 300m high. Several antennas are placed on a mast so that the antennas of the highest frequency range are placed on the top. The directional pattern should usually be omnidirectional in the horizontal plane, whereas in the vertical plane the beam should be narrow and shaped to give equal field strength at different distances. The mast disturbs antennas, except the one on the top. The antennas lower in the mast have to be made of several elements. There are usually three or four elements in the horizontal plane and several elements in the vertical plane. The vertical pattern is realized by adjusting the phase and amplitude of the elements. The antenna elements are often dipoles with a reflector. Slot antennas are also used at UHF. Tetrodes and parallel-connected transistor amplifiers are used as the output stages of the VHF transmitters. At UHF, klystrons work as output stages.

Because frequencies used for the FM, DAB, and TV need an almost free LOS path, one transmitter can cover typically an area with a radius of about 70 km. Therefore, about 40 stations are needed to cover all of Finland, which has a land area of 338,000 km<sup>2</sup> as well as scattered islands. Figure 12.1 shows the locations of FM stations and their coverage areas. At the outer limit of the coverage area, the field strength is 0.5 mV/m (54 dB $\mu$ V/m). Reception is often possible at distances 20 km to 30 km greater than these limits. The *equivalent isotropic radiated power* (EIRP), or the transmitted power that would be needed in the case of an isotropic antenna to give the same field strength as the actual antenna, is usually a few tens of kilowatts for FM transmissions. Total real radiated power is much less than *EIRP*. The polarization of FM signals is horizontal. In Lapland, circular polarization is also used. DAB transmissions are vertically polarized.

EIRP of TV transmissions can be as high as 1,000 kW. The polarization of TV signals is mainly horizontal; in the VHF I range vertical polarization is also used. In addition to the main transmission stations, many substations are needed to cover the whole country. A substation receives the signal from a main station, converts the frequency of the signal, and transmits it to those viewers who are unable to receive the signal from any main station. The coverage of the TV-1 and TV-2 networks is more than 99.9% of the population.

MF stations are in Helsinki (558 kHz) and Pori (963 kHz). The antennas are short (compared to wavelength) monopoles and the output stages are tetrodes. The HF station in Pori operates in several bands. The



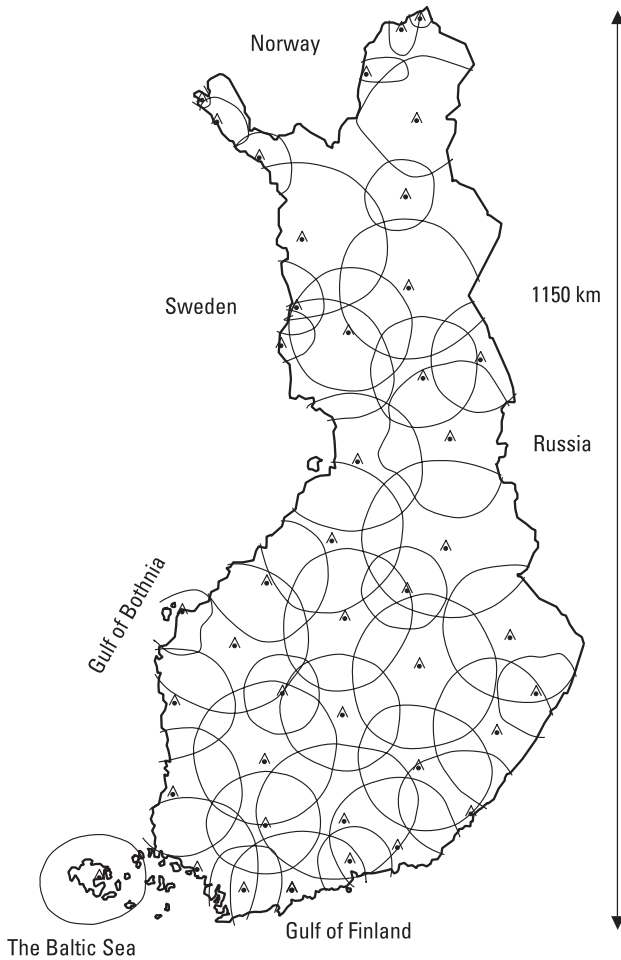


**Figure 12.1** FM radio stations and their coverage areas in Finland (338,000 km<sup>2</sup>).

antennas are horizontal dipole arrays. Reception of these HF signals is possible even in Australia.

In addition to YLE, many local FM radio stations operate in Finland. They use vertical polarization. In urban areas cable network companies distribute TV programs received from satellites.

### 12.1.2 Broadcasting Satellites

A satellite can be used as a platform for a broadcasting station. One single transmitter onboard a satellite can cover a whole country or continent.

Broadcasting and most other communication satellites are placed on *geosynchronous Earth orbit* (GEO) at the height of 35,800 km above the equator. At that height the orbiting time is equal to the rotation time of the Earth, 23 hours and 56 minutes. Then the satellites seem to be stationary and the antennas on Earth can be fixed. Positions of the satellites have to be corrected every now and then due to disturbances in the gravitational field. The amount of the steering gas limits the lifetime of satellites to about 10 years.

*Broadcasting satellite service* (BSS) satellites transmit (downlink) at frequencies from 11.7 GHz to 12.5 GHz into Europe. *Fixed satellite service* (FSS) satellites transmitting in the bands 10.7 to 11.7 GHz and 12.5 to 12.75 GHz also send radio and TV programs. The band 11.7 to 12.5 GHz is divided into 40 channels having a separation of 19.18 MHz. The width of the channels is 27 MHz and they are interleaved in orthogonal polarizations. BSS satellites send circularly polarized waves and FSS satellites linearly polarized waves. Analog TV programs are frequency modulated. Several digitally modulated TV programs fit in one 27-MHz band. The programs are sent to broadcasting satellites (uplink) in the band 17.3 to 18.1 GHz and to FSS satellites in the band 14.0 to 14.5 GHz. Due to crowding of the 12-GHz band, 20-GHz (downlink) and 30-GHz (uplink) bands will be introduced for the broadcasting service.

The microwave unit of a broadcasting satellite includes antennas and transponders. A transponder consists of a low-noise receiver, mixers and oscillators for frequency conversion, and power amplifiers. To improve reliability, transponders often have parallel units; for example, a broken power amplifier can be replaced with another unit. The power transmitted is typically about 100W so that an antenna having a diameter of 0.5m can be used for reception. The beam of the satellite antenna is shaped according to the service area. Figure 12.2 shows a typical footprint of a TV satellite.

In Finland, TV programs can be received from more than 20 satellites. The maximum elevation angle of geostationary satellites is only  $21^\circ$  in the most southern part of Finland. Because transmissions are usually directed to Central Europe, especially in the northern Finland, a large receiving antenna may be necessary.

### Example 12.1

A geostationary satellite transmits with a power of  $P_t = 100\text{W}$ . The width of the circular antenna beam is  $3^\circ$ . The beam can be assumed ideal so that the normalized pattern level is 1 within the beam and 0 outside the beam. Find the power density at a distance of  $r = 40,000$  km. What is the power received with a 0.5-m dish?



**Figure 12.2** Typical footprint of a GEO TV satellite beam directed at Central Europe.

### Solution

The beam area is approximately  $\Omega_A = (\pi/4)(3\pi/180)^2 = 2.15 \times 10^{-3}$  steradians (see Section 9.1). The directivity is  $D = 4\pi/\Omega_A = 5,840$ . The power density at a distance of  $r$  is  $S = (DP_t)/(4\pi r^2)$ . Thus,  $S = (5,840 \times 100)/[4\pi \times (4 \times 10^7)^2] \text{ W/m}^2 = 2.90 \times 10^{-11} \text{ W/m}^2$ , that is,  $-105.4 \text{ dBW/m}^2$ . The atmosphere is assumed to be lossless. The effective area of a 0.5-m antenna having an aperture efficiency of 0.6 is  $A_{ef} = 0.6\pi \times 0.25^2 \text{ m}^2 = 0.118 \text{ m}^2$ . The power received is  $P_r = A_{ef} S = 3.42 \times 10^{-12} \text{ W}$ , that is,  $-114.7 \text{ dBW}$  or  $-84.7 \text{ dBm}$ .

## 12.2 Radio Link Systems

Radio link systems convey telephone and data traffic, TV and radio signals to broadcasting stations, and so on. Stations may be terrestrial or space borne. In this section, only fixed links are considered. Short communication links allowing user mobility are the topic of Section 12.3.

### 12.2.1 Terrestrial Radio Links

A radio link system typically consists of terminal stations and repeater stations, as shown in Figure 12.3. There are several frequency bands reserved for

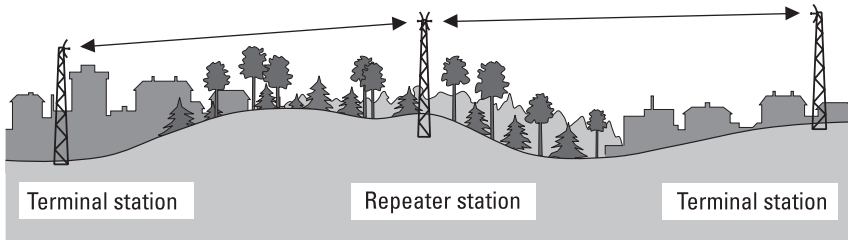


**Figure 12.3** A point-to-point radio link system (horizontal distances not in scale).

fixed terrestrial point-to-point radio links, including 7/8, 13, 15, 18, 23, 38, and 58 GHz. Bands below about 2 GHz are nowadays reserved for other applications, such as mobile communication. Below 10 GHz the curved surface of the Earth or the height of masts (60m to 80m) limits the length of a hop to about 50 km. At frequencies higher than 10 GHz, the atmospheric attenuation and especially the attenuation due to rain limits the hop length. For example, at 23 GHz the maximum hop length is about 10 km and at 58 GHz (near the oxygen resonance) about 1 km.

The reliability of a radio link system is important. Between two stations, the first Fresnel ellipsoid should be free from obstacles to avoid excessive propagation loss. The curved surface of the Earth, the ground profile between the stations, and the bending of rays have to be taken into account when planning the heights of antennas. The statistical nature of the bending of rays and rain attenuation must be considered in the link budget. Diversity techniques can reduce the adverse effects of multipath propagation; space diversity in which two antennas are at different heights is a common technique.

Radio link antennas are usually parabolic reflectors. At millimeter-wave range, low-profile array antennas are also used [1]. The half-power beamwidth is typically  $1^\circ$  to  $3^\circ$ . Often antennas are protected against weather with a radome. Repeater stations have transponders, which change the frequency so that successive hops do not interfere with each other.

Radio links are either analog or digital. Analog links use FDM; digital links use TDM. Standard capacities of digital links are 2, 8, 34, 140, and 155 Mbit/s, or multiples of these bit rates. A 2-Mbit/s signal is composed of the content of 32 channels with 64 kbit/s. Low- and medium-capacity (34 Mbit/s or less) long-haul links below 10 GHz often use the QPSK modulation. In high-capacity links more complicated modulation methods such as 16QAM and 64QAM are needed. The modulation method of short-haul links above 10 GHz is often 4FSK.

Point-to-multipoint radio links are used in *wireless local loops* (WLLs) and *local multipoint distribution systems* (LMDSs), which offer a wireless access to fixed telecommunication networks. Point-to-multipoint links are often a good alternative to cable.

### 12.2.2 Satellite Radio Links

When the link stations on satellites are placed in geostationary orbit, three satellites can cover the whole globe, excluding the polar regions.

The *International Telecommunications Satellite Organization* (INTELSAT) was founded in 1964. In 2000, its 144 member states approved the privatization of INTELSAT. The geostationary satellites of INTELSAT are placed over the Atlantic, Indian, and Pacific Ocean. They convey voice, data, Internet, and video traffic. The first geostationary communication satellite was INTELSAT-1, Early Bird, which was placed in orbit in 1965. Its capacity was 240 voice channels or one TV channel. Satellites from fifth to ninth generation were in operation in 2002. Figure 12.4 illustrates INTELSAT-6, which has a capacity of 36,000 voice channels and three TV channels. It has 48 transponders having a total bandwidth of 3.3 GHz. The antenna system includes 4- and 6-GHz zonal reflector antennas, 4- and 6-GHz horn antennas that cover the whole globe seen from the satellite, two steerable 14/11-GHz (uplink/downlink) spot antennas, and two omnidirectional antennas for telemetry and command signals. Figure 12.5 shows the beams of an Atlantic satellite. The transmitting power of the 4-GHz beam is 5W to 15W; the 11-GHz spot beams have transmitting powers of 20W and 40W. Due to the vast service area, the ground stations have large 30-m antennas.

Many countries, including the United States, Canada, Australia, Indonesia, and Japan, as well as regional organizations have their own communication satellites. European countries have formed the *European Telecommunications Satellite Organization* (EUTELSAT). INTERSPUTNIK is a satellite organization of the eastern European countries.

## 12.3 Wireless Local Area Networks

A *wireless local area network* (WLAN) is a data communication system that can be used as an alternative to or as an extension of a wired LAN. A WLAN can cover a building or campus. A wireless network covering a larger area

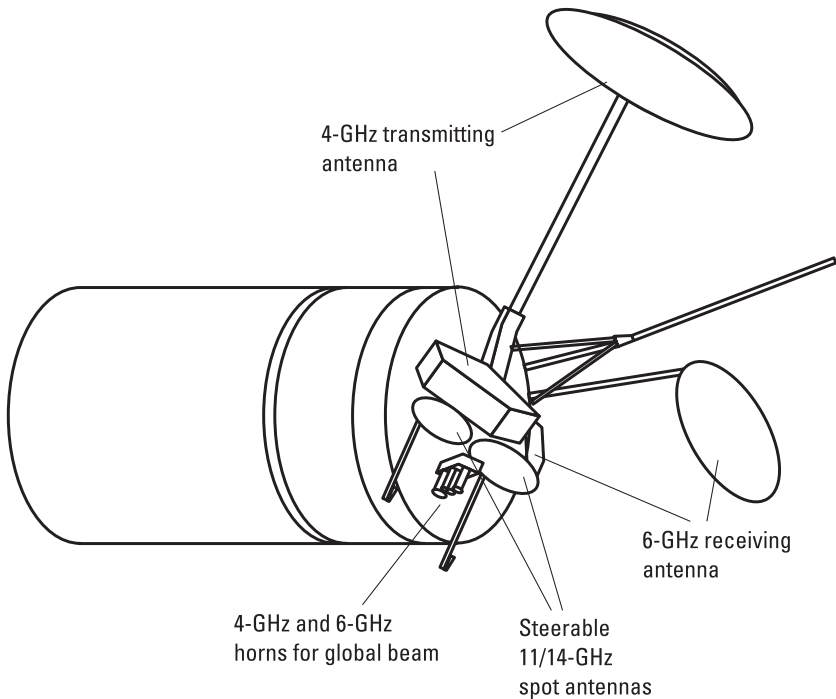


**Figure 12.4** INTELSAT-6 satellite.

is called a *wireless wide area network* (WWAN) or a *wireless metropolitan area network* (WMAN). A network covering only a small range is called a *wireless personal area network* (WPAN).

Computers, printers, robots, and so on can be connected to a wireless network by infrared or radio links. Most WLANs use radio waves and are also called *radio local area networks* (RLANs). Radio waves can penetrate most walls and floor surfaces, whereas these solid objects block infrared. WLANs offer many advantages over traditional wired networks, for example, user mobility, installation speed, and flexibility.

Many standards are available for WLANs. IEEE 802.11, Bluetooth, and HomeRF operate in the unlicensed *industrial, scientific, and medical* (ISM) band, 2,400 to 2,483.5 MHz. Bluetooth and HomeRF are more like WPANs than WLANs. HiperLAN/2 is a high-performance standard operating in the 5-GHz band that was developed by the *European Telecommunications Standards Institute* (ETSI). DECT is a standard for cordless phones that can also be used for WLANs.

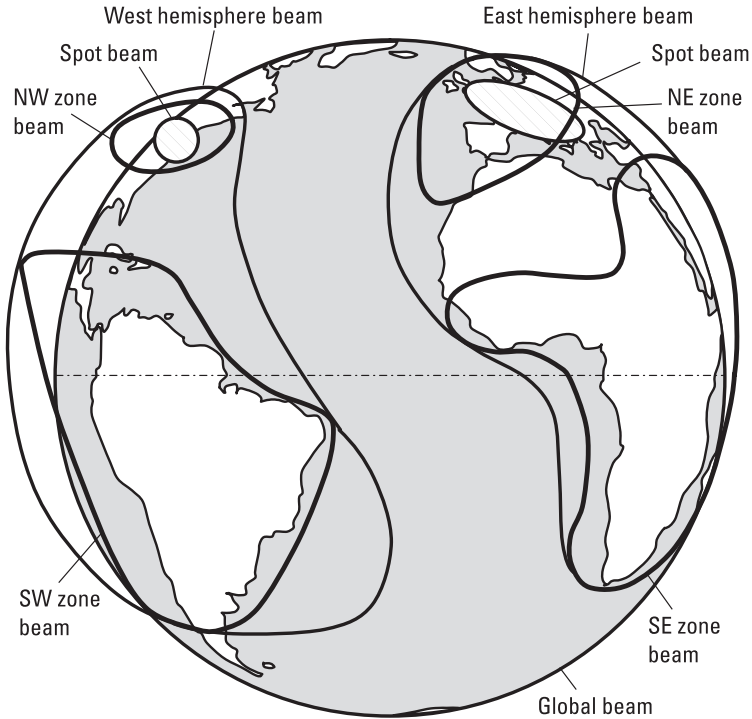


**Figure 12.5** Coverage areas of an INTELSAT satellite over the Atlantic Ocean.

No license is required for low-power transmitters operating in the 2.45-GHz band. In addition to WLANs, several other applications, including microwave ovens and *radio frequency identification* (RFID) systems, use this band. To reduce interference between different users, spread spectrum techniques can be used. There are two types of spread spectrum techniques: *direct sequence spread spectrum* (DSSS) and *frequency hopping spread spectrum* (FHSS) [2].

In DSSS, a digital bit stream representing the source data is multiplied by a pseudorandom (PN) code with a bit or chip rate much higher than that of the data. Thus this product has a much higher symbol rate than the original data, causing the spectrum to spread. In the receiver, the original data can be recovered by multiplying the received signal with the same PN code. Only the signal with the same PN code despreads. To an unintended receiver, a DSSS signal appears as wideband noise.

In FHSS, the transmitter changes carrier frequency in a pattern known to the receiver. To an unintended receiver, an FHSS signal appears to be short-duration impulse noise.

## 12.4 Mobile Communication

Mobile communication [3–5] has grown faster during the last decade than any other application of radio engineering. Optical fibers and copper cables cannot compete with freely propagating radio waves in this application. In addition to cellular mobile systems, which are the main topic of this section, a moving person can use satellite systems or pager systems for voice or data transfer. The geostationary satellites of *International Mobile* (earlier Maritime) *Satellite Organization* (INMARSAT) offer communication services for ships, airplanes, and trucks. The operating frequencies between the satellites and mobile users are 1.6/1.5 GHz (uplink/downlink). Several other systems based on satellites on *low Earth orbit* (LEO) have been launched since 1998. Compared to the GEO systems, many more satellites are needed in the LEO systems, but shorter path lengths allow the use of handheld terminals.

In a cellular network, the coverage areas of the base stations form a “cellular” structure. To offer a good availability both in densely and sparsely populated areas, cells of different sizes are needed. To avoid interference, adjacent cells use different frequencies. The same frequencies can be reused in cells, which are far enough from each other. Also, the power levels of transmitters should be controlled to reduce interference. When a mobile phone moves from one cell to another, the network has to take care of this handover without interruption. (Cellular systems can be used also for rough locating because the cell, in which the mobile unit locates, is known. The accuracy may be enhanced by using measurements performed by more than one base station.)

In the development of cellular mobile systems, three generations can be distinguished: first generation analog systems, second generation digital systems, and third generation wideband systems. In addition to voice transfer, the second generation systems are usable also for low bit rate data services. Third generation systems support wideband multimedia services. The following introduces an example of each generation.

*Nordic Mobile Telephone* (NMT) represents the first generation. It was developed by the Nordic countries: Denmark, Finland, Norway, and Sweden. The NMT 450 network, operating in the 450-MHz band, was launched in 1981. In response to congestion, the upgraded NMT 900 network, which had a larger capacity, started in 1986. NMT networks are still in operation in many countries outside Scandinavia. Several other analog systems have been in use around the world, including AMPS in the United States and TACS in the United Kingdom. However, due to emerging digital systems, many first generation networks have been closed down.



In NMT 450, the transmitting frequencies of mobile phones (receiving frequencies of base stations) are 453 to 457.5 MHz, and the transmitting frequencies of base stations (receiving frequencies of mobile phones) are 463 to 467.5 MHz. Thus, the duplex frequency is 10 MHz. In NMT 900, the transmitting and receiving frequencies are 890 to 915 MHz and 935 to 960 MHz, and the duplex frequency is 45 MHz. A frequency channel is assigned for each user in a cell, that is, the access method is the *frequency division multiple access* (FDMA). The channel spacing is 25 kHz. Thus, NMT 450 has 180 channels and NMT 900 has 1,000 channels. The modulation method is FM. The *mobile telephone exchange* (MTX) is a central component of the NMT network. Each MTX is responsible for a group of base stations. The MTX determines the frequencies and transmitting powers of mobile phones, and takes care of the handovers from one base station to another. One base station covers an area with a radius of 0.5 km to 20 km.

*Global System for Mobile Communications* (GSM) represents the second generation. It is a digital cellular standard developed at first by CEPT and later by ETSI. Originally, the acronym GSM came from the name of the study group Groupe Spécial Mobile, which was formed to develop a common European standard. The first GSM networks were launched in 1991. GSM was rapidly accepted worldwide. Other second generation standards include *Personal Digital Cellular* (PDC) operating in Japan, American standards IS-95 and IS-136, and *Trans-European Trunked Radio* (TETRA), which is a standard for private mobile networks.

GSM (or GSM 900) operates in the same frequency range as NMT 900 (i.e., 890–915 MHz and 935–960 MHz). The access method is a combination of the FDMA and TDMA. There are 124 carrier frequencies, which are spaced 200 kHz apart. Each frequency channel is divided into eight time slots for different users. Mobile phones and base stations transmit short bursts of data. The bit rate during a burst is 270.833 kbit/s. The length of a burst is 0.577 ms or 156.25 bit periods. Consequently, a TDMA frame of eight bursts lasts 4.615 ms. Effects of multipath fading are alleviated by using slow frequency hopping, that is, the carrier frequency changes from one frame to another. The modulation method of the carrier is a *Gaussian minimum shift keying* (GMSK). To reduce the number of bit errors, channel coding and interleaving is used. In channel coding, redundancy bits are added in order to detect and correct errors. Interleaving disperses a series of consecutive bit errors to several blocks, making error correction easier.

Figure 12.6 shows the architecture of a GSM network. The mobile station is connected to a *base transceiver station* (BTS) via a radio link. The *base station controller* (BSC) controls a group of BTSs and manages their

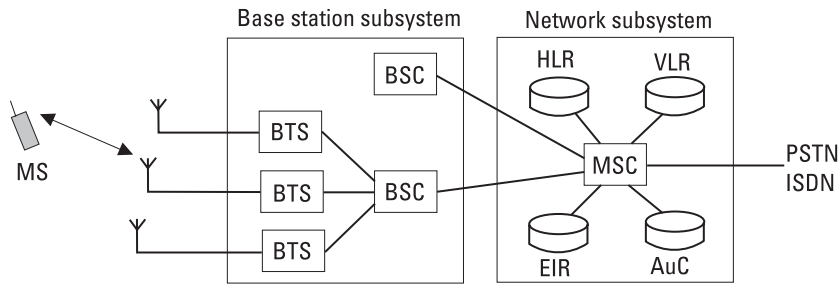


**Figure 12.6** Architecture of GSM network. (MS = mobile station; HLR = home location register; VLR = visitor location register; EIR = equipment identity register; AuC = authentication center; PSTN = public switched telephone network; ISDN = integrated services digital network.)

radio resources. The *mobile-services switching center* (MSC) performs the switching functions of the network and provides a connection to other networks. MSCs also take care of the registration, authentication, and location updating of subscribers. Received power levels are continuously monitored. MSCs and BSCs make decisions about handovers using these received signal strengths. Transmitter power levels are also controlled according to the signal strengths; the maximum transmitter power of a handheld phone is  $2\text{W}$ , and thus the maximum average power is  $(2\text{W})/8 = 0.25\text{W}$ .

Digital Cellular System, DCS 1800 or GSM 1800, is an upgraded version of GSM 900. Mobile units transmit at frequencies from 1,710 to 1,785 MHz and base stations at 1,805 to 1,880 MHz. The number of frequency channels is 374. GSM 1800 is especially useful in metropolitan areas where the cells are small.

GSM supports data transfer at the speed of 9.6 or 14.4 kbit/s. An extension to the GSM standard, *High-Speed Circuit Switched Data* (HSCSD), permits using three time slots per frame, allowing a data speed of 43.2 kbit/s. *General Packet Radio Service* (GPRS) and *Enhanced Data Rates for GSM Evolution* (EDGE) are further extensions of GSM, which may operate in the existing GSM networks. GPRS is better suited for data transfer than GSM or HSCSD, which are circuit-switched systems. In GPRS, data is transmitted in packets and more than one timeslot per TDMA frame may be allocated for a user. In EDGE, the eight-level phase modulation, 8PSK, is used. One 8PSK symbol contains 3 bits of data, allowing a higher transfer rate than the GMSK modulation of GSM.

The standardization work for the third generation systems is ongoing. Within ITU these systems are called *International Mobile Telecommunications*

2000 (IMT-2000), whereas *Universal Mobile Telecommunications System* (UMTS) is used in Europe [6]. Third generation systems will operate in the 2-GHz band and will provide data rates up to 2 Mbit/s. A *wideband code division multiple access* (WCDMA) will be one of the access methods of the third generation systems.

## 12.5 Radionavigation

Radionavigation means determining position, speed, or some other quantity using radio waves for navigation, such as for steering a vehicle. Radionavigation is used in aviation, in shipping, and on land [7]. Radionavigation systems can be divided into two groups:

1. *Base station systems.* The positions of stations on the ground or on satellites are known. The position of a vehicle can be determined by measuring distances, differences in distances (hyperbolic systems), or directions to the base stations.
2. *Autonomous systems.* Doppler navigation is an example of autonomous navigation: Antenna beams are directed from an airplane to ground. The speed of the plane is obtained from the measured Doppler shifts. The position of the plane is calculated by integrating the velocity vector.

Hyperbolic systems, satellite systems, and systems used in aviation are treated in this section. In addition to these systems, radio beacons, broadcasting stations, and base stations of mobile phone systems are used for navigation. By taking a bearing to two beacons, the position of the vehicle can be solved. The null in the radiation pattern of a loop or Adcock antenna can be used for bearing.

### 12.5.1 Hyperbolic Radionavigation Systems

In a hyperbolic system, differences in distances to the base stations are measured. The difference in distance for a pair of stations corresponds on a plane surface to a hyperbola, on which the vehicle is located. The position is obtained from the intersection of two such hyperbolas.

Both pulsed and continuous signals are usable: The difference of the arrival times of pulses,  $\Delta t$ , or the phase difference of continuous waves,  $\Delta\phi$ , from two stations determine a hyperbola. The transmitted signals from

different stations have to be time- or phase-synchronized to each other. On the line between two stations, a time difference of 1 ms corresponds to 150 km and a phase difference of  $360^\circ$  corresponds to  $\lambda/2$ .

In the example in Figure 12.7, stations A, B, and C transmit pulses simultaneously. (In practice, this would cause interference.) The pulse from station A arrives at the receiver on the vehicle 2 ms earlier than the pulse from station B and 1 ms earlier than the pulse from station C.

Decca, Loran-C, and Omega are hyperbolic radionavigation systems used in shipping and aviation. Only Loran-C is in use at present. Decca was closed down in 2000 after having been in operation more than 50 years. Decca consisted of chains having four stations, which transmitted in the 100-kHz range. Navigation was based on the measurement of phase differences. The operating range of a Decca chain was a few hundred kilometers and it had an accuracy range of 5m to 50m. The worldwide Omega system was closed down in 1997. It consisted of eight stations, which operated at about 10 kHz. The determination of position was based on the measurement of phase differences, and it had an accuracy range of from 2 to 4 km.

Loran-C (for long-range navigation) is a hyperbolic system that is based on the differences in arrival times of pulses transmitted by the base stations.

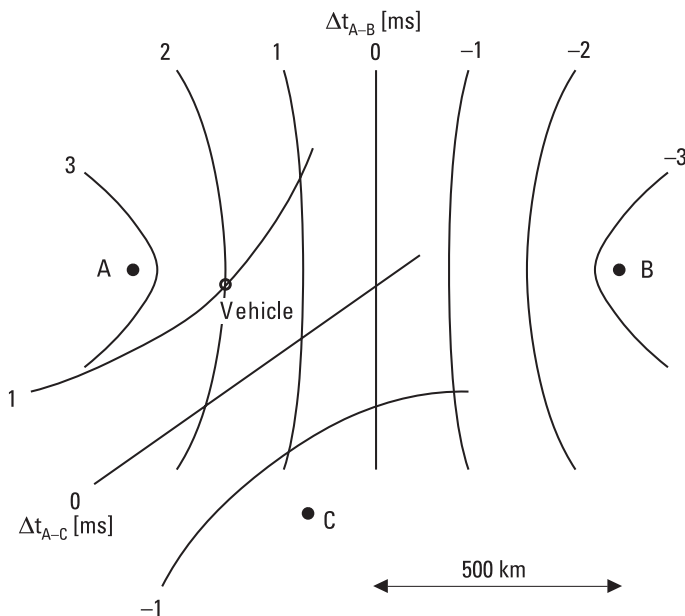


**Figure 12.7** Hyperbolic navigation system.

Loran-C consists of chains, which have one master station and two to five slave stations. The stations are located about 1,000 km apart. There are about 30 chains around the world.

The carrier frequency of Loran-C pulses is 100 kHz. Transmitted pulse power is typically 400 kW. The shape of the pulse is well defined, as shown in Figure 12.8. Both the envelope of the pulses and the phase of the carrier are used to determine time differences. The transmission sequence of a chain starts with nine pulses from the master station. The pulses are 1 ms apart, except the ninth pulse, which is 2 ms apart from the eighth pulse. Then, after a given delay, each slave station transmits eight pulses. Because of the delay, signals are always received from the stations in the same order in spite of the location of the receiver. The length of the pulse pattern is 30 to 100 ms. Figure 12.8 shows an example of a received pulse pattern. Adjacent chains have different repetition frequencies, which helps in the identification of the chain.

The signals of Loran-C system propagate to a distance of about 2,000 km as surface waves. Reflections from the ionosphere come at least  $30 \mu\text{s}$  later than the surface waves and do not disturb if only the beginning of the pulse is used for timing. Navigation accuracy is about 250m at a distance

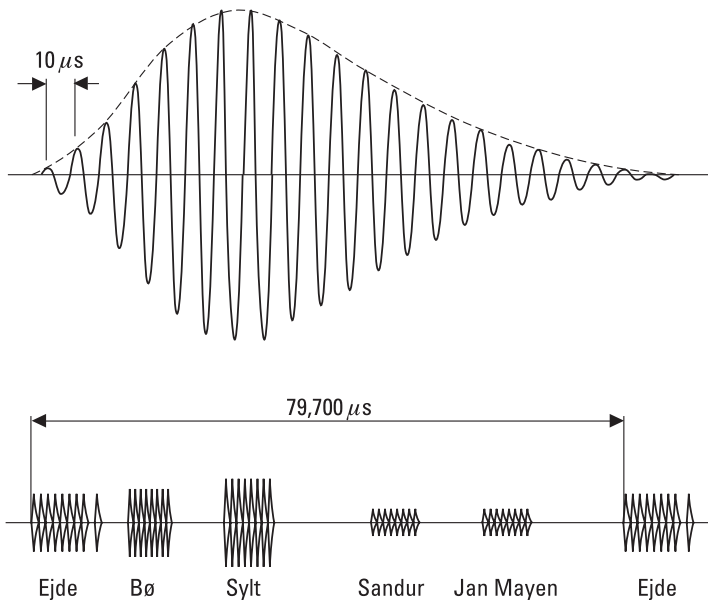


**Figure 12.8** Pulse of Loran-C, and pulse pattern of the Norwegian Sea chain received in Helsinki.

of 1,000 km. Reflections from the ionosphere can be used for navigation at distances greater than 2,000 km but with inferior accuracy.

## 12.5.2 Satellite Navigation Systems

A global navigation system is realized best by positioning the stations on satellites. Satellite navigation has several advantages:

- Vast areas can be covered with a few satellites, which makes the maintenance of the system economical.
- Navigation accuracy is better because the radio frequency used can be higher than in terrestrial systems.
- Three-dimensional navigation is possible.

In addition to navigation, satellite systems are used for locating, surveying, and transferring time signals.

Transit and GPS are briefly described below. Many other satellite-based navigation and location determination systems are in operation. The *Global Navigation Satellite System* (GLONASS) and Tsikada are the Russian counterparts of GPS and Transit. Cospas-Sarsat is a worldwide rescue system, which can locate rescue transmitters.

Transit was the first satellite navigation system and was operating between 1964 and 1997. It was initially maintained by the U.S. Navy. Six satellites in polar orbits at the altitude of 1,075 km transmitted at frequencies of about 150 and 400 MHz. The use of two frequencies made it possible to correct the effect of the ionospheric delay. Transit navigation was based on the Doppler effect. The position of a receiver was determined from the measured Doppler shift,  $f_D$ , as illustrated in Figure 12.9. The longitude was obtained from the rate of change in  $f_D$ , and the latitude from time of passage when  $f_D = 0$ . The location accuracy for an immobile vehicle was 50m.

The *Global Positioning System* (GPS) is maintained by the U.S. Department of Defense. Full operational status was reached in 1995. GPS includes 24 satellites, of which three are spare. Satellites are placed on six orbits at the height of about 20,000 km (orbiting time: 12 hours), as shown in Figure 12.10. At least five satellites are high enough above the horizon for any location on the globe.

GPS satellites transmit at two carrier frequencies,  $L1 = 1,575.42$  MHz and  $L2 = 1,227.60$  MHz. Using both frequencies, the ionospheric delay can be taken into account. The signal contains information about the orbit and

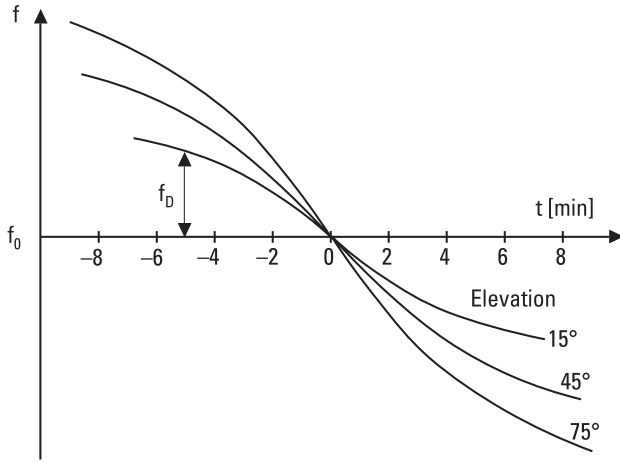


**Figure 12.9** Principle of Transit satellite navigation. The elevation is the maximum angle from the horizon during a passage.

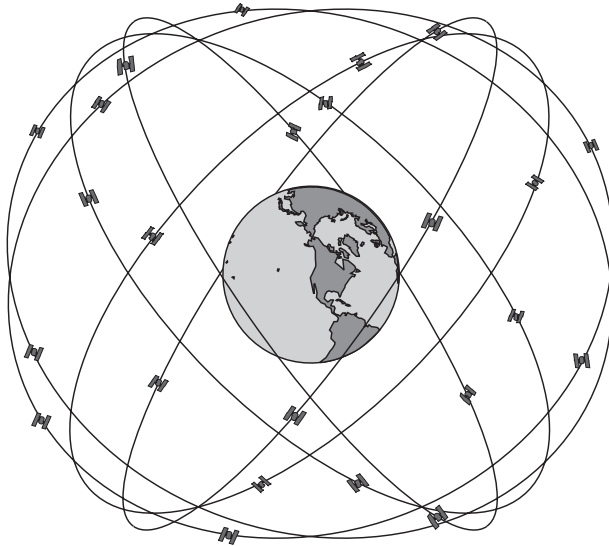


**Figure 12.10** Orbits of GPS satellites.

clock correction, and general notices. Timing of signals is based on accurate atomic clocks.

GPS is based on the measurement of the distances between the user and satellites. The distance is determined from the time of propagation from

the satellite to the receiver. The coordinates of the receiver can be calculated from distances to three satellites and from the coordinates of the satellites. The clock error of the receiver can be eliminated by using four satellites.

The GPS signal is PSK modulated with two pseudorandom codes, precise, or P, code and coarse/acquisition, or C/A, code, which have rates of 10.23 and 1.023 Mbit/s, respectively. The received code is compared to a similar code generated in the receiver, as illustrated in Figure 12.11. The delay of the generated code is adjusted until the correlation is at maximum. The transit time from the satellite to the receiver is the sum of the delay and a multiple of the length of the code. Figure 12.11 also shows the autocorrelation function of a pseudorandom code. Correlation is near zero if the phase difference is more than one bit. An error of one-hundredth bit period in the peak of the autocorrelation function corresponds to errors of 30 cm and 3m in the distance to the satellite with P and C/A codes, respectively.

The uncertainties of the clocks on the satellites and in the receiver, the uncertainties in orbital parameters, the propagation delays in the atmosphere and receiver, and multipath propagation are sources of error that impair navigation accuracy. The absolute accuracy of position is typically some tens of meters. The relative accuracy, that is, the difference in position for two receivers, is better, about 2m to 5m, because most of the errors are the same for both receivers. This is utilized in the *differential GPS* (DGPS), in which fixed stations monitor their positions and send correction signals to nearby GPS receivers. In surveying, the accuracy can be further improved by using the phase of the carrier and a long measurement time. The accuracy may be as good as about 1 cm.

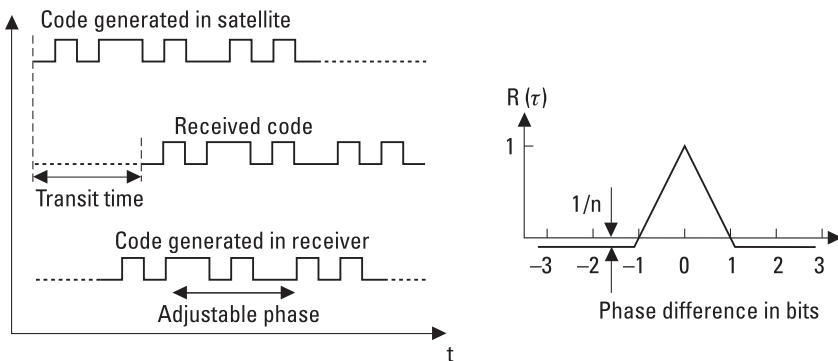


**Figure 12.11** Determination of the transit time from a satellite to the receiver, and the autocorrelation function of a pseudorandom code. The code length is  $n$  bits.



The European Union has a definite plan to deploy a new satellite navigation system called Galileo starting in 2005. The Galileo system should be ready for full operation in 2008 when all 30 satellites are orbiting at the altitude of 24,000 km.

### 12.5.3 Navigation Systems in Aviation

In addition to hyperbolic and satellite navigation systems, many other radio-navigation systems are in use in aviation.

*VHF Omnidirectional Range (VOR)* is based on omnidirectional beacons operating in the range of 108 to 118 MHz. The carrier is amplitude or frequency modulated at 30 Hz so that the phase of modulation depends on the azimuth angle. Two subcarriers 9,960 Hz apart from the carrier are frequency modulated at 30 Hz and are angle-independent reference signals. The receiver on an aircraft measures the phase difference of the 30-Hz signals and thus reveals the direction of the beacon.

*Distance Measuring Equipment (DME)* operates in the range of 962 to 1,213 MHz and is usually located with a VOR beacon. Its frequency can be “paired” with VOR or ILS. The distance between an interrogator on an aircraft and a transponder at a ground station is obtained from the time it takes for the signal to propagate from the aircraft to the ground station and back, as shown in Figure 12.12. The interrogator sends a pair of pulses. The transponder delays its response by 50  $\mu$ s and changes the frequency by 63 MHz.

The *Instrument Landing System (ILS)* and *Microwave Landing System (MLS)* are landing systems that give guidance for airplanes approaching a runway. ILS was introduced in the 1940s. It consists of three radio systems, as indicated in Figure 12.13: localizer, glide slope, and marker signals. The localizer signal (108–112 MHz) provides lateral guidance. The right side of the antenna pattern, as seen by an approaching aircraft, is modulated at

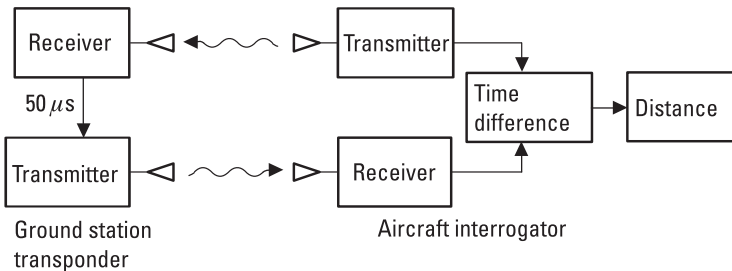
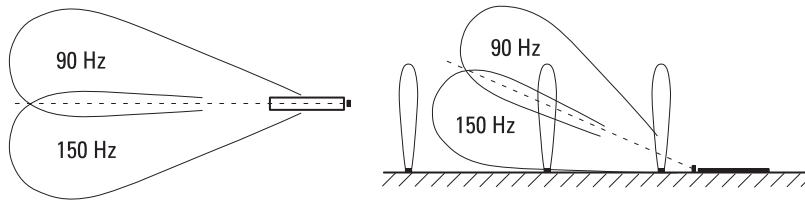


Figure 12.12 Operating principle of DME.



**Figure 12.13** ILS localizer, glide slope, and marker beams.

150 Hz, and the left side at 90 Hz. On the correct track, the 90 and 150 Hz signals are of equal intensity. The glide slope signal (329–335 MHz) provides vertical guidance. The upper part of the pattern is modulated at 90 Hz and the lower part at 150 Hz. The intensities of the modulating signals are equal in the optimum glide angle, which is typically  $2.5^\circ$  to  $3^\circ$ . Marker beacons at 75 MHz provide information on the distance from the runway.

MLS is a precision landing system that will replace ILS. MLS allows different glide angles and curved approach paths, and has many other advantages over ILS. Navigation is based on five signals: (1) the scanning azimuth signal,  $\pm 40^\circ$  or  $\pm 60^\circ$ ; (2) the scanning elevation signal, maximum scan  $0.9^\circ$  to  $30^\circ$ ; (3) the back-azimuth signal for missed approaches; (4) *precision DME* (DME/P); and (5) data signals. With the exception of DME/P, all MLS signals are transmitted on a single frequency through time-sharing. The operating range, 5,031 to 5,091 MHz, contains 200 channels. Figure 12.14 shows how the azimuth angle of an approaching plane is measured. The narrow beam produced by a phased antenna array sweeps at a fixed scan rate, and the receiver on the plane measures the time interval between sweeps,

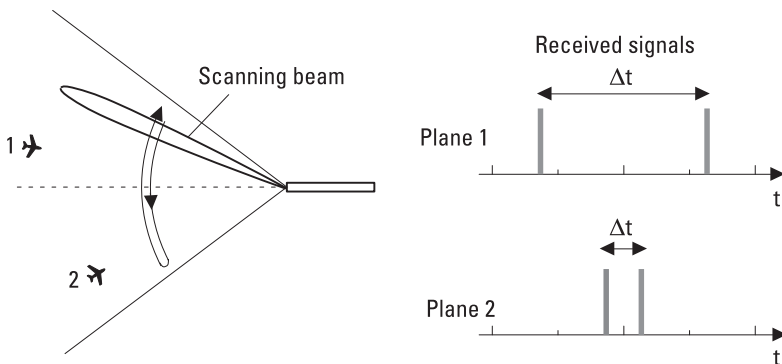


**Figure 12.14** Azimuth signal of MLS.

$\Delta t$ . The position of the plane is obtained from the measured azimuth, elevation, and distance.

*Traffic-alert and collision-avoidance systems* (TCAS) are based on transponders, which warn pilots about potential midair collisions. There are three versions of the system: TCAS I indicates potential threats, TCAS II gives simple advice such as “climb” or “descend,” and TCAS III gives more detailed advice.

## 12.6 Radar

The technique to detect and locate reflecting objects—targets—by using radio waves was first called *radio detection and ranging* [8]. Eventually, this expression was reduced to the acronym *radar*. The serious development of radar began in the mid-1930s and progressed rapidly during World War II.

The applications of radar are numerous: Surveillance radar is used in air-traffic control; tracking radar continuously tracks aircraft or missiles; weather radar reveals rain clouds and their movements; police speedometers are used in traffic control; collision-avoidance radar may be installed on all kinds of vehicles; surface-penetrating radar can locate buried objects or interfaces beneath the Earth’s surface or within visually opaque objects; and so on. Radar is applied in navigation (Section 12.5), in remote sensing of the environment (Section 12.7), in radio astronomy (Section 12.8), and in various sensors (Section 12.9).

Radar is either monostatic or bistatic. In monostatic radar the same antenna transmits and receives; in bistatic radar these are at separate locations. According to the waveforms used, radar can be divided into pulse radar, Doppler radar, and frequency-modulated radar. The basic principles of these different types of radar and the surveillance and tracking radar are treated in this section.

### 12.6.1 Pulse Radar

Pulse radar transmits a repetitive train of short-duration pulses, which reflect from the target back to the receiver. The distance to the target can be calculated from the speed of radio waves in the medium, which in most cases is with a good approximation of the speed of light in vacuum and the time  $\Delta t$  it takes for the pulses to propagate back and forth:

$$R = \frac{c\Delta t}{2} \quad (12.1)$$

The resolution of the pulse radar is

$$\Delta R = \frac{c\tau}{2} \quad (12.2)$$

where  $\tau$  is the length of the pulse. Typically  $\tau$  is in microseconds. Echoes from two objects, which are in radial direction closer than  $\Delta R$  to each other, merge in the receiver. To avoid ambiguities in the measurement of distance, the pulse repetition rate,  $f_p = 1/T$ , should be so low that all the echoes produced by a given pulse have traveled back to the receiver before the next pulse is sent.

Figure 12.15 shows the block diagram of a monostatic pulse radar (the transmitter and receiver of a bistatic radar are located at different sites). The transmitter is often based on a magnetron oscillator, whose peak power may be one megawatt. Usually, the same antenna is used both in transmitting and receiving. A duplexer isolates the sensitive receiver during the high-power pulses transmitted and directs the echoes to the receiver. The direction of the target is obtained from the direction of the narrow main beam of the antenna. The antenna may be a reflector antenna, which is rotated mechanically, or a phased array, whose main beam direction is scanned electronically. The output voltage of the superheterodyne receiver is compared

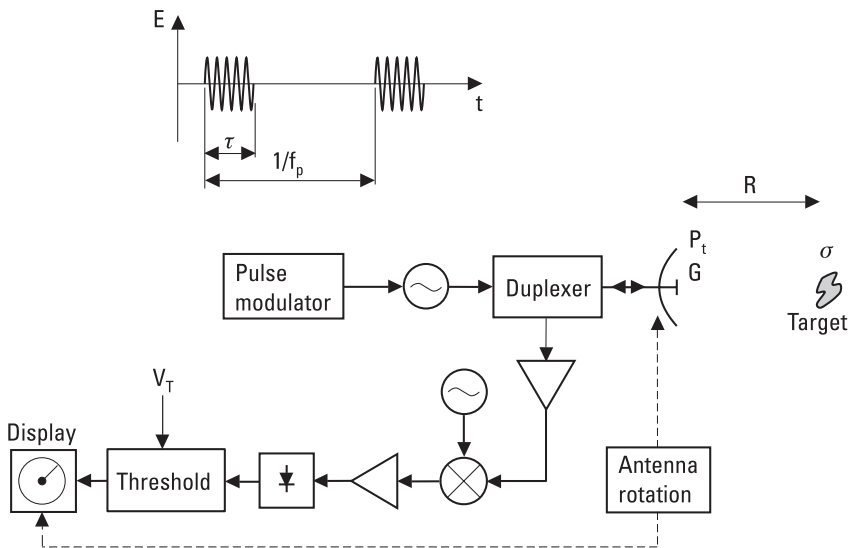


Figure 12.15 Block diagram of pulse radar.

to an adjustable threshold voltage,  $V_T$ . An output voltage higher than  $V_T$  is interpreted as a target. A too-low  $V_T$  increases the probability that noise is interpreted as a target; a too-high  $V_T$  reduces the probability of observing a weak target. The display may be a *plan position indicator* (PPI), in which the echo signal modulates an electron beam rotating synchronously with the antenna. Thus, the display shows the surroundings of the radar in polar form.

The power density produced by the radar at a distance of  $R$  is

$$S = \frac{P_t G}{4\pi R^2} \quad (12.3)$$

where  $P_t$  is the transmitted power (during a pulse) and  $G$  is the gain of the antenna. The radar cross section of a target,  $\sigma$ , is the fictional area intercepting that amount of power that, when scattered equally in all directions, produces an echo at the radar equal to that from the target. In other words,

$$\sigma = \frac{\text{power reflected towards radar/unit solid angle}}{\text{incident power density}/4\pi}$$

The radar cross section of a target depends on the frequency and polarization, as well as on the direction of observation. In case of monostatic radar, the power density produced by the target at the radar is (same  $R$  in both directions)

$$S_r = \frac{P_t G}{4\pi R^2} \times \frac{\sigma}{4\pi R^2} \quad (12.4)$$

and the power received is (same  $G$  both in transmitting and receiving mode)

$$P_r = S_r A_{ef} = S_r \frac{G\lambda^2}{4\pi} = \frac{P_t G^2 \lambda^2 \sigma}{(4\pi)^3 R^4} \quad (12.5)$$

If  $P_{r,min}$  is the minimum received power, which is reliably interpreted as a target, the maximum operating range of the radar is

$$R_{max} = \left[ \frac{P_t G^2 \lambda^2 \sigma}{P_{r,min} (4\pi)^3} \right]^{1/4} \quad (12.6)$$

This equation is called the radar equation. Because of the two-way propagation loss, doubling the transmitted power increases the maximum range only by 19%.

The minimum power  $P_{r,min}$  or the sensitivity of the radar is

$$P_{r,min} = kT_s B_n \frac{S}{N} \quad (12.7)$$

where  $T_s$  is the system noise temperature,  $B_n$  is the noise bandwidth of the receiver, and  $S/N$  is the signal-to-noise ratio corresponding to the threshold voltage. Usually the IF filter determines the noise bandwidth, which should be about  $1/\tau$ . If the bandwidth were narrower, the received pulses would distort. If it were broader, the sensitivity would be reduced.

The radar equation (12.6) is based on many idealizations. The atmospheric attenuation reduces the maximum operating range, especially at high microwave and millimeter-wave frequencies. The radar cross section of the target often changes rapidly, fluctuates, and thus has a statistical nature. Also noise and other interfering signals are statistical. Therefore, instead of exact figures, only probabilities can be estimated for a given radar measuring a target of a given type. The maximum operating range for radar may be calculated by assuming a certain probability of detection and a certain probability of false alarms.

The performance of pulse radar may be improved considerably by pulse integration, pulse compression, and moving target indication. Even if the beam of the antenna is scanning rapidly, several pulses are received from a target during each scan. The sensitivity of the radar can be improved by summing these pulses. The summing, or integration, is performed either coherently at IF or noncoherently after detection. An ideal coherent integration of  $n$  pulses having equal amplitudes improves the  $S/N$  by a factor of  $n$ . A noncoherent integration is not as effective as the coherent integration but it is much simpler to realize.

In pulse compression, the transmitted pulse is long and its carrier frequency or phase is modulated. In the receiver, the pulse is then compressed to a short impulse, for example, by using a filter whose delay is frequency dependent. Pulse compression combines the advantages of high-energy pulses and short pulses, that is, a large operating range and a good resolution.

The echoes originating from fixed objects in the radar's surroundings, clutter, may mask the detection of more interesting weak targets. The effect of clutter may be reduced by the use of a *moving target indicator* (MTI). Figure 12.16 shows the principle of a simple MTI in which echoes of

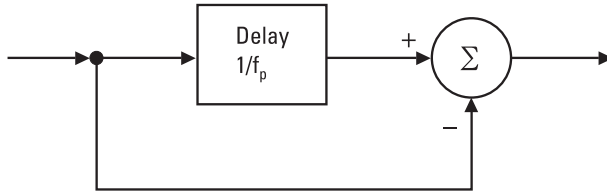


**Figure 12.16** MTI based on a delay line.

successive pulses are compared. For a fixed target, the echoes are similar, giving no output. Moving targets can be detected because the distance of a moving target changes from one pulse to the next and there is a phase difference between successive received pulses. However, if the distance of a target changes by a multiple of the wavelength during the delay  $1/f_p$ , the phase difference is zero and the target cannot be detected. Such blind speeds can be avoided by using two or more different pulse repetition frequencies. The delay circuit may be an analog filter or a digital shift register.

### Example 12.2

The properties of an air surveillance radar are: transmitted power  $P_t = 250$  kW, antenna gain  $G = 40$  dB, pulse length  $\tau = 1 \mu\text{s}$ , system noise temperature  $T_S = 500\text{K}$ , wavelength  $\lambda = 0.1\text{m}$ . The radar cross section of the target is  $\sigma = 1 \text{m}^2$  and the  $S/N$  required for detection is  $S/N = 13 \text{dB} = 20$ . Find the maximum operating range.

### Solution

The noise bandwidth is about  $1/\tau = 1 \text{MHz}$ . From (12.7) we obtain the minimum power  $P_{r,min} = 1.38 \times 10^{-23} \times 500 \times 10^6 \times 20\text{W} = 1.38 \times 10^{-13}\text{W}$ . Substituting this in (12.6) gives  $R_{max} = [250 \times 10^3 \times 10^8 \times 0.1^2 \times 1/(1.38 \times 10^{-13} \times 4^3 \pi^3)]^{1/4} \text{m} = 174 \text{km}$ .

## 12.6.2 Doppler Radar

The block diagram of a simple Doppler radar, called *continuous wave* (CW) radar, is shown in Figure 12.17. The radar transmits a continuous and unmodulated wave at a frequency of  $f_0$ . If the radial velocity of the target is  $v_r$ , the frequency of the reflected wave is  $f_0 + f_D$  where the Doppler frequency is

$$f_D = \pm \frac{2v_r}{\lambda} \quad (12.8)$$

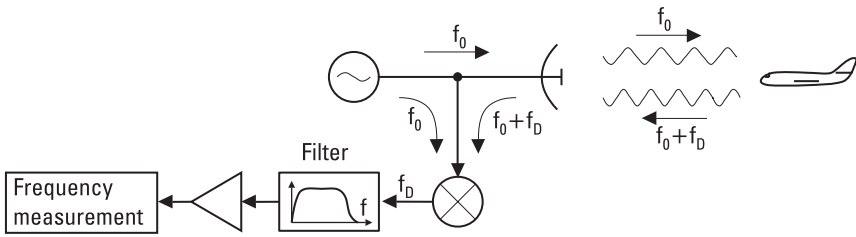


**Figure 12.17** Simple Doppler radar.

Doppler frequency is positive for an approaching target and negative for a receding target. Mixing the transmitted and received signals produces an output frequency of  $|f_D|$ . Thus, the sign of  $f_D$  is lost in mixing. The filter removes the dc component due to fixed targets. To obtain a good resolution in velocity measurement, the signal should be produced with an oscillator having low phase noise.

Figure 12.18 shows a more sophisticated Doppler radar. It has two antennas, one for transmission and one for reception, which reduces the leakage of power from the transmitter to the receiver. The local oscillator

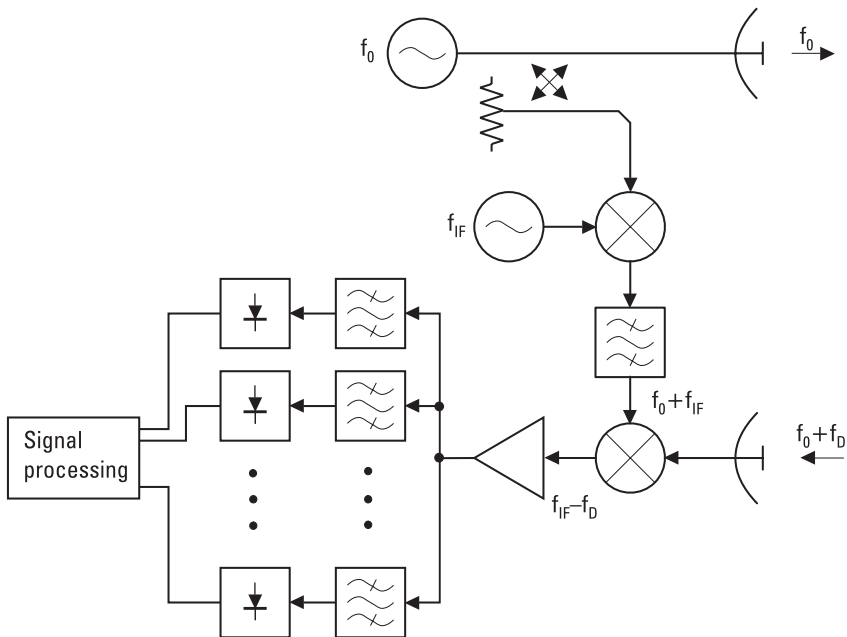


**Figure 12.18** Doppler radar having separate antennas for transmission and reception.



frequency is shifted from  $f_0$  to  $f_0 + f_{IF}$ . Now the output frequency  $f_{IF} - f_D$  reveals the sign of Doppler frequency. The higher output frequency also reduces the effect of low-frequency noise. The use of a filter bank consisting of narrow-band filters improves the signal-to-noise ratio compared to the simple radar of Figure 12.17.

Doppler radar is used for many kinds of velocity measurements: in traffic control, to measure ascent speeds of aircrafts, and so on. They are also used to detect intruders.

Doppler radar is not able to measure the distance to a target. However, pulsed Doppler radar may measure both the distance and the radial velocity. The pulse repetition rate is so high that the velocity of the target can be extracted from the phase shifts of the pulses, but at the expense of ambiguity in distance measurement.

### 12.6.3 Frequency-Modulated Radar

Conventional pulse radar is not suitable for measuring short distances because for that the pulses should be extremely short. FM radar, or FM-CW radar, is better suited for such measurements. FM-CW radar can be used as airplane altimeters, to measure liquid surface heights in containers and the thickness of different layers, and so on.

FM-CW radar transmits a continuous wave whose frequency is modulated. The distances of reflecting objects are obtained from the frequency difference,  $f_d$ , of the transmitted and received signals. If the frequency is modulated with a triangular wave, as shown in Figure 12.19, the absolute value of the frequency difference is, except near the turning points, directly proportional to the distance  $R$ :

$$f_d = \frac{2R|df/dt|}{c} = \frac{4R\Delta f f_m}{c} \tag{12.9}$$

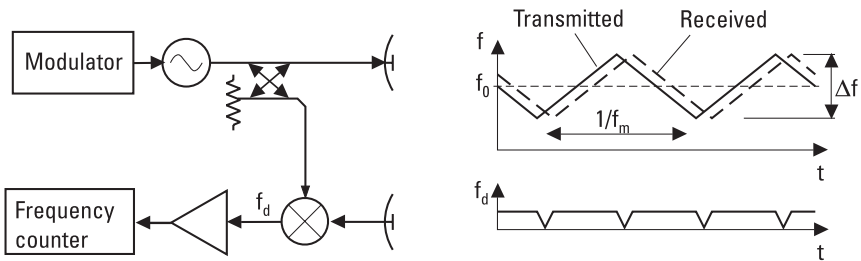


**Figure 12.19** Block diagram and frequency waveforms of FM-CW radar.

where  $\Delta f$  is the maximum change of the transmitted frequency and  $f_m$  is the modulation frequency. Equation (12.9) is valid only if the reflecting object is stationary. Other modulating waveforms can also be used.

### Example 12.3

The frequency of FM-CW radar, as shown in Figure 12.19, is modulated with a triangular wave between 3.0 and 3.2 GHz. The modulation frequency is 50 Hz. The output frequency is 1,200 Hz. Find the distance of the target.

### Solution

Now  $\Delta f = 3.2 \text{ GHz} - 3.0 \text{ GHz} = 200 \text{ MHz}$ ,  $f_m = 50 \text{ Hz}$ , and  $f_d = 1,200 \text{ Hz}$ . From (12.9) we solve  $R = cf_d / (4\Delta ff_m) = 3 \times 10^8 \times 1,200 / (4 \times 200 \times 10^6 \times 50) \text{ m} = 9 \text{ m}$ . This distance is too short to be measured with pulse radar.

## 12.6.4 Surveillance and Tracking Radars

Surveillance radar covers for example an air space surrounding an airport, whereas tracking radar follows a target continuously. Surveillance and tracking radar are usually pulse radar, and they differ from each other mainly by their beam shape and scanning techniques.

The beam of surveillance radar is usually scanned in the horizontal plane mechanically by rotating the antenna or electronically by using a phased array. In the circular scanning shown in Figure 12.20(a) the beam is fan-shaped, that is, narrow in the horizontal plane and broader in the vertical plane. If the beam is cosec<sup>2</sup>-shaped in the vertical plane, a target flying at a constant height produces an echo having a constant strength. A simple conical scanning reveals only the azimuth angle of the target. Stepped circular scanning [Figure 12.20(b)], and nodding circular scanning [Figure 12.20(c)], also give information on the elevation angle. Now the antenna may have a symmetrical pencil beam.

Tracking radar is used to track the paths of airplanes, missiles, rockets, and so on. Often tracking radar has a surveillance mode in which the radar seeks targets for tracking. As the target moves, the direction of the antenna has to be changed. In a conical scanning [Figure 12.20(d)], the axis of the beam makes a cone. If the target is not on the axis of the cone, the amplitude of the received pulses is modulated at the scanning rate. An error signal is generated from this modulation to correct the direction of the cone axis.

Monopulse radar has four beams, as shown in Figure 12.20(e). Now an error signal can be derived from a single pulse by comparing the amplitudes

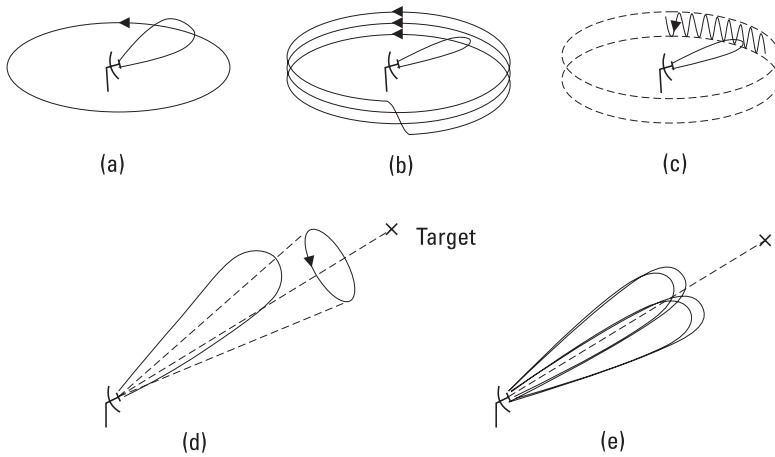


**Figure 12.20** Scanning techniques: (a) circular scanning; (b) stepped circular scanning; (c) nodding circular scanning; (d) conical scanning; and (e) monopulse.

from all four beams. Therefore, the fluctuation of the radar cross section causing amplitude modulation does not impair the tracking accuracy. A multibeam antenna can be realized by placing an array of feed antennas on the focal plane of a reflector antenna.

## 12.7 Remote Sensing

Remote sensing means measuring or observing of atmosphere or surface of the Earth by using electromagnetic waves without any physical contact with the object and the analysis of these measurements. Radio astronomy investigating other celestial bodies is a separate field and is treated in Section 12.8.

Aerial photography has been carried out for more than one hundred years. Optical pictures taken from satellites have good resolution, at its best about 1m. Radio waves have been used for remote sensing since the 1960s. Radio waves have some advantages over visible light and infrared waves: Darkness and clouds do not prevent measurements; radio waves penetrate deeper in the vegetation and soil; and higher radio frequencies give information on the upper layers and lower radio frequencies on the deeper layers. However, the resolution of radio images is poorer than that of optical images.

Remote-sensing methods may be divided into passive and active methods. Passive remote sensing is called radiometry, in which thermal emission from the ground or atmosphere is measured with a sensitive receiver,

a radiometer. In active remote sensing, radar techniques are used: objects are at first illuminated with the radar signal and then the reflected or scattered signal is measured.

Remote sensing using radio waves may reveal many properties of our environment [9–11]. Subjects that can be studied are numerous: ground profile, vegetation, moisture content of soil, water content of snow, oil leakages from ships, wind speed and direction, temperature and water vapor profiles of atmosphere, abundance of ozone and other molecules in the upper atmosphere, and so on.

Measurements can be carried out with instruments on the ground, on aircraft, or on satellites. The American Seasat (launched in 1978), Nimbus-7 (1978), and TOPEX/Poseidon (1992), the Canadian Radarsat (1995), and the European ERS-1 (1991), ERS-2 (1995), and ENVISAT (2002) are examples of remote-sensing satellites carrying radiometers or radar onboard. Several sounders for the measurement of the temperature profile and the contents profiles of water vapor, ozone, and many pollutants are planned.

### 12.7.1 Radiometry

All matter emits electromagnetic energy. A body in a thermodynamic equilibrium emits energy at the same rate as it absorbs energy. A blackbody is an object that absorbs all the energy that is incident on it, that is, the reflection coefficient is zero at all frequencies. If an antenna is pointing toward the surface of a blackbody at a temperature of  $T$ , the power coupled to the antenna in a bandwidth of  $B$  is (see Section 11.2.2)

$$P = kTB \quad (12.10)$$

Most natural bodies are “gray.” The power coupled to the antenna from a gray body is obtained by replacing the physical temperature  $T$  in (12.10) by the brightness temperature

$$T_B = eT \quad (12.11)$$

where  $e$  is the emissivity, or the power transmission coefficient, of the surface. The emissivity is related to the voltage (electric field) reflection coefficient of the surface as

$$e = 1 - |\rho|^2 \quad (12.12)$$

The emissivity depends on the electrical properties of the object ( $\epsilon_r$ ,  $\sigma$ ), on the roughness of its surface, and on the angle, frequency, and polarization

of the measurement. For a blackbody the emissivity is 1, for an ideal conductor it is 0, and for other objects it is between these limits. Thus,  $T_B$  is always smaller than or equal to the physical temperature. If the temperature of the object is not constant as a function of depth from the surface,  $T_B$  depends on the temperature distribution within a few skin depths. Radiometry is based on the fact that different objects have different temperatures and emissivities, and thus the measured brightness temperature may give a lot of information on the object.

Figure 12.21 shows a radiometer measuring the brightness temperature of the ground surface. In an ideal case, the noise signal is not attenuated by the atmosphere ( $L = 0$  dB), the brightness temperature of the sky is  $T_i = 0$ K, and the thermal noise from the ground having a brightness temperature of  $T_B$  fills the whole antenna beam and is independent of direction. Then the antenna noise temperature is  $T_A = T_B$ . In practice, the atmosphere attenuates the signal and itself produces thermal noise, the surface reflects noise from the sky ( $T_i \neq 0$ K), and a part of the antenna pattern is not pointing toward the surface. The noise coming to the antenna can be characterized by a direction-dependent antenna noise temperature  $T_{AP}(\theta, \phi)$ . The measured antenna noise temperature is obtained by weighing  $T_{AP}(\theta, \phi)$  by the normalized radiation pattern  $P_n(\theta, \phi)$ :

$$T_A = \frac{\iint_{4\pi} T_{AP}(\theta, \phi) P_n(\theta, \phi) d\Omega}{\iint_{4\pi} P_n(\theta, \phi) d\Omega} \tag{12.13}$$

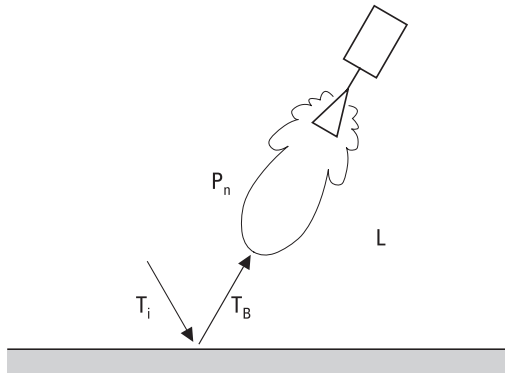


**Figure 12.21** Radiometer measuring the brightness temperature of ground.

The brightness temperature  $T_B$  can be best figured out from the measured  $T_A$ , if  $T_i$  and  $L$  are small. This situation realizes well in the frequency range of 1 to 10 GHz, because at these frequencies the sky looks very “cold” and the attenuation of the atmosphere is small enough.

A microwave image of a terrain is acquired by placing a radiometer on an airplane or a satellite and by scanning the beam of the antenna. The emissivity of a rough ground surface is usually close to 1, whereas water has much lower emissivity, about 0.4. Therefore, the brightness temperature of a sea surface is  $T_B = eT_{water} + (1 - e)T_{sky} \approx 100\text{K}$  to  $150\text{K}$ . Metallic objects reflecting the cold sky are also easily distinguished. At longer wavelengths the emissivity is sensitive to the soil moisture content, but the effects due to the surface roughness and vegetation may reduce the accuracy. Combining radiometric measurements at many frequencies and at both polarizations with infrared measurements may enhance the accuracy.

Radiometry can also be applied for the measurement of thicknesses of different layers. For example, a layer of ice or oil on the sea surface can be detected because the layer works as a matching element between the wave impedances of air and water. The reflection coefficient has a minimum and the brightness temperature a maximum when the thickness of the layer is a quarter (or an odd number of quarters) of wavelength.

Thermal emission of atmospheric gases can be used to study both the lower and upper atmosphere. The oxygen resonance at 60 GHz reveals the height profile of the temperature. The height profiles of the contents of water vapor, ozone ( $\text{O}_3$ ), and many other molecules can be retrieved from the measured spectral lines, which these molecules have at microwave and millimeter-wave ranges. The emission or absorption spectrum of a molecule that is not interacting with its surroundings is composed of a set of narrow spectral lines. The collisions of molecules broaden these lines. Therefore, molecules at lower altitudes and higher pressures emit broader spectral lines than those at higher altitudes and lower pressures. Because the pressure versus altitude is well known, the content profile of a molecule may be obtained from the shape of its spectral line. A spectral line and the corresponding height distribution of stratospheric ozone are shown in Figure 12.22.

The depletion of the ozone layer first observed in the 1980s is alarming and requires constant monitoring. Global monitoring of the atmosphere can best be carried out with radiometers onboard satellites. A proper geometry for the measurement of upper atmosphere is achieved with a limb sounder, a satellite instrument that has a narrow-beam antenna directed toward the horizon. Height profiles can be measured by scanning the antenna.

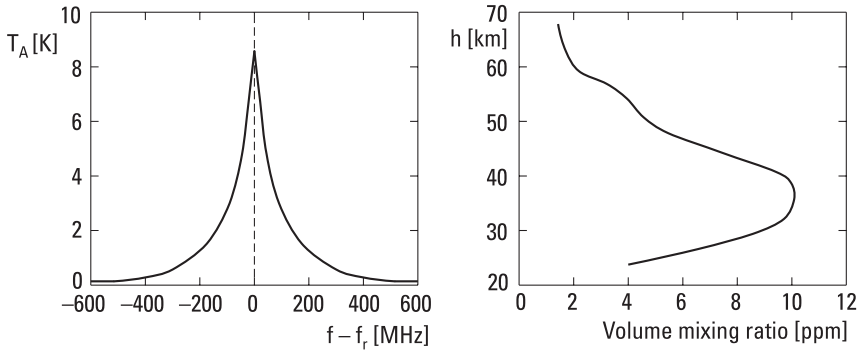


**Figure 12.22** Spectral line of ozone centered at 110.836 GHz (background noise of atmosphere removed) and height profile corresponding to this line.

*Example 12.4*

A ground surface having a temperature of 295K and an emissivity of 1 is covered with a quarter-wave layer of lossless material having a relative permittivity of 5. Find the antenna temperature measured with a radiometer pointing perpendicularly to the surface. Assume that the brightness temperature of sky is 0K.

*Solution*

The wave impedance of the layer is  $Z_{layer} = \sqrt{\mu/\epsilon} = \sqrt{\mu_0/\epsilon_0}/\sqrt{\epsilon_r} = 376.7/\sqrt{5} \Omega = 168.5 \Omega$ . Because now the ground is like a blackbody (emissivity  $e = 1$ ), its wave impedance  $Z_{ground} = 376.7 \Omega$  equals the wave impedance of free space,  $\eta_0$ . The layer operates as a quarter-wave transformer (see Section 4.3.3) that transforms  $Z_{ground}$  to a value of  $Z_t = Z_{layer}^2/Z_{ground} = 75.4 \Omega$ . The reflection coefficient between the free space and this impedance is  $\rho = (\eta_0 - Z_t)/(\eta_0 + Z_t) = 0.666$ . The brightness temperature of the ground is  $T_B = eT = (1 - |\rho|^2)T = 164K$ . This is also the antenna temperature seen by the radiometer, because the lossless layer itself does not emit thermal radiation and the sky is cold. Without the layer, the antenna noise temperature would be 295K.

**12.7.2 Total Power Radiometer and Dicke Radiometer**

A radiometer is a sensitive receiver that measures absolute noise power levels accurately and that is calibrated to display the brightness temperature.

Figure 12.23 shows a block diagram of a total power radiometer. It is a superheterodyne receiver, whose IF signal is fed to a detector. The mixer

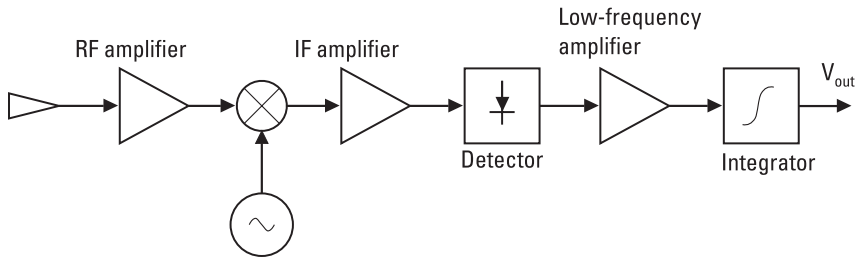


**Figure 12.23** Total power radiometer.

usually converts both the upper and lower sideband to IF. The measurement bandwidth is determined by the noise bandwidth of the IF stage,  $B_n$ . The detected signal is integrated to average the noisy output voltage  $V_{out}$ , shown in Figure 12.24. The output voltage includes both dc and ac components. The dc component is directly proportional to the system noise temperature:

$$V_{dc} = G_S (T_A + T_R) \quad (12.14)$$

The ac component,  $V_{ac}$ , comes from the statistical nature of noise. The ratio of the rms value of  $V_{ac}$  to the dc component  $V_{dc}$  is  $1/\sqrt{B_n \tau}$  [9, 12], where  $\tau$  is the integration time of the detector output voltage. The sensitivity of a radiometer is defined as the minimum change of the antenna

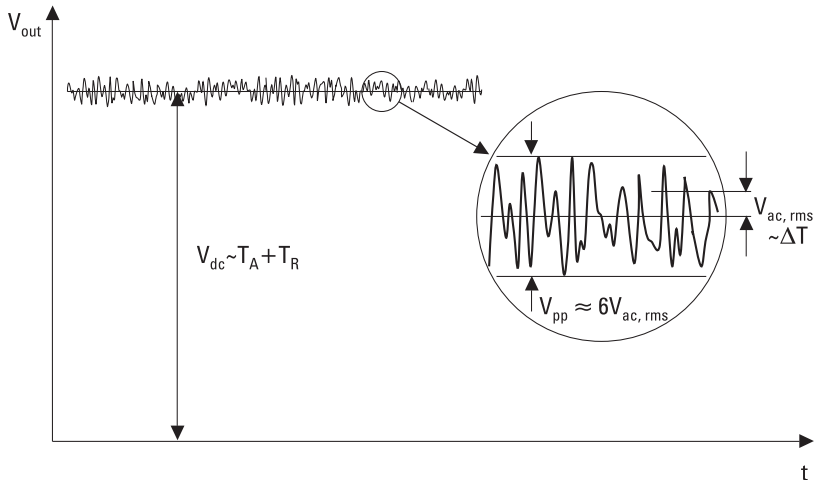


**Figure 12.24** Output voltage of a total power radiometer.



noise temperature that can be detected. For a total power radiometer, the sensitivity is

$$\Delta T = \frac{T_A + T_R}{\sqrt{B_n \tau}} \tag{12.15}$$

A change of  $\Delta T$  at the input produces at the output a change equal to the rms value of  $V_{ac}$ . The sensitivity can also be defined to be that change at the input that produces a change equal to the peak-to-peak value of the output voltage,  $V_{pp}$ . The peak-to-peak value is about six times the rms value.

The variations of the system gain,  $G_S$ , reduce the accuracy of a measurement. The gains of the amplifiers, mixer, and detector may depend on temperature and supply voltages. The effect of slow variations can be taken into account by calibrating the radiometer frequently with loads having known brightness temperatures. Rapid gain fluctuations deteriorate the sensitivity of the total power radiometer:

$$\Delta T = (T_A + T_R) \sqrt{\frac{1}{B_n \tau} + \left(\frac{\Delta G_S}{G_S}\right)^2} \tag{12.16}$$

where  $\Delta G_S$  is the rms value of the gain fluctuations. However, tight temperature control of the radiometer components successfully mitigates these problems.

Figure 12.25 shows the block diagram of the Dicke radiometer, in which the influence of gain variations is reduced. The receiver switches continuously between the antenna and a noise source that has a constant

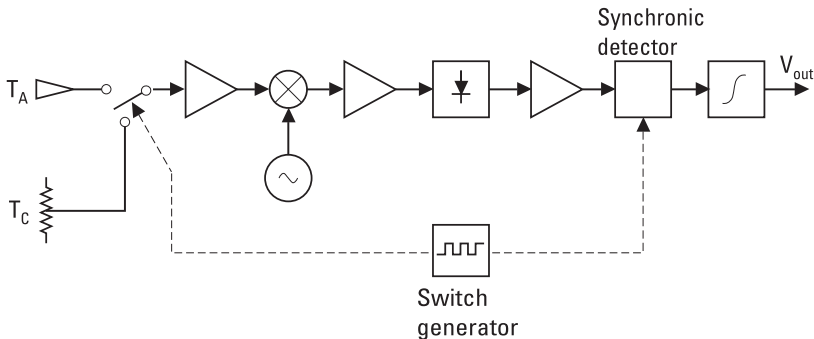


Figure 12.25 Dicke radiometer.

temperature,  $T_C$ . Gain variations are assumed to be small between switching. The output of the diode is detected synchronously with the switch generator so that the output voltage,  $V_{out}$ , is proportional to the difference between  $T_A$  and  $T_C$ . If the radiometer is balanced, that is,  $T_A = T_C$ , gain variations have no influence on the output. A Dicke radiometer may be balanced by injecting excess noise into the antenna branch (usually  $T_A < T_C$ ), by changing the IF gain synchronously with a switch generator, or by adjusting the temperature  $T_C$ . Because only half of the time is used for an effective measurement, the sensitivity,  $\Delta T$ , of the Dicke radiometer is twice of that of the total power radiometer:

$$\Delta T = \frac{2(T_A + T_R)}{\sqrt{B_n \tau}} \quad (12.17)$$

### Example 12.5

A Dicke radiometer has a noise temperature  $T_R = 500\text{K}$  and a bandwidth  $B_n = 10\text{ MHz}$ . A blackbody having a temperature of  $300\text{K}$  should be measured with a resolution of  $0.2\text{K}$ . Find the required integration time.

### Solution

The system noise temperature  $T_S = T_A + T_R = 800\text{K}$ . To obtain a sensitivity  $\Delta T = 0.2\text{K}$ , we solve for the required integration time from (12.17) as  $\tau = (2T_S/\Delta T)^2/B_n = (2 \times 800/0.2)^2/10^7$  seconds =  $6.4$  seconds.

## 12.7.3 Remote-Sensing Radar

*Side-looking airborne radar* (SLAR), *synthetic-aperture radar* (SAR), scatterometer, and altimeter are radars used for remote sensing.

SLAR is pulse radar that is usually placed on an airplane. It produces microwave images of ground at the side of the flight track. The beam of the antenna is broad in the vertical direction and narrow in the horizontal direction, as shown in Figure 12.26. If the plane flies at an altitude of  $5\text{ km}$ , for example, the image may cover a range from  $4\text{ km}$  to  $15\text{ km}$  at the side of the track. The resolution in the direction perpendicular to the flight track depends on the pulse length  $\tau$  as

$$\Delta R_r = \frac{c\tau}{2 \sin \theta} \quad (12.18)$$

where  $\theta$  is the angle of incidence. Thus, directly below the flight track at small  $\theta$  angles the resolution is bad. In the direction along the flight track,

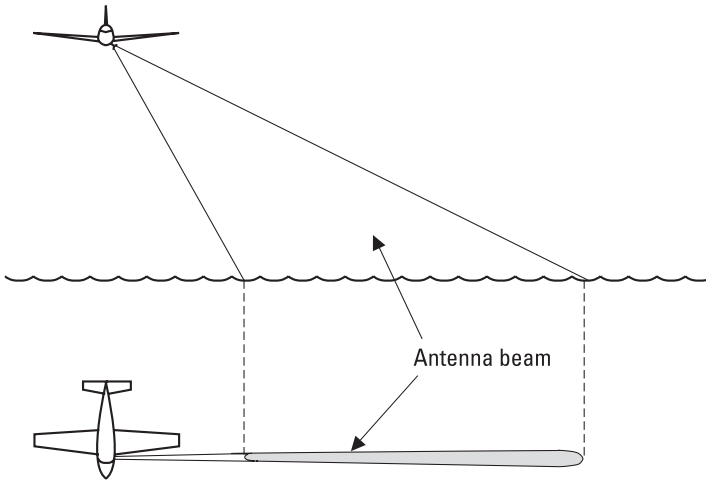


**Figure 12.26** SLAR.

the resolution depends on the beamwidth of the antenna. If the dimension of the antenna is  $D$  in the horizontal direction, the beamwidth is about  $\lambda/D$  and the along-track or cross-range resolution at a distance of  $R$  is

$$\Delta R_{cr} = \frac{R\lambda}{D} \quad (12.19)$$

The cross-range resolution gets worse as  $R$  increases and, therefore, SLAR onboard a satellite would need a very large antenna to obtain good resolution.

To overcome the limited cross-range resolution of SLAR, satellite remote-sensing radar is based on the principle of a synthetic aperture. Synthetic-aperture radar is pulse radar that uses the motion of the satellite (or some other vehicle) to synthesize the effect of a large antenna aperture. Echoes of several pulses are processed coherently to produce high-resolution images. If the pulses transmitted over a section of flight track having a length of  $s$  are processed, the resolution of this synthetic aperture equals that of an antenna having a width of  $2s$ . Because a single-point target is in the view of the real antenna over a track section  $s \approx R\lambda/D$ , the theoretical beamwidth of the synthetic-aperture radar is

$$\theta_s = \frac{\lambda}{2s} = \frac{D}{2R} \quad (12.20)$$

and the theoretical cross-range resolution is

$$\Delta R_{cr} = R\theta_s = \frac{D}{2} \quad (12.21)$$

It is not practical to improve the resolution by using a smaller antenna because echoes would get weaker and various sources of error over a long section  $s$  would limit the resolution to a value higher than given by (12.21).

The reflectivity of the ground or sea surface depends on frequency, polarization, and the angle of incidence. At higher frequencies, echoes depend on the roughness of surface, whereas at lower frequencies, waves penetrate into ground and echoes are sensitive to the humidity of soil. By combining dual-polarization measurements made at different frequencies and angles of incidence, SLAR and SAR measurements provide multifaceted information for agriculture, forestry, geography, oceanography, and so on.

Scatterometers and altimeters are remote-sensing radar that do not produce images. A scatterometer is radar calibrated for the measurement of scattering. Scatterometers on satellites are used for the measurement of winds over the oceans. Sea waves correlate with the wind, and scattering in turn is sensitive to the height and shapes of the waves. Thus, by measuring scattering from different angles, the speed and direction of wind may be retrieved.

An altimeter is based on the measurement of the two-way propagation time of an echo. Altimeters provide information of the shape of the globe, ocean currents, ice coverage of glaciers, and so on.

## 12.8 Radio Astronomy

For a long time, only the optical window of the atmosphere covering visible light and the shortest infrared and longest ultraviolet waves was available for astronomers. In 1932, the American engineer Karl Jansky observed noise coming from the Milky Way as he was studying interference in communication produced by thunderstorms. In the late 1930s, the American amateur astronomer Grote Reber built a parabolic reflector and made the first rough map of the radio sky. After World War II, microwave technology became available to astronomers, and eventually radio astronomy developed into an important part of astronomy. A very important milestone was the observation of the interstellar neutral hydrogen at 1,420 MHz in 1953.

The atmosphere is nearly transparent (to zenith) from about 10 MHz to tens of GHz. Thus, the radio window covers about four decades of spectrum, whereas the width of the optical window is less than one decade. The reflection from the ionosphere sets the lower frequency limit. At millimeter and submillimeter waves the attenuation of gases becomes prohibitive, and telescopes must be placed on satellites.

The Sun, planets, gas and dust clouds of the Milky Way, pulsars, radio galaxies, quasars, and cosmic background radiation are subjects studied in radio astronomy [12]. Radio telescopes are also used for *searching extraterrestrial intelligence* (SETI).

### 12.8.1 Radio Telescopes and Receivers

Signals from radio astronomical sources are very weak. Thus, a large radio telescope and a sensitive receiver are crucial. A large telescope gathers waves from a large area and has a good angular resolution. The telescope should be situated at a high altitude and in a dry climate, especially if it is used at submillimeter wavelengths. The location should also be selected so that the level of man-made interference is low. The accuracy of the reflector surfaces should be better than  $\lambda/10$ , which is a formidable requirement for a large telescope operating at high frequencies. Surface errors reduce the gain and deteriorate the radiation pattern of the antenna.

Radio telescopes are typically parabolic reflector antennas. The telescope of the *National Radio Astronomy Observatory* (NRAO) in Green Bank, West Virginia, which started its operation in 2000, is the largest fully steerable telescope. The size of this offset-fed reflector, shown in Figure 12.27, is  $100\text{m} \times 110\text{m}$ . It is usable even at millimeter wavelengths. Other large parabolic reflectors are the 100-m telescope of the Max Planck Institute in Effelsberg, Germany, the 76-m telescope of the University of Manchester in Jodrell Bank, England, the 64-m telescope of CSIRO near Parkes, Australia, and the 45-m telescope of the Nobeyama Radio Observatory, Japan, which operates up to 100 GHz. The 30-m telescope of the Institut de Radioastronomie Millimétrique at Pico Veleta, Spain, and the 15-m James Clerk Maxwell telescope at Mauna Kea, Hawaii, are so accurate that they can be used even at submillimeter wavelengths.

Due to gravitation, construction of steerable parabolic reflectors much larger than 100m is not practical on Earth. However, even fixed telescopes can cover large parts of the sky. The 305-m spherical reflector at Arecibo, Puerto Rico, is situated in a mountain valley. Moving the feed antenna allows observations up to  $20^\circ$  from the zenith. A large telescope can also be

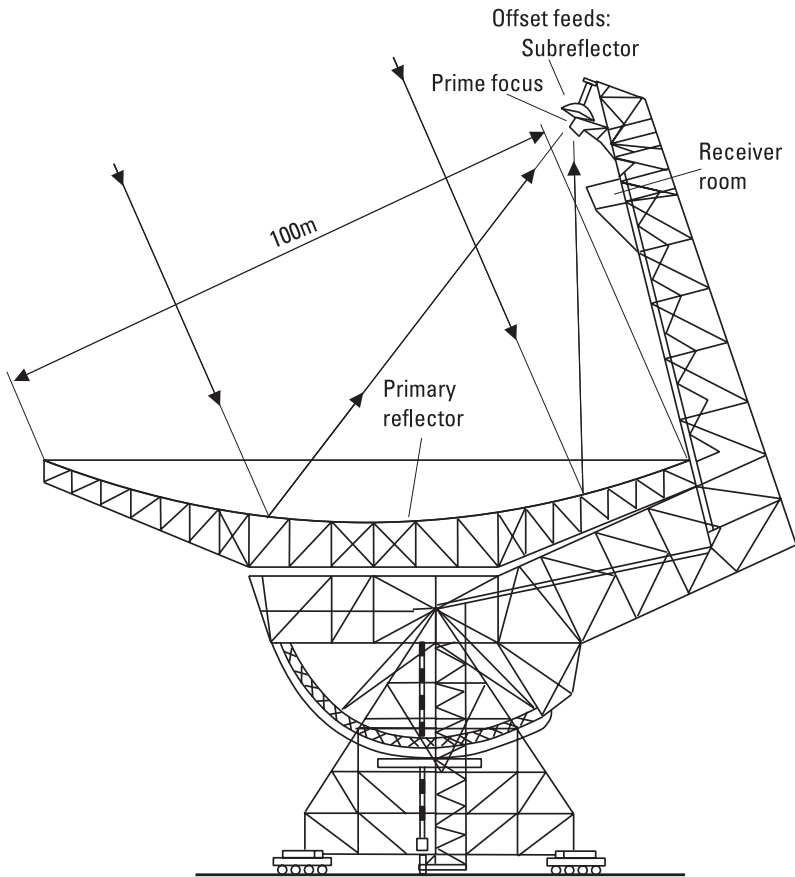


**Figure 12.27** Large steerable radio telescope of NRAO in Green Bank. (After: [13].)

made of a tilting flat reflector, which directs the waves to a fixed segment of a parabola.

Even the largest radio telescopes, as measured in wavelengths, are very small compared to optical telescopes and have correspondingly an inferior resolution. The angle resolution may be improved by an aperture synthesis, in which signals from several telescopes are combined. The *Very Large Array* (VLA) of the NRAO in New Mexico consists of 27 parabolic reflectors, each 25m in diameter. The antennas can be moved on three tracks 21 km long, so that a Y-shaped configuration is formed on the plain. By taking advantage of the Earth's rotation and combining measurements made in 8 hours, an angle resolution equal to that of a continuous 40-km telescope may be obtained.

In *very long baseline interferometry* (VLBI) radio telescopes are separated by intercontinental distances or may even be in space. Signals cannot be compared in real time but are recorded with accurate time signals from atomic standards for later processing. The achievable resolution is far better than that of optical telescopes. The Japanese satellite HALCA was launched in 1997 and makes VLBI measurements with its 8-m telescope at 1.6 GHz, 5 GHz, and 22 GHz. It is in an elliptical orbit with an apogee height of 21,000 km.

The sensitivity of the receiver is very important in radio astronomical measurements. Doubling of the system noise temperature increases the time needed for a measurement by a factor of four. At microwave frequencies, cooled transistor amplifiers (HEMT) are used as the front ends of the receivers. At millimeter and submillimeter wavelengths, receivers are based on Schottky mixers, SIS mixers, cooled bolometric mixers, or bolometers. Often an array of receivers is placed on the focal plane of the reflector.

Figure 12.28 shows a block diagram of a cooled Schottky-mixer receiver operating in the 100-GHz frequency range. Signal from the reflector first enters a quasi-optical calibration and beam-switching system. Calibration is based on two absorbing loads at known temperatures, one at the ambient temperature ( $T_H$ ), the other inside a cooled dewar ( $T_C$ ). Beam switching produces two adjacent beams in the sky by using a segmented, rotating mirror and two fixed mirrors. The radio source to be observed is in one of the beams while the other beam looks at the cold sky. The purpose of beam switching is to reduce the influence of the fluctuations caused by the atmosphere. The front-end components, feed horn, filter for LO injection, mixer, and the first IF amplifier are cooled to 20K with a closed-cycle helium refrigerator. The local oscillator is a phase-locked Gunn oscillator. The IF

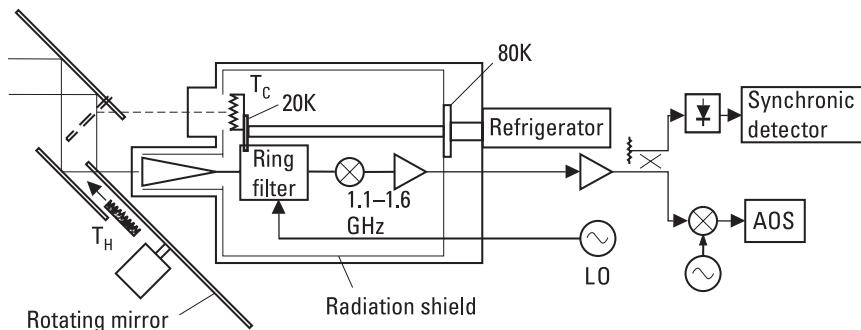


**Figure 12.28** Cooled 100-GHz Schottky-mixer receiver.

signal is fed both to a detector operating synchronously with the beam switching and to an *acousto-optical spectrometer* (AOS) for spectrum analysis.

### 12.8.2 Antenna Temperature of Radio Sources

The flux  $S$  of a radio source is calculated by integrating the brightness  $B_S$  over the solid angle  $\Omega_S$  covered by the source:

$$S = \iint_{\Omega_S} B_S(\theta, \phi) d\Omega \quad (12.22)$$

The unit of flux is jansky (Jy); one jansky is  $10^{-26} \text{ Wm}^{-2} \text{ Hz}^{-1}$ .

Some radio sources are like points in the sky, and some sources are extended. If the radio source is a point source and in the middle of the antenna beam, the received power in the frequency band  $\Delta f$  is

$$P_r = \frac{1}{2} A_{ef} S \Delta f \quad (12.23)$$

For an extended source, the flux  $S$  has to be replaced with the flux  $S_o$  observed by the antenna.  $S_o$  is obtained by weighing the right side of (12.22) with the normalized directional pattern  $P_n(\theta, \phi)$ . If the brightness of the radio source is constant over the whole antenna beam, the received power is

$$P_r = \frac{1}{2} A_{ef} B_S \Omega_A \Delta f \quad (12.24)$$

where  $\Omega_A = \iint_{4\pi} P_n(\theta, \phi) d\Omega$  is the solid angle of the beam. Now the observed flux is  $S_o = B_S \Omega_A$ .

The received power may be written using the antenna noise temperature  $T_A$  as

$$P_r = k T_A \Delta f \quad (12.25)$$

Combining this with (12.23) gives

$$T_A = \frac{A_{ef} S_o}{2k} \quad (12.26)$$



If the brightness temperature of the source,  $T_B$ , is constant over the whole beam, then  $T_A = T_B$ . For a small source ( $P_n \approx 1$  over the whole source), the antenna noise temperature is

$$T_A = \frac{\Omega_S}{\Omega_A} T_B \quad (12.27)$$

Above, the influence of the atmospheric loss was not taken into account. Because the fluxes of radio sources are values defined outside the atmosphere, the measured results have to be corrected with the attenuation of the atmosphere.

### Example 12.6

A point source having a flux of 2 Jy is measured with a 13.7-m radio telescope. Find the antenna noise temperature produced by the source and the required integration time  $\tau$ . The attenuation of the atmosphere is  $L = 0.8$  dB, the aperture efficiency is  $\eta_{ap} = 0.6$ , the noise temperature of the Dicke receiver is  $T_R = 100\text{K}$ , and the bandwidth is  $\Delta f = 300$  MHz.

### Solution

The physical area of the aperture is  $A = \pi D^2/4 = 147.4 \text{ m}^2$ . The effective area  $A_{ef} = \eta_{ap} A = 0.6 \times 147.4 \text{ m}^2 = 88.4 \text{ m}^2$ . The flux at the antenna is  $S = 2 \times 10^{-0.08} \text{ Jy} = 1.66 \text{ Jy}$ . From (12.26), the antenna noise temperature produced by the source is  $T_{A,source} = 88.4 \times 1.66 \times 10^{-26}/(2 \times 1.38 \times 10^{-23})\text{K} = 53 \text{ mK}$ . The sensitivity of a Dicke radiometer is  $\Delta T = 2T_S/\sqrt{\tau\Delta f}$ . The antenna noise temperature produced by the atmosphere is  $T_{A,atm} = (1 - 1/L) T_{phys} = (1 - 10^{-0.08}) \times 290\text{K} = 49\text{K}$ , assuming that the physical temperature of the atmosphere,  $T_{phys}$ , is 290K. Thus, the system noise temperature is  $T_S = T_{A,atm} + T_R = 49\text{K} + 100\text{K} = 149\text{K}$ . The integration time depends on the required  $S/N$  (note that now signal is also noise).  $S/N = 1$  or  $T_A = \Delta T$  is achieved if  $\tau = (2T_S/T_A)^2/\Delta f = 0.11$  second. The integration time needed for  $S/N = 10$  is 100 times longer, nearly 11 seconds.

## 12.8.3 Radio Sources in the Sky

The radio sky is very different from the sky we see at optical wavelengths. Point sources, radio “stars,” are not ordinary stars, which are relatively weak emitters of radio waves. The most significant similarities are the plane and the center of the Milky Way, which can be seen clearly in both optical and radio pictures.

Radio sources have different frequency dependencies. The radiation produced by thermal sources obeys Planck's radiation law. Nonthermal sources often emit synchrotron radiation, which is produced by electrons spiraling in a magnetic field. The intensity of synchrotron radiation decreases as frequency increases. Both thermal and synchrotron radiation have a broad, continuous spectrum and are called continuum radiation. Some sources emit only at discrete frequencies and have a line spectrum. Atoms and molecules emit spectral lines as their energy levels change, that is, when the atom or molecule after excitation returns to equilibrium.

There are many radio sources in our solar system, in our galaxy, and outside it. Moreover, from all directions comes a weak background radiation, which corresponds to the radiation from a blackbody at a temperature of 2.7K; see Figure 12.29. The intensity of the cosmic background radiation is at maximum at millimeter wavelengths, but on Earth it can best be observed in microwave range, where the noise level is the lowest. The discovery of background radiation in 1964 was proof in favor of the Big Bang theory, which assumes that the universe was born in a huge explosion. After its birth, the universe is believed to have expanded and cooled, and now we can observe the remnant of this explosion. The background radiation obeys extremely accurately Planck's law and is very isotropic. However, some anisotropy had to be in the young universe because galaxies have formed. In 1992, the *Cosmic Background Explorer* (COBE) satellite launched by NASA observed these anisotropies: The brightness of background radiation had tiny fluctuations whose relative amplitude was one part in one hundred thousand (1:100,000). The aim of successive space missions, such as the

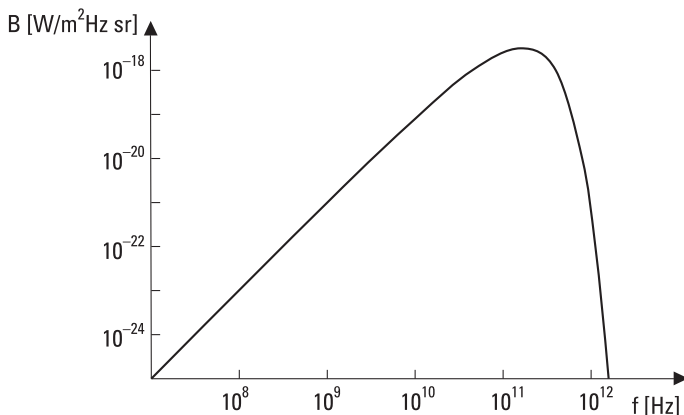


**Figure 12.29** Spectrum of the cosmic background radiation.

*Microwave Anisotropy Probe* (MAP), launched in 2001, and Planck Surveyor, scheduled for launch in 2007, is to measure these fluctuations with a much better angle resolution and with a better receiver sensitivity.

Although stars are weak radio sources, the Sun is an exception because of its vicinity. The radiation from the Sun at frequencies higher than 30 GHz resembles the radiation of a blackbody at a temperature of about 6,000K. At lower frequencies the brightness temperature may be as high as  $10^{10}$  K and depends on the activity of the Sun. When the Sun is active and there are plenty of sunspots, there are variations in the intensity of radiation. The sunspots are a source of slow variations and the flares are a source of rapid variations.

The planets and the Moon radiate almost as a blackbody. Jupiter is an exception: Below microwave frequencies it radiates more than a blackbody at the same temperature. The intensity of Jupiter's radiation varies in a complicated manner and is related to the position of its moon Io. Before the time of spacecraft, planets were studied using radar techniques. For example, the rotation times of Mercury and cloud-covered Venus were determined with radar in the 1960s. The surface of Venus was mapped more accurately in the beginning of the 1990s with SAR on the Magellan spacecraft. The rings of Saturn, its moon Titan, and asteroids have also been studied with radar.

Gas and molecular clouds, remnants of supernovas, and pulsars are radio sources in our galaxy. The continuum radiation of the Milky Way consists of synchrotron radiation and thermal radiation from ionized hydrogen. The synchrotron radiation dominates at frequencies lower than about 1 GHz and the thermal radiation at higher frequencies.

At 1,420 MHz ( $\lambda = 21$  cm) interstellar neutral hydrogen emits a spectral line, which has been used to map the structure of the Milky Way. By measuring radial velocities of hydrogen clouds in different directions using the Doppler shift, it has been concluded that we live in a spiral galaxy. Even the center of the Milky Way can be studied using radio waves, which penetrate through dust clouds.

In addition to hydrogen, many different molecules, both inorganic and organic, have been observed in interstellar clouds, in which new stars are born. More than 80 different molecules have been found, the most complicated of which has 13 atoms [14]. The line spectra of molecules are produced by changes in the rotational energy states and occur at millimeter and submillimeter wavelengths. Lines may be either emission or absorption lines. An absorption line is produced when a cloud absorbs a narrow band of frequencies from continuum radiation coming from background. The measurement of

the spectral lines reveals the distribution of molecules and dynamics of clouds. Figure 12.30 shows a measured spectrum of a molecular cloud in Orion [15].

Pulsars, originally called pulsating stars, are swiftly rotating neutron stars. They emit radiation in two narrow beams that sweep space like the beams from a lighthouse. The periods of short pulses received from pulsars range from one-thousandth of a second to a few seconds. The periods are very stable but are in some cases increasing as the neutron star slows down.

Radio galaxies and quasars (quasistellar objects) are radio sources outside our galaxy. The nearest normal galaxies have been mapped using radio waves. The radio emission of an ordinary galaxy is only a small fraction of its optical emission. In radio galaxies, the intensities of radio and optical emissions are of the same order. Quasars look like point sources. Their optical spectra show such large red shifts or recession velocities that the most distant quasars must be located near the edge of the known universe, or they are seen as they looked in the early universe. The intensities of both optical and radio emissions change with periods as small as one day, indicating that the quasars are small. The huge radiation of such a small object can be explained only by assuming that matter is falling down a black hole.

## 12.9 Sensors for Industrial Applications

Microwaves can be used for many kinds of measurements in industry [16–19]. The electrical properties of matter determine how radio waves propagate in it and reflect from interfaces. Electrical properties in turn depend on physical properties such as moisture, density, composition, and temperature. The

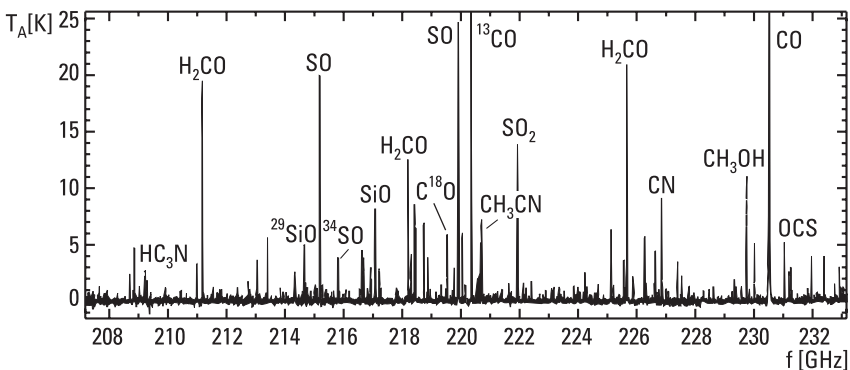


**Figure 12.30** Spectral lines of an interstellar molecular cloud. (After: [15].)

advantages of microwave sensors are that measurements can be carried out without touching the object and that microwaves penetrate into the material. Different types of sensors and their applicability are treated here.

### 12.9.1 Transmission Sensors

A typical transmission sensor has two horn antennas, a transmitter, and a receiver. Waves pass through the object placed between the antennas. The phase shift due to the change in propagation velocity and the attenuation due to loss in the material are measured. Transmission sensors are simple and can be used for the measurement of materials moving on a conveyor belt, for example, or in a large tube. They are used to measure the moisture content of grain, coal, sand, and so on.

### 12.9.2 Resonators

A microwave resonator may be a cavity, strip-line, slot-line, parallel-wire line, or coaxial-line resonator. Resonators based on a slot or parallel-wire line may be used to measure liquid, granular, or pasty materials. Strip-line resonators are suitable for measuring sheets and material layers. Cavity resonators may be used as gas analyzers and to measure bars and materials flowing in tubes. Resonators may be used for many kinds of measurements: the moisture content of paper (see Figure 12.31), veneer, and air, the thickness of paper mass, the fiber orientation in paper, the thickness of plastic bars

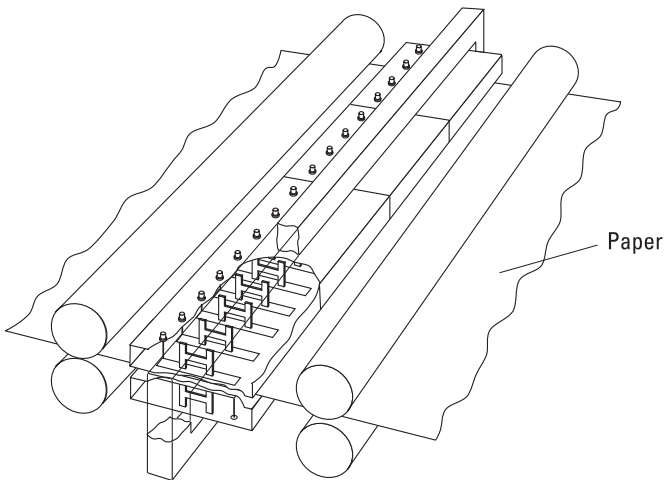


**Figure 12.31** Strip-line resonator array for measuring paper moisture profile. (After: [17].)

and metal sheets, the burning energy value of peat, the water content of snow, and so on.

### 12.9.3 Reflection Sensors

The complex reflection coefficient of an object depends on the relative permittivity  $\epsilon_r$  and its distribution within a few skin depths from the surface. If the object is layered, the thickness and permittivity of the layers may be solved from the frequency response of the reflection coefficient. An open end of a coaxial cable or waveguide, which is pressed on the surface of the object, is a simple reflection sensor. The reflection coefficient depends on the end capacitance and conductance, which in turn are functions of  $\epsilon_r$ . Measurement of ground moisture and testing of materials are applications of reflection sensors.

### 12.9.4 Radar Sensors

Radar sensors can measure the amplitude of reflection, propagation time, or Doppler shift. Applications of radar sensors are numerous: door openers, movement detectors in burglar alarms, surface height detectors in vessels (applicable also when there is danger of explosion or foam on the surface), measuring power line vibrations, detecting rot in trees (see Figure 12.32), detecting pipes, cables, ancient relics, and mines in the ground, measuring marsh depth, and more.

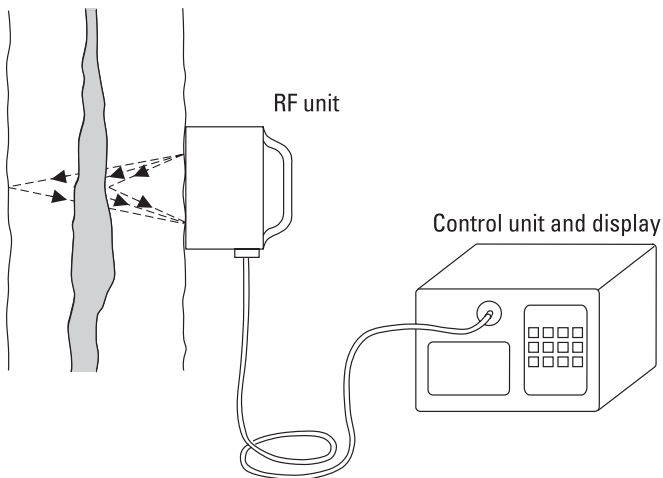


**Figure 12.32** Impulse radar used to measure rot in trees.

### 12.9.5 Radiometer Sensors

Radiometer sensors provide information on the physical temperature and emissivity of an object. If one is known, the other may be found from the measured brightness temperature. A radiometer can make measurements through steam and smoke. By measuring also the reflection coefficient, the accuracy can be improved. The depth profile of temperature may be obtained by using several frequencies.

### 12.9.6 Imaging Sensors

In microwave tomography, the changes in amplitude and phase distribution caused by the object are measured as shown in Figure 12.33. The three-dimensional distribution of the permittivity may then be determined. In microwave holography, the shape of the object is resolved by measuring the scattered field. Imaging sensors can be used to search for objects in the ground, inside ceilings, or in security inspections.

## 12.10 Power Applications

Radio waves can be used for heating lossy materials. Often losses are caused by polar molecules such as water molecules, which the electric field turns back and forth. In many dielectric materials  $\mu'' = 0$  and  $\sigma = 0$ , and according to (2.99) the power absorbed is

$$P = \frac{\omega}{2} \int_V \epsilon'' \mathbf{E} \cdot \mathbf{E}^* dV = \frac{\omega}{2} \int_V \epsilon'' |E|^2 dV \quad (12.28)$$

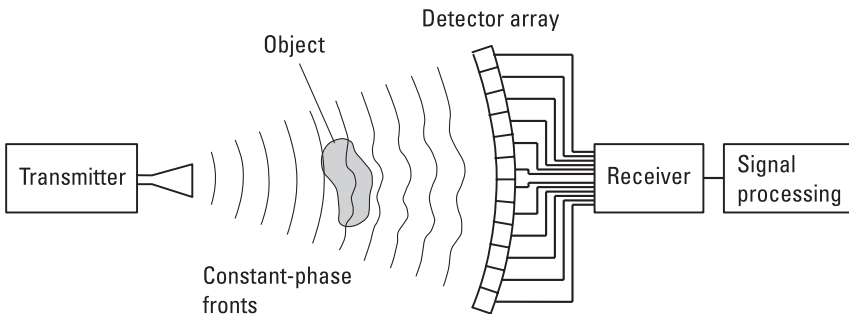


**Figure 12.33** Measurement of permittivity distribution using microwave tomography. (After: [16].)

where  $E$  is the electric field within the material. Figure 12.34 shows how the electric field  $E$  inside bodies of different shapes is related to the field  $E_0$  in the surrounding air.

Frequencies of 27 MHz and 2.45 GHz are allocated for power applications in Europe. Microwave ovens in the 2.45-GHz range are the most common power application. The oven shown in Figure 12.35 is a large cavity resonator within which many resonance modes are excited to realize a field that is as even as possible. The household ovens have a magnetron oscillator and their power is typically 600W to 1,000W. In industry, radio-frequency power is used to dry lumber, bake bread, vulcanize rubber, seam plastic, dry concrete, and so on.

## 12.11 Medical Applications

Radio waves are used in thermography, diathermy, and hyperthermia. Diathermy and hyperthermia are based on the absorption of radio-frequency

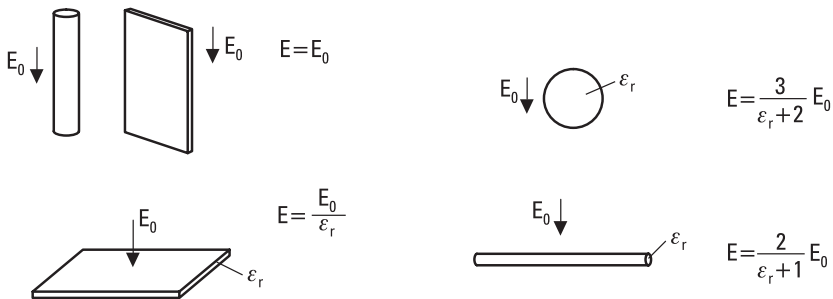


**Figure 12.34** Electric field  $E$  inside bodies of different shapes.  $E_0$  is electric field in the surrounding air.

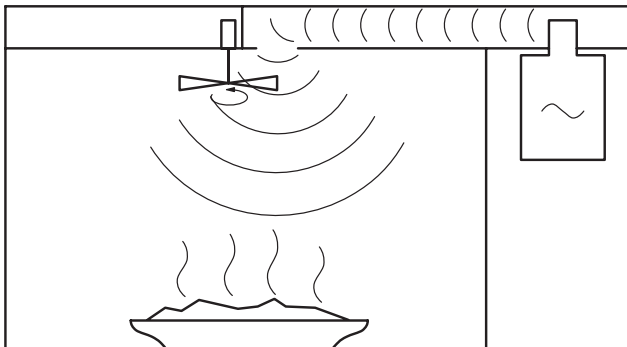


**Figure 12.35** Microwave oven.



energy by a tissue, whereas in thermography, the thermal emission of the tissue is measured.

### 12.11.1 Thermography

According to Planck's law, the maximum intensity of thermal radiation is at infrared wavelengths if the temperature of a blackbody is 310K, the temperature of a human being. However, a human being can easily be detected with a microwave radiometer also. At microwaves, the human body is a gray object: at 3 GHz the emissivity of skin is about 0.5 and at 30 GHz over 0.9 [20].

The skin depth  $\delta_s$  given in (2.69) is a measure of how deep the waves penetrate into the material. At a depth of  $\delta_s$  from the surface, the field has attenuated by a factor of  $e$  from its original value at the surface. Correspondingly, the skin depth determines from how deep the thermal radiation of the tissue can be detected. The skin depth depends on the frequency and electric properties of the material. In bone and fatty tissue, water content is low and, thus, the skin depth is large. Muscles and skin have much higher water content and smaller skin depth, as shown in Figure 12.36 [21].

Thermography offers a noninvasive technique for early detection of cancer. A tumor having a temperature 1°C to 5°C higher than its surround-

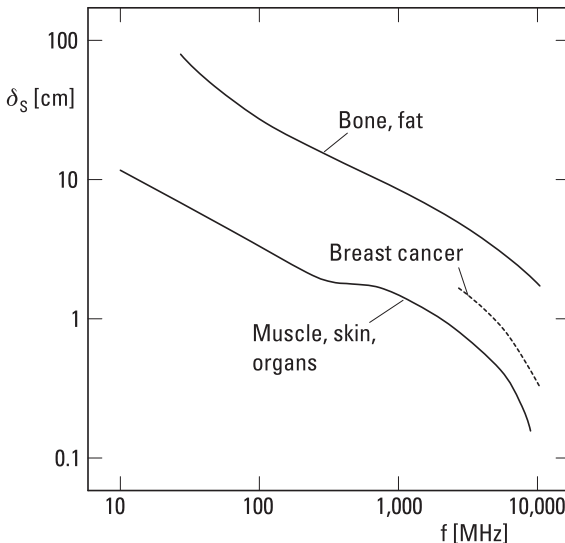


**Figure 12.36** Skin depth for different tissues. (After: [21].)

ings can be detected with a microwave radiometer if the tumor is close enough to the surface. At RF a tumor can be detected from a depth of a few centimeters; at microwave frequencies a tumor can be detected only if it is on the skin or just below it. The antenna of the radiometer may be a large focusing antenna or a contact antenna pressed on the skin.

### 12.11.2 Diathermy

In diathermy, the temperature of a tissue or body is elevated by radio-frequency energy. Frequencies for diathermy are 27 MHz and 2.45 GHz. The temperature of the tissue is raised to between 39°C and 45°C. Higher temperatures, which kill cells, must be avoided. The power density may be 100 to 1,000 mW/cm<sup>2</sup>. The power is focused to a restricted area and sensitive parts of body, such as eyes, are protected. Raising the temperature has many positive effects: Blood vessels become distended and circulation quickens, muscles relax, the threshold of pain gets higher, the stretching ability of a connective tissue increases, the penetration ability of cell membranes increases, and metabolism and enzyme reactions speed up. Diathermy is used for relieving muscle tension and as a pretreatment for physical therapy.

### 12.11.3 Hyperthermia

Microwave hyperthermia is used to treat cancer. A tissue containing a tumor is heated without destroying the healthy cells surrounding the tumor. This is possible because at 41°C to 45°C the cancer cells are destroyed more readily than the healthy cells [22]. Because the power density is high (1 W/cm<sup>2</sup>) and the skin absorbs well, a burn may arise in the skin on top of the tumor. To be able to focus the energy into the tumor, microwave frequencies have to be used.

## 12.12 Electronic Warfare

Radar and wireless communication have many important military applications. There are also many other ways to utilize radio engineering techniques or knowledge for military purposes: jamming enemy communication and radar, stealth technology, signal intelligence, and so on. These applications go under the name *electronic warfare* (EW). Electronic warfare can be defined as military action involving the use of electromagnetic energy to determine, exploit, reduce, or prevent the use of the electromagnetic spectrum by the

enemy, and as action that retains effective use of this spectrum, but sometimes also as military action where an electromagnetic weapon is used against personnel. EW is divided into three categories:

- *Electronic support* (ES), formerly *EW support measures* (ESM);
- *Electronic attack* (EA), formerly *electronic countermeasures* (ECM);
- *Electronic protection* (EP), formerly *electronic counter-countermeasures* (ECCM).

### 12.12.1 ES

ES is defined as actions taken to search for, intercept, locate, record, and analyze radiated electromagnetic energy for the purpose of exploiting it in support of military operations, especially for the purpose of immediate threat recognition. ES involves *signal intelligence* (SIGINT), which is divided into *electronics intelligence* (ELINT) and *communications intelligence* (COMINT). Detection, identification, evaluation, and location of foreign electromagnetic radiation from radar, communication radios, and so on are called electronic reconnaissance.

In ELINT wideband monitoring receivers covering, typically, frequency ranges from 20 to 500 MHz and from 0.5 to 40 GHz, as well as omnidirectional or rotating antennas are used to detect the presence of a radar signal. A high-gain steerable antenna is used to find the rough direction of the signal source. The signal is then analyzed and characterized using a sophisticated channelized receiver and analyzer, and compared to known radar signals in a signal library. Direction-finding antenna systems consisting of an array of antenna elements and utilizing, for example, interferometric or *time difference of arrival* (TDOA) techniques, are used at several receiving sites in order to locate the transmitting radar. Similarly, in COMINT communication signals in the HF, VHF, and UHF ranges are characterized and their sources located.

### 12.12.2 EA

EA is a division of EW involving actions taken to prevent or reduce an enemy's effective use of the electromagnetic spectrum by either passive or active means. EA involves, for example, radar or communication link jamming, high-power *electromagnetic pulse* (EMP), stealth technology, and the use of chaff to make fake radar targets.

Active EA involves jamming, high-power microwave weapons, and EMP. Jamming is deliberate radiation of wideband RF noise for the purpose

of preventing or reducing an enemy's effective use of radar or communication link. The high-power microwave weapon or electromagnetic weapon is a class of *directed energy weapons* (DEW), and it is any device that can produce a directed microwave field of such intensity that targeted items of electronic equipment experience damage. EMP is often related to the electromagnetic radiation from a nuclear explosion, but it may also be caused by non-nuclear means, such as radio equipment; the resulting strong electric and magnetic fields may damage electronic systems.

Passive EA includes the use of chaff or decoys and stealth technology. Chaff is highly microwave-reflective material, such as sections of thin metallic stripes or wires with a resonant length, dispensed over a large volume to present a false radar target in order to protect a battleship or aircraft. A decoy is a passive dummy target or a radio repeater that appears as a false radar target. Stealth technology is used to reduce the radar cross section of an aircraft, ship, or ground facility by shaping the object and covering its surfaces with layers of absorbing composite materials.

### 12.12.3 EP

This division of EW involves actions taken to ensure effective use of the electromagnetic spectrum despite the enemy's use of electronic warfare by protecting equipment and facilities. EP involves technologies, such as shielding, that make electronic equipment robust against jamming, electromagnetic weapons, and EMP.

## References

- [1] Sehm, T., A. Lehto, and A. Räsänen, "A High-Gain 58-GHz Box-Horn Array Antenna with Suppressed Grating Lobes," *IEEE Trans. on Antennas and Propagation*, Vol. 47, No. 7, 1999, pp. 1125–1130.
- [2] Prasad, R., *CDMA for Wireless Personal Communications*, Norwood, MA: Artech House, 1996.
- [3] Gibson, J. D., (ed.), *The Mobile Communications Handbook*, New York: IEEE Press, 1996.
- [4] Lee, W. C. Y., *Mobile Communications Engineering: Theory and Applications*, 2nd ed., New York: McGraw-Hill, 1998.
- [5] Rappaport, T. S., *Wireless Communications, Principles, and Practice*, Upper Saddle River, NJ: Prentice Hall, 1996.
- [6] Holma, H., and A. Toskala, (eds.), *WCDMA for UMTS, Radio Access for Third Generation Mobile Communications*, Chichester, England: John Wiley & Sons, 2000.

- [7] Kayton, M., (ed.), *Navigation: Land, Sea, Air, & Space*, New York: IEEE Press, 1990.
- [8] Skolnik, M. I., *Introduction to Radar Systems*, 2nd ed., New York: McGraw-Hill, 1981.
- [9] Ulaby, F. T., R. K. Moore, and A. K. Fung, *Microwave Remote Sensing, Vol. I, Microwave Remote Sensing Fundamentals and Radiometry*, Reading, MA: Addison-Wesley, 1981.
- [10] Ulaby, F. T., R. K. Moore, and A. K. Fung, *Microwave Remote Sensing, Vol. II, Radar Remote Sensing and Surface Scattering and Emission Theory*, Reading, MA: Addison-Wesley, 1982.
- [11] Ulaby, F. T., R. K. Moore, and A. K. Fung, *Microwave Remote Sensing, Vol. III, From Theory to Applications*, Dedham, MA: Artech House, 1986.
- [12] Kraus, J. D., *Radio Astronomy*, 2nd ed., Powell, OH: Cygnus-Quasar Books, 1986.
- [13] Kraus, J. D., and R. J. Marhefka, *Antennas for All Applications*, 3rd ed., New York: McGraw-Hill, 2002.
- [14] Payne, J. M., "Millimeter and Submillimeter Wavelength Radio Astronomy," *Proc. of the IEEE*, Vol. 77, No. 7, 1989, pp. 993–1017.
- [15] Phillips, T. G., and J. Keene, "Submillimeter Astronomy," *Proc. of the IEEE*, Vol. 80, No. 11, 1992, pp. 1662–1678.
- [16] Nyfors, E., and P. Vainikainen, *Industrial Microwave Sensors*, Norwood, MA: Artech House, 1989.
- [17] Fischer, M., P. Vainikainen, and E. Nyfors, "Dual-Mode Stripline Resonator Array for Fast Error Compensated Moisture Mapping of Paper Web," *1990 IEEE MTT-S International Microwave Symposium Digest*, 1990, pp. 1133–1136.
- [18] Fischer, M., P. Vainikainen, and E. Nyfors, "Design Aspects of Stripline Resonator Sensors for Industrial Applications," *Journal of Microwave Power and Electromagnetic Energy*, Vol. 30, No. 4, 1995, pp. 246–257.
- [19] Toropainen, A. P., "New Method for Measuring Properties of Nonhomogeneous Materials by a Two-Polarization Forward-Scattering Measurement," *IEEE Trans. on Microwave Theory and Techniques*, Vol. 41, No. 12, 1993, pp. 2081–2086.
- [20] Edrich, J., "Centimeter- and Millimeter-Wave Thermography—A Survey on Tumor Detection," *The Journal of Microwave Power*, Vol. 14, No. 2, 1979, pp. 95–103.
- [21] Myers, P. C., N. L. Sadowsky, and A. H. Barrett, "Microwave Thermography: Principles, Methods and Clinical Applications," *The Journal of Microwave Power*, Vol. 14, No. 2, 1979, pp. 105–113.
- [22] Storm, F., "Hyperthermia," *Proc. of the IEEE MTT-S International Microwave Symposium*, 1981, pp. 474–475.

# 13

## Biological Effects and Safety Standards

RF radiation does not ionize molecules in biological tissue, because the energy quantum  $hf$  is only 4 meV at 1 THz, while the minimum energy to ionize those molecules is about 12 eV. Therefore, according to the information and understanding of today, RF radiation cannot cause mutations leading to, for example, cancer. However, RF radiation may have other hazards: So-called thermal hazards are known for sure.

The biological effects of RF radiation have been studied through experiments with animals and models, and through epidemiological research. Effects may be divided into two classes: thermal effects and nonthermal effects [1]. Firmly observed thermal effects are the following:

- Cataracts;
- Increase of tissue temperature (see diathermy and hyperthermia in Section 12.11);
- Burns.

In addition, heat is known to weaken sperm, so this is also a possible side effect of strong RF radiation. Furthermore, RF radiation is suspected of causing instability in blood pressure and pulse rate, and changes in breathing due to thermal effects.

Nonthermal effects are subjective (like sensitivity to electricity) and include headache, tiredness, insomnia, irritation, weak appetite, loss of

memory, and so on. The origin of these effects is not known, neither are they unambiguously proven.

Dosimetry is a field of research studying how radiation is absorbed into a tissue. The absorption of RF radiation depends on the skin depth  $\delta_s$  of the tissue, on the size of the object in wavelengths, and on the polarization of radiation [2, 3]. Depending on whether the electric field, the magnetic field, or the propagation vector of the incident wave is parallel to the longitudinal axis of the object, the polarization is said to be E-, H-, or k-polarization.

To measure absorption we use the specific absorption rate (SAR), which has a unit of watts per kilogram. The SAR depends strongly on the size of the object. According to model measurements, the SAR on E-polarization of an average-sized person is as shown in Figure 13.1 [4]. At 70 MHz there is a strong resonance. Various parts of the body have their own resonance frequencies; the human head has a resonance at about 400 MHz. Because of resonance and depending on the tissue type, hot spots may appear in the human body exposed to RF radiation; however, these hot spots are not very pronounced due to high losses in the human body.

In practice, nearly all human beings are exposed to RF radiation from, for example, mobile phones [5]. A person in a certain profession may be exposed to a considerably higher power density. The industrial personnel working with RF heaters or dryers is a good example of this. A faulty

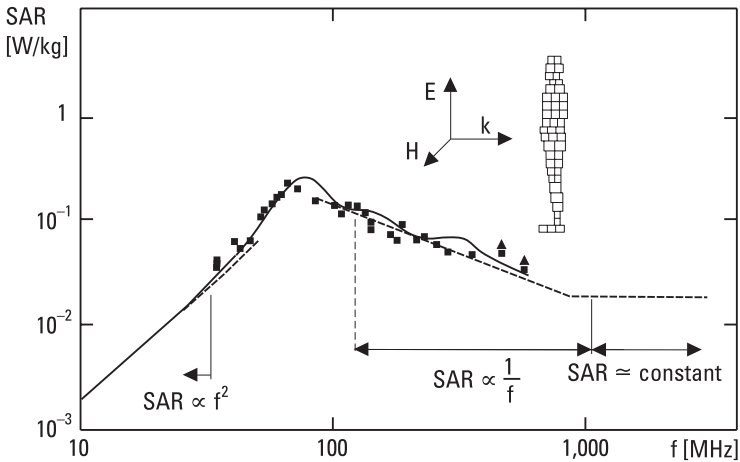


**Figure 13.1** Average SAR in plane wave conditions with power density of  $10 \text{ W/m}^2$  calculated using a block model of size of an average human being. Measurement points are obtained with experimental models with human shape but artificial tissues. (After: [4].)

microwave oven may expose its user to a high RF radiation dose. However, we do not know any incidence where a person has been permanently harmed by leakage radiation from a microwave oven. When an oven is mechanically damaged, however, its leakage radiation should be checked before the oven is used.

We consider harmless all the appliances that have maximum power below 100 mW. Table 13.1 lists typical sources of RF radiation.

Most countries use both national and international safety standards. The standards set limits on RF radiation power density or field strengths to which people in the general public and specific personnel dealing with strong RF radiation sources may be exposed.

In 1998 the *International Commission on Non-Ionizing Radiation Protection* (ICNIRP) developed new guidelines for limiting exposure to time-varying electric, magnetic, and electromagnetic fields [6], based on which

**Table 13.1**  
Sources of RF Radiation in Finland

Source	Frequency (MHz)	Max. Average Power	Application
RF heater/dryer	13.56	250 kW	Drying glue
	27.12	25 kW	
Diathermy equipment	27.12	500W	Diathermy
MRI equipment	1–100	100W	MR imaging, diagnostics
MF broadcasting station	0.525–1.605	600 kW	Radio broadcasting
HF broadcasting station	5.95–26.1	500 kW	Radio broadcasting
FM broadcasting station	87.5–108	50 kW	Radio broadcasting
VHF broadcasting station	174–230	8 kW	TV broadcasting
UHF broadcasting station	470–790	16 kW	TV broadcasting
Mobile base station	450	320W	Mobile
	900	80W	communications
	1,800	50W	
Radar	1,200	2 kW	Air and sea surveillance,
	3,000		military
	9,000		applications, meteorology
Microwave oven	2,450	1,500W	Cooking
Microwave dryer	2,450	5 kW	For example, drying of concrete
Microwave heater	2,450	50 kW	Drying of materials



the Commission of the European Union in 1999 issued a directive concerning limiting acceptable exposure to electromagnetic fields to between 0 Hz and 300 GHz. Table 13.2 provides these limits. It is worth noticing that, because of the human body's resonance, the frequency range from 10 to 400 MHz is considered more harmful than other frequency ranges. In Finland, the Radiation and Nuclear Safety Authority supervises the safety of RF equipment.

**Table 13.2**

Limits of Exposure to RF Radiation as Electric and Magnetic Field Strengths and as Equivalent Power Densities (Frequency  $f$  Must Be Introduced in Megahertz)

Frequency Range	Electric Field [V/m]	Magnetic Field [A/m]	Equivalent Power Density [ $\text{W}/\text{m}^2$ ]
3–150 kHz	87	5	—
0.15–1 MHz	87	$0.73/f$	—
1–10 MHz	$87/f^{1/2}$	$0.73/f$	—
10–400 MHz	28	0.073	2
400–2,000 MHz	$1.375f^{1/2}$	$0.0037f^{1/2}$	$f/200$
2–300 GHz	61	0.16	10

Source: [6].

## References

- [1] Johnson, C., and A. Guy, "Nonionizing Electromagnetic Wave Effects in Biological Materials and Systems," *Proc. of the IEEE*, Vol. 60, No. 6, 1972, pp. 692–718.
- [2] Durney, C., "Electromagnetic Dosimetry for Models of Humans and Animals: A Review of Theoretical and Numerical Techniques," *Proc. of the IEEE*, Vol. 68, No. 1, 1980, pp. 33–39.
- [3] Gandhi, O., "State of the Knowledge for Electromagnetic Absorbed Dose in Man and Animals," *Proc. of the IEEE*, Vol. 68, No. 1, 1980, pp. 24–32.
- [4] Hagmann, M. J., O. P. Gandhi, and C. H. Durney, "Numerical Calculation of Electromagnetic Energy Deposition for a Realistic Model of Man," *IEEE Trans. on Microwave Theory and Techniques*, Vol. MTT-27, No. 9, 1979, pp. 804–809.
- [5] Jokela, K., et al., "Radiation Safety of Handheld Mobile Phones and Base Stations," Radiation and Nuclear Safety Authority of Finland, STUK-A161, 1999.
- [6] International Commission on Non-Ionizing Radiation Protection (ICNIRP), "Guidelines for Limiting Exposure to Time-Varying Electric, Magnetic, and Electromagnetic Fields (Up to 300 GHz)," *Health Physics*, Vol. 74, No. 4, 1998, pp. 494–522.

# Appendix A: Vector Operations

$$\nabla(fg) = f\nabla g + g\nabla f$$

$$\nabla \cdot (f\mathbf{A}) = \mathbf{A} \cdot \nabla f + f\nabla \cdot \mathbf{A}$$

$$\nabla \cdot (\mathbf{A} \times \mathbf{B}) = \mathbf{B} \cdot (\nabla \times \mathbf{A}) - \mathbf{A} \cdot (\nabla \times \mathbf{B})$$

$$\nabla \times (f\mathbf{A}) = (\nabla f) \times \mathbf{A} + f\nabla \times \mathbf{A}$$

$$\nabla \times (\mathbf{A} \times \mathbf{B}) = \mathbf{A}\nabla \cdot \mathbf{B} - \mathbf{B}\nabla \cdot \mathbf{A} + (\mathbf{B} \cdot \nabla)\mathbf{A} - (\mathbf{A} \cdot \nabla)\mathbf{B}$$

$$\nabla(\mathbf{A} \cdot \mathbf{B}) = (\mathbf{A} \cdot \nabla)\mathbf{B} + (\mathbf{B} \cdot \nabla)\mathbf{A} + \mathbf{A} \times (\nabla \times \mathbf{B}) + \mathbf{B} \times (\nabla \times \mathbf{A})$$

$$\nabla \cdot \nabla f = \nabla^2 f$$

$$\nabla \cdot \nabla \times \mathbf{A} = 0$$

$$\nabla \times \nabla f = 0$$

$$\nabla \times \nabla \times \mathbf{A} = \nabla(\nabla \cdot \mathbf{A}) - \nabla^2 \mathbf{A}$$

Gauss' theorem  $\oint_S \mathbf{A} \cdot d\mathbf{S} = \int_V \nabla \cdot \mathbf{A} \, dV$

Stokes' theorem  $\oint_{\Gamma} \mathbf{A} \cdot d\mathbf{l} = \int_S (\nabla \times \mathbf{A}) \cdot d\mathbf{S}$

In rectangular coordinate system

$$\nabla f = \mathbf{u}_x \frac{\partial f}{\partial x} + \mathbf{u}_y \frac{\partial f}{\partial y} + \mathbf{u}_z \frac{\partial f}{\partial z}$$

$$\nabla^2 f = \frac{\partial^2 f}{\partial x^2} + \frac{\partial^2 f}{\partial y^2} + \frac{\partial^2 f}{\partial z^2}$$

$$\nabla \cdot \mathbf{A} = \frac{\partial A_x}{\partial x} + \frac{\partial A_y}{\partial y} + \frac{\partial A_z}{\partial z}$$

$$\nabla \times \mathbf{A} = \mathbf{u}_x \left( \frac{\partial A_z}{\partial y} - \frac{\partial A_y}{\partial z} \right) + \mathbf{u}_y \left( \frac{\partial A_x}{\partial z} - \frac{\partial A_z}{\partial x} \right) + \mathbf{u}_z \left( \frac{\partial A_y}{\partial x} - \frac{\partial A_x}{\partial y} \right)$$

$$\nabla^2 \mathbf{A} = \mathbf{u}_x \nabla^2 A_x + \mathbf{u}_y \nabla^2 A_y + \mathbf{u}_z \nabla^2 A_z$$

In cylindrical coordinate system

$$\nabla f = \mathbf{u}_\rho \frac{\partial f}{\partial \rho} + \mathbf{u}_\phi \frac{1}{\rho} \frac{\partial f}{\partial \phi} + \mathbf{u}_z \frac{\partial f}{\partial z}$$

$$\nabla^2 f = \frac{1}{\rho} \frac{\partial}{\partial \rho} \left( \rho \frac{\partial f}{\partial \rho} \right) + \frac{1}{\rho^2} \frac{\partial^2 f}{\partial \phi^2} + \frac{\partial^2 f}{\partial z^2}$$

$$\nabla \cdot \mathbf{A} = \frac{1}{\rho} \frac{\partial}{\partial \rho} (\rho A_\rho) + \frac{1}{\rho} \frac{\partial A_\phi}{\partial \phi} + \frac{\partial A_z}{\partial z}$$

$$\nabla \times \mathbf{A} = \mathbf{u}_\rho \left( \frac{1}{\rho} \frac{\partial A_z}{\partial \phi} - \frac{\partial A_\phi}{\partial z} \right) + \mathbf{u}_\phi \left( \frac{\partial A_\rho}{\partial z} - \frac{\partial A_z}{\partial \rho} \right) + \mathbf{u}_z \frac{1}{\rho} \left[ \frac{\partial (\rho A_\phi)}{\partial \rho} - \frac{\partial A_\rho}{\partial \phi} \right]$$

In spherical coordinate system

$$\nabla f = \mathbf{u}_r \frac{\partial f}{\partial r} + \mathbf{u}_\theta \frac{1}{r} \frac{\partial f}{\partial \theta} + \mathbf{u}_\phi \frac{1}{r \sin \theta} \frac{\partial f}{\partial \phi}$$

$$\nabla^2 f = \frac{1}{r^2} \frac{\partial}{\partial r} \left( r^2 \frac{\partial f}{\partial r} \right) + \frac{1}{r^2 \sin \theta} \frac{\partial}{\partial \theta} \left( \sin \theta \frac{\partial f}{\partial \theta} \right) + \frac{1}{r^2 \sin^2 \theta} \frac{\partial^2 f}{\partial \phi^2}$$

$$\begin{aligned}\nabla \cdot \mathbf{A} &= \frac{1}{r^2} \frac{\partial}{\partial r} (r^2 A_r) + \frac{1}{r \sin \theta} \frac{\partial}{\partial \theta} (\sin \theta A_\theta) + \frac{1}{r \sin \theta} \frac{\partial A_\phi}{\partial \phi} \\ \nabla \times \mathbf{A} &= \frac{\mathbf{u}_r}{r \sin \theta} \left[ \frac{\partial}{\partial \theta} (\sin \theta A_\phi) - \frac{\partial A_\theta}{\partial \phi} \right] + \frac{\mathbf{u}_\theta}{r} \left[ \frac{1}{\sin \theta} \frac{\partial A_r}{\partial \phi} - \frac{\partial}{\partial r} (r A_\phi) \right] \\ &\quad + \frac{\mathbf{u}_\phi}{r} \left[ \frac{\partial}{\partial r} (r A_\theta) - \frac{\partial A_r}{\partial \theta} \right]\end{aligned}$$



# Appendix B: Physical Constants and Material Parameters

## Physical Constants

Name	Symbol	Value
Speed of light in vacuum	$c$	299,792,458 m/s
Permittivity of vacuum	$\epsilon_0$	$8.854 \times 10^{-12}$ As/Vm
Permeability of vacuum	$\mu_0$	$4\pi \times 10^{-7}$ Vs/Am
Wave impedance in vacuum	$\eta$	376.7 $\Omega$
Boltzmann's constant	$k$	$1.381 \times 10^{-23}$ J/K
Planck's constant	$h$	$6.626 \times 10^{-34}$ Js
Charge of electron (magnitude)	$e$	$1.602 \times 10^{-19}$ As
Mass of electron	$m_e$	$9.109 \times 10^{-31}$ kg

## Conductivity of Some Materials at 20°C

Material	$\sigma$ [S/m]
Aluminum	$3.8 \times 10^7$
Brass (66% Cu, 34% Zn)	$2.6 \times 10^7$
Copper	$5.8 \times 10^7$
Germanium	2.2
Glass	$10^{-12}$
Gold	$4.1 \times 10^7$
Iron	$1.0 \times 10^7$
Nickel	$1.4 \times 10^7$
Porcelain	$2 \times 10^{-13}$
Quartz	$1.3 \times 10^{-18}$
Seawater	4
Silicon	$1.2 \times 10^3$
Silver	$6.2 \times 10^7$
Tin	$8.8 \times 10^6$
Water, distilled	$2 \times 10^{-4}$

## Dielectric Constant (Relative Permittivity) of Some Materials (at 10 GHz If Not Otherwise Stated)

Material	$\epsilon_r$	$\tan \delta$
Alumina (Al <sub>2</sub> O <sub>3</sub> )	9.7	$2 \times 10^{-4}$
RT/duroid®5880	2.20	$9 \times 10^{-4}$
RT/duroid®6010LM	10.2	$2.3 \times 10^{-3}$
Gallium arsenide	13.0	$6 \times 10^{-4}$
Glass	4–10	$2 \times 10^{-3}$ – $2 \times 10^{-2}$
Ice (fresh water)	3–4	$10^{-3}$
Polyethylene	2.3	$10^{-3}$
Polystyrene	2.54	$5 \times 10^{-4}$
Porcelain	5.5	$1.5 \times 10^{-2}$
Quartz (fused)	3.78	$10^{-4}$
Sapphire	$\epsilon_\rho = 9.4, \epsilon_z = 11.6$	$10^{-4}$
Seawater (20°C)	54	0.7
Seawater (1 GHz, 20°C)	69	1.4
Silicon	11.9	$10^{-3}$ – $10^{-2}$
Styrox	1.05	
Teflon	2.06	$3 \times 10^{-4}$
Water, distilled (20°C)	60	0.5
Water, distilled (1 GHz, 20°C)	80	0.06

# List of Acronyms

ac	alternating current
ADC	analog-to-digital converter
AGC	automatic gain control
AM	amplitude modulation
AMPS	Advanced Mobile Phone System
AOS	acousto-optical spectrometer
ASK	amplitude-shift keying
AuC	authentication center
AWGN	additive white Gaussian noise
BAW	bulk acoustic wave
BER	bit error rate
BiCMOS	bipolar complementary metal-oxide-semiconductor
BSC	base station controller
BSS	broadcasting satellite service
BTS	base transceiver station
CAD	computer-aided design
CCIR	Comité Consultatif International des Radiocommunications; International Radio Consultative Committee
CDMA	code division multiple access
CEPT	Conference Européenne des Administration des Postes et des Telecommunications; European Conference of Postal and Telecommunications Administrations
CMOS	complementary metal-oxide-semiconductor
COBE	Cosmic Background Explorer



COFDM	coded orthogonal frequency division multiplex
COMINT	communications intelligence
CW	continuous wave
DAB	digital audio broadcasting
DAC	digital-to-analog converter
dc	direct current
DCS	Digital Cellular System
DDS	direct digital synthesis
DECT	Digital European Cordless Telecommunications
DEW	directed energy weapon
DGFET	dual-gate field-effect transistor
DGPS	differential GPS
DME	Distance Measuring Equipment
DPSK	differential phase-shift keying
DRO	dielectric resonator oscillator
DSB	double sideband
DSBSC	double-sideband suppressed carrier
DSSS	direct sequence spread spectrum
DVB	digital video broadcasting
EA	electronic attack
ECCM	electronic counter-countermeasures
ECM	electronic countermeasures
EDGE	Enhanced Data Rates for GSM Evolution
EHF	extremely high frequency
EIR	equipment identity register
EIRP	equivalent isotropic radiated power
ELINT	electronics intelligence
EMC	electromagnetic compatibility
EMP	electromagnetic pulse
ENVISAT	Environment Satellite
EP	electronic protection
ERS	European Remote Sensing Satellite
ES	electronic support
ESA	European Space Agency
ESM	electronic support measures
ETSI	European Telecommunications Standards Institute
EUTELSAT	European Telecommunications Satellite Organization
EW	electronic warfare
FDM	frequency division multiplexing

---

FDMA	frequency division multiple access
FET	field-effect transistor
FHSS	frequency hopping spread spectrum
FM	frequency modulation
FSK	frequency-shift keying
FSS	fixed satellite service
GEO	geosynchronous Earth orbit
GLONASS	Global Navigation Satellite System
GMSK	Gaussian minimum shift keying
GPRS	General Packet Radio Service
GPS	Global Positioning System
GSM	Global System for Mobile Communications (formerly Groupe Spécial Mobile)
HALCA	Highly Advanced Laboratory for Communication and Astronomy
HBT	heterojunction bipolar transistor
HEMT	high electron mobility transistor
HF	high frequency
HFET	heterostructure field-effect transistor = HEMT
HiperLAN	High-Performance Radio Local Area Network
HLR	home location register
HSCSD	High Speed Circuit Switched Data
ICNIRP	International Commission on Non-Ionizing Radiation Protection
IEEE	Institute of Electrical and Electronics Engineers
IF	intermediate frequency
IFRB	International Frequency Registration Board
ILS	Instrument Landing System
IMPATT	impact-ionization avalanche transit time
IMT	International Mobile Telecommunications
INMARSAT	International Mobile (formerly: Maritime) Satellite Organization
INTELSAT	International Telecommunications Satellite Organization
ISDN	Integrated Services Digital Network
ISI	intersymbol interference
ISM	industrial, scientific, medical
ITU	International Telecommunication Union
ITU-R	ITU Radiocommunication Sector

LEO	low Earth orbit
LF	low frequency
LMDS	local multipoint distribution system
LNA	low-noise amplifier
LO	local oscillator
LOS	line-of-sight
LUF	lowest usable frequency
MAP	Microwave Anisotropy Probe
MEMS	microelectromechanical system
MESFET	metal-semiconductor field-effect transistor
MF	medium frequency
MIM	metal-insulator-metal
MIMO	multiple-in-multiple-out
MLS	Microwave Landing System
MMIC	monolithic microwave integrated circuit
MOSFET	metal-oxide-semiconductor field-effect transistor
MRI	magnetic resonance imaging
MS	mobile station
MSC	mobile-services switching center
MSK	minimum-shift keying
MTI	moving target indicator
MTX	mobile telephone exchange
MUF	maximum usable frequency
NASA	National Aeronautics and Space Administration
NMT	Nordic Mobile Telephone
NRAO	National Radio Astronomy Observatory
PA	power amplifier
PAE	power added efficiency
PDC	Personal Digital Cellular
PLL	phase-locked loop
PM	phase modulation
PMR	Private Mobile Radio
PN	pseudorandom noise
PPI	plan position indicator
PSK	phase-shift keying
PSTN	Public Switched Telephone Network
QAM	quadrature amplitude modulation
QPSK	quadrature phase-shift keying
RF	radio frequency

---

RFID	radio frequency identification
RLAN	radio local area network
SAR	specific absorption rate
SAR	synthetic-aperture radar
SAW	surface acoustic wave
SETI	search for extraterrestrial intelligence
SHF	super high frequency
SIGINT	signal intelligence
SIS	superconductor-insulator-superconductor
SLAR	side-looking airborne radar
SSB	single sideband
TACS	Total Access Communications System
TCAS	Traffic-Alert and Collision-Avoidance System
TDD	time division duplexing
TDM	time division multiplexing
TDMA	time division multiple access
TDOA	time difference of arrival
TE	transverse electric
TED	transferred electron device
TEM	transverse electric and magnetic
TETRA	Trans-European Trunked Radio
TM	transverse magnetic
UHF	ultra high frequency
UMTS	Universal Mobile Telecommunications System
VCO	voltage-controlled oscillator
VHF	very high frequency
VLA	Very Large Array
VLBI	very long baseline interferometry
VLF	very low frequency
VLR	visitor location register
VOR	VHF omnidirectional range
VSF	vestigial sideband
VSWR	voltage standing wave ratio
WARC	World Administrative Radio Conference
WCDMA	wideband code division multiple access
WLAN	wireless local area network
WLL	wireless local loop
WMAN	wireless metropolitan area network
WPAN	wireless personal area network

WRC	World Radiocommunication Conference
WWAN	wireless wide area network
YIG	yttrium iron garnet

## About the Authors

**Antti V. Räisänen** received a Diploma Engineer (M.Sc.), a Licentiate of Science (Tech), and a Doctor of Science (Tech) in electrical engineering from Helsinki University of Technology (HUT), Finland, in 1973, 1976, and 1981, respectively. Dr. Räisänen was appointed to the professor chair of radio engineering at HUT in 1989, after previously having held the same position as an acting professor. He has held visiting scientist and professor positions at the Five College Radio Astronomy Observatory (FCRAO), the University of Massachusetts, Amherst, the Chalmers University of Technology, Göteborg, Sweden, at the Department of Physics, University of California, Berkeley, the Jet Propulsion Laboratory and California Institute of Technology, Pasadena, and the Paris Observatory and University of Paris 6.

Currently, Dr. Räisänen is supervising research in millimeter-wave components, antennas, receivers, and microwave measurements at HUT Radio Laboratory and MilliLab. He has authored or coauthored about 400 scientific or technical papers and five books: *Microwave Measurement Techniques*, *Radio Engineering, RF and Microwave Techniques*, *Millimeter-Wave Techniques*, and *Fundamentals of Radio Engineering* (with A. Lehto, published by Otatiето, in 1991, 1992, 1994, 1997, and 2001, respectively, all in Finnish). He also coauthored a chapter, “Radio-Telescope Receivers” with M. E. Tiuri, in J. D. Kraus, *Radio Astronomy, Second Edition* (Cygnus-Quasar Books, 1986). In 1994 he was elected to the grade of Fellow of the Institute of Electrical and Electronics Engineers (IEEE) with the citation “for contribution to and leadership in millimeter-wave receiver technology.” In 1998 he

received the EIS Award with a citation “for raising education and research of radio engineering in Finland to the top international level.” The Smart and Novel Radios Research Unit (SMARAD), led by Dr. Räsänen at HUT, obtained in 2001 the national status of Center of Excellence in Research from The Academy of Finland after competition and international review. Dr. Räsänen was the secretary general of the Twelfth European Microwave Conference in 1982. He was the chairman of the IEEE MTT/AP chapter in Finland from 1987 to 1992. He was the conference chairman for the Twenty-Second European Microwave Conference in 1992, and for the ESA Workshop on Millimetre Wave Technology and Applications in 1998. From 1997 to 2000 he served as vice-rector for research and international relations of HUT. Currently he serves as an associate editor of the *IEEE Transactions on Microwave Theory and Techniques*.

**Arto Lehto** received a Diploma Engineer (M.Sc.), a Licentiate of Science (Tech), and a Doctor of Science (Tech) in electrical engineering from HUT, in 1981, 1986, and 1990, respectively. Since 1981 he has held different teaching and research positions at HUT. Currently he is the docent of radio engineering at HUT. Dr. Lehto has authored and coauthored more than 80 scientific or technical papers about antenna measurement techniques, low-profile antennas, and millimeter-wave components. He has also authored or coauthored eight books (all in Finnish and published by Otatieto): *Micro-wave Measurement Techniques* (1991 with A. V. Räsänen), *Radio Engineering* (1992 with A. V. Räsänen), *RF and Microwave Techniques* (1994 with A. V. Räsänen), *Exercises for Radio Engineering* (1996 with J. Louhi), *Milli-meter-Wave Techniques* (1997 with A. V. Räsänen), *Radar Engineering* (1998 with O. Klemola), *Fundamentals of Radio Engineering* (2001 with A. V. Räsänen), and *Exercises for RF and Microwave Techniques* (2002 with V. Möttönen). He also coauthored a chapter, “Antenna Measurements” with P. Vainikainen, in J. D. Kraus and R. J. Marhefka, *Antennas for All Applications, Third Edition* (McGraw-Hill, 2002).

# Index

- $1/f$  noise, 276
- 16QAM, 302
- ABCD matrix, 100
- acousto-optical spectrometer (AOS), 349
- adapters, 139
- additive white Gaussian noise (AWGN), 275
- admittance matrices, 97–101
- Ampère's law, 12, 41
- amplifiers, 184–93
  - current waveforms, 192
  - defined, 184
  - dynamic range, 191
  - FET, 190
  - gain, 186, 189
  - HEMT, 189
  - low-noise, 184–91
  - noise factor, 188
  - nonlinearities and, 191–92
  - output stability, 187
  - power, 191–92
  - reflection, 192–93
  - small-signal, 184–91
  - stability, 186–87
  - two-port as, 184
- amplitude demodulators, 291–92
  - DSB, 292
  - envelope detector, 291
- amplitude modulation (AM), 288–90
  - defined, 288
  - quadrature (QAM), 292, 302, 303, 304
  - signal, 289
  - spectrum, 289, 290
- amplitude modulators, 290–91
  - mixer, 290
  - SSB, 291
- amplitude-shift keying (ASK) modulation, 298
- analog modulation, 288–97
- analog-to-digital converter (ADC), 274
- angles of incidence, 30, 31
- antenna arrays, 239–42
  - adaptive, 242
  - defined, 239
  - directional patterns, 241
  - illustrated, 239
  - microstrip, 241
  - pattern, 240
  - phased, 242
- antennas, 205–45
  - analysis and measurement, 207
  - aperture, 213, 225–31
  - bandwidth, 212
  - bow-tie, 237, 238
  - concepts, 205–12



- antennas (continued)
  - dielectric rod, 237, 238
  - dipole, 217–22
  - directional patterns, 208, 209
  - directivity, 209–10
  - effective area, 210–11
  - electric field amplitude produced by, 243
  - far-field region, 206
  - gain, 210
  - helix, 223, 224
  - horn, 213, 232–34
  - impedance, 212
  - isotropic, 208
  - lens, 237, 238
  - link between, 242–45
  - log-periodic, 222
  - long-wire, 223–24
  - loop, 222–23
  - matching of, 242
  - microstrip, 237–38
  - monopole, 217–22
  - need for, 205
  - noise, 275
  - noise temperature, 284–87
  - phase pattern, 211
  - polarization, 211–12
  - power available from, 244
  - power density produced by, 243
  - properties, 207
  - radiating current element, 214–16
  - radiating near-field region, 206
  - radiation calculation, 212–14
  - radiation efficiency, 210
  - radiation pattern, 208
  - radiation resistance, 212
  - reactive near-field region, 206
  - as reciprocal devices, 205–6
  - reflector, 234–36
  - rhombic, 223, 224–25
  - slot, 237, 238
  - space around, 206
  - spherical coordinate system, 207
  - surrounded by black surface, 285
  - temperature of radio sources, 349–50
  - traveling-wave, 223–25
  - wire, 217–25
  - Yagi, 221–22
- apertures
  - circular, properties of, 230, 231
  - large, 228
  - line source, directional pattern, 231
  - line source properties, 230
  - phase, 230
  - radiation from, 225–31
  - radiation pattern, 229
  - rectangular, normalized directional pattern, 229
- applications, 307–61
  - broadcasting, 307–12
  - electronic warfare, 359–61
  - medical, 357–59
  - mobile communications, 317–20
  - power, 356–57
  - radar, 328–36
  - radio astronomy, 345–53
  - radio link systems, 312–14
  - radionavigation, 320–28
  - remote sensing, 336–45
  - sensors, 353–56
  - wireless LANs (WLANs), 314–16
- Armstrong, Edwin, 8
- attenuation
  - in clear atmosphere, 250
  - from knife-edge diffraction, 256
  - from rain/fog, 250–51
  - of standard waveguides, 51
  - tropospheric, 249–52
  - value, 136
- attenuators, 136–38
  - adjustable waveguide, 137
  - coaxial, 137
  - fixed, 137
  - ideal, 136
  - microstrip, 137
  - waveguide, 137
  - See also* Passive devices
- automatic gain control (AGC), 274
- available power gain, 111–12
- aviation navigation, 326–28
  - DME, 326
  - ILE, 326–27
  - MLS, 327–28
  - TCAS, 328
  - VOR, 326
  - See also* Radionavigation

- bandpass filters, 154
  - design example, 165–66
  - elements, 167
  - illustrated, 165
  - microstrip layouts of, 167
  - from waveguide cavities, 168
  - See also* Filters
- bandstop filters, 167
- bandwidth
  - antenna, 212
  - noise, 278, 305
- Bessel functions, 293
- biological effects, 363–66
- bipolar transistors, 177, 181
- bit error rate (BER), 299
  - of PSK systems, 303
  - S/N and, 303
- boundary conditions, 20–22
- bow-tie antennas, 237, 238
- branch-line coupler, 127
- brightness temperature, 338–39
- broadcasting, 307–12
  - defined, 307
  - in Finland, 308–10
  - frequency ranges for, 308
  - satellites, 310–12
  - transition, 307–8
- broadcasting satellite service (BSS), 311
- bulk acoustic wave (BAW) filters, 169
- Butterworth response, 156
  
- Carson's rule, 294
- cavity resonators, 149–53, 354
  - cavity length, 150
  - couplings, 149
  - cylindrical cavity, 153
  - defined, 149
  - quality factor, 152, 153
  - rectangular, 150
  - See also* Resonators
- Chebyshev response, 156–57
  - component value calculation, 158
  - element values, 159
  - insertion loss, 157
- Chebyshev transformer, 92
- circular waveguides, 37, 52–55
  - conductor losses, 53
  - illustrated, 52
  - relative bandwidth, 53
  - See also* Waveguides
- circulators, 134
- coaxial attenuator, 137
- coaxial lines, 37, 58–61
  - air-filled, 60
  - characteristic impedance, 59
  - conductor loss, 59–60
  - defined, 58
  - dielectric loss, 60
  - electric field, 59
  - example, 60–61
  - at high frequencies, 60
  - illustrated, 58
  - low-/high-impedance matching, 93
  - magnetic field, 59
  - TEM wave mode, 59
  - See also* Transmission lines
- coaxial-to-microstrip transition, 139
- coded orthogonal frequency division multiplex (COFDM), 308
- comb-line filters, 168
- computer-aided design (CAD) package, 191
- connectors, 138–39
  - defined, 138
  - illustrated, 139
  - See also* Passive devices
- coplanar waveguide, 37
- Cosmic Background Explorer (COBE), 351
- coupled resonators, 144–47
  - equivalent circuits, 145
  - one coupling, 145–46
  - quality factor, 146
  - two couplings, 146–47
  - See also* Resonators
- cutoff frequency, 46
  - defined, 42
  - of rectangular/circular waveguides, 55
  - of TE<sub>01</sub> wave mode, 55
- cutoff wavelength, 42
  - in circular waveguide, 54
  - in rectangular waveguide, 46
- cylindrical coordinate system, 39, 368
  
- Decca, 321
- De Forest, Lee, 7

- detectors, 198–201
  - diode, 198–201
  - equivalent circuit, 200
  - operation, 198
  - response, 201
- diathermy, 359
- Dicke radiometer, 342–43
- dielectric resonator oscillator (DRO), 154
- dielectric resonators, 153–54
  - defined, 153
  - illustrated, 154
  - See also* Resonators
- dielectric rod antennas, 237, 238
- differential PSK (DPSK), 301
- Digital Audio Broadcasting (DAB), 308
- Digital Cellular System (DCS 1800), 319
- digital modulation, 297–304
  - ASK, 298
  - bandwidth efficiency, 303
  - comparison, 302–4
  - FSK, 298, 299–300
  - PSK, 298, 300–301
  - QAM, 302
  - See also* Modulation
- digital-to-analog converter (DAC), 273
- Digital Video Broadcasting (DVB), 308
- diode detectors, 198–201
- diode mixers, 195
- diodes, 172–77
  - Gunn, 176
  - IMPATT, 176–77
  - negative resistance for oscillators, 181
  - p-n*, 172–74
  - Schottky, 174–76
  - tunnel, 173
  - See also* Semiconductor devices
- dipole antennas, 217–22
  - $3\lambda/2$ -long, 219
  - current distribution, 217, 218
  - folded, 219
  - half-wave, 218
  - Hertz, 215, 219
  - illustrated, 217
  - length, 218, 219
  - log-periodic, 222
  - omnidirectional, 221
  - See also* Antennas
- direct-conversion transmitters, 272
- direct digital synthesis (DDS), 273
- directed energy weapons (DEW), 361
- directional couplers, 116–17, 119–27
  - branch-line, 127
  - coupling, 119–20
  - defined, 116
  - directivity, 119–20
  - illustrated, 119
  - Lange, 126
  - microstrip, 124–27
  - ports, 116
  - for reflection coefficient magnitude measurement, 120
  - ring, 126–27
  - scattering matrix, 120–22
  - uses, 116–17
  - waveguide, 122–24
  - See also* Passive devices
- direct sequence spread spectrum (DSSS), 316
- Distance Measuring Equipment (DME), 326
- distributed components, 115
- Doppler radar, 332–34
  - block diagram, 332, 333
  - distance to target and, 334
  - Doppler frequency, 332–33
  - with two antennas, 333
  - for velocity measurements, 334
  - See also* Radar
- dosimetry, 364
- double-sideband suppressed carrier (DSBSC) modulation, 289
- DSB demodulator, 292
- DSB mixers, 196, 281, 282
- DSB modulation, 289, 290
- dual-gate FET (DGFET), 195
- effective area, 210–11
- electric fields
  - coaxial line, 59
  - line integral of, 15
  - of plane waves, 26
  - ratio, 23
  - tangential components, 29
  - See also* Magnetic fields

- electric flux, 15
- electric flux density, 12
- electric polarization, 17–18
- electric quantities, 11
- electric vector potential, 212, 214
- electric wall, 22
- electromagnetic capability (EMC), 6
- electromagnetic fields
  - creation of, 16
  - fundamentals, 11–33
  - as vector quantities, 26
- electromagnetic spectrum, 2
- electronic attack (EA), 360–61
- electronic protection (EP), 360, 361
- electronic support (ES), 360
- electronic warfare (EW), 359–61
  - categories, 360
  - defined, 360
  - EA, 360–61
  - EP, 361
  - ES, 360
- electron tubes, 171
- energy
  - conservation principle, 32
  - power and, 31–33
  - propagation velocity of, 44
  - stored, 152
  - time-averaged stored electric, 32
- equivalent isotropic radiated power (EIRP), 309
- equivalent noise temperature, 277, 279, 280, 304
- EUTELSAT, 314
- extremely high frequency (EHF) waves, 3
- fading
  - flat, 261
  - frequency-selective, 261
  - large-scale, 260–61
  - scattering and, 265
  - small-scale, 262
- Faraday rotation, 131–33, 267
- Faraday's law, 12
- far-field region, 206
- ferrite devices, 128–34
  - circulators, 133–34
  - defined, 128
  - Faraday rotation, 131–33
  - isolators, 133–34
  - properties, 128–31
  - See also* Passive devices
- filters, 154–69
  - bandpass, 154, 165, 167
  - bandstop, 167
  - BAW, 169
  - comb-line, 168
  - defined, 154
  - design of, 155, 161–66
  - highpass, 154
  - ideal, 154–55
  - insertion loss method, 155–61
  - interdigital, 168
  - lowpass, 158–61, 163
  - microwave, 161–69
  - practical, 166–69
  - realization difficulties, 161
  - reflection coefficient, 155
  - SAW, 169
  - uses, 155
- Finland
  - broadcasting in, 308–10
  - FM radio stations, 310
  - RF radiation sources, 365
- fin line, 37
- flat fading, 261
- Fleming, John Ambrose, 7
- flicker noise, 276
- FM-CW radar, 334–35
  - block diagram, 334
  - defined, 334
  - example, 335
  - See also* Radar
- folded dipole, 219
- Fraunhofer region, 206
- frequency allocation, 4–6
  - for frequency band 10–10.7 GHz, 6
  - world regions for, 5
- frequency demodulators, 295, 296
  - frequency discriminator, 296
  - PLL as, 296
- frequency division duplexing (FDD), 275
- frequency division multiple access (FDMA), 318

- frequency division multiplexing (FDM), 304
- frequency hopping spread spectrum (FHSS), 316
- frequency modulation (FM), 183, 292–94
  - Bessel functions, 293
  - defined, 288
  - spectrum, 293, 294
  - with VCO, 294
- frequency modulators, 294–95
- frequency multipliers, 197–98
  - defined, 197–98
  - efficiency, 198
  - nonlinear element, 198
- frequency-selective fading, 261
- frequency-shift keying (FSK) modulation, 299–300
  - coherent demodulator, 300
  - noncoherent demodulator, 299
  - realization, 299
  - waveform, 298
- Fresnel ellipsoid, 255
- Fresnel region, 206
- gain, 105
  - amplifier, 186, 189
  - antenna, 210
  - available power, 111–12
  - insertion, 112
  - maximum available power, 112, 186
  - power, 111
  - transducer power, 111
  - of two-port, 111–12
- Galileo system, 326
- Gauss' theorem, 12, 13
  - defined, 367
  - in sourceless space, 41
- General Packet Radio Service (GPRS), 319
- geosynchronous Earth orbit (GEO) satellites, 311, 312
- Global Navigation Satellite System (GLONASS), 323
- Global Positioning System (GPS), 323–25
  - defined, 323
  - frequencies, 323
  - satellite orbits, 324
  - signal, 325
- Global System for Mobile Communications (GSM), 318–19
  - BSC, 318, 319
  - BTS, 318
  - defined, 318
  - GSM 900, 318
  - MSC, 319
  - network architecture, 319
- ground-wave propagation, 248, 267–70
  - electric field strength, 269
  - surface electric properties, 268
- group velocity, 65–66
- Gunn diode, 176
- Gunn oscillators, 181
- Hartley oscillator, 294, 295
- helix antennas, 223, 224
- Helmholtz equation, 22–26
  - in cylindrical coordinate system, 39
  - defined, 23
  - plane wave solution, 22–26
  - solution, 23
  - in sourceless medium, 38
- Hertz, Heinrich, 7, 215
- Hertz dipole, 215, 219
- heterojunction bipolar transistors (HBTs), 178
- heterojunction field-effect transistors (HFETs), 179
- high electron mobility transistors (HEMTs), 179
- highpass filters, 154
- High-Speed Circuit Switched Data (HSCSD), 319
- horn antennas, 213, 232–34
  - conical, 232
  - corrugated, 234
  - defined, 232
  - diagonal, 234
  - directivities of, 233
  - E*-plane, 232, 233
  - H*-plane, 232
  - illustrated, 232
  - Potter, 234
  - pyramidal, 232
  - types of, 232
  - See also* Antennas

- Hülsmeier, Christian, 8
- hyperbolic radionavigation systems,  
320–26  
Decca, 321  
illustrated, 321  
Loran-C, 321–23  
*See also* Radionavigation
- hyperthermia, 359
- impact ionization avalanche transmit time.  
*See* IMPATT diode; IMPATT oscillators
- IMPATT diode, 176–77  
defined, 176  
illustrated, 177  
structures, 176, 177  
*See also* Diodes
- IMPATT oscillators, 181–82
- impedance matching, 69–95  
coaxial line, 93  
concepts, 69  
input, 78  
load, 81  
with lumped reactive elements, 79–86  
methods, 78–95  
output, 78  
purpose, 78  
quarter-wave transformer, 89–94  
resistive, 94–95  
Smith chart and, 74–78  
with tuning stubs, 86–89  
with two reactive elements, 82
- impedance matrices, 97–101
- insertion gain, 112
- insertion loss method, 155–61  
Chebyshev response, 156–57  
defined, 155  
maximally flat response, 156, 157  
*See also* Filters
- Instrument Landing System (ILS), 326–27
- INTELSAT, 314, 315, 316  
coverage areas, 316  
defined, 314  
INTELSAT-6 satellite, 315
- interdigital filters, 168
- International Mobile Satellite Organization (INMARSAT), 317
- International Mobile Telecommunications 2000 (IMT-2000), 319–20
- International Telecommunication Union (ITU), 5
- intersymbol interference (ISI), 261
- ionosphere, 247–48  
defined, 265  
electron density in, 266  
propagation via, 248, 265–67  
radio hop, 267  
wave propagation illustration, 268
- isolators, 133–34  
defined, 133  
illustrated, 133  
operation, 133  
*See also* Passive devices
- Jansky, Karl, 8
- Kirchoff's law, 181
- knife-edge diffraction, 256
- Kuroda identities, 161–64  
illustrated, 162  
parallel stubs transformation with, 163, 164  
using, 161–62
- Lange coupler, 126
- Laplace's equations, 41, 59
- Larmor frequency, 129
- lens antennas, 237, 238
- load  
length, 135  
line termination with, 70  
matching, with quarter-wave transformer, 90  
matching of, 83, 84, 85  
mismatched, 69–74  
normalized impedance, 71  
reflection coefficient, 94  
voltage, solving, 108
- load impedance, 70, 78  
matching, 81, 83, 84, 85  
mixer, 196  
oscillators, 180
- local multipoint distribution systems (LMDSs), 314
- log-periodic antennas, 222

- long-wire antennas, 223–24
- loop antennas, 222–23
- Loran-C, 321–23
  - defined, 321–22
  - pulse of, 322
  - signals, 322–23
- Lorentz's force law, 11
- LOS path, 255–57
  - example, 257
  - knife-edge obstacle on, 256
  - receiving antenna in, 255
- low Earth orbit (LEO), 317
- lowest usable frequency (LUF), 267
- low-loss lines, 72
- lowpass filters, 158–61
  - Chebyshev, element values, 159
  - design, 163
  - frequency scaling and transformations, 160
  - insertion-loss frequency response, 161
  - microstrip layout, 167
  - prototypes, 158
  - realization, 166
- lumped components, 115
- lumped reactive elements
  - illustrated, 80
  - load matching with, 83, 84
  - matching with, 79–86
- magnetic current density, 14
- magnetic fields
  - coaxial line, 59
  - electron precessing in, 129
  - line integral of, 15
  - of plane wave, 23
  - ratio of, 23
  - tangential components, 29, 30
- magnetic field strength, 12
- magnetic flux, 15
- magnetic flux density, 21, 130
- magnetic quantities, 11
- magnetic vector potential, 212, 213
- magnetic wall, 22
- Marconi, Guglielmo, 7
- Mason's rule, 109–11
  - defined, 109
  - example, 110–11
- material parameters, 372
- maximally flat response, 156, 157
  - element values, 159
  - insertion loss, 157
- maximum available power gain, 112, 186
- maximum usable frequency (MUF), 267
- Maxwell, James Clerk, 6–7, 12
- Maxwell's equations, 11–17
  - III equation, 20, 38
  - IV equation, 20, 38
  - in case of harmonic time dependence, 14–15
  - defined, 11
  - in differential form, 12
  - illustrated, 16
  - in integral form, 13–14
  - interpretations of, 15–17
  - as radio engineering basis, 16
- media
  - boundary between, 20
  - fields in, 17–19
- medical applications, 357–59
  - diathermy, 359
  - hyperthermia, 359
  - thermography, 358–59
- metal-insulator-metal (MIM) structure, 80, 202
- metal-oxide-semiconductor field-effect transistors (MOSFETs), 178
- metal-semiconductor field-effect transistors (MESFETs), 178
- microelectromechanical systems (MEMS) technology, 141
- microstrip antennas, 137–38
- microstrip attenuator, 137
- microstrip directional couplers, 124–27
  - branch-line, 127
  - illustrated, 125
  - Lange, 126
  - multielement, 125
  - ring, 126–27
  - single-element, 125
  - See also* Directional couplers
- microstrip lines, 61–65
  - characteristic impedance, 62
  - cross section, 61
  - defined, 37, 61

- dielectric loss, 64
- dielectric resonator coupled to, 154
- discontinuities, 64
- example, 64–65
- loss sources, 64
- TEM wave mode propagation in, 61
- width, 63, 64
- See also* Transmission lines
- Microwave Anisotropy Probe (MAP), 352
- microwave circuits
  - monolithic, 201–2
  - with  $n$  ports, 98
  - ports, 101
  - reciprocal, 102
  - scattering matrices, 103–4
  - theory, 97–112
- microwave filters, 161–69
  - design of, 161–66
  - practical, 166–69
- Microwave Landing System (MLS), 327
- Mie scattering, 263
- minimum-shift keying (MSK), 300
- mixers, 194–97
  - as amplitude modulator, 290
  - balanced, 197
  - defined, 194
  - diode, 195
  - double-balanced, 197
  - as downconverters, 195
  - DSB, 196, 281, 282
  - Gilbert cell, 197
  - load impedances, 196
  - noise factor/temperature, 281
  - operation of, 195
  - single-ended, 197
  - SSB, 196, 197, 281, 282
- mobile communications, 317–20
- modulation, 287–304
  - AM, 288–92
  - analog, 288–97
  - ASK, 298
  - digital, 297–304
  - DSB, 289, 290
  - DSBSC, 289
  - FM, 292–95
  - FSK, 298, 299–300
  - PM, 295–97
  - PSK, 298, 300–301
  - QAM, 292, 302
  - schemes, 287
  - SSB, 289, 290
  - VSB, 289, 290
- monolithic microwave circuits (MMICs), 201–2
  - defined, 201
  - designing, 202
  - illustrated, 202
- monopole antennas, 220–22
  - defined, 220
  - illustrated, 220
  - omnidirectional, 221
  - short, 221
  - top-loaded, 220
  - in VLF/LF ranges, 221
  - Yagi, 221–22
  - See also* Antennas
- monopulse radar, 335–36
- Motley-Keenan model, 263
- multipath propagation, 257–63
  - in cellular mobile radio systems, 260–63
  - defined, 257
  - in urban environment, 261
  - See also* Propagation
- multiple-in-multiple-out (MIMO) systems, 262
- multisection transformer, 94
- National Radio Astronomy Observatory (NRAO), 346–47
- noise, 275–87
  - $1/f$ , 276
  - antenna, 275, 284–87
  - AWGN, 275
  - bandwidth, 278, 305
  - from human activity, 287
  - measure, 280
  - polarization of, 286
  - properties, 276
  - quantum, 276
  - receiver, 275–84
  - shot, 276
  - from space, 287
  - thermal, 276, 287
  - types, 275



- noise factor, 188
  - of chain, 279–80
  - of mixer, 281
  - as S/N ratio, 278
- noise power, 275, 277
  - available, 277–78
  - defined, 275
- noise temperature
  - antenna, 284–87
  - DSB, 281
  - equivalent, 277, 279, 280, 304
  - frequency vs., 284
  - of mixer, 281
  - of sky, 286
  - SSB, 282
  - system, 304
- nonthermal effects, 363–64
- Nordic Mobile Telephone (NMT), 317–18
- optical depth, 279
- optical fibers, 56–58
  - defined, 56
  - example, 57–58
  - loss mechanisms, 58
  - multimode, 57
  - properties, 58
  - structures, 56
- oscillators, 180–84
  - bipolar transistors in, 181
  - defined, 180
  - equivalent circuit, 180
  - Gunn, 181
  - Hartley, 294, 295
  - IMPATT, 181–82
  - load impedance, 180
  - microstrip layout, 183
  - modeling, 180
  - negative resistance for, 181
  - output powers, 182
  - YIG resonator coupled to, 184
- parabolic reflector antennas, 234–35
- parallel polarization, 29, 31
- parallel-wire line, 37
- passive devices, 115–39
  - adapters, 139
  - attenuators, 136–38
  - circulators, 134
  - connectors, 138–39
  - directional couplers, 116–17, 119–27
  - ferrite, 128–34
  - isolators, 133–34
  - phase shifters, 138
  - power dividers, 116, 117–19
  - standardized symbols, 116
  - terminations, 135–36
- perpendicular polarization, 30, 31
- phase-locked loop (PLL), 272
- phase modulation (PM), 295–97
  - defined, 288
  - phasor representation, 297
  - signal, 297
  - See also* Modulation
- phase pattern, 211
- phase shifters, 138
- phase-shift keying (PSK) modulation
  - BER, 303
  - differential (DPSK), 301
  - illustrated, 300
  - quadrature phase (QPSK), 301
  - realization, 300
  - signal spectra, 299
  - waveform, 298
  - See also* Digital modulation
- phase velocity, 43, 65
- physical constants, 371
- plane waves
  - electric field of, 26
  - group velocity, 66
  - magnetic field of, 23
  - polarization of, 26–28
  - propagation, 24
  - propagation velocity, 24
  - reflection of, 28–31
  - transmission of, 28–31
- plasma frequency, 267
- plate capacitor, 18
- p-n* diode, 172–74
  - defined, 172–73
  - forward-biased, 173–74
  - illustrated, 173
  - reversed-biased, 173
- polarization
  - antenna, 211–12

- circular, 27–28
  - elliptic, 27
  - horizontal, 259
  - linear, 27
  - of noise, 286
  - parallel, 29, 31
  - perpendicular, 30, 31
  - of plane waves, 26–28
- power
- applications, 356–57
  - complex, 32
  - current element, 216
  - energy and, 31–33
  - noise, 275, 277
  - reflection coefficient, 155
- power amplifiers, 191–92
- power dividers, 116, 117–19
- defined, 116
  - equivalent circuits, 118
  - ports, 116
  - resistive, 118
  - T-junctions, 117–18
  - Wilkinson, 118, 119
- See also* Passive devices
- power gain, 111
- available, 111–12
  - maximum available, 112, 186
- Poynting's theorem, 32–33
- propagation, 247–70
- aided by scattering, 263–65
  - along LOS path, 248
  - beyond radio horizon, 249
  - deterministic models, 262
  - in ferrite, 132
  - as ground (surface) wave, 267–70
  - ground-wave, 248
  - mechanisms, 247–49
  - multipath, 257–63
  - in plasma, 265
  - of radio waves, 247–70
  - stochastic models, 262
  - in troposphere, 254
  - velocity, 65
  - via ionosphere, 248, 265–67
- pulse radar, 328–32
- block diagram, 329
  - defined, 328
  - example, 332
  - maximum operating range, 330
  - performance, 331
  - power density, 330
  - pulse compression, 331
  - radar cross section, 330
  - resolution, 329
- See also* Radar
- quadrature amplitude modulation (QAM), 292, 302
- 16QAM, 302
  - multistate, 303, 304
- quadrature phase shift keying (QPSK), 301
- quality factor, 142–44
- cavity resonators, 152, 153
  - coupled resonators, 146
  - defined, 142–43
  - solving, from input admittance vs. frequency, 147
- See also* Resonators
- quantum noise, 276
- quarter-wave transformer, 89–94
- defined, 89
  - illustrated, 89
  - matching load with, 90
  - multiple-reflection analysis of, 91
  - problem, 92
  - reflection coefficient, 93
- See also* Impedance matching
- quasioptical components, 116
- quasioptical waveguide, 37
- radar, 328–36
- bistatic, 328
  - defined, 328
  - Doppler, 332–34
  - FM-CW, 334–35
  - monopulse, 335–36
  - monostatic, 328
  - pulse, 328–32
  - remote-sensing, 343–45
  - SAR, 343–45
  - sensors, 355
  - SLAR, 343–45
  - surveillance, 335
  - tracking, 335

- radiating current element, 214–16
  - components, 215–16
  - defined, 214–15
  - illustrated, 214
  - power, 216
- radiating near-field region, 206
- radiation efficiency, 210
- radiation resistance, 212
- radio astronomy, 345–53
  - radio sources, 350–53
    - radio sources antenna temperature, 349–50
  - receivers, 348–49
  - telescopes, 346–48
- radio engineering, 4
  - activities, 4
  - history of, 6–8
  - time harmonic phenomena, 14
- radio frequencies, allocation, 4–6
- radio frequency (RF) waves, 3
- radio link budget, 304–6
- radio-link hop planning, 258
- radio links, 312–14
  - analog/digital, 313
  - point-to-point, 313, 314
  - satellite, 314
  - terrestrial, 312–14
- radiometers, 340–43
  - defined, 340
  - Dicke, 342–43
  - measuring brightness temperature, 338
  - total power, 340–42
- radiometry, 337–40
- radionavigation, 320–28
  - in aviation, 326–28
  - hyperbolic, 320–23
  - satellite, 323–26
- radio sources
  - antenna temperature of, 349–50
  - frequency dependencies, 351
  - in sky, 350–53
- radio systems, 271–306
  - link budget, 304–6
  - modulation/demodulation, 287–304
  - noise, 275–87
  - receivers, 271–75
  - transmitters, 271–75
- radio telescopes, 346–48
  - illustrated, 347
  - NRAO, 346
  - VLA, 347
  - VLBI, 348
- radio waves
  - bending (refraction) of, 252–55
  - direct, 258
  - ducting of, 255
  - as part of electromagnetic spectrum, 1–4
  - propagation of, 247–70
  - ranges of, 3
  - reflected, 258
  - remote sensing with, 337
  - velocity, 65–66
- Rayleigh probability distribution, 261
- reactive near-field region, 206
- receivers, 271–75
  - direct-conversion, 274
  - noise, 275–84
  - QAM, 292
  - radio astronomy, 348–49
  - superheterodyne, 273
  - See also* Radio systems; Transmitters
- rectangular coordinate system, 368
- rectangular waveguide, 35–36, 44–52
  - air-filled, 46
  - illustrated, 45
  - metal, 46
  - slotted line made with, 74
  - TE wave modes, 44–50
  - TM wave modes, 50–52
  - See also* Waveguides
- reflection
  - from ground, 257–60
  - from mismatched load, 69–74
  - of plane wave, 28–31
  - sensors, 355
  - total, 31
- reflection amplifiers, 192–93
  - defined, 192
  - illustrated, 193
  - power gain, 192
- reflection coefficient, 29, 31
  - filter, 155
  - input, solving, 107, 108

- load, 94
- magnitude measurement, 120
- of matching transformers, 93
- power, 155
- total, 91
- voltage, 70, 75, 107
- reflector antennas, 234–36
  - aperture blockage, 236
  - Cassegrainian, 235
  - parabolic, 235–36
  - pattern, 236
  - uses, 234
  - See also* Antennas
- refraction, 252–55
- remote sensing, 336–45
  - active, 337
  - defined, 336
  - passive, 336–37
  - radar, 343–45
  - radiometers, 340–43
  - radiometry, 337–40
  - with radio waves, 337
- resistive matching, 94–95
  - applications, 95
  - with attenuator, 94
  - defined, 94
- resonance
  - frequency, 143
  - modes, 151, 152
  - phenomenon, 142
- resonators, 141–54, 354–55
  - cavity, 149–53, 354
  - coupled, 144–47
  - defined, 141
  - dielectric, 153–54
  - equivalent circuits of, 145
  - illustrated, 142
  - loss, 146
  - power absorbed in, 144
  - power loss, 144
  - quality factor, 142–44
  - selectivity measurement, 144
  - strip-line, 354
  - transmission line section as, 147–49
  - types of, 354
  - uses, 354–55
- RF radiation, 365–66
  - absorption of, 364
  - limits of exposure, 366
  - sources, 365
- rhombic antennas, 223, 224–25
  - defined, 223
  - illustrated, 225
  - See also* Antennas
- Richard's transformation, 161, 162
- ring coupler, 126–27
- satellite navigation systems, 323–26
  - Galileo, 326
  - GPS, 323–25
  - Transit, 323, 324
- satellite radio links, 314
- satellites, 310–12
  - broadcasting, 310–12
  - BSS, 311
  - GEO, 311, 312
- scattering
  - cause of, 263
  - cross section, 263, 264
  - defined, 263
  - fading and, 265
  - Mie, 263
  - propagation aided by, 263–65
  - tropospheric, 264, 265
- scattering matrices, 101–4
  - defined, 101
  - directional coupler, 120–22
  - of lossless circuit, 121
  - with normalized waves, 102
  - of simple circuits, 103–4
- Schottky diode, 174–76
  - defined, 174
  - as detector/mixer, 175
  - equivalent circuit, 174
  - illustrated, 174
  - I-V* characteristic, 174, 175
  - junction capacitance, 175
  - See also* Diodes
- Schottky-mixer receiver, 348
- scintillation, 251–52
- semiconductor devices, 172–79
  - advantages, 171–72
  - circuits based on, 171–202

- semiconductor devices (continued)
  - diodes, 172–77
  - drawing symbols based on, 172
  - transistors, 177–79
- sensors, 353–56
  - imaging, 356
  - radar, 355
  - radiometer, 356
  - reflection, 355
  - resonators, 354–55
  - transmission, 354
- shot noise, 276
- side-looking airborne radar (SLAR), 343–45
  - cross-range resolution, 344
  - defined, 343
  - illustrated, 344
  - measurements, 345
  - See also* Remote sensing
- signal flow graphs, 104–9
  - defined, 104
  - nodal points, 105
  - simplification of, 106
  - solving input reflection coefficient with, 107
  - solving load voltage with, 108
  - three-port, 105
  - two-port, 105
- single-sideband (SSB) mixers, 196, 197, 281, 282
- slot antennas, 237, 238
- Smith chart, 74–78
  - amplifier gain/noise circles on, 189
  - defined, 74
  - illustrated, 76
  - matching of load with shunt susceptance with, 87
  - to obtain tuning stubs length, 88
  - output stability circles on, 187
  - use illustration, 77
- Snell's law, 29, 253
- specific absorption rate (SAR), 364
- spherical coordinate system, 207, 368–69
- SSB modulation, 289, 290
- SSB modulator, 291
- Stokes' theorem, 14, 367
- superhigh frequency (SHF) waves, 3
  - surface acoustic wave (SAW) filters, 169
  - surveillance radar, 335
  - suspended microstrip, 37
  - synthetic-aperture radar (SAR), 343–45
- TE<sub>01</sub> wave mode, 53–55
  - attenuation, 54
  - attenuation constant, 53
  - cutoff frequency, 55
- TE<sub>10</sub> wave mode, 47–49
  - characteristic impedance, 48
  - conductor loss for, 49
  - power propagation, 48
  - waveguide frequency range, 49
  - wave impedance, 47
- TE<sub>101</sub> mode, 153
- TEM waves, 40–41
  - coaxial line, 59
  - defined, 40
  - phase constant, 62
  - propagation velocity, 44
  - wave equations for, 40
- terminations, 135–36
- terrestrial radio links, 312–14
- TE waves, 42–44
  - attenuation of, 43
  - defined, 42
  - in rectangular waveguide, 44–50
  - transverse field distributions (circular waveguide), 54
  - transverse field distributions (rectangular waveguide), 52
  - wave impedance, 45
  - wavelength, 44
- thermal noise
  - from atmospheric attenuation, 287
  - defined, 276
  - See also* Noise
- thermography, 358–59
- Tigerstedt, Eric, 7
- time division duplexing (TDD), 275
- time division multiplexing (TDM), 304
- time harmonic fields, 14
- T-junctions, 117, 123–24
- TM<sub>110</sub> mode, 153
- TM waves, 42–44
  - attenuation of, 43

- defined, 42
- longitudinal electric fields, 53
- propagation velocity, 44
- in rectangular waveguide, 50–52
- transverse field distributions (circular waveguide), 54
- transverse field distributions (rectangular waveguide), 52
- wave impedance of, 51
- wavelength, 44
- total power radiometer, 340–42
  - block diagram, 341
  - output voltage, 341
  - rapid gain fluctuations, 342
  - See also* Radiometers
- tracking radar, 335
- traffic-alert and collision-avoidance systems (TCAS), 328
- transceivers, 274–75
- transducer power gain, 111
- transfer functions, 105
  - linear circuit, 194
  - linear small-signal condition, 194
  - nonlinear circuit, 194
- transferred electron device (TED), 176
- transistors, 177–79
  - bipolar, 177
  - HEMT, 179
  - HFET, 179
  - MESFET, 178
  - MOSFET, 178
  - See also* Semiconductor devices
- Transit, 323, 324
- transmission
  - coefficient, 29
  - of plane wave, 28–31
- transmission lines, 35–68
  - coaxial, 37, 58–61
  - comparison, 36
  - defined, 35
  - equations for, 38–40
  - fin, 37
  - illustrated, 36
  - joint, 103–4
  - lossless, 103, 108
  - low-loss, 72
  - microstrip, 37, 61–65
  - model, 66–68
  - parallel-wire, 37
  - passive devices, 115–39
  - standing wave in, 74
  - transmission line section
    - equivalent circuit, 148
    - reactance vs. frequency, 149
    - as resonator, 147–49
  - transmission matrix, 100
    - calculation, 104
    - of two-port, 100
  - transmission sensors, 354
  - transmitters, 271–75
    - direct-conversion, 272
    - low-power, 272
    - QAM, 292
    - See also* Radio systems; Receivers
  - transverse electric modes. *See* TE waves
  - transverse electromagnetic waves. *See* TEM waves
  - transverse magnetic modes. *See* TM waves
  - traveling-wave antennas, 223–25
  - troposphere, 247
    - attenuation, 249–52
    - bending of radio waves in, 252–55
    - propagation in, 254
    - refraction index, 252
    - scattering, 264, 265
    - turbulence in, 251
  - tuning stubs
    - characteristic impedance, 86
    - lengths, obtaining, 88
    - matching of load with normalized admittance, 88
    - matching with, 86–89
    - open-circuited, 86
- tunnel diode, 173
- ultrahigh frequency (UHF) waves, 3
- Universal Mobile Telecommunications System (UMTS), 320
- vector operations, 367–69
- vector potentials, 225–26
- Very Large Array (VLA), 347
- very long baseline interferometry (VLBI), 348

- vestigial sideband (VSB) modulation, 289, 290
- VHF Omnidirectional Range (VOR), 326
- voltage
  - load, solving, 108
  - reflection coefficient, 70, 75, 107
  - sensitivity, 199
  - total, 99, 102
  - wave normalization, 101
- voltage-controlled oscillator (VCOs), 272, 294
- Walfisch-Bertoni model, 262–63
- waveguide attenuator, 137
- waveguide-cavity filters, 168
- waveguide directional couplers, 122–24
  - directivity frequency response, 123
  - illustrated, 123
  - magic T-junction, 123–24
  - See also* Directional couplers
- waveguides, 35–68
  - attenuation, 51
  - circular, 37, 52–55
  - comparison, 36
  - coplanar, 37
  - defined, 35
  - equations for, 38–40
  - illustrated, 36
  - isolator, 133
  - passive devices, 115–39
  - quasioptical, 37
  - rectangular, 35–36, 44–52
  - standard, 50
- waveguide-to-coaxial adapter, 139
- wave impedance
  - defined, 23
  - TE wave mode, 45
- wave modes, 39–40
  - defined, 39–40
  - TE, 42–44
  - TEM, 40–41
  - TM, 42–44
- wideband code division multiple access (WCDMA), 320
- Wilkinson power divider, 118, 119
- wireless LANs (WLANs), 314–16
  - defined, 314
  - DSSS, 316
  - FHSS, 316
  - radio waves, 315
  - standards, 315
- wireless local loops (WLLs), 314
- wireless metropolitan area networks (WMANs), 315
- wireless personal area networks (WPANs), 315
- wireless wide area networks (WWANs), 315
- World Radiocommunication Conferences (WRCs), 5
- Yagi antennas, 221–22
- YIG resonator, 183, 184
- Y-junction circulators, 134